THE ELECTRICAL CONDUCTIVITY OF MELTER TYPE SLAGS

RODNEY HUNDERMARK

This thesis is submitted in fulfilment of the requirements for a Masters of Science degree

June 2003

Department of Chemical Engineering

University of Cape Town

DECLARATION

I declare that this thesis, submitted for the degree of Master of Science in Engineering at the University of Cape Town is my own work except where otherwise referenced. It has not been submitted prior to this at any other university for any other degree or examination.

Rodney Hundermark

ABSTRACT

This thesis details an investigation into the factors affecting the electrical conductivity of slags containing some or all of the following components: Al_2O_3, CaO, Cr_2O_3, FeO_x, MgO and SiO_2. The interest in the electrical properties of these slags originated from problems being experienced in the electrical control of the melter type furnaces of the platinum producers in South Africa.

A large amount of literature on the electrical conductivity of slags was collected and analysed. The key research areas identified through the literature review were: the effect of iron oxide on slag conductivity in terms of ionic and electronic mechanisms, the effect of oxidation state on the conductivity of iron-containing slags and the effect of chromium on the electrical conductivity of melter type slags. Measurements of the electrical conductivities of various slags were conducted in order to gain an understanding of these effects.

Electrical conductivity was measured using a two-electrode technique. Two different conductivity cell designs were used. The first was referred to as a deep cell technique, where there was approximately 25mm of slag height in a crucible and the electrodes were immersed to a depth of 8mm. The deep cell technique was used in measurements of the electrical conductivity of slags at a fixed oxidation state and a range of temperatures. Platinum electrodes and crucibles were used where the temperature range of the measurements did not exceed 1550 °C. Molybdenum electrodes and crucibles were used up to temperatures of 1700 °C.

The second cell design was referred to as a shallow cell technique where a thin layer of slag (3-4mm) was placed in a magnesia crucible and the electrodes were immersed to a depth of 2mm. The shallow cell technique was used for measurements of the electrical conductivity of iron-containing slags at a fixed temperature but varying oxidation states. The thin layer of slag allowed for quick equilibration with the gases (air, CO, CO_2 and N_2) used to control the atmosphere in the furnace. Platinum electrodes were used in the shallow cell technique.

The impedance of the conductivity cell was measured using a Fluke PM6304 RCL meter. Usually measurements were made at 100 kHz (in the range where the real part of the impedance was typically independent of the frequency), although some measurements were carried out at a range of frequencies (from 50 Hz to 100 kHz).

The effect of iron oxide on slag conductivity was examined by the addition of FeO_x (up to 30wt%) to three Al_2O_3-CaO-MgO-SiO_2 slags of varying basicity. The slags were classified according to their basicities and termed low, intermediate and high basicity slags and their mole fraction $(CaO+MgO)/(Al_2O_3+SiO_2)$ ratios were 0.63, 0.86 and 1.22 respectively. The experiments were carried out using the deep cell technique in the temperature range 1400 to 1550 °C. The slag conductivity increased with temperature and increasing basicity at a given iron content. The addition of iron oxide to the slags brought about increases in the electrical conductivities (from ~0.1–0.3 $(\Omega.cm)^{-1}$ for iron-free slags up to 0.8-0.9 $(\Omega.cm)^{-1}$ for slags containing ~30wt% FeO_x at 1500 °C). The increases were ascribed to the increase in ionic and electronic conduction. The activation energy for conduction decreased with increasing iron content (from ~180 kJ/mole for iron-free slags to ~110 kJ/mole for slags containing ~30wt% FeO_x).

The effect of iron oxide on slag conductivity was further characterised by carrying out measurements of the response of the slag conductivity to changes in oxidation state. These experiments were carried

out using the shallow cell technique. Measurements were made on the low, intermediate and high basicity slags with 20, 30 and 40wt% FeO_x as well as on a calcium ferrite slag containing 25wt% CaO. Typically experiments were started in air and the slag was then reduced at intervals by using different ratios of CO_2 and CO gas flows. The typical response of the conductivity to the changing oxidation state was that, starting in air, it would increase, reach a maximum at Fe^{3+}/Fe_{total} fractions of 0.3 to 0.5 and then decrease under more reduced conditions. The magnitude of the conductivity at a given iron content and oxidation state typically increased with increasing basicity (for example, the conductivities at 1450 °C of the low, intermediate and high basicity slags containing 30wt% FeO_x at a ferric fraction of 0.3 were approximately 0.5, 0.75 and 1.05 $(\Omega.cm)^{-1}$ respectively). One of the focuses of the investigation into the oxidation state dependence of the conductivity was the effect of basicity on the electronic conduction mechanism. Data were available in the literature for the oxidation state dependence of the conductivity of iron silicate slags, therefore the information on the calcium ferrite slag was of interest as it provided data at the other extreme of basicity. It was apparent from the measured conductivities that the electronic and ionic contributions to the conductivity increased with increasing basicity at a given iron content. It was further proposed that the basicity and the manner in which it affected the co-ordination of the ferric and ferrous ions in the slag would be important in determining the conduction mechanisms operating in the slag and define the response of the conductivity to varying oxidation state.

The effect of chromium on the electrical conductivity of slags was determined by the addition of chromium (0.5, 1, 2, 4, 6 and 8wt%) to the low basicity slag containing 20wt% FeO_x. The low basicity slag composition was very similar to that of the industrial furnace type slags (typical compositions (wt%): Al_2O_3: ~5, CaO: 5-15, FeO_x: 5-30, MgO: 15-25, SiO_2: 40-60). The deep cell technique was employed and measurements were made in Pt crucibles up to 1550 °C and in Mo crucibles up to 1700 °C. The measurements in the Pt crucibles showed that the addition of chromium to the slag brought about a decrease in the electrical conductivity of the slag. It was postulated that the decrease in conductivity was caused by the precipitation of a spinel phase which contained Al, Cr, Fe and Mg ions. The corresponding decrease in the amounts of conducting Fe and Mg cations in the liquid phase therefore decreased the conductivity. Measurements were therefore made using Mo crucibles and electrodes up to temperatures of 1700 °C in the hope that the spinels would melt and the effect of chromium in the liquid phase could be identified. Measurements were made on slags containing 0, 2 and 4wt% Cr_2O_3 and again the conductivity decreased with increasing chromium. Unfortunately molybdenum dissolved into the slag and other unpublished work suggested that the molybdenum would promote the formation of solid phases even at the higher temperatures. Therefore it was not possible to conclusively determine the effect of chromium in slags above their liquidus temperatures.

Modelling of the electrical conductivity of slags was based on slag composition, temperature and oxidation state. The modelling made use of regression techniques to obtain correlations between functions of the slag composition and the electrical conductivity. A large amount of literature data was used in the modelling in addition to the experimental data measured in this investigation.

Initially iron-free Al_2O_3-CaO-MgO-SiO_2 slags were examined as ionic conduction is the only mechanism operating. Of interest was that the temperature dependence of the conductivity data for Al_2O_3-CaO-MgO-SiO_2 slags was found to obey a compensation law (where the activation energy for conduction and the natural logarithm of the pre-exponential factor are linearly related). The correlation developed

for the conductivity of Al_2O_3-CaO-MgO-SiO_2 containing slags in the temperature range 1350-1750 °C is given below:

$$\ln\kappa = \left(31.6 - \frac{68048}{T}\right)X_{Al_2O_3} + \left(-2.2 + \frac{9006}{T}\right)X_{CaO} + \left(10.5 - \frac{15049}{T}\right)X_{MgO} + \left(17.1 - \frac{40544}{T}\right)X_{SiO_2}$$

where X represents the mole fractions of the components and T is in Kelvins.

Thereafter the electrical conductivity of iron-containing slags was modelled. It was desired to incorporate the understanding of the oxidation state dependence of the conductivity into the model. Therefore the approach in the modelling of these systems was similar to that for the iron-free slags, however knowledge of the ferric and ferrous fractions in the slags was required. It was noted that the magnitudes of the model parameters for Al_2O_3, CaO, MgO and SiO_2 were similar in the iron-free and iron-containing models, therefore the iron-free data and the iron-containing data were combined and a unified model was developed. The correlation is given below for the electrical conductivity of slags containing two or more of the following components: Al_2O_3, CaO, FeO_x, MgO and SiO_2:

$$\ln\kappa = \left(19.9 - \frac{47348}{T}\right).X_{Al_2O_3} + \left(15.4 - \frac{24087}{T}\right).X_{CaO} + \left(9.2 - \frac{14151}{T}\right).X_{MgO} + \left(-0.5 - \frac{7478}{T}\right).X_{SiO_2}$$
$$+ \left(10.0 - \frac{9140}{T}\right)X_{FeO}.Fe^{2+} + \left(65.4 - \frac{82447}{T}\right).X_{FeO}{}^2.Fe^{2+}.Fe^{3+} + (-2.6 + \frac{6642}{T}).X_{FeO}.Fe^{3+}$$

where X represents the mole fractions of the components, T is in Kelvins and Fe^{2+} and Fe^{3+} are the fractions of ferrous and ferric ions respectively.

The correlation predicted the correct trends in the change in electrical conductivity with changing oxidation state. In many cases the magnitude of the electrical conductivity of slags at oxidised conditions was quite different from literature values. This was largely due to the relative lack of data for the conductivity of iron-containing slags at oxidised conditions.

The electrical conductivity of slags containing chromium was modelled by estimating the change in the liquid phase composition due to the precipitation of spinels. The altered liquid phase composition was then substituted into the correlation above in order to obtain estimates of the conductivity. The trend of decreasing conductivity with increasing chromium content in the slag was correctly identified through this approach. Assumptions were made that the contributions of spinel phase and Cr ions in the liquid phase were negligible.

In conclusion it is considered that a very good understanding of the factors affecting the electrical conductivity of slags was achieved. The correlations developed should provide a good estimate of a slag's conductivity based on composition, temperature and oxidation state. Improvements could be made in modelling the electrical conductivity by bringing in more fundamental aspects such as mathematical descriptions of the slag structure and better understanding of the electronic conduction mechanism (although this is likely to require further experimental work to quantify iron ion distributions and co-ordinations).

ACKNOWLEDGEMENTS

My thanks go to:

Anglo Platinum and specifically Waterval Smelter for providing the support that enabled me to carry out this work. I feel very privileged to have been able to conduct the research for the project in Melbourne, Australia. Specifically, I would like to thank Mr Wayne Venter for his support of the project. I would also like to thank Dr Tom Hara for his assistance and his suggestion of the title.

Dr Sharif Jahanshahi and Dr Shouyi Sun for their excellent supervision of the project. As a result of their guidance and sharing of knowledge throughout the entire research process, the project has been a valuable learning experience and resulted in this thesis.

Prof Peter Gaylard for his input into the thesis and for assistance in dealing with the administration of completing the degree through the University of Cape Town.

The University of Cape Town for permitting me to complete the degree in an unconventional way.

AMIRA International who brokered the P479A project and without whom this research project would not have been possible. The support of the other P479A sponsors (Impala Platinum, Lonmin, Kumba Resources, BHP Steel and Rio Tinto) is also acknowledged.

The staff at CSIRO Minerals for their assistance, guidance and friendship. My thanks go specifically to Rowan Davidson and Justen Bremmel for always being willing to help out with the furnace and auxiliary equipment. Also, to Colin Nexhip, Steve Wright, Michael Somerville, Ty Tran and Ling Zhang, thanks for all the technical advice and very useful discussions. To the library staff for their assistance with tracking down obscure technical literature. To Rosalie Louey and Sarah Buckler for their encouragement with writing up. To Steve Peacock for all the XRF analyses carried out. To Neill Bartie and Trina Lau for their good humour and friendship.

On a more personal note, I would like to thank all my friends at Monash Bushwalking Club (MBC) for the many great times we had in the Victorian outdoors. And to Dalene, I hope you enjoy the book.

TABLE OF CONTENTS

LIST OF TABLES

LIST OF FIGURES

LIST OF SYMBOLS AND ABBREVIATIONS

Symbol	Variable	Value	Units
A	cross sectional area of current path		cm^2
$A_{\kappa \text{ or } D}$	pre-exponential factor for conduction or diffusion		
a	jump distance		cm
a.c.	alternating current		
C	capacitance		F
c	concentration		$mol.cm^{-3}$
c_+	fraction of conducting ions of higher valence		
c_-	fraction of conducting ions of lower valence		
D_i	self/tracer diffusion coefficient		$cm^2.s^{-1}$
d.c.	direct current		
e	electron charge	$1.602x10^{-19}$	C
EIS	electrochemical impedance spectroscopy		
$E_{\kappa \text{ or } D}$	activation energy for conduction or diffusion		$kJ.mol^{-1}$
E_H	activation energy for hopping		$kJ.mol^{-1}$ or eV
F	Faraday constant	96485.3	$C.mol^{-1}$
f	frequency		Hz
f_0	frequency at which Z" = 0		Hz
$Fe^{3+}(IV)$	tetrahedrally co-ordinated ferric ion		
$Fe^{3+}(VI)$	octahedrally co-ordinated ferric ion		
G	cell constant		cm^{-1}
k_B	Boltzmann's constant	$1.3807x10^{-23}$	$J.K^{-1}$
L	inductance		H
l	length of current path		cm
LT	liquidus temperature		°C
M_s	molecular weight of slag		$g.mol^{-1}$
N	density of conducting species		cm^{-3}
N_A	Avogadro's number	$6.022x10^{23}$	mol^{-1}
N_{SiO2}	mole fraction of silica		
p_{O2}	oxygen partial pressure		atm
Q	thermopower coefficient		$\mu V.°C^{-1}$

R	resistance		Ω
R	universal gas constant	8.314	$J.mol^{-1}.K^{-1}$
$R_{external}$	external resistance due to leads and electrodes		Ω
$R_{measured}$	measured resistance		Ω
R_{slag} / R_s	resistance offered by slag or solution respectively		Ω
RCL	resistance (R) / capacitance (C) / inductance (L)		
r_i	ionic radius of cation *i*		Å
S_T^*	vibrational entropy of transport		$\mu V.°C^{-1}$
T	temperature		°C or K
u	mobility of cation		$cm^2.V^{-1}.s^{-1}$
VHT	very high temperature		
x	fraction of ferric / total iron ($Fe^{3+}/(Fe^{2+} + Fe^{3+})$)		
z	charge on ion		
Z	complex impedance		Ω
Z'	real part of complex impedance		Ω
Z''	imaginary part of complex impedance		Ω
α	equivalent electronic conductivity		$\Omega^{-1}cm^2.(iongr\ Fe^{3+})^{-1}$
χ_i	volume fraction of phase *i*		
ρ_s	slag density		$g.cm^{-3}$
σ	electrical conductivity in solid phase		$(\Omega.cm)^{-1}$
σ_{eff}	effective electrical conductivity in multiphase system		$(\Omega.cm)^{-1}$
σ_i	electrical conductivity of phase *i*		$(\Omega.cm)^{-1}$
ν_o	longitudinal optical phonon frequency		s^{-1}
ω	angular frequency		$rad.s^{-1}$
ß	spin degeneracy factor		
$\Delta R/\Delta t$	rate of change in measured resistance		Ω/min
θ	phase angle		degrees (°)
κ	specific electrical conductivity		$(\Omega.cm)^{-1}$ or S/cm
κ_i	partial electrical conductivity of species *i*		$(\Omega.cm)^{-1}$
κ_c	electrical conductivity of conducting phase		$(\Omega.cm)^{-1}$
κ_d	electrical conductivity of dispersed phase		$(\Omega.cm)^{-1}$
κ_{eq}	electrical conductivity of slag in equilibrium with gas		$(\Omega.cm)^{-1}$

Chapter 1

INTRODUCTION

1.1. Background

In order to place the project in context the following was considered important. In 1999 the three major platinum producers in South Africa (Anglo Platinum, Impala Platinum and Lonmin) sponsored the AMIRA research project P479A entitled 'Slags, Refractories and Processes'. The research was to be carried out at CSIRO Minerals as an extension of the previous P479 project. There was a possibility that postgraduate students from the South African companies could undertake masters or doctorate degrees as part of the overall project. This particular research project for a masters degree came about in this way.

The interest in the electrical conductivity of the melter type slags arose due to problems encountered in the operation of the six-in-line electric furnaces (melters) of the platinum producers. Many of the furnace problems were thought to have arisen from the increase of chromium in the ore being processed by the operations. Over the past ten years, the ore and hence concentrate being treated by the smelters has slowly been changing in composition. The majority of the ore processed used to come from the Merensky reef of the Bushveld Complex in the Northwest Province of South Africa. The electric furnaces of the platinum producers were designed primarily for the treatment of concentrate arising from Merensky ore. However, as the mining operations have expanded and the demand for platinum increased, more of the chromium-rich UG2 reef has been mined. The UG2 reef occurs from 60-400m below the Merensky reef in the Bushveld Complex and is typically lower in base metal grade than the Merenksy reef. The increased blending of the UG2 ore has contributed the additional chromium to the operations.

Specific furnace problems, which arose as a result of the changing feedstock, involved the electrical control of the furnaces, difficulties in tapping and bottom build-up. In terms of the electrical control, the immersion depths of the electrodes were adversely affected by increased slag conductivity. The consequences of having reduced immersion depths of the electrodes included reduced smelting rates, increased furnace roof temperatures and increased bottom build-ups. It was therefore of interest to obtain an understanding of how the slag chemistry affected the electrical conductivity of the slag.

The research project was set out such that a literature review was completed to identify the areas where knowledge was lacking and thereby focus the investigations carried out in the project. The scope of the research project was broader than merely concentrating on the types of slags

treated by the platinum producers (typical compositions (wt%): Al_2O_3: ~5, CaO: 5-15, FeO_x: 5-30, MgO: 15-25, SiO_2: 40-60). However, the determination of the effect of chromium on the electrical properties of slags was one of the specific goals of the project. The justification for the broad scope of the investigation was that a better understanding of the factors affecting the electrical conductivity of slags would be obtained and this would lead to a broader application of the knowledge. One example where such knowledge would possibly be of value is in the case of the platinum producers where the treatment of converter slags in slag cleaning furnaces is likely to take place.

Initially, the necessary experimental techniques were developed and verified against the known conductivities of various aqueous solutions and slags. Thereafter work began on the slags of interest as well as on the modelling of the conductivity of slags. Much of the work is fundamental in nature and the challenge for the future will be to apply the knowledge, although hopefully through the development of a conductivity model, calculation of the slag conductivity based on composition will mean one less variable.

1.2. General notes

It will be noted that a thermodynamic modelling package called MPE (Multi Phase Equilibria) has been used extensively throughout this project. The software package has been developed at CSIRO Minerals and more details concerning its operation may be found in the following reference: Zhang *et al.* (2002). Briefly, given starting compositions of various phases (matte/metal, slag, gas) and temperature and pressure inputs, MPE will predict the equilibrium conditions at the required pressure and temperatures. MPE was used mainly for the calculation of liquidus temperatures and phase distributions in this work.

Throughout this report the symbol used for the specific electrical conductivity is kappa (κ) and the units are expressed in $(\Omega.cm)^{-1}$ or $\Omega^{-1}.cm^{-1}$ which is the same as S/cm. The reason for the choice of these units is that they are used in almost all other literature concerning the specific electrical conductivity of slags even though the SI units are S/m. To convert from $(\Omega.cm)^{-1}$ or S/cm to S/m one must multiply by 100. Also, the specific electrical conductivity will be referred to as the electrical conductivity or simply the conductivity interchangeably. Where molar or equivalent electrical conductivities are discussed, they will be explicitly indicated. The same applies to thermal conductivities.

Chapter 2

LITERATURE REVIEW

The objectives of the literature survey were to:

a. collect and analyse the data and theory related to the electrical conductivities of slags

b. gain an understanding of the manner in which various factors such as slag composition, temperature and oxidation state affect the electrical conductivity

c. evaluate the various methods of measuring electrical conductivities

d. identify research questions

The chapter has been organised in the following manner. The measurement techniques used for determination of electrical conductivity of slags are discussed first as they give an idea of how the conductivity data discussed later in the chapter were obtained. The slags of interest are typically silicate slags so a brief introduction to silicate slag structure is provided. The mechanisms of electrical conduction and the effect of temperature on conductivity are covered next. Thereafter the conductivity data found in the literature are discussed. As there was a modelling component related to the project, a considerable amount of data was investigated. Finally several research questions are identified and approaches suggested for investigation of these research areas.

2.1. Measurement techniques

2.1.1. Basic principle and common techniques

The basic principle in measuring electrical conductivity is that a substance of unknown conductivity is placed in a well defined conductivity cell. A current is passed through the substance by means of immersed electrodes and the resistance offered by the substance is measured. The conductivity cell has a characteristic cell constant (G) which is determined beforehand by means of a calibration with substances of known conductivity. The specific electrical conductivity (κ) of the substance can then be determined using the following formula:

$$\kappa = \frac{G}{(R_{measured} - R_{external})} = \frac{G}{R_{substance}}$$

$$G = \frac{l}{A}$$

The external resistance is due to the resistance of the leads and the electrodes and is obtained by measuring the resistance of the short-circuited electrodes. In some cases authors have done this by immersing the electrodes in mercury. The cell constant is dependent on the equivalent length of the current path (l) between the electrodes and inversely proportional to the equivalent cross sectional area (A) of the current path. Ideally G should remain constant irrespective of the slag being tested, the slag container and the electrodes. Schiefelbein (2000) identified eleven techniques, seven low accuracy techniques and four high accuracy techniques. Neither Schiefelbein (2000) nor Schiefelbein and Sadoway (1997) specifically mention the levels of accuracy in techniques classified as 'low accuracy' and 'high accuracy'. However, with low accuracy techniques such as the two-electrode, four-electrode and central electrode techniques, the cell constant may vary with the slag being tested, the slag container or the electrodes. This occurs because the current path taken is not confined and is a function of the electrical properties of the liquid being tested, hence calibration is unreliable. It follows from this that the conductivity cell geometry and the calibration of the cell present major sources of error in the low accuracy techniques. With high accuracy techniques such as the co-axial cylinder and digitated electrode techniques, there is no variance in the cell constant. The author also noted that in selecting a particular technique it is necessary to take into account the desired accuracy, the compatibility of the liquid and the materials to construct the conductivity cell, the conductivity of the liquid and the range of limits of the measuring instrument.

In the literature on the conductivity of slags, the most commonly employed techniques were the two-electrode technique and the central-electrode or crucible technique. The two-electrode technique consists of two parallel electrodes of known diameter and spacing which are immersed into the slag to a known depth. In most cases where this technique has been used, the cell constants for cells of various dimensions ranged from 0.5 to 1.5 cm^{-1}. According to the Slag Atlas (1995) the spacing between the electrodes should be less than the distance from the electrodes to the crucible wall and from the tips of the electrodes to the bottom of the crucible to avoid or minimise wall effects. The two-electrode technique was applied to a very wide variety of slag systems, although materials of construction of the cells were usually platinum, platinum-rhodium alloys or molybdenum.

The central-electrode technique involves a rod / wire electrode centrally located and immersed to a known depth in the slag contained in a crucible which forms the other electrode. For various dimensions of cells, the cell constants varied from 0.1 to 3.2 cm^{-1}. Usually the central-electrode technique was used for slags containing high proportions of iron and the materials of construction of the cell were either iron or molybdenum. In some cases the central-electrode technique was used to measure the conductivity of very high conductivity slags such as liquid FeO. For example, the measurements by Inouye *et al.* (1953) were made in a cell with a constant of 0.128 cm^{-1}. This meant that for the liquid FeO conductivity of approximately 320 $(\Omega.cm)^{-1}$ at 1480 °C, the measured resistance was only 0.0004Ω. The authors used a four wire connection to the crucible and central electrode which eliminated the majority of the external resistance however, it would be more ideal if the cell constant is larger such that the measured resistance is larger in magnitude.

Exceptions to the above two techniques were the work of Schiefelbein and Sadoway (1997) who developed a high accuracy experimental technique suitable for measurements on slags using coaxial cylinders and the work of Hoster and Pötschke (1983) and Winterhager *et al.* (1966) who used ring electrode systems. Summaries of the various techniques are given in the Slag Atlas (1995) and by Schiefelbein (2000).

The two-electrode, central-electrode and the ring-electrode techniques were classified by Schiefelbein as low accuracy for the reasons mentioned above. In most cases authors have reported estimated errors of 5-10% in the conductivity values.

2.1.2. Techniques used for oxidation state dependence work

There have only been three thorough investigations into the oxidation state dependence of the conductivity of the slags of interest. The first was carried out by Pastukhov *et al.* (1966) who performed measurements on liquid FeO_x, FeO_x-SiO_2 and Al_2O_3–CaO–FeO_x–SiO_2 slags. The measurements on the highly conductive liquid FeO_x and FeO_x-SiO_2 slags were carried out using a modified central electrode technique. An iron crucible was used as one electrode on which a lid with two openings was welded. A corundum (Al_2O_3) cylindrical tube was then immersed through one of the openings and touched the bottom of the iron crucible. A cylindrical molybdenum electrode was then immersed in the column of slag (30-45mm in height) inside the corundum tube. A cell constant of 40-70 cm^{-1} was found. The other opening in the lid was used to supply the gases for controlling the oxidation state of the slag7. Equilibrations with the gas took around 1 hour.

The measurements on the Al_2O_3–CaO–FeO_x–SiO_2 slags were carried out using a variation of the two-electrode technique. A zirconia boat was used with a thin layer of slag (3-4mm). The electrode spacing was 40 – 50 mm. The authors wanted a small amount of slag such that equilibration with gases was quick and the cell constant was sufficiently high that relatively high conductivity slags could be tested.

The measurements by Engell and Vygen (1968) were carried out in a platinum crucible with a volume of 20 cm^3. The conventional two-electrode technique was used with 0.5mm Pt electrodes. The work was carried out at 1600 °C. The atmosphere in the furnace was controlled using oxygen, oxygen-nitrogen and CO_2–CO mixtures. The oxygen partial pressure was varied from 1 atm down to 6×10^{-6} atm. For the slag to come to equilibrium at a particular oxygen partial pressure took 4-6 hours. This meant that for a slag where the oxygen partial pressure was varied 8 times, the overall experiment time was up to 48 hours. At the more reducing conditions, it is possible that there was significant contamination of the Pt crucible by the iron in the slag as a result of the duration of the experiments.

The work by Fontana *et al.* (1984) used the conventional two-electrode technique. A Pt / 20% Rh alloy crucible and two Pt / 40% Rh alloy wires were used. The atmosphere was controlled by using mixtures of CO_2 and CO but no mention is made of equilibration times. Measurements were made at both constant p_{O2} and also constant CO_2/CO ratios. The temperature dependence of the conductivity was also measured at each oxygen partial pressure.

2.1.3. *Measurement instruments*

In most cases, the actual measurements of the resistances were carried out using an a.c. bridge in conjunction with an oscilloscope. Various designs of bridges have been used and reviews of these are given by Solomons (1979) and Robbins (1969). Jowsa and Gzielo (1988) compared measurements using an a.c. bridge, a voltmeter-ammeter and galvanostatic method for an Al_2O_3–CaO–MnO–SiO_2 slag and a calcium fluoride slag. The authors found good agreement between the three methods but their results differed markedly from other authors measurements on calcium fluoride slags of the same composition. When comparing the applicability of the three methods, they found that voltmeter-ammeter gave quick results provided the constants for the system were properly matched to the slag composition (in terms of finding the resonance frequency). The bridge method gave greater accuracy but the measurements took longer as the bridge had to be balanced. The galvanostatic measurement (where a d.c. pulse is used) also gave high accuracy results but the system was complex to set up, however it had the advantage of not requiring checking for frequency dependence.

In some investigations the authors have made use of electrochemical impedance spectroscopy (EIS) in order to determine the frequency dependence of the melts: Hino *et al.* (1992), Schiefelbein (2000), Segers *et al.* (1978), Fontana *et al.* (1985) and Kim and Sadoway (1992). A brief description of the frequency dependence of the conductivity of slags is given below in Section 2.1.5.

In the current investigation, an automatic programmable RCL meter was available. This allowed automatic measurements at a range of frequencies where the complex impedance was measured and resolved into its real and imaginary parts. Equivalent circuits for the system measured were also displayed indicating the resistive, the capacitive and the inductive components of the impedance.

2.1.4. *Calibration techniques*

For the low accuracy techniques, the conductivity cell needs to be calibrated in order to obtain the cell constant. This is done by measuring for liquids of known conductivity. Potassium chloride (KCl) solutions are the commonly accepted standard materials used in the calibration of electrolytic cells and the conductivity is known very accurately at various concentrations and temperatures. Janz and Tomkins (1977) reviewed conductivity cell calibration practices in 1977 and concluded that the demal values of Jones and Bradshaw (1933) were the most widely used. The demal concentration scale was introduced as mass can be more accurately measured than volume and it was not dependent on atomic weights of the elements. Kohlrausch and co-workers (1898, 1916) produced standards which were based on volume rather than mass of solvent and were regarded to be slightly less accurate (error of 0.54% as reported by Janz and Tomkins). Recently in a IUPAC technical report, Pratt *et al.* (2001) have published primary standards for electrolytic conductivity cells based on molality as the errors in atomic weights are far smaller than the accuracies of conductivity cells in current times. The dependence of the standards on temperature is also given which is an improvement on the demal scale where conductivities were only given for 0, 18 and 25 °C. Janz and Tomkins (1977) also gave a table of cell constants measured using KCl and

various molten salt standards at temperatures from 25 °C for the KCl up to 1073 °C for the molten salts. The cell constants varied by ± 0.8%.

A paper by Riebling and Logel (1965) is often cited for the calibration of the two-electrode technique for slags. The authors investigated the effect of liquid depth, frequency, immersion depth and capacitance. They found that for an immersion depth of 8mm, the liquid depth needed to be greater than 25mm for the cell constant to be independent of the depth. The authors noted that for the more concentrated KCl solution (1N), capacitive effects appeared and were ascribed to polarisation. To obtain reactance free impedances, the impedance was extrapolated to infinite frequency by plotting the measured impedance versus the reciprocal of the frequency squared (Ω vs $1/f^2$). For the less concentrated solutions, it was found that the impedance was independent of frequency at 10 kHz. Probably as a result of the dependence of the impedance on the frequency, the authors found that the cell constant varied with the measured resistance. In order to account for this variation, the data was plotted on a log-log scale and found to obey a linear relationship.

2.1.5. Effect of frequency on conductivity measurements

To provide some starting point to the discussion it is worth mentioning observations made by Segers *et al.* (1978). They found that the frequency at which the imaginary part of the impedance was zero (resonant frequency or f_0) occurred at 150 kHz, 60 kHz and 10 kHz for aqueous KCl solutions, aqueous potassium nitrate solutions and silicate slags respectively. This suggested that for a given experimental setup, the frequency dependence of the measurements depended on the liquid being measured.

Other authors have found similar results for calibrations with aqueous KCl solutions. Rennie *et al.* (1972) found that for more concentrated KCl solutions there was a large increase in the measured capacitance and attributed this to polarisation. They followed Riebling and Logel's method of extrapolation of the measured resistances to infinite frequency. (Their measurements on slags were made at 10 kHz as they found greatest precision at that frequency and the slag resistance was independent of frequency down to 2 kHz).

Robbins (1969) examined the effect of frequency on measured resistance in a review of the measurement of the electrical conductivity of molten fluorides by 16 other investigators. His findings can be summarised as follows:

- In many cases the effect of frequency on the measured resistance was not stated.
- In some cases a linear relationship was found between the measured resistance and $f^{-1/2}$. Theoretical justification for this was given by Warburg (as cited in Robbins) and Neumann (as cited in Robbins) based on Fick's laws of diffusion. Measured resistances would then be extrapolated to infinite frequency on a plot versus $f^{-1/2}$.
- In the case of measurements on methanol solutions by Nichol and Fuoss (as cited in Robbins), linear dependency was found between the measured resistance and f^{-1}.
- Buckle and Tsaoussoglou (as cited in Robbins) found that at higher frequencies the measured resistance became independent of the frequency. They suggested that extrapolation to infinite frequencies would bring about errors and that for a given setup,

the frequency dependence should be studied and the resistance measured in a frequency independent region.

Electrical conductivity measurements on slags have been carried out at a large range of frequencies. In most cases the measuring frequency was between 1 kHz and 10 kHz and authors claimed that polarisation was minimised at such frequencies. This assumption seems fair, given that the resonant frequency of silicate slags has been found to be around 10kHz (Segers (1978)). However, Keller *et al.* (1979b) found on measuring conductivities of CaO-SiO_2 slags, that the measured resistance became independent of the frequency in the range 30-100 kHz. Engell and Vygen (1968) also found that the measured resistance was independent of the frequency in the range 40 – 100 kHz for CaO-FeO_x-SiO_2 slags and consequently made measurements at 50 kHz. A table summarising the frequencies at which measurements were made on slags is provided in Appendix A.1.

Work has also been carried out by Hino *et al.* (1992), Schiefelbein (2000), Segers *et al.* (1978), Fontana *et al.* (1985) and Kim and Sadoway (1992) on the frequency dependence of conductivity measurements of slags. As mentioned above, Segers *et al.* (1978) stated that in silicate slags the resonant frequency occurred at around 10 kHz. A graph is given by Fontana *et al.* (1985) showing the impedance plot for a CaO-MnO-SiO_2 slag. At low frequencies the plot is characteristic of diffusion processes. At higher frequencies, the imaginary part of the impedance approaches zero and then changes from being capacitive to inductive at the resonant frequency (f_0). The resonant frequency was between 1 and 10 kHz. Hino *et al.* (1992) measured impedance responses for a CaO-Al_2O_3 slag at the interface with molten copper or iron. The authors give an explanation of an equivalent circuit diagram for a slag and the theoretical impedance plot for the diagram. Amongst other aspects, it is shown that at the resonant frequency the measured resistance is the resistance due to the slag. Schiefelbein (2000) and Kim and Sadoway (1992) performed electrochemical impedance spectroscopy (EIS) measurements on CaO-MgO-SiO_2 slags and molten fluorides respectively. In both cases the impedance was measured and the resistances of the molten slag or fluoride were taken where the imaginary part of the complex impedance was zero. The authors do not mention the value of the resonant frequency.

2.1.6. Summary of measurements techniques and conclusions

In conclusion it was decided that the two-electrode technique would be the most appropriate to use. Calibrations were to be carried out using KCl standard solutions. The conductivity values used for the KCl solutions were those reported by Dobos (1975) (based on Kohlrausch standards). The slightly lower accuracy of the Kohlrausch standards (in comparison to those of Jones and Bradshaw (1933)) was deemed acceptable for the level of overall accuracy required in the investigation. As for the frequency dependence of the slags, it was decided that a scan should be carried out to determine the frequency response and if feasible, determine the resistance at the resonant frequency or in a range where the resistance is independent of the frequency.

The reasons for the above decisions were that:

- the technique would give results of sufficient accuracy (5-10%) given the time and financial limitations on the project
- the materials of construction for the cell were readily available and were compatible with the slags being tested
- the technique had previously been applied in measurements on the oxidation state dependence of slag conductivity.

Although very high accuracy measurements would have been desirable, it was not the purpose of this investigation to develop an extremely accurate measurement technique but rather to obtain results of sufficient accuracy to adequately conduct the research. It was attempted to obtain the maximum accuracy from the technique used. The major sources of error were identified as being inaccurate calibration, conductivity cell geometry and not accounting for the frequency dependence of the resistance. In order to minimise these errors, great care was taken in preparation of calibration standards, and in setting up of the cell (including electrode immersion depth, electrode spacing and alignment of the electrodes). As mentioned above the frequency dependence of the resistance measurements will be taken into account. Further sources of error, how they are handled and detailed error analyses are discussed in Sections 3.6.5 and 3.7.5.

2.2. Silicate slag structure

Some of the earlier electrical conductivity measurements (Bockris *et al.* (1948, 1952)) on binary silicates were performed in order to elucidate more information about the silicate slag structure. In this study, it will be attempted to explain the factors affecting the electrical conductivity in terms of the slag structure. This eases visualisation and interpretation of electrical conductivity data and mechanisms. It is also possible to relate the slag structure to other physicochemical properties such as viscosity. The following is therefore included as a very basic introduction to silicate slag structure, although some detail has been given on the effect of ferric and ferrous ions on the slag structure.

In molten silicate slags, it is commonly accepted that the melt is composed of networks of silica tetrahedra i.e. SiO_4^{4-}. The more silica tetrahedra bonded to each other, the more polymerised the melt. Highly polymerised melts have high viscosities as the large anionic units have low mobilities. The addition of uni- and divalent metal oxides e.g. K_2O, Na_2O, Li_2O, BaO, PbO, SrO, CaO, MnO, FeO and MgO tends to bring about depolymerisation of the silicate network by the donation of oxygen ions. Thus, these metal oxides are regarded as network modifiers.

Addition of higher valence metal oxides has varying effects. In some cases higher valence metal oxides such as Al_2O_3 and P_2O_5 will also form tetrahedra which enhance the polymerisation. In other cases, higher valence metal oxides such as Fe^{3+} and Ti^{4+} can enhance or decrease the polymerisation depending on the coordination of the ions. The role of ferric and ferrous ions in silicate melts has been investigated by Mysen *et al.* (1984). The authors used Mössbauer and Raman spectroscopy on quenched samples to investigate iron redox equilibria and melt structure in alkaline earth metal silicates. They found that as Fe^{3+}/Fe_{total} increased from 0.3 to 0.5, the ferric ions changed from octahedral to tetrahedral co-ordination. These measurements were on low iron content containing melts (5 and 10 wt% FeO_x), but it is expected that similar structural changes occur in high iron containing slags. Therefore at reduced conditions ferric ions are

octahedrally co-ordinated while at oxidised conditions it is likely that ferric ions will at least partly be tetrahedrally co-ordinated. Ferrous ions remain octahedrally co-ordinated.

There are thought to be three different ways in which oxygen ions can be bonded in melts. The first is called a bridging oxygen ion (O^0) and is bonded to two silicon ions. The second type is called a non-bridging oxygen (O^-) and is bound to only one silicon ion. The third type is an 'oxide' or free oxygen ion (O^{2-}) which is not bonded to a silicon ion.

More comprehensive descriptions of silicate slag structure are widely available, for example see Mysen *et al.* (1984), Mysen *et al.* (1985), Mills (1993), Slag Atlas (1995) and Masson (1965, 1984). Where applicable, mention will be made of the slag structure in terms of its effect on the electrical conductivity.

2.3. Mechanisms for electrical conduction

It will be shown in this section that there are two distinct mechanisms for electrical conduction within melts. The first is ionic conduction and arises from the movement of basic metal cations such as Mg^{2+} and Ca^{2+}. The second is electronic conduction which arises from the exchange of electrons or holes between transition metal ions of differing valencies. Both mechanisms contribute to the overall conductivity of a melt, although the dominant mechanism depends on the presence and amount of transition metals such as Fe, Mn and Ti.

2.3.1. Ionic conduction

The primary mechanism for conduction in slags where transition metals are absent is by the motion of basic metal cations, and is termed ionic conduction. This type of conduction commonly takes place in silicate slags. The magnitude of electrical conductivity where ionic conduction predominates is low (up to 1 $(\Omega.cm)^{-1}$ except in the case of binary alkali metal oxide silicates which are more conductive).

Bockris *et al.* (1948, 1952) conducted work on binary metal oxide – silicate systems (CaO, MnO, Al_2O_3, K_2O, Na_2O, Li_2O, BaO, SrO and MgO binary silicates). The composition ranges tested were in the liquid regions of the binary silicates in the temperature ranges 1050 – 1500 °C for the alkali metal silicates and 1400 - 1750 °C for the alkali earth metal silicates. The authors concluded that the conductivity in the melts investigated was entirely due to the metal cations. Evidence for ionic conduction was that the order of magnitude of conductance was the same as for typical liquid ionic conductors (as opposed to typical semiconductors), the temperature coefficient for conductance was positive, the passage of current produced electrolysis and Faraday's laws for electrolysis were obeyed.

Further relevant conclusions drawn by Bockris *et al.* (1952) regarding ionic conduction in binary silicates were that:

The activation energy for electrical conductance was lower than the activation energy for viscous flow in all of the systems studied, indicating that different processes govern the viscosity and electrical conductivity. It is unlikely that current is carried by the negatively charged complexes containing silica and oxygen as they have very low mobilities relative to the cations. Oxygen ions are also unlikely to participate in conduction as they have a high affinity for the silica network and the metal cations. It is only likely for free oxygen ions (O^{2-})

to be found in melts where O/Si > 4, that is when all the silicon ions are present as the orthosilicate ion (SiO_4^{4-}).

Bockris *et al.* (1952) employed the ion-oxygen attraction (I) values as a basis on which to compare the effects of different cations. (The ion-oxygen attraction function was introduced by Dietzel (1942) where $I = 2z / l^2$ and z = valency of the cation and $l = (r_{cation} + r_{oxygen})$ where r is the ionic radius of the cation and oxygen respectively. The ionic radii vary with co-ordination number therefore the co-ordination of the ions must also be known). The following table is provided for convenience:

Table 1: Classification of cations according to ion-oxygen attraction values after Bockris *et al.* (27)

Dietzel's classification	Cation	Cation radius	Co-ordination number	Ion-oxygen attraction (I)	κ_{1750} at 1:1 $M_xO_y:SiO_2$
Network modifiers	K^+	1.50	9	0.24	2.4
	Na^+	0.95	6	0.36	4.8
	Li^+	0.60	6	0.50	5.5
	Ba^{2+}	1.35	6	0.53	0.6
	Sr^{2+}	1.13	6	0.62	0.63
	Ca^{2+}	0.99	6	0.70	0.83
	Mn^{2+}	0.80	6	0.83	1.8
Intermediate	Fe^{2+}	0.75	6	0.87	1.82
	Mg^{2+}	0.65	6	0.95	0.72
Network formers	Al^{3+}	0.38	4	1.89	
	Ti^{4+}	0.35	4	2.61	

The alkali and alkaline earth metals are regarded as network modifiers as they tend to break down (depolymerise) the silicate network by the donation of oxygen ions. This can be represented by the following reaction:

$$\text{-Si-O-Si-} + O^{2-} \rightarrow \text{-Si-}O^- + {}^-O\text{-Si-}$$

The alkali metal oxides have low I values (0.24 – 0.50). The conductivities of these melts are relatively high. The oxygen ions are bound tightly to the silica network and the metal cations are free to move within the network. The activation energy for conduction is small.

The alkaline earth metal oxides, excluding Mg^{2+}, also have low I values (0.53 - 0.70) but have lower conductivities than the alkali metal oxides. Bockris *et al.* (1952) suggested that the reason for this was that the higher ion-oxygen attraction of the divalent cations becomes significant. As the melt becomes more depolymerised, the divalent cations become associated with the silicate anions to form ion-pairs. Therefore a higher activation energy is required for a cation to be separated from an ion-pair and transferred to the next one.

Mn^{2+}, Fe^{2+} and Mg^{2+} were classified as intermediate between network modifying and network forming. Bockris *et al.* (1952) suggested that the abnormalities with these cations were probably due to the varying type of electronic structure of the ions, polarisability and tendency to covalency. Mills (1993) mentioned that ordering of the melt is likely to occur with divalent cations, as two O^- bonds need to be satisfied. As a result of Mg^{2+} being a very small

cation, more ordering of the melt is required than with larger cations. Therefore $MgO-SiO_2$ has a lower conductivity than expected.

The specific electrical conductivity in ionically conducting melts can be represented by the following equation (see Engell and Vygen (1968) and the Slag Atlas (1995)):

Equation 1: $$\kappa = F \sum z_i c_i u_i$$

where z is the charge on ion i
c is the concentration of ion i
u is the mobility of ion i
F is the Faraday constant

With the aid of Equation 1 one can therefore qualitatively explain the conductivities of simple silicate melts. The polymerisation of the silica and oxygen ions into a network means that those ions will have very low mobilities and therefore contribute very little to the conductivity. The basic metal cations which do not form part of the silicate network, have considerably higher mobilities than the network and therefore contribute most to the conductivity.

In support of the findings of ionic conduction, measurements have been made on the tracer diffusivities of some of the basic metal oxides in slags. One example is that of Keller and co-workers (1979a, 1979b, 1982) who measured tracer diffusivities for Ca, Si and O in a $CaO-SiO_2$ slag at 1600 °C. The tracer diffusivities of the Ca, Si and O ions were 4.6×10^{-6}, 7.6×10^{-7} and 8.3×10^{-7} cm^2/s respectively. This showed that the diffusion of the Ca ions was an order of magnitude higher than the Si and O ions. The partial electrical conductivity of a species in a melt can be related to the self or tracer diffusion coefficient (D_i) by means of the Nernst - Einstein equation:

Equation 2: $$\kappa_i = \frac{z_i^2 c_i F^2 D_i}{R T}$$

Goto (1984) reviewed the electrical properties of metallurgical slags (K_2O, Li_2O, CaO, FeO_x binary silicates and $FeO_x-CaO-SiO_2$, $CaO-Al_2O_3-SiO_2$, $Na_2O-CaO-SiO_2$ and $K_2O-BaO-SiO_2$ ternary slags) and based on several measurements of diffusivities and transference numbers concluded that the alkali and alkali earth metal cations are the main charge carriers in melts not containing iron. In high iron-containing slags, electronic conduction occurs.

2.3.2. Electronic conduction

In slags containing transition metals the possibility of electronic conduction arises as a result of electron or hole exchange between metal ions of differing valencies. As the transition metal content in a melt increases, the electronic contribution to the overall electrical conductivity increases significantly. At low transition metal content, ionic conduction is dominant. When electronic conduction is dominant, it gives rise to much higher electrical conductivities as the mobility of electrons or holes is high relative to ions. To gain a better understanding of the mechanism, iron oxide will be considered as this was the transition metal of interest.

Electrical conductivity measurements were made by Inouye *et al.* (1953) on wüstite below and above its melting point. It is known that solid wüstite is a p-type semiconductor. The authors suggested that since the order of magnitude of the specific conductivity of liquid wüstite was the same as for the solid, a similar mechanism for conduction should occur in the liquid.

Following the conclusions of Inouye *et al.* (1953) about the applicability of conduction mechanisms in solid and liquid iron oxides, it was considered of value to investigate the electrical properties of solid iron oxides. Gleitzer (1997) presented a very comprehensive review of the electrical properties of these iron oxides. Summarised very briefly, solid wüstite is regarded as a p-type semiconductor with charge transfer taking place by means of small polaron hopping. Small polaron hopping conduction refers to the exchange of electrons or holes between ions of different valency e.g. Fe^{2+} and Fe^{3+} (where the electron/hole and its distortion on the lattice/network is called a small polaron). For a more comprehensive explanation of small polarons in solids see Elliot (1998) and Shluger and Stoneham (1993).

Small polaron hopping in wüstite was expressed in terms of the following equation (Gartstein and Mason (1982)):

Equation 3: $$\sigma = \frac{N c_+ c_- e^2 a^2 \nu_0}{k_B T} \exp\left(-\frac{E_H}{k_B T}\right)$$

where σ specific electrical conductivity in solid
N density of conducting ions per cm^3
c_+ fraction of conducting ions of higher valence
c_- fraction of conducting ions of lower valence
e electron charge
a jump distance
ν_0 longitudinal optical phonon frequency
E_H hopping activation energy
k_B Boltzmann's constant

The authors referred to the values c_+ and c_- as the electrical valences and they were not the same as the chemical valence values for Fe^{3+} and Fe^{2+}. The values for c_+ and c_- were calculated from measurements of the thermoelectric coefficient (also called thermopower or Seebeck coefficient) which were related by the following equation:

Equation 4: $$Q = \frac{-k_B}{e}\left[\ln\beta\frac{c_+}{c_-} + \frac{S_T^*}{k_B}\right]$$

where Q thermoelectric coefficient
β spin degeneracy factor
S_T^* vibrational entropy of transport

In Equation 4 the entropy term (S_T^*) is considered to be negligible and the spin degeneracy factor has a value of 2. Spin degeneracy refers to the two possible spin states that electrons possess (see Constable and Roberts (1997)). Therefore from the measurements of the conductivity and thermoelectric coefficient of wüstite at various oxidation states / stoichiometries, the authors were able to show that small polaron hopping was likely to be

the mechanism of conduction. The activation energy for conduction was approximately 15.4 kJ/mol.

Nell and Wood (1991) made measurements of the thermopower and electrical conductivity of magnetite and other spinels in the temperature range 600 to 1400 °C. They justified the use of the small polaron conduction mechanism in magnetite and made use of the relationships shown in Equation 3 and Equation 4 above. Wu and Mason (1981) modelled cation distributions in magnetite and provided justification that hopping conduction in magnetite only occurred between octahedrally co-ordinated Fe^{3+} and Fe^{2+} sites. Therefore the values c_+ and c_- were related to the fractions of Fe^{3+} and Fe^{2+} ions in octahedral co-ordinations. Based on this mechanism for the conduction, Nell and Wood modelled the cation distributions of spinels of interest in geological systems.

In terms of representing the conduction mechanism in slags containing transition metals, the application of a model is complicated by the presence of both ionic and electronic conduction. Engell and Vygen (1968) approached this problem by considering the two mechanisms separately. As mentioned above, they accounted for the ionic contribution based on Equation 1, and then considered two limiting case scenarios for the electronic contribution. The first case was that the electronic conduction occurred by electron exchange between stationary conduction sites by a tunneling mechanism. The second case involved bimolecular reaction between ferric and ferrous ions dependent on the collision number.

The first case was synonymous with the small polaron hopping conduction mechanism mentioned above. The authors found discrepancy between their measured results and the model and ascribed the difference to the assumption that the conduction centres were stationary and that the transfer distance between the conduction sites was not dependent on the concentration.

In the second limiting case the authors therefore investigated the possibility that the rate of conduction was diffusion controlled. This involved modelling the electron exchange between ferric and ferrous ions as a collision number dependent bimolecular reaction. The concept of a collision number dependent bimolecular reaction stems from collision theory, which can be used to describe the mechanism and rate of a chemical reaction. Briefly, if two molecules collide and have sufficient excess energy (activation energy), then reaction will occur. The rate of the reaction is governed by the number of collisions multiplied by a factor which describes the fraction of the total number of molecules that have sufficient energy to bring about activation (for further details see, for example, Levenspiel (1972)). The logic behind the application of this model was that the electron exchange was very rapid in comparison to the diffusion of the ferric and ferrous ions which facilitated the electron exchange. Therefore the diffusion would be the rate limiting step. Engell and Vygen (1968) derived the following expression for the electronic conduction based on a diffusion controlled bimolecular reaction:

Equation 5: $$\kappa_e = \frac{4(2a)^3}{\pi} N_A F u_{Fe^{2+}} c_{Fe}^2 x(1-x)$$

Where a transfer distance

u_{Fe2+} mobility of ferrous ion

x ferric / total iron fraction

The authors had measured the densities and the ferric and ferrous contents of their slags. They had also estimated the mobilities of the ferrous ions. They were thus able to fit their conductivity data to the model and found that a transfer distance of a = 2.8 Å gave good agreement between the results and the model. However, the transfer distance (a) calculated was relatively large and almost the same as the average distance between iron ions (as calculated from the concentration). This suggested that the diffusion was not important.

In the case of high titania content slags, Desrosiers *et al.* (1980) suggested that the conductivity could be described by the random walk model of electrons introduced by Rice (1962). This involves electrons 'hopping' between Ti^{3+} and Ti^{4+}. It is considered that similar electron / hole transfer mechanisms will occur in both iron and titania – rich slags.

2.3.3. Measures of ionic and electronic contribution

Measurements have been carried out on the current efficiencies (C_+) in FeO_x-SiO_2, CaO-FeO_x, FeO_x-MnO-SiO_2 and CaO-FeO_x-SiO_2 melts by Simnad *et al.* (1954), Dancy and Derge (1966), Dukelow and Derge (1960) and Dickson and Dismukes (1962) respectively. This was used as a measure of the relative ionic and electronic contributions to the overall conductivity. C_+ = 100% means that the conduction is purely ionic and C_+ = 0% means that conduction is purely electronic. The experiments involved measuring the amount of iron formed on or lost from the cathode or anode of an electrochemical cell when a known amount of current was passed through the cell. It should be noted that all of the current efficiency measurements were carried out in iron crucibles using an iron central electrode. Therefore the slags would all have been at relatively reduced conditions.

Simnad *et al.* (1954) found that in iron silicate slags, in the temperature range 1250 to 1400 °C, the current efficiency was independent of temperature. Dickson and Dismukes (1962) came to a similar conclusion concerning the current efficiencies of CaO-FeO_x-SiO_2 melts. Figure 1 below shows the findings of the current efficiency measurements and the following is evident:

From around 90-100% FeO_x, the current efficiency in all systems was reported to be constant between 2-10%. This suggests that the majority of the conduction was electronic with a small amount of ionic conduction occurring.

In the system FeO_x-SiO_2 as measured by Simnad *et al.* (1954), from 10-40 mol% SiO_2 (90-60mol% FeO_x) the current efficiency increased linearly from around 10% up to around 90%. The current efficiency then remained constant at ~90% where SiO_2 > 40mol%.

In the system CaO-FeO_x-SiO_2 as measured by Dickson and Dismukes (1962), different ratios of CaO/(CaO + SiO_2) were investigated with increasing iron oxide content. It should be noticed that for constant iron oxide content, as the ratio increased, the electronic contribution becomes higher (the current efficiency lower).

In the system CaO-FeO_x as measured by Dancy and Derge (1966), current efficiency measurements were made of melts containing up to ~23 mol% CaO. It should be noted that at a given level of FeO_x, the current efficiencies were significantly lower than in the FeO_x-SiO_2 system. This indicates that more electronic conduction takes place. The data also fits in with the observed trend in the CaO-FeO_x-SiO_2 system.

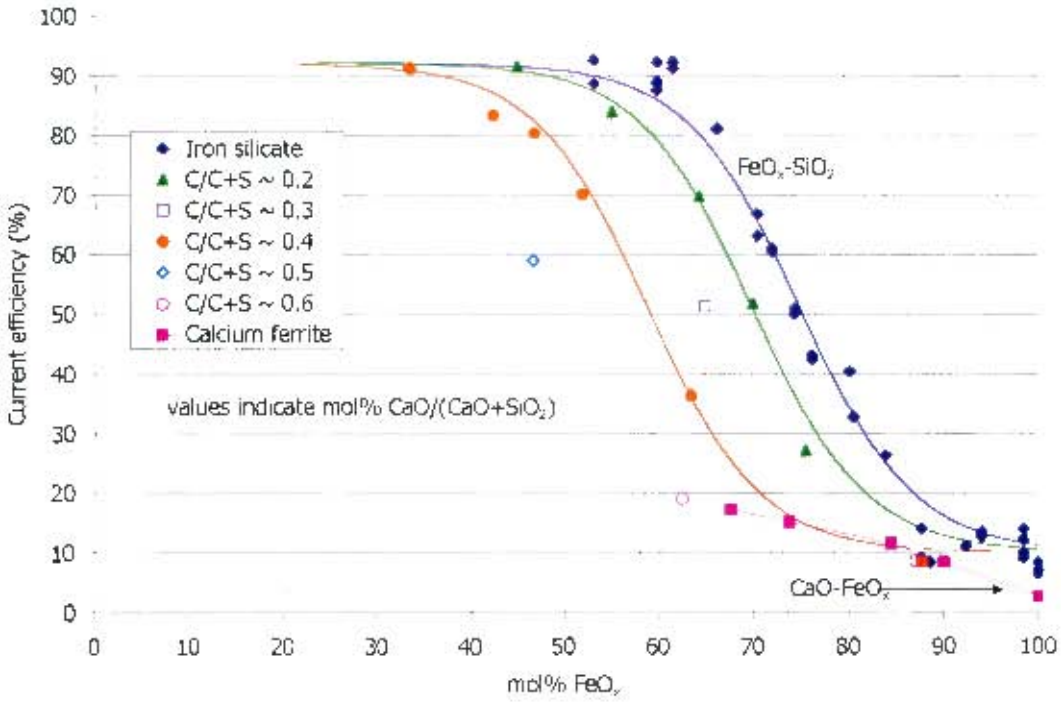

Figure 1: Current efficiency vs %FeO_x for melts containing FeO_x, CaO and SiO_2. Measurements on FeO_x-SiO_2 by Simnad *et al.* (1954), CaO-FeO_x data by Dancy and Derge (1966) and data on CaO-FeO_x-SiO_2 by Dickson and Dismukes (1962). Curves are included to enhance visualisation. Temperatures of measurements are from 1300 – 1400 °C for silicates and around 1200 °C for calcium ferrites.

Three observations can be drawn from the above results. The first is that basicity of the melt affects the relative ionic and electronic contributions, where the higher the basicity, the more electronic conduction takes place. The melt would be more depolymerised with higher levels of CaO and it is possible that the mobilities of both holes and ions would be increased. The second observation is that the addition of CaO to wüstite will bring about the generation of more Fe_2O_3 (Fe^{3+}) while the addition of SiO_2 will maintain the majority of the iron as wüstite. This suggests that the iron redox equilibrium affects the relative electronic contribution. This redox equilibrium is related to the oxidation potential in terms of the relative amounts of the valencies of the metal ions. The last observation is that in the FeO_x-SiO_2 system, significant ionic conduction is attributable to the Fe^{2+} ion.

2.3.4. Summary

It has been established that electrical conduction in slags can occur through ionic or electronic mechanisms or contribution from both. In slags containing no transition metals the ionic mechanism will dominate. The ionic mechanism is dependent on the concentration, mobilities and valences of the ions in the slag. The electronic mechanism will occur in slags containing transition metals where electron exchange occurs between transition metal ions of different valencies. In slags containing iron oxide, a combination of ionic and electronic conduction will occur.

2.4. Effect of temperature

The effect of temperature on the electrical conductivities of slags is discussed next as most of the literature deals with the temperature dependence of the conductivity in a similar fashion. The electrical conductivities of all the slags studied in the literature increased with increasing temperature. It is commonly accepted that the variation with temperature of electrical conductivities of melts above their liquidus temperatures, can be expressed in terms of the Arrhenius relationship (sometimes referred to as the Rasch-Hinrichsen law (Bockris *et al.* (1952) and Winterhager *et al.*(1966)):

Equation 6: $\kappa = A_\kappa \exp(-\frac{E_\kappa}{RT})$

Thus by evaluating log κ or ln κ vs 1/T, one can obtain values for the activation energy (E_κ) and the constant (A_κ). Bockris *et al.* (1948) interpreted the temperature dependence of the conductivity as being related to a metal cation positioned in an "energy well" in the interstices of the silicate network. The height of the energy well is related to E_κ and the probability of the cation escaping from the well is proportional to $\exp(-E_\kappa/RT)$. Therefore as the temperature is increased, the likelihood of the cation to escape and jump in response to an applied potential will increase.

In most cases authors have made use of the Arrhenius relationship to describe the temperature dependence of the conductivity. A notable exception was provided by Hoster and Pötschke (1983) who studied the Al_2O_3-CaO-FeO_x-SiO_2 system. Their data suggested that for the CaO-SiO_2 binary with CaO/SiO_2 ratios of 0.6 and 0.3, the temperature dependence was not Arrhenian and there was a greater dependence of the conductivity on temperature. For more basic slags (lime-silica ratios of 1.0 and 1.5), the temperature dependence was Arrhenian despite being two phase at some of the temperatures investigated. Bockris *et al.* (1948) studied the same system over a larger temperature range and noted that there were inflections at some compositions in the CaO-SiO_2 system, however above and below the inflections, the relation between ln k and 1/T was linear. Bockris *et al.* made use of the Arrhenius relationship to describe the temperature dependence.

MacKenzie (1962) reviewed electrochemical measurements on binary liquid silicates and presented the data as shown in Figure 2. It was found that the activation energies for alkali metal silicates (~10 kcal/mole or ~40 kJ/mole) were markedly lower than for the alkaline earth metal silicates (15-50 kcal/mole or 60-210 kJ/mole). Furthermore, the activation energies for the binary alkaline earth metal silicates decreased with increasing metal oxide addition. This suggested that for melts containing alkaline earth metal cations, the activation energy for conduction was related to the composition.

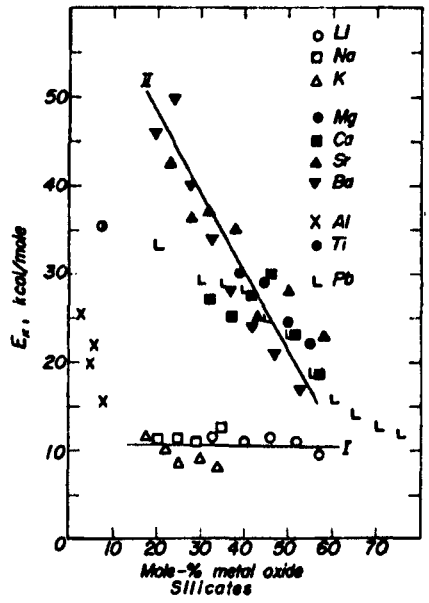

Figure 2: Activation energies for electrical conduction in binary liquid silicates after MacKenzie (1962)

Jiao and Themelis (1988), in their work on correlating slag composition and conductivity, provided a table showing that the activation energies for systems not containing iron occurred within the range 62 – 200 kJ/mole. For systems containing greater than 15wt% FeO_x, the activation energies were in the range 20 – 80 kJ/mole. In general, the higher the electrical conductivity of the slag, the lower the activation energy for that system.

For slags containing iron oxide, of particular interest was data reported by Pastukhov *et al.* (1966) who added FeO_x sequentially to an Al_2O_3–CaO–SiO_2 system. At around 15% FeO_x the authors reported that electronic conduction became the dominant mechanism, and at the same composition, the activation energy for conduction decreased significantly.

In summary, the temperature dependence of the electrical conductivity of most slags is well described by the Arrhenius relationship. The activation energy for conduction is significantly lower for binary alkali earth metal silicates than for binary alkali metal silicates. Also systems containing large amounts of iron have lower activation energies.

2.4.1. Compensation law

The compensation law will be shown to be valid for the electrical conductivity of Al_2O_3-CaO-MgO-SiO_2 containing slags in the modelling Chapter 6. In order to provide further background concerning the compensation law the following is provided in relation to silicate glasses and melts. (The compensation law occurs in a vast range of processes including thermal denaturation of proteins, catalytic reactions, evaporation of metals and semiconduction (Kemeny and Rosenberg (1973))). The compensation law is very often found to be obeyed where the property being studied e.g. diffusion, viscosity, electrical conductivity is exponentially related to temperature e.g. by the Arrhenius relationship. Where the compensation law is obeyed, the activation energy for the property (diffusion, viscosity, electrical conductivity) is linearly related to the logarithm of the pre-exponential factor. For example in the case of diffusion the compensation law is expressed as the following:

Equation 7: $E_D = a + b \cdot \log A_D$

Where E_D is the activation energy for diffusion

$\log A_D$ is the logarithm of the pre-exponential factor for diffusion

a and *b* are coefficients unique to particular systems

Winchell (1969) proposed that diffusion data in silicates obeyed the compensation law. The author examined diffusion data in a wide range of silicate systems and many different diffusing species. Dosdale and Brook (1983) showed that ionic conduction and diffusion in ionic crystals should be expected to be compensated. The authors also mentioned that an analogous expression called the Meyer-Neldel rule is used in the case of electronic conductivity. Zhang and Jahanshahi (1998a,b) and Urbain *et al.* (1981) made use of the compensation between the activation energy and pre-exponential factor for viscosity in silicate melts, in order to help describe the temperature dependence of the melt viscosity.

There have been many attempts to provide an explanation for the basis of the compensation law. For example, Winchell (1969) suggested that for diffusion in silicates the law arose on the basis of the absolute reaction rate theory. Fortner *et al.* (1995) suggested that the Meyer-Neldel rule for conductivity in liquid semiconductors arose as a result of multiphonon hopping conductivity. Chakraborty (1995) in a review on diffusion in silicate melts emphasised that the compensation law is merely an empirical observation and not based on any theory. It was considered outside the scope of this review to provide a comprehensive investigation into the origins of the compensation law or Meyer-Neldel rule. However, the validity of the compensation law can be questioned owing to four factors (Kemeny and Rosenberg (1973)). The factors are:

- Inadequate data over a sufficient range of temperatures and number of Arrhenius lines
- The logarithmic compression accidentally produces an apparent compensation law
- Biased sets of data are chosen
- The law cannot be derived from first principles of statistical mechanics or thermodynamics.

In further discussion of the applicability of the compensation law, Harris (1973) considered the effect of experimental errors in the application of the Arrhenius equation to temperature dependence data. He concluded that if the range of the experimentally obtained compensation effect was double the uncertainty in the activation energy, then the intrinsic relation between ln A and E was probably valid.

In summary, it was not surprising that a compensation effect was observed for the electrical conductivity in silicate melts given that the conductivity is exponentially related to temperature. As suggested by Chakraborty (1995), the compensation law can also be a useful tool in checking newly measured data by comparing it with a suitable compensation plot. The compensation law could also be useful in the modelling of electrical conductivity data.

2.5. Review of electrical conductivity data available

There is a large amount of literature available on the electrical conductivities of silicate slags with wide composition ranges (see Slag Atlas (1995) from which much of the literature under

examination was referenced and sourced). As was done in the Slag Atlas (1995), the approach in dealing with this amount of data was to categorise the slags according to the type of components and the number of components. Therefore single components were considered first, then binary silicates and so on. The slag components of interest were Al_2O_3, CaO, MgO, SiO_2, FeO_x and Cr_2O_3, however some data on slags containing TiO_2, MnO, NiO, CuO and alkali metals have also been considered. No data on metal fluorides were considered. The data on slags containing transition metals other than FeO_x will be treated separately towards the end of the section.

The reason for examining the large amount of data in the literature was that a modelling component was planned for this work, therefore it was necessary to scrutinise the relevant data. The other advantage of going through the data was that a good understanding would be obtained of the factors affecting the electrical conductivity of slags. In all cases it was attempted to only consider data where the conductivity was measured above the slag's liquidus temperature. Liquidus temperatures were estimated from phase diagrams for binary and ternary systems and calculated using MPE (see Zhang *et al.* (2002)) for higher order systems. The reason for considering only liquid phase data was that the effect of a solid phase differed amongst various systems, therefore treating data below the liquidus temperatures would lead to inconsistencies depending on the nature of the solid phases present. The conductivity of multiphase systems will be investigated in more depth in section 2.9.

Data have been presented at discrete temperatures and it should be borne in mind that the majority of the temperature dependence data have been regarded as Arrhenian in nature. In considering data, it was always attempted to obtain discrete data points as opposed to estimating data points from iso-conductivity lines on phase diagrams. Where data have been estimated from iso-conductivity plots on phase diagrams, this will be mentioned.

It has been attempted to consider as much of the available data as possible. Therefore most of the references in the Slag Atlas (1995) have been obtained as well as more recent references not covered in the Slag Atlas. In some cases literature was not easily available and either the data reported in the Slag Atlas were used or the data were omitted. However, in the slag systems of interest, it is considered that the data presented below is representative of the trends in the literature and approaches the true conductivities of the slags in those systems.

2.5.1. Single component systems

Electrical conductivity data were obtained for the single components of interest. An early investigation into the electrical conductivities of molten oxides was carried out by van Arkel *et al.* (1953). A review of the properties of oxide melts is given by Mackenzie (1962) which includes a section on pure metal oxides. The pertinent findings are summarised below.

2.5.1.1 Al_2O_3

The electrical conductivity for pure liquid alumina ranges from around 0.8 to 1.3 $(\Omega.cm)^{-1}$ from 2150 to 2500 °C respectively (Slag Atlas (1995)). Earlier measurements gave the conductivity as 15 $(\Omega.cm)^{-1}$ and 3.84 $(\Omega.cm)^{-1}$ at the melting point of ~2050°C (van Arkel *et al.* (1953) and Fay (1966) respectively). Mackenzie suggested that pure alumina is an ionic conductor based on the low conductivity of the liquid phase and the large increase in conductivity on fusion.

2.5.1.2CaO

The electrical conductivity value reported for pure molten CaO was that of van Arkel *et al.* (1953). The reported conductivity value at the melting point of CaO (2580 °C) was 40 $(\Omega.cm)^{-1}$, however the uncertainty in the value was ±50%. Mackenzie concluded that molten CaO was an ionic conductor.

2.5.1.3FeO_x

In this thesis, FeO_x refers to a liquid phase containing a specified amount of iron oxide with unspecified amounts of ferric and ferrous ions unless explicitly stated. All FeO_x mole% values have been calculated as equivalent stoichiometric FeO so that comparisons can be made where no indication was given of the oxidation state of the slag. The three types of solid iron oxide also need to be distinguished more carefully. The notation used for the three types of solid iron oxide is the following: wüstite or $Fe_{1-x}O$ refers to the relatively reduced state of iron oxide, magnetite is represented by Fe_3O_4 and haematite is referred to as Fe_2O_3.

Considering liquid iron oxide first, Inouye *et al.* (1953) measured the electrical conductivity of wüstite in an iron crucible below and above the melting point. The conductivity ranged from approximately 78 to 325 $(\Omega.cm)^{-1}$ in the temperature range 1300-1500 °C. The conductivity increase over the melting point (~1370 °C) was not an order of magnitude change and led the authors to conclude that the conduction mechanism in the solid was likely to be applicable to that in the liquid. They therefore concluded that liquid wüstite was a p-type semiconductor. The electrical conductivity of solid wüstite varies from 80 to 240 $(\Omega.cm)^{-1}$ from 600 to 1300 °C and depends on the stoichiometry / oxidation state (see Gartstein and Mason (1982)).

Pastukhov *et al.* (1966) measured the electrical conductivity of a pure FeO_x melt over a range of oxidation states at 1470 °C. The conductivity varied from ~140 to 360 $(\Omega.cm)^{-1}$ in the range $p_{O2} = 10^{-11}$ to 10^{-8} atm. The dependence of conductivity on the state of oxidation of the slag will be discussed further in section 2.7.

The electrical conductivity of magnetite at room temperature is around 200 $(\Omega.cm)^{-1}$ (see Gleitzer (1997)) and varies from 200-250 $(\Omega.cm)^{-1}$ at ~1520 °C depending on its oxidation state (see Mason and Bowen (1981b)). Conduction mechanisms in magnetite were discussed in section 2.3.2.

The electrical conductivity of haematite is considerably lower than wüstite and magnetite. For example, measurements by Geiger and Wagner (1965) showed that the conductivity of haemetite in air was ~1 $(\Omega.cm)^{-1}$ at 1100 °C and increased to approximately 8 $(\Omega.cm)^{-1}$ in equilibrium with magnetite at 1100 °C.

2.5.1.4MgO

The electrical conductivity of pure molten MgO at its melting temperature of 2800 °C was reported as 35 $(\Omega.cm)^{-1}$ ± 50% by van Arkel *et al.* (1953). MgO was regarded by Mackenzie (1962) as an ionic conductor.

2.5.1.5 SiO_2

Silica has a very low electrical conductivity ranging from approximately 10^{-5} to 10^{-4} $(\Omega.cm)^{-1}$ in the temperature range 1000 to 2700 °C (Panish (1959)). The structure of silicate melts was described above. As a result of the polymerised network of silica tetrahedra, it should be evident that the mobilities of the anions are limited.

2.5.1.6 Cr_2O_3

The electrical conductivity of pure molten Cr_2O_3 at its melting temperature of 2275 °C was reported as 65 $(\Omega.cm)^{-1}$ ± 50% by van Arkel *et al.* (1953). Measurements on solid hot pressed or sintered Cr_2O_3 showed the conductivity to be 0.1 to 1 $(\Omega.cm)^{-1}$ in the temperature range of 1400-1650 °C (Hagel and Seybolt (1961)). The activation energy for the conductivity above temperatures of 1400 °C has been reported as 1.8 eV or 173 kJ/mole (cited in Young *et al.* (1987)) Extrapolating the conductivity to the melting temperature of 2275 °C, the conductivity increase on fusion is from ~15 to 65 $(\Omega.cm)^{-1}$ suggesting that chromium is a semiconductor. The dependence of the conductivity of solid Cr_2O_3 on oxygen partial pressure provides further evidence for semiconduction. Young *et al.* (1987) measured thermopower and electrical conductivity of sintered pressed Cr_2O_3 compacts. At low oxygen partial pressures the conduction behaviour was n-type and changed to p-type at higher oxygen partial pressures.

2.5.2. Binary systems

Bockris *et al.* (1948, 1952) conducted measurements on binary silicates in order to gain a better understanding of the silicate slag structure (as seen in Section 2.2). The authors systematically examined the electrical conductivities of binary silicates containing Li_2O, Na_2O, K_2O, MgO, CaO, SrO, BaO, MnO, Al_2O_3 and TiO_2. Various other authors have studied some of these binary silicates. In light of the modelling requirement of the project, the data considered for the binary silicates Al_2O_3-SiO_2, CaO-SiO_2, FeO_x-SiO_2 and MgO-SiO_2 are presented below. The conductivities of calcium ferrite slags were also considered.

2.5.2.1 Al_2O_3-SiO_2

The electrical conductivity of Al_2O_3-SiO_2 melts is considerably lower than for the other metal oxides considered. At a temperature of 1700°C, Bockris *et al.* (1948) measured the conductivity which ranged from 0.001 to 0.003 $(\Omega.cm)^{-1}$ for additions of up to 8mol% Al_2O_3. The addition of alumina initially increased the conductivity up to a composition of 5mol% and therafter the conductivity decreased. Alumina is regarded as being amphoteric, therefore a network former in acidic slags and a network modifier in basic slags (for example, see the effect of alumina on the viscosity of slags: Zhang and Jahanshahi (2000)). Where the alumina acts as a network former, it will decrease the electrical conductivity of melts. Alumina is usually tetrahedrally-coordinated (AlO_4^{5-}) and these tetrahedra can fit into the silicate network and enhance the polymerisation.

2.5.2.2 CaO-SiO_2

Numerous measurements have been made on the electrical conductivity of this binary silicate. The data considered are shown in Figure 3 below:

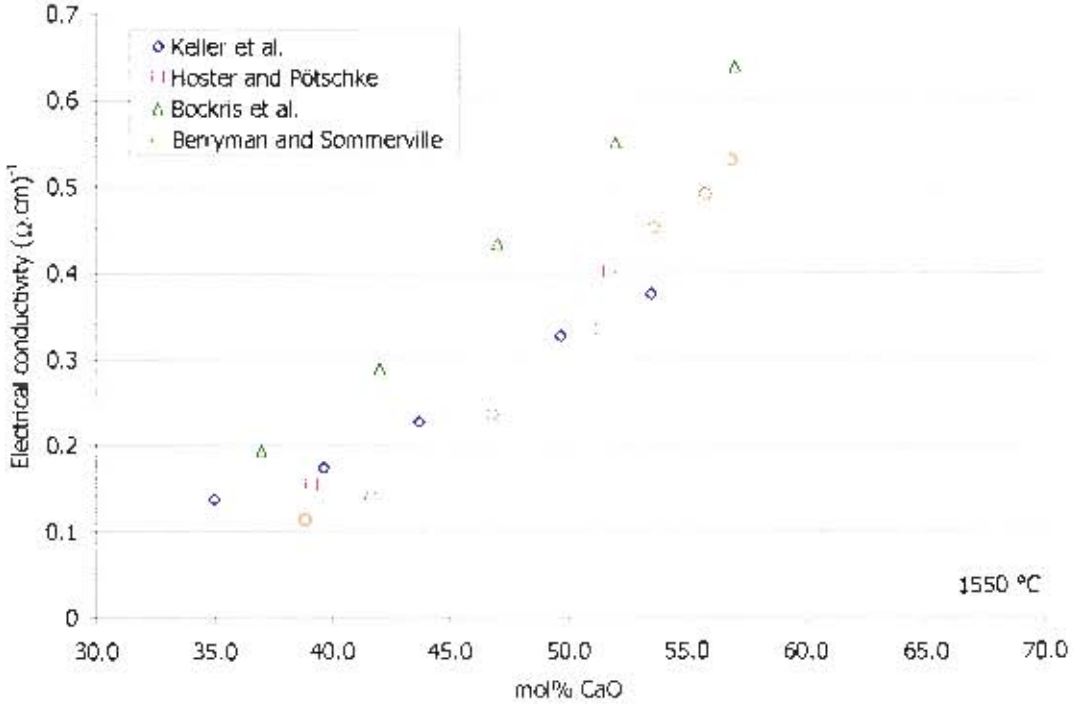

Figure 3: Electrical conductivity of CaO-SiO_2 slags at 1550 °C. Measurements by Keller *et al.* (1979b), Hoster and Pötschke (1983), Bockris *et al.* (1948) and Berryman and Sommerville (1988).

It is clear from Figure 3 that increasing the amount of CaO brings about an increase in the conductivity. The oxygen ions donated by the metal oxide will depolymerise the silicate network allowing for higher mobility of the metal cations as has been explained in more detail in section 2.3.1.

The variation in the conductivity values is likely to have arisen from the slightly different measuring setups used by the different authors. The data recommended in the Slag Atlas (1995) was that of Keller *et al.* (1979b), although no reason was given for this. The material of construction of the conductivity cells was molybdenum in the work of Bockris *et al.* (1948), Berryman and Sommerville (1988) and Hoster and Pötschke (1983). Bockris *et al.* used a two-electrode technique, Berryman and Sommerville used a central-electrode technique and Hoster and Pötschke used a ring electrode system. Keller *et al.* (1979) used a two-electrode technique and platinum crucibles and electrodes.

Hoster and Pötschke (1983) considered the temperature dependence of the electrical conductivity non-Arrhenian for the composition at 39 mol% CaO (mol% CaO/SiO_2 ratio of 0.64).

2.5.2.3 FeO_x-SiO_2

Most of the conductivity measurements on iron silicate slags were carried out in iron crucibles with an iron central electrode. The measurements by Victorovich *et al.* (1984) were carried out in molybdenum crucibles under argon and the analysed ferric contents were up to 2wt%. As a result of this the slags would all be at relatively reduced conditions. The exceptions were the measurements made by Fontana *et al.* (1984) and Pastukhov *et al.* (1966) on the

oxidation state dependence of the conductivity of iron silicates (from $p_{O_2} = 10^{-11}$ to 10^{-6} atm). The results of several authors are shown in Figure 4 for slags with up to 50 mol% SiO_2. The temperature of these measurements ranged from 1300 to 1400°C. The electrical conductivity of pure wüstite as measured by Inouye *et al.* (1953) is also shown. The p_{O_2} dependent conductivity data of Fontana *et al.* and Pastukhov *et al.* are connected by vertical lines for a given slag. The arrow indicates the direction of increasing p_{O_2}.

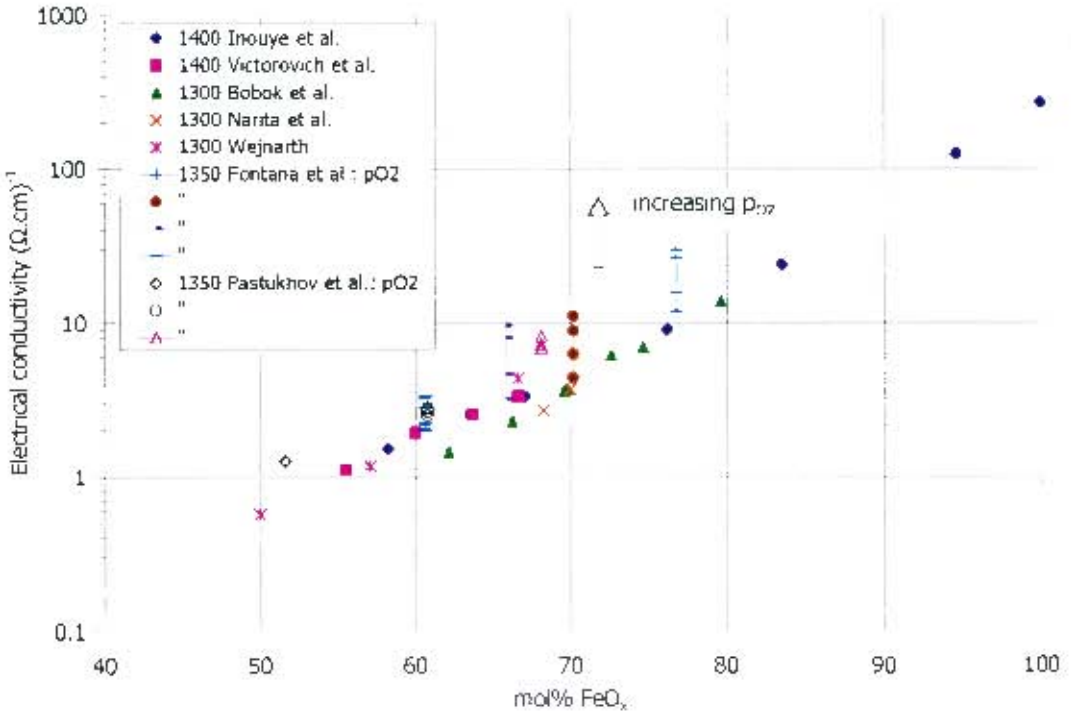

Figure 4: Electrical conductivity of FeO_x-SiO_2 slags at 1300, 1350 and 1400 °C. Measurements by Inouye *et al.* (1953), Victorovich *et al.* (1984), Bobok *et al.* (1982), Narita *et al.* (1975), Wejnarth (1934a), Fontana *et al.* (1984) and Pastukhov *et al.* (1966). The last two mentioned investigated the effect of oxidation state on the conductivity.

The general trends of interest in Figure 4 are that the conductivity increases by more than two orders of magnitude with increased iron oxide content from 50 to 100 mol%. The conductivity appears to vary exponentially with increasing iron oxide content (note the logarithmic scale in Figure 4). For a given slag the electrical conductivity increases with increasing p_{O_2}. The increase in the conductivity with increasing p_{O_2} can be understood in terms of the relative quantities of ferric and ferrous ions. At more oxidising conditions (p_{O_2} = 10^{-6} atm) there should be more ferric ions and therefore more sites for electronic conduction as discussed in section 2.3.

It is also of interest to compare Figure 1 and Figure 4. From Figure 1 it was evident that the conduction mechanism in FeO_x-SiO_2 was predominantly electronic where FeO_x > 90 mol% and predominantly ionic for FeO_x < ~60 mol%. Silica additions brought about an increase in the ionic contribution at the expense of the electronic contribution. This is reflected clearly in the large decrease in the conductivity with increasing silica.

2.5.2.4 MgO-SiO_2

The only data considered for this binary silicate were that of Bockris *et al.* (1952) where the conductivity increased from 0.34 to 1.00 $(\Omega.cm)^{-1}$ with MgO contents from 38.5 to 55 mol% at 1750 °C. As was explained in section 2.3.1 the addition of MgO would bring about depolymerisation of the silicate network and increase the conductivity.

2.5.2.5 CaO-FeO_x

The reason for the interest in calcium ferrite slags was that comparison with iron silicate slags would provide insight into the effect of basicity on the electrical conductivity of slags. Calcium ferrite slags provide data on the high basicity extreme and iron silicates on the low basicity extreme. The other benefit of studying calcium ferrite slags was that the slags have relatively low liquidus temperatures at both oxidising and reducing conditions, therefore data were available on the conductivity under these conditions. The data are shown in Figure 5.

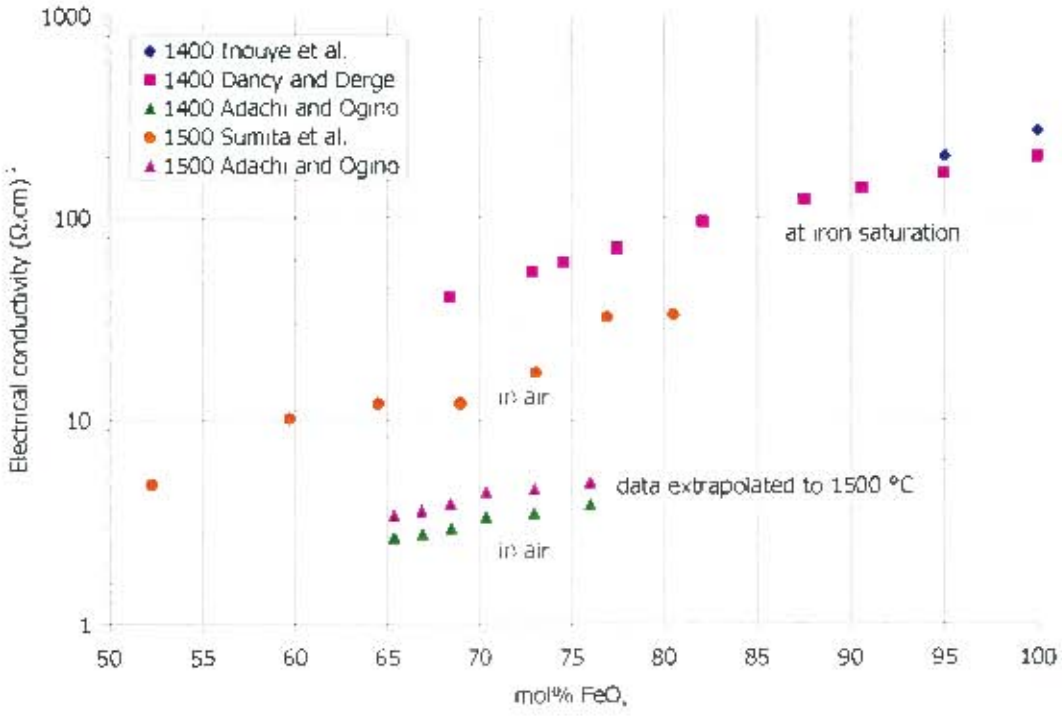

Figure 5: Electrical conductivity of CaO-FeO_x slags at reduced and oxidised conditions at 1400 °C and 1500 °C. Measurements by Inouye *et al.* (1953), Dancy and Derge (1966), Adachi and Ogino (1957), Sumita *et al.* (1983).

The electrical conductivity of CaO-FeO_x slags under reduced conditions (as measured in an iron crucible) at 1400 °C was high and ranged from 40 to above 200 $(\Omega.cm)^{-1}$ from 68 to 100 mol% FeO_x. The data are comparable to the current efficiency data in Figure 1 as those measurements were also carried out by Dancy and Derge (1966) in iron crucibles. Therefore at the reduced conditions the majority of the conduction was by the electronic mechanism. Dancy and Derge (1966) explained the decrease in the conductivity with increasing CaO content as a result of the decreased electronic component and the increase in ionic contribution of the Ca^{2+} ions. The authors suggested that Ca^{2+} ions substituted for

octahedrally co-ordinated Fe^{2+} ions but the calcium ions could not take part in electronic exchange.

The conductivity of the $CaO-FeO_x$ slags in air at 1400 °C was an order of magnitude lower than the conductivity at the reduced conditions for the equivalent amount of FeO_x (calculated as stoichiometric FeO). The likely reason for this was that the majority of the iron was present as ferric ions in air and not much electronic conduction took place. Adachi and Ogino (1957) suggested that the ferric ions were not present in the form of ferrite anions and the conduction mechanism was considered ionic.

Sumita *et al.* (1983) reported the electrical conductivity for calcium ferrite slags in air at 1500 °C and obtained higher values than the values extrapolated from the data given by Adachi and Ogino (1957) from 1300 to 1400 °C. Sumita *et al.* (1983) explained the decrease in the conductivity with increasing CaO content in terms of a change in co-ordination of the ferric ions from octahedral to tetrahedral as well as a decrease in the overall iron concentration. The tetrahedrally co-ordinated ferric ions formed complex anions such as FeO_4^{5-} or $Fe_2O_5^{4-}$ which did not contribute to the conductivity. To provide some justification for this interpretation, the authors performed Mössbauer spectroscopy on a quenched $CaO.Fe_2O_3$ sample and found the ratio of Fe^{3+}(VI) to Fe^{3+}(IV) was 1. They then described the change in co-ordination of the ferric ions in terms of the amount of CaO added. This was based on the assumption that for 100% Fe_2O_3 all the ferric ions were octahedrally co-ordinated. The ratio of Fe^{3+}(VI) to Fe^{3+}(IV) then decreased monotonically with addition of CaO. The authors further related the electrical conductivity in terms of the following parameter:

Equation 8:
$$\kappa_p = \frac{2}{r_{Ca^{2+}}}.[at.\%Ca^{2+}] + \frac{2}{r_{Fe^{2+}}}.[at.\%Fe^{2+}] + \frac{3}{r_{Fe^{3+}}}.[at.\%Fe^{3+}(VI)]$$

Where r is the ionic radius of the cation in Å. Sumita *et al.* (1983) found a linear relationship between this parameter and the measured conductivity data.

2.5.3. Ternary silicate systems

The ternary silicate systems considered were $Al_2O_3-CaO-SiO_2$, $Al_2O_3-FeO_x-SiO_2$, $Al_2O_3-MgO-SiO_2$, $CaO-FeO_x-SiO_2$, $CaO-MgO-SiO_2$ and $FeO_x-MgO-SiO_2$.

2.5.3.1 $Al_2O_3-CaO-SiO_2$

A large amount of data was available for this ternary system. The data considered for modelling purposes are presented in Figure 6 below. There was no specific criterion for choosing the data and most of the available data were considered.

It is clear from Figure 6 that an increase in the lime content in the range 31 to 58 mol% resulted in an increase in the electrical conductivity from around 0.05 to 0.3 $(\Omega.cm)^{-1}$. The increase in the alumina content from 0 to 25 mol% at both constant CaO/SiO_2 content and constant SiO_2 content brought about a decrease in the conductivity although this is not very clear from the graph.

The bulk of the data was sourced from Winterhager *et al.* (1966) and is considered the most reliable data. The authors found that the addition of alumina decreased the electrical conductivity and in the concentration ranges of interest (Al_2O_3/CaO ratio < 0.49), the

majority of the current was carried by Ca^{2+} ions. The alumina was considered to be present in less mobile alumino-silicate anions. The authors constructed an iso-conductivity ternary diagram for the system which is shown in Figure 7. The iso-conductivity lines ran parallel to the lime composition.

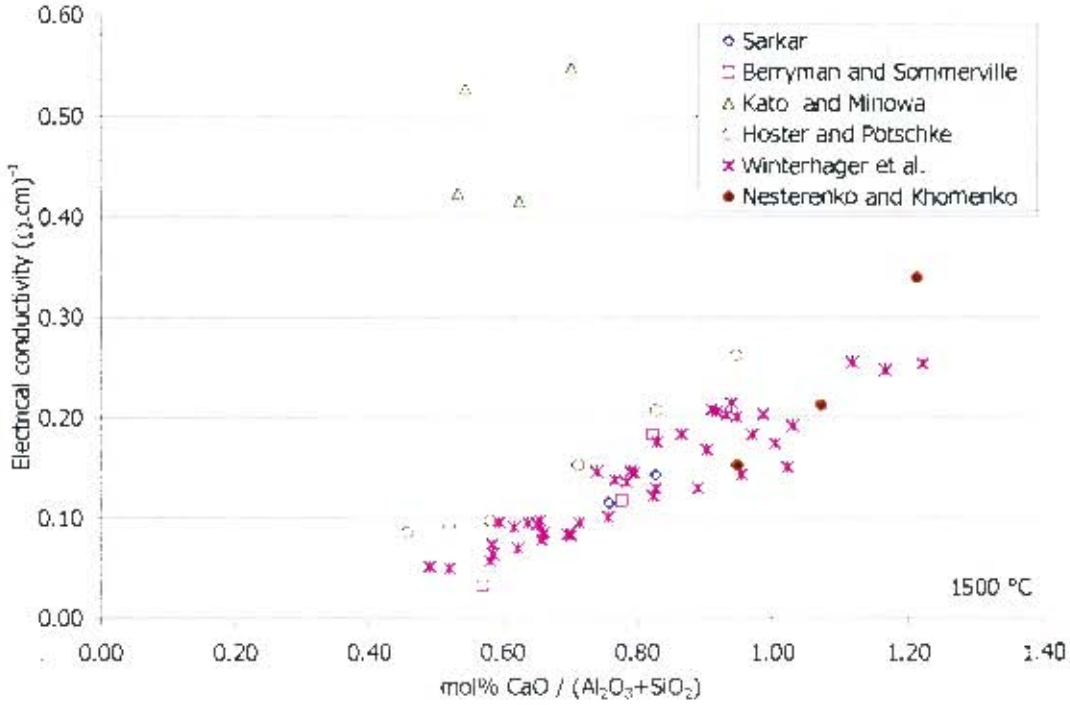

Figure 6: Electrical conductivity of Al_2O_3-CaO-SiO_2 slags at 1500 °C. Measurements by Sarkar (1989), Kato and Minowa (1969), Hoster and Pötschke (1983), Winterhager *et al.* (1966) and Nesterenko and Khomenko (1985). Data by Berryman and Sommerville (1988) at 1527°C.

Referring back to Figure 6, the data of Sarkar were in good agreement with that of Winterhager *et al.*. The conductivity values of Hoster and Pötschke (1983) were slightly higher than those of Winterhager *et al.*. Hoster and Pötschke commented that the reason for this was their finding that the temperature dependence of the conductivity was not Arrhenian in nature and was more strongly dependent on temperature. The data of Kato and Minowa (1969) were considerably higher than other authors' data for similar compositions and were therefore not considered for modelling. The reason for such a large discrepancy was not evident from the description of the measurement technique they used.

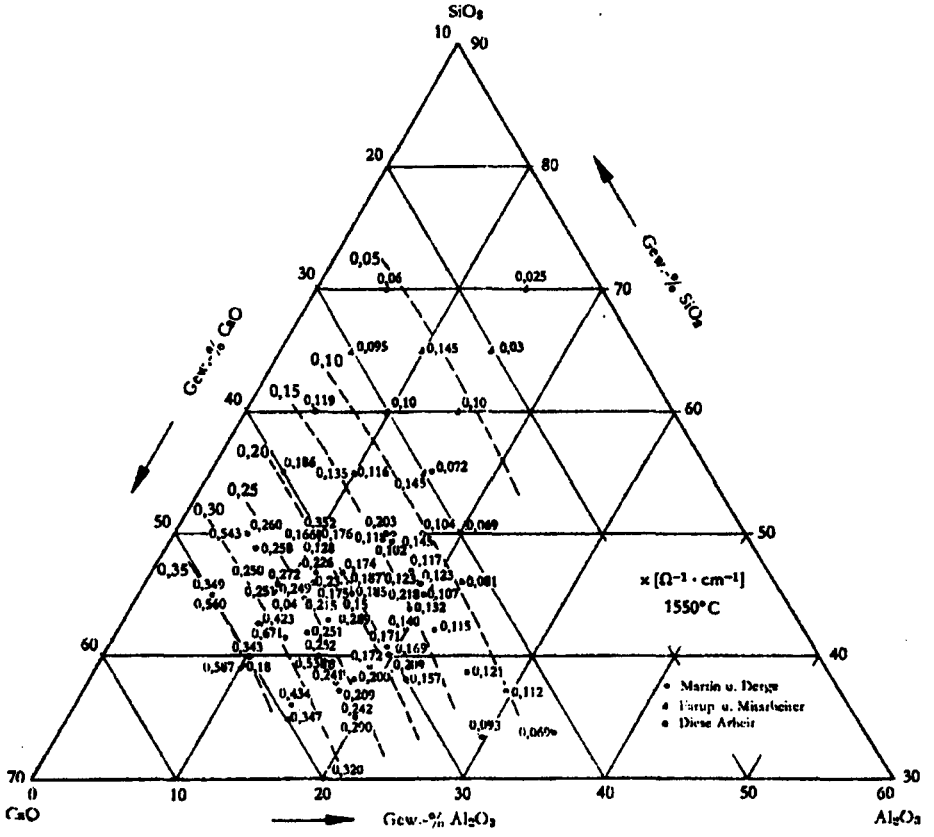

Figure 7: Iso-conductivity ternary diagram for Al_2O_3-CaO-SiO_2 system at 1550 °C after Winterhager *et al.* (1966). Open circles represent the data of Winterhager *et al.*

Winterhager *et al.* (1966) related the electrical conductivity to the composition by use of the following expression:

Equation 9: $$\kappa_{ZI} = \frac{(I_{Ca^{2+}} . at\%\ Ca^{2+})}{(I_{Si^{4+}} . at\%\ Si^{4+}) + (I_{Al^{3+}} . at\%\ Al^{3+})}$$

The I values refer to the ion-oxygen attraction values as developed by Dietzel (see Table 1 for values). The authors found good agreement between the function and their conductivity results at a temperature of 1550 °C. This is shown in Figure 8: Conductivity of Al_2O_3-CaO-SiO_2 at 1550 °C correlated as function of composition: κ_{ZI} = [(0.7 * At% Ca^{2+}) + (0.95 * At% Mg^{2+})] / [(2.83 * At% Si^{4+}) + (1.9 * At% Al^{3+})], after Winterhager *et al.* (1966). Some Al_2O_3-CaO-MgO-SiO_2 data are also included..

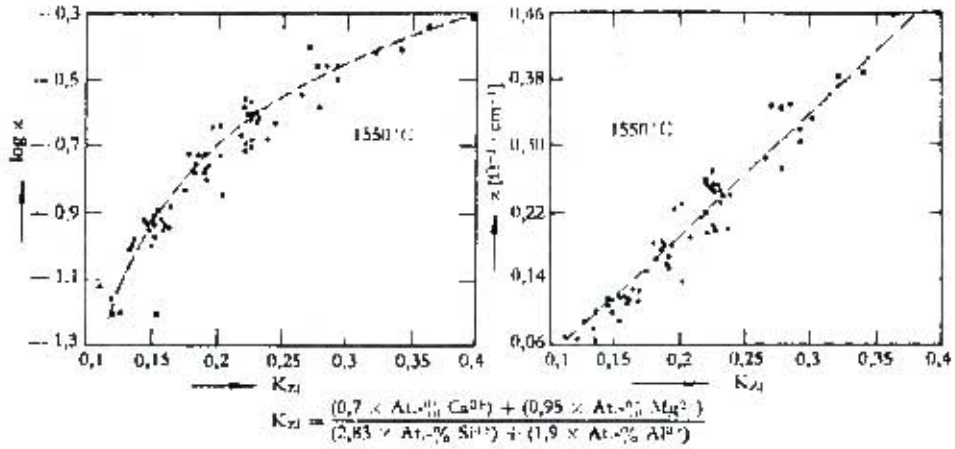

Figure 8: Conductivity of Al_2O_3-CaO-SiO_2 at 1550 °C correlated as function of composition: κ_{ZI} = [(0.7 * At% Ca^{2+}) + (0.95 * At% Mg^{2+})] / [(2.83 * At% Si^{4+}) + (1.9 * At% Al^{3+})], after Winterhager *et al.* (1966). Some Al_2O_3-CaO-MgO-SiO_2 data are also included.

2.5.3.2 Al_2O_3-FeO_x-SiO_2

Several conductivity measurements have been carried out on this ternary system in iron crucibles, therefore the iron oxide is relatively reduced. The data are presented in Figure 9.

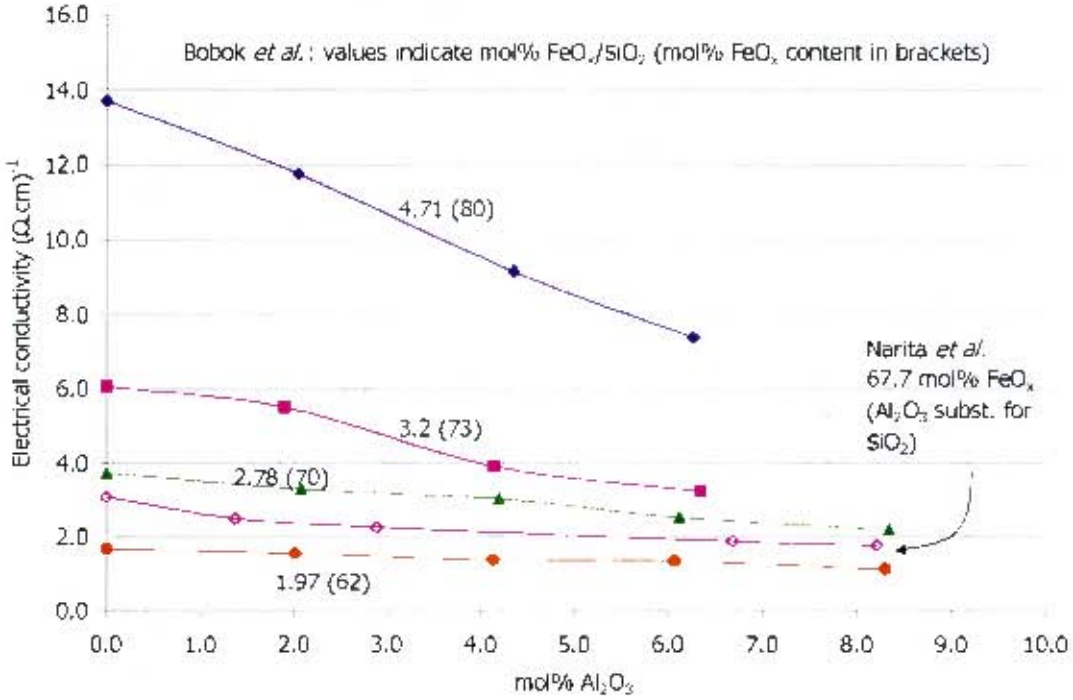

Figure 9: Electrical conductivity of Al_2O_3-FeO_x-SiO_2 slags at 1300 °C. Measurements by Bobok *et al.* (1982) and Narita *et al.* (1975).

The conductivity data measured by Bobok *et al.* (1982) was at constant FeO_x/SiO_2 ratios with addition of alumina. The data measured by Narita *et al.* (1975) was at a constant iron oxide level of 67.7 mol% and alumina substituted for silica. In all cases the alumina addition

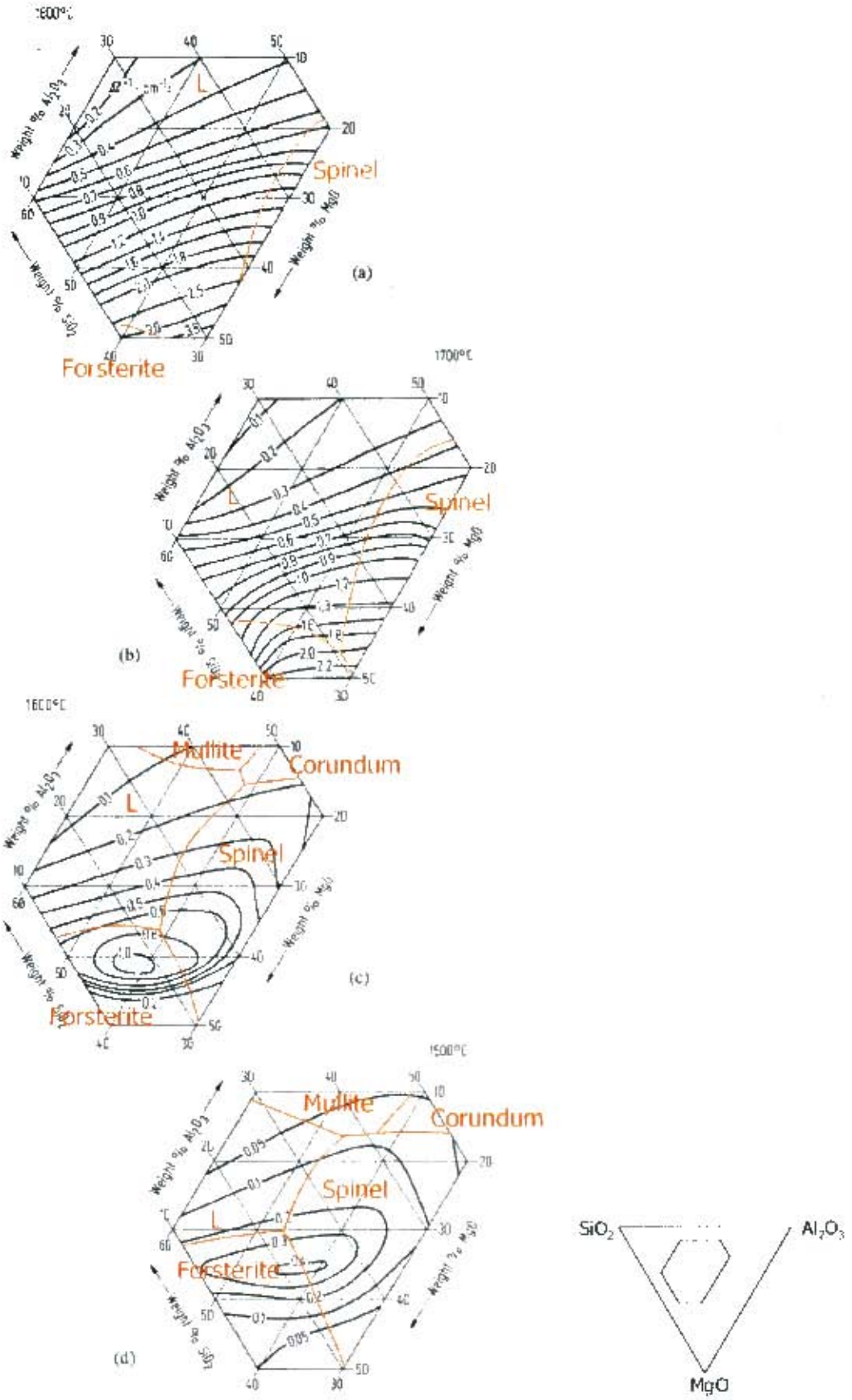

Figure 10: Iso-conductivity ternary diagrams for Al_2O_3-MgO-SiO_2 system at (a) 1800°C, (b) 1700°C, (c) 1600°C and (d) 1500°C after Liutikov and Tsylev (from Slag Atlas (1995))

There are several noticeable trends in Figure 10. The liquid region decreases in size markedly with decreasing temperature. The conductivity in two phase regions is complex and will not be considered in much detail here. In the liquid regions, the electrical conductivity of the slags increases with increasing MgO content. The additions of both SiO_2 and Al_2O_3 decrease the conductivity although the silica reduces the conductivity more so than alumina. These trends fit in with the explanation of the network forming characteristics of Al^{3+} and Si^{4+} ions and the network modifying characteristics of Mg^{2+} cations. It should be noted that data was not estimated from the iso-conductivity contours for the purposes of modelling.

Rennie *et al.* (1972) measured the conductivity at a range of temperatures for two slags in the system (compositions were wt%: 24%Al_2O_3-31%MgO-43%SiO_2 and 33%Al_2O_3-23%MgO-44%SiO_2). Their data agreed reasonably with the values of Liutikov and Tsylev. Downing and Urban (1966) also measured a composition in this ternary (30%Al_2O_3-30%MgO-40%SiO_2) and their conductivity values at each temperature agreed well with the values of Liutikov and Tsylev when measured in a graphite crucible (as opposed to the results when measured in a tungsten crucibles).

2.5.3.4CaO-FeO_x-SiO_2

As with the binary CaO-FeO_x and FeO_x-SiO_2 systems, data are available for the ternary CaO-FeO_x-SiO_2 at a range of oxidation states. Oxidation state dependence of the conductivity of compositions in this ternary were also reported by Fontana *et al.* (1984) at 1350 °C and Engell and Vygen (1968) at 1600 °C. In an attempt to highlight the important aspects related to this ternary system, data are presented in Figure 11 and Figure 12.

With reference to Figure 11, the measurements of Bobok *et al.*, Narita *et al.*, Adachi and Ogino (from Slag Atlas (1981)) and Wejnarth were all made in iron crucibles therefore the slags were at relatively reduced conditions. The measurements of Adachi and Ogino (1957) were performed in air using a Pt crucible to contain the slag. The measurements of Fontana *et al.* were performed at a range of oxygen partial pressures (p_{O2} = 10^{-11} to 10^{-6} atm) in a Pt crucible.

The trends which are clear from Figure 11 are that increasing the iron oxide content of the slag from 10 to 75 mol% increases the conductivity from 0.05 to 20 $(\Omega.cm)^{-1}$. The oxidation state also plays a role in determining the conductivity. With increasing p_{O2} from 10^{-11} to 10^{-6} atm, the conductivity increased by a factor of 2, as indicated by the data of Fontana *et al.*

However, the data of Adachi and Ogino (1957) showed that the conductivity in air was relatively low in comparison to the conductivity of slags at more reduced conditions. The measurements in air can be explained by the fact that the majority of the iron was present as ferric ions. The authors analysed the slags after measurements were made and found that 88-95% of the iron oxide was present as Fe_2O_3. As was mentioned in section 2.2 on silicate slag structure, it was likely that the ferric ions were tetrahedrally co-ordinated (Mysen *et al.* (1984)) and therefore enhanced the polymerisation of the slag and decreased the conductivity. This does not contradict the trend shown for the data of Fontana *et al.* as the relative proportions of ferric and ferrous ions present at p_{O2} = 10^{-6} atm are significantly different to the proportions in air. Further data on the electrical conductivity of CaO-FeO_x-SiO_2 slags in air was reported by Morinaga *et al.* (1975) for a temperature of 1500 °C.

The oxidation state dependent conductivity data of Engell and Vygen (1968) at 1600 °C provides a clearer picture of the situation. Their measurements were carried out through a range of oxygen partial pressures so the change in conductivity with oxidation state could clearly be seen. These data will be evaluated in section 2.7.

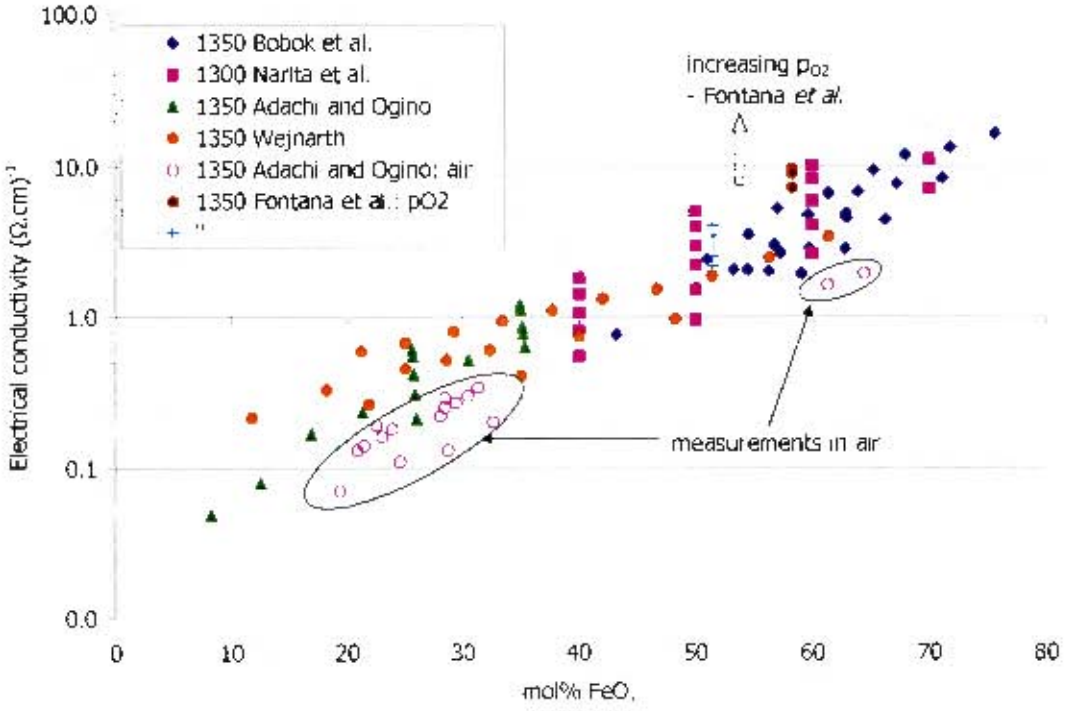

Figure 11: Electrical conductivity of $CaO-FeO_x-SiO_2$ slags at 1300 and 1350 °C and at a range of oxidation states. Measurements by Bobok *et al.* (1982), Narita *et al.* (1975), Adachi and Ogino (from Slag Atlas (1981)) and Wejnarth (1934a) at iron saturation, Adachi and Ogino (1957) in air and Fontana *et al.* (1984) at a range of oxidation states. The data of Narita *et al.* (1975) were estimated from an iso-conductivity diagram at constant iron content with increasing CaO/SiO_2 ratios.

In order to give some indication of how the lime and silica contents of the slag affect the conductivity, the data at 1350°C of Bobok *et al.* (1982), Adachi and Ogino (from Slag Atlas (1981)) and Wejnarth (1934a) was plotted in Figure 12 at various lime-silica ratios.

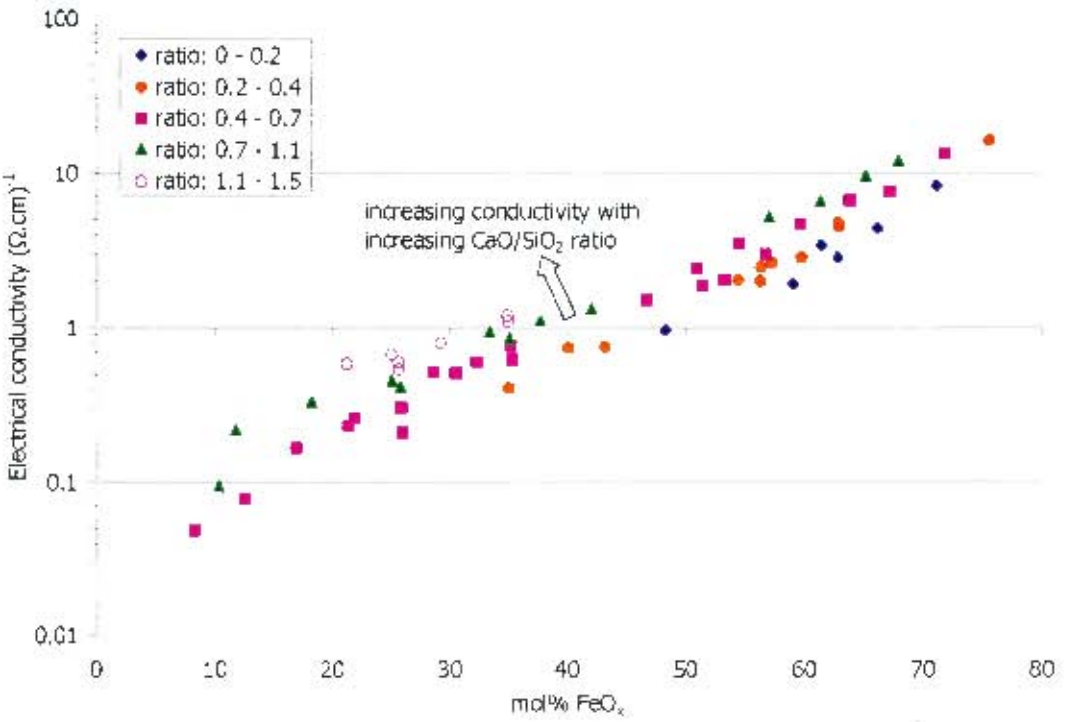

Figure 12: Electrical conductivity of $CaO-FeO_x-SiO_2$ slags at 1350 °C depicting effect of increasing lime-silica ratio. Measurements by Bobok *et al.* (1982), Adachi and Ogino (from Slag Atlas (1981)) and Wejnarth (1934a) organised into ranges of $CaO-SiO_2$ ratios.

The general trend evident from Figure 12 is that the electrical conductivity of slags at the same iron oxide content increases as lime replaces silica. This is explained by two reasons. Firstly the trend is in agreement with the current efficiency data of Dickson and Dismukes (1962) presented in Figure 1. As the lime content of a slag is increased, the electronic contribution to the overall conductivity increases. The reason for the increase in the electronic contribution is that the ferric ion content of the slags increases and provides more sites for electron / hole exchange. The other effect of replacement of silica by lime is that the ionic contribution of Ca^{2+} ions is significantly higher than that of silicate anions (for example see effect of CaO in the $CaO-SiO_2$ binary in Figure 3).

Hoster and Pötschke (1983) also carried out work on the ternary system in question. The authors started with the binary $CaO-SiO_2$ slag at varying CaO/SiO_2 ratios and added iron oxide. The work was carried out from 1450 to 1650 °C and was therefore not compared with the data presented above. The authors' data are presented in Figure 13. It is clear from the data that the electrical conductivity increased with increasing FeO_x content and increasing CaO/SiO_2 ratios. The explanation for these trends is similar to the explanation given for the slags above. As has been mentioned previously, Hoster and Pötschke maintained that the temperature dependence of slags with $CaO/SiO_2 \leq 0.6$ was not Arrhenian and the conductivity was more strongly related to temperature. The authors also correlated the conductivity as a function of the composition and temperature. This will be discussed later in this chapter.

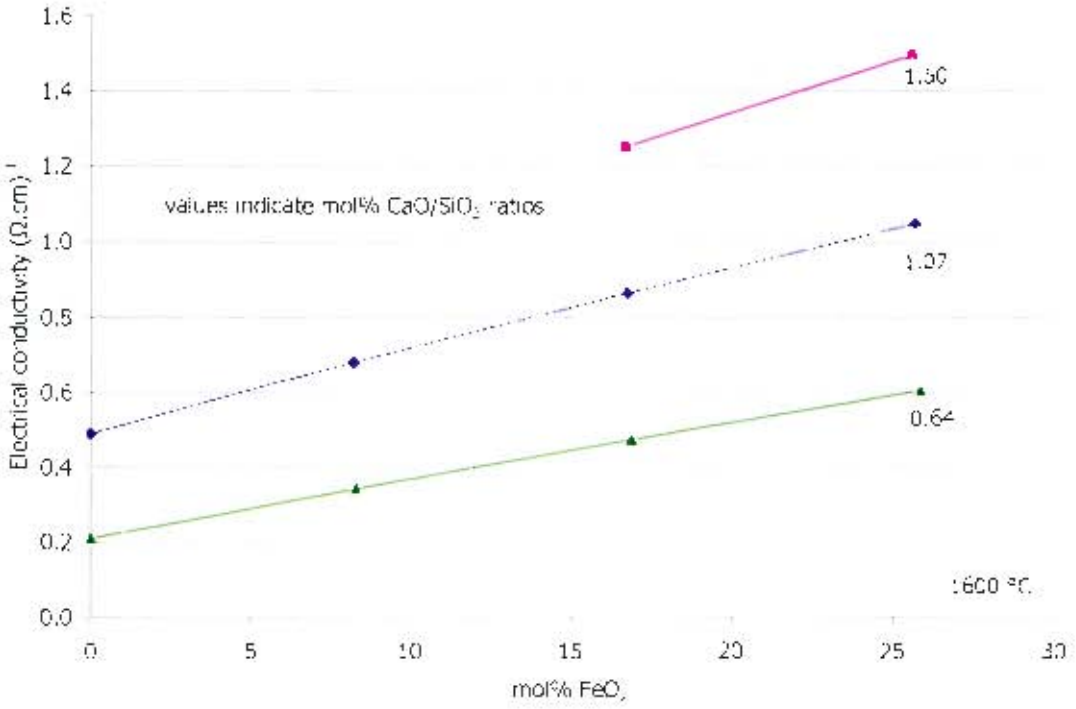

Figure 13: Electrical conductivity of CaO-FeO_x-SiO_2 slags at 1600 °C with various CaO/SiO_2 ratios and increasing FeO_x content. Measurements by Hoster and Pötschke (1983).

2.5.3.5 CaO-MgO-SiO_2

Relatively few data were available for this ternary system. The majority of the data for this system was presented (Slag Atlas (8)) as iso-conductivity lines on a ternary diagram with a couple of discrete points by other authors. This is reproduced in Figure 14.

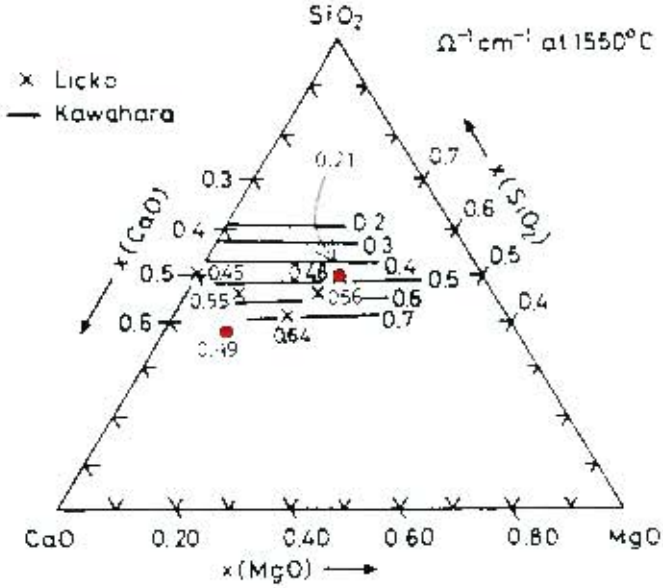

Figure 14: Electrical conductivity data at 1550 °C for CaO-MgO-SiO_2 system plotted on ternary diagram (after Slag Atlas (1995)). Iso-conductivity lines reported by Kawahara *et al.* (1983). Other data by Licko and Danek (as cited in Slag Atlas (1995)) (crosses) and Schiefelbein and Sadoway (1997) (red circles).

The data presented in Figure 14 need to be considered carefully. The iso-conductivity lines of Kawahara *et al.* (1983) suggested that the conductivity in the CaO-MgO-SiO_2 slags was equally dependent on the lime and magnesia contents. For a given level of SiO_2, the substitution for each other of CaO and MgO showed little effect on the conductivity within the liquid region. The data of Licko and Danek appeared to confirm the findings of Kawahara *et al.*.

The measurements by Schiefelbein and Sadoway (1997) were carried out using their high accuracy coaxial cylinders technique. The authors directly compared their results with those of Kawahara *et al.* and ascribed the higher conductivity values of Kawahara *et al.* to the lower accuracy measurement technique used by those authors. However, despite the difference in the absolute value of the measured conductivity, Schiefelbein and Sadoway's data seem to agree with the trend of increasing conductivity with increasing CaO and MgO.

Given the large difference in the values of the conductivity between the high accuracy and low accuracy techniques, the only data point considered for this system was the value of 0.21 $(\Omega.cm)^{-1}$ as measured by Schiefelbein and Sadoway. The data point of Schiefelbein and Sadoway with a value of 0.49 $(\Omega.cm)^{-1}$ is possibly below the liquidus temperature of the slag at 1550 °C (liquidus temperature according to phase diagram is >1600 °C) and is not considered further.

2.5.3.6 FeO_x-MgO-SiO_2

This system was studied by Victorovich *et al.* (1984). The authors started with iron silicate slag compositions and substituted MgO for FeO such that the silica content was constant. Their data are presented in Figure 15. Their data for iron silicate slags are also included in the graph for comparison with the MgO containing slags. The experiments were carried out at reduced conditions in molybdenum crucibles under an argon atmosphere. The ferric iron content in the final slags was analysed and found to be under 2wt% Fe_2O_3 for all slags.

Victorovich *et al.* (1984) chose to interpret their results at the liquidus temperatures of the slags instead of analysis at constant temperatures. They argued, that at constant temperatures, the degree of superheat (difference between the constant temperature and the liquidus temperature) for different slags would change the distribution of silicate anions. Therefore interpretation of the conductivity data would need to involve distinguishing between the effect of cationic composition and structural changes. In the context of the current investigation, the results will be interpreted at constant temperature.

Victorovich *et al.* (1984) suggested that no electronic conduction took place and that the conductivity was entirely due to Fe^{2+} and Mg^{2+} cations. Given the low ferric iron contents measured in the slags, this was considered a good assumption. Therefore, considering the results in Figure 15, it is seen that at a constant iron oxide content, the conductivity increases as MgO replaces SiO_2. This can be understood in terms of the additional Mg^{2+} cations being available to carry current. The other possibility is that the MgO increased the amount of ferric in the slag and therefore enhanced the electronic contribution.

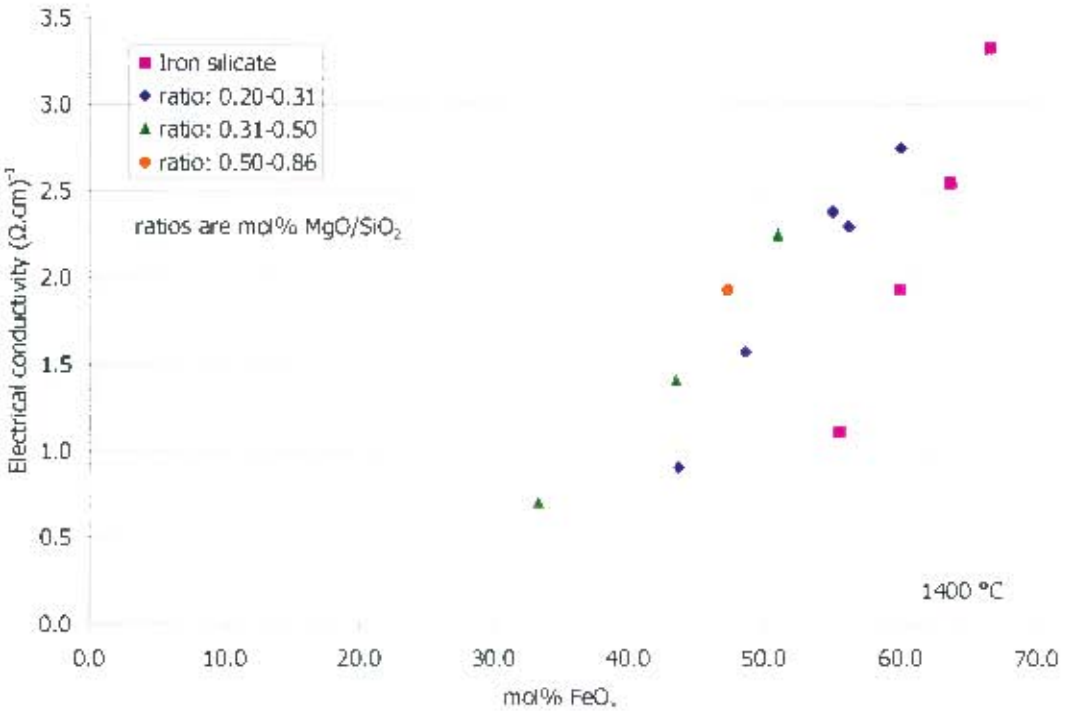

Figure 15: Electrical conductivity of FeO_x-MgO-SiO_2 and FeO_x-SiO_2 slags at 1400 °C at reduced conditions. Measurements by Victorovich *et al.* (1984).

2.5.4. Quaternary silicate systems

The quaternary systems studied were Al_2O_3-CaO-FeO_x-SiO_2, Al_2O_3-CaO-MgO-SiO_2 and CaO-FeO_x-MgO-SiO_2. The data available for other quaternaries were limited.

2.5.4.1 Al_2O_3-CaO-FeO_x-SiO_2

The only conductivity data considered for this system were those measured by Pastukhov *et al.* (1966). The authors studied the effect of oxidation state on the electrical conductivity of a 20%Al_2O_3-40%CaO-40%SiO_2 slag with increasing iron oxide content. The results of the oxidation state work will be shown later in the chapter. The authors also looked at the increase in the conductivity of the abovementioned slag in air with iron oxide additions. The results are shown in Figure 16.

The authors found that the electrical conductivity increased dramatically with increasing FeO_x content. The activation energy for conduction decreased with increasing FeO_x content. The large increase in the conductivity was ascribed to increasing electronic conduction with increasing iron oxide content. This also explained the large drop in the activation energy at around 15wt% Fe_2O_3.

It should be emphasised that the above measurements were in air, the rest of the experimental setup for these particular measurements was not entirely clear from the paper. The magnitude of the conductivities of the higher iron containing slags was surprising given that the majority of the iron should be ferric in air. The values are of comparable magnitude to those for calcium ferrite slags in air at 1500 °C (see Figure 5). Unfortunately, there are no other suitable data with varied alumina content for this system, therefore comparisons are not possible to investigate the effect of alumina on the system.

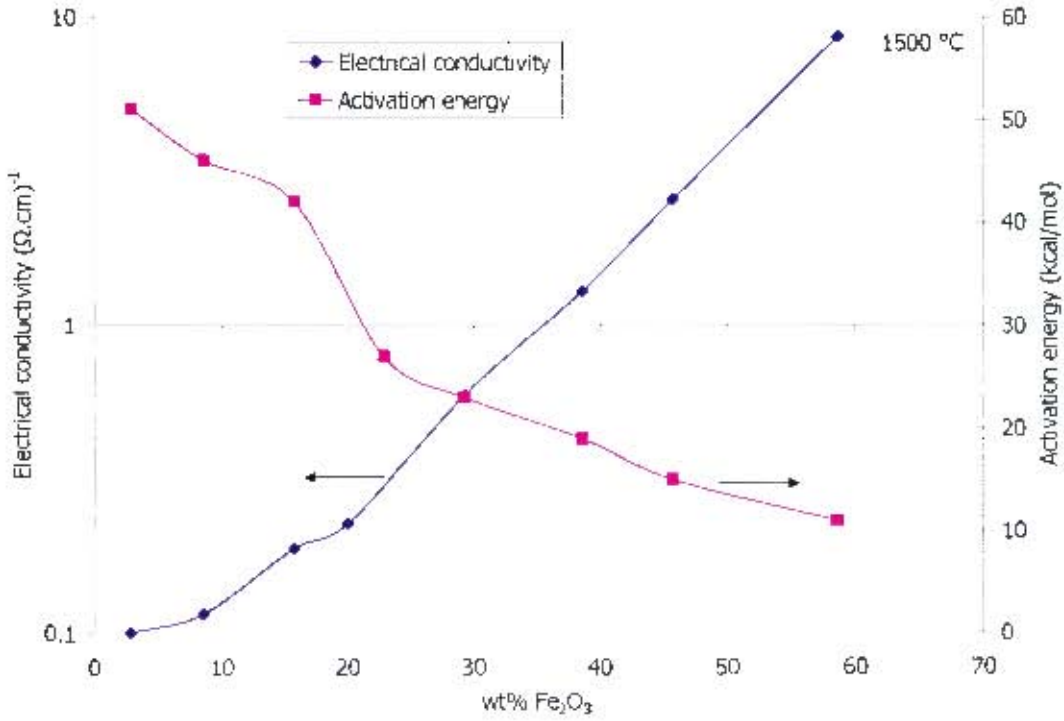

Figure 16: Electrical conductivity and activation energy of Al_2O_3-CaO-FeO_x-SiO_2 slag in air at 1500 °C with increasing iron oxide content. Measurements by Pastukhov *et al.* (1966).

2.5.4.2 Al_2O_3-CaO-MgO-SiO_2

There was a lot of conductivity data for slags in this quaternary system. The data of various authors is presented in Figure 17 as a function of mol% (CaO+MgO)/(Al_2O_3+SiO_2).

The data of Adachi and Ogino, Rennie *et al.*, Sarkar and Ossin *et al.* was for high alumina containing slags (>~10 mol% or > ~20wt%). Most of the data of Winterhager *et al.* and Nesterenko and Khomenko were for slags with lower alumina contents (up to 3mol%). The measurements were made using a variety of techniques including the ring-electrode technique and the two-electrode technique although Sarkar used parallel plates instead of wires.

The general trend observed in Figure 17 is that an increase in the CaO and MgO contents brought about an increase in the conductivity. This is in accordance with the network modifying properties of the Ca^{2+} and Mg^{2+} cations: the silicate network is depolymerised allowing for enhanced mobilities of the divalent cations. It is assumed that the role of alumina in the slag is that of a network former, therefore it will enhance the polymerisation of the network.

Winterhager *et al.* (1966) once again correlated their data as a function of the composition as given in Figure 8: Conductivity of Al_2O_3-CaO-SiO_2 at 1550 °C correlated as function of composition: κ_{ZI} = [(0.7 * At% Ca^{2+}) + (0.95 * At% Mg^{2+})] / [(2.83 * At% Si^{4+}) + (1.9 * At% Al^{3+})], after Winterhager *et al.* (1966). Some Al_2O_3-CaO-MgO-SiO_2 data are also included. and Equation 9. Figure 8: Conductivity of Al_2O_3-CaO-SiO_2 at 1550 °C correlated as function of composition: κ_{ZI} = [(0.7 * At% Ca^{2+}) + (0.95 * At% Mg^{2+})] / [(2.83 * At% Si^{4+})

+ (1.9 * At% Al^{3+})], after Winterhager *et al.* (1966). Some Al_2O_3-CaO-MgO-SiO_2 data are also included. included their data for the quaternary system.

Sarkar (1989) related the conductivity of the high alumina blast furnace type slags to an empirical measure of the basicity ratio. This is shown in Figure 18 and includes the two data points measured by Sarkar for the Al_2O_3-CaO-SiO_2 system.

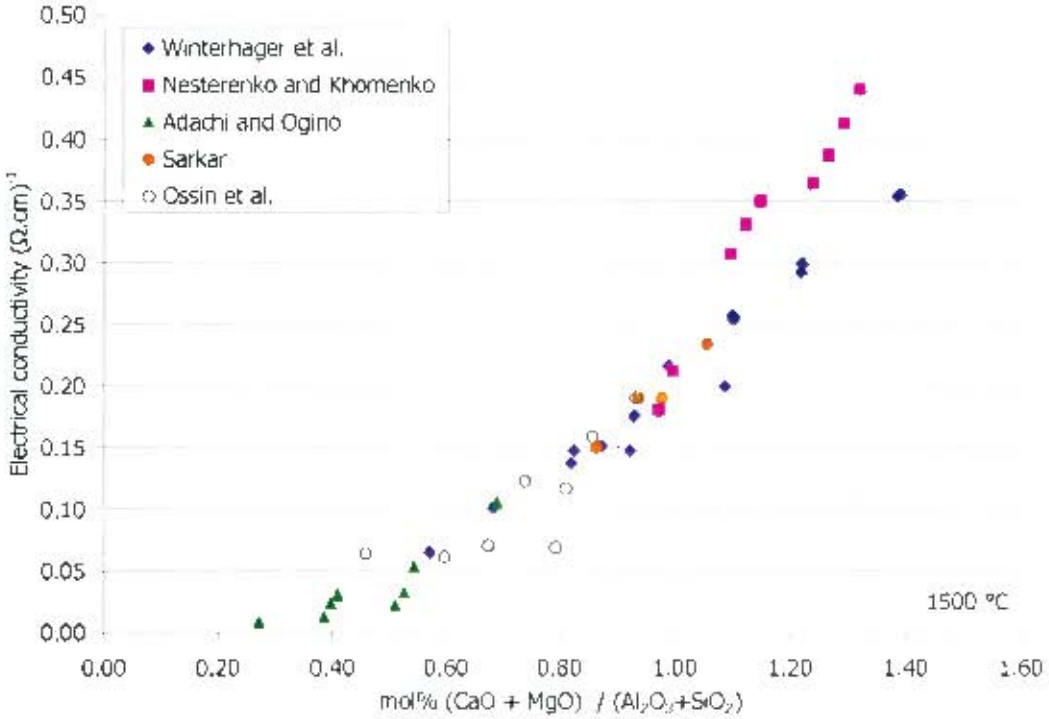

Figure 17: Electrical conductivity of Al_2O_3-CaO-MgO-SiO_2 system at 1500 °C. Measurements by Winterhager *et al.* (1966), Nesterenko and Khomenko (1985), Adachi and Ogino (from Slag Atlas (1995)), Sarkar (1989) and Ossin *et al.* (1971).

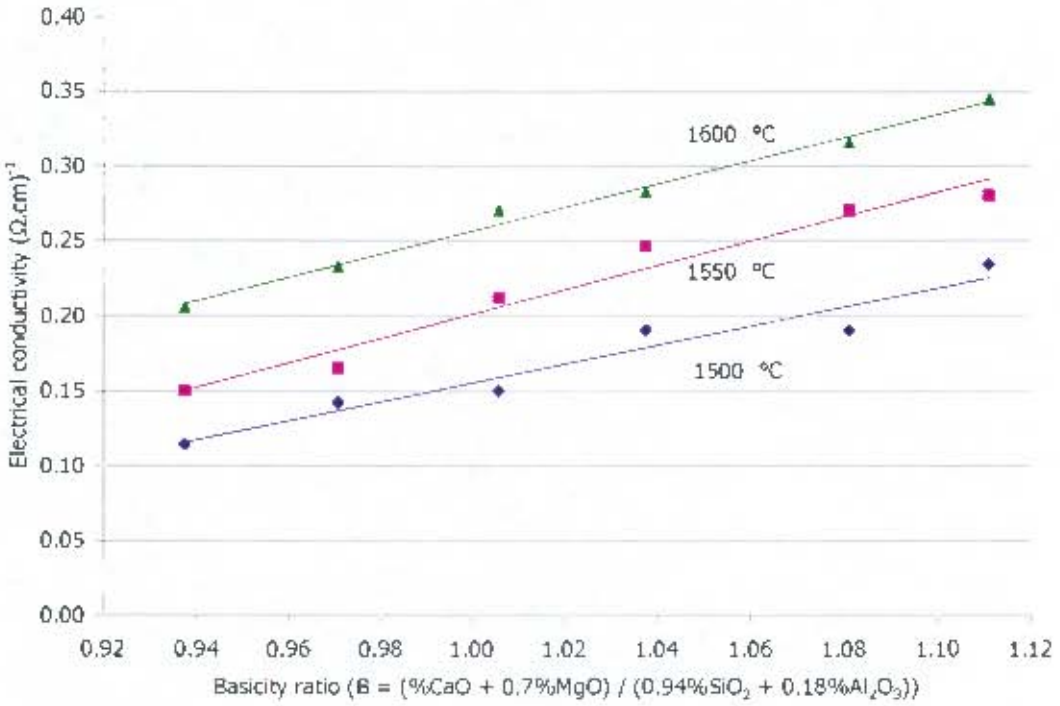

Figure 18: Electrical conductivity measurements for high alumina blast furnace slags at 1500, 1550 and 1600 °C as a function of the empirical basicity ratio according to Sarkar (1989)

2.5.4.3 $CaO-FeO_x-MgO-SiO_2$

There were only two major investigations into the electrical conductivities of slags in this quaternary. The first was by Bobok *et al.* (1982) where MgO was added to slags with constant $(CaO+FeO_x)/(SiO_2)$ ratios. The work was carried out at 1140 to 1320 °C, so the slags with higher MgO contents were possibly below their liquidus temperatures. The data at 1300 °C is plotted in Figure 19. The measurements were carried out in an iron crucible, therefore the slags were fairly reduced. The ferric content was analysed and found to be around 5-8wt% which equated to Fe^{3+}/Fe_{total} ratios of 0.08 to 0.2 which rose with increasing CaO content.

Two trends may be observed in Figure 19. For a given mol% $(CaO+FeO_x)/SiO_2$ ratio, the electrical conductivity increased with increasing MgO addition. This was to some extent surprising given that the addition of MgO would dilute the iron oxide content. However, if the majority of the conduction was ionic, then addition of another ionic conductor would increase the conductivity. The other trend was that as iron oxide content increased, the electrical conductivity increased. The difference between the conductivities at constant iron oxide contents is dependent on the amounts of CaO and MgO in the slags. Thus with greater CaO and MgO content, there is more ionic conduction as well as greater ferric content which increases the electronic contribution.

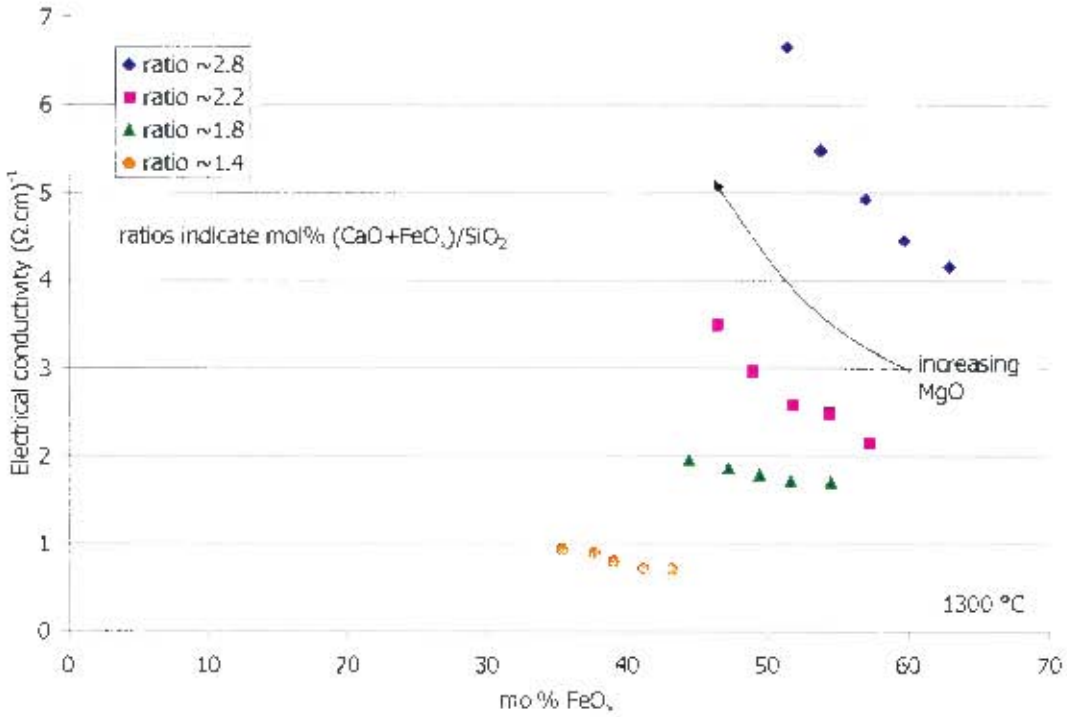

Figure 19: Electrical conductivity of CaO-FeO_x-SiO_2 slags with MgO additions at 1300 °C. Measurements by Bobok *et al.* (1982).

The other literature concerning this quaternary system was published very recently by Ducret *et al.* (2002). The measurements were made using the high accuracy coaxial cylinders technique developed by Schiefelbein and Sadoway (1997). The initial slag was a CaO-MgO-SiO_2 slag and then iron oxide was added to the slag in 5, 10, 15 and 20wt% increments. It was not clear from the paper at what oxidation state the work was carried out, however the conductivity cell was made from molybdenum (according to Schiefelbein and Sadoway (1997)). This suggests that the work may have been conducted at reducing conditions (given that molybdenum oxidises very readily at high temperature and therefore it is advisable to maintain the slag at reduced conditions).

The conductivity was measured at a range of temperatures at each iron oxide level, so the activation energy data could be calculated. The increase in the conductivity with increasing iron oxide content is clearly seen in Figure 20 for a temperature of 1450 °C. The activation energy also decreased with increasing iron oxide content. The authors explained the increase in the conductivity with iron oxide content by suggesting that the FeO_x donated both ionic and electronic charge carriers. Evidence for electronic conduction was suggested as a result of measurements of the electronic transference number which was found to increase with increasing iron content. The electronic transference number at the highest FeO_x content of 16 mol% was 0.3 at a temperature of 1425 °C.

Ducret *et al.* correlated the conductivity for the slags they measured as a function of the compositions. The correlation given for a temperature of 1425 °C was the following:

Equation 10: $\kappa_{1425} = -0.138 - 0.361.X_{SiO2} + 1.186.X_{FeO} + 0.917.(X_{FeO} + X_{MgO} + X_{CaO})$

The X denotes mole fractions. The first term containing X_{FeO} indicated the electronic contribution and the second term containing X_{FeO} indicated the ionic contribution of the iron

oxide. The iron oxide content range investigated by Ducret *et al.* was only up to ~16 mol% FeO_x and a linear correlation between conductivity and FeO_x content was found to be satisfactory. Based on the conductivities of higher iron oxide-containing melts, the linear correlation would not suffice at higher iron-oxide contents.

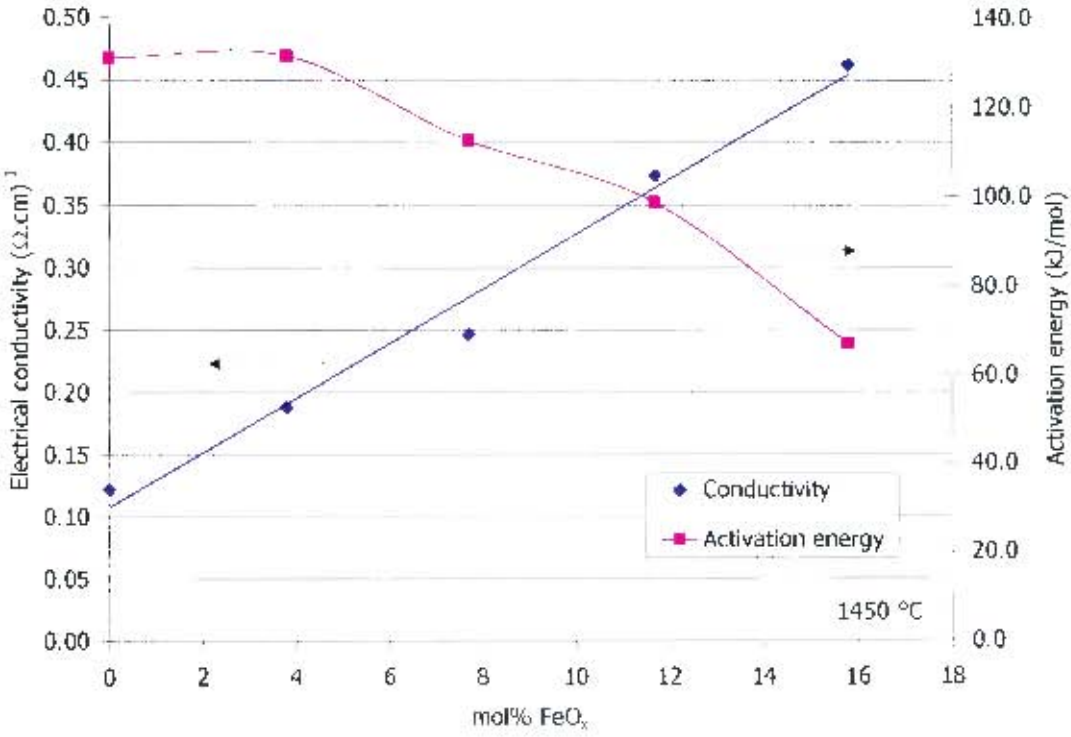

Figure 20: Electrical conductivity of CaO-MgO-SiO_2 slag with FeO_x added at 1450°C. Measurements by Ducret *et al.* (2002)

2.5.5. Higher order systems

The higher order system of interest is the system: Al_2O_3-CaO-FeO_x-MgO-SiO_2. There was a reasonable amount of data on this system, including oxidation state-dependent conductivity measurements by Fontana *et al.* (1984). The oxidation state work will be presented in section 2.7. The most comprehensive work on this system was that by Hejja *et al.* (1994). The data was also the most relevant to the investigation as slag compositions were fairly similar to the industrial melter type slags of the project sponsors. The authors performed experiments on slags within the following composition ranges (wt%): Al_2O_3: 5%, CaO: 13 – 19%, FeO_x: 13 - 27%, MgO: 13 – 19%, SiO_2: 40 – 46%. The authors studied the effects of changing the CaO content, the MgO content, the FeO_x content and the oxygen potential on the electrical conductivity as well as the liquidus temperature and viscosity.

The electrical conductivity values were in the range 0.17 to 0.30 $(\Omega.cm)^{-1}$. The general trends observed by the authors are qualitatively summarised in Table 2 below:

Table 2: Qualitative summary of the findings of Hejja *et al.* (1994) for the system Al_2O_3–CaO–FeO-MgO–SiO_2

Increase in	Electrical conductivity	Liquidus temperature	Viscosity
CaO	increases	decreases	decreases
MgO	increases	increases	decreases
CaO + MgO	increases	increases	decreases
FeO_x	increases	decreases	decreases
Ferric / ferrous ratio	increases	increases	increases

The qualitative findings are in line with the effects of the various components in simpler systems.

2.5.6. Chromium containing slag systems

There is relatively little literature concerning the effect of chromium on the electrical conductivity of slags. The major reason for this is that chromium containing slags tend to have very high liquidus temperatures, so carrying out electrical conductivity measurements involves experimental difficulties as a result of the high temperatures required. The most systematic and comprehensive study carried out on chromium containing slags was that by Liutikov and Tsylev (1963). The authors investigated the addition of chromium to Al_2O_3-MgO-SiO_2 slags which are of interest to ferrochrome producers. The authors had previously studied the Al_2O_3-MgO-SiO_2 system which was discussed in section 2.5.3.3.

Liutikov and Tsylev added from 0 to 12wt% Cr_2O_3 to slags with MgO/Al_2O_3 = 1 where SiO_2 was varied from 30 to 60 wt%. The electrical conductivity of the slags was measured at temperatures of 1800, 1700, 1600 and 1500 °C. The results were presented in the form of iso-electrical conductivity contours on pseudoternary diagrams. For ease of reference the diagrams were reproduced from the Slag Atlas (1995) and are shown in Figure 21.

The authors also studied additions of Cr_2O_3 to slags at 1800 °C with Al_2O_3/SiO_2 = 1 and MgO varied from 10 to 50wt% and to slags with MgO/SiO_2 = 1 and Al_2O_3 added from 10 to 50 wt%. The results for these compositions are also shown as iso-electrical conductivity contours on pseudoternary diagrams. These are shown in Figure 22.

The phase boundaries shown in the diagrams were estimated using MPE (see Zhang *et al.* (2002)) with a specified oxidation state of p_{CO2}/p_{CO} = 2. The oxidation state is important because the relative quantities of the divalent and trivalent chromium ions determine the stability of the spinel phase. The estimated phase boundary is believed to be reasonably accurate and thus the results have been interpreted in terms of the phase boundary.

The trends which can be seen in Figure 21 (a) to (d) are the following. The liquid region is very small at 1500 and 1600 °C but increases as the temperature is increased to 1700 and 1800 °C. The liquid region is larger at higher silica contents which is in agreement with the lower liquidus temperatures of compositions within the cordierite ($2MgO.2Al_2O_3.5SiO_2$) phase region. The addition of chromium in small amounts stabilises the spinel phase. Considering the diagrams at 1700 and 1800 °C, the electrical conductivity appears to increase with increasing Cr_2O_3 additions while the slag is still fully liquid. When spinel phase starts forming, the conductivity reaches a plateau and then decreases with further chromium addition and spinel formation.

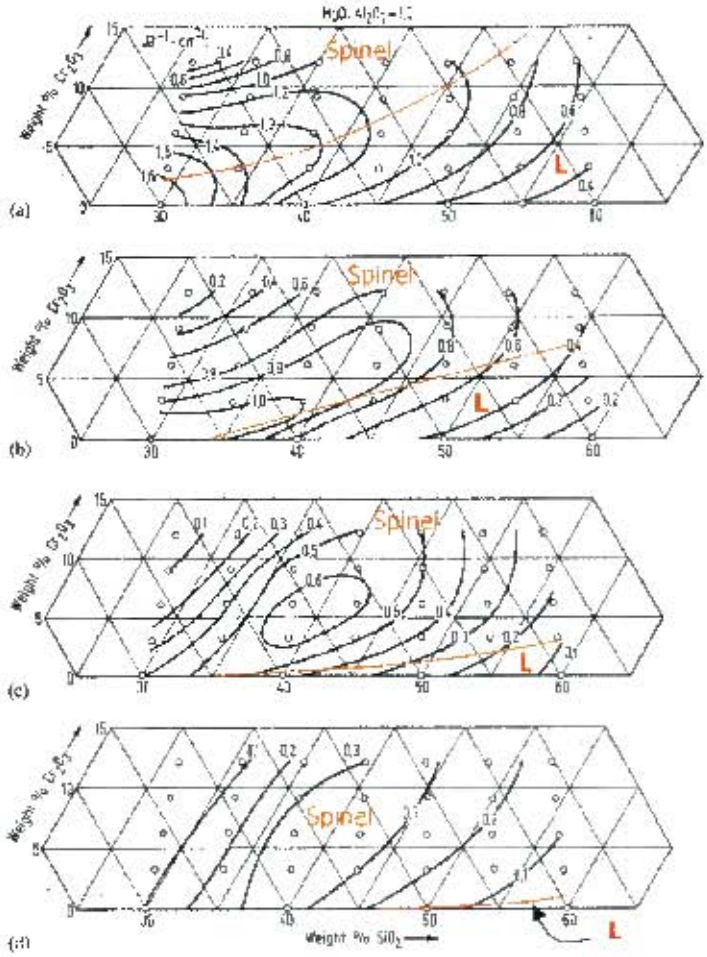

Figure 21: Iso-electrical conductivity contours of Al_2O_3-Cr_2O_3-MgO-SiO_2 system with MgO/Al_2O_3 = 1 at temperatures of (a) 1800°C, (b) 1700°C, (c) 1600°C and (d) 1500°C. Measurements and diagrams by Liutikov and Tsylev (1963), diagrams reproduced from Slag Atlas (1995). Phase boundary estimated using MPE (Zhang *et al.* (2002)) for oxidation state of p_{CO2}/p_{CO} = 2.

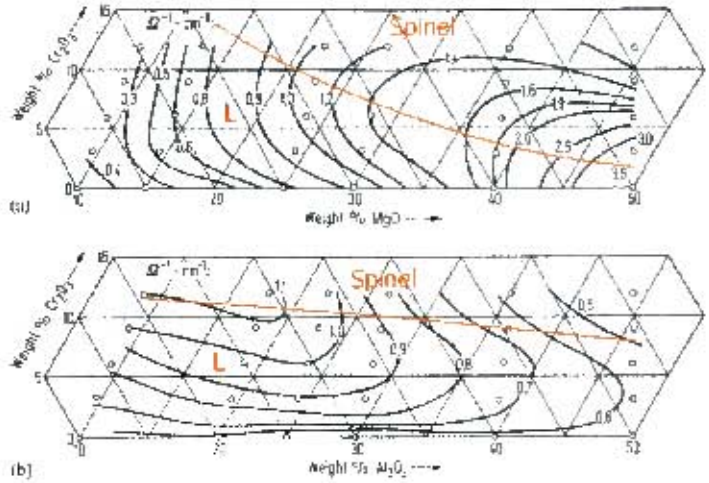

Figure 22: Iso-electrical conductivity contours of Al_2O_3-Cr_2O_3-MgO-SiO_2 system at 1800 °C with (a) Al_2O_3/SiO_2 = 1 and (b) MgO/SiO_2 = 1. Measurements and diagrams by Liutikov and Tsylev (1963), diagrams reproduced from Slag Atlas (1995). Phase boundary estimated using MPE (Zhang *et al.* (2002)) for oxidation state of p_{CO2}/p_{CO} = 2.

The trends apparent in Figure 22 (a) are the following. The addition of MgO causes the liquidus temperature and the electrical conductivity to increase. Below 40% MgO, the addition of Cr_2O_3 initially brings about a sharp increase in the conductivity and then the increase becomes more gradual. Once spinel phase starts forming the conductivity reaches a plateau and then starts decreasing. Above 40% MgO, the addition of Cr_2O_3 decreases the conductivity and spinel phase forms at very low chromium contents. The conductivity decreases with further chromium addition.

The trends apparent in Figure 22 (b) are the following. The addition of Al_2O_3 does not significantly change the estimated phase boundary or affect the electrical conductivity at 0% Cr_2O_3. The addition of Cr_2O_3 initially brings about a sharp increase in the conductivity and then the increase becomes more gradual. At higher alumina contents (>25%) the conductivity starts decreasing with further chromium additions. Once spinel phase starts forming the conductivity flattens and then starts decreasing.

Liutikov and Tsylev (1963) concluded that chromium was present as Cr^{2+} and Cr^{3+} ions and that the ratio between the ions depended on the distribution of the mineral phases. Therefore the authors suggested that where the composition was in the cordierite region (see chromium-free phase diagram), there was more divalent chromium. The Cr^{2+} ion was thought to behave similarly to MgO therefore bringing about an increase in the conductivity as a result of network modifying properties. Where the slag composition was in the spinel region, the trivalent chromium ion was more prevalent and brought about polymerisation of the slag by formation of complex compounds with Al_2O_3.

Rennie *et al.* (1972) investigated the addition of Cr_2O_3, Fe_2O_3 and CaO to Al_2O_3-MgO-SiO_2 slags with the following compositions (wt%): A: 24%Al_2O_3, 31%MgO, 43%SiO_2 and B: 33%Al_2O_3, 23%MgO, 44%SiO_2. The authors made measurements in platinum crucibles in air from 1500 to 1640°C and in molybdenum crucibles under argon up to 1800 °C. The addition of 7% Cr_2O_3 to slags A and B increased the liquidus temperatures to between 1700 and 1800 °C (estimated by Rennie *et al.*). The measurements in the Pt crucibles were below the liquidus temperatures for the chromium containing slags. Measurements were therefore obtained at higher temperatures in the molybdenum crucibles for slag A+7% Cr_2O_3 and slag A+6% Fe_2O_3+12%Cr_2O_3 (experimental difficulties were experienced for slags with the B composition due to reaction of Cr_2O_3 and Fe_2O_3 with the Mo crucibles and unstable resistance readings). The results, as calculated from the temperature dependence data given in the paper, are shown in Figure 23.

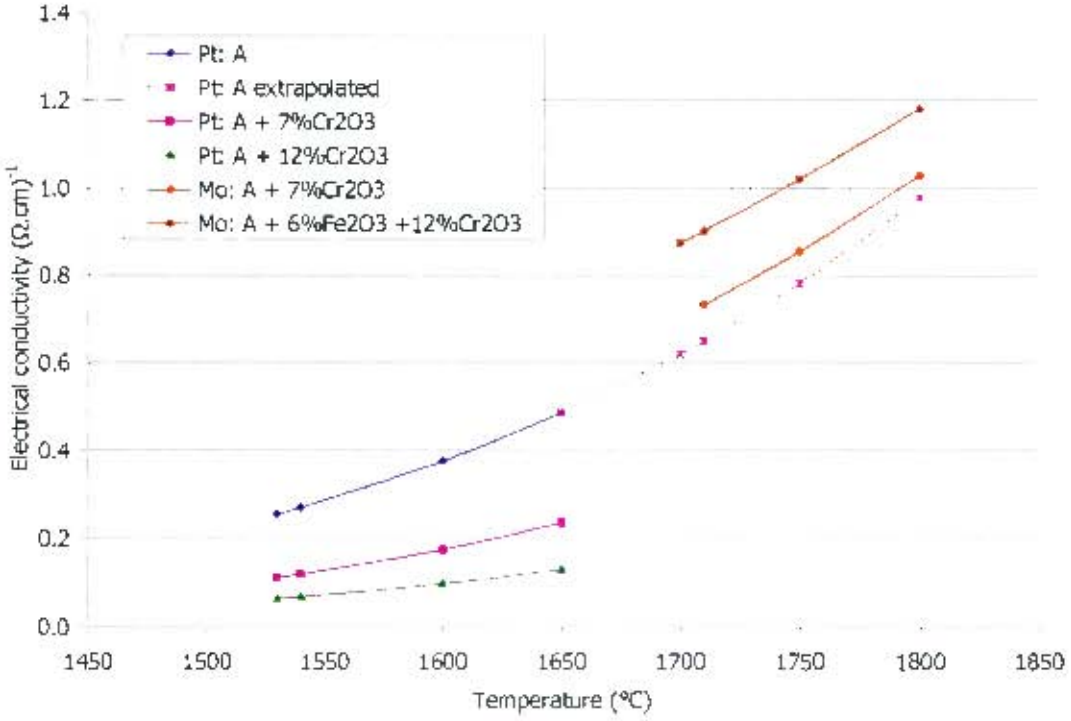

Figure 23: Electrical conductivity of Al_2O_3-MgO-SiO_2 slags with additions of Cr_2O_3 and Fe_2O_3 in Pt and Mo crucibles. Measurements by Rennie *et al.* (1972).

As can be seen in Figure 23 the electrical conductivities of the A+7%Cr_2O_3 and A+12%Cr_2O_3 slags in Pt crucibles were significantly lower than the conductivity of slag A. Rennie *et al.* reasoned that the primary phase for the chromium containing slags was MgO.$(Al,Cr)_2O_3$ therefore the formation of the phase reduced the number of cations available for conduction. These results agree with the findings of Liutikov and Tsylev.

Figure 23 also shows the measurements of the conductivities of the chromium containing slags in molybdenum crucibles. The conductivity for slag A (measured in Pt crucible) was extrapolated to the higher temperatures to allow for comparison. The electrical conductivities for slag A+7%Cr_2O_3 was slightly higher than for slag A, while the conductivity of A+6% Fe_2O_3+12%Cr_2O_3 was significantly higher than for slag A. Rennie *et al.* commented that the activation energies for slag A+7%Cr_2O_3 below (Pt) and above (Mo) its liquidus temperature were very different. The authors suggested that the reason for the differences between the measurements in the platinum and molybdenum crucibles was that the inert atmosphere in the Mo crucible experiments promoted the conversion of Cr^{3+} to Cr^{2+} (unlike in the Pt crucible experiments where air was used). Directly as a result of this, and indirectly, as chromite spinel was destabilised, more conducting cations would be available in the slag, therefore increasing the electrical conductivity. The other comment was that there was up to 1% Mo in the analysed slags which the authors suggested could also have increased the conductivity.

Downing and Urban (1966) also studied the effect of Cr_2O_3 on a slag containing 30%Al_2O_3, 20%CaO, 30%MgO and 20%SiO_2. The additions of both 5.5 and 15 wt% brought about decreases in the conductivity up to temperatures of 1700 °C. The liquidus temperatures for both slags were calculated using MPE (Zhang *et al.* (2002)) and found to be above 1800 °C even at reducing conditions.

Kato and Minowa (1969) studied the addition of up to 1.38mol% Cr_2O_3 to a base slag with the following composition (mole fractions): 0.084 Al_2O_3, 0.473 CaO, 0.443 SiO_2. It is not clear what gas atmosphere was used. The electrical conductivity was reported to increase from 0.5 to 1 $(\Omega.cm)^{-1}$ at 1500 °C with the addition of the 1.38mol% Cr_2O_3. The liquidus temperature of the slag exceeded 1800 °C (estimated using MPE (Zhang *et al.* (2002)) with the addition of the Cr_2O_3 as a result of the presence of spinel phase. The large increase in the conductivity was surprising given that the slag was below its liquidus temperature. However, given that no MgO or FeO was present in the slag, it was possible that the Cr_2O_3 was dissolved in the slag and increased the conductivity.

2.5.6.1 Summary of the effect of chromium

From the literature concerning the effect of chromium on the electrical conductivity of slags, the following conclusions can be drawn. The addition of chromium to slags quickly brings about formation of a spinel phase. The spinel phase has a very high melting temperature, therefore measurements on chromium containing slags need to be carried out at relatively high temperatures (up to 1800°C). This introduces experimental difficulties in terms of materials of construction for the conductivity cell and the low resistances at the high temperatures.

The data of Liutikov and Tsylev (1963), Rennie *et al.* (1972) and Downing and Urban (1966) suggested that where chromium was added to slags below their liquidus temperatures, the chromium would bring about the formation of spinel phase and lock up conducting cations. Therefore the conductivity of the slags would decrease. Above the liquidus temperature, the conducting cations would be released from the spinel phase and increase the conductivity.

In other words, dissolved Cr_2O_3 in $MgO-Al_2O_3-SiO_2$ melts tends to increase the conductivity, but below the liquidus temperature, the formation of chromite solids leads to a decrease in the conductivity. Co-addition of 6% Fe_2O_3 and 12% Cr_2O_3 to a slag above 1700 °C appeared to increase the conductivity of the slag. However, the effect of Cr in iron oxide – containing slags, particularly at higher levels of FeO_x, is not known.

It is likely that the oxidation state of the slag will play an important role in chromium containing slags. The reason for this follows from Liutikov and Tsylev's suggestions that Cr^{2+} is likely to be a network modifier while Cr^{3+} is a network former. Therefore the former will increase the electrical conductivity, while the latter will polymerise the slag and decrease the conductivity.

2.5.7. Systems containing other transition metals – MnO and TiO_2

2.5.7.1 MnO

For systems containing manganese, Segers *et al.* (1978, 1983) systematically studied the conductivities of the systems $CaO-MnO-SiO_2$, then $CaO-MgO-MnO-SiO_2$ and then $Al_2O_3-CaO-MgO-MnO-SiO_2$. Other conductivity measurements were provided by Woollacott *et al.* (1974) for the system $Al_2O_3-CaO-MgO-MnO-SiO_2$ with 10mol% Al_2O_3. Min'ko and Nevedomskii (1991) studied the electrical conductivities of three industrial furnace slags containing around 17wt% MnO.

The electrical conductivity data at 1500 °C of the above authors has been presented as a function of the mol% MnO content in Figure 24. The most obvious trend that can be seen is that the electrical conductivity increases dramatically with increasing Mn content above 50 mol%. Also the electrical conductivities of slags containing MnO are higher than those not containing transition metals (compare with Figure 17 for the Al_2O_3–CaO–MgO–SiO_2 system where the maximum conductivity at 1550 °C for a high basicity slag is ~0.45 $(\Omega.cm)^{-1}$). Woollacott *et al.* (1974) suggested that there was a possibility of electronic conduction between Mn^{2+} and Mn^{3+} ions.

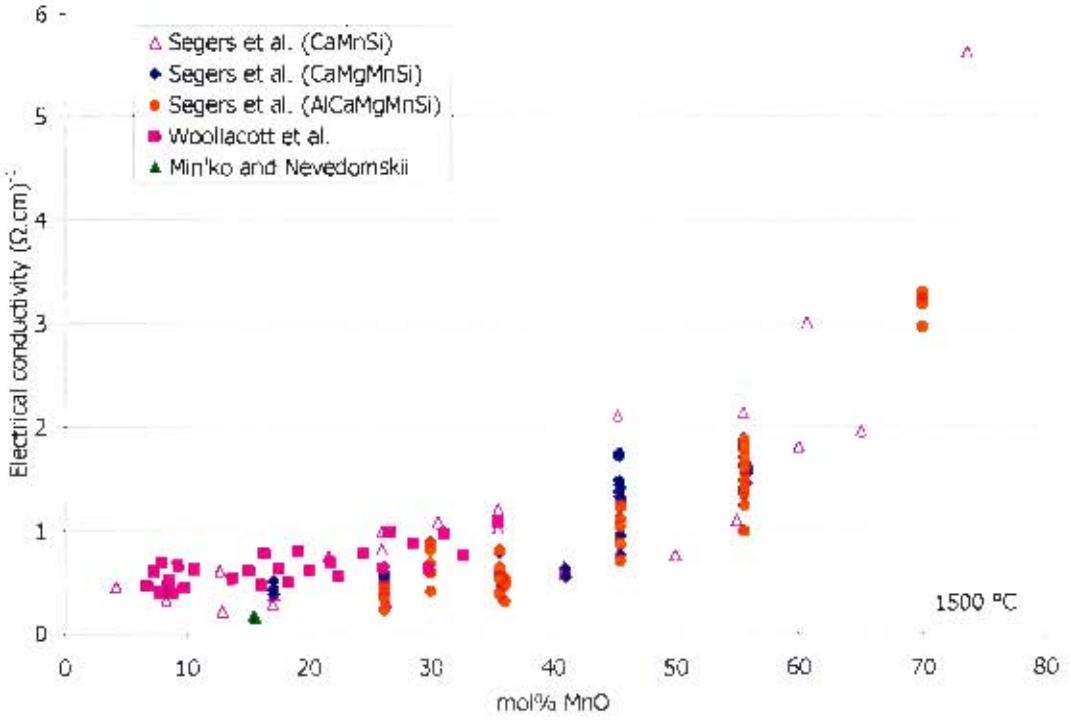

Figure 24: Electrical conductivity of manganese containing slags at 1500 °C. Measurements by Segers *et al.* (1978, 1983), Woollacott *et al.* (1974) and Min'ko and Nevedomskii (1991).

The variations in conductivity at constant MnO content are due to differing slag chemistries. At constant MnO contents, substitution of network modifying cations (CaO and MgO) for network forming ions (Al_2O_3 and SiO_2) resulted in an increase in the conductivity. The simplest system where this effect can be seen is the CaO-MnO-SiO_2 system studied by Segers *et al.* (1978). CaO was substituted for MnO at constant silica contents. The results are shown in Figure 25 for conductivities at 1500 °C. As the plot suggests, at any given Mn/Ca ratio, increasing SiO_2 always results in a decrease in the conductivity.

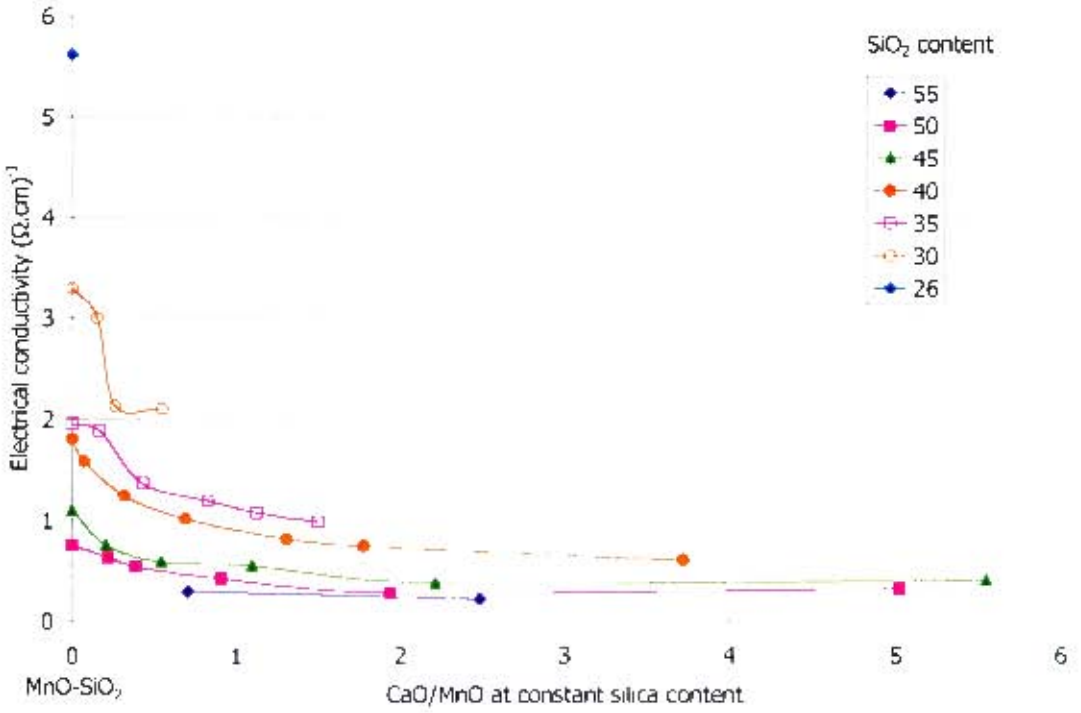

Figure 25: Electrical conductivity of CaO-MnO-SiO_2 slags at 1500 °C. Measurements by Segers *et al.* (1978). Compositions based on molar percentages and ratios.

Segers *et al.* (1983) compared the effects of MgO and CaO on the electrical conductivity at constant MnO and SiO_2 contents and concluded that where the molar ratio MgO/(MgO+CaO) was greater than 0.25, the effects of MgO and CaO were very similar. Slight differences were observed where the ratio was less than 0.25. The other comment was that at a constant SiO_2 content of 35 mol%, the influence of MgO was complex.

Of interest in the Al_2O_3–CaO–MgO–MnO–SiO_2 system is that replacing SiO_2 with Al_2O_3 results in a decrease in the electrical conductivity. Segers *et al.* (1983) suggested that the melt became more polymerised with the alumina than the silica as a result of the formation of a silica free anionic network of alumina. This occurred where the molar ratio $Al_2O_3/(Al_2O_3 + SiO_2)$ was greater than 0.5. This may also be due to the formation of solid phases such as mullite ($Al_2O_3.SiO_2$).

In comparison to slags containing iron, manganese containing slags have much lower conductivities. It is still considered that part of the conduction is due to the electronic mechanism. MnO is an oxide of the 3d transition metals (as is FeO_x) and also has semi-conducting properties. The reason that the electronic contribution is much smaller is that the Mn^{2+} ion is far more stable than the higher valence ions of manganese, whereas in the case of iron, the oxidation of ferrous to ferric ions is much easier.

2.5.7.2TiO_2

Desrosiers *et al.* (1980) measured electrical conductivities of industrial slags with high titania content. The authors examined various grades of ilmenite ($FeO.TiO_2$) smelting slags containing up to 5wt% each of Al_2O_3 and MgO. Van der Colf and Howat (1979) conducted measurements on a limited range of slag compositions in the system Al_2O_3–CaO–MgO–SiO_2–

TiO_2. A slag containing 24 mol% TiO_2 was found to have electrical conductivities of $\kappa \approx 1.2 - 3.0$ $(\Omega.cm)^{-1}$ over a temperature range of 1400 – 1600 °C. The results of the authors mentioned are shown in Figure 26 below.

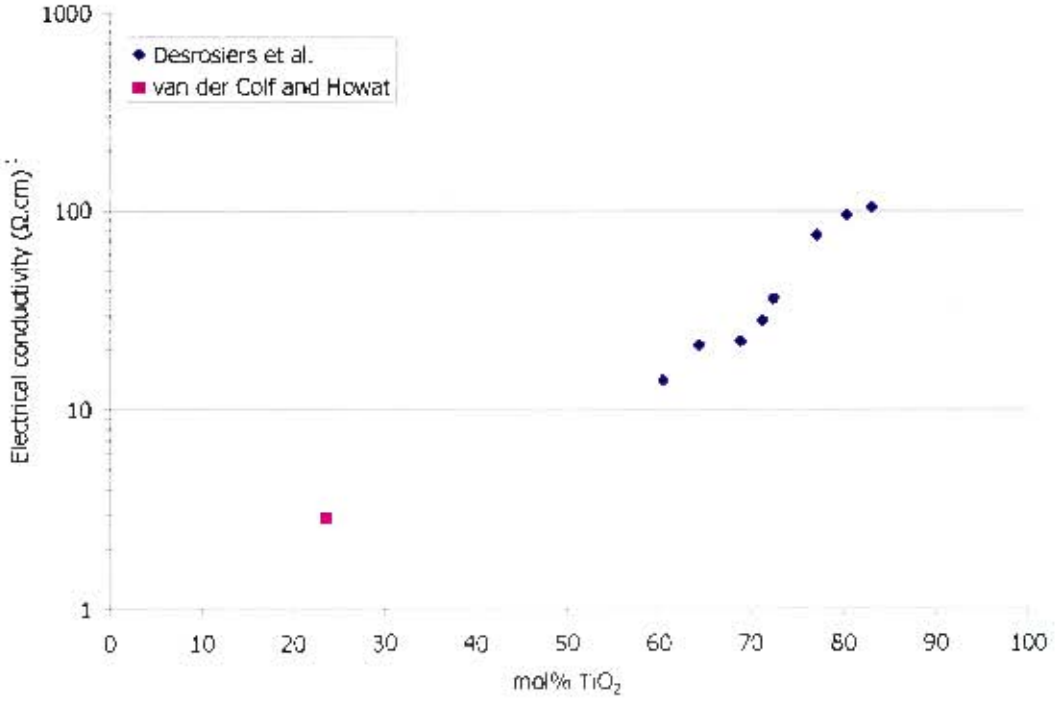

Figure 26: Electrical conductivity vs mol % TiO_2 at 1600 °C. Measurements by Desrosiers *et al.* (1980) on primarily FeO_x-TiO_2 slags with ~5% each of Al_2O_3 and MgO. Measurements by van der Colf and Howat (1979) on Al_2O_3-CaO-MgO-SiO_2-TiO_2 slags.

It is evident from Figure 26 that TiO_2 containing slags exhibit very high electrical conductivities. The behaviour of titania appears to be similar to that of FeO_x and it was considered by Desrosiers *et al.* (1980) that semiconduction occurred between Ti^{3+} and Ti^{4+} ions by a hopping mechanism. Desrosiers *et al.* provided a comparison between their work and previous work carried out on titanium-containing slags. The comparison is shown in Figure 27.

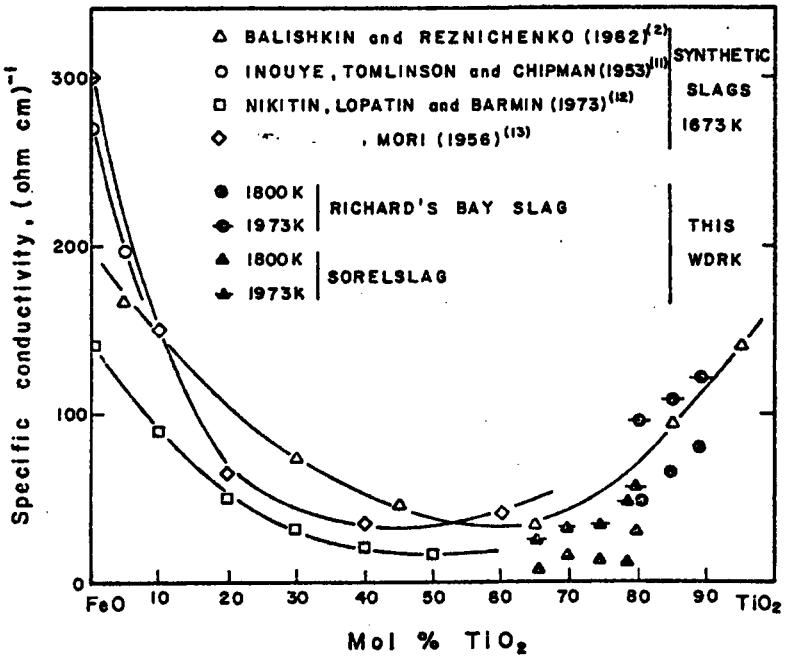

Figure 27: Electrical conductivity of FeO_x-TiO_2 slags after Desrosiers *et al.* (1980)

From Figure 27 it is evident that the electrical conductivity of iron and titania-containing slags is very high. Addition of titania to iron oxide melts reduces the conductivity up to approximately 60mol% TiO_2. Thereafter the conductivity increases with further titania addition.

Sommerville and Bell (1980) provided a good review of the electrical (and other) properties of slags containing TiO_2. Similar conclusions regarding the conductivity of titania containing slags were obtained.

2.6. Effect of slag chemistry / basicity

It should be apparent from the literature data presented in the previous section 2.5 that the slag chemistry plays a very important role in determining the electrical conductivity. The classification of metal oxides in terms of their ion-oxygen attractions gives a useful way of explaining their properties. The transition metals pose more complex relationships owing to their presence in different valencies.

Several authors have tried to relate the slag composition and the electrical conductivity in terms of a basicity ratio or function of the composition. Sarkar (1989), who investigated high alumina blast furnace slags, found a linear relationship between an empirical basicity ratio and the conductivity for the range of compositions tested. Winterhager *et al.* (1966) related the composition to the conductivity in terms of the ratio of the partial ion-oxygen attractions for the network modifying cations to the network forming cations.

Mills (1993) attempted to relate various physicochemical properties as functions of the optical basicity and the NBO/T ratio. (Briefly, the NBO/T ratio refers to the ratio of number of non-bridging oxygen ions to the number of tetrahedrally co-ordinated atoms (see Mills (1993) for exact definition and calculation)). In the case of electrical conductivity, it was concluded that the

degree of depolymerisation was the primary factor governing the conductivity. Melts containing FeO_x and TiO_x were not considered.

The two different mechanisms for conduction present complications in representing data in terms of a basicity ratio e.g. FeO is less basic than CaO yet because of electronic conduction, addition of FeO gives rise to much higher electrical conductivities. In order to deal with this situation, melts containing no transition metals will be represented by means of a basicity ratio or optical basicity. For melts containing transition metals, one needs to take into account the amount of transition metal present, the basicity and the state of oxidation.

2.7. Effect of slag oxidation state

The significant work that has been carried out on the effect of oxidation state on the slag conductivity in iron-containing slags is that of Pastukhov *et al.* (1966), Engell and Vygen (1968) and Fontana *et al.* (1984). The three studies found that the conductivity varied with the oxidation state as a result of the changing amounts of ferric and ferrous ions in the slag. Measurements by Fontana *et al.* (1984) were made at reduced conditions. The measurements by Engell and Vygen (1968) and Pastukhov *et al.* (1966) were made over a range of reduced and oxidised conditions. Gudenau and Petry (1981) reported results for the effect of oxidation state on the conductivity of a $CaO\text{-}FeO_x\text{-}SiO_2$ slag. Hejja *et al.* (1994) also presented some oxidation state dependent conductivity results for the system $Al_2O_3\text{-}CaO\text{-}FeO_x\text{-}MgO\text{-}SiO_2$.

As mentioned in section 2.3, it was also considered worthwhile examining the literature concerning the oxidation state dependence of some of the solid state systems. The simplest system (pure FeO_x) will be considered first. Thereafter the effects of other slag chemistries will be covered.

2.7.1. FeO_x

Experiments were conducted by Pastukhov *et al.* (1966) on the variation in the electrical conductivity at 1470 °C of pure liquid wüstite with oxidation state. Gartstein and Mason (1982) analysed the conductivity data of Hillegas (as cited by Gartstein and Mason) for the solid wüstite phase. The results are shown in Figure 28. From the graph it is clear that as the oxidation state increased, the electrical conductivity of liquid and solid wüstite increased.

Hillegas had also measured the thermoelectric coefficient for solid wüstite. Gartstein and Mason analysed this data in terms of the small polaron hopping conduction mechanism (see section 2.3.2 and Equation 4). From this they were able to calculate the distribution of the conducting cations (c_+ and c_-). The increase in the oxidation state brought an increase in the c_+ / c_- ratio and the conductivity increased. The conduction in solid wüstite was well described by the small polaron mechanism.

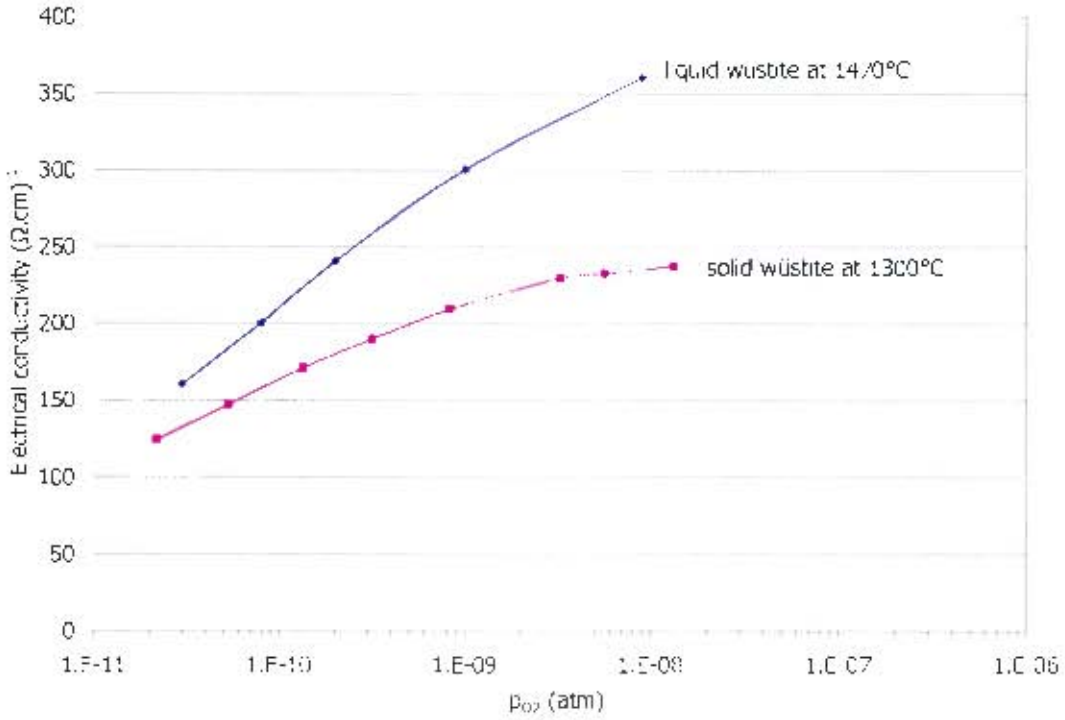

Figure 28: Electrical conductivity of pure solid and liquid wüstite at 1300 and 1470°C respectively at a range of oxygen partial pressures. Measurements on liquid wüstite by Pastukhov *et al.* (1966), data on solid wüstite from Gartstein and Mason (1982) who analysed the data of Hillegas (as cited in Gartstein and Mason).

Similar measurements of the conductivity and thermoelectric coefficient have been carried out for solid magnetite by many authors including Nell and Wood (1991) and Mason and Bowen (1981b). The oxidation state dependent data of Mason and Bowen (1981b) is shown below:

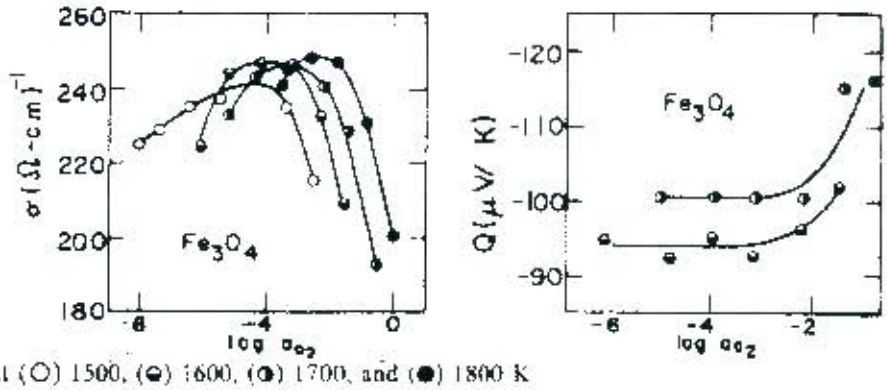

at (○) 1500, (◒) 1600, (◑) 1700, and (●) 1800 K

Figure 29: Oxidation state dependence of electrical conductivity (σ) and thermoelectric coefficient (Q) of magnetite at indicated temperatures, after Mason and Bowen (1981b)

From Figure 29 it is evident that the conductivity and thermoelectric coefficient of magnetite were both dependent on the oxygen partial pressure. Wu and Mason (1981) showed for magnetite that the cation distribution (c_1 and c_2) could be calculated from the thermoelectric coefficient and that the electrical conductivity could be calculated with knowledge of the cation distribution. As for solid wüstite, the conduction mechanism was considered to be

small polaron hopping conduction, however in wüstite the conduction was p-type and in magnetite it was n-type.

Solid state conduction will not be investigated further as the conduction mechanisms in slags are of more interest in this investigation. However, Gleitzer (1997) gives an excellent review of the electrical properties of iron oxides and there are many studies into the conductivity and conduction mechanisms in spinels and other solid phases.

2.7.2. FeO_x-SiO_2

Pastukhov *et al.* (1966) and Fontana *et al.* (1984) carried out measurements on the electrical conductivity of iron silicate slags with varying oxygen partial pressures. The results that were obtained are shown in Figure 30.

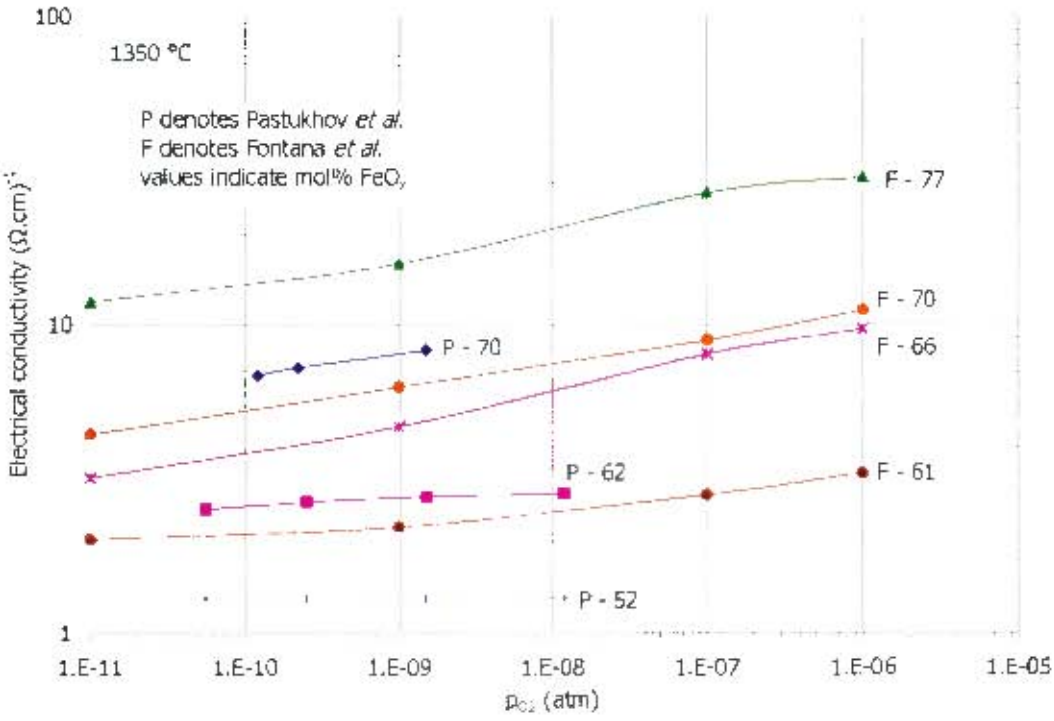

Figure 30: Variation in electrical conductivity at varying oxidation states at 1350 °C for the system FeO_x-SiO_2. Measurements by Pastukhov *et al.* (1966) and Fontana *et al.* (1984)

From Figure 30 it is clear that the electrical conductivity of iron silicate slags increased with increasing oxidation state with the exception of the slag containing 52mol% FeO_x (it is possible that at the reduced conditions slag P-52 is below its liquidus temperature, however, the data were included for illustration that the slag conductivity did not vary with oxidation state). The increase in the oxidation state will convert some of the ferrous ions to ferric ions and provide more sites for electron / hole exchange.

It is of interest to compare the FeO_x-SiO_2 data provided in Figure 1 and the data in Figure 30 above. It appears that where the majority of the conductivity is ionic (FeO_x < 60 mol%), there is no variation of the conductivity with the oxidation state. When electronic contribution becomes significant (FeO_x > 60 mol%), an increase in the oxygen partial pressure brings about an increase in the overall conductivity.

At higher oxygen partial pressures it was likely that magnetite would form at the temperatures at which the work was carried out. The data presented in Figure 30 was also presented in Figure 4 to show the comparison between the oxidation state dependent data and that of other authors where measurements were made at iron saturation.

2.7.3. $CaO\text{-}FeO_x\text{-}SiO_2$

Engell and Vygen (1968) carried out work on this system at 1600 °C. Fontana *et al.* (1984) carried out experiments on two slags of this composition at 1350 °C. Gudenau and Petry (1981) carried out work on one slag at 1400 °C.

Engell and Vygen studied a slag with a molar CaO/SiO_2 ratio of 0.79. They added FeO_x to the slag and measured the oxidation state dependence of the slag conductivity. The authors also measured the quantities of ferric and ferrous iron in the slag for given oxygen partial pressures and presented their results as a function of the ferric / total iron ratio. The results of Engell and Vygen are shown in Figure 31.

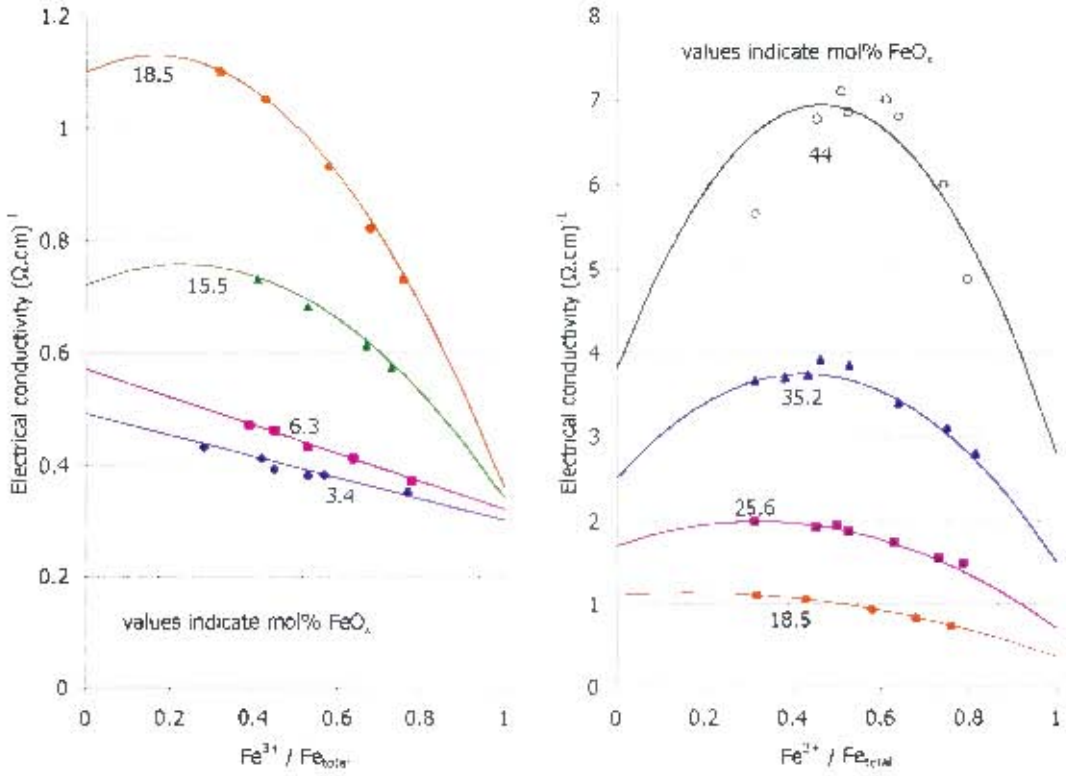

Figure 31: Oxidation state dependence of electrical conductivity of $CaO\text{-}FeO_x\text{-}SiO_2$ slags at 1600 °C with molar CaO/SiO_2 ratio of 0.79 and addition of FeO_x. Measurements by Engell and Vygen (1968).

It should be noted that the trend lines shown in Figure 31 were fitted by the authors and the fitting parameters were interpreted in terms of the proposed conduction mechanisms. (The modelling of the data will be discussed in more detail in Section 2.8). From Figure 31 the following was evident:

The electrical conductivity increased greatly with increasing iron content. At low iron contents, the conductivity did not vary much with oxidation state. The fitted parameters

indicated that only ionic conduction took place with iron contents of 3.4 and 6.3 mol%. At iron contents of 15.5 mol% and above the conductivity varied significantly with changing oxidation state. The conduction mechanism at the extremes (Fe^{3+}/Fe_{total} = 0 and 1) was considered to be exclusively ionic. Between the extremes the conductivity was the sum of the ionic and electronic contributions. A peak in the conductivity was obtained at varying oxidation state depending on the total iron content. The electronic contribution for the higher iron-containing slags was greatest at around Fe^{3+}/Fe_{total} = 0.5 where there would be the most number of sites for electron exchange. Engell and Vygen (1968) suggested that the tetrahedral co-ordination of ferric ions at higher ferric fractions resulted in decreased mobility of these cations as they form part of the silicate network. Therefore lower conductivities were observed at more oxidised conditions than at reduced conditions (where the ferrous ions are octahedrally co-ordinated and more mobile).

Fontana *et al.* (1984) carried out two experiments on $CaO-FeO_x-SiO_2$ slags at 1350°C. The results are shown in Figure 32 together with one of the measurements on an iron silicate slag with 60 mol% FeO_x.

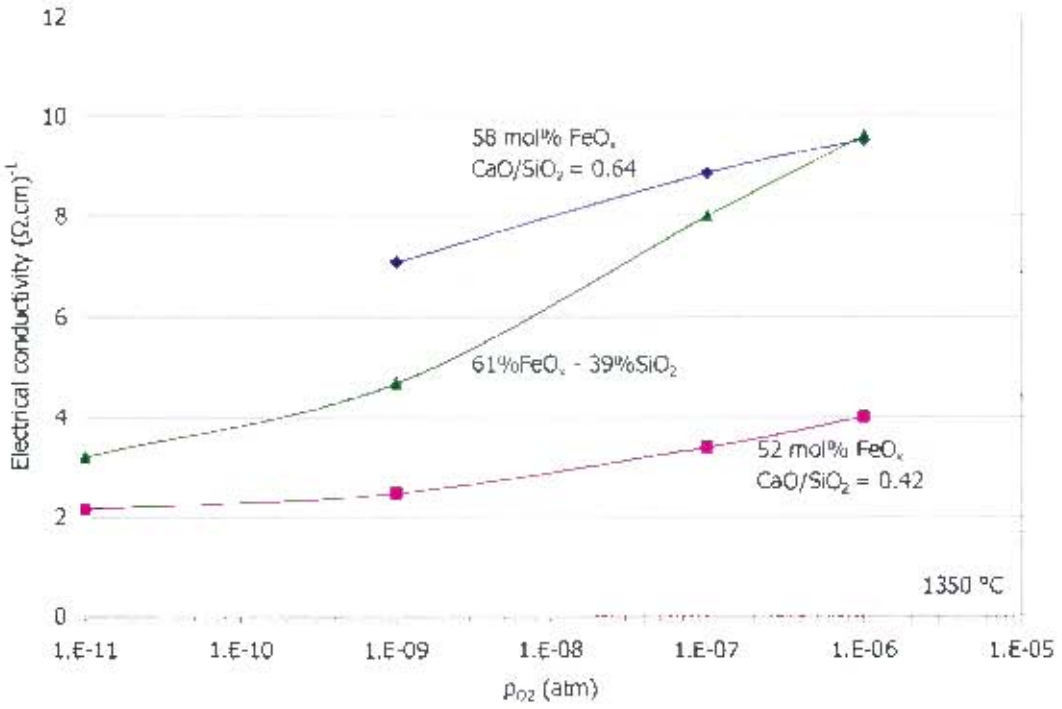

Figure 32: Oxidation state dependence of electrical conductivity of $CaO-FeO_x-SiO_2$ slags at 1350°C, iron oxide contents and molar CaO/SiO_2 ratios as indicated. Measurements by Fontana *et al.* (1984), iron silicate slag conductivity given for comparison.

The measurements presented in Figure 32 once again show the trends that the electrical conductivity increases with increasing iron oxide content and increasing oxidation state (up to $p_{O2} = 10^{-6}$ atm). Unfortunately the conductivity was not measured at more oxidising conditions but it would be expected that the conductivity would reach a maximum and then start decreasing. The results for an iron silicate slag measured by the authors have also been presented to show that the slag chemistry (basicity) plays a role in determining both the magnitude of the electrical conductivity and the response to oxidation state.

Gudenau and Petry investigated the oxidation state dependence of the conductivity of a slag containing 20wt% FeO_x with a CaO/SiO_2 ratio of 0.7. Their data are presented in Figure 33. The oxidation state was expressed in terms of the ferric/total iron ratio. It can be seen in the figure that the electrical conductivity increased as the slag became more reduced. The trend is in agreement with that of Engell and Vygen for lower iron containing slags. (16.9 mol% FeO_x in Gudenau and Petry's slag compared with 15.5 and 18.5 mol% FeO_x in Engell and Vygen slags)

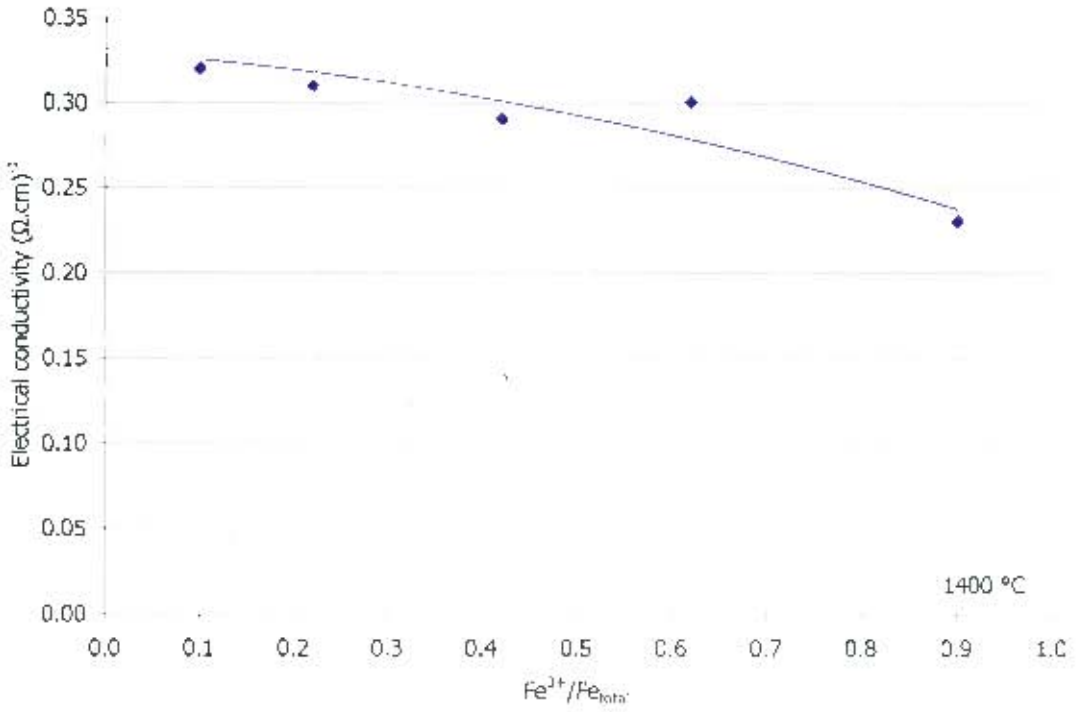

Figure 33: Electrical conductivity of $CaO-FeO_x-SiO_2$ slag at 1400°C where oxidation state was varied, FeO_x = 20wt% and CaO/SiO_2 ratio = 0.7. Measurements by Gudenau and Petry (1981)

2.7.4. Al_2O_3-CaO-FeO_x-SiO_2

Pastukhov *et al.* (1966) measured the oxidation state dependence of the conductivities of slags in the 20%Al_2O_3–40%CaO–40SiO_2 system where iron was added. In slags with iron oxide contents of 0.6 and 7.5mol% no change in conductivity was observed as the p_{O_2} changed. Where the Fe content was 13.9mol% and above, the electrical conductivity was affected when the p_{O_2} was changed. There was a maximum in the conductivity at $p_{O_2} = 10^{-7}$ atm and then the conductivity dropped as the oxygen partial pressure was increased further. The results are shown in Figure 34. It should be noted that electronic conduction becomes significant at much lower FeO_x levels (15 – 20%) in the quaternary system than in the binary FeO_x-SiO_2 system. It is likely that this is brought about by the presence of CaO. As seen in Figure 12, the addition of CaO to the FeO_x-SiO_2 system brought about an increase in the electronic contribution at lower total FeO values. CaO promotes a higher Fe^{3+}/Fe^{2+} ratio which enhances the electronic mechanism.

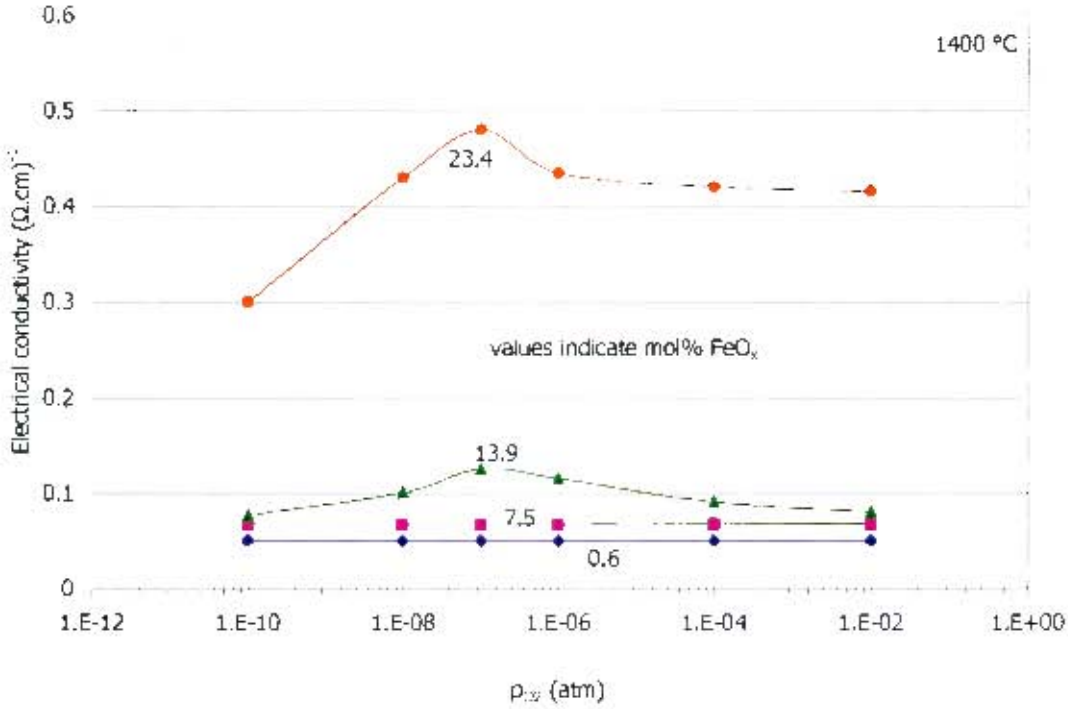

Figure 34: Oxidation state dependence of electrical conductivity of Al_2O_3–CaO-FeO_x-SiO_2 slags at 1400 °C with increasing iron oxide content. Measurements by Pastukhov *et al.* (1966).

The reasons given for the shape of the curve were:

An increase in the oxygen partial pressures from 10^{-10} to 10^{-7} atm brings about higher conductivity as a result of an increase in the ferric / ferrous ratio and therefore increased p-type semiconduction (electronic contribution). The sharp decrease from $p_{O2} > 10^{-8}$ to 10^{-6} atm is a result of Fe_2O_3 being formed. The conductivity then remains fairly constant as p_{O2} increases from 10^{-6} to 10^{-2} atm as Fe_2O_3 is stable at these partial pressures.

2.7.5. Al_2O_3-CaO-FeO_x-MgO-SiO_2

Measurements of the oxidation state dependence of the conductivity of slags in this system were made by Hejja *et al.* (1994) and Fontana *et al.* (1984). The data obtained by Hejja *et al.* for a slag with 15.4wt% total iron showed that the conductivity increased slightly going from oxidising to reducing conditions. (A similar trend to that presented by Gudenau and Petry in Figure 33 was obtained).

Fontana *et al.* studied slags with low iron contents with varying basicities (expressed as (CaO+MgO)/(Al_2O_3+SiO_2) ratios). Their data is shown in Figure 35. The following trends could be seen. The electrical conductivity increased with increasing total iron content. The conductivity of the slag with 30 mol% FeO_x and a basicity ratio of 0.76 increased with increasing p_{O2}. The conductivities of the slags with lower iron contents increased from $p_{O2} = 10^{-11}$ to 10^{-7} atm and then decreased from $p_{O2} = 10^{-7}$ to 10^{-6} atm. This trend agreed with the trend shown by Pastukhov *et al.* in Figure 34. The authors mentioned that electronic conduction was likely to take place in iron containing slags and therefore the conductivity would vary with oxidation state.

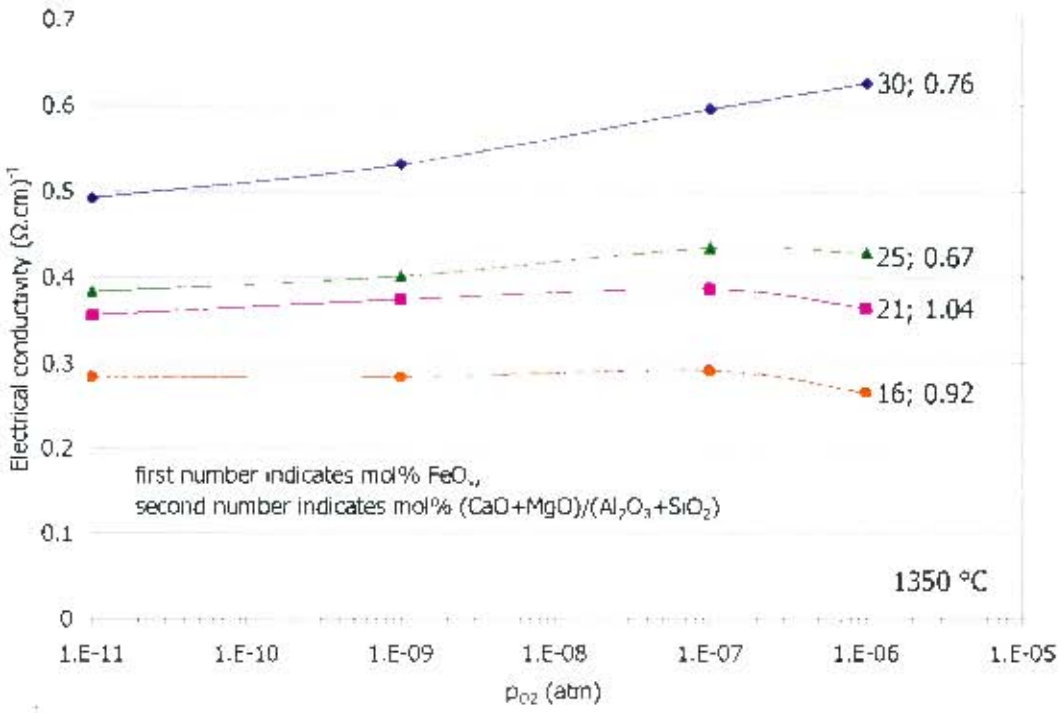

Figure 35: Oxidation state dependence of electrical conductivities of Al_2O_3-CaO-FeO_x-MgO-SiO_2 slags at 1350 °C with varying chemistries and iron oxide contents. Measurements by Fontana *et al.* (1984)

2.7.6. Summary of findings about the oxidation state dependence of electrical conductivity of iron containing slags

From the review of the literature data the following was evident:

The electronic conduction mechanism operates in slags containing iron, but the fraction of electronic conduction is a function of the total iron content and the basicity of the slag. At low iron content (<15mol%), there is very little, if any, electronic conduction. At higher iron contents (greater than approximately 15mol% and depending on slag chemistry), electronic conduction becomes important. The oxidation state of the slag determines the amounts of ferric and ferrous ions in the slag and therefore the amount of electronic conduction.

It is expected that the electrical conductivity will be greater at reduced conditions than at oxidised conditions owing to the greater mobilities of ferrous ions in comparison to ferric ions. This is as a result of the ferric ions being tetrahedrally co-ordinated at oxidised conditions and forming part of the silicate network (and hence restricting their mobilities).

The conductivity reaches a maximum at an intermediate oxidation state. This is likely to be where the most number of sites for electronic conduction occur i.e. equal quantities of ferric and ferrous ions.

2.8. Mathematical models for electrical conductivity

It is clear that the overall electrical conductivity of a slag containing iron oxide (or other transition metal) comprises contributions from the electronic and ionic mechanisms. In slags not containing transition metals, only ionic conduction will occur. As there is a change in ionic contribution in iron containing slags with variation in oxidation state, the mechanisms need to be considered together.

2.8.1. Ionic conduction – transition metal free slags

As mentioned in Section 2.3.1 the ionic conduction mechanism can be represented by the following equation:

Equation 1: $\kappa = F\sum z_i c_i u_i$

Therefore if one has measured the density of the slag and measured the mobility of each of the conducting cations, then the total conductivity can be calculated. The density is required to calculate the partial concentration of each species in the slag. Measuring the mobilities of the conducting cations is not simple. The mobility can be calculated from the self or tracer diffusion coefficients for the cations from the following equation (which follows from the Nernst-Einstein equation, see Equation 2):

Equation 11: $u_i = \frac{z_i F D_i}{RT}$

Goto *et al.* (1977) compared measured tracer diffusion coefficients with the diffusion coefficients calculated from the electrical conductivity using the Nernst-Einstein equation. Assuming a transference number of one for the conducting cations, the calculated D values were lower than the measured D values. The authors proposed that neglecting the interactions between the conducting cations and the rest of the components in the slag led to the lower calculated D values.

From the above discussion, it is evident that modelling the conductivity on this basis is difficult as the self or tracer diffusion coefficient for each component in the slag is required. Also the relationship between the partial conductivity and the diffusion coefficient appears to be more complex.

The correlation of Winterhager *et al.* (1966) appeared to give good representation of their data and was also not entirely empirical given the inclusion of the ion-oxygen attraction values (I). The expression for the conductivity was related to a function of the ratio of the partial ion-oxygen attractions for the network modifying cations to the network forming cations. It is summarised below:

Equation 12: $\kappa_{ZI} = \frac{\sum I_{\text{network modifier}} . at\%_{\text{network modifier}}}{\sum I_{\text{network former}} . at\%_{\text{network former}}}$

The empirical basicity ratio given by Sarkar (1989) was similar in principle to that of Winterhager *et al.*

2.8.2. Mixed ionic and electronic conduction – transition metal containing slags, oxidation state neglected in model

2.8.2.1 Jiao and Themelis

Jiao and Themelis (1988) developed empirical correlations between slag conductivity and composition and temperature. The slags were classified into ferrous and non-ferrous smelting slags. For ferrous smelting slags the data considered were those of Segers *et al.* (1983) for manganese containing slags. The following correlation was given for slags at 1500 °C:

Equation 13: $\kappa_{1500} = -3.34 + 6.41X_{CaO} + 6.75X_{MgO} + 8.06X_{MnO}$

The correlation was deemed valid for compositions in the following mole fraction ranges:

SiO_2: 0.35 – 0.50 CaO: 0 – 0.47 MnO: 0.08 – 0.56 MgO: 0 – 0.20

A correlation of similar form was given for the activation energy for conduction also based on the data of Segers *et al.*. Note that the relationship between the conductivity and the composition is linear.

For non-ferrous smelting slags at 1400 and 1500 °C, the following correlations were given:

Equation 14: $\ln \kappa_{1400} = -5.21 + 9.92X_{FeO} + 5.94(X_{CaO} + X_{MgO})$

Equation 15: $\ln \kappa_{1500} = -4.45 + 9.15X_{FeO} + 5.34(X_{CaO} + X_{MgO})$

The correlation was for slags with compositions in the following mole fraction ranges:

SiO_2: 0.17 – 0.49 CaO: 0 – 0.47 FeO: 0.11 – 0.83 MgO: 0 – 0.25

Al_2O_3: 0 – 0.03

It should be noted that the data considered in the development of this correlation were those of Inouye *et al.* (1953), Wejnarth (1934a), Victorovich *et al.* (1984), Fontana *et al.* (1984) and Hejja (as cited by Jiao and Themelis (1988)). The relation between the conductivity and the composition is exponential. The silica and alumina contents were neglected as their contribution to the conductance was assumed to be negligible. Mention was made of the effect of the oxidation potential on the conductivity for slags containing FeO_x. The authors found that conductivity values predicted by the correlation were within 20% of the measured values used to develop the correlation.

2.8.2.2 Hoster and Pötschke

Hoster and Pötschke (1983) also provided an empirical correlation between the conductivity and slag composition and temperature for the slags that they studied. Given that they studied CaO-SiO_2 slags with additions of either Al_2O_3 or FeO_x, the correlation given in their paper accounted for the conductivity of both iron free and iron containing slags. The authors had also made some measurements on MgO containing slags and maintained that effect of MgO was very similar to that of CaO. This explains the MgO term which appears in the basicity ratio. The correlation and the conditions under which it applies are shown below:

For slags where $CaO/SiO_2 \leq 0.6$, the conductivity is given by Equation 16 in the temperature range 1450 to 1650 °C

Equation 16: $\kappa = (0.0108.\ln T - 0.074).\%FeO + (0.025.\%FeO + 0.0035.T - 4.915).B^{2.3488}$

where $B = (\%CaO + \%MgO)/(\%SiO_2 + 0.11\%Al_2O_3)$

For slags where $CaO/SiO_2 > 0.6$, the conductivity is given by Equation 17 in the temperature range 1450 to 1650 °C

Equation 17:
$$\kappa = -0.216e^{-0.0353.\%FeO - 0.0363.\%Al_2O_3} + (-19.32e^{0.0057.\%FeO - 0.0086.\%Al_2O_3} + 2.714e^{0.0061.\%FeO - 0.009.\%Al_2O_3}.\ln T).B$$

where $B = (\%CaO+\%MgO)/(\%SiO_2)$ and $0.6 \leq B \leq 2$

It should be noted that these correlations are based on conductivity data in systems which were two phase at some temperatures.

2.8.3. Mixed ionic and electronic conduction – transition metal containing slags, oxidation state considered in model

Pastukhov *et al.* (1966) defined the overall electrical conductivity for iron oxide containing slags with the following relationship:

Equation 18: $\kappa_{total} = \kappa_i + \kappa_e = \kappa_i + K.p_{O2}^{m}$

therefore $\log \kappa_e = \log (\kappa_{total} - \kappa_i) = \log K + m.\log p_{O2}$

where the subscripts *i* and *e* refer to ionic and electronic contributions respectively

K and *m* define the dependence of the electronic contribution on the p_{O2}

The authors then analysed their data in terms of finding a value for κ_i such that a straight line was found for the relationship $\log (\kappa_{total} - \kappa_i) = \log K + m.\log p_{O2}$. Therefore the values of K and m could be found. The authors suggested that *m* should have the value of $^1/_6$ based on the reaction: $\frac{1}{2}O_2 = O^{\circ} + V_{Fe} + 2\oplus$ where O° is an oxygen ion bonded to the lattice, V_{Fe} is an iron vacancy and $\oplus$ is a hole. The values that they found for *m* were in the range 0.11 to 0.18. This method of analysis provided satisfactory agreement with the data for iron oxide and iron silicate melts, however for the Al_2O_3-CaO-FeO-SiO_2 slag, the relationship only applied to the conductivity at the reducing conditions (see Figure 34 for the 23.4mol% FeO_x slag).

Fontana *et al.* (1984) applied a similar approach to the modelling of their data for the iron silicate slags. The difference in their treatment lay in the use of the thermodynamic model of Goel *et al.* (1980) for iron silicate slags to obtain the relationship between Fe^{3+}, Fe^{2+} and the oxygen partial pressure. The following expression was obtained:

Equation 19:
$$\kappa_{total} = \frac{C\rho_s}{M_s}(1 - N_{SiO_2}) + \frac{\rho_s\, k}{M_s}(\alpha - C).p_{O_2}^{\,n}$$

where C is the equivalent ionic conductivity due to Fe^{2+} ions

α is the equivalent electronic conductivity due to Fe^{3+} ions

ρ_s is the slag denstiy

M_s is the molar mass of the slag

N_{SiO2} is the silica mole fraction

k and n are the coefficients determined from the model of Goel *et al.* (1980) for the ratio of ferric and ferrous ions at given oxidation states

The first term was the ionic contribution to the conductivity and the second term was the electronic contribution. Knowing *k,n*, ρ_s, M_s and N_{SiO2} and plotting log (κ_{total} – ionic term) vs log p_{O2}, the values of C and α could be obtained from the intercept given that the slope of

the line should be *n*. The authors found that α was 3 to 10 times higher than C and increased strongly with iron content. The temperature did not have a very large effect on the electronic component.

Engell and Vygen (1968) modelled their oxidation state dependent conductivity data as a function of the ferric/total iron content. The overall conductivity was represented by the following equation:

Equation 20: $\kappa = \kappa_0 - ax + bx(1-x)$

Where κ overall conductivity
$\kappa_0 - ax$ ionic contribution
$bx(1-x)$ electronic contribution
x ferric / total iron fraction i.e. $Fe^{3+} / (Fe^{3+} + Fe^{2+})$

The electrical conductivity data shown in Figure 31 was fitted by means of parabolas in order to give the best representation of the data and to obtain values for κ_0, *a* and *b*. The values for κ_0, *a* and *b* were then related to the conduction mechanisms as follows:

The value of κ_0 was used to determine the mobilities of Ca^{2+} and Fe^{2+} cations based on the assumption that the only ionic contribution was from Ca^{2+} and Fe^{2+}. This was done using the relationship in Equation 1 i.e. $\kappa_0 = 2\ F\ \Sigma\ (c_{Ca2+}.u_{Ca2+} + c_{Fe2+}.u_{Fe2+})$. The authors suggested that the ratio of the mobilities of Ca^{2+} and Fe^{2+} would remain constant based on the assumption that the ionic radii of the cations were similar and they had the same co-ordination (octahedral). The mobilities of both cations were therefore able to be calculated. The mobilities of the cations were then related to the self diffusion coefficients using the relationship given in Equation 11. The authors reported good agreement between the calculated diffusion coefficients and coefficients measured elsewhere.

From the value of *a*, the value for the mobility of ferric cations could be calculated based on the relationship $a = 2.F.c_{Fe}.(u_{Fe2+} - u_{Fe3+})$. The authors discussed the structural aspects relating to ferric ions and how they can be present in both octahedral and tetrahedral co-ordinations. It was suggested that if the ferric ions were only present in tetrahedral co-ordination and therefore helped polymerise the silicate network, then the calculated mobilities were too high. If all the ferric ions were present in octahedral co-ordination then where the total iron content was greater than 27mol%, the silicate network would be fully depolymerised and free oxygen ions would also be likely to contribute to the conductivity. It was concluded that the structural aspects of the ferric ions could not be deduced exclusively from the conductivity measurements.

In the discussion of electronic conduction mechanisms in Section 2.3.2, the approaches of Engell and Vygen (1968) in modelling the electronic contribution were mentioned. Ultimately the authors related the coefficient *b* to the relationship given in Equation 5. They determined that a transfer distance of 2.8 Å gave the best agreement with the values of *b*. However, as the authors mentioned, the transfer distance was very similar to the average iron-iron distance, therefore a diffusion controlled mechanism was in doubt.

2.8.4. Summary of modelling

For slags not containing transition metals, the conductivity should be able to be related to a function of the composition. Ideally it would include the ion-oxygen attraction values of the ions in the slag. Modelling of the temperature dependence of the slag conductivity also needs to be investigated more carefully as no satisfactory models were given in the literature. Hoster and Pötshcke's model included temperature dependence however they did not relate temperature in terms of the Arrhenius relationship. Almost all other literature has found the Arrhenius relationship to be applicable.

In the modelling of slags containing iron oxide, Jiao and Themelis (1988) suggested that the model of Engell and Vygen was more realistic than those of Pastukhov *et al.* and Fontana *et al.*. The reason for this was that the ionic contribution included a term (ax) to account for the decrease in the partial ionic conductivity due to the ferrous ions as the slag became more oxidised. The other point relevant here is that the models of Pastukhov *et al.* and Fontana *et al.* were only applied successfully to slags at more reducing conditions, while the model of Engell and Vygen gave better representation of the change in conductivity over a wide oxidation state range.

In terms of modelling the electronic contribution to the overall conductivity, the two models of Engell and Vygen (1968) are both considered reasonable, however neither give completely satisfactory explanation of the conductivity results. This is because they do not comprehensively explain the mechanisms and structural aspects and many assumptions are required to apply them.

2.9. The effect of solid phases

It should be noted that in the preceding discussion of the electrical conductivity data in slags, only fully liquid systems were generally considered. The reason given for this was that the effect of a solid phase could significantly affect the electrical conductivity of a slag depending on the nature and the amount of the solid phase. In order to gain better insight into the effects of solid phases the literature on the subject was briefly examined. There is a large amount of literature dealing with the electrical conductivity of multiphase systems, especially within the geosciences. The literature examined is by no means comprehensive in terms of what is available, however it is considered that the important factors affecting the conductivity of multiphase systems have been identified.

There are two main considerations in terms of the effect of solids on the conductivity of the slags of interest. The first is the effect of a dispersed solid phase as in the case of the chromium containing slags where spinels are likely to form. In that case, the bulk phase is assumed to be the liquid and the solid phase is quite dilute. The second consideration is that where melting of a slag occurs from below the solidus to above the liquidus temperature.

2.9.1. Electrical conductivity of dispersions

Banisi *et al.* (1993) gave a review of the electrical conductivity of dispersions. The authors classified the investigations into the effects of dispersions into four categories: classical solutions, ordered arrangements of the dispersed phase, non-empirical approximations and

empirical approximations. Only the classical solutions were considered starting with the Maxwell model which considers conducting, uniform spheres dispersed in a conducting medium. Thereafter several other models were considered which took into account shape factors for the dispersed phase. The authors applied Maxwell's model to show the effect of the amount of dispersed phase (called phase holdup), the difference in conductivity between the conducting phase (κ_c) and the dispersed phase (κ_d) on the resultant conductivity of the mixture (κ_m). Their findings are presented in Figure 36.

The results confirm the logic that if the dispersed phase has a higher conductivity than the conducting phase, then the mixture conductivity will increase and vice versa. Also the greater the amount of dispersed phase, the greater its effect on the mixture conductivity.

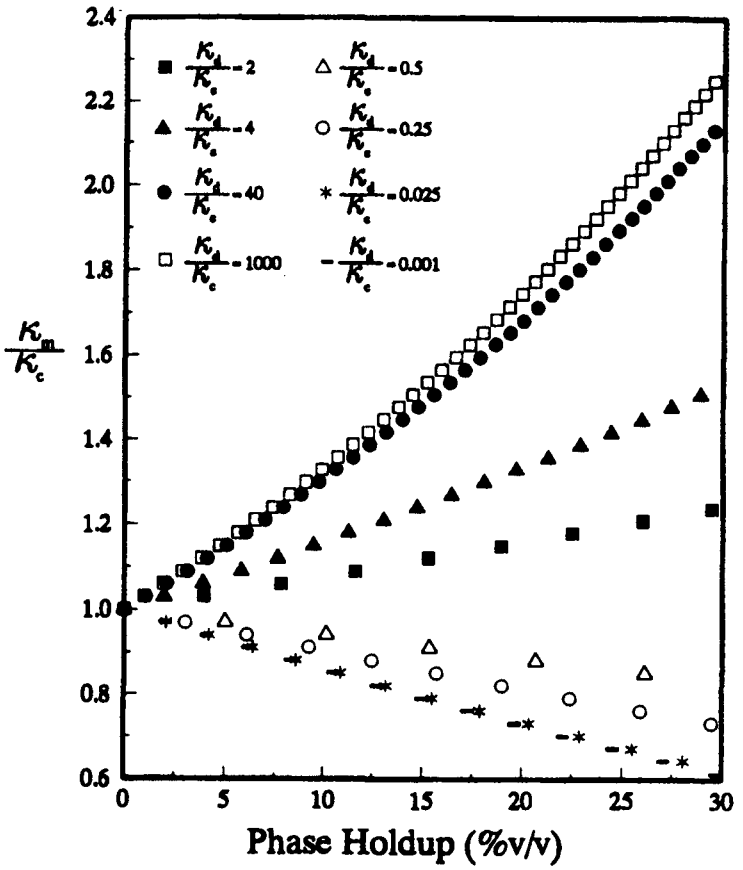

Figure 36: Effect of a dispersed phase (of conductivity κ_d) on the conductivity of a conducting phase (κ_c) resulting in the mixture conductivity (κ_m) using Maxwell's model after Banisi *et al.* (218). Phase holdup refers to the volume of dispersed phase over the volume of the conducting phase.

2.9.2. Electrical conductivity of partially molten systems

Bockris *et al.* (1948, 1952) studied the conductivity of various binary silicate slags below and above their liquidus temperatures and qualitatively explained the changes in conductivity observed. Bockris *et al.* (1952) presented a graph for a $CaO.SiO_2$ slag which is reproduced in Figure 37 for ease of reference. There was a large difference in the conductivity in the solid and in the liquid. The conductivity on cooling to the liquidus temperature was higher than the conductivity of heating to the liquidus temperature. Segers *et al.* (1978) presented a very

similar curve for a slag in the system CaO-MnO-SiO_2. Bockris *et al.* (1952) suggested that where a melt crystallises the drop in the conductivity is due to the locking up of conducting cations in the crystal lattice. Conduction can then only occur via lattice defects such as interstitial cations and vacant lattice sites. However where the melt is glass forming and supercooling occurs, then the glassy state retains some of the disorder present in the liquid state.

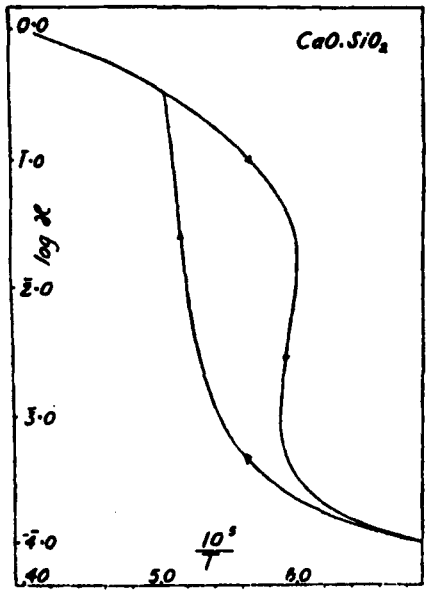

Figure 37: Change in conductivity when heating and cooling to the slag liquidus temperature after Bockris *et al.* (1952)

Bockris *et al.* (1948) also mentioned that the increase in the conductivity over the liquidus temperature could give an indication of the type of conduction mechanism. Where there was a small increase in the conductivity (less than an order of magnitude), then the conduction mechanism in both the solid and liquid was likely to be semiconduction. If the increase was larger then it was likely that ionic conduction was taking place.

In order to quantify the conductivity of partially molten systems, the use of mixing models is common. Glover *et al.* (2000) provided a review of some of the mixing models used to describe the conductivity of mixtures of two conducting phases. The authors provided a table summarising the more common mixing models for electrical conductivity and also provided a graphical comparison of the models which is reproduced in Figure 38. The parallel model considers solid layers lying parallel to the direction of current flow. The perpendicular model considers solid layers lying normally to the direction of current flow. The random model considers arbitrary shaped and oriented solid fractions. The Hashin-Shtrikman upper and lower bound models were derived from effective medium theory (as cited by Glover *et al.*) The authors concentrated on Archie's law which was empirically derived for clean porous sandstone saturated in saline solutions. The original Archie's law ($\sigma_{eff} = C.\sigma_2.\chi_2^m$) was only valid for one conducting phase so the authors then proposed a modified Archie's law which was valid for two conducting phases ($\sigma_{eff} = \sigma_1(1-\chi_2)^p + \sigma_2.\chi_2^m$ where $p = \log(1-\chi_2^m)/\log(1-\chi_2)$). In all of the models one needs to know the volume fractions of each phase and the conductivity of each phase.

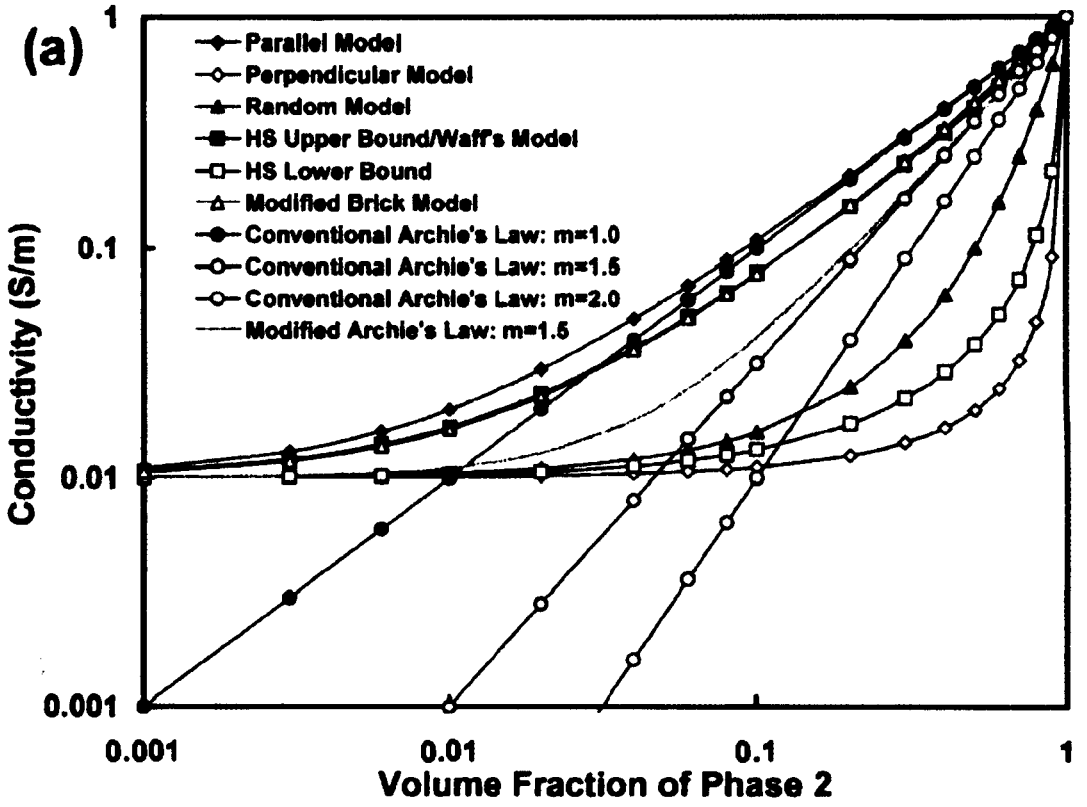

Figure 38: Comparison of mixing models for describing electrical conductivity of two phases as a function of the volume fraction of phase 2. Phase 1 conductivity = 0.01 S/m and phase 2 conductivity = 1 S/m. Diagram after Glover *et al.* (2000)

The effect of partial melting has been investigated widely in the geosciences. A paper of interest was that by Partzsch *et al.* (2000) who studied the melting of crustal rocks by means of laboratory experiments. They made measurements of the electrical conductivity of gabbro-norite rock samples from below the solidus to a partially molten state. Quenched samples were obtained at a range of temperatures and the phases present were identified and the melt volume fraction was estimated. Their findings are shown in Figure 39.

The authors found that at temperatures above the solidus the grain surfaces were wetted, however melt volume fractions of 0.1 were required for interconnection of the melted areas. An increase in the conductivity of an order of magnitude was observed on formation of the interconnected melt network. Partzsch *et al.* modelled the melting process by means of a modified brick layer model (MBLM). The model considers a unit cube (melt) inside of which is a smaller cube of edge length *a* (solid). The melt and the solid are connected along the faces of the cubes. The electrical conductivity of the composite can then be calculated as a function of the melt fraction and the conductivities of the solid and the liquid.

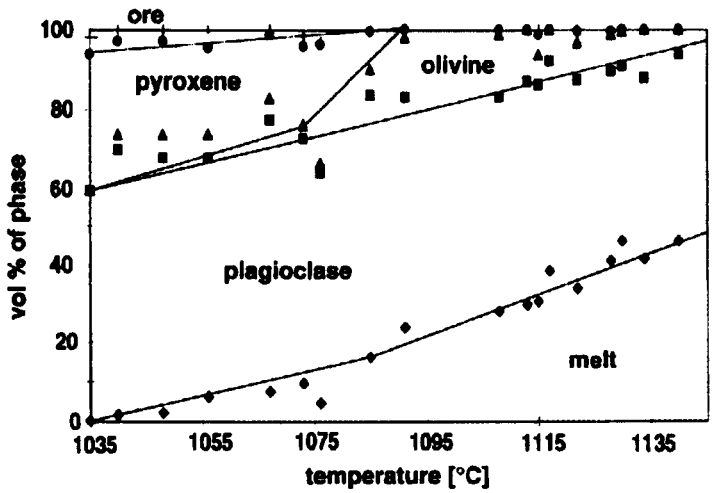

Figure 39: Volume fraction of phases on partial melting of a gabbro-norite rock sample after Partzsch *et al.* (2000)

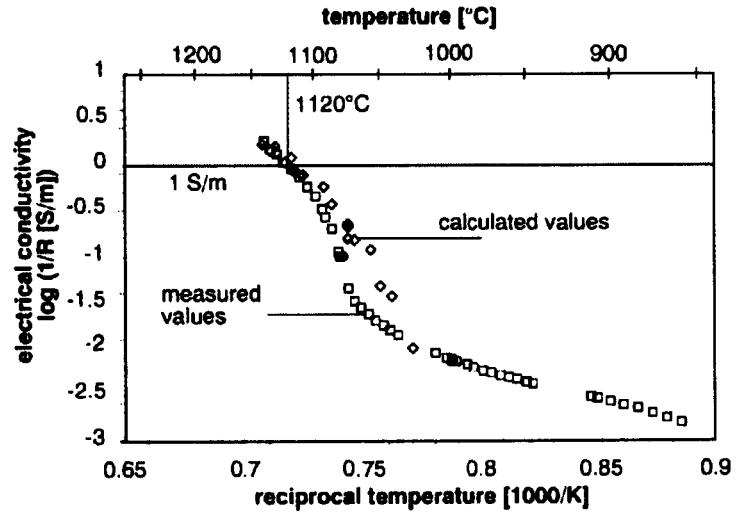

Figure 40: Measured and calculated change in electrical conductivity of gabbro-norite rock sample during melting, after Partzsch *et al.* (2000)

2.10. Research questions and hypotheses

The aim of the literature review was to obtain an understanding of the factors affecting the electrical conductivity of slags, to determine how the conductivity had been measured and modelled previously and to isolate areas in which more work was required. As a result of this, the following research questions arose. They have been categorised into experimental considerations and modelling considerations:

2.10.1. Experimental considerations

- The industrial slags of interest have up to 30wt% FeO_x with around 5% Al_2O_3, 5-10% CaO, 15-25%MgO and 40-60% SiO_2. There is fairly good understanding of the conductivity in the iron-free Al_2O_3-CaO-MgO-SiO_2 system. For slags with up to 30%FeO_x there could be significant electronic contribution (see Figures 31, 33, 34 and 35). There is not a clear understanding of the contributions from the ionic mechanism and electronic mechanism in slags containing these amounts of FeO_x (up to 30wt%). Therefore quantitative prediction of the conductivity is not feasible at this stage. Experimental work is required to provide further information on how the addition of iron affects the conductivity.
- In iron-containing slags it is known that the oxidation state of the slag is an important factor affecting the electrical conductivity. The oxidation state-dependent conductivity measurements reported in the literature were conducted primarily on slags of relatively low basicities. The effect of slag basicity was not systematically studied or evident from the literature. Therefore, how does the slag chemistry affect the oxidation state dependence of the slag conductivity or in other words the electronic mechanism?
- How will chromium affect the electrical conductivity of the melter type slags? The measurements reported in the literature concerning the effect of chromium were on slags in the system Al_2O_3-MgO-SiO_2. Given that the melter type slags contain iron and are likely to have some electronic conduction, what is the effect of chromium?

2.10.2. Modelling considerations

- Both ionic and electronic conduction occur in slags containing transition metals. Therefore what is the best way of accounting for the relative contributions by the ionic and electronic conduction mechanisms? In systems where only ionic conduction takes place, it seems possible that a measure of the basicity can give a good indication of the conductivity. However where transition metals are present, the presence of electronic conduction complicates the concept of basicity and application thereof.
- How can the temperature dependence of the electrical conductivity be accounted for? It is commonly accepted that the Arrhenius relationship satisfies the dependence of conductivity on temperature. Are the pre-exponential factor and the activation energy related to the slag composition? Given that the compensation law (relating ln A_k and E_k) is valid for viscosity and diffusion in silicate systems, will it be applicable for the conductivity?

- Can changes in the activation energy for conduction be used as an indication of whether ionic or electronic conduction is dominant?
- In chromium containing slags, can the presence of spinel phase be modelled in terms of theoretical relationships where the conductivity and volume fraction of each phase present in the slag is known?

2.10.3. Approaches

The approach taken to investigate the research questions was to measure the electrical conductivity of the slags of interest using suitable techniques. From the literature review of experimental techniques used it appeared that the two-electrode technique would be satisfactory. It was hoped that through the experimental approach taken, answers could be obtained for both the experimental and modelling considerations.

In terms of determining the effect of addition of iron oxide at low total iron contents, synthetic slags of varying basicity (but relevant in composition to the melter type slags) were prepared. Iron oxide was then incrementally added to the master slags and the conductivity was measured at a range of temperatures. In this way, the relationship between the total iron content and the conductivity could be established. Also the activation energies could be obtained and possibly provide an answer for the second and third modelling questions.

In determining the oxidation state dependence of the electrical conductivity, it was first necessary to find a suitable technique to allow for reasonably short equilibration times with the gas atmosphere in the furnace. The electrical conductivity of slags of varying basicity and iron content would then be measured as a function of the oxygen partial pressure. Given that data were available for the oxidation state dependence of the conductivity of iron silicate slags, it was deemed to be of value to make similar measurements for calcium ferrite slags. Therefore data would be available at both extremes of basicity as well as some intermediate basicities.

In determining the effect of chromium on the electrical conductivity of the melter type slags, the approach was to add chromium to synthetic slags of interest and determine the electrical conductivity as a function of temperature. It was likely that very high temperatures (>1600°C) would be required to make measurements above the liquidus temperatures of the higher chromium containing slags. Oxidation state runs were not carried out on chromium-bearing slags as the presence of both iron and chromium (both multivalent and influenced by oxidation state) in the slags would increase the number of unknowns and interpretation of results would be speculative. Also measurement of chromium redox equilibria in the slags of interest wa considered difficult given the small amounts of chromium involved and the problems associated with fully dissolving samples for wet chemical analysis.

2.10.4. Hypotheses

It is postulated that the addition of iron oxide to a slag will bring about an increase in both the ionic and electronic conduction mechanisms. At low iron content, the majority of the conduction is by ionic means, therefore the slag basicity will be the most important factor determining the conductivity. Once the iron oxide content is sufficiently high that electronic

conduction is possible, the conductivity is likely to vary exponentially with increased iron oxide content i.e. the iron content will be the most important factor determining the conductivity.

It is postulated that the effect of basicity on the oxidation state dependence of the conductivity will be governed by the amounts of ferric and ferrous ions in the slag. Therefore, the manner in which the basicity affects the ferric and ferrous contents will determine the effect on oxidation state dependence of the conductivity. The basicity will also affect the magnitude of the conductivity, where higher basicity slags will have higher conductivities because of the presence of more conducting cations and a more depolymerised silicate network.

From the literature concerning chromium containing slags, it was evident that presence of chromium in slags significantly raised the liquidus temperature of the slag. The literature suggested that where slags were below their liquidus temperatures, the chromium addition would decrease the electrical conductivity of the slags due to the formation of solid phases which removed conducting cations from the liquid state. Above the liquidus temperature, the effect of chromium was likely to be determined by the oxidation state of the chromium ions. If the chromium was present as trivalent ions, then slag polymerisation was likely to occur and the conductivity would decrease. If the chromium was present as divalent ions, then the Cr^{2+} ions would act as network modifiers, depolymerise the silicate network and increase the conductivity. Therefore in the case of the melter type slags (which are relatively reduced), it is postulated that the addition of chromium will decrease the conductivity where the slags are below their liquidus temperatures and increase the conductivity where the slags above their liquidus temperatures.

Chapter 3

MATERIALS AND METHODS

The two-electrode technique was chosen for this study. Two slightly different experimental setups were used in order to achieve the desired experimental objectives. These setups were classified as:

a. *Deep cell* technique for general slag conductivity measurements and determination of temperature dependence. The deep cell setup refers to a depth of slag of approximately 20mm or greater.

b. *Shallow cell* technique for measurements of the oxidation state dependence of slag conductivity at a single temperature. The shallow cell setup refers to a slag depth of 3-4mm.

In both cases, the same furnace and auxiliary equipment was used. The differences lie in the crucibles used, the calibration of the setup and the gas atmospheres applied. The descriptions of the furnace and the auxiliary equipment will be given first and thereafter the specific setups and their calibrations will be explained.

In the investigation of chromium containing slags, conductivity measurements at very high temperatures (up to 1700 °C) were desired. This required the use of a different furnace and materials of construction for the conductivity cell. The two furnaces will be referred to as the standard furnace and the very high temperature (VHT) furnace.

This chapter is written to provide an accurate record of the experimental procedures employed. Also included are some of the observations made during both successful and unsuccessful experiments in the hope that future work in this field may avoid the problems encountered during this investigation.

3.1. Furnaces

A schematic of the standard furnace and associated equipment is provided in Figure 41. The furnace used for the majority of the experiments was a vertical tube furnace (Ceramic Engineering, Sydney). The furnace was heated by four U-shaped $MoSi_2$ elements and the temperature was controlled by a Eurotherm controller (model 902). The maximum operating temperature of the furnace was around 1700 °C, although in practice the maximum obtainable temperature inside the tube was around 1550 °C. The vertical tube had an internal diameter of 80mm and was approximately 950mm in length. The tube was made from Pythagoras (a mullite type ceramic with ~60% Al_2O_3, ~37% SiO_2, ~3% alkali). The tube was fitted with water-cooled stainless steel end caps which were sealed by O-rings. The gas inlet was located on the bottom end cap and the gas outlet was located on the top end cap. The top end cap had a port for the measurement thermocouple, a sight glass and a port into which the rubber stopper with the

electrodes was plugged. Temperature in the tube was measured by a Pt-Pt/13%Rh (ASTM type R) thermocouple protected by a closed-end 5x3mm alumina tube (the accuracy of the thermocouple was checked by comparison with the freezing point of copper – see Appendix B1 for details). The thermocouple and the electrode tips were positioned such that they were in the middle of the hot zone of the furnace. The hot zone of the furnace was approximately 50mm in height in which the temperature did not vary by more than ± 2°C at 1400°C (see Appendix B2 for temperature profile of the hot zone). It was assumed that there was a negligible thermal gradient over the crucible and slag as the crucible would be positioned in the middle of the hot zone.

The bottom end cap was fitted with a port through which the alumina rod and pedestal could be moved. The crucible was supported by the pedestal which had been cast at the top of the closed end alumina rod (using Moral Quickcast, Shinagawa Thermal Ceramics). The alumina rod passed through the bottom end cap through an O-ring system and connected to a programmable linear motion actuator. The actuator (NSK, model no. XY-FS0050-901) had a 500mm stroke and could position and move the crucible vertically with a precision of 0.1mm.

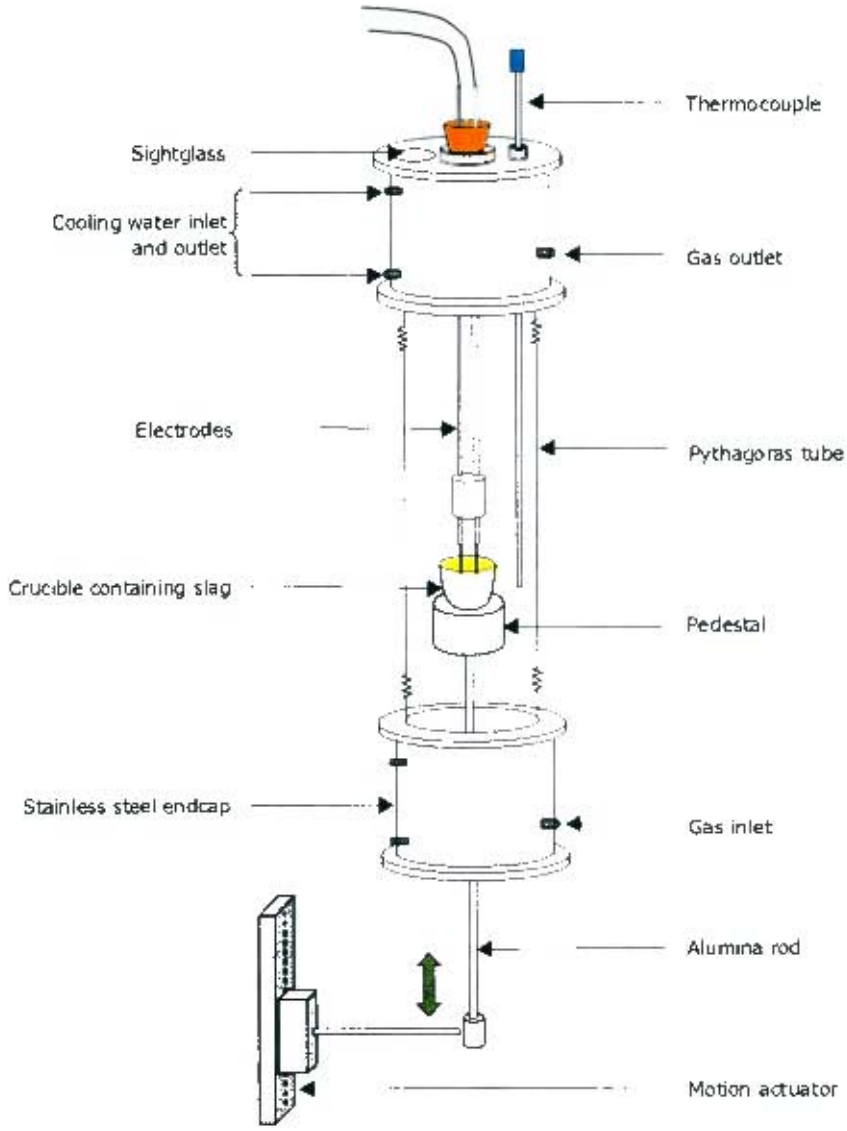

Figure 41: Schematic of vertical tube furnace

VHT furnace

The very high temperature (VHT) furnace was of similar design to the one described above, however, there were some differences in order to facilitate the higher temperatures required. The heating was provided by four Kanthal super 1800 molybdenum disilicide elements. The vertical tube was made from pure alumina (instead of Pythagoras) and it had an internal diameter of 50mm. The thermocouple had to be inserted into the rod supporting the crucible. Temperature was controlled by a Eurotherm 902 temperature controller.

3.2. Electrodes

The electrodes were made up from two platinum wires of 0.5mm diameter (Engelhard-Clal) with 1mm diameter Pt wire tips (Engelhard-Clal) spot welded onto the end. The wires were in excess of 700mm in length, while the tips were approximately 30mm in length. The reason for the larger diameter tips was to minimise polarisation by having larger electrode surface areas in contact with the slag and hence a lower current density.

The electrodes were sheathed in two twin bore alumina tubes such that the tips extended precisely the same distance from the tubes' bottom ends. The twin bore tubes were held rigidly in place by means of a rubber stopper (through which two holes had been drilled) at the top and were cemented a set distance apart at the lower end by means of a castable ceramic spacer (Moral Quickcast , Shinagawa Thermal Ceramics). Figure 42 shows the setup of the electrodes:

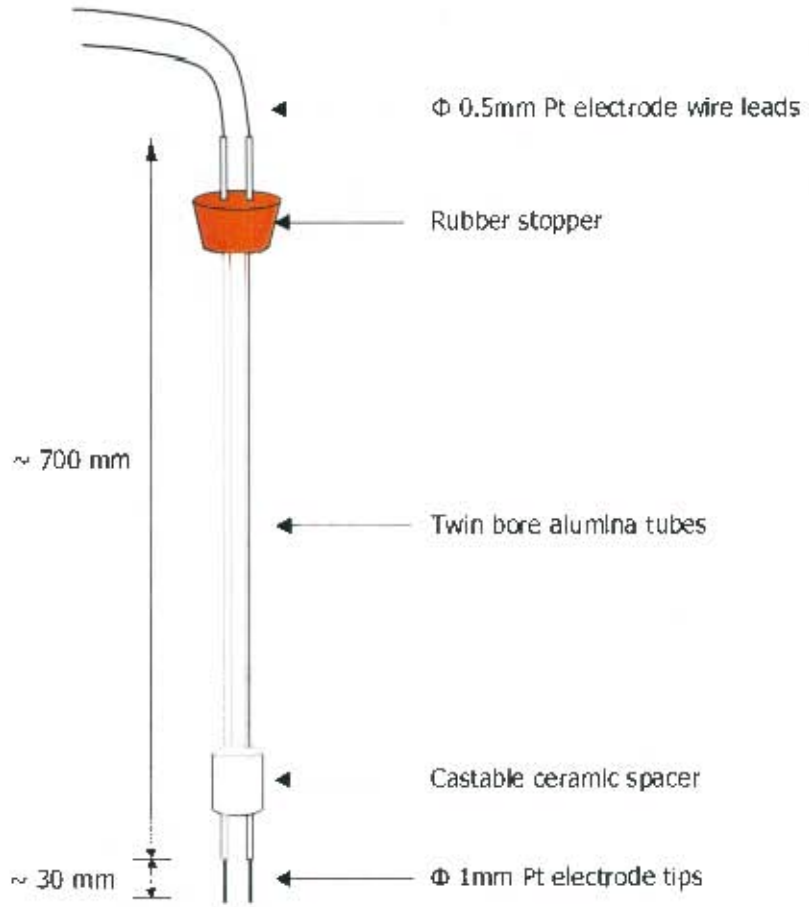

Figure 42: Schematic of electrode setup

In all experiments except the calcium ferrite experiments, the electrode spacing was maintained at 10mm (centre to centre) as measured using vernier calipers. Owing to the flexibility of the 0.5mm Pt wire leads, the electrode spacing was sometimes found to vary by ± 0.5mm either in the process of placing the electrodes in or removing them from the furnace. This was taken into account when applying the calibration and analysing the results.

In the set of experiments on the high conductivity calcium ferrite slag, the electrodes were set at a distance of 25mm apart. In order to maintain the electrodes at this spacing it was necessary to develop a spacer to hold the electrodes apart. This was accomplished by using a short section of 5x3mm alumina tube with holes drilled through it using a dental drill. The spacer is depicted in Figure 43 below:

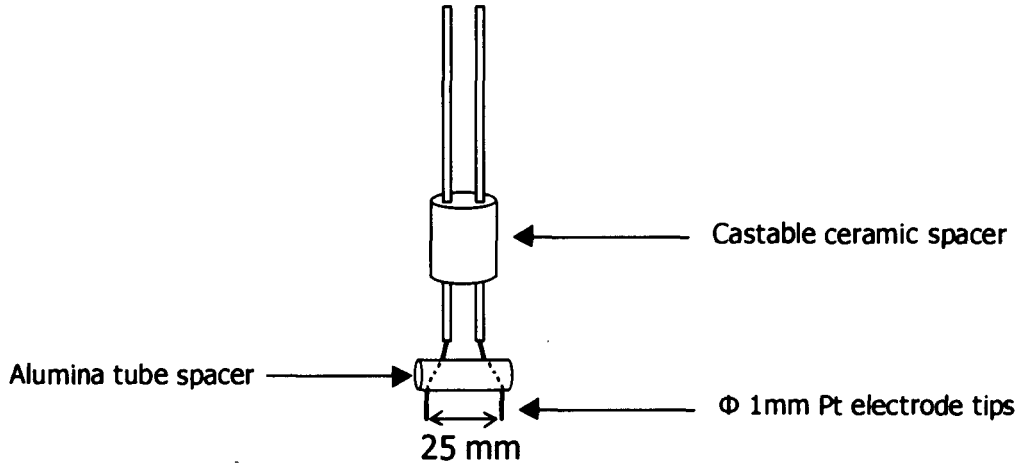

Figure 43: Schematic of electrode spacer for high conductivity slag

The electrodes were stationary in the furnace and the tips of the electrodes were positioned so that they were in the hot zone of the furnace. The crucible containing the slag was raised until contact was made with the electrodes. The point of contact was detected by a large decrease in the measured resistance and a stable reading of the resistance. The surface of the slag could therefore be detected to within 0.1mm.

In most cases at the end of an experimental run there was very little slag frozen on the electrode tips. However, in some cases where the electrodes had been withdrawn when the slag was close to its liquidus temperature and hence very viscous, there were slag accretions on the electrodes. To avoid contamination of the next slag being tested, large accretions of slag were broken off using pliers and the remainder was dissolved by placing the electrode tips in a mixture of diluted HCl and HF acid which was heated on a hotplate in a fume cupboard.

Periodically the electrode tips were changed when they had become worn either through mechanical damage such as bending or chemical attack by slags over extended periods of time. In these cases the tips were cut off and new lengths of 1mm diameter Pt wire were spot welded onto the ends of the 0.5mm diameter wire such that the dimensions remained constant. A new calibration with aqueous solutions was carried out when the electrode tips were changed. The calibration procedures are detailed in Sections 3.6.2 and 3.7.2.

In the case of the measurements at very high temperature, molybdenum electrodes were required. The molybdenum wire used for the electrodes had a diameter of 1.5 mm and the electrodes were 60cm long. The electrode spacing was 10mm and the electrodes were immersed to a depth of 8 mm in the slag.

3.3. Instruments

Two instruments were used to make measurements on the molten slags. The first was an RCL meter which was used for all of the measurements. The second was an electrochemical impedance spectrometer which was used in one series of measurements to obtain the frequency response for a particular slag and to provide comparison with the RCL meter measurements.

3.3.1. RCL meter

The instrument with which the measurements were taken was a Fluke Programmable Automatic RCL meter (model PM6304). The instrument was connected to the electrodes by means of a 4-wire lead with heavy duty Kelvin clips (model PM9541B). This meant that there was a four-wire measurement up to the connection with the electrodes. The connection to the electrodes was made in the same place each time such that the distance from the connection to the electrode tips was constant (~ 730mm – see Figure 42)

The RCL meter could be operated on its own or connected via an RS232 interface to a computer. When connected to a computer, the meter could be controlled remotely using supplied software (Fluke ComponentView Software for Microsoft Windows®). This allowed frequency scans or continuous data measurement at specified settings.

The instrument was able to measure in the following frequency ranges: 50Hz, 60Hz, 100Hz, 120Hz, from 200Hz to 20kHz in 100Hz steps and then 100kHz. The amplitude of the applied voltage could be set at 50mV, 1V or 2V.

The range of measurement capability was the following:

Resistance	R or Z:	0.0000 Ω to 200 MΩ
Capacitance	C:	0.00pF to 15.9μF at 100kHz
Inductance	L:	0.00μH to 318μH at 100kHz

The instrument automatically determined an equivalent circuit for the slag being measured. For most slags the equivalent circuit at low frequencies was a resistor in series with a capacitor and at high frequencies the equivalent circuit was a resistor in series with an inductor. During calibration with aqueous solutions the equivalent circuit was a resistor in parallel with a capacitor at all frequencies. The reasons for this are explained later.

The majority of the measurements were carried out at 100 kHz with an applied voltage of 1V. Under these measurement conditions the accuracy of the reported resistance (within the range 1Ω to 1MΩ) was ± 0.4%. The reason for the selection of the 100 kHz frequency parameter was that the measured resistance for most of the slags was independent of the frequency from around 1 kHz to around 100 kHz. The frequency response of various slags will be discussed in more detail below. The reason for using an applied voltage of 1V was

that one obtained the best accuracy from the instrument and the readings were more stable than at the other voltages. At the lower test voltage of 50mV the accuracy of the instrument was ±2%; so even though the lower voltage would probably be better in terms of reducing polarisation, there would be greater uncertainty in the measurement.

The basic principle of operation of the meter involves placing a low voltage with constant current across the electrodes. The resultant voltage developed across the electrodes as a result of the slag resistance is then measured based on dual-slope integration of the unknown voltage. As the applied current is known, the resistance can be calculated. The principle of operation is summarised in slightly more detail below (refer to the block diagram below (Figure 44)):

The four-wire leads from the instrument are connected to the electrodes by means of the Kelvin grips. A sinusoidal ac voltage is generated by the source in the instrument and routed along the high drive (HD) wire to an electrode. The amplitude, frequency and phase of the voltage are controlled by the signal synthesiser and the CPU in the instrument according to the settings selected. The low drive (LD) wire is connected to the other electrode and is forced electronically to near ground voltage level and current passes through this wire. The high sense (HS) and low sense (LS) wires sense the voltages at each of the electrodes as a result of the current passing through the slag. The sensed voltages are amplified and filtered and are then converted to equivalent dc voltages in the multiplying DAC (digital-to-analog converter) by multiplying the voltages by a digital reference sine wave from the signal synthesiser. The dc voltages are then converted to digital equivalents using a dual slope ADC (analog-to-digital converter) which consists of the dual slope integrator and the counter. The reference voltage and current signals, the measured voltage and current signals and the gains used are then processed in the CPU according to pre-defined algorithms and the measured impedance is given.

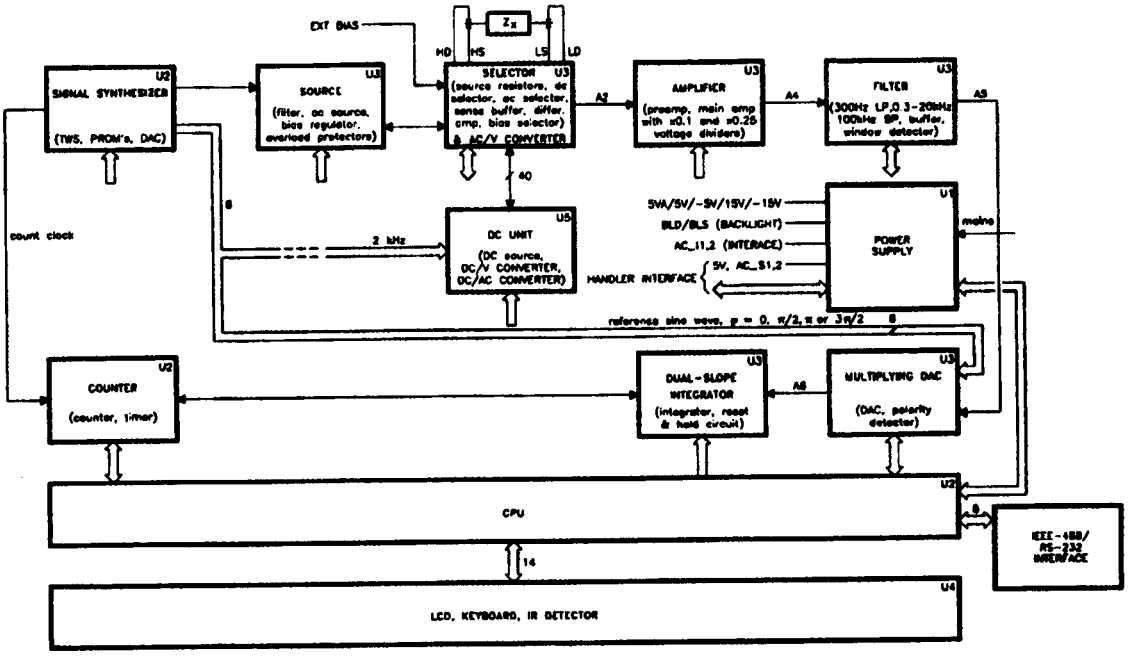

Figure 44: Block diagram of RCL meter

3.3.2. Impedance spectrometer

Electrochemical impedance spectroscopy (EIS) was used for one set of measurements on a slag. The principle of operation of these types of spectrometers is that the impedance of a conductivity cell is measured over a wide range of frequencies and the response of the impedance provides information regarding the electrochemical processes occuring within the cell. The main reasons for the test were to compare the results with measurements from the RCL meter and to observe the response at frequencies outside the range of the RCL meter. There is a considerable amount of additional information that one can obtain by close analysis of electrochemical measurements, however the focus of this project was to obtain the electrical conductivity of slags and not to get heavily involved in analysing impedance spectra.

The spectrometer used was a Schlumberger/Solartron 1255 Frequency Response Analyser (waveform generator) in conjunction with a Schlumberger/Solartron 1286 Electrochemical Interface (potentiostat). The spectrometer was connected up to the two electrodes by means of leads with crocodile clips. The spectrometer was connected to a computer from which it was controlled using Zview2 software by Scribner Associates Inc. Impedance measurements were carried out at frequencies of 0.01Hz to 1MHz at applied voltages of 1mV, 5mV and 100mV and analysed using the Zview software.

For the run where EIS was used, there was excellent agreement between the results from the two instruments i.e. RCL meter and the EIS. The results of the effect of frequency on the measurements of slag conductivities are presented in Section 3.6.4.

3.4. Gas flows and calibrations

In many of the experiments the atmosphere in the furnace needed to be controlled to obtain the desired partial pressure of oxygen (p_{O2}) and therefore the correct oxidation state of the slag. Gases were cleaned, dried, measured and mixed before being delivered to the bottom of the tube furnace. The gases were removed from the top of the furnace and vented into the laboratory's main scrubber / gas extraction system.

High purity CO_2 (BOC food grade – 99.8%), CO (Linde CO2.5 grade – 99.5%), N_2 (BOC grade 4.0 high purity – 99.99%) and Ar (grade 4.7 high purity – 99.997%) were available in the laboratory. Prior to use, the gases were dried by passing them through silica gel and magnesium perchlorate. They were then deoxidised by passing them through copper turnings at 500°C in a horizontal Kanthal wound furnace. The flow rates of the gases were controlled by mass flow controllers (MKS, model no. 1179A) with various flow capacities (200, 1000 and 5000 cc/min). The flow measurement was based on the differential heat transfer between temperature sensing elements in a laminar flow of the gas. The controllers were calibrated by means of bubble flow meters for each different type of gas. Occasionally checks were made that the flow rates were accurate. In all cases the desired ratio of flow rates were obtained to within ± 2%. The calibration curves for the three mass flow controllers are supplied in Appendix B3.

Where an inert atmosphere was required, either N_2 or Ar was used at a flow rate of approximately 1l/min. In cases where the oxygen potential was being controlled, the ratio of CO_2 flow to CO flow was kept constant with a total flow of 1 l/min of the combined gases.

3.5. Slag compositions and preparation

In most cases, master slags containing alumina, lime, magnesia and silica were prepared. Transition metals such as iron or chromium were then added to the master slag to give the desired slag composition. The compositions of the various master slags (transition metal free) have been plotted on a phase diagram for 5% Al_2O_3-CaO-MgO-SiO_2 in Figure 45. For ease of reference the different compositions have been classified according to their basicities as low (L), intermediate (I) and high basicity (H) - the wt% (CaO+MgO) / (Al_2O_3 + SiO_2) ratio is given as an indication of the basicity. The intended compositions for all the slags tested are given in Table 3.

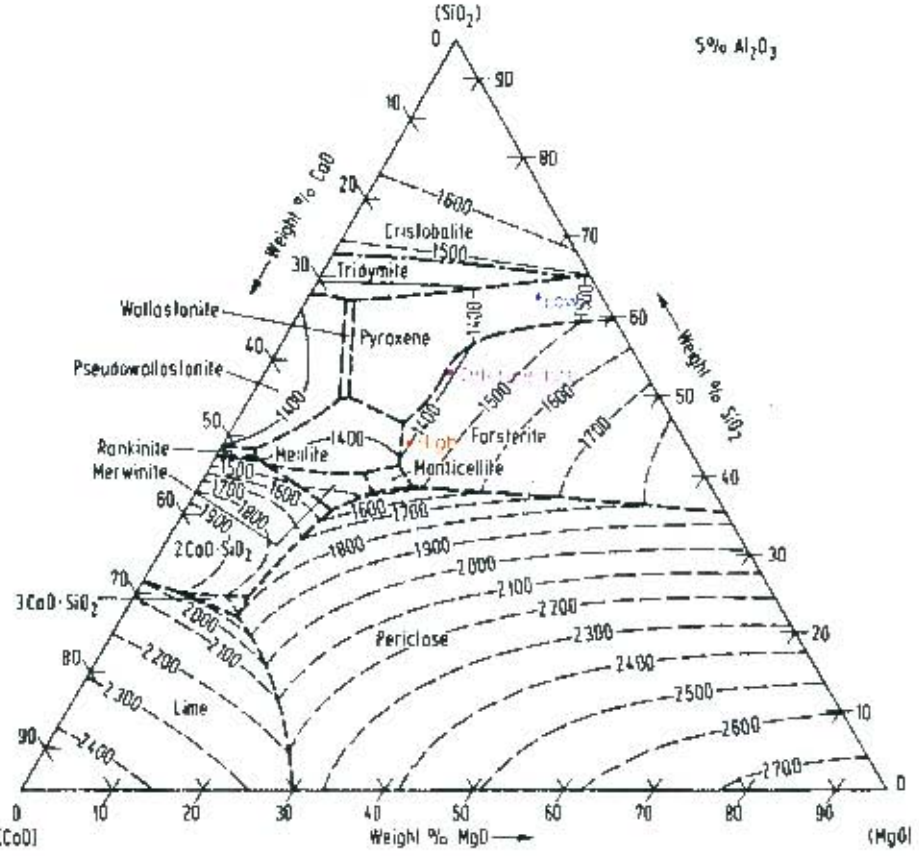

Figure 45: Phase diagram showing approximate compositions of master slags. Diagram after Slag Atlas (1995)

Table 3: Compositions of master slags

Slag name	Composition (wt%)							Basicity	Measurements
	Al_2O_3	CaO	Cr_2O_3	FeO_x	MgO	SiO_2	Total		
L0	6.3	6.3	-	0.0	25.0	62.5	100	0.45	T, F, H
L10	5.6	5.6	-	10.0	22.5	56.3	100	0.45	T,F, IA
L15	5.3	5.3	-	15.0	21.3	53.1	100	0.45	T, O, F, IA
L20	5.0	5.0	-	20.0	20.0	50.0	100	0.45	T, O, F, IA
L30	4.4	4.4	-	30.0	17.5	43.8	100	0.45	O, F, IA
L40	3.8	3.8	-	40.0	15.0	37.5	100	0.45	O, F
I0	6.3	20.0	-	0.0	20.0	53.8	100	0.67	T, F
I10	5.6	18.0	-	10.0	18.0	48.4	100	0.67	T, F, IA
I20	5.0	16.0	-	20.0	16.0	43.0	100	0.67	T, O, F, IA
I30	4.4	14.0	-	30.0	14.0	37.6	100	0.67	T, O, F, IA
I40	3.8	12.0	-	40.0	12.0	32.3	100	0.67	O
H0	5.0	30.0	-	0.0	20.0	45.0	100	1.00	T, F, H
H10	4.5	27.0	-	10.0	18.0	40.5	100	1.00	T, F, IA
H15	4.3	25.5		15.0	17.0	38.3	100	1.00	T, F, IA
H20	4.0	24.0	-	20.0	16.0	36.0	100	1.00	T, O, F, H, IA
H30	3.5	21.0	-	30.0	14.0	31.5	100	1.00	T, O, F, IA
H40	3.0	18.0	-	40.0	12.0	27.0	100	1.00	O, F
Cr0	5.0	5.0	0.0	20.0	20.0	50.0	100	0.45	T, VHT, F, IA
Cr0.5	5.0	5.0	0.5	19.9	19.9	49.8	100	0.45	T, IA
Cr1	5.0	5.0	1.0	19.8	19.8	49.5	100	0.45	T, IA
Cr2	4.9	4.9	2.0	19.6	19.6	49.0	100	0.45	T, H, VHT, F, IA
Cr4	4.8	4.8	4.0	19.2	19.2	48.0	100	0.45	T, VHT, F, IA
Cr6	4.7	4.7	6.0	18.8	18.8	47.0	100	0.45	T, IA
Cr8	4.6	4.6	8.0	18.4	18.4	46.0	100	0.45	T, IA
CF	-	25.0	-	75.0	-	-	100	-	O

Guide to slag names

L - low basicity slag, number after is wt% FeO_x

I - intermediate basicity slag, number after is wt% FeO_x

H - high basicity slag, number after is wt% FeO_x

Cr - chromium containing slags, number after is wt% Cr_2O_3

CF - calcium ferrite slag

Guide to measurement symbols

T - temperature dependence

O - oxidation state dependence

F - frequency dependence

H - conductivity profile on heatup from low temperature

VHT - measurements at very high temperature (up to 1700 °C)

IA - experiments conducted under an inert atmosphere

The reasons for the choices of the slag compositions were as follows:

The low basicity slag was chosen for its similar composition to the industrial melter type slags (although the iron level in the industrial slags varied from 10 to 30wt% FeO_x). The intermediate basicity slag was chosen as it had been tested by Hejja *et al.* (1994), therefore comparisons could be made with the measurements of those authors. It was of interest to study the effect of basicity and therefore a higher basicity slag was required. Ideally the MgO content of the slag would be similar to the low and intermediate basicity slags, therefore lime was substituted for silica to give the high basicity composition. The liquidus temperatures of the slag were also borne in mind when deciding on the system. The liquidus temperatures for the slags were 1425, 1336 and 1402 °C for the low, intermediate and high basicity slags respectively (temperatures calculated using MPE (see Zhang *et al.* (2002)). The effect of iron oxide addition and the oxidation state dependence of the conductivity were investigated using the low, intermediate and high basicity slags. The effect of chromium on the electrical conductivity was tested using the low basicity slag as it was similar in composition to the industrial melter type slags. As explained in section 2.5.2.5, a calcium ferrite slag was investigated as conductivity measurements on this slag would provide information on the high basicity extreme in comparison to iron silicate slags. The specific calcium ferrite slag was selected for being liquid over a wide range of oxidation states at 1300 °C.

Alumina (May and Baker – 99%+), calcium carbonate (Aldrich Chemical Company – 99%+), magnesia (Ajax Chemicals – 96%+, up to 1.5% Ca) and silica (Consolidated Chemical Company – 99.6%) were used to prepare the master slags. The reagents were kept dry in an oven at 160°C. They were weighed on an accurate scale (Sartorius, model no. MCI LC620P, accuracy ± 0.001g) in the desired proportions. The reagents were well mixed before being melted in a platinum crucible in a muffle furnace in air. The furnace was kept at approximately 1500-1550 °C (about 100°C above most of the slags' liquidus temperatures). The molten slag was then quenched by pouring it onto a steel launder. The slag was then crushed in a ring mill to promote homogeneity and a sample of each master slag was submitted for analysis.

For FeO_x-containing slags, the iron oxide was added in one of three ways. Where wüstite was required, it was prepared by thermal decomposition of ferrous oxalate (Aldrich Chemical Company – 99%+) at around 1000°C under a nitrogen atmosphere and then quickly cooled to below 500° (in accordance with method by Hejja *et al.* (1994)). Wüstite was used in the measurements where the temperature dependence of the slags was being tested, therefore slags L0, L10, L15, L20, L30, I0, I10, I20, I30, H0, H10, H15, H20 and H30. For example the iron oxide-free slag L0 was tested, then a specified amount of wüstite was added to the slag in the crucible to obtain the next slag (L10). Slag L10 was then tested and then more wüstite was added to obtain slag L20. The wüstite powder was placed on top of the frozen slag in the crucible. The contents of the crucible were heated to the starting temperature of the experiment (1400-1500°C) and left for approximately 30 minutes to equilibrate before conductivity measurements were started. It was assumed that this was sufficient time for the slag to become homogeneous. The conductivity values measured suggested that this was the case i.e. no unexpected decreases or increases with time and temperature.

In cases where the oxidation state of the slags was being tested, iron oxide was added as haematite (slags L15, L20, L30, L40, I20, I30, I40, H20, H30 and H40). The reason is that the

measurements were initially carried out in air and then reduced. The specified amount of haematite powder (Aldrich Chemical Company – 99%+) was well mixed in with the master slag to give the desired composition.

In the case of the chromium testwork, a master slag containing iron in a reduced state was required (slag Cr0). Here iron (Aldrich Chemical Company – 99.9%+) and haematite were added in stoichiometric proportions to give wüstite. The slag was melted in an MgO crucible in an inert atmosphere in a tube furnace and held at the slag's liquidus temperature for about 2 hours. The slag was carefully removed from the MgO crucible and was then crushed in a ring mill. A sample was submitted for analysis. The electrical conductivity of Slag Cr0 was then tested in a Pt crucible. Then chromium was introduced into the slag using Cr_2O_3. The Cr_2O_3 powder (Aldrich Chemical Company – 99%+) was dried and the correct amount was placed on top of the frozen Slag Cr0 in the crucible to obtain Slag Cr0.5. As before, the contents of the crucible were left to equilibrate at the starting temperature of the experiment for approximately 30 minutes. In terms of the chromium mixing into the rest of the slag, it was assumed that a uniform distribution would be obtained. This judgement was based on drop quench work conducted by N. Bartie (unpublished work, 2002) on samples of melter type slags containing Cr_2O_3. Bartie found that spinel crsytal compositions varied little from centre to edge suggesting that the chromium was well distributed. A photomicrograph of the frozen slag Cr8 was obtained which showed that the chromium spinels were well distributed throughout the slag sample. This suggested that the addition of the chromium in this way was feasible in terms of achieving a uniform slag composition. This is discussed further in Section 4.4.

Where possible, slags were sampled before and after the experiments. In all of the oxidation state dependence experiments, initial and final samples were analysed. In experiments where sequential additions of iron or chromium were made to a slag, it was only possible to analyse the initial and final compositions and unfortunately not the intermediate compositions. Therefore the initial slags L0, I0, H0, Cr0 were analysed, and then after all the FeO_x or Cr_2O_3 additions, slags L20, I30, H30 and Cr8 were analysed.

The calcium ferrite slag (Slag CF) was prepared using dried calcium carbonate and haematite powders. The components were mixed in the desired proportions and the mixture was then pre-melted in a Pt crucible at 1350°C and quenched on a steel launder. The slag was crushed in a ring mill, sampled and was ready for use.

3.6. Deep cell setup

This setup employed the standard two-electrode technique. It was used for conductivity measurements of slags containing 30wt% FeO_x or less and where the oxygen potential was not being varied. It was also used for the testwork on the chromium containing slags. Slags containing greater than 30wt% FeO_x were considered to be too conductive and the external resistance of the circuit would contribute too much to the measured resistance. Temperatures were typically varied from 1400 to 1550 °C at 25 °C intervals such that sufficient data were obtained to apply the Arrhenius relation. This setup was used for all the T and H measurements (refer to Table 3). For some slags the frequency dependence of the conductivity (F measurements in Table 3) was also measured. The reason for the interest in the frequency dependence of the conductivity was to identify the frequency range in which measurements

should be made. Electrochemical Impedance Spectroscopy (EIS) was used once to compare with the frequency response of the RCL meter measurements.

3.6.1. Crucible

A platinum crucible was used in this setup. At the temperatures of interest (1400-1550°C), the platinum crucible was reasonably inert to attack from the slags (except for minimal alloying of iron with Pt in iron containing slags). The crucible was egg cup shaped and approximately 40mm in diameter (top) and 35mm high. The volume of the crucible was approximately 25 cm^3 and usually 45 to 50g of slag was used (giving a slag depth of approximately 25mm).

In one set of experiments on the chromium containing slags, measurements were made in magnesia crucibles but there was excessive dissolution of MgO from the crucibles at the higher temperatures (> 1500 °C).

In the set of measurements on the chromium containing slags at very high temperatures, molybdenum crucibles were required. The crucibles were fabricated from 40mm Mo rod. Therefore the crucibles had an OD of 40mm, ID of 36mm and a height of 40mm.

3.6.2. Calibration

Calibrations of the conductivity cell were carried out with potassium chloride solutions of 0.01 ± 0.0006 N, 0.1 ± 0.004N and 1 ± 0.045N concentrations. The reasons for the choice of potassium chloride standards were given in the section 2.1. The various concentrations of solutions were made up using the correct quantities of AR grade potassium chloride salt (Ajax Chemicals, 99.8% purity) dissolved in distilled water in 250ml A-grade volumetric flasks (± 0.15ml). The potassium chloride salt was weighed using a Mettler AE200 scale which had an accuracy of ± 0.1 mg. The temperatures of the KCl solutions were measured before the calibration so that the conductivity was known from literature values. The conductivity values for the KCl solutions were the Kohlrausch standards (1898) as reported by Dobos (1975). Volumes of approximately 30 ml of KCl solution were placed in the Pt crucible such that the liquid depth was similar to the slag depth, and the cell constant was independent of the liquid depth.

For convenience calibrations were usually carried out on the laboratory bench. The electrodes were held in a fixed position by a clamp attached to a stand. The electrode spacing was maintained at 10mm. The crucible was supported on a platform which could be jacked up and down very precisely. The height of the platform was measured using vernier calipers to an accuracy of 0.01mm. The crucible containing the liquid was raised until contact with the electrodes was made as observed by a sudden large decrease in the measured resistance and a stable resistance reading. The height of the platform was noted and then the platform was raised until the electrodes were immersed to the desired level. The resistance was noted and sometimes frequency scans were carried out. Initially measurements were taken at depths of 4, 8 and 12mm, however in later calibrations and experiments, measurements were only taken at immersion depths of 8mm.

The resistances measured for each of the three solutions at each depth were recorded. The external resistance of the leads and electrodes was determined beforehand by joining the electrodes at the tips and taking a resistance measurement. The external resistance at room temperature was around 1.42Ω. A calibration plot was then generated by plotting the natural logarithm of known conductivities of the KCL solutions versus the natural logarithm of the resistances of the solutions. The following relationship arose:

Equation 21: $\ln \kappa_{KCl} = -\ln(R_{measured} - R_{external}) - \ln G$

As was found by Riebling and Logel (1965), the cell constant was dependent on the value of the resistance measured. This meant that although the plot of ln κ vs ln (R_{meas}-R_{ext}) should have a slope of −1 and the intercept should be ln G, the slope varied slightly from −1. In most cases the slope was around −0.98 to -1.02.

A typical calibration plot is given in Figure 46 below for a calibration in a Pt crucible:

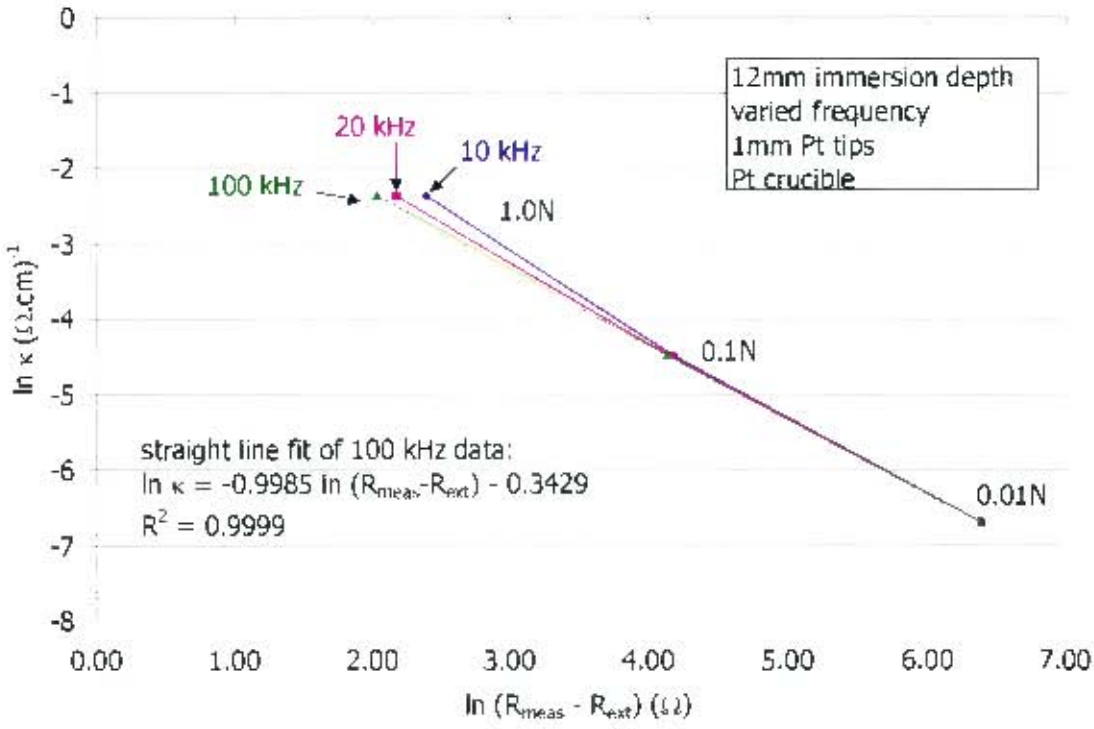

Figure 46: Typical calibration plot and effect of frequency on calibration with KCl solutions

It is clear from the above graph that the resistances of the more concentrated KCl solutions (>0.1N) were dependent on the measuring frequencies. Riebling and Logel (1965) attributed this dependence to polarisation and / or ion pair phenomena. At a measurement frequency of 100 kHz, it appeared that 1N KCl solution was independent of the frequency. This was in fair agreement with Segers *et al.* (1978) who found that for KCl solutions, f_0 occurred at frequencies around 150 kHz. Therefore all calibrations were carried out at a frequency of 100 kHz. Typical values for the cell constant at various depths and 100 kHz are given in the table below:

Table 4: Variation of cell constants with depth of immersion

Depth (mm)	Slope	Intercept	R^2	Cell constant (cm^{-1})
4	-1.008	0.573	0.99976	1.77
8	-0.998	-0.015	0.99995	0.99
12	-0.999	-0.343	0.99995	0.71

The calibration of the electrodes was carried out periodically, usually when the electrode tips were replaced. The change in the calibration over time and different electrode tips was not large but is reflected in Table 5:

Table 5: Change in calibration data with time

Date	Slope	Intercept	Cell constant (cm^{-1})
Aug 2001	-0.998	-0.015	0.99
Nov 2001	-1.010	0.052	1.05
Apr 2002	-1.013	0.024	1.02
average	-1.007	0.020	1.02
standard deviation	0.008	0.034	0.034

When the above calibration data were applied to the same measured resistance (worst case scenario where the measured resistance is small), the calculated electrical conductivities were within approximately 4%. The fact that the values for the cell constant were very similar for separate measurements indicated the repeatability of the calibration technique.

Application of cell calibration data to measurement of slag conductivity

The calibration was applied to the slag conductivity measurements by substituting the measured resistance into the formula:

Equation 22: $\kappa_{slag} = e^{slope \cdot \ln(R_{measured} - R_{external}) + intercept}$

The external resistance of the electrodes was measured from room temperature up to the temperatures at which the slag conductivity measurements were being made. The electrodes were short-circuited by twisting their ends together and measuring the resultant resistance using the RCL meter. The external resistance increased with temperature as expected and from 1400 – 1500 °C varied in the range 2.4 – 2.6 Ω. The change in the external resistance with temperature is shown in Appendix B4.

In order to obtain some assurance that the experimental technique was accurate for measurements at high temperatures on slags, measurements were made on three slags of the same compositions as Winterhager *et al.* (1966) (slags 55, 56 and 57). For ease of reference the compositions of the slags are given below:

Table 6: Composition of Winterhager *et al.* (1966) slags 55, 56 and 57

Composition (wt%)	Slag		
	55	56	57
Al_2O_3	4.8	4.6	4.4
CaO	33.7	32.3	30.7
MgO	13.4	16.9	21.1
SiO_2	48.1	46.2	43.8
Total	100	100	100

The results of these comparisons are given below:

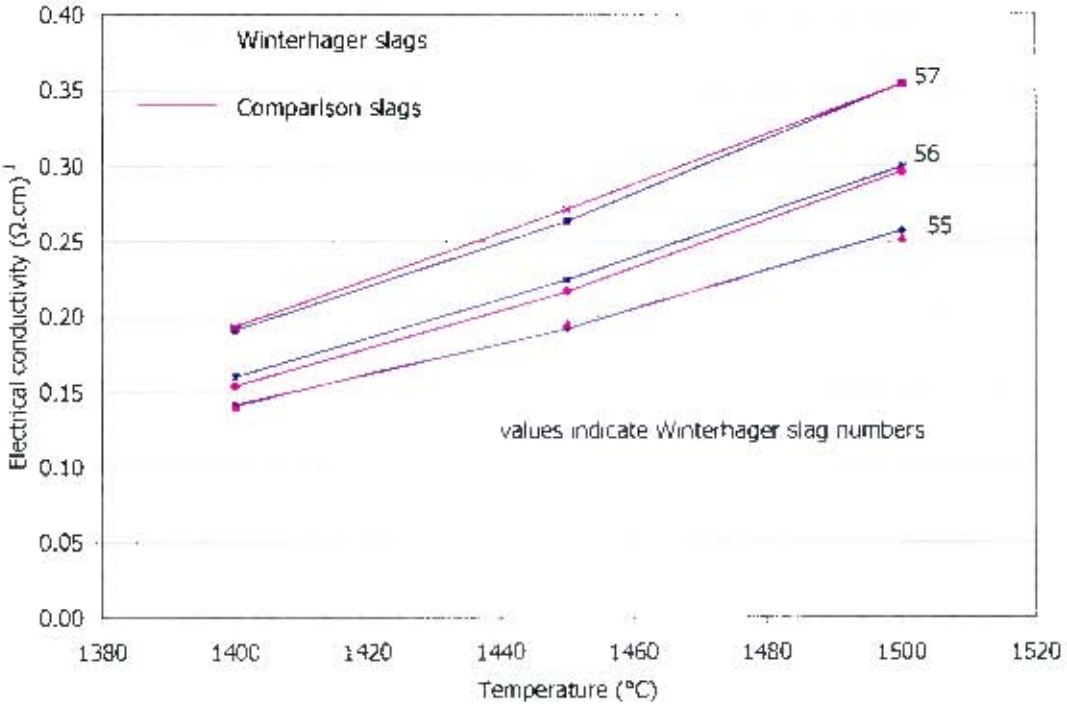

Figure 47: Comparison of results with Winterhager *et al.* (1966) measurements

The results measured were in very good agreement with those of Winterhager *et al.*. The difference in the values ranged from 0.05 to 4%. Thus the calibration of the conductivity cell and use of the cell at high temperature was deemed acceptable.

3.6.3. Experimental procedure

The slag to be tested was prepared as described in section 3.5. Fifty grams of the milled slag were weighed into the Pt crucible. The crucible was placed on top of the pedestal. The pedestal and the associated bottom end plate were then securely bolted onto the bottom end cap. The pedestal was then connected up to the motion actuator. The pedestal and crucible were raised to near the bottom of the hot zone using the motion actuator (but not high enough to touch the electrodes).

The electrodes and associated top end plate and thermocouple were then bolted onto the top end cap. The electrodes were connected to the Kelvin grips of the RCL meter and the

thermocouple connection was joined. By means of the sight glass it was ensured that the electrodes and the crucible were properly aligned. The furnace was now sealed and ready to be heated up.

The ramp rate during the heat-up was usually 360°C/hour. This meant that it took over four hours to reach the starting measuring temperature of around 1400°C inside the tube. To reduce the time for heat up, the furnace was often heated overnight to 800 °C and then the following morning it would be ramped up to the starting measuring temperature.

For slags containing FeO_x an inert atmosphere was required so that the iron remained in its reduced state (iron oxide additions were made as wüstite in all of these measurements). Nitrogen was used for this purpose. Where an inert atmosphere was required, often the slag would only be placed in the furnace (at 800 °C) in the morning, the nitrogen was then applied and then the pedestal was slowly raised up to the high temperature zone.

Once the furnace was at temperature (usually 1400 °C inside the tube although sometimes higher depending on the liquidus temperature of the slag), the RCL meter was switched on and allowed to warm up for a couple of minutes. The crucible was then raised very slowly while the RCL meter was being monitored. The resistance of the open circuit electrodes fluctuated between 200-400 kΩ, however when the electrode tips were 1-2mm above the slag surface, the resistance would decrease and fluctuate around 100-150 kΩ (similar observations were noted by Bockris *et al.* (1952)). When the electrodes touched the slag, the reading on the RCL meter would drop dramatically (usually to a value in tens of Ω) and the reading would be stable. The point of contact could be observed repeatedly to within 0.1mm. The electrodes were then immersed to the desired depth and the RCL meter was then controlled by a laptop computer connected via the RS-232 cable.

Initially experiments were carried out at immersion depths of 4, 8 and 12 mm, however by doing this, one was not able to obtain an online measurement of the conductivity. Most of the later measurements were conducted only at a depth of 8mm and the electrodes could be left in the slag and the resistance monitored continuously for the duration of an experiment. This facilitated easy observations of a steady equilibrium condition being established. For example, if the temperature was increased, one saw the resistance drop over a couple of minutes and then stabilise at a constant resistance. The controlling software allowed measurements at various time intervals. Usually measurements were recorded every 30 seconds.

Once the resistance had stabilised after the electrodes had been immersed, the temperature setpoint of the furnace was raised to give a 25 °C rise in temperature in the tube. The measurements recorded by the computer would then be observed to see when equilibrium was reached and the temperature would be raised again. This was repeated until the temperature range up to 1550 °C had been measured. In several cases (where time allowed) measurements were also made while cooling the slag down at set intervals. From these results it was possible to calculate the activation energy of the slag according to the Arrhenius relationship. The results of a typical experimental run for slag H0 were as follows:

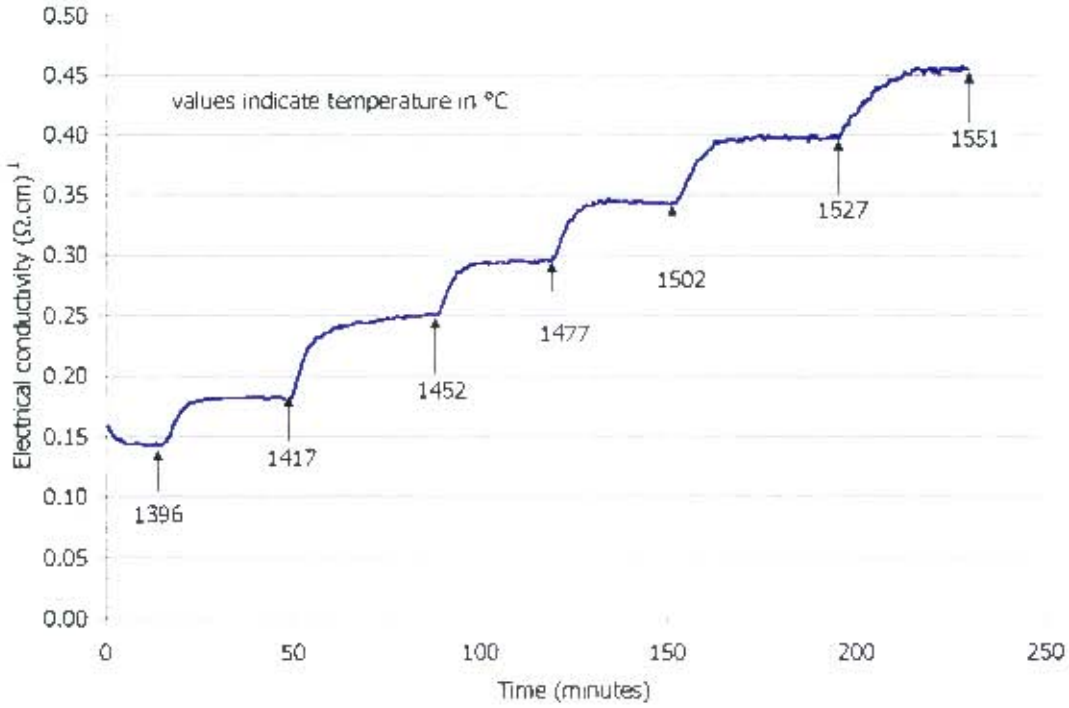

Figure 48: Temperature dependence of slag H0

With a couple of slags the electrodes were left immersed in the slag and the furnace was cooled down to 800 °C overnight. The frozen slag was then heated up the next morning while taking resistance measurements at certain temperature intervals. This enabled one to obtain the heat-up curve for the slag and gave information concerning melting of phases until the liquidus temperature was reached.

3.6.4. Frequency dependence of slag conductivity

Using the experimental setup described above, the frequency dependence of a slag was measured using both the RCL meter and the electrochemical impedance spectrometer. The slag tested was the high basicity slag containing no iron: H0. The EIS measurements were made at 1500°C and an applied voltage amplitude of 100 mV. The measurements by the RCL meter were made at 1550 °C. There was no specific reason for carrying out the measurements at different temperatures. The following three graphs show the results of this experiment:

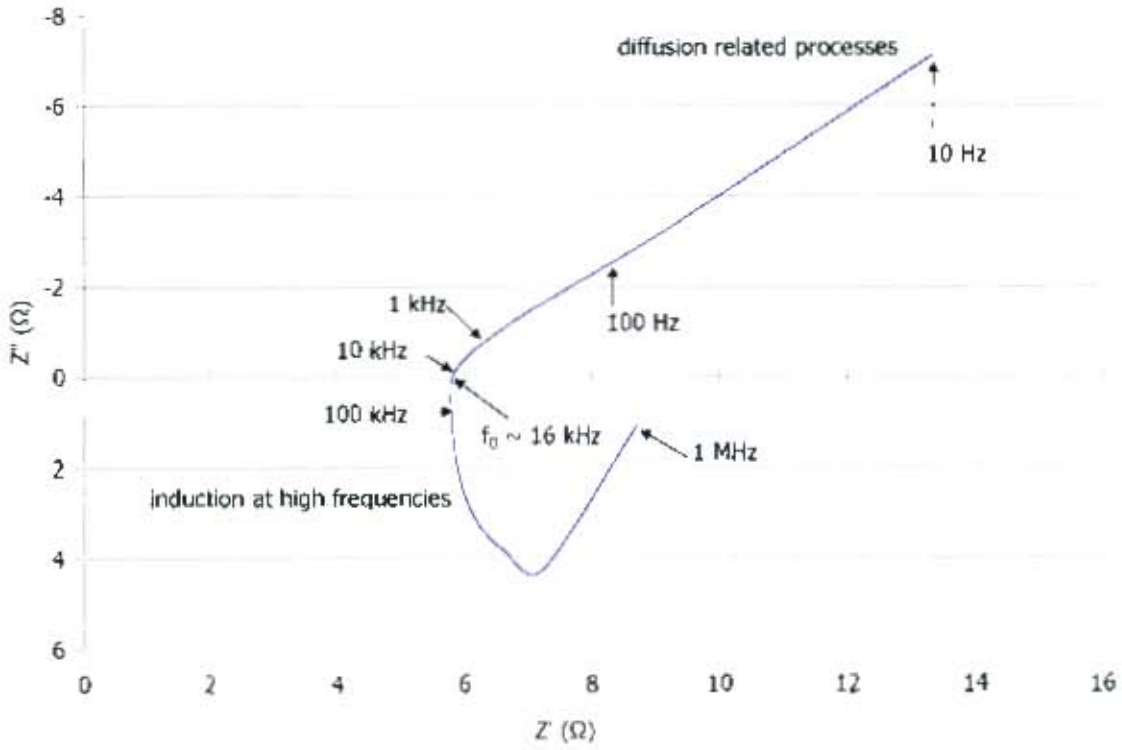

Figure 49: EIS measurements on high basicity slag with 0% FeO_x at 1500 °C

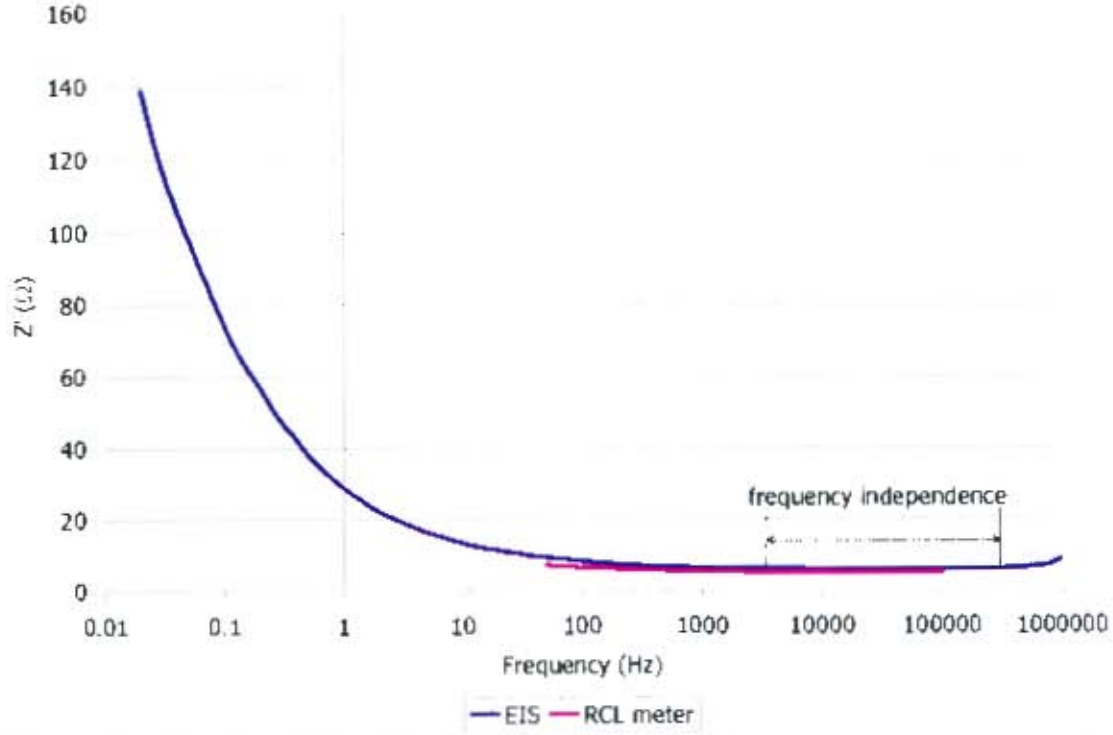

Figure 50: Influence of frequency on real part of complex impedance for high basicity slag with 0% FeO,

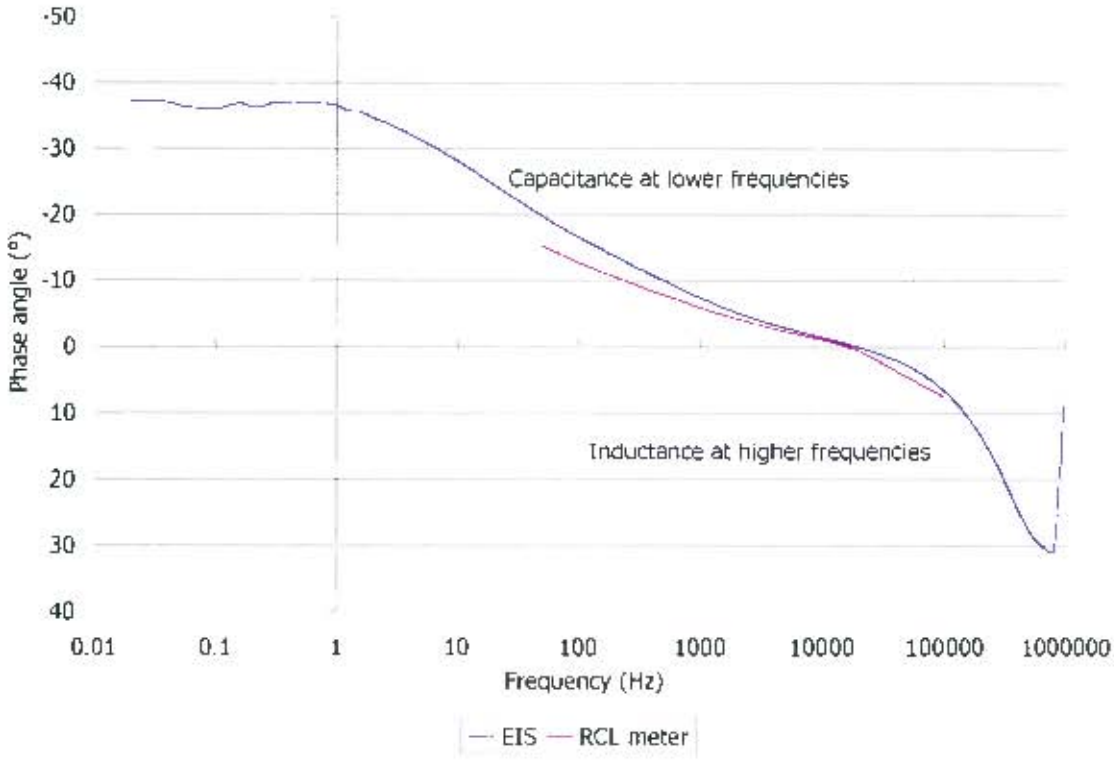

Figure 51: Influence of frequency on phase angle measured impedance of slag H0

The complex impedance plot presented in Figure 49 had the same basic features as a graph presented by Fontana *et al.* (1985) who made EIS measurements on a CaO – MnO – SiO_2 slag at 1398 °C. The features at low frequency are characteristic of a diffusion controlled process. The imaginary part of the impedance then decreases to 0 as the frequency increases to approximately 16 kHz (referred to as f_0 or the resonant frequency). The real part of the complex impedance (Z') at f_0 is attributed to the resistance of the slag only, that is at f_0 $Z' = R_{slag}$. Above 16 kHz, inductance of the leads starts occurring, however Z' remains constant up to approximately 200 kHz. This can be seen in Figure 50 and Figure 51 where from approximately 8 kHz to 200 kHz, Z' varies by less than 1%, but Z'' changes from negative to positive indicating the change from capacitance to inductance respectively. This is fortunate in that one can make measurements at higher frequencies and the inductance of the leads and electrodes contribute very little to Z'. The modulus of the impedance does change though. Macdonald and Johnson (1987, pp. 212-213) provides an explanation for this situation.

Figure 50 and Figure 51 are also used to compare the measurements by the RCL meter with those of the spectrometer. In Figure 50, it should be borne in mind that the slight difference in magnitude of Z' is due to the higher temperature of measurements with the RCL meter (1550 °C as opposed to 1500 °C). It was found that the temperature did not affect the value of f_0 as can be seen in Figure 51. Unfortunately it was not possible for the RCL meter to measure at frequencies between 20 kHz and 100 kHz which gave rise to the straight line from f_0 to 100 kHz and an apparent deviation from the curve by the EIS. (The specific model of RCL meter had this limitation as noted in Section 3.3.1)

As the measured resistance was reasonably independent of the frequency from 8 kHz to 200 kHz, it seemed possible that one could measure the resistance at any frequency within the

frequency independent range. It would therefore not be required to determine the frequency response of each slag before measurements were made to determine the resonant frequency. In order to check that this would not bring about large errors, the frequency response of the high basicity slags was examined. The following two graphs show the results:

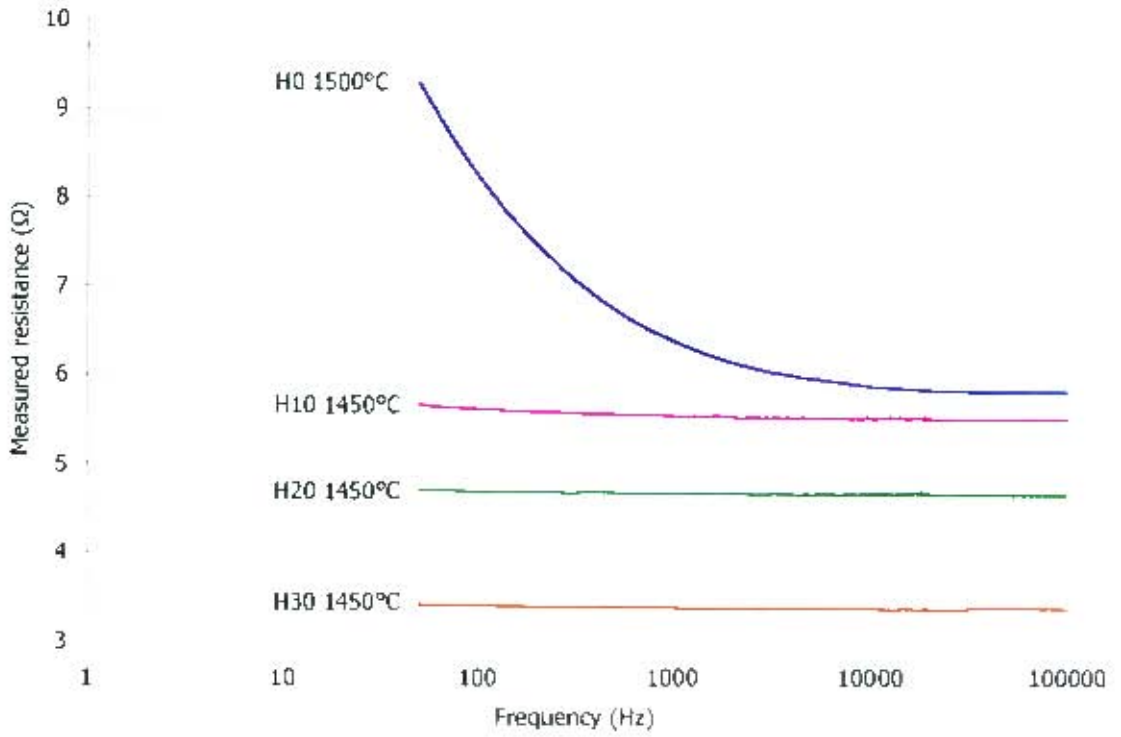

Figure 52: Frequency response of the high basicity slags – real part

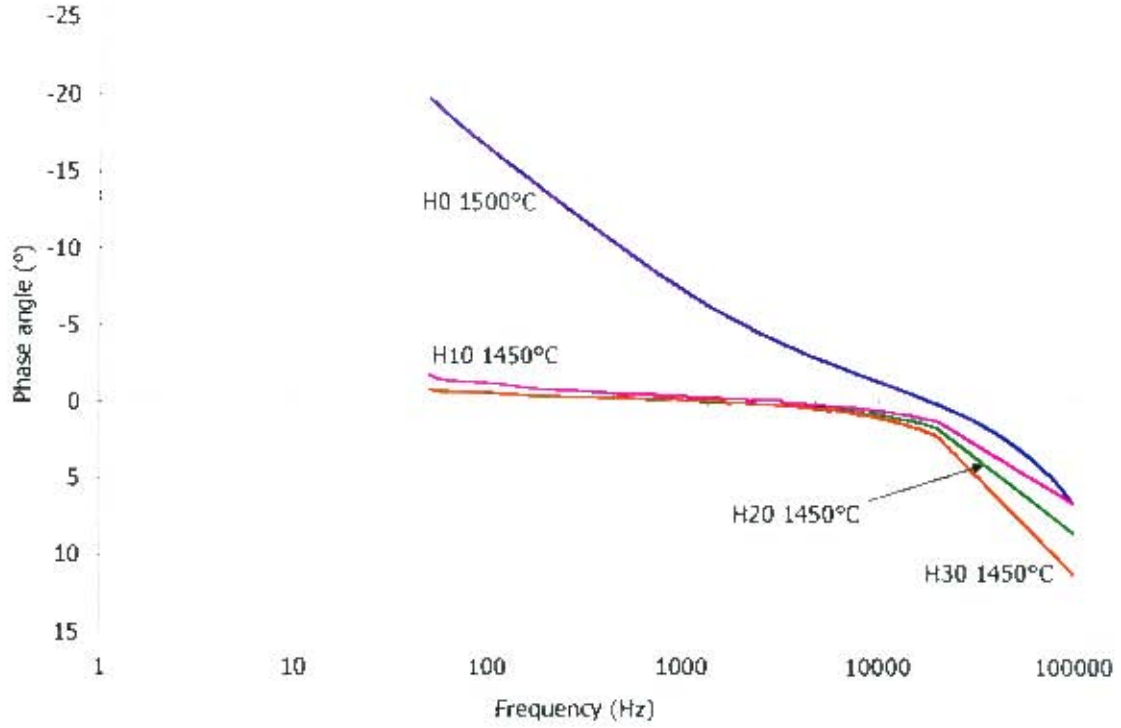

Figure 53: Frequency response of the high basicity slags – phase angle

From Figure 52 it is evident that the real part of the impedance remained frequency independent from approximately 1 kHz to 100 kHz as the iron content of the slags was raised. However, the phase angle varied with frequency and iron content as can be seen in Figure 53. The phase angle has been used as an indication of the imaginary part; where the phase angle is negative, the imaginary part is capacitive; where the phase angle is positive, the imaginary part is inductive; the resonant frequency occurs where the phase angle is zero. It was concluded that the resistance could be measured at a frequency of 100 kHz and the difference between the resistances measured at f_0 and 100 kHz would be less than 0.6%.

3.6.5. Error analysis

In order to obtain an estimate of the error associated with the conductivity measurements, the factors which affected the accuracy of the results were considered. It was necessary to examine the effect of both the calibration at room temperature and the actual measurements at high temperature.

In the calibration of the conductivity cell, errors could have arisen as a result of the following: the preparation of the potassium chloride solutions, the use of the Kohlrausch standard conductivity values, the temperature at which the calibrations were carried out, the electrode spacing, the immersion depth, the alignment of the electrodes relative to the crucible, the measuring frequency, the instrumental error in the measured resistance and the error in measuring the resistance of the shorted electrodes.

As the calibrations with the KCl solutions were carried out under well controlled conditions, the errors which could arise from the cell geometry (electrode spacing, immersion depth and electrode alignment) were minimised. The cell geometry error in the cell constant was estimated from the theoretical cell constant equation given by Attwood (1949) for two infinite parallel wires:

Equation 23:
$$G = \frac{\ln\left[\frac{S}{D} + \sqrt{\left(\frac{S}{D}\right)^2 - 1}\right]}{\pi.\lambda}$$

where G is the cell constant cm^{-1}
S is the electrode spacing cm
D is the electrode diameter cm
λ is the immersion depth cm

This expression was used by Downing and Urban (1966), Persson and Treilhard (1973), Fontana *et al.* (1984) and Eric *et al.* (1991). The expression gives a reasonable estimate of the cell constant (~1.2 cm^{-1} as opposed to ~1 cm^{-1}) and it is therefore assumed that performing error propagation using the expression will be appropriate. The relative error in the cell constant owing to geometric factors is calculated to be around 2% under the controlled conditions for the calibration (assuming the following errors: S: 1 ± 0.02 cm, D: 0.1 ± 0.005 cm and λ: 0.8 ± 0.005 cm).

The error in the cell constant due to the concentration, temperature and hence known conductivity of the KCl solutions was estimated to be approximately 6%. This was calculated by considering the uncertainty in the preparation of the solutions, the uncertainty in the Kohlrausch values and the temperature of the solutions at time of measurement. The instrumental error was also considered.

In measurements on the slags at high temperature, sources of error included: the temperature of the slag, the electrode spacing, the immersion depth, the alignment of the electrodes, the frequency of measurement, the instrumental error and the error in the external resistance.

Related to the possible error in the immersion depth was the fact that the electrodes were left in the melt so that an online measurement was available. This meant that as the temperature was raised the thermal expansions of the melt, crucible and electrodes were not taken into account in terms of the immersion depth. Bockris *et al.* (1948) found that over a temperature range of 1200-1700 °C, the melt height changed by 1.8mm (although this is dependent on the overall slag height). This equates to 0.54mm over a 150°C range. Therefore to take this into account, the expression for the cell constant in Equation 23 was applied to the cell geometry for the melts at high temperature. This also included the greater uncertainty in the alignment of the electrodes and the crucible in the furnace and the possibility of the electrode spacing changing slightly. This introduces a further relative error of approximately 7% in the cell constant (assuming the following errors: S: 1 ± 0.05 cm, D: 0.1 ± 0.005 cm and λ: 0.8 ± 0.05 cm)

Assuming that all the relative errors in the cell constant are additive, the maximum error in measuring the conductivity of the slags from 1400-1550°C is expected to be around 15% (2% for geometric factors in calibration, 6% in the use of the calibration solutions and 7% due to geometric factors in the high temperature measurement). This is the worst case scenario and the error is expected to be significantly lower than that. The reason that the error is expected to be lower than 15% is because the experiments were carried out under well controlled conditions, therefore much of the error in terms of the cell geometry falls away. The error in conductivity measurements reported by other authors is generally estimated to be around 5-8%.

3.6.6. Reproducibility of experiments

In several experiments repeat runs were carried out in order to show reproducibility in measuring the conductivity using the deep cell technique. The duration of experiments prevented multiple repeats from being performed for every experiment. However, the following examples show that the measured results are generally reproducible within 10-15%.

Repeat measurements were performed on slag Cr2 and slag L0. The repeat experiments were carried out independently of the initial experiments, therefore fresh slag was used and the electrodes were set up prior to each experiment. The results of these experiments are shown in Figure 54 and Figure 55.

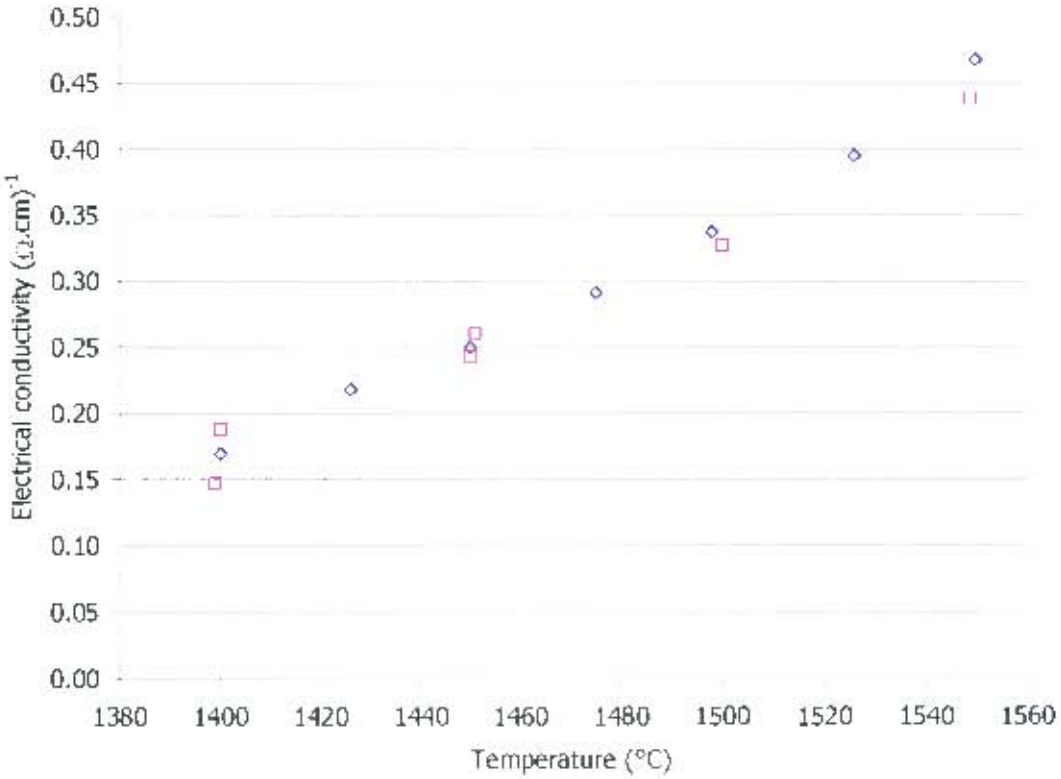

Figure 54: Reproducibility of conductivity measurements on slag Cr2. Approximate slag composition (wt%): Al_2O_3: 4.9, CaO: 4.9, Cr_2O_3: 2, FeO_x: 19.6, MgO: 19.6, SiO_2: 49.

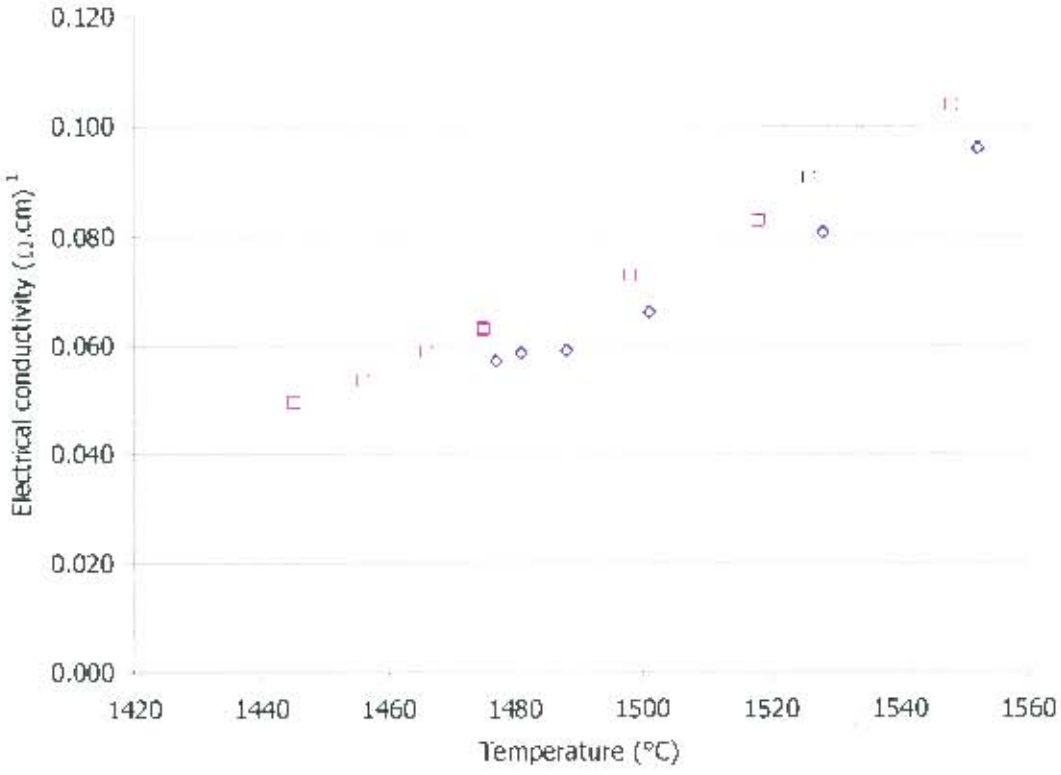

Figure 55: Reproducibility of conductivity measurements on slag L0. Approximate slag composition (wt%): Al_2O_3: 6.3, CaO: 6.3, MgO: 25, SiO_2: 62.5.

As can be seen in both graphs, the agreement between the original and repeated runs was good. In order to give some numerical comparison of the agreement, the relative standard deviation for the measurements on slag Cr2 at discrete temperatures was around 4%. The relative standard deviation for the measurements on slag L0 at discrete temperatures was around 8%.

The errors in the conductivity measurements are in a range found to be acceptable in the literature for the two-electrode technique (for example, see Riebling and Logel (1965) - 5% and Ossin *et al.* (1971) – 10%)

3.7. Shallow cell setup

The shallow cell setup was used to test the oxidation state dependence of the slag conductivity. This setup was used for slags containing significant amounts of iron. The principle of the setup was that slags at either a reduced or oxidised state would be sequentially oxidised or reduced such that the slag conductivity could be measured over a broad range of ferric - ferrous contents. The oxidation state dependence measurements of the slag conductivity are referred to as O measurements in Table 3.

For conductivity measurements where the oxygen potential was being varied, the major concern was how long it would take the slag to come to equilibrium at a particular oxygen partial pressure. The literature review provided some information as to equilibration times. Engell and Vygen (1968) found that equilibration times of 4-6 hours at each oxidation state at 1600°C were necessary for a setup very similar to the one described in section 3.6 above. Bearing in mind the large number of measurements to be taken in this investigation, the lower slag temperatures and the time constraints, it was not feasible to use the setup described in section 3.6 above. Therefore alternatives were investigated.

It was necessary to have good slag-gas contact so that equilibrium could be reached in reasonable amounts of time and it was also desired that the measurements be as accurate as possible. Therefore it was postulated that by blowing the oxidising / reducing gas directly into the melt by means of a lance would give good stirring and slag-gas contact and reduce equilibration times. However, a crucible with tall walls was required such that when gas was bubbled through the melt, the slag would not spill over the side of the crucible and damage the furnace. This necessitated the use of tall MgO crucibles (40mm ID and 100mm high). Gas was bubbled directly into the melt through an alumina lance. Once gas had been bubbled for a time, the lance would be removed from the furnace and the electrodes would be placed in the furnace. A measurement would be taken and then the electrodes would be removed and the lance placed back in the furnace. The bubbling of gas would then be resumed. This setup was rejected after several attempts for a number of reasons:

- One could not easily tell when equilibrium was reached due to the intermittent measurements.
- The swapping of the lance and the electrodes brought about thermal shock of both the lance and the electrode sheaths. The swapping also made it more likely that the electrode spacing could be changed in the process of removing the electrodes from and placing them in the furnace.

- Significant amounts of alumina from the lance and magnesia from the crucible dissolved into the slag and changed the slag chemistry.

The next alternative was to use a smaller amount of slag and therefore not need to blow gas into the melt with a lance as the normal gas flow through the furnace was sufficient. The use of metallic crucibles was not feasible because one would obtain significant current flow through the crucible walls. Therefore a non-metallic, non-reactive crucible was required. As most of the slags being tested contained around 20wt% MgO, magnesia crucibles were deemed suitable. A technique similar to that of Pastukhov *et al.* (1966) was envisaged where a boat type crucible was used. Egg-cup shaped MgO crucibles were available and these were used for the measurements on all the oxidation state dependent silicate slags. The calcium ferrite type slag was tested in an MgO boat.

3.7.1. Crucibles

3.7.1.1 Silicate slags

The egg-cup shaped MgO crucibles had a height of 47mm and diameter of 35mm. Usually the height of the crucibles was reduced to 20-25mm to reduce restrictions to the flow of gas to the slag-gas interface. In these experiments approximately 3.5g of slag was used. The slag depth was approximately 3mm and with the large slag-gas contact surface area, equilibration times were reduced to less than one hour. Increase of the MgO content in the slag varied from 3-8 wt% with more MgO crucible dissolution as the iron content increased. This was borne in mind when analysing results.

3.7.1.2 Calcium ferrite slag

As the conductivity of the calcium ferrite type slag was very high, magnesia boat crucibles were used. Using the boat crucible enabled a wider electrode spacing (25mm as opposed to 10mm, see Figure 43) and a narrower current path and hence the cell constant was high. This was important to ensure that the overall measured resistance was not dominated by the external resistance of the circuit. Once again the benefit of using a small amount of slag was required for reasonable equilibration times. Two grams of slag were used in the experiments which gave rise to a liquid depth of approximately 2.5mm. The boat dimensions were 50mm long, 8mm wide and 6mm high. The amount of MgO that dissolved into the slag was from 1 to 2%.

3.7.2. Calibration

3.7.2.1 Silicate slags

The same KCl solutions and laboratory bench equipment were used in the calibration of this setup (see Section 3.6.2). Initially, it was decided that a volume of $1cm^3$ of solution would be used in the calibration. The reason for this choice was that the slag density was estimated to be around 3.5 g/cm^3, therefore a calibration with 1 cm^3 of KCl solutions would result in a liquid depth similar to that of the slag. The volume of solution was measured by means of an A-grade pipette of $1cm^3$ volume and placed in the crucible. The cell constant was then determined by measuring the resistances of the various concentrations of KCl solutions at an

immersion depth of 2mm. The electrode spacing in this setup was also 10mm. As with the previous setup, a calibration plot was drawn up and cell constant determined. A cell constant value of approximately 4.5 cm^{-1} was obtained.

However, on closer examination of the density data for the silicate slags, it was found that the density varied significantly with the iron content of the slag and ranged from 2.7 to 3.3 g/cm^3. (The density values of the iron-free master slags were estimated from the Slag Atlas (1995) and then corrected for the amount of iron added). As 3.5g of slag was used in the experiments, the volume of slag in the crucible was then more than 1 cm^3 (typically 1.1-1.4 cm^3 with lower volumes at higher iron oxide contents). Therefore it was necessary to apply a correction to the calibration. This was done by carrying out a second set of calibrations using 1.5 cm^3 of KCl solutions. A 1 cm^3 pipette and a 0.5 cm^3 pipette were used to measure the volume of solution accurately. A second calibration plot was drawn up and the cell constant determined. The cell constant was approximately 3.5 cm^{-1} for a 2mm immersion depth. Then depending on the calculated volume that 3.5g of a particular slag would fill, an interpolation of the two cell constants provided the calibration data for the intermediate volume. The calibration slopes and intercepts are noted for each slag in the Results chapter.

3.7.2.2 Calcium ferrite slag

Here also the same solutions and equipment were used. The amount of KCl solution used in the calibration was 0.5 cm^3. The reason for this volume was that 2g of slag was used in the experiment and the density of the calcium ferrite slag was estimated to be around 4 g/cm^3 at 1300 °C (estimated from the Slag Atlas (1995)).

The calibration was carried out in much the same way as in section 3.6.2 with a calibration plot being generated. The immersion depth used was 1mm. The cell constant was approximately 17 cm^{-1}.

3.7.3. Experimental procedure

The experimental procedure for this setup was very similar to the procedure explained in Section 3.6.3. The major difference was that instead of varying the temperature, the oxygen partial pressure in the furnace was varied while the temperature was held constant at 1450°C (1300°C for the calcium ferrite slag).

In most cases, the iron was added to the master silicate slags in the form of haematite. Therefore the furnace was heated up in a normal air atmosphere to 1450 °C (1300 °C for the calcium ferrite slag). The crucible was raised until contact was made between the slag and the electrodes, as observed by a sharp decrease in the resistance and a stable reading. Then the crucible was raised by 2mm to the correct immersion depth (or 1mm in the case of the calcium ferrite slag). The logging of the measurements by the computer was then started. Readings were taken at 30 second intervals.

It usually only took around 20 minutes for the slag to come to equilibrium in air. Once equilibrium was reached, the gas atmosphere would be changed to a CO_2-CO mixture at a particular ratio (the gas mixture was prepared and mixed as specified in section 3.4.). The resistance readings were then monitored until a constant resistance reading was obtained. This was assumed to indicate that equilibrium at that partial pressure of oxygen had been

reached. The CO_2/CO ratio was then changed again and the resistance measurements were repeated. In this way, the gas atmosphere was controlled at the following ratios (in order): 80, 20, 10, 5, 2 and 1 (slightly different ratios of 70, 22.5, 7, 2.25 and 0.7 were applied to the calcium ferrite slag). In some cases where time permitted at the end of the experiment, a mixture of CO and N_2 was applied to the furnace. In these cases the FeO_x would be reduced to iron and there was a large increase in the conductivity.

A typical profile throughout an oxidation state run is provided in Figure 56 for slag H40:

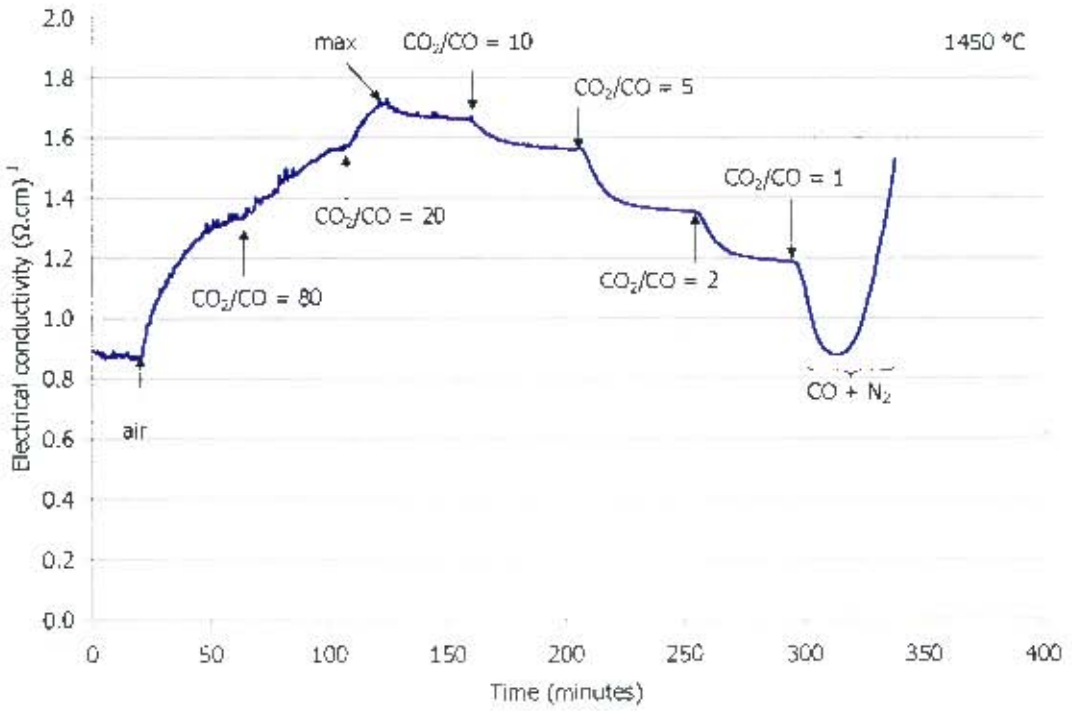

Figure 56: Oxidation state dependence of slag H40 at 1450 °C

A number of features should be noted from the figure above. Measurements were made every 30 seconds but the time has been expressed in minutes. The arrows and labels indicate where it was estimated that equilibrium had been reached for each CO_2/CO ratio. Thereafter the gas mixture was changed to the next ratio of CO_2/CO and allowed to equilibrate. The experiment was started in air and then reduced at various CO_2/CO ratios.

Determination of equilibrium

It was considered important to give a clearer explanation of exactly how equilbrium conditions were determined. It was found that when changing from one oxidation state to another, the approximate time for equilibration was usually between 30 to 60 minutes. Therefore, after 30 minutes, the measured resistances would be observed, and based on the rate of change of the resistance over the previous five minutes, a decision would be made as to whether the system was at equilibrium. In order to illustrate this point rate of change in $R_{measured}$ during the experiment on slag H40 was calculated as a moving average over five minutes for the duration of the experiment. In essence, a first derivative (denoted $\Delta R/\Delta t$ as actual changes have been calculated) of the function of R vs time has been calculated and

where ($\Delta R/\Delta t$) = 0 for a period of about 5 minutes, equilibrium was considered to have been achieved.

Figure 57 below shows the average rate of change for the experimental data on Slag H40 (compare with Figure 56).

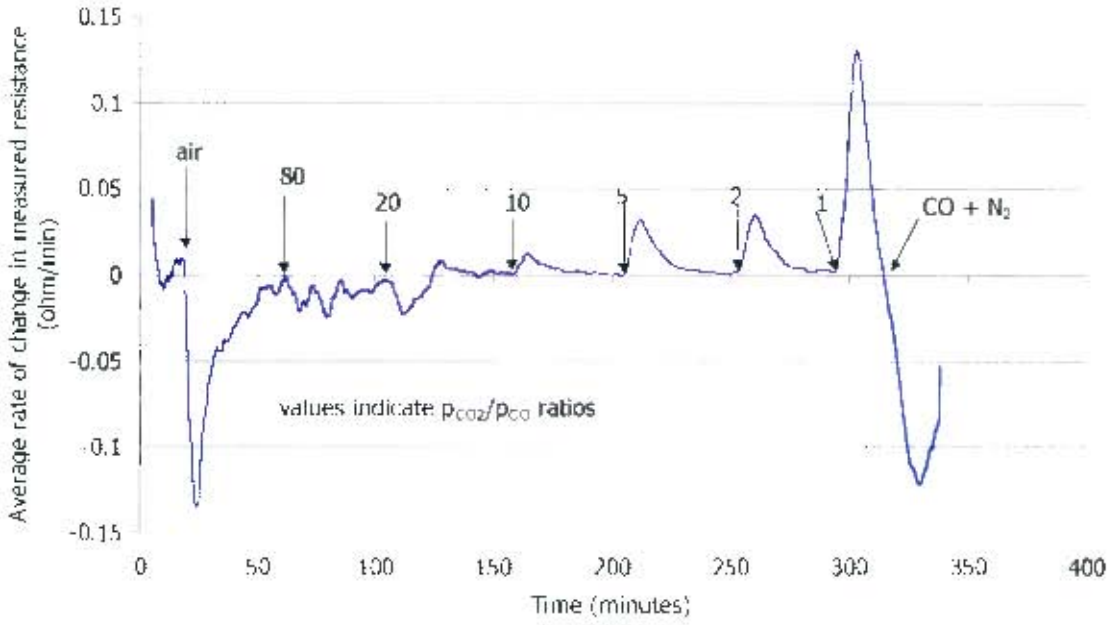

Figure 57: Slag H40: Average rate of change in measured resistance with time (5 point moving average)

From Figure 57 it can be seen that the average rate of change in the measured resistance approaches zero when the slag is in equilibrium with the gas for a given p_{CO_2}/p_{CO} ratio. The average rate of change in the measured resistance can be used to estimate how close the conductivity measurement was to equilibrium. Data is shown in Table 7 indicating the measured resistance at the point of equilibrium, the average rate of change in the resistance measured, the conductivity calculated at the equilibrium resistance and how much the conductivity would have changed if left for an additional 30 minutes at each oxidation state.

Table 7: Equilibrium data calculated from oxidation state experiment on Slag H40 based on average rate of change in measured resistance with time

p_{CO_2}/p_{CO}	Time	$R_{measured}$	Average ($\Delta R/\Delta t$)	κ_{eq}	κ_{30}	%change
ratio	minutes	Ω	(Ω/min)	$(\Omega.cm)^{-1}$	$(\Omega.cm)^{-1}$	
air	19	7.61	0.000	0.865	0.864	-0.2
80	63	5.89	-0.001	1.328	1.341	1.0
20	106	5.41	-0.004	1.556	1.620	4.1
10	158	5.24	0.000	1.658	1.653	-0.3
5	203	5.41	0.000	1.558	1.550	-0.5
2	254	5.83	0.002	1.350	1.323	-2.0
1	295	6.28	0.003	1.185	1.156	-2.5
$CO + N_2$	315	7.54	0.001	0.877	0.874	-0.4

From the data presented in Table 7 it is apparent that most of the equilibrium conductivity measurements were very good (<3 change% if left for 30 minutes), with the exception of the one at a p_{CO2}/p_{CO} ratio of 20 where the conductivity was likely to be higher by 4.1%. This magnitude of change has a relatively minor effect on the variation of conductivity vs the ferric fraction: see Figure 57a.

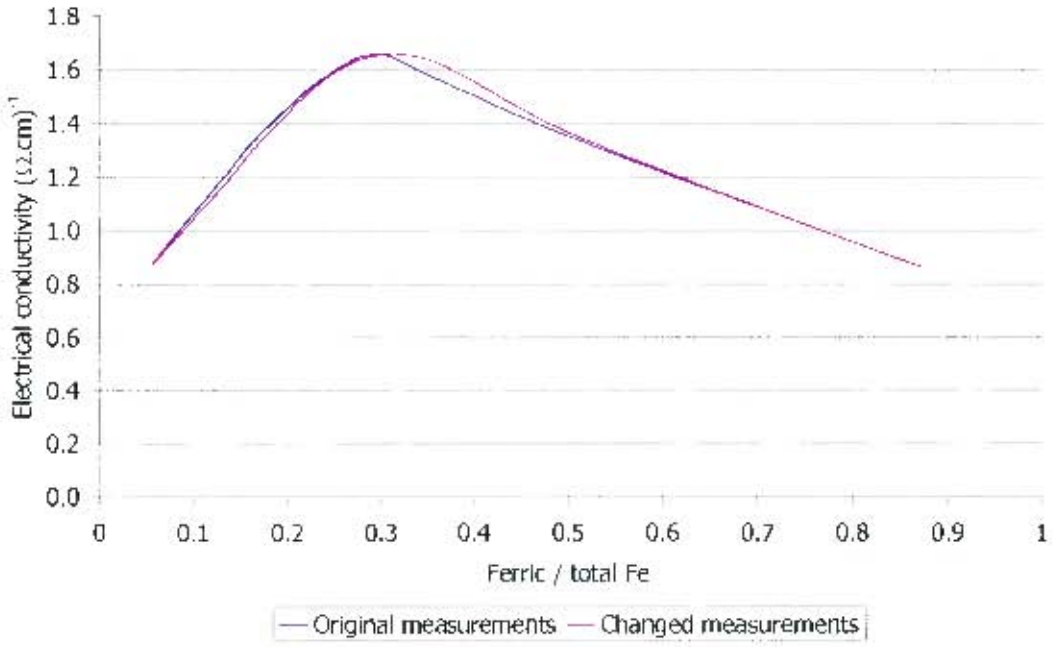

Figure 57a: Expected changes to curve of conductivity vs ferric fraction for slag H40 based on an additional 30 minutes of equilibration time at each p_{CO2}/p_{CO} ratio.

This was the approach used in determining equilibrium in all the experiments and it is suggested that the results obtained are a reasonable indication of the conductivity at those equilibrium conditions. Duplicate experiments all showed very similar trends with respect to the shape of the resistance vs time curve and the position of equilibrium conditions. In a couple of instances, the equilibrium points were possibly judged prematurely and a longer time for equilibration should have been allowed. However, the criteria for judging equilibrium was based on the average rate approaching zero and where premature decisions have been made, it is likely that the reported value for the conductivity at that equilibrium is very close to the real value. The purpose of carrying out repeat experiments was to validate the findings in the initial experiments. Unfortunately reversing an experiment i.e. starting from oxidising conditions, going to reducing conditions and then back to oxidising conditions was not possible given the use of MgO crucibles. The slags dissolved MgO during the course of the experiments, therefore reversing the readings would lead to differences in measured resistances. It should be pointed out that reverse experiments were carried out using a platinum crucible, however, the formation of a solid crust on the surface of the slag resulted in very long equilibration times and eventually the suspension of the particular experiments.

3.7.4. Effect of frequency

The effect of frequency on the measured resistance was only checked with the RCL meter for a few of the slags being tested in the MgO crucibles. The frequency dependence of the

measurements on the calcium ferrite slag was not checked. The frequency dependence results for slag H40 at 1450 °C are presented below:

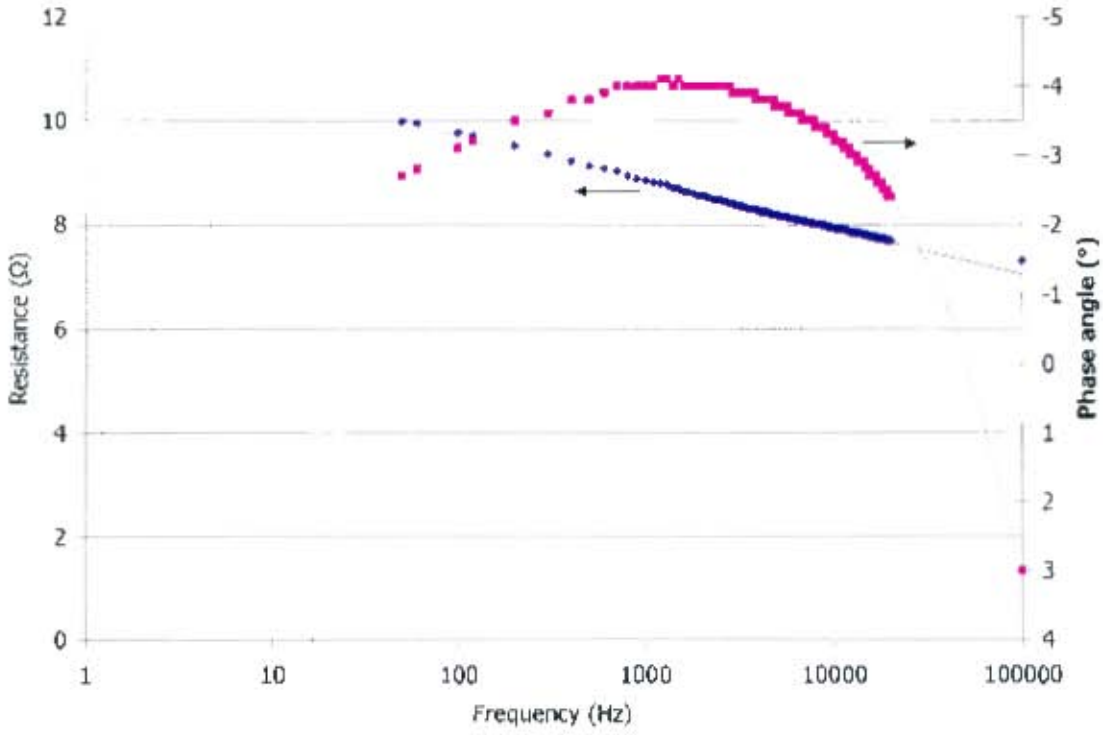

Figure 58: Frequency dependence of slag H40 in air at 1450 °C

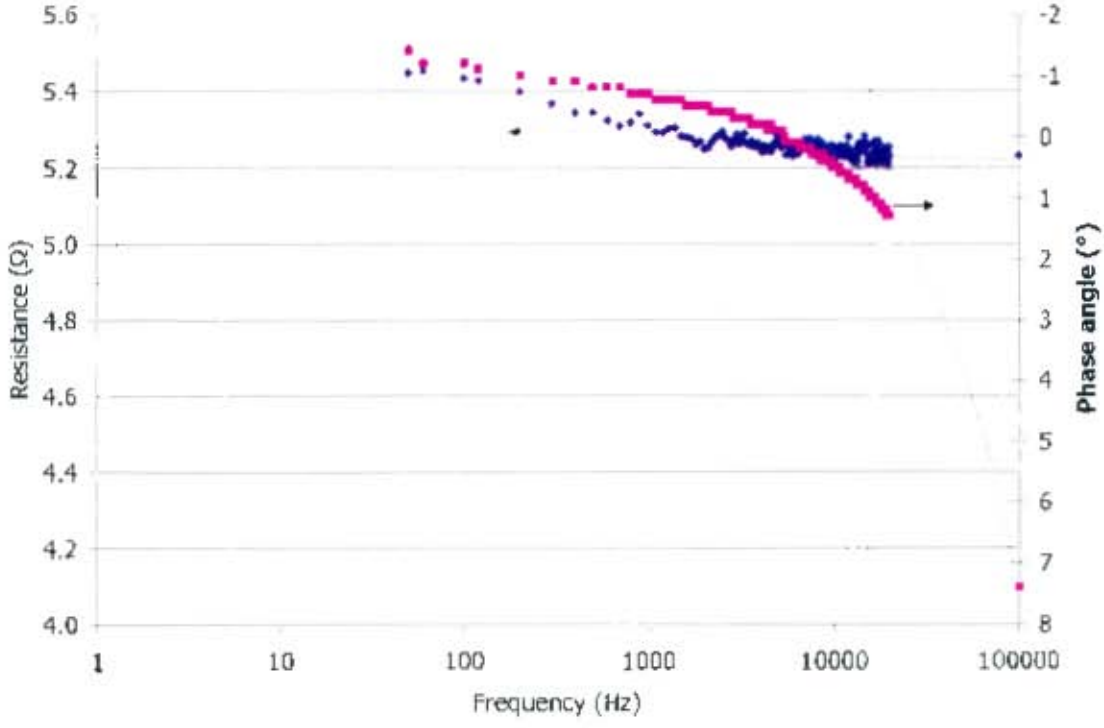

Figure 59: Frequency dependence of slag H40 at CO_2/CO = 10 at 1450 °C

The above graphs show that the frequency dependence of slag H40 changes as the oxidation state of the slag changes. Initially in air, the resonant frequency occurred between 20 and 100 kHz (see Figure 58). The resistance also appeared to be dependent on the frequency even at 100 kHz, dropping from 7.68Ω at 20 kHz to 7.3Ω at 100 kHz. At a more reduced condition (CO_2/CO ratio = 10), the resonant frequency dropped down to 5.4 kHz and the resistance appeared to be independent of the frequency from approximately 2 kHz.

Similar trends were seen with measurements on slag H30.

3.7.5. Error analysis

The errors that possibly arose in this experimental setup include all the errors mentioned for the deep cell technique (see Section 3.6.5). However, there are additional errors which need to be considered for the shallow cell setup.

The shallow cell setup required the use of magnesia crucibles. There was slight attack of the crucible by the slag. The dissolution of MgO into the slag would change the slag chemistry and affect the conductivity either because of the additional Mg^{2+} cations introduced into the liquid slag or the increase in the magnesia content caused precipitation of a solid phase. Samples were taken before and after each run so the total amount of magnesia that entered the slag was known. However, it was not known when the magnesia dissolved in terms of the oxygen potential or the duration of the experiment.

Another source of error was the difference in the surface tension of the slags and the KCl solutions. It was noticed that the slags wetted the walls of the crucibles which suggested that the liquid depth in the crucible dropped during the course of an experiment. The walls of the crucibles were wetted to different degrees depending on the slag compositions and the durations of the experiments.

A similar approach to the one used in calculating the error for the deep cell setup was used to calculate the error for the shallow cell setup. The relative error in the cell constant due to the cell geometry during the calibration was estimated to be around 3%. The Attwood expression (Equation 23) was used again and gave a good estimation of the cell constant (4.76 cm^{-1} in contrast to the measured 4.5 cm^{-1}). The relative error in the cell constant due to the temperature and known conductivity of the KCl solutions remained around 6%.

To account for the changes in the cell geometry at high temperature, including the wetting of the crucible walls and resultant change in immersion depth of the electrodes, the Attwood expression was applied again. For an uncertainty in the immersion depth of 0.3mm, the relative error in the cell constant was approximately 15%.

Assuming that the relative errors in the cell constant are additive, the total relative error in the shallow cell technique is around 25% (3% from geometric factors during calibration, 6% from the use of the KCl solutions and 15% from geometric factors during high temperature measurement). This refers to the absolute values of the conductivity measured as opposed to the relative values of the conductivity for an experiment on a slag. Therefore, although the absolute values of the conductivity may not be very accurate, the change in the conductivity with oxidation state should be accurately measured. Since the effect of oxidation state on

slag conductivity was of interest, the relatively large uncertainty in the absolute values of the conductivity was deemed acceptable.

In many cases repeat runs on specific slags were carried out to gain confidence in the absolute values of the conductivity. The other check in place to ensure reasonably accurate conductivity values was the comparison with conductivity measurements using the deep cell technique. For the slags containing 20 and 30wt% FeO_x, conductivity was measured using both techniques, although the deep cell measurements were only at reduced conditions.

3.7.6. Reproducibility of experiments

As mentioned above, repeat runs were carried out for some of the slags where the shallow cell technique was being used. The details of the initial and repeated runs are presented in the Results chapter.

3.8. Analytical methods

The majority of the slags were analysed by the CSIRO Minerals analytical laboratory. The technique used to analyse most of the slags was XRF (X-ray Fluorescence).

For certain slags where the oxidation state was varied, the ferric and ferrous iron contents of the slags were determined by the author by titrations using the potassium dichromate method. The potassium dichromate method involves the following procedure. For the ferrous iron content, approximately 50 mg of slag was digested in HCL and HF under a N_2 atmosphere to prevent oxidation of the ferrous ions. The solution was then titrated against potassium dichromate using sodium diphenylamine sulfonate as the indicator. To calculate the ferric iron content the total iron content was determined. This was done by digesting the slag sample in HCL and HF. Once dissolved, the ferric iron was reduced to ferrous iron by the addition of stannous chloride. Excess stannous chloride was oxidised with mercuric chloride. The solution was then titrated as for the ferrous iron. The ferric content was then calculated from the difference between the total iron and ferrous iron contents.

Chapter 4

RESULTS

The objective of the experimental work was to obtain answers to the research questions and therefore obtain a better understanding of the factors affecting the electrical conductivity of slags. The aim of the temperature dependent experiments was to determine the effect of iron oxide addition on the electrical conductivity and the activation energy for conduction. The aim of the oxidation state dependent experiments was to determine the effects of slag chemistry and iron oxide content on the electronic and ionic mechanisms for conduction. The aim of the experiments in which chromium was added to the low basicity slag was to determine the effect of chromium on the electrical conductivity of the slag.

The results have been categorised according to the slag type i.e. low, intermediate or high basicity slags, calcium ferrite slag and chromium-containing slags.

- The first three sections contain the results of the temperature dependent and oxidation state dependent conductivity experiments on the low, intermediate and high basicity slags. The composition of the low basicity slag was the following (wt%): Al_2O_3: 6.25, CaO: 6.25, MgO: 25, SiO_2: 62.5 and FeO_x additions from 0 to 40%). The composition of the intermediate basicity slag was the following (wt%): Al_2O_3: 6.25, CaO: 20, MgO: 20 and SiO_2: 53.75 with FeO_x additions from 0 to 40%. The composition of the high basicity slag was the following (wt%): Al_2O_3: 5, CaO: 30, MgO: 20 and SiO_2: 45 with FeO_x additions from 0 to 40%. Therefore the mol% $(CaO+MgO)/(Al_2O_3+SiO_2)$ ratios of the low, intermediate and high basicity slags were 0.63, 0.86 and 1.22 respectively. The temperature dependent conductivity measurements were made in the range from 1400 to 1550 °C. The oxidation state measurements were in the range of $p_{O2} = 10^{-11}$ to 0.21 atm at a fixed temperature of 1450 °C.
- The fourth section presents the results of the conductivity measurements when chromium was added to the low basicity slag containing 20wt% FeO_x. Chromium was added sequentially to the master slag to obtain levels of 0.5, 1, 2, 4, 6 and 8 wt% Cr_2O_3. The measurements on each slag were in the range of 1400 to 1550 °C. In a secondary series of experiments, the conductivities of slags containing 0, 2 and 4 wt% Cr_2O_3 were measured in the temperature range 1400 to 1700 °C.
- The final section contains the results of the experiment on the calcium ferrite slag. The experiment was conducted on a slag containing 25% CaO and 75% FeO_x to determine the oxidation state dependence of the conductivity. The temperature of the experiment was 1300 °C and the oxidation state was varied from 10^{-10} to 0.21 atm.

4.1. Low basicity slags

The intended (as opposed to analysed) master composition (wt%) of the low basicity slag was Al_2O_3: 6.25%, CaO: 6.25%, MgO: 25%, SiO_2: 62.5%. Iron oxide was added to the master slag to obtain iron levels in the slag of 10, 15, 20, 30 and 40wt%. The analysed compositions of all the slags were very similar to the intended compositions. The analysed compositions are shown in Appendix C.1.1.

The experiments on slags L0, L10, L15 and L20 were performed using the deep cell technique and the effect of temperature on the conductivity was of interest. For these experiments, the iron oxide was added in the form of wüstite and the experiments were conducted under a nitrogen atmosphere. The experiments were carried out in the temperature range of 1400 to 1550 °C.

Measurements were performed on slags L15, L20, L30 and L40 using the shallow cell setup to determine oxidation state dependence of the conductivity of the slags. In these cases, the iron oxide was added in the form of haematite and the experiments were started in air. The slag was then reduced while conductivity measurements were made. The experiments were carried out at a constant temperature of 1450 °C.

4.1.1. Deep cell measurements – temperature dependence

In the temperature dependence measurements of the conductivity on the low basicity slags containing 0, 10, 15 and 20wt% FeO_x, the deep cell technique was used. As mentioned in section 3.6, the deep cell setup made use of platinum electrodes and crucibles. The experiments were conducted under a nitrogen atmosphere. The resistance of the slag was measured using an RCL meter. The slag conductivity was then calculated using the following formula:

Equation 24: $\kappa_{slag} = e^{slope.\ln(R_{measured} - R_{external}) + intercept}$

Where *slope* and *intercept* were obtained from the calibration with the KCl solutions

$R_{external}$ was the resistance of the shorted electrodes and leads

The measured resistances are dependent on the slag resistance in addition to the external resistance. The external resistance was around 2.5 Ω at 1400 °C and the overall resistance was in the range 3.5 to 25 Ω for slag conductivities ranging from 0.05 to 1 $(\Omega.cm)^{-1}$. All the measured resistances and calculated conductivities for the low basicity slags are shown in Appendix C.1.2.

The iron-free master slag (Slag L0) had a liquidus temperature of approximately 1450 °C as estimated from the 5% Al_2O_3-CaO-MgO-SiO_2 phase diagram (see Figure 45). Therefore the starting temperature for measurements on this slag was approximately 1475 °C. The progress of the experiment is presented in Figure 60.

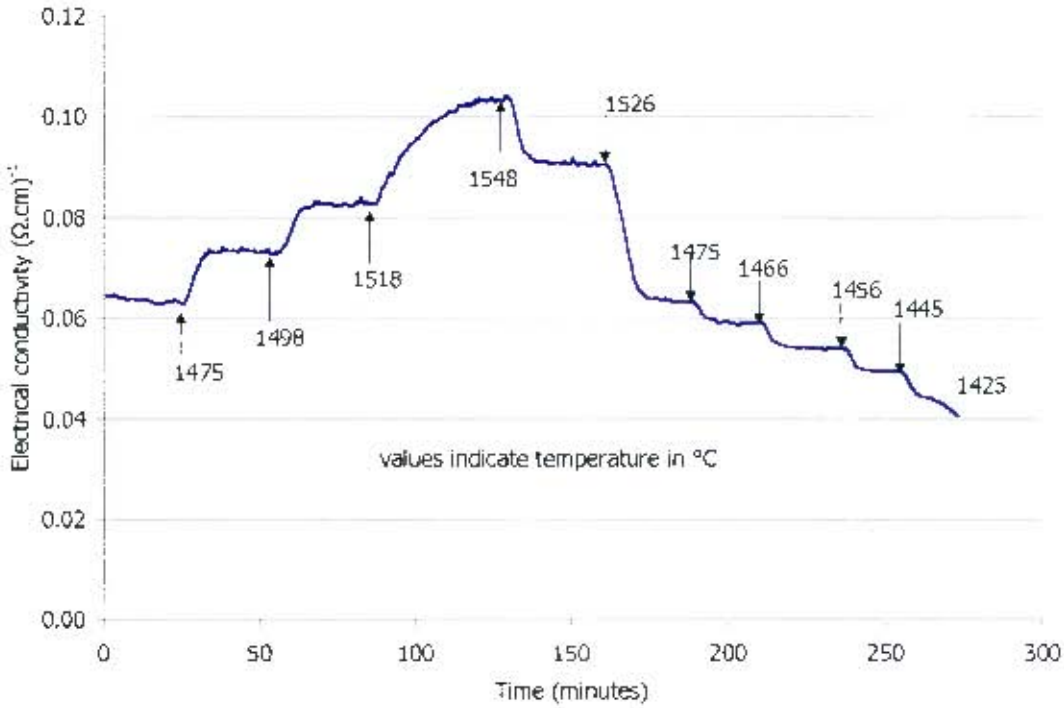

Figure 60: Progress of temperature dependence experiment on Slag L0. Composition: Al_2O_3: 6.25%, CaO: 6.25%, MgO: 25%, SiO_2: 62.5%

The trend shown in Figure 60 is going to be explained in more detail. After starting at 1475 °C and allowing the slag to come to thermal equilibrium, the setpoint of the furnace was raised to approximately 1500 °C. There was a step increase in the slag conductivity as a result of the temperature increase. The increase in the conductivity occurred within 5-10 minutes after the increase in the setpoint and thereafter the slag approached thermal equilibrium more slowly. A period of around 20 to 30 minutes was allowed for the slag to reach thermal equilibrium. The resistance reading used to calculate the conductivity was the one at the end of the equilibration time. Thereafter the furnace setpoint was increased or decreased to the next temperature. The exception to this was the increase in the setpoint to around 1550 °C. As a result of this temperature being near the maximum operating range of the furnace, it took longer for the furnace to reach and maintain the temperature. Therefore the equilibration took longer for the temperature of 1548 °C. Overall, the experiment took between 4 to 6 hours to complete which was a typical duration for an experiment.

Readings were taken at approximately 20 °C intervals on heating up to ~1550 °C (the upper limit of the furnace) and then on cooling down to the estimated liquidus temperature. When the temperature of the slag dropped from 1445 to 1425 °C, the conductivity did not reach a steady value and continued decreasing. This was regarded as an indication that the liquidus temperature was reached. The apparent liquidus temperature was therefore between 1445 and 1425 °C. The liquidus temperature of slag L0 calculated using MPE (see Zhang *et al.* (2002)) was 1425 °C. The numerical values of the resistances measured and the conductivities calculated are presented in Table 8. The calibration data used in the calculation is also provided. It should be noted that the results have been tabulated in the order that the measurements were made.

Table 8: Slag L0 results: Temperature dependence of electrical conductivity. Composition (wt%): Al_2O_3: 6.25%, CaO: 6.25%, MgO: 25%, SiO_2: 62.5%

Temperature	Resistance measured	Electrical conductivity
°C	Ω	$(\Omega.cm)^{-1}$
1475	18.3	0.063
1498	16.2	0.073
1518	14.6	0.083
1548	12.3	0.104
1526	13.6	0.091
1475	18.2	0.063
1466	19.4	0.059
1456	21.0	0.054
1445	22.5	0.050
Calibration slope		-1.013
Calibration intercept		0.024

The progress of the experiment on slag L10 was similar to that presented in Figure 60, although the apparent liquidus temperature was between 1455 and 1432 °C. The conductivity values for slag L10 are shown in Table 9 below:

Table 9: Slag L10 results: Temperature dependence of electrical conductivity. Composition (wt%): Al_2O_3: 5.6%, CaO: 5.6%, FeO_x: 10, MgO: 22.5%, SiO_2: 56.3%

Temperature	Resistance measured	Electrical conductivity
°C	Ω	$(\Omega.cm)^{-1}$
1474	13.1	0.095
1498	11.3	0.115
1524	9.9	0.138
1540	9.2	0.153
1500	11.1	0.118
1477	12.7	0.098
1455	14.2	0.085
Calibration slope		-1.013
Calibration intercept		0.024

The progress of the experiments on slags L15 and L20 were very similar to that presented in Figure 48. The results obtained for slags L15 and L20 are provided in Table 10. The resistance values measured have been omitted from the table but these values are available in Appendix C.1.2. The calibration data used for slag L0 and L10 were used in the calculation of the conductivity for slags L15 and L20.

Table 10: Slag L15 and L20 results: temperature dependence of electrical conductivity. Slag L15 composition (wt%): Al_2O_3: 5.3%, CaO: 5.3%, FeO_x: 15, MgO: 21.3%, SiO_2: 53.1%

L15		L20	
Temperature	Electrical conductivity	Temperature	Electrical conductivity
°C	$(\Omega.cm)^{-1}$	°C	$(\Omega.cm)^{-1}$
1451	0.134	1424	0.242
1474	0.154	1449	0.287
1499	0.181	1473	0.328
1524	0.209	1498	0.375
1550	0.244	1521	0.430
1502	0.185		
1455	0.137		
1427	0.114		

The tabulated results of the slag conductivity measurements mentioned above are shown in Figure 61.

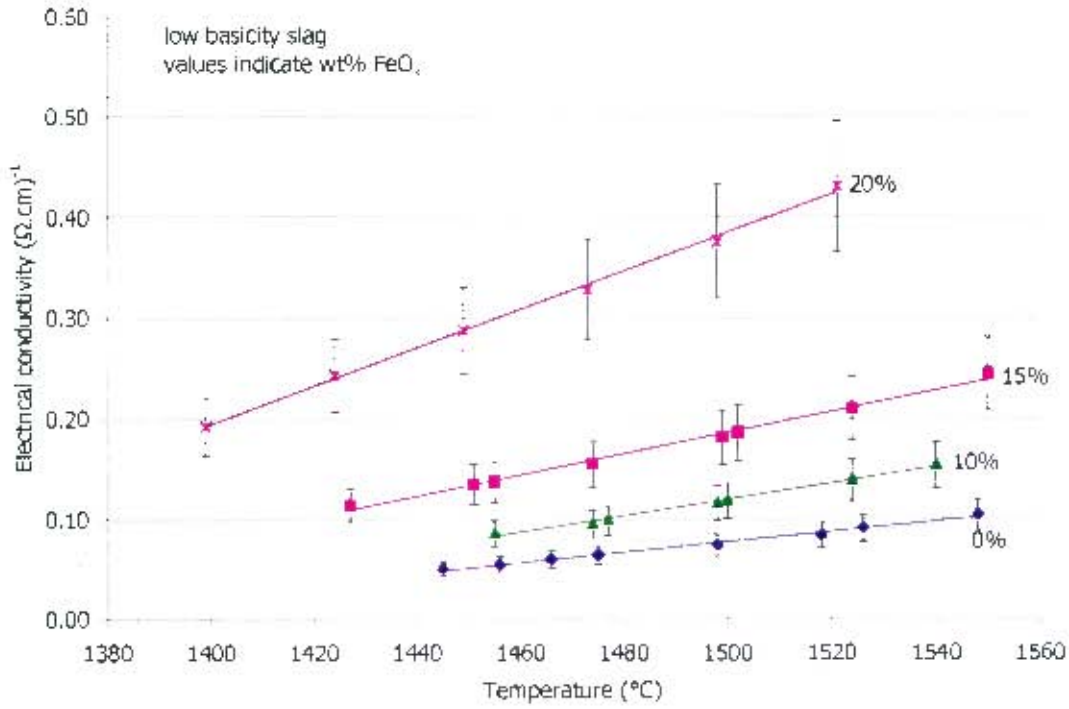

Figure 61: Temperature dependence of the electrical conductivity of low basicity slags with FeO_x additions. Low basicity master slag composition (wt%): Al_2O_3: 6.25%, CaO: 6.25%, MgO: 25%, SiO_2: 62.5% with additions of 10, 15 and 20% FeO_x.

The electrical conductivity increased with temperature and the addition of FeO_x. The trend lines are included to aid visualisation. The error bars indicate the 15% uncertainty in the measured values. Where there are multiple conductivity values at a similar temperature for the same slag, one value was measured while heating and the other on cooling. Activation energies were calculated for the slag conductivities but will be presented and discussed in section 5.2. It is possible that slag L20 was at a slightly different oxidation state than slags L10 and L15 as a result of the different method of preparation of the iron oxide. Slag L20 and slag Cr0 had the same composition and the slag was prepared in a magnesia crucible where

iron and haematite were added in stoichiometric proportions to obtain wüstite (details given in section 3.5).

4.1.2. Shallow cell measurements – oxidation state dependence

The oxidation state dependence of the conductivities of slags L15, L20, L30 and L40 was tested using the shallow cell setup. The iron oxide was added to the master slag L0 in the form of haematite to obtain the desired amount of iron in the slags. Magnesia crucibles were used to contain the slags. As discussed in section 3.7.1, the reason for using magnesia crucibles was that a non-conductive container was required such that there was not a parallel conduction path given the small amount of slag used in the experiments. There was some attack of the crucible by the slags and the magnesia content of the slags increased. The slags were analysed both before and after the experiments to determine the MgO increase. The pertinent data from the analyses has been summarised in Table 11. The full analyses are available in Appendix C.1.1.

Table 11: MgO gain during oxidation state experiments on low basicity slags

Slag name	MgO gain	Duration	Final p_{CO2}/p_{CO}	Basicity (molar basis)		FeO_x content (wt%)	
	wt%	hours	ratio	Initial	Final	Initial	Final
L15	1.8	4.9	1	0.62	0.68	14.6	13.6
L20	3.2	5.4	1	0.62	0.73	19.4	18.0
L30	4.0	7.0	2	0.62	0.77	29.3	26.3
L30 rep 1	4.9	5.5	10	0.62	0.81	29.3	25.6
L30 rep 2	4.9	4.5	$CO + N_2$	0.62	0.81	29.3	26.8
L40	4.5	6.0	10	0.61	0.80	37.8	35.3
L40 rep 1	4.8	5.5	$CO + N_2$	0.61	0.83	37.8	34.2
L40 rep 2	5.9	5.5	$CO + N_2$	0.61	0.87	37.8	33.8

The durations of the experiments (typically 5 to 7 hours) and the final oxidation states of the slags are noted as these factors were likely to determine the amount of MgO dissolved (1.5 to 5wt%). The increase in the MgO content brought about dilution of the other components in the slag. As the iron oxide content was of most interest, the initial and final FeO_x contents are also given. It should be noted that the initial FeO_x content in slag L40 was 37.8 wt% and lower than the intended 40wt%.

It was apparent that more MgO dissolved into the slags with the higher iron oxide contents. For example, the MgO content of slag L15 changed from 19.8 to 21.6wt%, while the MgO content of slag L40 changed from 13.7 to 18.2wt%. This was expected as the addition of FeO_x to the slags diluted the other components, hence the effective MgO content of the slag was further away from magnesia saturation and more MgO dissolved. Also, the reduced vicosity of the high iron containing slags may have led to increased diffusion and therefore increased solubility. The effect of the gain in MgO will be discussed in more detail in section 5.3.

4.1.2.1 Slag L15

The calculated conductivities for the oxidation state experiment on Slag L15 are shown in Figure 62. The conductivity increased as the oxidation state of the slag became more

reduced. The absolute value of the conductivity at the more reduced conditions (~0.17 to 0.18 $(\Omega.cm)^{-1}$ at p_{CO_2}/p_{CO} = 1 to 5) is higher than the value obtained in the temperature dependence experiment (~0.13 $(\Omega.cm)^{-1}$ at 1450°C from Table 10).

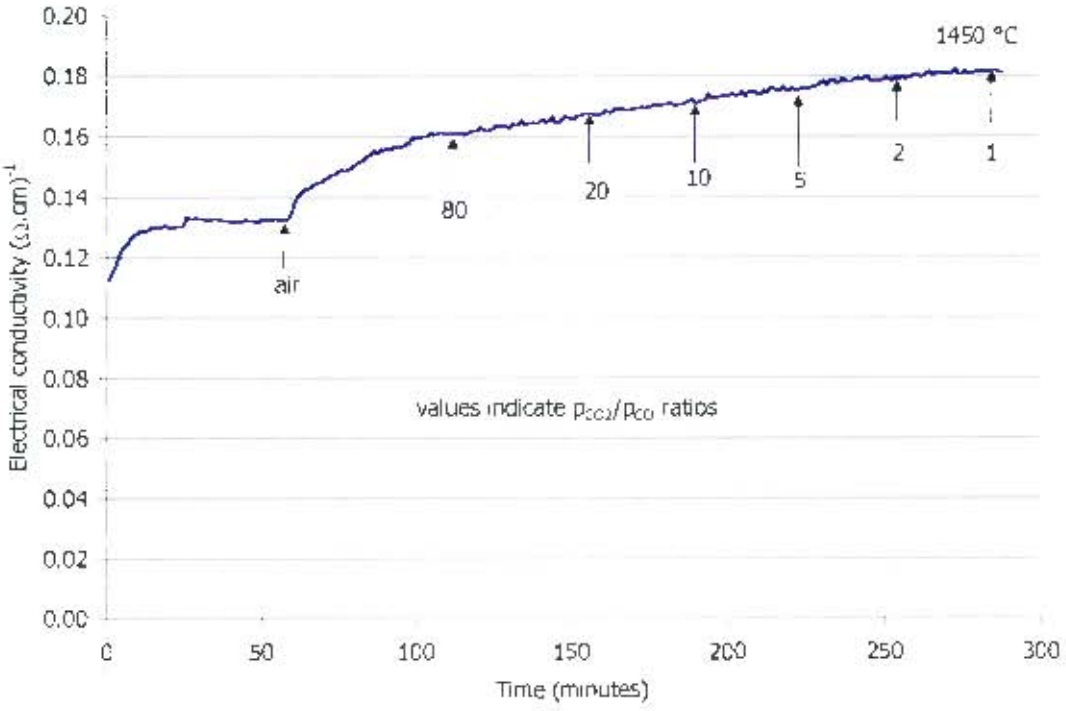

Figure 62: Progress of oxidation state experiment on Slag L15 at 1450 °C showing calculated conductivity values. Slag L15 composition (wt%): Al_2O_3: 6, CaO: 5, FeO_x: 15, MgO: 20, SiO_2: 54.

The numerical values of the resistance measured and conductivity calculated are provided in Table 12 for slag L15. The calibration data used is also included. The oxygen partial pressure values were calculated from the p_{CO_2}/p_{CO} ratios and temperature using the free energy data for the reaction $CO_{(g)} + \frac{1}{2}O_{2\,(g)} = CO_{2\,(g)}$ as cited by Mackey (1982): $\Delta G° = -67500 + 20.75\,T$ (T in K and $\Delta G°$ in cal/mol).

Table 12: Slag L15 results: oxidation state dependence of electrical conductivity at 1450 °C

Slag L15

p_{CO_2}/p_{CO}	p_{O_2}	Resistance measured	Electrical conductivity
	atm	Ω	$(\Omega.cm)^{-1}$
air	2.1E-01	31.0	0.132
80	5.6E-05	26.0	0.161
20	3.5E-06	25.1	0.167
10	8.7E-07	24.7	0.170
5	2.2E-07	24.1	0.175
2	3.5E-08	23.6	0.180
1	8.7E-09	23.4	0.181
Calibration slope			-1.02
Calibration intercept			1.37

It was considered important to show again how the conductivity was determined for each equilibrium point. The progress of the experiment on slag L15 is shown in Figure 63 in terms of the average rate of change in the measured resistances (as was done in Figure 57). From Figure 63 it is evident that the system came to equilibrium as. Referring to Figure 63, the experiment was started in air using haematite as the source of iron. The slag was allowed to equilibrate in air until the average rate of change in the measured resistances approached 0 at around 50 minutes. The p_{CO2}/p_{CO} ratio was then changed to 80 and the slag was once again left to equilibrate. After approximately a further 55 minutes, ($\Delta R/\Delta t$) approached zero, indicating equilibrium and the p_{CO2}/p_{CO} ratio was changed to 20. This procedure was continuec until measurements had been made at each of the desired p_{CO2}/p_{CO} ratios. The criteria by which it was judged that equilibrium was reached, were a duration of around 30 to 60 minutes for equilibrium to be achieved (based on experience from other tests) and then the average rate of change in the measured resistance being zero or close to zero for around 5 minutes.

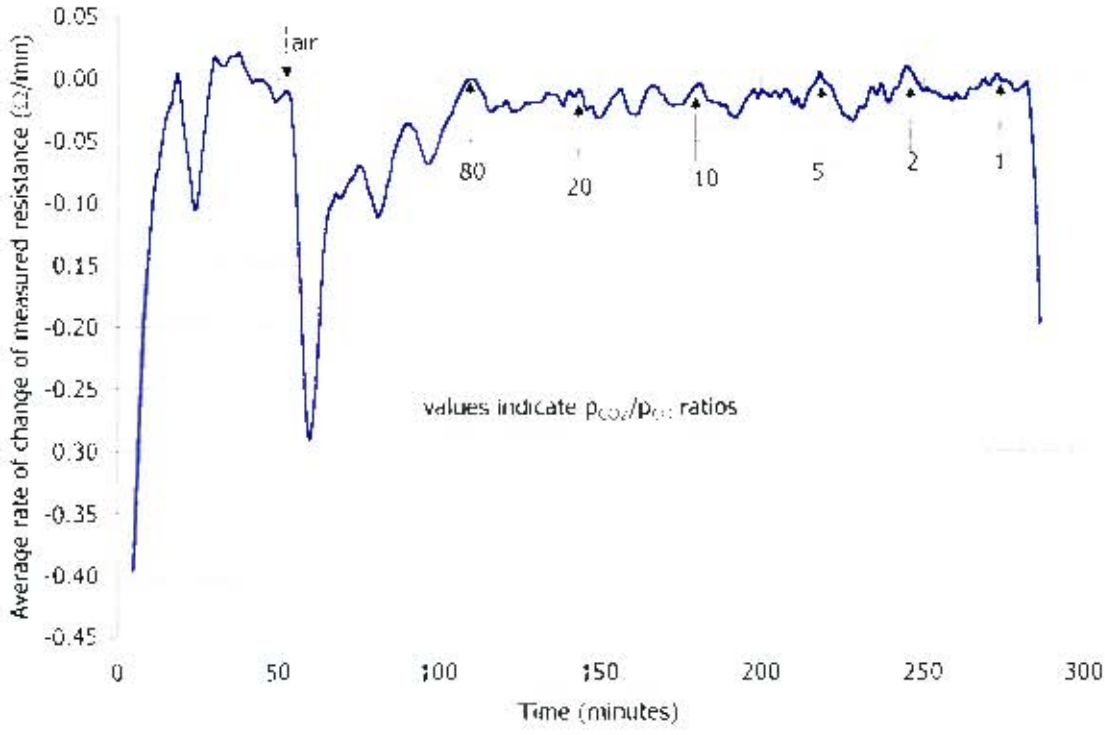

Figure 63: Average rate of change in resistances measured during the oxidation state experiment on Slag L15 at 1450 °C. Slag L15 composition (wt%): Al_2O_3: 6, CaO: 5, FeO_x: 15, MgO: 20, SiO_2: 54. Five point moving average.

As was done in Table 7 for Slag H40, the percentage change in the conductivity at each equilibrium point for Slag L15 was calculated if the slag had been left to equilibrate for longer at each p_{CO2}/p_{CO} ratio. The data in Table 13 was obtained. It can be seen from the table that the measurements were taken very close to the equilibrium points and no significant change in the conductivity would occur, with the exception of the point at p_{CO2}/p_{CO} = 20 which was possibly determined prematurely. However, the change in the conductivity if the slag had been allowed to equilibrate for longer was around 4.5%.

Table 13: Equilibrium data calculated from oxidation state experiment on Slag L15 based on average rate of change in measured resistance

p_{CO2}/p_{CO}	Time	$R_{measured}$	average $\Delta R/\Delta t$	k_{eq}	k_{3D}	%change
ratio	minutes	Ω	Ω/min	$(\Omega.cm)^{-1}$	$(\Omega.cm)^{-1}$	
air	51	31.00	-0.015	0.132	0.134	1.7
80	105	26.02	-0.021	0.161	0.165	2.8
20	149	25.09	-0.032	0.167	0.175	4.5
10	180	24.69	-0.007	0.170	0.172	1.0
5	214	24.10	-0.014	0.175	0.179	2.0
2	249	23.57	-0.006	0.180	0.181	0.9
1	279	23.36	-0.010	0.181	0.184	1.5

4.1.2.2Slag L20

The progress of the experiment on slag L20 is shown in Figure 64. The experiment was carried out in the same manner as for the experiment on slag L15. The equilibrium conditions were again based on the average rate of change in the measured resistance and the results are shown in Appendix C.1.3.

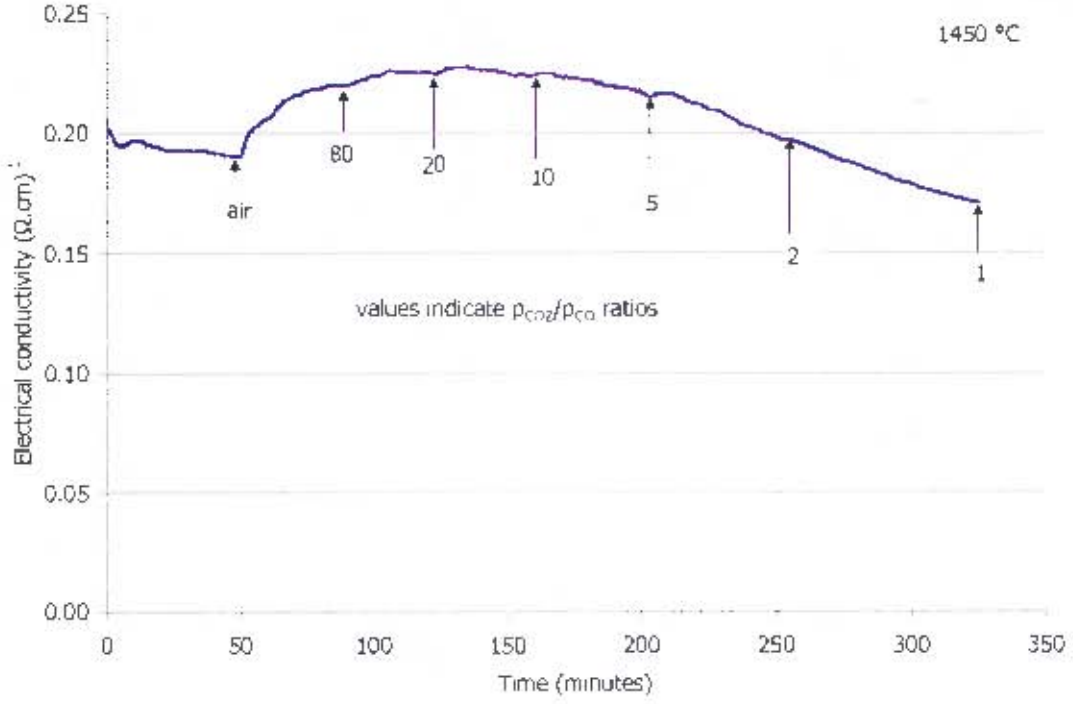

Figure 64: Progress of oxidation state experiment on slag L20 at 1450 °C. Approximate composition of slag L20: Al_2O_3: 6, CaO: 5, FeO_x: 20, MgO: 19, SiO_2: 50.

The electrical conductivity of slag L20 initially increased as the oxidation state became more reduced and reached a maximum between p_{CO2}/p_{CO} = 20 and 10. However, when the p_{CO2}/p_{CO} ratio was decreased below 10, the conductivity started to decrease. The absolute values of the conductivity at the more reduced conditions (~0.17 to 0.22 $\Omega^{-1}.cm^{-1}$ at p_{CO2}/p_{CO} = 1 to 5) was lower than the value from the temperature dependence measurement in Table

10 (~0.29 $\Omega^{-1}.cm^{-1}$ at 1450°C). The reason for examining the conductivity values at those particular oxidation states is that slag was quite reduced in the temperature dependent conductivity measurements. A possible reason for the discrepancy between the values was the lower accuracy of the shallow cell technique. The numerical values of the resistance measured and the conductivity calculated are provided in Table 14.

Table 14: Slag L20 results: oxidation state dependence of electrical conductivity at 1450 °C. Approximate composition (wt%) : Al_2O_3: 6, CaO: 5, FeO_x: 20, MgO: 19, SiO_2: 50.

Slag L20

P_{CO2}/P_{CO}	P_{O2}	Resistance measured	Electrical conductivity
	atm	Ω	$(\Omega.cm)^{-1}$
air	2.1E-01	22.8	0.190
80	5.6E-05	20.1	0.220
20	3.5E-06	19.6	0.225
10	8.7E-07	19.7	0.224
5	2.2E-07	20.2	0.217
2	3.5E-08	21.9	0.198
1	8.7E-09	25.0	0.171
Calibration slope			-1.02
Calibration intercept			1.40

4.1.2.3 Slag L30

Three runs were performed on slag L30 in the same manner as described for Slag L15. The progress of the experiments is shown in Figure 65. The initial run is shown in blue, the first repeat in purple and the second repeated run in green. The determination of equilibrium conditions was carried out in the same manner as described for Slag L15 above and the results are shown in Appendix C.1.3.

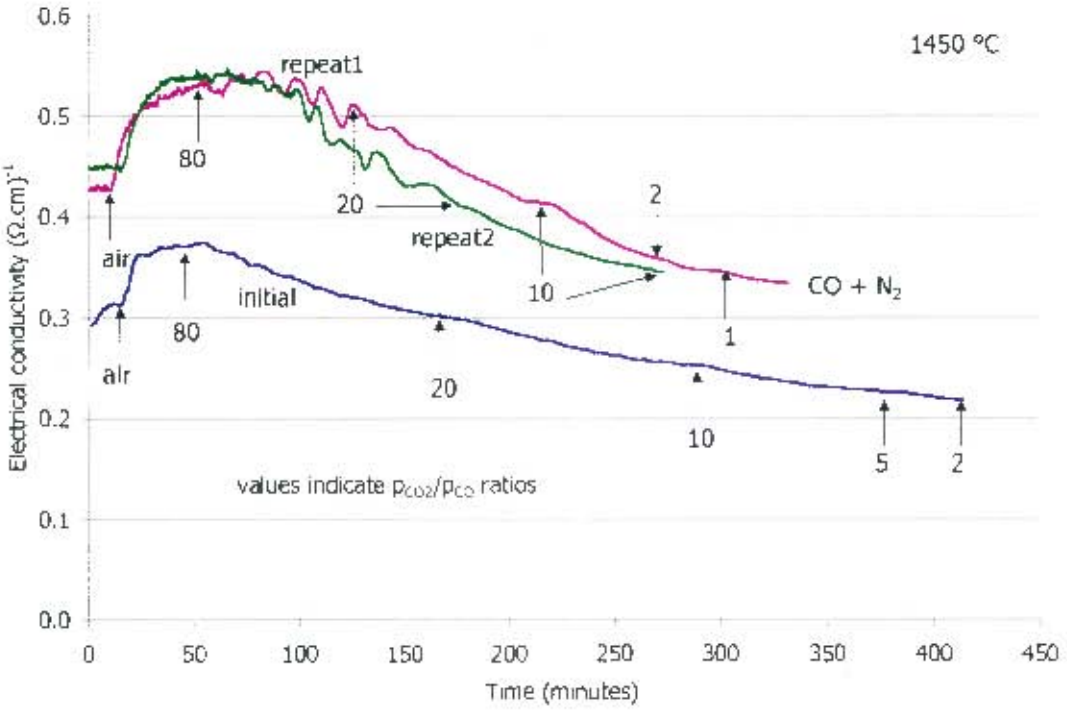

Figure 65: Progress of oxidation state experiments on slag L30 at 1450 °C – initial and repeat runs. Approximate composition of slag L30 (wt%): Al_2O_3: 5, CaO: 5, FeO_x: 30, MgO: 16, SiO_2: 44.

There was a significant difference in the absolute values of the conductivity for the initial run and the repeats but a similar response of the conductivity to the oxidation state was observed in all three runs. Starting in air, the conductivity increased as the slag became reduced and reached a maximum between p_{CO2}/p_{CO} = 80 and 20. Below a ratio of 20, the conductivity decreased with further reduction and the conductivity value at the most reducing condition was lower than the value in air. The reason for the fluctuation of the conductivity in the repeated runs between p_{CO2}/p_{CO} = 80 and 20 is not known. The numerical results for the three runs are shown in Table 15. The p_{CO2}/p_{CO} value for $CO+N_2$ was calculated using the p_{O2} value calculated by MPE (see Zhang *et al.* (2002)) just before iron saturation occurred.

10 (~0.29 $\Omega^{-1}.cm^{-1}$ at 1450°C). The reason for examining the conductivity values at those particular oxidation states is that slag was quite reduced in the temperature dependent conductivity measurements. A possible reason for the discrepancy between the values was the lower accuracy of the shallow cell technique. The numerical values of the resistance measured and the conductivity calculated are provided in Table 14.

Table 14: Slag L20 results: oxidation state dependence of electrical conductivity at 1450 °C. Approximate composition (wt%) : Al_2O_3: 6, CaO: 5, FeO_x: 20, MgO: 19, SiO_2: 50.

Slag L20

P_{CO2}/P_{CO}	P_{O2}	Resistance measured	Electrical conductivity
	atm	Ω	$(\Omega.cm)^{-1}$
air	2.1E-01	22.8	0.190
80	5.6E-05	20.1	0.220
20	3.5E-06	19.6	0.225
10	8.7E-07	19.7	0.224
5	2.2E-07	20.2	0.217
2	3.5E-08	21.9	0.198
1	8.7E-09	25.0	0.171
Calibration slope			-1.02
Calibration intercept			1.40

4.1.2.3 Slag L30

Three runs were performed on slag L30 in the same manner as described for Slag L15. The progress of the experiments is shown in Figure 65. The initial run is shown in blue, the first repeat in purple and the second repeated run in green. The determination of equilibrium conditions was carried out in the same manner as described for Slag L15 above and the results are shown in Appendix C.1.3.

Table 15: Slag L30 results for initial and repeat runs: oxidation state dependence of electrical conductivity at 1450 °C. Approximate composition (wt%): Al_2O_3: 5, CaO: 5, FeO_x: 30, MgO: 16, SiO_2: 44.

Slag L30 initial

p_{CO2}/p_{CO}	p_{O2}	Resistance measured	Electrical conductivity
	atm	Ω	$(\Omega.cm)^{-1}$
air	2.1E-01	15.3	0.313
80	5.6E-05	13.4	0.370
20	3.5E-06	15.9	0.301
10	8.7E-07	18.3	0.252
5	2.2E-07	20.1	0.227
2	3.5E-08	20.8	0.217
Calibration slope			-1.02
Calibration intercept			1.44

Slag L30 repeat 1

p_{CO2}/p_{CO}	p_{O2}	Resistance measured	Electrical conductivity
	atm	Ω	$(\Omega\ cm)^{-1}$
air	2.1E-01	12.0	0.428
80	5.6E-05	10.3	0.525
20	3.5E-06	10.5	0.508
10	8.7E-07	12.3	0.415
2	3.5E-08	14.1	0.347
1	8.7E-09	14.7	0.331
0.1	2.2E-11	15.8	0.303
Calibration slope			-1.02
Calibration intercept			1.44

Slag L30 repeat 2

p_{CO2}/p_{CO}	p_{O2}	Resistance measured	Electrical conductivity
	atm	Ω	$(\Omega\ cm)^{-1}$
air	2.1E-01	11.5	0.448
80	5.6E-05	10.1	0.533
20	3.5E-06	11.9	0.431
10	8.7E-07	14.2	0.345
Calibration slope			-1.02
Calibration intercept			1.44

A possible reason for the difference in the conductivity values in the three runs was a slight misalignment of the electrodes with the crucible. From measurements in aqueous solutions it was found that when the electrodes were far off centre, the cell constant decreased by up to 20% which could have been the case in this experiment. It was decided to average only the results of the two repeat runs in order to obtain a single curve for the oxidation state experiment. The conductivity data from the initial run was omitted owing to the misalignment of the electrodes the crucible.

A sample was obtained of the slag from the second repeated run by cooling the slag while still maintaining the gas atmosphere at p_{CO2}/p_{CO} = 10. A titration was then carried out on the sample in order to determine the ferric and ferrous iron content. The ferric / total Fe fraction was found to be 0.17. The reason for doing the titration and the interpretation of the ferric fraction is discussed in Section 5.3.

4.1.2.4 Slag L40

Three runs were conducted on Slag L40. The progress of the experiments with time is shown in Figure 66 below. Again the determination of equilibrium was based on monitoring the rate of change in the measured resistances and the results are shown in Appendix C.1.3.

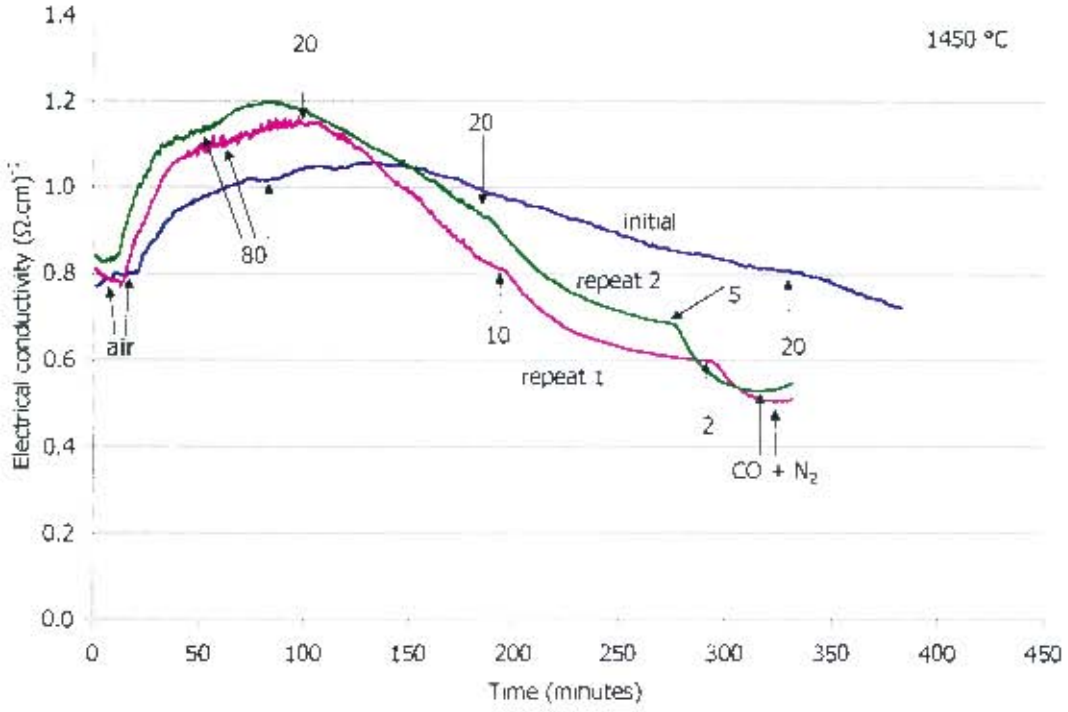

Figure 66: Progress of oxidation state experiments on Slag L40 at 1450 °C – initial and repeat runs. Approximate composition of slag L40: Al_2O_3: 5, CaO: 4, FeO_x: 38, MgO: 15, SiO_2: 38.

The initial run (blue line) took a very long time (around 2.5 hours) to come to equilibrium at p_{CO2}/p_{CO} = 20. The first repeated run (repeat 1 – purple line) was prematurely changed over from p_{CO2}/p_{CO} = 20 to 10 as the plateau in the maximum of the conductivity was mistaken for an indication of the equilibrium condition (the measurement at the ratio of 20 for repeat 1 was therefore omitted). The second repeat run (repeat 2 – green line) had a very similar trend to the initial run although the absolute values of the conductivity were slightly higher. The reason for the very long equilibration times between p_{CO2}/p_{CO} = 100 and 20 was suspected to be as a result of a solid layer forming on the surface of the slag. This will be discussed further in Sections 4.3.2.2 and 5.3 where justification for this reason is given.

Starting in air, the conductivity increased to a maximum between p_{CO2}/p_{CO} = 100 and 20 and then decreased at more reducing conditions. The value of the conductivity in air was higher than the value at the reducing conditions. The differences in the absolute values of the conductivities were considered acceptable in light of the expected accuracy of the shallow cell technique.

The numerical results for the initial and second repeated run are given in Table 16.

Table 16: Slag L40 results for initial and repeated runs: oxidation state dependence of electrical conductivity at 1450 °C. Approximate composition (wt%): Al_2O_3: 5, CaO: 4, FeO_x: 38, MgO: 15, SiO_2: 38.

Slag L40 initial

P_{CO2}/P_{CO}	P_{O2}	Resistance measured	Electrical conductivity
	atm	Ω	$(\Omega.cm)^{-1}$
air	2.1E-01	7.8	0.802
80	5.6E-05	6.7	1.015
20	3.5E-06	7.8	0.805
10	8.7E-07	8.4	0.723
Calibration slope			-1.02
Calibration intercept			1.48

Slag L40 repeat 1

P_{CO2}/P_{CO}	P_{O2}	Resistance measured	Electrical conductivity
	atm	Ω	$(\Omega.cm)^{-1}$
air	2.1E-01	8.0	0.783
80	5.6E-05	6.4	1.103
10	8.7E-07	7.7	0.824
2	3.5E-08	9.6	0.600
0.1	4.7E-11	10.9	0.504
Calibration slope			-1.02
Calibration intercept			1.48

Slag L40 repeat 2

P_{CO2}/P_{CO}	P_{O2}	Resistance measured	Electrical conductivity
	atm	Ω	$(\Omega.cm)^{-1}$
air	2.1E-01	7.7	0.827
80	5.6E-05	6.3	1.132
20	3.5E-06	7.1	0.938
5	2.2E-07	8.7	0.688
0.1	4.7E-11	10.5	0.528
Calibration slope			-1.02
Calibration intercept			1.48

4.1.2.5 All oxidation state dependence results for low basicity slags

The conductivity results for the low basicity slags were plotted against the oxygen partial pressures rather than the P_{CO2}/P_{CO} ratios. This was considered more meaningful as other authors' measurements were reported in terms of the P_{O2} or the ferric / total FeO_x ratio (Pastukhov *et al.* (1966), Fontana *et al.* (1984) and Engell and Vygen (1968)). As mentioned above, the P_{O2} values at the very reduced conditions (where $CO+N_2$ was used) were assumed to be determined by iron saturation and were estimated using MPE (see Zhang *et al.* (2002)) by finding the values of the P_{O2} just before iron saturation occurs for a given slag. The results are plotted in Figure 67.

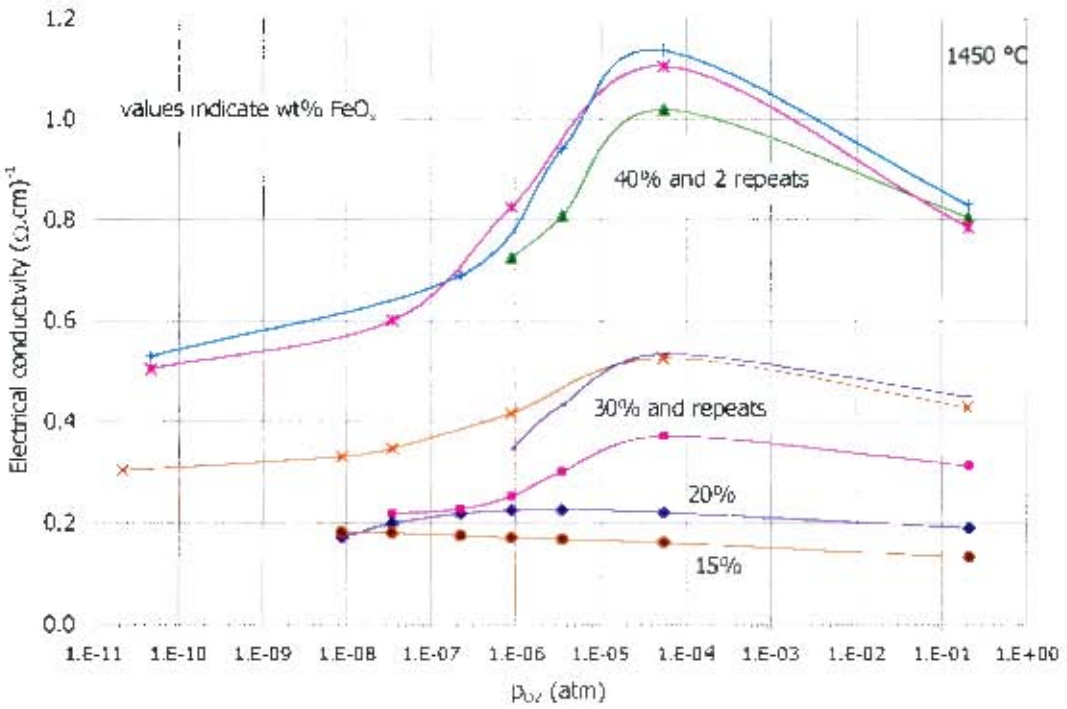

Figure 67: Variation of low basicity slag conductivity with oxidation state and iron oxide content at 1450 °C. Slag composition (wt%): Al_2O_3: 6, CaO: 6, MgO: 25, SiO_2: 63 with FeO_x additions as indicated.

The following trends are apparent from Figure 67. The conductivity of the slags increased with increasing iron oxide content. The effect of the variation in the oxidation state was more pronounced as the FeO_x content of the slags increased. The conductivity of the 15wt% FeO_x slag increased with decreasing p_{O2} and reached a maximum at 10^{-8} atm where the experiment was ended at that oxidation state. The conductivity of the 20wt% FeO_x slag increased with decreasing p_{O2}, reached a maximum at around 4×10^{-6} atm and then decreased at more reducing conditions. The conductivity of the 30wt% FeO_x slag increased with decreasing p_{O2} until it reached a maximum at around 6×10^{-5} atm. Thereafter the conductivity decreased with further reduction and the conductivity values at the reduced conditions were lower than in air. The conductivity of the 40wt% FeO_x slag followed the same trends as the 30wt% FeO_x slag and the peak in the conductivity also occurred at around $p_{O2} = 6 \times 10^{-5}$ atm.

The repeatability of the response of the electrical conductivity to oxidation state was good in terms of the similar shapes observed for the curves of repeated runs. The repeatability of the absolute values of the conductivity at a particular oxidation state was fair (within 20%). As mentioned above, the large difference in the conductivity values for slag L30 was considered to have been a result of misalignment of the electrodes and the crucible in the case of the intial run. Error bars have not been shown on the diagram as the diagram loses clarity.

Similar trends were reported by Engell and Vygen (1968) for the variation of slag electrical conductivity with oxidation state and iron oxide addition. Their slags had a molar CaO/SiO_2 ratio of 0.79. The molar basicity ratio of the low basicity slag varied from around 0.62 at the start of an experiment to values between 0.68 and 0.80 at the end owing to the dissolution

of MgO (see Table 11 for more details). Unfortunately the data of Engell and Vygen (1968) cannot be directly compared as their work was carried out at 1600 °C. It was not feasible to carry out comparative experiments at 1600 °C with the shallow cell technique, as the attack of the MgO crucibles would have resulted in significant changes in the slag chemistry.

4.2. Intermediate basicity slags

The intended master composition (wt%) of the intermediate basicity slag was Al_2O_3: 6.25%, CaO: 20%, MgO: 20%, SiO_2: 53.75%. Iron oxide was added to the master slag to obtain iron levels in the slag of 10, 20, 30 and 40wt%. The analysed compositions of all the slags were very similar to the intended compositions and are shown in Appendix C.2.1.

Experiments on slags I0, I10, I20 and I30 were performed using the deep cell technique and the effect of temperature on the conductivity was of interest. For these experiments, the iron oxide was added in the form of wüstite and the experiments were conducted under a nitrogen atmosphere. The experiments were carried out in the temperature range of 1400 to 1550 °C.

Measurements were performed on slags I20, I30 and I40 using the shallow cell setup to determine oxidation state dependence of the conductivity of the slags. In these cases, the iron oxide was added in the form of haematite and the experiments were started in air. The slag was then reduced while conductivity measurements were made. The measurements were made at a constant temperature of 1450 °C.

4.2.1. Deep cell measurements – temperature dependence

The standard deep cell technique was used to test the temperature dependence of the electrical conductivity of slag I0. The slag had an expected liquidus temperature of slightly below 1400 °C (see pseudo-ternary diagram in Figure 45), therefore measurements were made on heating from 1400 up to 1550 °C and on cooling back down to 1400 °C. The typical response to temperature was observed and is shown in Figure 68.

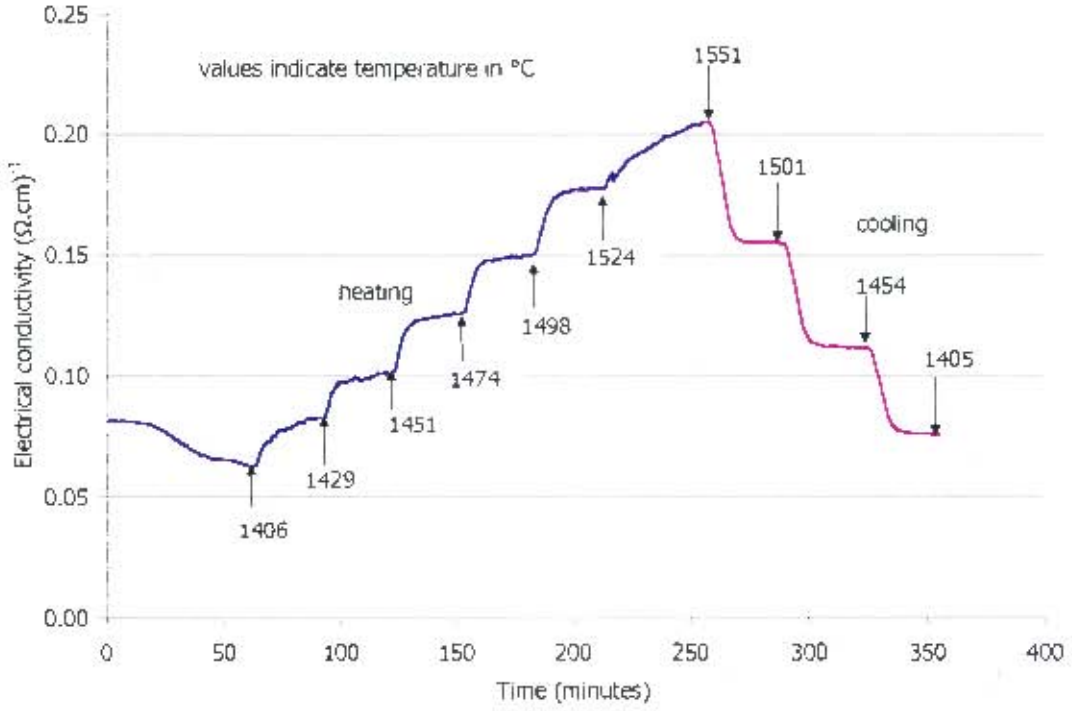

Figure 68: Temperature dependence of conductivity of slag I0. Approximate composition of slag I0 (wt%): Al_2O_3: 6, CaO: 20, MgO: 20, SiO_2: 54.

The electrical conductivity of the slag increased as the temperature increased. The longer equilibration time when approaching 1550°C was due to the longer time that it took the furnace to heat up to the temperature (as explained in Section 4.1.1). The conductivity values on cooling were close to but slightly higher than the values recorded on heating. As with the experiments on the low basicity slag, the typical duration of an experiment was from 4 to 6 hours.

Iron oxide was added to slag I0 in the form of wüstite to obtain slags I10, I20 and I30. Very similar trends to the ones shown in Figure 48 and Figure 68 were obtained and will not be shown. The values of the conductivity of these slags on heating and cooling agreed very well. The numerical values of the conductivities calculated for all the intermediate basicity slags are presented in Table 17. The data are presented in the chronological order in which they were measured for a given slag. The calibration data used in the calculation of the conductivity were a slope of −1.013 and an intercept of 0.024. The raw values of the resistances measured are shown in Appendix C.2.2.

Table 17: Intermediate basicity results: temperature dependence of electrical conductivity. Approximate slag compositions (wt%): Al_2O_3: 6, CaO: 20, MgO: 20, SiO_2: 54 with FeO_x additions of 10, 20 and 30% (in the form of wüstite). Measurements conducted under nitrogen.

I0		I10		I20		I30	
Temperature °C	Electrical conductivity $(\Omega.cm)^{-1}$	Temperature °C	Electrical conductivity $(\Omega.cm)^{-1}$	Temperature °C	Electrical conductivity $(\Omega.cm)^{-1}$	Temperature °C	Electrical conductivity $(\Omega.cm)^{-1}$
1407	0.062	1407	0.115	1407	0.267	1405	0.519
1429	0.082	1426	0.134	1426	0.309	1429	0.596
1450	0.102	1449	0.156	1450	0.353	1452	0.667
1474	0.126	1475	0.185	1475	0.400	1477	0.746
1498	0.151	1500	0.221	1499	0.452	1501	0.833
1525	0.180	1525	0.255	1523	0.509	1523	0.916
1550	0.208	1550	0.291	1551	0.582	1551	1.046
1501	0.156	1503	0.219	1501	0.464	1504	0.849
1454	0.112	1454	0.159	1453	0.355	1453	0.679
1405	0.076	1403	0.112	1403	0.271		

The tabulated conductivity results for the intermediate basicity slags above are more easily visualised in Figure 69.

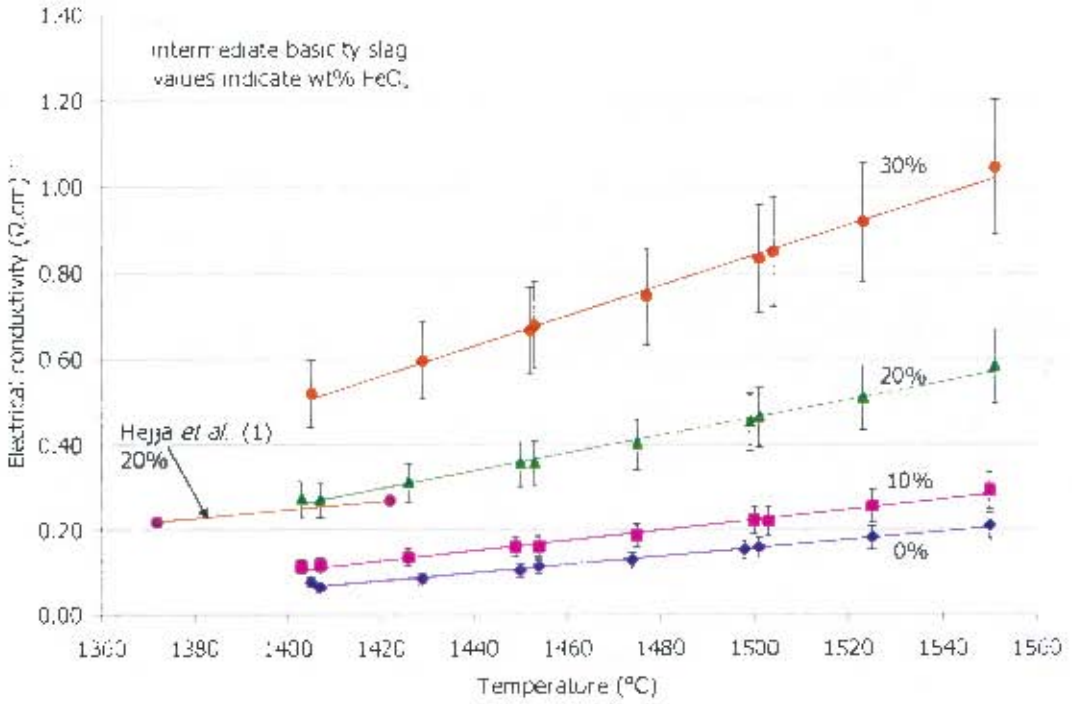

Figure 69: Temperature dependence of the conductivity of slags I0, I10, I20 and I30. Master slag composition: Al_2O_3: 6, CaO: 20, MgO: 20, SiO_2: 54 with addition of 10, 20 and 30 wt% FeO_x.

From Figure 69 it is apparent that additions of FeO_x to the master slag brought about increases in the conductivity. The electrical conductivity of all the slags increased with increasing temperature. Where there are multiple data points at similar temperatures, one was the conductivity value on heating and the other on cooling. The trend lines are included to aid visualisation. The error bars indicate the ±15% uncertainty in the measurements.

Table 19: Slag I20 results: oxidation state dependence of electrical conductivity at 1450 °C. Approximate slag composition (wt%): Al_2O_3: 6, CaO: 16, FeO_x: 20, MgO: 15, SiO_2: 43.

Slag I20

p_{CO2}/p_{CO}	p_{O2}	Resistance measured	Electrical conductivity
	atm	Ω	$(\Omega.cm)^{-1}$
air	2.1E-01	13.3	0.353
80	5.6E-05	12.3	0.392
20	3.5E-06	12.2	0.393
10	8.7E-07	12.7	0.374
5	2.2E-07	13.4	0.352
2	3.5E-08	13.7	0.343
1	8.7E-09	13.9	0.337
0.05	1.9E-11	14.5	0.320
Calibration slope			-1.02
Calibration intercept			1.41

The peak in the conductivity occurred at a p_{CO2}/p_{CO} ratio of 20 and the value of the conductivity at reduced conditions was lower than the value in air. The absolute value of the conductivity at around p_{CO2}/p_{CO} = 1 to 5 was in good agreement with the value from the temperature dependence experiment (~0.35 $\Omega^{-1}.cm^{-1}$ at 1450 °C from Table 17).

4.2.2.2Slag I30

The progress of the experiment on slag I30 is shown in Figure 70. The description of the experimental progress is very similar to that given in Section 4.1.2.1 for slag L15. The only expection is that at the end of the experiment the gas atmosphere was changed to CO + N_2. It is postulated that the very reducing gas atmosphere reduced the ferric to ferrous iron leading to a decrease in the conductivity and thereafter the ferrous ions were reduced to metallic iron which brought about the rise in the conductivity. This explains the U-shape section of the curve at around 350 minutes.

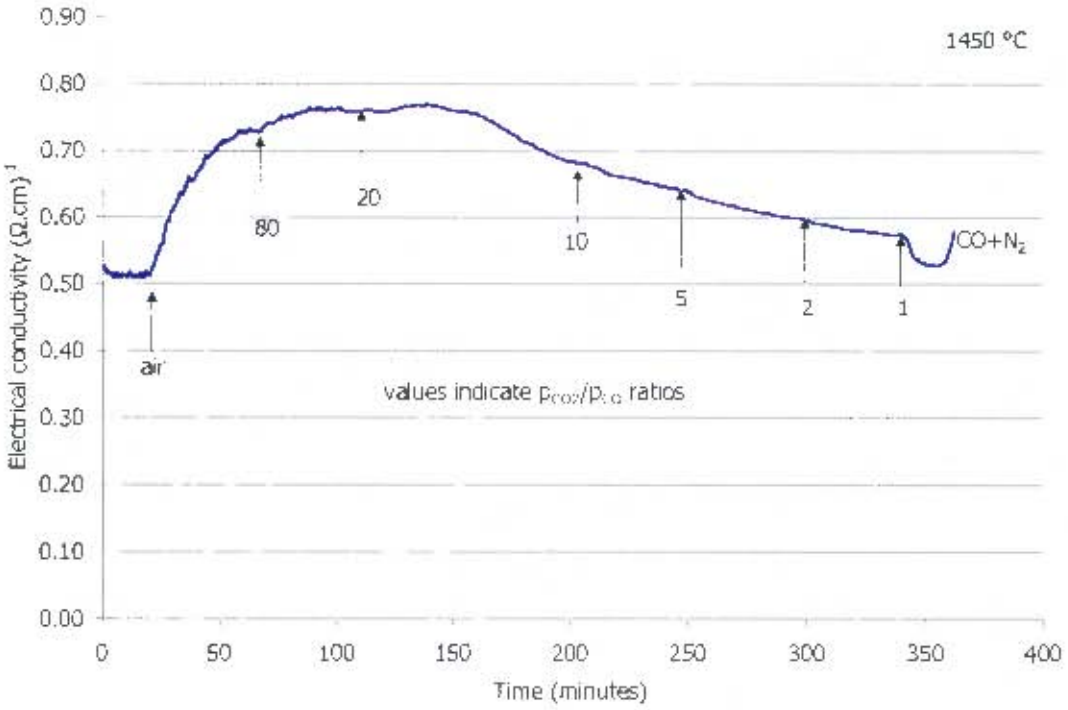

Figure 70: Progress of oxidation state experiment on slag I30 at 1450 °C. Approximate slag composition (wt%): Al_2O_3: 6, CaO: 14, FeO_x: 30, MgO: 13, SiO_2: 37.

The conductivity increased from around 0.51 $(\Omega.cm)^{-1}$ in air to a maximum of around 0.76 $(\Omega.cm)^{-1}$ at a p_{CO2}/p_{CO} ratio of 20. The conductivity then decreased with further reduction of the slag and reached a value of around 0.57 to 0.65 $(\Omega.cm)^{-1}$ at ratios of 1 to 5. This value was slightly lower than the value of ~0.67 $(\Omega.cm)^{-1}$ at 1450 °C obtained in the temperature dependence experiment. The reason for the lower value could possibly have come about as a result of the decrease in the iron content of the slag from 30.2wt% to 25.6wt% (see Table 18), although the increase in the MgO content also needs to be considered. The effect of MgO will be discussed in more detail in Section 5.3.

Table 20: Slag I30 results: Oxidation state dependence of electrical conductivity at 1450 °C. Approximate slag composition (wt%): Al_2O_3: 6, CaO: 14, FeO_x: 30, MgO: 13, SiO_2: 37.

Slag I30

p_{CO2}/p_{CO}	p_{O2}	Resistance measured	Electrical conductivity
	atm	Ω	$(\Omega.cm)^{-1}$
air	2.1E-01	10.5	0.514
80	5.6E-05	8.2	0.729
20	3.5E-06	8.0	0.760
10	8.7E-07	8.6	0.683
5	2.2E-07	9.0	0.644
2	3.5E-08	9.4	0.600
1	8.7E-09	9.7	0.574
0.1	4.7E-11	10.3	0.527
Calibration slope			-1.02
Calibration intercept			1.45

In terms of the decision as to when equilibrium was reached was again examined in terms of the rate of change in the measured resistances. The relevant graph for Slag I30 is shown in Figure 71.

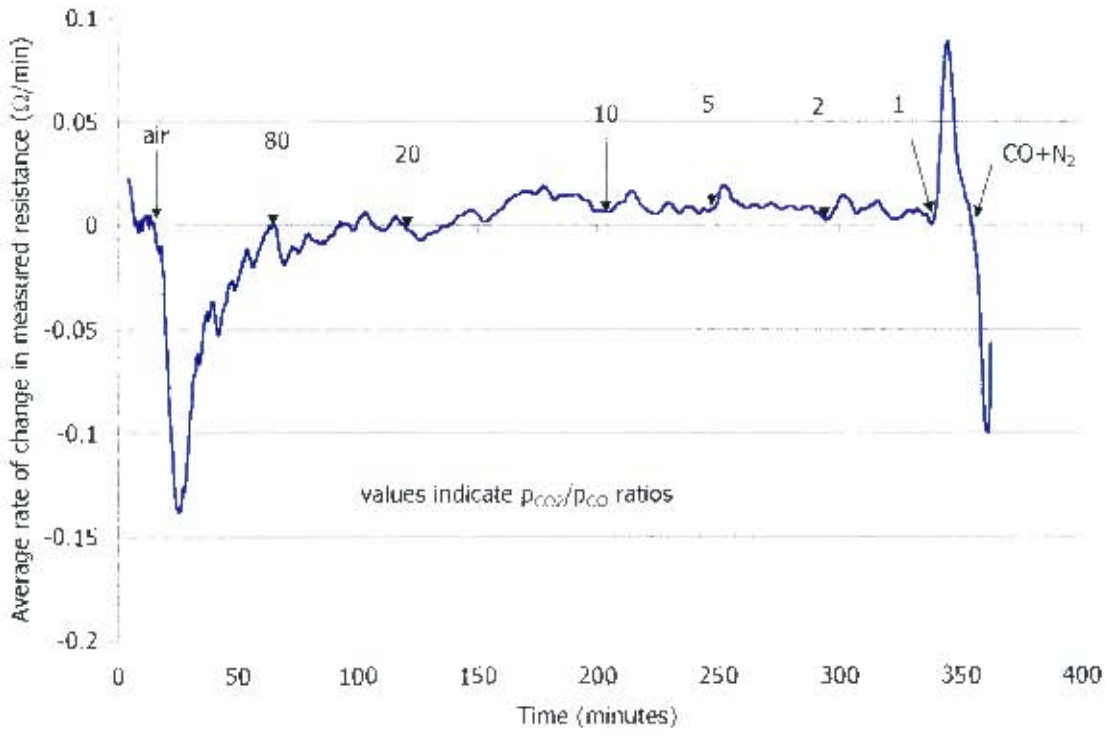

Figure 71: Average rate of change in resistances measured during the oxidation state experiment on Slag I30 at 1450 °C. Slag I30 composition (wt%): Al_2O_3: 6, CaO: 14, FeO_x: 30, MgO: 13, SiO_2: 37.

From the data presented in Figure 71, it is seen that where the average rate of change in the measured resistances approached zero, then the system was identified as being at or very close to equilibrium. The numerical values of the conductivity at the various oxidation states are provided in Table 20. The assessment of equilibrium conditions is presented in

Table 21.

Table 21: Equilibrium data calculated from oxidation state experiment on Slag I30 based on average rate of change in measured resistance with time

p_{CO2}/p_{CO}	Time	$R_{measured}$	Average ($\Delta R/\Delta t$)	κ_{eq}	κ_{30}	%change
ratio	minutes	Ω	(Ω/min)	$(\Omega.cm)^{-1}$	$(\Omega.cm)^{-1}$	
air	20	10.53	0.001	0.514	0.512	-0.4
80	66	8.23	0.000	0.729	0.727	-0.2
20	115	8.00	0.002	0.760	0.754	-0.9
10	202	8.59	0.007	0.683	0.660	-3.4
5	244	8.96	0.007	0.644	0.622	-3.5
2	293	9.41	0.003	0.600	0.592	-1.3
1	336	9.72	0.002	0.574	0.570	-0.7
$CO + N_2$	356	10.34	-0.002	0.527	0.530	0.7

From Table 21 and Figure 71 it can be seen that most of the equilibrium conductivity points were identified correctly. The conductivities at the conditions of p_{CO2}/p_{CO} were possibly judged prematurely. However, the change in the conductivity that would occur after 30 minutes would only be around 3 – 3.5 % and the original conductivity values are considered accurate enough.

In order to obtain a comparision of the shallow cell and the deep cell techniques, an experiment was conducted on slag I30 where the deep cell was used in an oxidation state experiment. After the temperature dependence experiment on slag I30 was completed (where the slag was still in a reduced state at 1450 °C), the atmosphere in the furnace was then changed from nitrogen to air. The response of the conductivity to the change in the oxidation state of the slag was recorded. The progress of this experiment is shown in Figure 72.

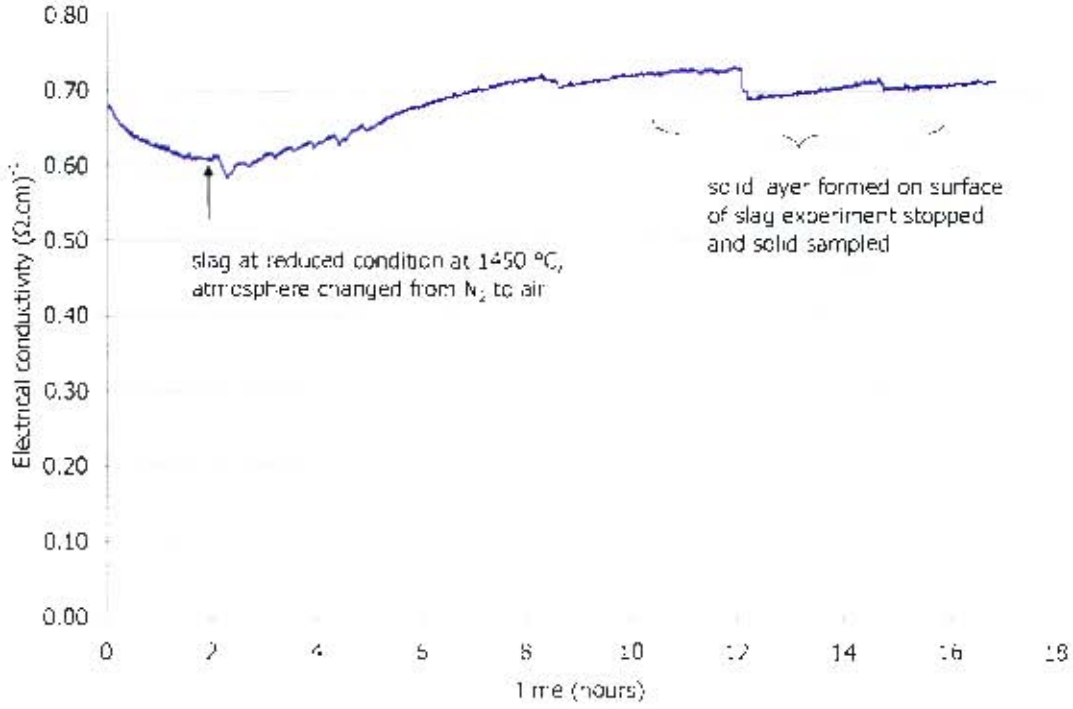

Figure 72: Slag I30: Deep cell experiment on oxidation state dependence of electrical conductivity at 1450 °C. Approximate slag composition: Al_2O_3: 6, CaO: 14, FeO_x: 30, MgO: 13, SiO_2: 37.

The conductivity initially dropped from around 0.67 $(\Omega.cm)^{-1}$ to around 0.61 $(\Omega.cm)^{-1}$. This was possibly due to a slight cooling effect by the air which was not preheated to 500 °C (the nitrogen was deoxidised by passing the gas through copper turnings at 500 °C). The other possibility was slight differences in the thermal conductivities of the gases at 1450°C caused additional surface cooling of the slag in the case of air. Data on the thermal conductivity of air has been found up to temperatures of 1450°C, but unfortunately not for nitrogen. At 600K (326.8 °C) the thermal conductivity of nitrogen (0.0441 W/m.K) is slightly lower than for air (0.0465 W/m.K).

Referring to Figure 39 again, the conductivity increased to approximately 0.73 $(\Omega.cm)^{-1}$ over a time period of about ten hours. This value of the peak in the conductivity was in fair agreement with the value from the shallow cell technique (0.76 $(\Omega.cm)^{-1}$ at p_{CO_2}/p_{CO} 20). The conductivity appeared to stabilise although there were some irregularities over time. The slag surface was observed through the sight glass on the top end cap of the furnace and a distinct solid layer was observed. The experiment was stopped and an attempt was made to obtain a sample of the solid layer. This was done by quickly withdrawing the electrodes from the furnace and quenching the material on the electrode tips in water. The solid layer frozen onto the electrodes was then mounted and polished and analysed using an electron microprobe (Jeol 8900). The analysis of the solid material is shown in Table 22 below. It should be noted that the value for oxygen is a calculated value based on the oxygen requirements for Al_2O_3, MgO and FeO (as Fe^{2+}).

Table 22: Analysis of solid layer on surface of slag I30

Element	wt%
Al	1.6
Ca	0.0
Fe	60.0
Mg	9.3
Si	0.0
O	24.9
Total	96.0

Based on the above analysis and assuming the 4% of mass not accounted for is due to oxygen associated with Fe^{3+} ions, then the composition is close to that magnetite (Fe_3O_4). The analysis suggested that the composition of the solid layer on the surface of slag I30 was very close to magnetite, although also included some magnesia. This is plausible given the high conductivity of the slag at the time when the solid was formed. The conductivity of magnetite at around 1400-1500 °C is around 200 $\Omega^{-1}.cm^{-1}$ (Gleitzer (1997), Nell and Wood (1989), Mason and Bowen (1981b)). The effect of a solid layer will be discussed further in Section 5.3.

4.2.2.3Slag I40

Two experiments were carried out on slag I40. The progress of the initial experiment on slag I40 and a repeat run are shown in Figure 73.

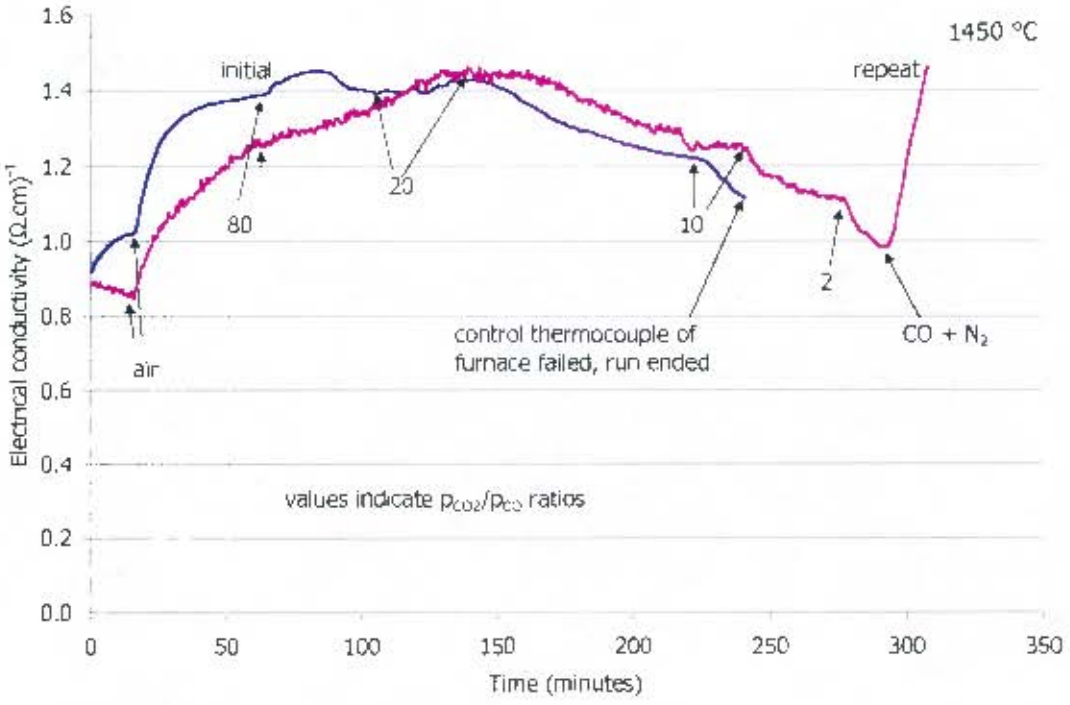

Figure 73: Progress of experiments on slag I40 – initial and repeat runs at 1450 °C. Approximate composition of slag I40 (wt%) : Al_2O_3: 5, CaO: 12, FeO_x: 40, MgO: 11, SiO_2: 32.

The reason a repeat run was performed on slag I40 was that during the initial run the control thermocouple of the furnace failed and the experiment had to be ended. The results of both

experiments agreed quite well in terms of the response to the oxidation state. The absolute values of the conductivity were in fair agreement, although the conductivity values at the more oxidised conditions were higher in the initial run than in the repeat run. The conductivity increased as the oxidation state was decreased, came to a maximum and then decreased with further reduction. The conductivity values in air were lower than at reduced conditions. During the initial run (blue line) the peak in the conductivity occurred between p_{CO2}/p_{CO} = 80 and 20 and then a secondary peak was observed between p_{CO2}/p_{CO} = 20 and 10. With the repeat run (purple line), the maximum conductivity occurred at around p_{CO2}/p_{CO} = 20 where there was a plateau. A secondary peak was not observed in the repeat run. The sharp increase at the end of the repeat experiment is ascribed to the reduction of the ferric and ferrous ions to metallic iron.

The results of the both experiments are shown in Table 23.

Table 23: Slag I40 results: oxidation state dependence of electrical conductivity at 1450 °C. Approximate composition of slag I40 (wt%) : Al_2O_3: 5, CaO: 12, FeO_x: 40, MgO: 11, SiO_2: 32.

Slag I40 initial

p_{CO2}/p_{CO}	p_{O2}	Resistance measured	Electrical conductivity
	atm	Ω	$(\Omega.cm)^{-1}$
air	2.1E-01	6.8	1.017
80	5.6E-05	5.7	1.386
20	3.5E-06	5.7	1.395
10	8.7E-07	6.1	1.220
Calibration slope			-1.02
Calibration intercept			1.49

Slag I40 repeat

p_{CO2}/p_{CO}	p_{O2}	Resistance measured	Electrical conductivity
	atm	Ω	$(\Omega.cm)^{-1}$
air	2.1E-01	7.6	0.856
80	5.6E-05	5.9	1.296
20	3.5E-06	5.6	1.432
10	8.7E-07	6.0	1.242
2	3.5E-08	6.4	1.114
0.1	8.7E-11	6.9	0.985
Calibration slope			-1.02
Calibration intercept			1.49

4.2.2.4 All oxidation state experiment results on intermediate basicity slags

The results of the oxidation state experiments on the intermediate basicity slags were also expressed in terms of the oxygen partial pressures and are shown in Figure 74.

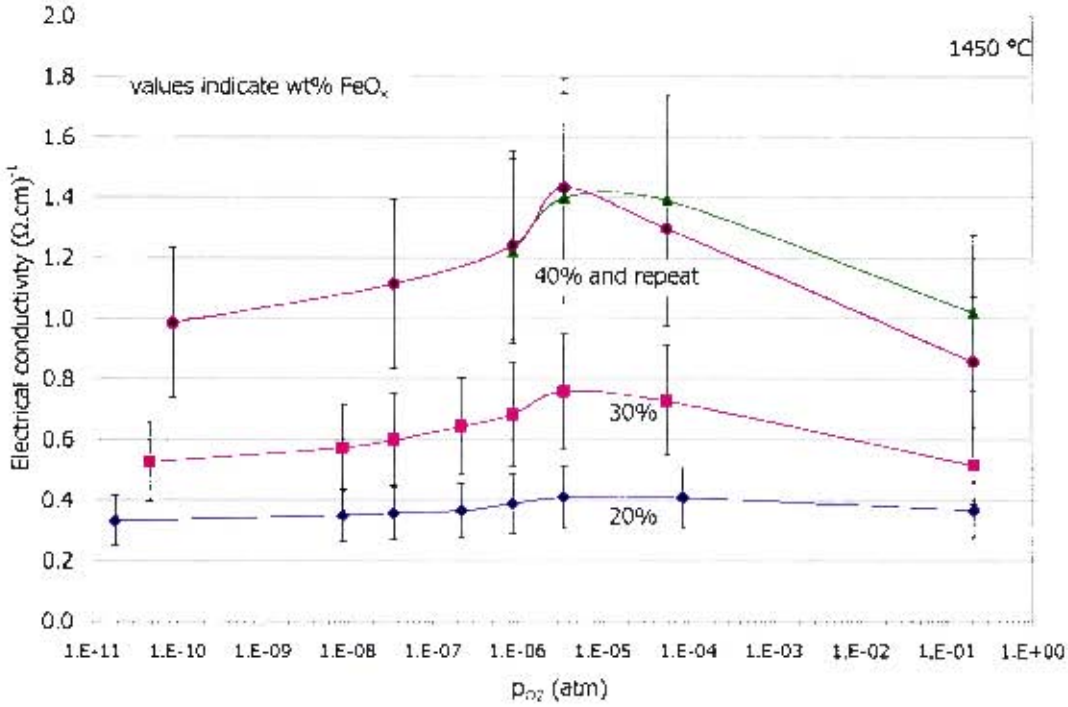

Figure 74: Variation of intermediate basicity slag conductivity with oxidation state and iron oxide content at 1450 °C. Composition of master slag: Al_2O_3: 6, CaO: 20, MgO: 20, SiO_2: 54 with additions of 20, 30 and 40wt% FeO_x.

The electrical conductivity of the intermediate basicity slags increased with iron oxide content. Starting from air, the conductivity increased as the p_{O2} decreased until it reached a maximum at around 4 x 10^{-n} atm. The conductivity then decreased as the atmosphere became more reducing. In the case of slag I20, the conductivity at the reduced conditions was lower than the value in air. For slag I30 and one of the I40 slags, the values of the conductivity in air were lower than at the reduced conditions.

The value of the conductivity for slag I20 at around p_{O2} = 10^{-8} to 10^{-7} atm (approximately 0.36 $\Omega^{-1}.cm^{-1}$) compared well with the value from the temperature dependence measurements (approximately 0.35 $\Omega^{-1}.cm^{-1}$). The conductivity value for slag I30 at around p_{O2} = 10^{-8} to 10^{-7} atm (approximately 0.60 $\Omega^{-1}.cm^{-1}$) was slightly lower than the value from the temperature dependence measurements (approximately 0.67 $\Omega^{-1}.cm^{-1}$). The repeatability of the variation of the conductivity with oxidation state for slag I40 was reasonable in terms of the maximum in the conductivity. The values of the conductivity in air for slag I40 were within the possible 25% error. The error bars indicate the possible ±25% uncertainty in the measurements (as calculated in the error analysis in section 3.7.4). It must be emphasised however, that for a given run, the relative change in the conductivity with oxidation state is more accurate than the possible 25% uncertainty in the absolute values of the run.

4.3. High basicity slag

As with the low and intermediate basicity slags, the high basicity slag was tested using the deep cell and the shallow cell technique. The first set of experiments examined the effect of temperature on the conductivity of slags H0, H10, H15, H20 and H30 using the deep cell setup. The second set of experiments examined the effect of oxidation state on the conductivity of slags H20, H30 and H40.

4.3.1. Deep cell measurements – effect of temperature

As the other high basicity slags were made up from the master slag H0, the intended and analysed compositions of slag H0 are provided in Table 24. The slag sample was milled in a ring mill and analysed using XRF.

Table 24: Intended and analysed compositions of the high basicity master slag H0

Slag H0	Intended		Analysed	
Component	wt%	mol%	wt%	mol%
Al_2O_3	5.0	2.7	5.3	2.9
CaO	30.0	29.2	28.7	28.2
MgO	20.0	27.1	19.6	26.8
SiO_2	45.0	40.9	45.8	42.1
Total	100	100.0	99.3	100.0
(C+M)/(A+S)	1.00	1.29	0.94	1.22

The lime and magnesia contents of the analysed slag were slightly lower than intended which meant that the wt% basicity ratio was 0.94 instead of 1.00.

The standard deep cell technique was used to test the conductivity of Slag H0. The slag had an expected liquidus temperature of around 1400 °C (see Figure 45), therefore measurements were made on heating from 1400 up to 1550 °C. The temperature dependence of slag H0 was shown in Figure 48 in section 3.6.3.

Iron oxide was added to Slag H0 in the form of wüstite to obtain slags H10, H15, H20 and H30. The temperature responses of the slags' conductivities were very similar to the trend shown in Figure 48 and will not be shown. The results of the conductivity vs temperature for the high basicity slags are shown in Table 25 and in Figure 75. The full results including the measured resistances are shown in Appendix C.3.2. The calibration data used in calculating the conductivities from the resistances measured were a slope of –1.013 and an intercept of 0.024. The data are presented in the chronological order in which they were measured.

Table 25: High basicity slags – temperature dependence of conductivities. Approximate composition of slags (wt%): Al_2O_3: 5, CaO: 29, MgO: 20, SiO_2: 46 with additions of 10, 15, 20 and 30% FeO_x

H0		H10		H15		H20		H30	
Temperature	Electrical conductivity	Temperature	Electrical conductivity	Temperature	Electrical conductivity	Temperature	Electrical conductivity	Temperature	Electrical conductivity
°C	$(\Omega.cm)^{-1}$	°C	$(\Omega.cm)^{-1}$	°C	$(\Omega.cm)^{-1}$	°C	$(\Omega.cm)^{-1}$	°C	$(\Omega.cm)^{-1}$
1396	0.143	1401	0.224	1408	0.301	1405	0.375	1407	0.645
1417	0.181	1430	0.277	1425	0.339	1427	0.423	1427	0.692
1457	0.249	1452	0.327	1452	0.389	1452	0.475	1450	0.763
1477	0.296	1477	0.381	1476	0.446	1475	0.545	1475	0.849
1502	0.343	1502	0.444	1500	0.520	1498	0.613	1501	0.950
1527	0.397	1526	0.517	1524	0.591	1524	0.691	1524	1.055
1551	0.455	1552	0.592	1546	0.664	1548	0.768	1550	1.193
				1503	0.537	1500	0.617	1453	0.797
				1456	0.420	1453	0.492		

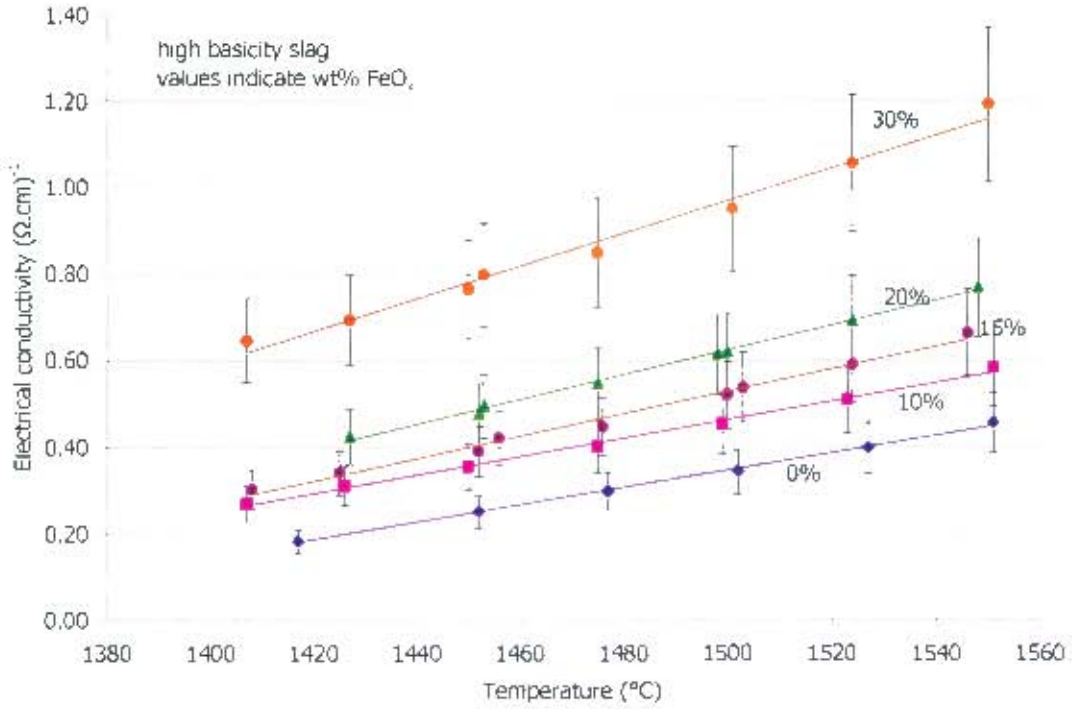

Figure 75: Temperature dependence of conductivity of high basicity slags with iron oxide addition. Approximate composition of slags (wt%): Al_2O_3: 5, CaO: 29, MgO: 20, SiO_2: 46 with additions of 10, 15, 20 and 30% FeO_x

The addition of FeO_x to the high basicity master slag brought about increases in the conductivity. Where there are multiple data points at one temperature for a particular slag, one was the conductivity value on heating and the other on cooling. The trend lines are included to aid visualisation. The electrical conductivity increased with increasing temperature. The error bars indicate the possible error of ±15% in the measurements. The activation energies for the slags were calculated from the Arrhenius relationship but will be presented and discussed in Section 5.2.

4.3.2. Shallow cell measurements – oxidation state dependence

The oxidation state dependence of the slag conductivity was tested for slags H20, H30 and H40. This was done using the shallow cell technique using MgO crucibles at 1450 °C. The determination of equilibrium conditions was based on monitoring of the average rate of change in the measured resistances (results shown in Appendix C.3.3). As a result of using the MgO crucibles, the MgO content of the slags increased with experiment duration and gas atmosphere. The pertinent data has been summarised in Table 26 below, The complete analysed compositions are available in Appendix C.3.1.

Table 26: MgO increase in oxidation state experiments on high basicity slags

Slag name	MgO gain	Duration	Final p_{CO_2}/p_{CO}	Basicity (molar basis)		FeO_x content (wt%)	
	wt%	hours	ratio	Initial	Final	Initial	Final
H20	3.8	6	$CO + N_2$	1.22	1.37	19.0	18.5
H30 initial	5.4	5	$CO + N_2$	1.21	1.52	29.6	23.8
H30 repeat	4.3	5.3	$CO + N_2$	1.21	1.43	29.6	23.1
H40	7.2	5.6	$CO + N_2$	1.20	1.61	37.9	32.3
H40 rep 1	4.2	2.9	10	1.20	1.47	37.9	34.7

Over the duration of the experiments, the high basicity slags picked up between 3.8 and 7.2 wt% MgO. The amount of MgO that dissolved into the slags was clearly related to the amount of iron in the slag. This was expected as the increase in iron brought about dilution of the other components. Therefore slag H40 had an initial MgO content of only 11.4wt% whereas slag H20 had an initial MgO content of 15.4wt%. From analysing the high and intermediate basicity slags' final MgO contents, it appeared that MgO level stabilised at around 18-20% for experiment durations of around 6 hours. The increase in the MgO content of the high basicity slags resulted in an increase in the basicity (molar% $(CaO+MgO)/(Al_2O_3+SiO_2)$ ratio) from around 1.21 up to 1.37 – 1.61.

4.3.2.1 Slag H20

The progress of the experiment on slag H20 is shown in Figure 76. There was relatively little variation in the conductivity with change in oxidation state. The value of the conductivity at the reduced conditions (~0.51 $\Omega^{-1}.cm^{-1}$ at ratios of 1 to 5) agreed well with the value from the temperature dependence measurements (~0.48 $\Omega^{-1}.cm^{-1}$ at 1450°C – see Table 25). The only major variation in the conductivity with oxidation state was changing from an air atmosphere to a p_{CO_2}/p_{CO} ratio of 80.

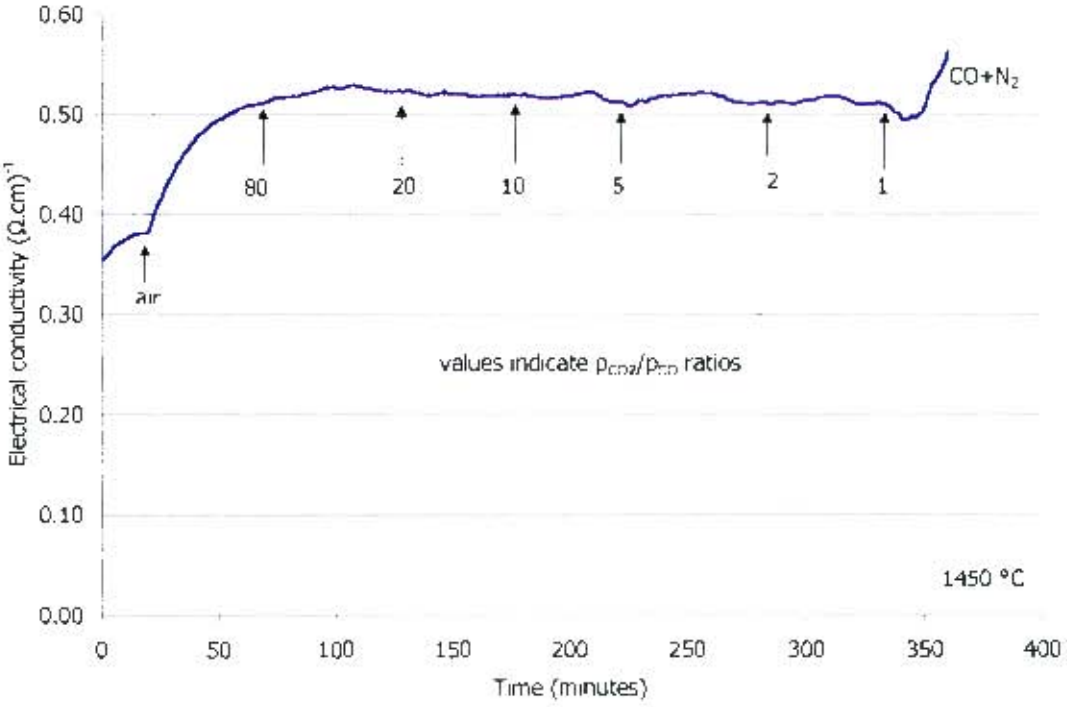

Figure 76: Oxidation state experiment on conductivity of slag H20 at 1450 °C. Approximate slag composition (wt%): Al_2O_3: 5, CaO: 23, FeO_x: 19, MgO: 16, SiO_2: 37.

The numerical results for the experiment are shown in Table 27.

Table 27: Slag H20 results: oxidation state dependence of conductivity at 1450 °C. Approximate slag composition (wt%): Al_2O_3: 5, CaO: 23, FeO_x: 19, MgO: 16, SiO_2: 37.

Slag H20

p_{CO2}/p_{CO}	p_{O_2}	Resistance measured	Electrical conductivity
	atm	Ω	$(\Omega.cm)^{-1}$
air	2.1E-01	13.1	0.381
80	5.6E-05	10.5	0.509
20	3.5E-06	10.3	0.522
10	8.7E-07	10.4	0.518
5	2.2E-07	10.5	0.511
2	3.5E-08	10.5	0.511
1	8.7E-09	10.5	0.510
0.1	4.5E-11	10.8	0.493
Calibration slope			-1.02
Calibration intercept			1.44

4.3.2.2 Slag H30

Two experiments were carried out on slag H30 using the shallow cell technique. The progress of both the runs is shown in Figure 77.

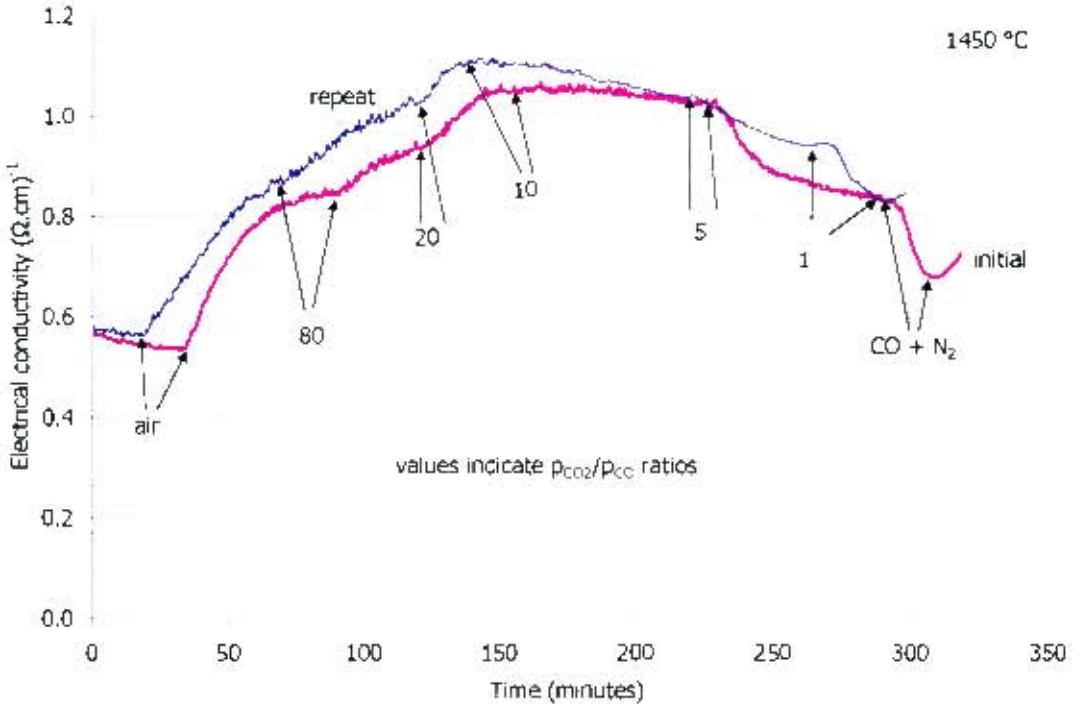

Figure 77: Progress of experiments on slag H30 – initial and repeat runs at 1450 °C. Approximate composition of slag (wt%): Al_2O_3: 4, CaO: 20, FeO_x: 30, MgO: 13, SiO_2: 31.

The agreement between the initial and repeat runs was good in terms of both the absolute values of the electrical conductivity and the response to the changes in oxidation state. The conductivity was around 0.55 $(\Omega.cm)^{-1}$ in air and then increased as the atmosphere became more reduced. The conductivity reached a maximum of around 1.05 - 1.1 $(\Omega.cm)^{-1}$ at a p_{CO2}/p_{CO} ratio of 10 and then decreased as the slag was reduced further. The results for both experiments are shown in Table 28.

Table 28: Slag H30 results: oxidation state dependence of conductivity at 1450 °C. Approximate composition of slag (wt%): Al_2O_3: 4, CaO: 20, FeO_x: 30, MgO: 13, SiO_2: 31.

Slag H30 initial

p_{CO2}/p_{CO}	p_{O2}	Resistance measured	Electrical conductivity
	atm	Ω	$(\Omega.cm)^{-1}$
air	2.1E-01	10.3	0.540
80	5.6E-05	7.6	0.845
20	3.5E-06	7.1	0.935
10	8.7E-07	6.6	1.053
5	2.2E-07	6.7	1.025
1	8.7E-09	7.6	0.830
0.1	9.2E-11	8.4	0.722
Calibration slope			-1.02
Calibration intercept			1.48

Slag H30 repeat

p_{CO2}/p_{CO}	p_{O2}	Resistance measured	Electrical conductivity
	atm	Ω	$(\Omega.cm)^{-1}$
air	2.1E-01	10.0	0.560
80	5.6E-05	7.4	0.874
20	3.5E-06	6.8	0.991
10	8.7E-07	6.4	1.109
5	2.2E-07	6.6	1.039
1	8.7E-09	7.0	0.945
0.1	9.2E-11	7.7	0.827
Calibration slope			-1.02
Calibration intercept			1.48

A comparison was possible between the results of the shallow cell technique and the deep cell technique as an oxidation state experiment was carried out on slag H30 using the deep cell technique. This experiment was carried out in the same manner as the one on slag I30 (see section 4.2.2.2). Approximately 60g of slag H30 (in a reduced state) was held in a Pt

crucible at 1450 °C under a nitrogen atmosphere and the usual procedure followed in terms of immersing the electrodes to 8mm. The atmosphere was then changed to an air atmosphere and the change in the conductivity was recorded by logging the data on the laptop computer. The trend in Figure 78 was observed.

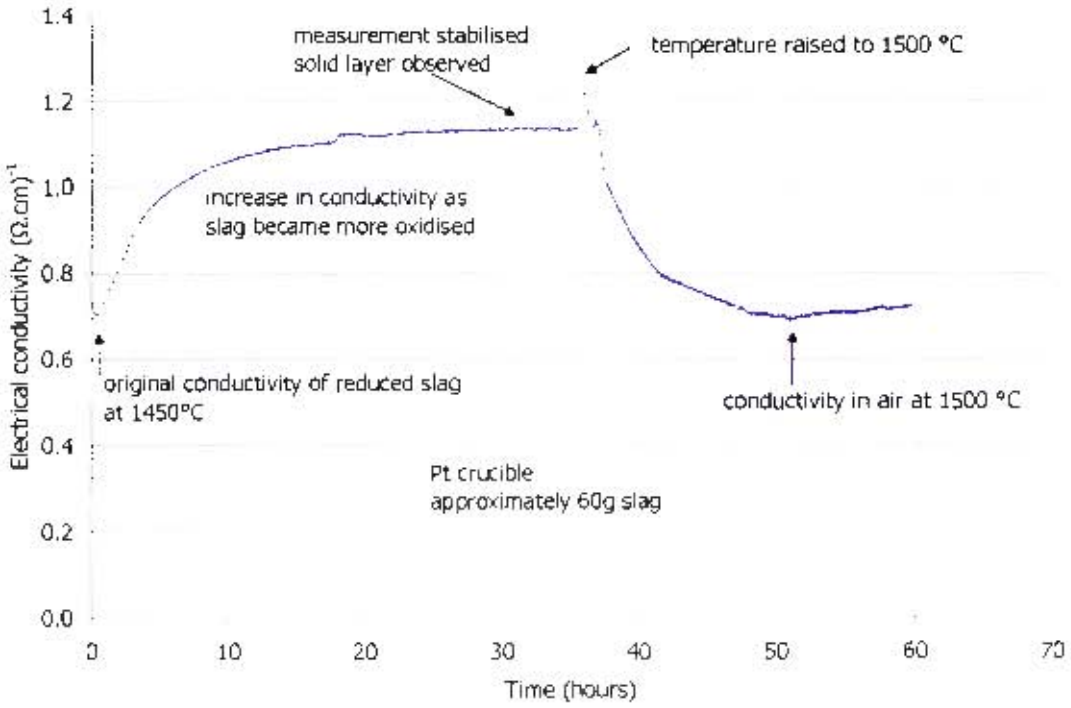

Figure 78: Variation in conductivity during oxidation of slag H30 using deep cell technique

Firstly, as a result of the amount of slag used in the experiment, the time taken for the slag to come to equilibrium with the gas atmosphere was very long (over 2 days). As the slag was initially in a reduced oxidation state it was expected that the slag conductivity would rise when exposed to the air atmosphere. This was observed, however, the conductivity then stabilised at approximately 1.13 $(\Omega.cm)^{-1}$ (from around 19 to 36 hours). The value of the peak in the conductivity from the deep cell measurements appeared to indicate that the shallow cell measurements were reasonably accurate. Also, the conductivity values at reduced conditions for both techniques were in reasonable agreement (~0.7 $(\Omega.cm)^{-1}$ for the deep cell and 0.72-0.83 $(\Omega.cm)^{-1}$ for the shallow cell).

As with slag I30, observations of the slag surface through the sight glass showed a distinct solid layer. It was reasoned that the solid surface was preventing further oxidation of the melt and explained the cause of the stable conductivity value. The temperature was raised to 1500 °C, the solid melted and the oxidation continued. The electrical conductivity of the slag at 1500 °C in air was approximately 0.69 $\Omega^{-1}.cm^{-1}$.

The fact that a solid layer formed on the surfaces of both slags I30 and H30 in the deep cell experiments was of interest. It is possible that similar surface layers were formed in the shallow cell measurements, however the differences between the experimental setups may be significant. In the shallow cell experiments the slag is initially in equilibrium with air and is then gradually reduced, whereas in the deep cell experiments the slag is initially in a reduced state and then oxidised. As a result of the lesser amount of slag in the shallow layer cell,

equilibration with gas phases is much quicker than in the deep layer cell. Therefore, even if a solid layer is formed in the shallow cell, equilibration of the slag with the gas is sufficiently rapid and the change in the conductivity can be be observed with changing oxidation state. However, in the deep cell experiments it is likely that the solid layer formed will significantly decrease mass diffusion between the gas and slag and to reach a final equilibrium will take very large amounts of time. Further, one of the other contributing factors which could also explain fewer crust formations in the shallow cell technique, is that the shallow cell crucible was smaller than the deep cell and fitted inside the pedestal used to hold the crucible. Therefore the radiant heat losses from both the surface and the sidewalls of the crucible are reduced for the shallow cell and the formation of a crust is reduced. Crusts on the surface during deep cell experiments could be observed, however, none were observed during shallow cell experiments.

In summary, it is felt that the agreement between the shallow and deep cell oxidation state dependent measurements was satisfactory in terms of the conductivities at reduced conditions and the maxima in the conductivities. As a result of the formation of a solid layer in the deep cell measurements, it was not possible to obtain a full oxidation state response, however, from the data obtained, it was possible to conclude that the shallow cell technique provided reasonably accurate results (within 20%).

4.3.2.3 Slag H40

The progress of the experiment on slag H40 was shown in Figure 56, but is shown again below in Figure 79 with the results of a repeat run. The agreement between the initial and repeat runs was very good in terms of both the absolute values of the conductivity and the response to the oxidation state. The repeat run (blue line) was stopped at $p_{CO2}/p_{CO} = 10$ so that a sample could be taken for analysis of ferric and ferrous contents. Starting from air, the conductivity increased with decreasing p_{CO2}/p_{CO} ratio until it reached a maximum between $p_{CO2}/p_{CO} = 20$ and 10. The conductivity then decreased at more reducing conditions. The large increase in the conductivity at the end of the initial run was thought to be due to the reduction of the ferric and ferrous ions to metallic iron.

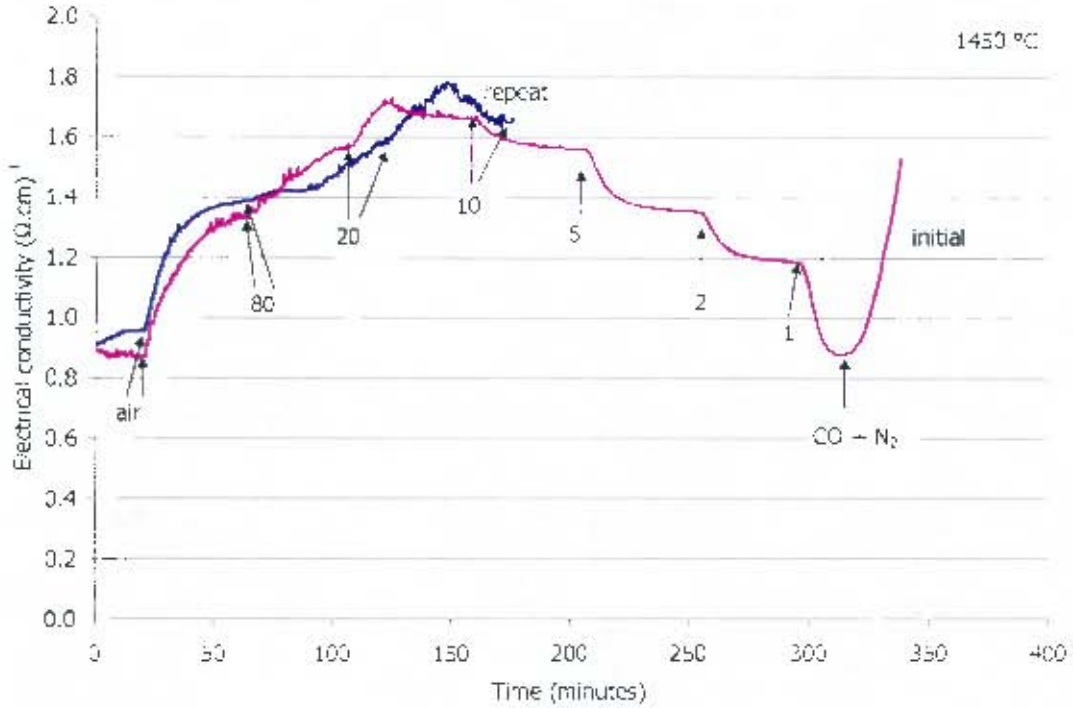

Figure 79: Progress of experiments on slag H40 – initial and repeat runs at 1450 °C. Approximate slag composition (wt%): Al_2O_3: 4, CaO: 17, FeO_x: 38, MgO: 12, SiO_2: 27.

As the experiment on the repeat run was stopped after approximately 2.9 hours, this enabled an opportunity to compare the MgO dissolution between the two runs. This is presented in Table 29 below:

Table 29: Analysed compositions of slag H40 and repeat

H40 and repeat	Initial analysed		H40		H40 repeat	
Components	wt%	mol%	wt%	mol%	wt%	mol%
Al_2O_3	4.0	2.4	3.8	2.2	3.3	2.0
CaO	16.9	18.9	17.5	18.3	17.6	18.9
FeO_x	37.9	33.0	32.3	26.4	34.7	29.1
MgO	11.4	17.6	18.6	27.1	15.6	23.2
SiO_2	27.0	28.1	26.6	26.0	26.7	26.8
Total	97.2	100.0	98.7	100.0	98.0	100.0
(C+M)/(A+S)	0.91	1.20	1.19	1.61	1.10	1.47
Basicity change			0.27	0.42	0.19	0.27
MgO gain			7.2	9.5	4.2	5.6
Final p_{CO_2}/p_{CO}			CO – N_2		10	
Duration (hours)			5.6		2.9	

The MgO gain in the initial run was 7.2wt%, while in the repeat run it was 4.2wt%. This indicated that the MgO gain was probably dependent on both the length of the experiment and the final oxidation state of the slag.

The numerical values of the conductivity results for both runs are shown in Table 30.

Table 30: Slag H40 results: Oxidation state dependence of conductivity at 1450 °C. Approximate slag composition (wt%): Al_2O_3: 4, CaO: 17, FeO_x: 38, MgO: 12, SiO_2: 27.

Slag H40 initial

P_{CO2}/P_{CO}	P_{O2}	Resistance measured	Electrical conductivity
	atm	Ω	$(\Omega.cm)^{-1}$
air	2.1E-01	7.6	0.865
80	5.6E-05	5.9	1.328
20	3.5E-06	5.4	1.556
10	8.7E-07	5.2	1.657
5	2.2E-07	5.4	1.558
2	3.5E-08	5.8	1.350
1	8.7E-09	6.3	1.185
0.13	1.5E-10	7.5	0.877
Calibration slope			-1.03
Calibration intercept			1.51

Slag H40 repeat

P_{CO2}/P_{CO}	P_{O2}	Resistance measured	Electrical conductivity
	atm	Ω	$(\Omega.cm)^{-1}$
air	2.1E-01	7.1	0.976
80	5.6E-05	5.7	1.414
20	3.5E-06	5.3	1.609
10	8.7E-07	5.2	1.679
Calibration slope			-1.03
Calibration intercept			1.51

A titration was carried out on the sample from the repeated run to determine the ferric and ferrous iron content. The titration technique used was described in Section 3.8. The ferric/total Fe fraction measured was 0.39. The interpretation of this ferric fraction will be discussed in Section 5.3.

4.3.2.4 All oxidation state dependence results for high basicity slag

The results of the high basicity slag conductivity variation with iron oxide content and oxidation state are shown in Figure 80. As was done previously, the P_{CO2}/P_{CO} ratios were expressed in terms of equivalent oxygen partial pressures.

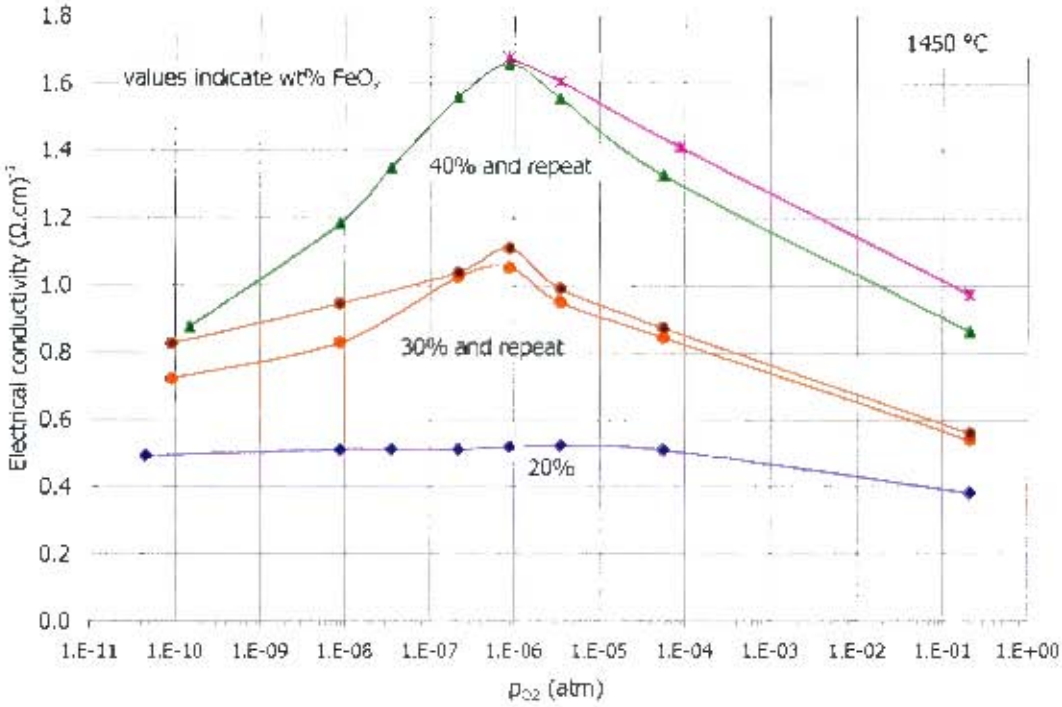

Figure 80: Variation of conductivity of high basicity slag with iron oxide content and oxidation state at 1450 °C. Approximate slag compositions: Al_2O_3: 5, CaO: 29, MgO:19, SiO_2: 46 diluted with 20, 30 and 40 wt% FeO_x.

The conductivity of the high basicity slags increased with iron oxide addition. Starting from p_{O2} = 0.21 atm (air), the conductivity increased with decreasing oxygen partial pressure until it reached a maximum at 4 x 10^{-6} atm for slag H20 and at 9 x 10^{-7} atm for both slags H30 and H40. The conductivity then decreased as the slag was reduced further. The conductivity values of the slags in air were lower than at the reduced conditions, although the conductivity of slag H40 was almost identical in air and at the reduced condition.

The value of the conductivity of slag H20 at p_{O2} = 10^{-8} to 10^{-6} atm (~0.51 $\Omega^{-1}.cm^{-1}$) was in good agreement with the value obtained from the temperature dependence measurements (~0.48 $\Omega^{-1}.cm^{-1}$ at 1450°C). The value of the conductivity of slag H30 at p_{CO2}/p_{CO} = 10^{-8} to 10^{-6} atm varied from 0.8 to 1.1 $\Omega^{-1}.cm^{-1}$. The conductivity value measured for the same slag from the temperature dependence measurements was approximately 0.8 $\Omega^{-1}.cm^{-1}$. The repeatability of the change in conductivity with oxidation state was very good in terms of the similar shapes the curves for repeated runs. The repeatability of the absolute values of the conductivity at particular oxidation states was fair (values within 15% of each other). Error bars representing the possible 25% error have been omitted to enhance the clarity of the diagram.

4.3.3. Heat-up profiles of slag H0 and H20

As was briefly mentioned in the Section 3.6.3, heat-up profiles were obtained for several slags. Two such experiments were carried out on the high basicity slag with no iron and on the high basicity slag with 20% FeO_x. These experiments were conducted using the deep cell technique in the following manner: the electrodes were left immersed in the slag at high

temperature (above the slag liquidus temperature) and the furnace was cooled down to 800 °C overnight. The frozen slag was then heated up the next morning while taking resistance measurements at certain temperature intervals. It was assumed that the volume changes on freezing and remelting made a negligible difference to the cell geometry and cell constant. The resultant graph is shown in Figure 81.

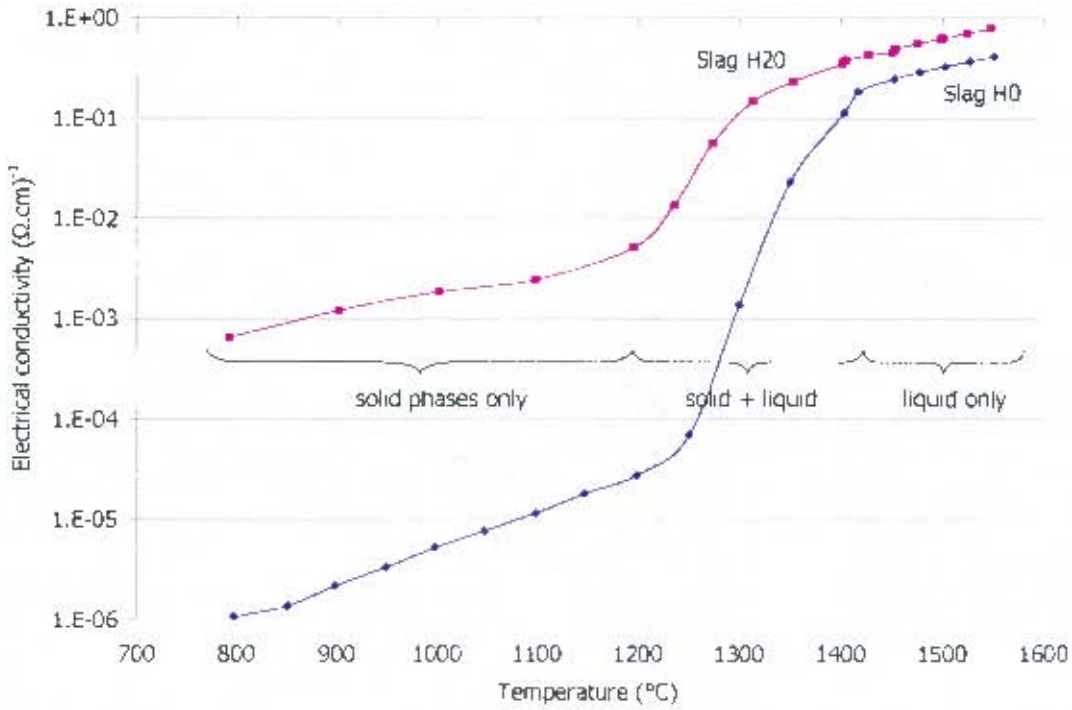

Figure 81: Heat-up profiles of the conductivities of slag H0 and slag H20. Slag H0 composition (wt%): Al_2O_3: 5, CaO: 29, MgO: 20, SiO_2: 46. Slag H20 composition (wt%): Al_2O_3: 4, CaO: 24, FeO_x: 20, MgO: 16, SiO_2: 36.

The main features evident in Figure 81 are that there is a very large increase in the conductivity as the slag melts, there are three distinct conductivity regions and the slag containing 20% FeO_x is more conductive than the iron-free slag both as a solid and a liquid. The three conductivity regions have been denoted as follows: solid phase region, solid and liquid phase region and liquid phase region. In each region there is a distinct slope in the conductivity – temperature curve. The regions have been loosely indicated in Figure 81. There is a large increase in the slope as the slag melts. It is likely to be related to the greater mobility that conducting ions have in the liquid phase. As mentioned briefly in Section 2.9, a large increase (orders of magnitude) in the conductivity of a slag on melting is characteristic of ionically conducting slags (in comparison to semiconducting systems where the change in conductivity on melting is less than an order of magnitude – see wüstite as an example in Section 2.5.1.3). The numerical results are shown in Table 31.

Table 31: Electrical conductivity of slags H0 and H20 on heating from 800 °C up to 1550 °C. Slag H0 composition (wt%): Al_2O_3: 5, CaO: 29, MgO: 20, SiO_2: 46. Slag H20 composition (wt%): Al_2O_3: 4, CaO: 24, FeO_x: 20, MgO: 16, SiO_2: 36.

Slag H0

Temperature	Electrical conductivity
°C	$(\Omega.cm)^{-1}$
797	1.06E-06
851	1.35E-06
898	2.14E-06
949	3.29E-06
998	5.15E-06
1047	7.52E-06
1098	1.13E-05
1147	1.78E-05
1199	2.73E-05
1251	6.87E-05
1300	1.34E-03
1350	2.26E-02
1403	1.13E-01
1417	1.83E-01
1452	2.44E-01
1477	2.84E-01
1502	3.23E-01
1527	3.64E-01
1551	4.04E-01

Slag H20

Temperature	Electrical conductivity
°C	$(\Omega.cm)^{-1}$
792	6.43E-04
902	1.20E-03
1002	1.84E-03
1098	2.43E-03
1196	5.09E-03
1236	1.36E-02
1274	5.65E-02
1313	1.46E-01
1353	2.31E-01
1401	3.47E-01
1404	3.73E-01
1405	3.75E-01
1427	4.23E-01
1450	4.41E-01
1452	4.75E-01
1453	4.92E-01
1475	5.45E-01
1498	6.13E-01
1500	6.17E-01
1524	6.91E-01
1548	7.68E-01

4.4. Chromium containing slags

The aim of the experiments on the chromium containing slags was to identify the effect that addition of chromium had on the electrical conductivity of melter type slags. As explained in the introduction, the feed to the electric furnaces of the platinum producers in South Africa is increasing in chromium content as a result of increased mining and treatment of UG2 ore. The chromium negatively effects the furnace operation. Currently the chromium level in the sponsors' slags vary from around 0.5% up to as much as 4% however higher chromium contents are possible and have been recorded.

The low basicity slag containing 20wt% FeO_x was selected for the testwork as it was similar in composition to the melter type slags (slag composition (wt%): Al_2O_3: 5, CaO: 5, FeO_x: 20, MgO: 20, SiO_2: 50). Additions of chromium were made to slag Cr0 to obtain levels of 0.5, 1, 2, 4, 6 and 8% Cr_2O_3. Conductivity measurements were initially on the chromium-free slag (designated slag Cr0). The slag was cooled and the specified amount of Cr_2O_3 powder required to increase the chromium content to 0.5% was placed on top of the frozen slag from the previous measurement. The slag was then heated up to the starting temperature for conductivity measurements (around 1400 °C) and a brief period of time (~30 minutes) was allowed for equilibration. It was assumed that the slag composition was uniform throughout the crucible after this equilibration time. The conductivity measurements were then carried out and thereafter the slag was then cooled down to room temperature. More Cr_2O_3 powder was then added to the slag to increase the chromium content of the slag to the next level (1%). The same equilibration procedure was employed again assuming that the slag composition was uniform throughout the crucible. In order to validate this assumption, two core samples were drilled from slag Cr8. Slag Cr8 was the last slag in the series hence the reason for analysing this slag. The first core sample was submitted for XRF analysis. The other core sample was mounted, polished and sectioned and examined under an optical microscope. The photomicrographs for the sample are shown in Figure 82 and Figure 83 below.

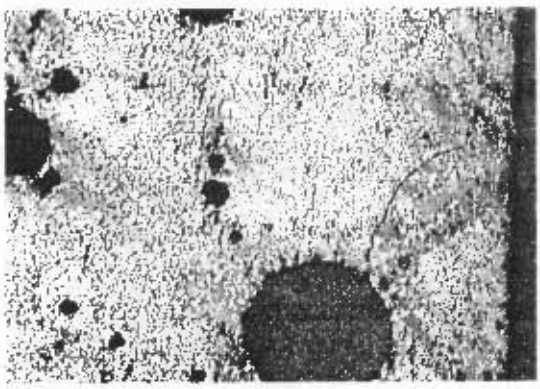

Figure 82: Photomicrograph of slag Cr8 – 2.5X magnification

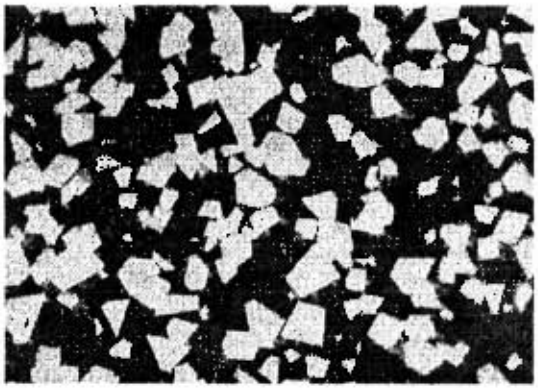

Figure 83: Photomicrograph of slag Cr8 – 50X magnification

Unfortunately the sample had to be slow cooled, therefore the phases present were not necessarily representative of the slag at high temperature. The height and width of the section of the sample shown in Figure 82 were approximately 2 x 3 mm respectively. This section was from the centre of the core sample which was drilled from the centre of the crucible. It is clear in Figure 82 that the spinel phase was very well distributed. The significant amount of spinel visible is likely to have been a result of spinel growth on slow cooling. Sections of the sample above and below the one shown had similar distributions of spinel. Figure 83 shows the distinctive shape of the spinel crystals.

The XRF analysis of the other core sample is given in Table 32:

Table 32: XRF analysis of core sample from slag Cr8

Slag Cr8	Intended composition		Analysed composition	
Components	wt%	mol%	wt%	mol%
Al_2O_3	4.6	7.7	4.6	7.7
CaO	4.6	4.9	4.7	5.0
Cr_2O_3	8.0	3.7	9.1	3.6
FeO	18.4	15.4	18.0	15.1
MgO	18.4	27.5	18.9	28.3
SiO_2	46.0	46.7	45.1	45.3
Total	100.0	100.0	100.3	100.0

The analysed composition showed that there was 9.1wt% Cr_2O_3 instead of the intended 8.0wt%. The rest of the components were close to their intended values. The reason for the excess chromium is not known, however this suggests that the chromium contents of the predecessors of slag Cr8 contained at least the quoted amount of chromium.

From the literature review (see Section 2.5.6) it was identified that the addition of chromium was likely to bring about precipitation of spinels at the temperatures of interest. Therefore changes of the conductivity vs temperature curves were expected as the spinels melted. The deep cell technique was used in all cases and the temperature dependence of the slags was measured from 1400 °C to approximately 1550 °C. The atmosphere used in all experiments was argon and therefor inert. The typical temperature dependence plots were obtained. An example of the conductivity vs temperature curve is shown in Figure 84 for slag Cr4.

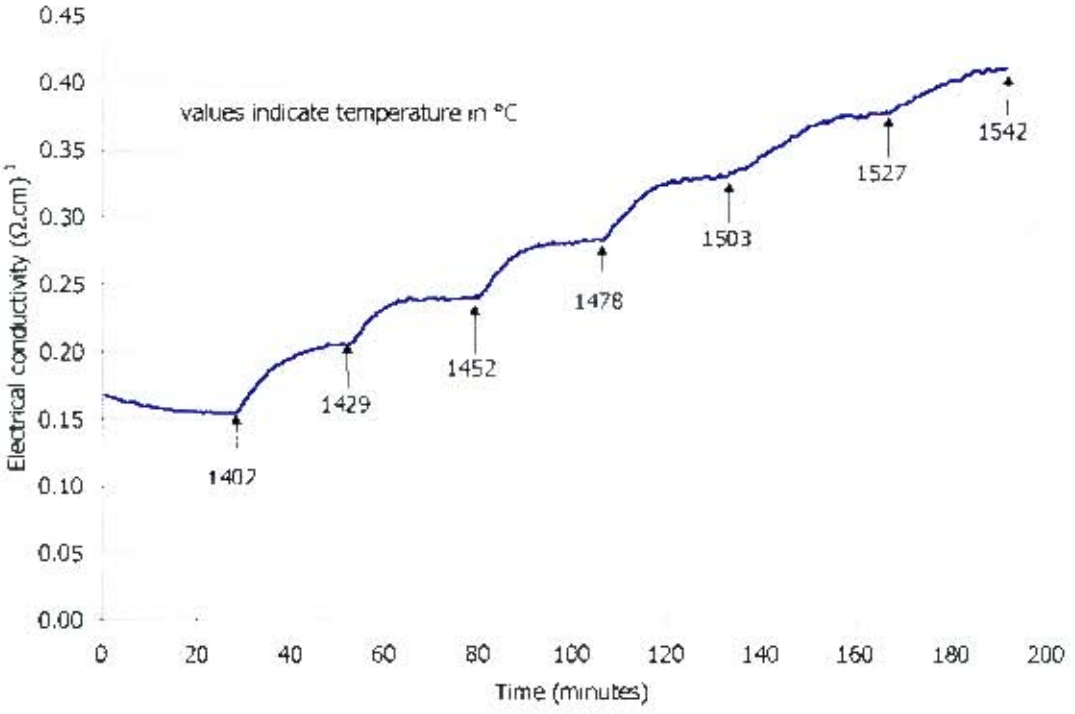

Figure 84: Temperature dependence of conductivity of slag Cr4. Approximate slag composition (wt%): Al_2O_3: 4.8, CaO: 4.8, Cr_2O_3: 4, FeO_x: 19.2, MgO: 19.2, SiO_2: 48. Argon atmosphere

The conductivity increased with temperature and the conductivity quickly stabilised at each temperature. This was important as it suggested that there were no significant amounts of spinel melting. It should, however, be noted that the relative amount of spinel is small in comparison to the overall sample and small changes in spinel content might not be noticed. This will be discussed further in Section 5.4.

The results of the temperature dependence of the conductivity of the chromium containing slags are shown in Table 33 and in Figure 85. The full results with the measured resistances and Arrhenius plots are shown in Appendix C4. The conductivity values were calculated using a calibration slope of −1.013 and an intercept of 0.024.

Table 33: Chromium containing slags: temperature dependence of electrical conductivity. Master slag composition (wt%): Al_2O_3: 5, CaO: 5, FeO_x: 20, MgO: 20, SiO_2: 50 with Cr_2O_3 additions as specified. Argon atmosphere

Slag Cr0		Slag Cr0.5		Slag Cr1		Slag Cr2	
0% Cr_2O_3		0.5% Cr_2O_3		1% Cr_2O_3		2% Cr_2O_3	
Temperature	Electrical conductivity	Temperature	Electrical conductivity	Temperature	Electrical conductivity	Temperature	Electrical conductivity
°C	$(\Omega.cm)^{-1}$	°C	$(\Omega.cm)^{-1}$	°C	$(\Omega.cm)^{-1}$	°C	$(\Omega.cm)^{-1}$
1399	0.192	1397	0.180	1400	0.191	1400	0.169
1424	0.242	1424	0.221	1425	0.232	1426	0.217
1449	0.287	1450	0.270	1450	0.279	1450	0.249
1473	0.328	1475	0.315	1475	0.329	1475	0.290
1498	0.375	1501	0.366	1500	0.379	1498	0.337
1521	0.430	1525	0.422	1526	0.444	1526	0.394
		1550	0.488	1550	0.517	1550	0.467

Slag Cr4		Slag Cr6		Slag Cr8	
4% Cr_2O_3		6% Cr_2O_3		8% Cr_2O_3	
Temperature	Electrical conductivity	Temperature	Electrical conductivity	Temperature	Electrical conductivity
°C	$(\Omega.cm)^{-1}$	°C	$(\Omega.cm)^{-1}$	°C	$(\Omega.cm)^{-1}$
1402	0.154	1403	0.155	1405	0.135
1429	0.205	1427	0.194	1428	0.184
1452	0.240	1451	0.225	1453	0.217
1478	0.284	1476	0.262	1476	0.250
1503	0.330	1502	0.302	1502	0.286
1527	0.377	1525	0.342	1526	0.332
1542	0.411	1549	0.388	1552	0.386

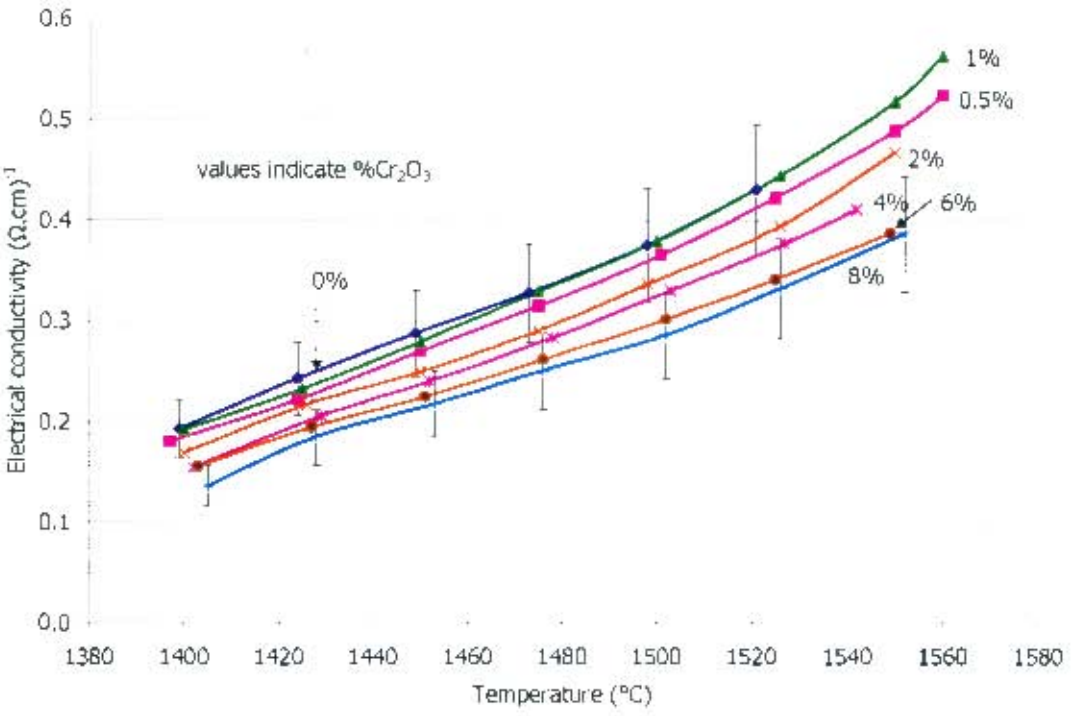

Figure 85: Temperature dependence of the electrical conductivity of the chromium containing slags – Pt crucible. Master slag composition (wt%): Al_2O_3: 5, CaO: 5, FeO_x: 20, MgO: 20, SiO_2: 50 with Cr_2O_3 additions as specified.

The conductivity of all the slags increased with temperature. The general trend apparent was that the addition of chromium brought about a decrease in the slag conductivity. The only exception to this was the slag containing 1% chromium (slag Cr1) whose conductivity lay between that of the chromium-free slag and the slag Cr0.5. There were no significant increases in the conductivity at higher temperatures. Error bars have been included for slag Cr0 and slag Cr8 to give an indication of the uncertainty in the measurements.

As was mentioned in section 3.6.1, MgO crucibles were used in one series of experiments on the chromium containing slags. There was significant dissolution of the crucible into the slag at the higher temperatures (T > 1500 °C) and the MgO content in the final slags was around 25 – 29wt% (instead of around 20wt%). The data obtained is presented in Figure 86. The values of the conductivity from the measurements in the MgO crucibles are regarded as being less accurate than those from the measurements using a Pt crucible as a result of the change in the slag chemistry. However, despite the change in slag chemistry, the decrease in the conductivity with addition of chromium was still evident. This showed that the effect of chromium addition on the electrical conductivity was reproducible.

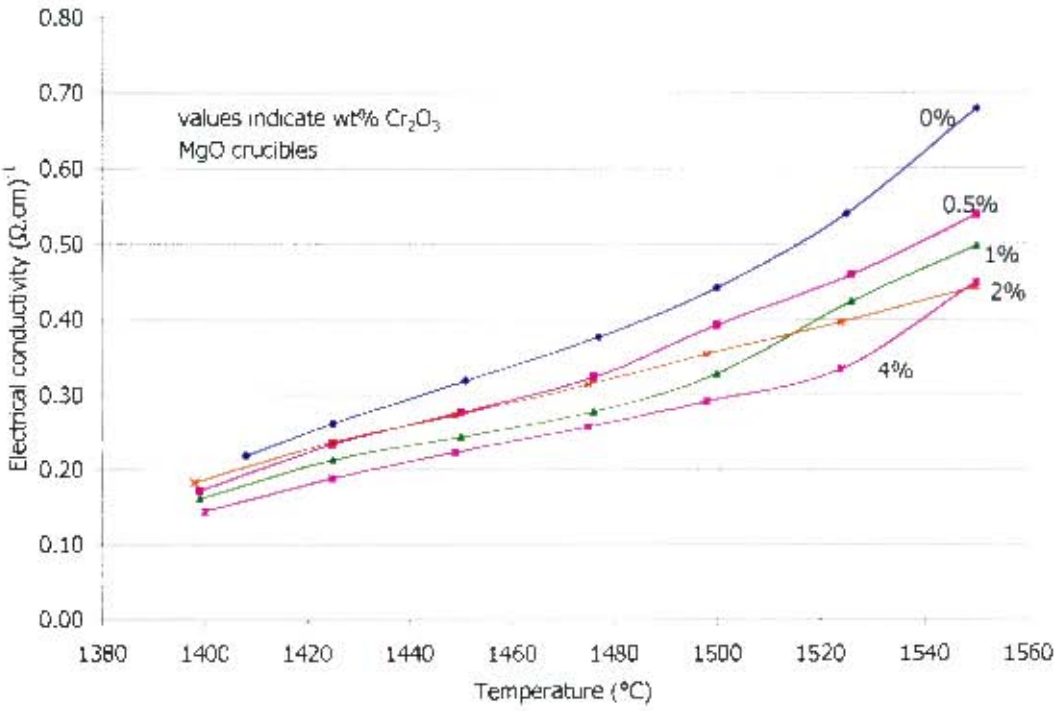

Figure 86: Temperature dependence of the electrical conductivity of chromium containing slags – MgO crucibles. Master slag composition (wt%): Al_2O_3: 5, CaO: 5, FeO_x: 20, MgO: 20, SiO_2: 50 with Cr_2O_3 additions as specified.

It was of interest to the sponsors of the project to obtain measurements of the conductivity of the chromium containing slags at temperatures higher than 1550 °C. In order to make these measurements it was necessary to make use of a different furnace which could attain temperatures of up to 1700 °C (referred to as the very high temperature (VHT) furnace). It was also necessary to make use of different materials of construction for the crucibles and the electrodes as the platinum would soften too much at 1700 °C. Therefore molybdenum was selected for the crucibles and the electrodes. Measurements were carried out on the chromium free slag and the slags containing 2 and 4wt% Cr_2O_3. The results are shown in Figure 87.

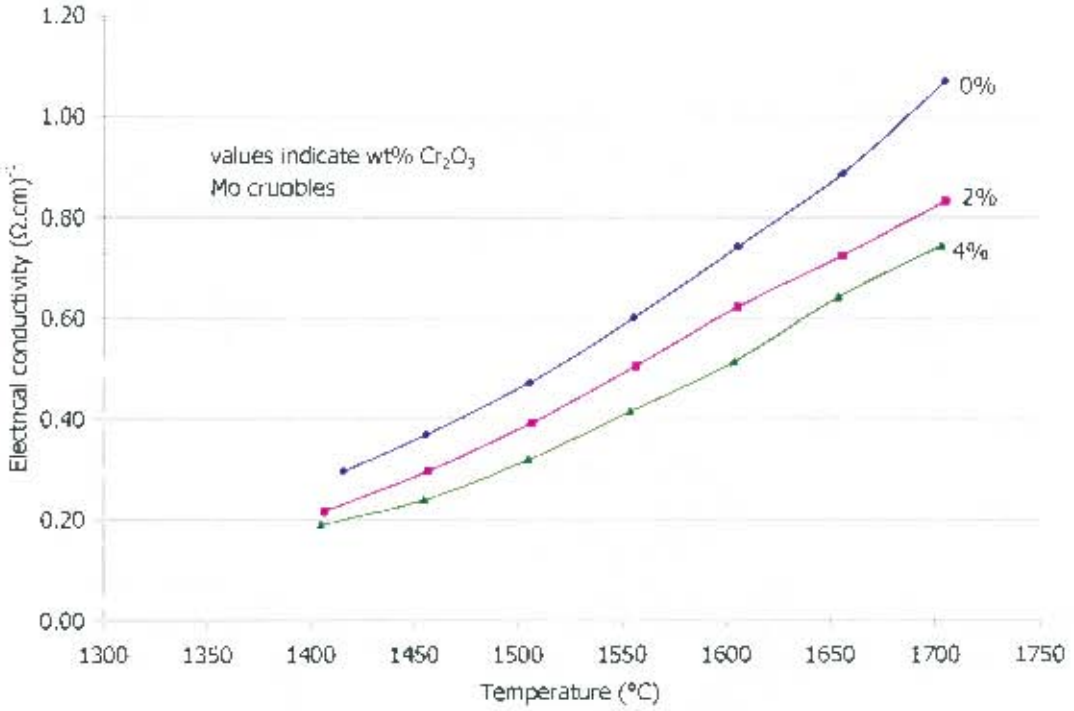

Figure 87: Temperature dependence of the electrical conductivity of chromium containing slags – molybdenum crucibles. Master slag composition (wt%): Al_2O_3: 5, CaO: 5, FeO_x: 20, MgO: 20, SiO_2: 50 with Cr_2O_3 additions as specified.

As expected, at the lower temperatures (up to 1600 °C), the electrical conductivity of the slag decreased as chromium was added. At temperatures higher than 1600 °c, there was no increase in the slag conductivity above that expected from a temperature rise. There was some reaction between the Mo and the slag and the final molybdenum content of the slags was around 1.5wt% Mo. The effect of the molybdenum is uncertain.

It was considered valuable to provide a comparison of the results of the measurements using the three different types of crucibles. The results for slag Cr0 and slag Cr4 are shown in Figure 88.

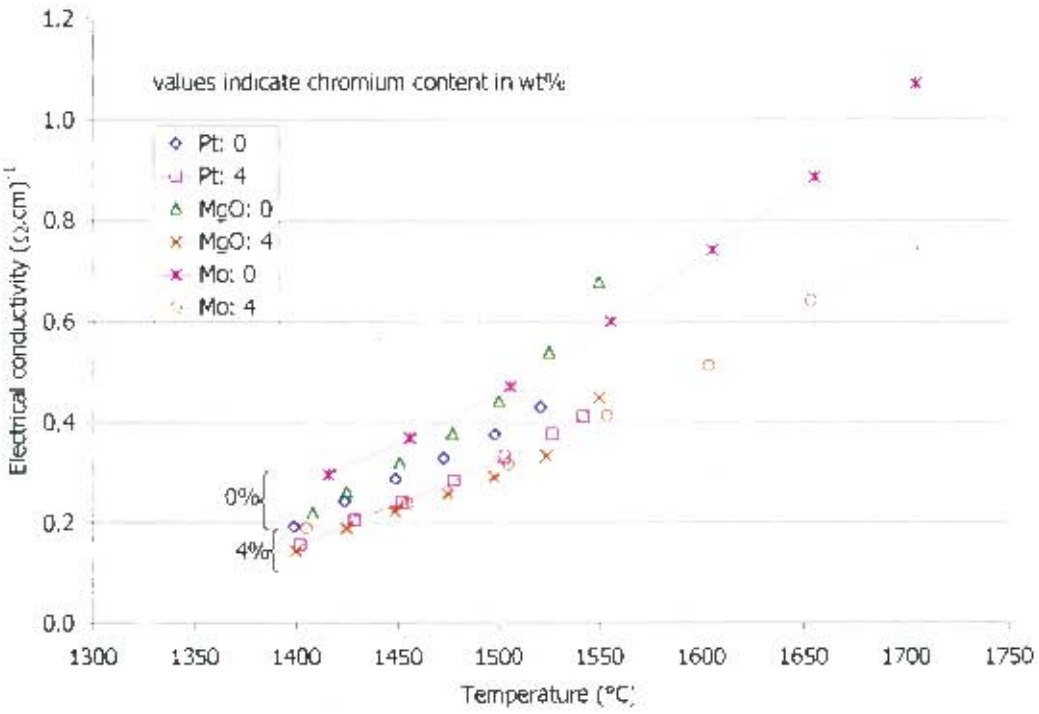

Figure 88: Comparison of electrical conductivity results on slag Cr0 and slag Cr4 from measurements in Pt, MgO and Mo crucibles. Master slag composition (wt%): Al_2O_3: 5, CaO: 5, FeO_x: 20, MgO: 20, SiO_2: 50 – chromium free and with 4% Cr_2O_3 addition.

The measurements on the chromium free slags were quite similar for the Pt and the MgO crucibles at around 1400 °C, although with increasing temperature MgO would have dissolved into the slag and increased the conductivity. The chromium free results for the Mo crucible were significantly higher at 1400 °C than for the other two crucibles. This was possibly as a result of the Mo that dissolved into the slag.

The results for the slag containing 4% chromium were very close to each other. The large increase at 1550 °C for the measurement in the MgO crucible is again likely to have resulted from the increase in the MgO content of the slag.

4.4.1. Heat-up profile of slag Cr2

A heat-up profile of the conductivity of the low basicity slag containing 2% Cr_2O_3 was obtained in same manner as described in Section 4.3.3 for the high basicity slags.

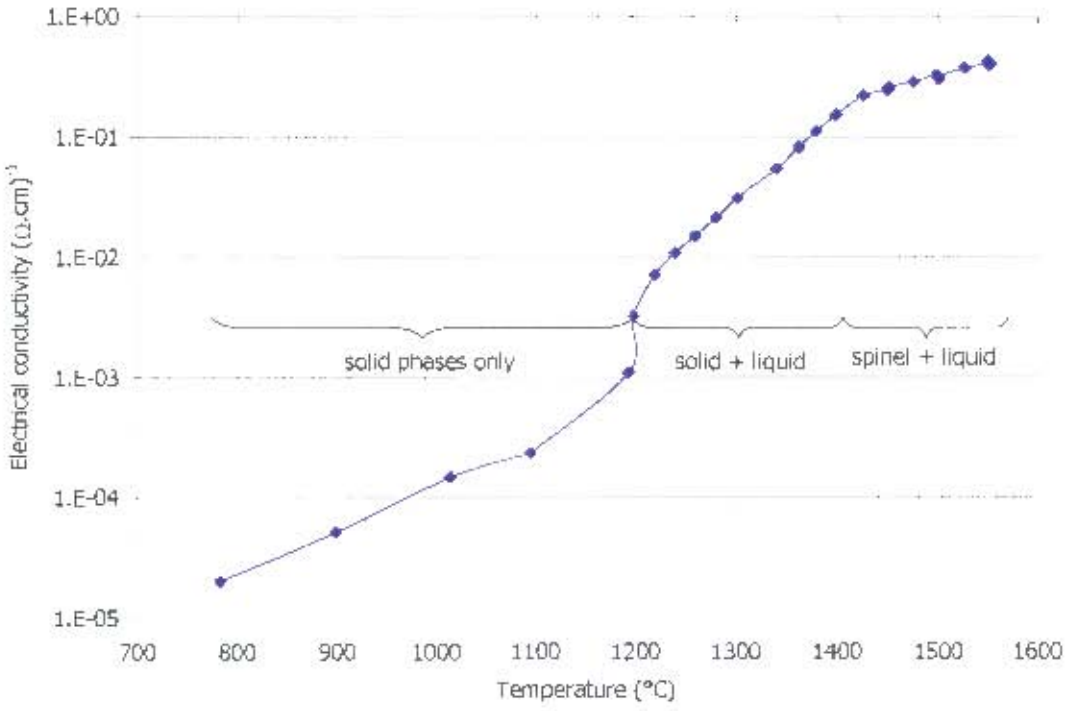

Figure 89: Heat-up profile for the electrical conductivity of slag Cr2 from 800 to 1550 °C. Approximate slag composition (wt%): Al_2O_3: 4.9, CaO: 4.9, Cr_2O_3: 2, FeO_x: 19.6, MgO: 19.6, SiO_2: 49.

As was found for the heat-up profiles of the high basicity slags (see Section 4.3.3), there were three distinct regions in the heat-up profile, which have been indicated in Figure 89. However, with the chromium containing slag, at the higher temperatures there would still have been spinel phase present even though slope of the conductivity vs temperature curve had flattened out. The importance of this will be discussed in Section 5.4.

4.5. Calcium ferrite slag

As indicated in the literature review (Chapter 2), there were data available on the oxidation state dependence of the conductivity of iron silicate slags and other silicate slags of varying basicity. However, there was no literature that specifically examined the oxidation state dependence of calcium ferrite slag conductivity. The electrical conductivity of calcium ferrite slags had, however, been measured in air and also at reduced conditions in iron crucibles. It was considered that measurements on the oxidation state dependence of the conductivity of calcium ferrite slags would therefore provide further understanding of the electronic conduction mechanism.

An initial and a repeat experiment were carried out on the calcium ferrite slag containing 25% CaO and 75% Fe_2O_3. The reasons for selection of this slag were provided in Section 2.5.2.5 and 3.5. The shallow cell technique was used for the measurements, although a magnesia boat was used instead of a circular crucible. The details of the conductivity cell were provided in section 3.7. Samples of the initial and final slags were analysed to determine the amount of magnesia that dissolved into the slag. The analysed slag compositions are shown in Table 34:

Table 34: Analysed compositions of calcium ferrite slags

Slag CF	Initial composition		Final composition - run1		Final composition - run2	
Components	wt%	mol%	wt%	mol%	wt%	mol%
Al_2O_3	0.2	0.2	0.4	0.4	0.4	0.4
CaO	23.5	45.9	26.3	47.2	26.5	47.0
Fe_2O_3	73.6	50.6	72.2	45.6	75.5	47.0
MgO	0.9	2.4	2.2	5.4	1.8	4.5
SiO_2	0.5	0.9	0.8	1.4	0.7	1.2
Total	98.6	100.0	101.8	100.0	105.0	100.0

In the above table the iron oxide content has been regarded as Fe_2O_3 hence the low mol% values for the Fe_2O_3 and the high total values for run1 and run2 (which were both at reduced conditions when analysed). The initial composition of the slag contained some alumina, magnesia and silica which was unexpected. It is possible that when ring milling the calcium ferrite slag there was still some contamination. There were no other significant minor elements in the sample. The final compositions of the initial run (run1) and the repeat run (run2) were as expected. The MgO content of the final analysed slags was around 2wt% as a result of using an MgO crucible.

The progress of the experiment of the initial run is provided in Figure 90.

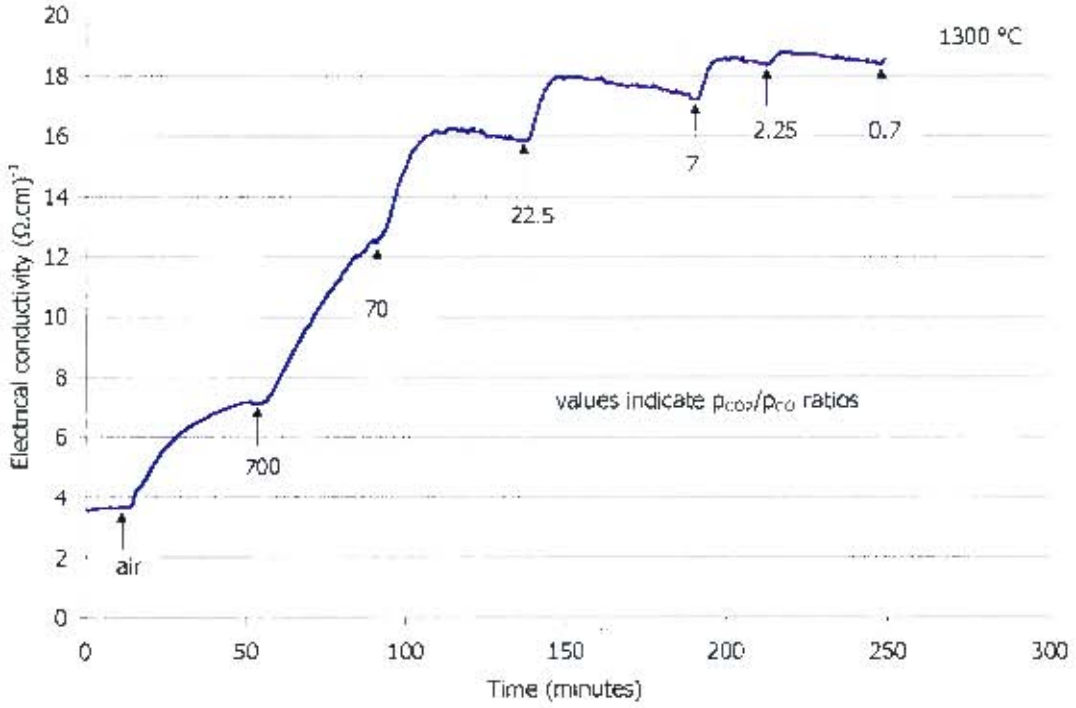

Figure 90: Progress of experiment on slag CF (25% CaO, 75% FeO_x) – initial run at 1300 °C.

A repeat run was carried out to show reproducibility of the results and after the p_{CO2}/p_{CO} ratio of 0.7, the atmosphere was changed to CO + N_2. This resulted in a dramatic increase of the conductivity as shown in Figure 91.

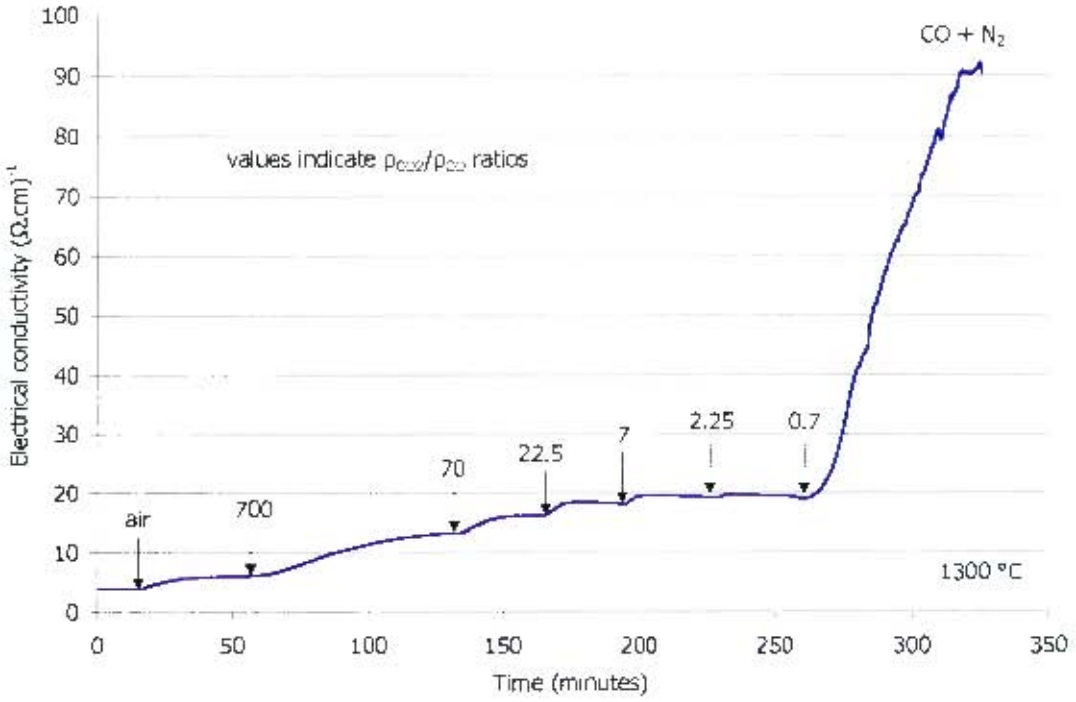

Figure 91: Progress of experiment on slag CF (25% CaO, 75% FeO_x) – repeat run at 1300 °C

The electrical conductivity of the calcium ferrite slags increased significantly as the oxidation state became more reduced. It should be noticed in Figure 90 that the conductivity increased when the

ratio was changed from 70 to 22.5 (for example) and then started decreasing with time. In the initial run, this occurred at ratios of 22.5, 7, 2.25 and 0.7. In the repeat run, this only occurred for ratios of 7, 2.25 and 0.7. It is not well understood why this should happen. A possibility was that MgO from the boat dissolved into the slag and decreased the conductivity (by reducing the amount of electronic conduction through dilution of iron ions). However, given the low MgO content in the final composition, this seems less plausible.

The oxygen partial pressures were calculated for each of the p_{CO2}/p_{CO} ratios and the results plotted. The value of the conductivity at iron saturation was omitted as the high conductivity was likely to be due to a highly conductive metallic phase and not entirely due to conduction through the slag. The results are shown in Figure 92:

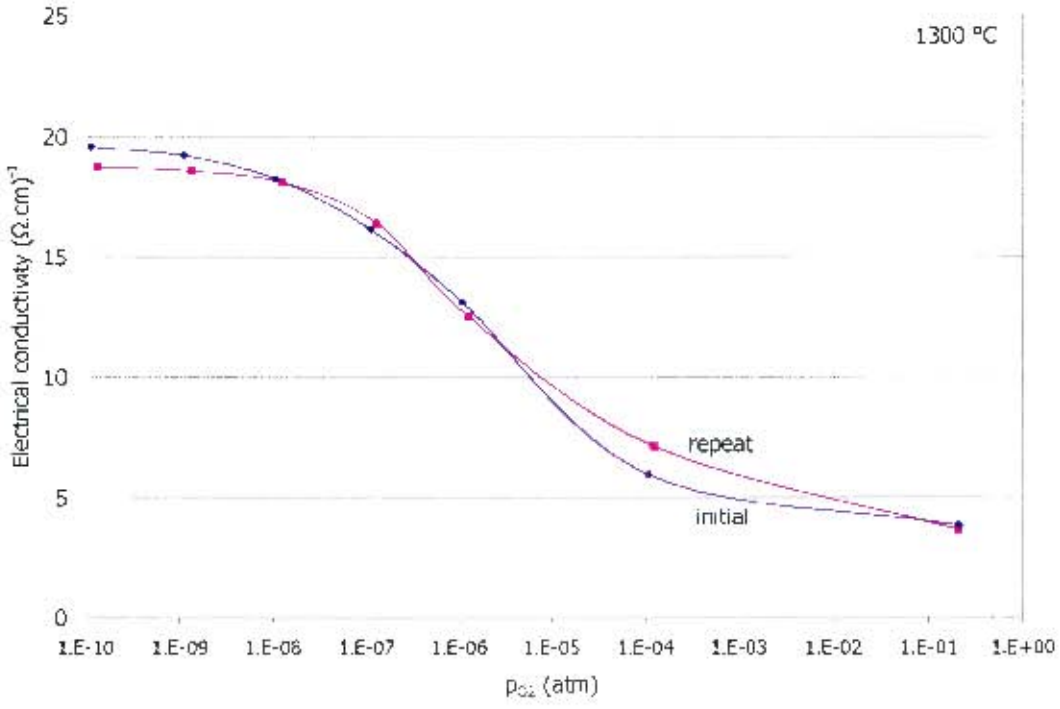

Figure 92: Electrical conductivity of calcium ferrite slag (25% CaO-75% FeO_x) at 1300°C vs p_{O2}

The agreement between the initial and repeat runs was good. The slight difference in the values of the conductivity between the two runs at $p_{O2} \approx 10^{-4}$ (p_{CO2}/p_{CO} = 700) was likely to have arisen as a result of the very low CO flow required to obtain the ratio of 700. (A flow rate of 1.4 ml/min of CO was required, so slight changes in the flow could have resulted in relatively large changes in the ratio).

As the slag became more reduced, the conductivity increased. The value of the conductivity in air (~3.7 $(\Omega.cm)^{-1}$) is higher than the values reported in the literature (Adachi (1957) ~2 $(\Omega.cm)^{-1}$ at 1300 °C). The conductivity value at the reduced conditions (~19 $(\Omega.cm)^{-1}$ at $p_{O2} \sim 10^{-11}$ atm) is lower than values reported in the literature for calcium ferrite slags in iron crucibles (see Dancy and Derge (1966) ~30 $\Omega^{-1}.cm^{-1}$). A possible reason for the difference in the values at reduced conditions is that the slags contained in iron crucibles were closer to iron saturation.

The numerical values for the conductivities for both runs are shown in Table 35.

Table 35: Electrical conductivity of calcium ferrite slag with 25% CaO and 75% FeO_x – initial and repeat runs at 1300 °C

Slag CF - initial run

p_{CO2}/p_{CO}	p_{O2}	Resistance measured	Electrical conductivity
	atm	Ω	$(\Omega.cm)^{-1}$
air	0.21	7.00	3.63
700	1.24E-04	4.78	7.12
70	1.27E-06	3.77	12.50
22.5	1.32E-07	3.46	16.38
7	1.27E-08	3.36	18.08
2.25	1.35E-09	3.34	18.55
0.7	1.34E-10	3.33	18.72

Slag CF - repeat run

p_{CO2}/p_{CO}	p_{O2}	Resistance measured	Electrical conductivity
	atm	Ω	$(\Omega.cm)^{-1}$
air	0.211057	6.77	3.81
700	1.08E-04	5.24	5.93
70	1.08E-06	3.71	13.10
22.5	1.12E-07	3.47	16.13
7	1.08E-08	3.35	18.21
2.25	1.12E-09	3.30	19.19
0.7	1.14E-10	3.29	19.53

4.6. Summary of experimental findings

Electrical conductivity measurements were carried out on Al_2O_3-CaO-FeO_x-MgO-SiO_2 slags with varying basicity and iron content. The basicities of the slags were termed low, intermediate and high and had the following respective values: wt%(CaO+MgO)/(Al_2O_3+SiO_2) ~ 0.43, 0.64 and 0.94. The FeO_x contents of the slags were varied from 0 up to 40wt%. An experiment was also carried out on a calcium ferrite slag with 25% CaO and 75% FeO_x. The results of the experimental work showed the following:

- The electrical conductivity of all the slags increased with increasing temperature in the range 1400 – 1550 °C.
- The addition of iron oxide to base slags containing Al_2O_3-CaO-MgO-SiO_2 significantly increased the electrical conductivity. In the case of the low basicity slag, an addition of 20wt% FeO_x to the base slag brought about an increase in the conductivity from around 0.05 to around 0.29 $(\Omega.cm)^{-1}$ at 1450 °C. Similarly, 20wt% FeO_x addition to the intermediate and high basicity slags raised the conductivity from 0.1 to 0.35 $(\Omega.cm)^{-1}$ and from 0.25 to 0.48$(\Omega.cm)^{-1}$ respectively at 1450 °C.
- The electrical conductivity of the iron oxide - containing silicate slags was dependent on the oxidation state of the slag. The higher the FeO_x content of the slag, the more dependent the conductivity was on the oxidation state. A typical response of the conductivity to the change in oxidation state of the slag was the following: starting in air, the conductivity would increase and reach a maximum at an oxygen partial pressure of around 10^{-7} to 10^{-4} atm (the p_{O2} at which the maximum occurred was dependent on the amount of iron oxide in the slag and the slag basicity). As the slag was reduced further the conductivity decreased. The pertinent conductivity values at various oxidation states for all of the slags tested have been summarised in Table 36. The oxygen partial pressures at which the maximum conductivity occurred have been noted. The reduced condition typically refers to the measurement of the conductivity just before iron saturation except in the case of slags L15 and L20 where the reduced condition refers to $p_{O2} = 8.7 \times 10^{-9}$ atm.

Table 36: Summary of results of oxidation state dependence of all slags' conductivities

Slag name	Electrical conductivity values $(\Omega.cm)^{-1}$			p_{O2} at κ_{max}
	air	maximum	reduced condition	atm
L15	0.132	0.181	0.181	8.7E-09
L20	0.190	0.225	0.171	3.5E-06
L30	0.428	0.525	0.303	5.6E-05
L40	0.802	1.084	0.528	5.6E-05
I20	0.353	0.393	0.320	3.5E-06
I30	0.514	0.760	0.527	3.5E-06
I40	0.937	1.413	0.985	3.5E-06
H20	0.381	0.522	0.493	3.5E-06
H30	0.550	1.081	0.774	8.7E-07
H40	0.920	1.668	0.877	8.7E-07

- The effect of chromium addition on the conductivity of the low basicity slag was tested by sequentially adding 0.5, 1, 2, 4, 6, 8 wt% Cr_2O_3 to the base slag. Experiments were carried

out in platinum, magnesia and molybdenum crucibles. In all the experiments the trend was that the chromium brought about a decrease in the electrical conductivity of the order of 0.01 $(\Omega.cm)^{-1}$ / wt% Cr_2O_3 added in the temperature range 1400 to 1550 °C. For example, the measurements in the Pt crucible showed that with 8% Cr_2O_3 addition to the low basicity slag, the conductivity dropped from 0.29 $(\Omega.cm)^{-1}$ to 0.22 $(\Omega.cm)^{-1}$ at a temperature of 1450 °C. The work carried out in molybdenum crucibles extended to temperatures of up to 1700 °C in the hope of identifying the change in conductivity when spinel phase melted out. No significant changes were found in comparison to the previous trends.

- The oxidation state dependence of the conductivity of a calcium ferrite slag was tested starting in air and then reduced to p_{O2} $\sim 10^{-10}$ atm. The conductivity was strongly dependent on the oxidation state of the slag and increased from a value of around 3.8 $(\Omega.cm)^{-1}$ in air to a value of around 19 $(\Omega.cm)^{-1}$ at an oxygen partial pressure of 1×10^{-10} atm.
- Several experiments were carried out on the heating of a solid slag at 800 °C to the molten state at around 1550 °C. A clear trend was observed in all the heat-up profiles where there were three distinct conductivity regions. At low temperatures where only solid phases were present, the conductivity was low (<0.01 $(\Omega.cm)^{-1}$), then when melting occurred there was a sharp increase in the conductivity (usually from around 0.01 to 0.1 $(\Omega.cm)^{-1}$ from 1200 to 1400 °C) and then where the slag became fully molten, the conductivity increased more gradually with temperature.

Chapter 5

DISCUSSION

The discussion has been divided into various sections according to the effect of various factors on the electrical conductivity and in order to directly address the research questions posed. The first section examines the effects of basicity and temperature on the conductivities of the FeO_x-free Al_2O_3–CaO–MgO–SiO_2 slags. The second section deals with the addition of iron oxide to the Al_2O_3–CaO–MgO–SiO_2 slags of varying basicities. The third section deals with the variation of slag conductivity with oxidation state for the iron containing slags. The final section examines the effect of chromium on the conductivity of the low basicity slag.

It was considered necessary in certain areas to compare the results measured in this work to other measurements reported in the literature. Therefore some of the data considered for modelling has been presented as part of the discussion. This also facilitated greater understanding of the conduction mechanisms and their effects on other factors such as temperature dependence of conductivity. The Discussion chapter approaches the electrical conductivity of slags from a more qualitative point of view and thereafter the Modelling chapter will deal with the conductivity from a quantitative view.

5.1. Effect of basicity and temperature on FeO_x-free slag conductivity

Several experiments were carried out on iron oxide-free slags. It was considered worthwhile investigating the effects of basicity and temperature on these slags first, before evaluating the effect of addition of FeO_x. Also, the iron oxide-free systems have been better characterised, therefore comparison with literature data will be more significant.

Figure 93 shows the comparison between the measured conductivities at 1500 °C for the low, intermediate and high basicity slags and the literature data for the Al_2O_3-CaO-MgO-SiO_2 system (range of slag compositions (mol%): Al_2O_3: 2-19, CaO: 5-51, MgO: 4-42, SiO_2: 34-64).

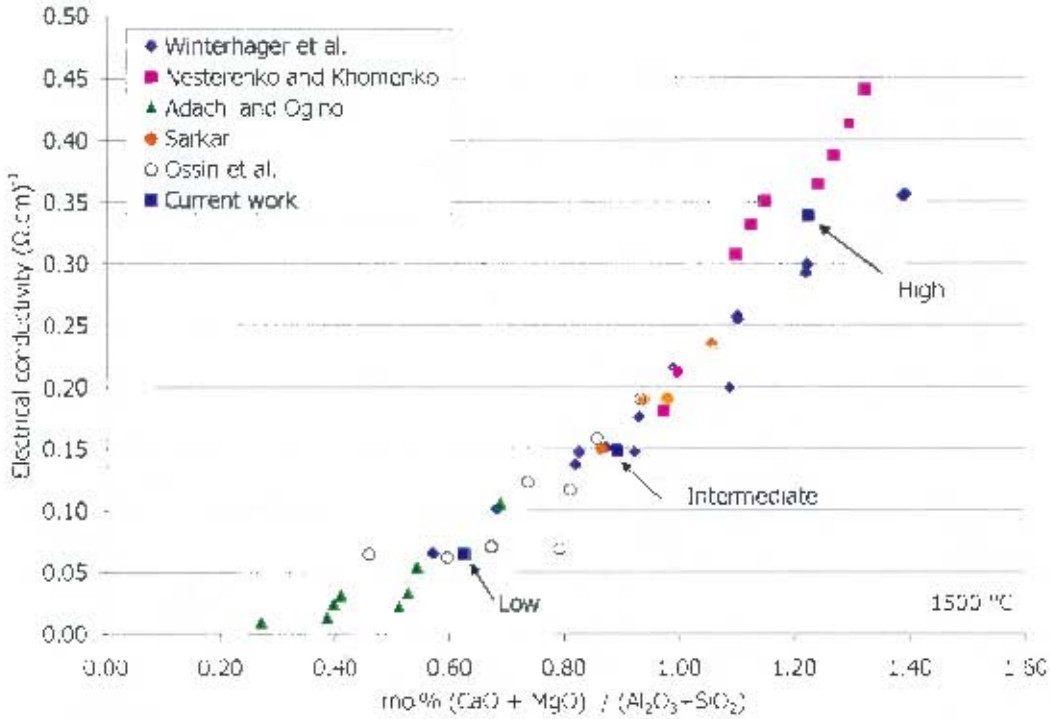

Figure 93: Comparison between measured electrical conductivities for low, intermediate and high basicity slags and literature data for Al_2O_3-CaO-MgO-SiO_2 system at 1500 °C. Literature data by Winterhager *et al.* (1966), Nesterenko and Khomenko (1985), Adachi and Ogino (from Slag Atlas (1995)), Sarkar (1989) and Ossin *et al.* (1971).

The agreement between the measured conductivities and the literature data was good. The increase in conductivity with increasing basicity was expected. As explained in the literature review, as the number of Ca^{2+} and Mg^{2+} cations increases, the anionic network becomes more depolymerised and the mobilities of the cations increase. The relation between the composition and the conductivity has been investigated further in the modelling chapter.

It was evident from the results shown in the previous chapter that the electrical conductivity of the slags increased with temperature. The effect of temperature on the conductivities of fully molten slags was well described by the Arrhenius relationship. It was found during the modelling of the temperature dependence of the conductivity of iron-free slags that the activation energy and pre-exponential factor were related by the compensation law. Details found in the literature concerning the compensation law were presented in section 2.4.1. The compensation law relationship found for the iron-free slags is shown in Figure 94. It should be noted that the data plotted in Figure 94 are for slags of a wide range of composition, with $(CaO+MgO)/(Al_2O_3+SiO_2)$ ratios from 0.2 to 1.4.

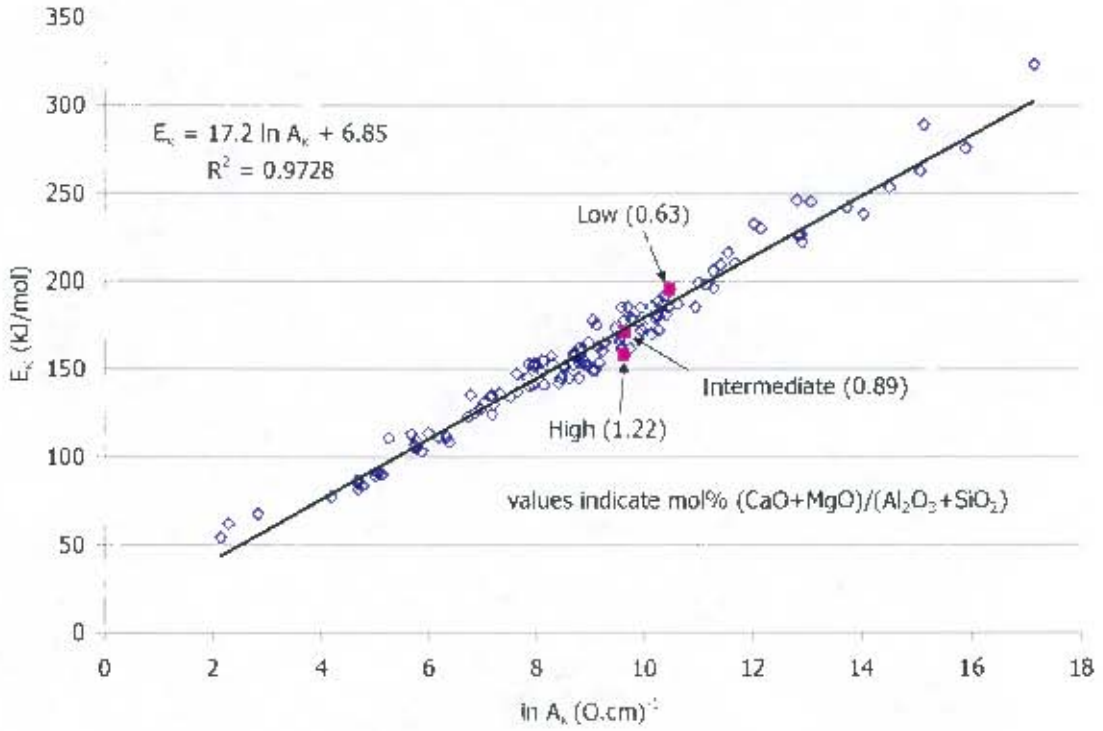

Figure 94: Compensation law relationship between activation energy for conduction and the natural logarithm of the pre-exponential factor for Al_2O_3, CaO, MgO and SiO_2 containing slags. Temperature dependence data for low, intermediate and high basicity slags from this work also shown.

It was suggested by Chakraborty (1995) that the compensation law could be used as a tool for checking the reliability of newly measured data. Therefore the temperature dependence data for the conductivities of the low, intermediate and high basicity slags measured in this work were also plotted on the compensation law plot. The agreement between the compensation law relationship and the current work suggested that the conductivity values measured and their temperature dependence were reliable. Quantifying the effect of temperature based on the slag composition will be dealt with in the modelling chapter.

In order to give a brief indication of the effect of the slag chemistry on the temperature dependence, the activation energy for conduction has been plotted as a function of the molar basicity ratio in Figure 95.

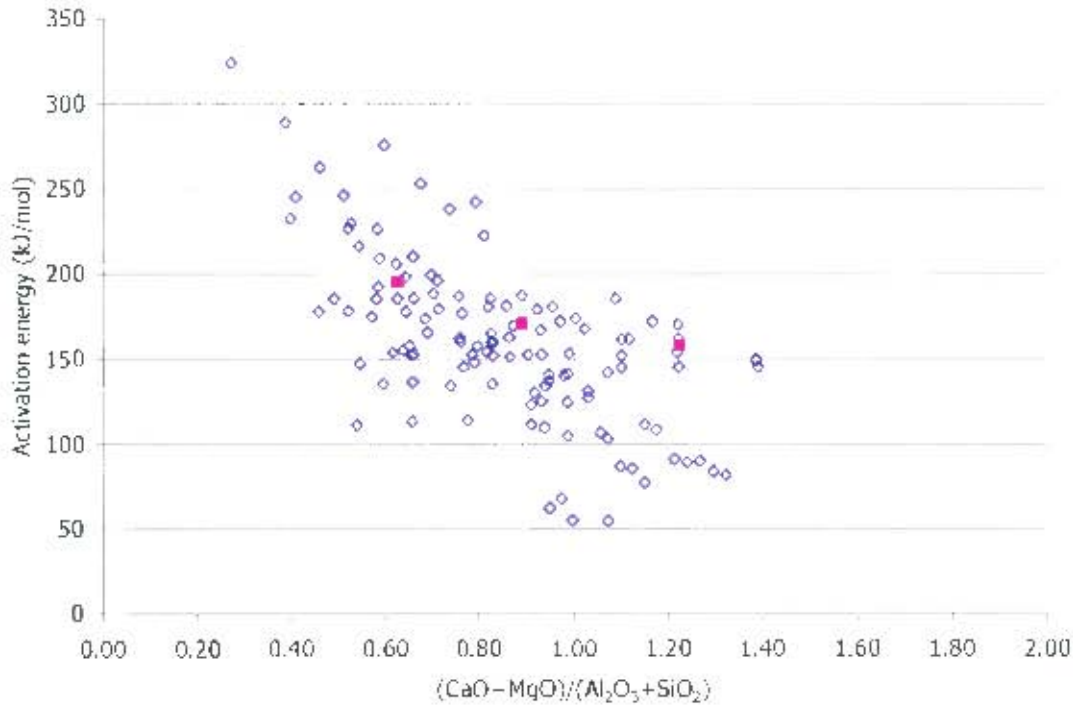

Figure 95: Activation energy for conduction vs mol% (CaO+MgO)/(Al_2O_3+SiO_2) for slags containing Al_2O_3, CaO, MgO and SiO_2. The purple squares indicate the present work (low, intermediate and high basicity slags: from left to right respectively)

The general trend evident in Figure 95 is that the higher the basicity of a slag, the lower the activation energy for conduction (ignoring the scatter). Therefore, if one now looks back to Figure 94, the differences in the extremes of the activation energies can be understood. The slags with high activation energies (>200 kJ/mol) are typically low basicity slags (ratio < 0.8) with high alumina contents (>10 mol%). The slags with lower activation energies (<150 kJ/mol) are typically high basicity slags (ratio > 1.0). The measurements on the slags in the current work appear to confirm the general trend mentioned. The trend can be interpreted in terms of silicate slag structure and the "energy well" concept of Bockris *et al.* (1948). Low basicity slags are more polymerised than high basicity slags, therefore the conducting cations are more firmly "held" in the "energy wells" in the interstices of the more closely bound anionic network. Therefore more energy must be provided to the cation for it to be able to escape and conduct. High basicity slags are less polymerised therefore the conducting cations require less energy to be activated as they are less tightly associated to the anionic network.

Summary of the effect of basicity and temperature on the iron-free slag conductivity

Slag conductivity increases with increasing temperature and basicity. Generally, low basicity slags will have higher activation energies for conduction than higher basicity slags. The temperature dependence parameters for Al_2O_3-CaO-MgO-SiO_2 containing slags appear to obey the compensation law, therefore there is a linear relationship between the activation energy for conduction and the natural logarithm of the pre-exponential function. The quantification of the effect of temperature and slag basicity for Al_2O_3-CaO-MgO-SiO_2 containing slags is considered further in the modelling chapter.

5.2. Effect of iron oxide addition

It was expected from the literature review that the addition of iron oxide to the master slags would significantly increase the electrical conductivity. The effect of the iron oxide addition to the master slags is shown in Figure 96. The conductivity values for the low, intermediate and high basicity slags at 1500 °C in N_2 are shown.

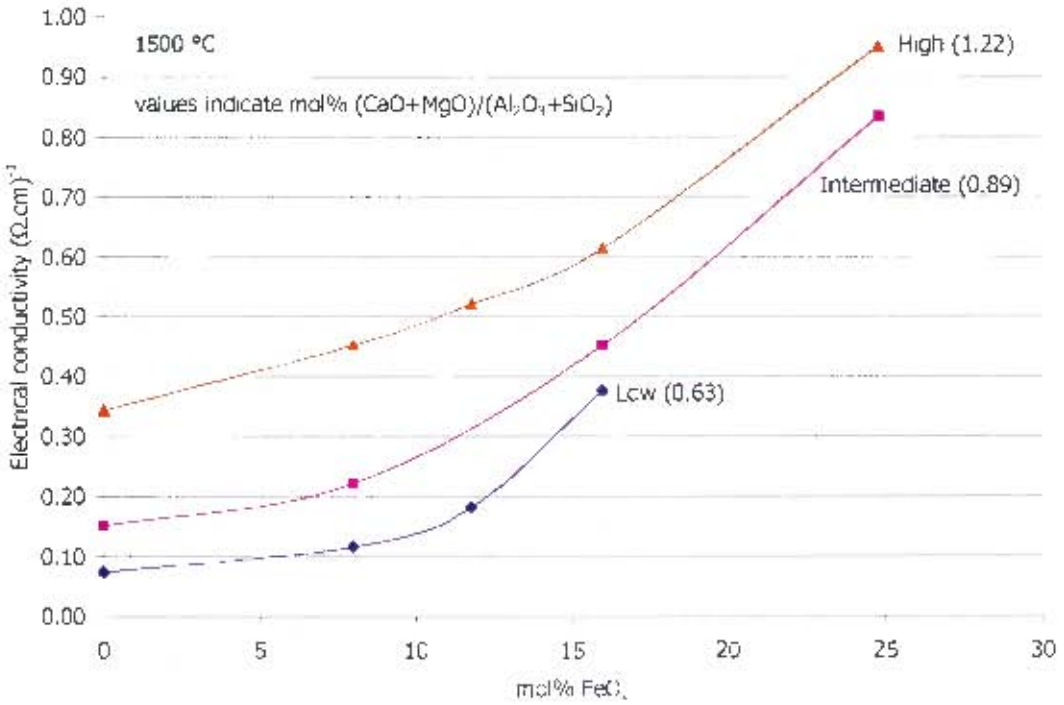

Figure 96: Effect of FeO_x addition on the electrical conductivity of low, intermediate and high basicity slags at 1500 °C in N_2.

The addition of FeO_x to the slags significantly increased the electrical conductivities. These increases were expected for two reasons. Firstly, the addition of iron oxide in a relatively reduced form (wüstite) meant that the majority of the iron ions were divalent. Bockris *et al.* (1952) suggested that ferrous ions are network modifiers and therefore will bring about depolymerisation of the silicate network (Dietzel's classification was intermediate between network forming and network modifying). The greater the depolymerisation of the network, the greater the cation mobilities and hence the conductivity. The basicity still plays an important role in determining the conductivity, as the Ca^{2+} and Mg^{2+} cations continue to promote the conductivity.

The second reason for expecting the increase in the conductivity with iron oxide addition was that electronic conduction should start to take place. Probably the clearest evidence for the onset of electronic conduction can be seen in the oxidation state dependence of the electrical conductivity of slags with higher iron oxide contents. For example, if one considers the results of the low basicity slag with additions of 15, 20, 30 and 40 wt% FeO_x, it was observed in Figure 67 that there was very little variation in the conductivity with changing oxidation state for the slag containing 15wt% FeO_x. As the FeO_x content was raised to 20wt% and higher, the change in oxidation state had a much greater effect on the conductivity, indicating enhanced electronic conduction. The oxidation state dependence of the slag conductivity will be discussed in more detail in the next section.

It was mentioned in the literature survey that Pastukhov *et al.* (1966) found that above approximately 10 mol% Fe, electronic conduction became important in Al_2O_3-CaO-FeO_x-SiO_2 slags. Therefore in the current slags at low levels of FeO_x (<15mol%), it is likely that there are insufficient ferric and ferrous cations to bring about electronic conduction, as the jump distances between cations are too great. However, above approximately 15mol% FeO_x, electronic conduction should be possible. Pastukhov *et al.* (1966) also suggested that the onset of electronic conduction could possibly be observed by a sharp drop in the activation energy for conductivity as the iron content is increased and electronic conduction occurs. Their data was shown in Figure 16 in the literature review.

Sun and Jahanshahi (2002) examined diffusion data and electrical conductivity data in iron-containing slags in an attempt to establish a link between oxygen transport and electronic conduction. The authors estimated the interatomic distance between iron ions based on the concentration of iron oxide in the slags. When the estimated bulk average of the Fe-Fe interatomic distance decreased to below approximately 6 Å, the activation energy for conduction decreased markedly. They suggested this could be explained by overlapping of iron orbitals where the iron interatomic distance was less than 6 Å. The approximate iron oxide content at which the estimated Fe-Fe spacing is 6Å is 16mol% FeO_x.

The change in activation energy with increasing iron content for the low, intermediate and high basicity slags is shown in Figure 97:

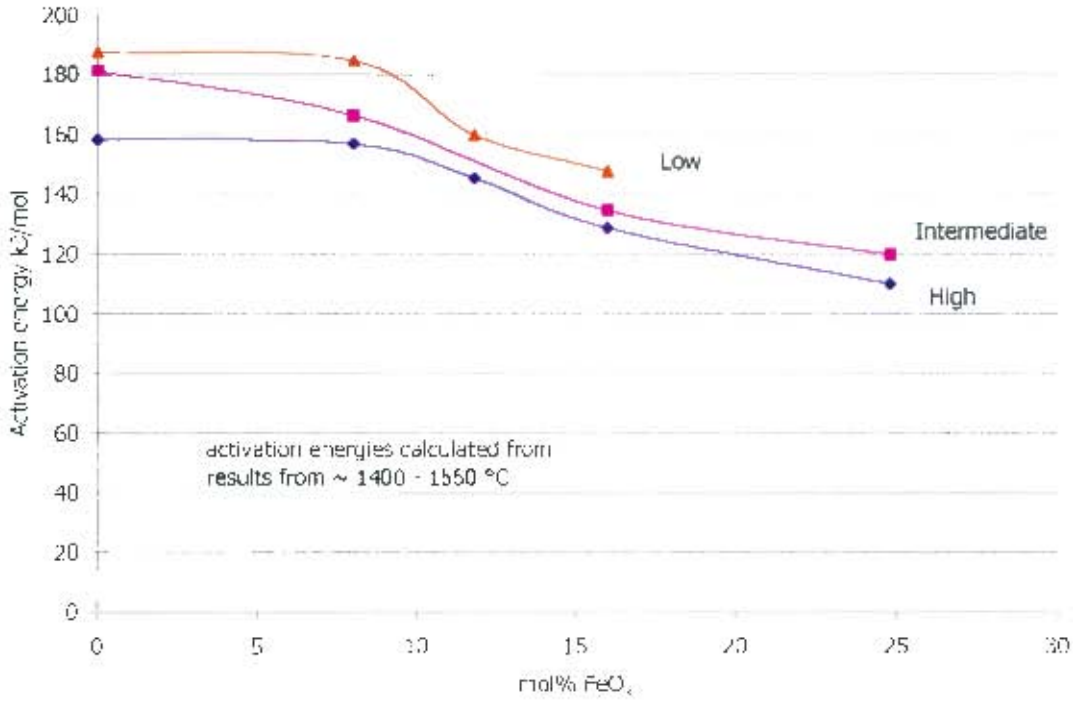

Figure 97: Variation of activation energy for conduction as FeO_x content is increased

It should be noted from Figure 97 that the activation energy for all three slags decreased markedly between 8 and 15 mol% FeO_x. The decrease was not as distinct as that found by Pastukhov *et al.* (1966), however the explanation for the decrease should still be valid i.e. as a result of the electronic mechanism.

In order to obtain a better understanding of how iron oxide addition and electronic conduction affected the temperature dependence of the slag conductivity, the data in the literature was investigated. It was observed from the data that an increase in FeO_x content of a slag resulted in a shift away from the compensation law relationship found for the iron-free Al_2O_3-CaO-MgO-SiO_2 slags. This is shown in Figure 98.

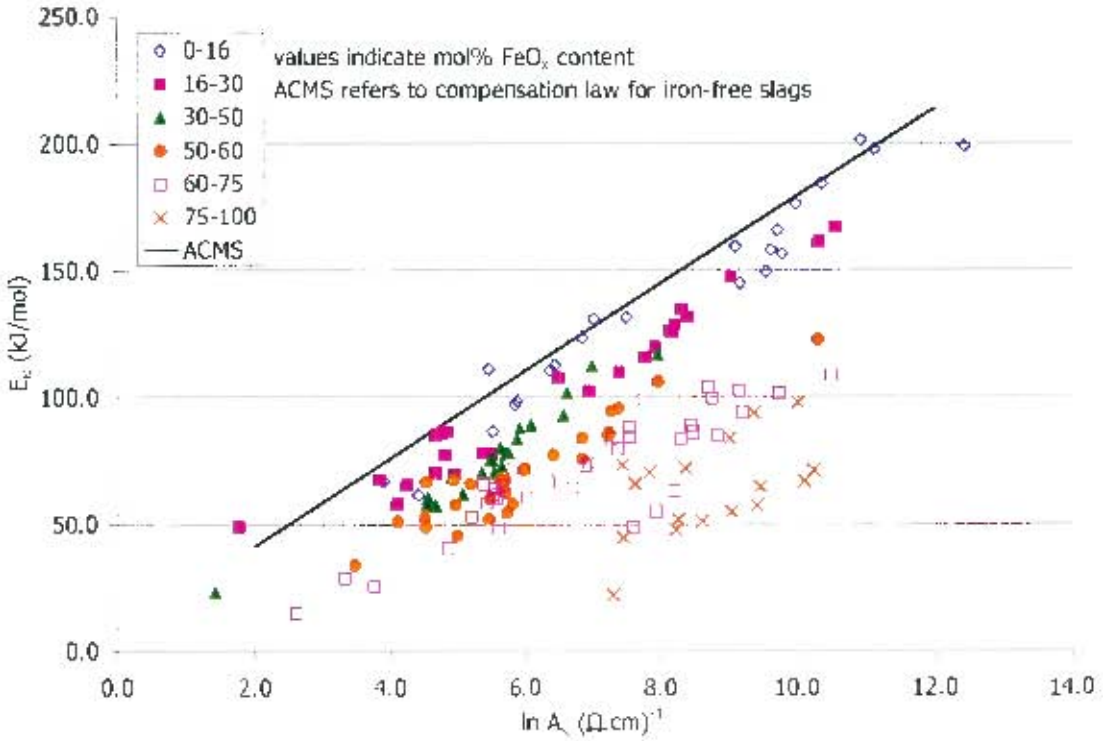

Figure 98: Plot of activation energy for conduction vs the natural logarithm of the pre-exponential factor for iron-containing slags. The values plotted above were obtained from the temperature dependent conductivity data reported in the literature. The line indicates the compensation law relationship found for the iron-free Al_2O_3-CaO-MgO-SiO_2 slags.

It is seen in Figure 98 that the greater the amount of iron oxide present in a slag, the further the temperature dependence data deviates from the compensation relationship for the iron-free slags. It is proposed that the electronic conduction mechanism brings about the shift away from the compensation relationship found for iron-free slags. However, it is possible that at constant iron oxide contents, new compensation relationships could be applied. Justification for this statement is that the Meyer-Neldel Rule (analogous to compensation law) applies in liquid semiconductors where the conductivity is related to temperature by the Arrhenius function (Fortner *et al.* (1995)). Fortner *et al.* (1995) considered the basis for the Meyer-Neldel rule and proposed that it could be explained by multiphonon hopping conduction or a statistical shift of the Fermi energy level. It was considered outside the scope of this work to attempt to infer the origin of the compensation law or Meyer-Neldel rule or infer further structural or physical phenomena based on the temperature dependence of the conductivity data.

For comparison of the conductivity results, Figure 99 shows the conductivity results of this work and of various authors' work as a function of the FeO, content.

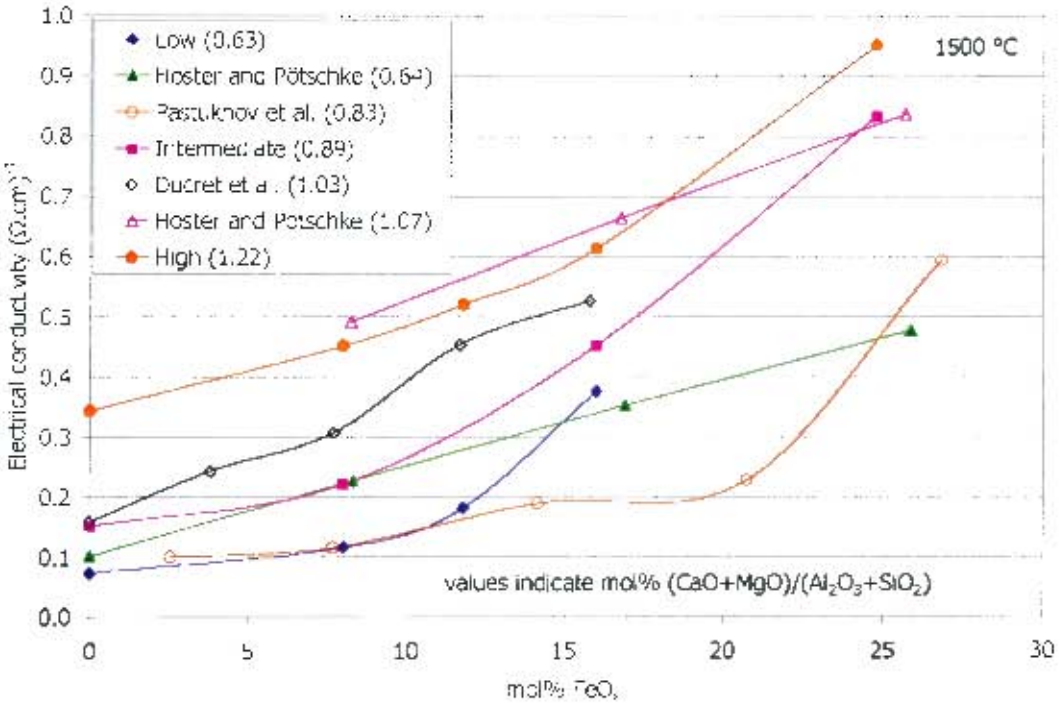

Figure 99: Comparison of current work and other authors' conductivity results at 1500 °C for FeO_x additions to slags. Measurements by Ducret *et al.* (2002) on CaO-FeO_x-MgO-SiO_2 system, Pastukhov *et al.* (1966) on Al_2O_3-CaO-FeO_x-SiO_2 system in air, Hoster and Pöstchke (1983) on CaO-FeO_x-SiO_2 system.

Direct comparisons between the data in Figure 99 are made difficult by the differences in the actual slag chemistries. However, to allow for comparison, the slag chemistries have been represented as the mol% (CaO+MgO)/(Al_2O_3+SiO_2) ratios. For the same iron oxide content, the electrical conductivity generally increases with basicity. All the authors' data increases with increasing iron oxide content. The data of Pastukhov *et al.* are not strictly comparable as the measurements were made in air.

The activation energies for conduction have also been compared to other authors' data in Figure 100. It should be noted that the activation energy data reported for Hoster and Pötschke (1983) was calculated from their conductivity data at discrete temperatures (given that Hoster and Pötschke did not relate the temperature dependence of their conductivity data using the Arrhenius function). The general trend evident in the graph is that the activation energy decreases with increasing iron content. At a particular iron oxide content, there is no clear trend between the basicity and the magnitude of the activation energy.

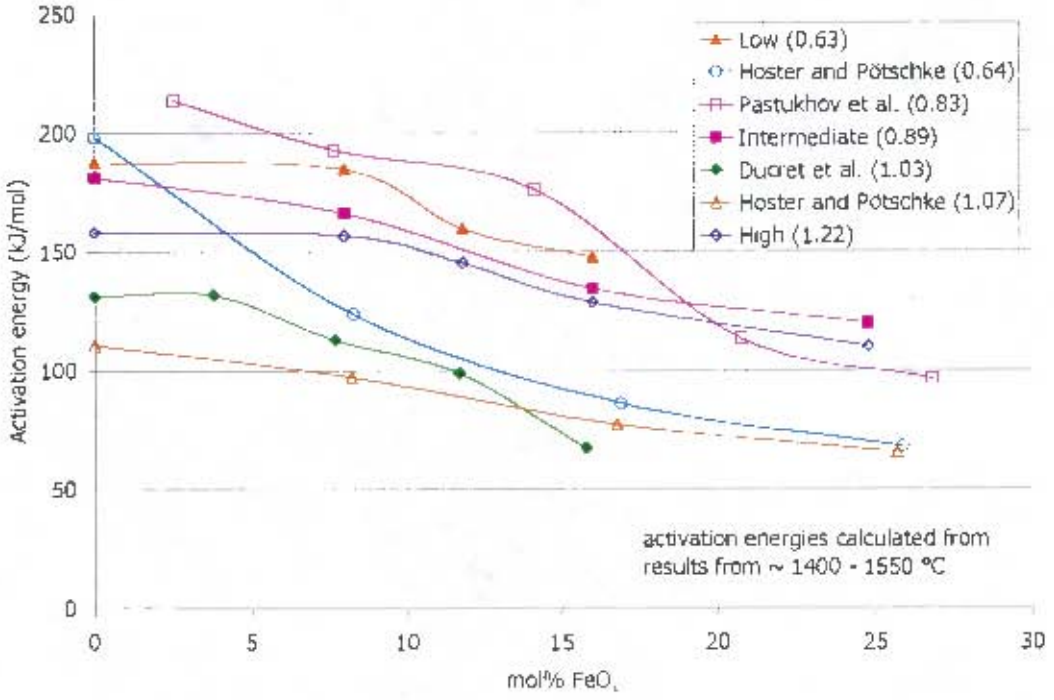

Figure 100: Comparison of activation energies for conduction in current work and other authors' data. Measurements by Ducret *et al.* (2002) on CaO-FeO_x-MgO-SiO_2 system, Pastukhov *et al.* (1966) on Al_2O_3-CaO-FeO_x-SiO_2 system in air, Hoster and Pöstchke (1983) on CaO-FeO_x-SiO_2 system.

The quantification of slag conductivity and temperature dependence with increasing iron oxide content will be more fully investigated in the modelling chapter.

5.3. Oxidation state dependence of conductivity of iron oxide – containing slags

The results of the oxidation state experiments on iron oxide–containing slags showed the dependence of the conductivity on the partial pressure of oxygen. This was expected as the quantities of ferric and ferrous ions in the melt depend on the oxygen partial pressure and the electronic mechanism is dependent on the ferric and ferrous content. It was seen in the literature review that previous work on the oxidation state dependence of the conductivity in iron-containing slags had been carried out at limited ranges of slag chemistry. Engell and Vygen's (1968) work was on slags with a molar CaO/SiO_2 ratio of 0.79. Pastukhov *et al.* (1966) carried out work on iron silicate slags and wt% $20Al_2O_3$-40CaO-$40SiO_2$ slags. Fontana *et al.* (1984) also conducted work on iron silicate slags, two CaO-FeO_x-SiO_2 slags and six Al_2O_3-CaO-FeO_x-MgO-SiO_2 slags, however the work on the latter slags was not systematic with regard to the effect of iron or basicity. Therefore it was not clear from the literature what the effect of basicity was on the oxidation state dependence of the conductivity.

Therefore in order to gain an understanding of how the basicity affected the oxidation state dependence of the conductivity, the following discussion is presented. Initially the conductivity results of the low, intermediate and high basicity slags containing the same amount of iron oxide were considered. Thereafter the effect of oxidation state on the conductivity of the calcium ferrite

slag was considered. In order to present a more complete picture of the effect of basicity, the data on the iron silicate slags reported by Pastukhov *et al.* (1966) and Fontana *et al.* (1984) were also considered. It should be noted that where multiple runs were carried out for a particular basicity slag and iron content, the results of the runs for that slag were averaged.

However, before the results of the oxidation state dependent experiments are discussed, it was considered important to evaluate the use of the shallow cell technique and the implications the technique had on the measured results. Another preliminary discussion on the calculation of ferric-ferrous fractions is also presented as much of the rest of the chapter relates conductivity to ferric and ferrous ion concentrations as opposed to oxygen partial pressures of p_{CO2}/p_{CO} ratios.

5.3.1. Implications of using the shallow cell technique

The shallow cell technique was deemed a very useful technique to obtain oxidation state dependent conductivity results in a relatively short space of time. However, the technique had its drawbacks and the variation in the results of duplicate experiments suggested that random errors could influence the measurements obtained. The implications of the identified random errors are discussed briefly below:

5.3.1.1 Effect of MgO dissolution

It was felt necessary to provide some discussion of the expected effects of the dissolution of MgO from the crucibles used in the oxidation state experiments on the conductivity. The effect of the MgO dissolution on the conductivity is likely to depend on the basicity and iron oxide content of the slag. In slags where the iron oxide content is low (<15 mol%) and the ionic conduction mechanism is dominant, it is likely that the conductivity will increase as more Mg^{2+} cations become available for conduction. In slags where the iron oxide content is higher (>15 mol%) and the electronic mechanism is more dominant, it is likely that the MgO addition will bring about dilution of the electronically conducting iron cations which would reduce the conductivity. However, the reduction in the electronic contribution may be offset by the increase in the ionic contribution owing to the increase in the number of Mg^{2+} cations. The other possible effect of MgO is on the relative proportions of ferric and ferrous cations at a constant p_{O2}. As an example of this, the ferric and ferrous quantities have been calculated for slag H40 based on the initial and final slag analyses using Larson and Chipman's data. This is shown in Table 37.

Table 37: Estimated ferric / total iron fractions for slag H40 considering change in slag composition due to dissolution of MgO crucible

			p_{CO2}/p_{CO}	over course of experiment, estimated change in		Fe^{3+}/Fe_{total} with MgO	Fe^{3+}/Fe_{total} without MgO
Slag H40	mol%			(C+M)/(A+S)	FeO_x	dissolution	dissolution
Component	initial	final	4900	1.2	33	0.89	0.89
Al_2O_3	2.4	2.2	80	1.3	32	0.51	0.50
CaO	18.9	18.3	20	1.4	31	0.42	0.38
FeO_x	33.0	26.4	10	1.47	30	0.38	0.33
MgO	17.6	27.1	5	1.51	29	0.33	0.28
SiO_2	28.1	26.0	2	1.55	28	0.28	0.21
Total	100.0	100.0	1	1.58	27	0.23	0.16
(C+M)/(A+S)	1.20	1.61	0.13	1.61	26.4	0.10	0.03

The information in Table 37 needs to be explained in more detail. The initial and final molar compositions have been given for the initial run on slag H40 in the first three columns on the left. In the next three columns the equilibrium conditions are given with estimates of the change in the molar $(CaO+MgO)/(Al_2O_3+SiO_2)$ ratios and the iron content at each p_{CO2}/p_{CO} ratio due to the dissolution of MgO from the crucible. From this information the ferric fractions were calculated for each equilibrium condition based on the initial composition and the estimated compositions. Therefore the last two columns compare the ferric fractions calculated for slag H40 where MgO dissolution was considered and where the MgO dissolution was not considered. The intermediate compositions were estimated as follows: as a repeat run was performed on slag H40 and ended at a p_{CO2}/p_{CO} ratio of 10, the compositions at that ratio are based on the analysed composition of the repeat run's sample. From calculations using MPE (see Zhang et al. (2002)), it seemed likely that the system was not at MgO saturation, therefore the linear increase in the basicity and decrease in the iron content were used as a first approximation. The p_{CO2}/p_{CO} ratio of 4900 is the equivalent of an oxygen partial pressure of 0.21 atm at 1450 °C.

From the analysis above, it was estimated that the maximum increase in the ferric fraction owing to the increased MgO was 0.07 (based on slag H40 which was the worst case). As mentioned above, the wet chemical analysis of the ferric fraction of the sample from the repeated run at a p_{CO2}/p_{CO} ratio of 10 gave the ferric fraction as 0.40 (as compared to 0.38 when considering MgO dissolution and 0.33 when not considering MgO dissolution). This suggested that the increase in the MgO content of the slags needed to be accounted for when determining the ferric fractions. Therefore the calculation of the ferric fractions based on the equilibrium conditions included an estimate of the effect of the MgO dissolution.

5.3.1.2 Reaction of FeO_x with the MgO crucible and formation of a thin surface layer

It is possible that FeO_x in the slag reacted with the MgO crucible to form a conducting layer around the surface of the crucible. The presence of this layer was not analysed for and difficulties would be encountered in accounting for the effect of this layer. Such difficulties include the electrical connectivity between the slag and the surface layer and also ascribing a numerical value for the conductivity to the surface layer. It is still considered that the current transport in the slag will be the rate limiting step and parallel current paths on a crucible surface layer will be contribute little to the overall conductivity.

5.3.1.3 Formation of solid phases in the slag

It is possible that solid phases form in the slag during the duration of an experiment especially in light of the changing oxidation state. The experiments were carried out at temperatures of 1450 °C so that the formation of solids such as magnetite and magnesio-ferrites spinels would be avoided. Simulations were carried out using MPE (see Zhang *et al.* (2002)) which suggested that formation of solid phases over the range of oxidation states tested would not occur. Possible reasons why crusts formed during the deep cell experiments have been explained above in Section 4.3.2.2.

5.3.1.4 Loss of iron to the electrodes

Given the length of the electrodes immersed (2mm) in the slag, significant losses of iron to the electrodes were not expected relative to the amount of iron in the bulk slag. The dilution

of the iron in the slag by MgO dissoluition was of more concern and has been accounted for by considering the changes in the slag chemistry.

5.3.1.5 Presence of gas bubbles in slag during reduction of sample

It was suggested that oxygen bubbles could possibly form when the slags were being reduced. This was considered unlikely given that the experiments were carried out under atmospheric pressure conditions and the partial pressures of oxygen at reduced conditions were very low. Possibly under higher pressure atmospheres, oxygen boil would be problematic.

5.3.1.6 Non-equilibrium

Differences between duplicate runs could have arisen from measurements taken where the system was not at equilibrium for a given set of conditions. In a couple of instances, the equilibrium points were possibly judged prematurely and a longer time for equilibration should have been allowed. However, the criteria for judging equilibrium was based on the average rate approaching zero and where premature decisions were made, it is likely that the reported value for the conductivity at that equilibrium is very close to the real value (within 5-8%). The purpose of carrying out duplicate experiments was to validate the findings in the initial experiments and thus provide a safeguard against measurements taken very far away from equilibrium. For example, in the case of the first repeat run on Slag L30, the measured resistances were oscillating at a p_{CO2}/p_{CO} ratio of 20. One of the local minima in an oscillation was mistakenly judged as the equilibrium condition. This misjudgement was identified when comparing with the second repeat run on Slag L30. Aside from this type of error in the judgement in equilibrium, it is considered that the majority of the decisions that equilibrium had been reached were correct. (The calculations of the variance of the conductivity from the time it was taken and what it could have been 30 minutes later are shown in Appendices C.1.3., C.2.3. and C.3.3. for all the slags. In all cases, the effect of the variation in the conductivity had a minimal impact on the conductivity vs ferric / total Fe trend.)

Further evidence to support the argument that equilibrium was reached is provided by the titrations carried out on samples of slags H40 (repeat) and L30 (repeat 2) both equilibrated at p_{CO2}/p_{CO} ratios of 10. The measured ferric and ferrous contents of the samples are compared to the values estimated based on the data of Larson and Chipman (1953):

Table 38: Comparison of titration measurements of ferric / total iron fraction vs estimated fractions based on data of Larson and Chipman (1953)

Sample	Measured Fe^{3+}/Fe_{total}	Calculated Fe^{3+}/Fe_{total}
H40 (repeat)	0.40	0.38
L30 (repeat 2)	0.17	0.22

The measured ferric/total Fe ratios are in reasonable agreement with the estimated values and suggest that the slags were in equilibrium with the gas.

5.3.2. Calculation of ferric/total iron fractions

It should be noted that interpretation of the results in terms of the oxygen partial pressure was considered less meaningful than expressing the conductivity in terms of the ferric and ferrous contents in the slag. Knowledge of the ferric and ferrous contents gives more insight into the structural aspects of the ionic and electronic contributions of the iron ions. In order to gain some appreciation of the effect of ferric and ferrous iron on the conductivity, it was therefore necessary to calculate the relative amounts present at each oxygen partial pressure. The literature was investigated to obtain estimates of the Fe^{3+} and Fe^{2+} contents based on oxygen partial pressures. Larson and Chipman (1953) measured the effect of oxygen partial pressure on the ferric/Fe_{total} fraction for a wide range of slags including iron silicates, calcium ferrites and CaO-FeO_x-SiO_2 slags of varying CaO/SiO_2 ratio. Timucin and Morris (1970) studied phase equilibria and thermodynamic properties in the CaO-FeO_x-SiO_2 system and included iron redox equilibria. The redox in MgO-containing slags was studied and a correlation was given by Yang and Belton (1998) which related $\log(Fe^{3+}/Fe^{2+})$ to $\log(p_{CO2}/p_{CO})$ and the molar (CaO+MgO)/SiO_2 ratio. However, the correlation was developed for low iron slags (up to 10wt% Fe). Mysen et al. (1984) also examined redox equilibria in CaO-FeO_x-MgO-SiO_2 melts but also only at low iron concentrations. The work of Larson and Chipman (1953) suggested that the Fe^{3+}/Fe_{total} fraction was dependent on the total iron content of the slag for low (mol% CaO/SiO_2 = 0.54) and high (mol% CaO/SiO_2 = 2.235) basicity slags. For intermediate basicity slags (mol% CaO/SiO_2 = 1.306), the ferric fraction was relatively independent of the total iron content.

In the end, the ferric and ferrous quantities were estimated from the data given by Larson and Chipman (1953). Several assumptions were made in estimating the ferric fraction. The temperature dependence of the ferric fraction at a given p_{CO2}/p_{CO} ratio was ignored. This assumption was necessary given that the measurements of Larson and Chipman were at 1550 °C and the measurements in this work were at 1450 °C. It was also assumed that the MgO would affect the Fe^{3+}/Fe_{total} fraction in a similar way to CaO, therefore the basicity was calculated as (CaO+MgO)/SiO_2. The measurements and discussion of Yang and Belton gave some indication that these assumptions were justified. Ultimately, the use of either Larson and Chipman's data or Yang and Belton's correlation gave rise to very similar results for the ferric fractions based on the p_{CO2}/p_{CO} ratos. For the sake of completeness, the conductivity results have been presented as a function of both oxygen partial pressure and ferric/total Fe fraction .

In order to give further justification for the estimation of the ferric fractions, several samples from the oxidation state dependent experiments were analysed by wet chemical methods to determine the amount of ferric and ferrous iron present. The analysis techinque was described in Section 3.8. A sample was obtained during the second repeat run on slag L30 at a p_{CO2}/p_{CO} ratio of 10. The Fe^{3+}/Fe_{total} fraction in the analysed slag sample was 0.17 and the predicted ferric fraction based on the data of Larson and Chipman was 0.22. A sample was also taken during the repeat run on slag H40 (approximate composition (wt%): Al_2O_3: 4, CaO: 17, FeO_x: 38, MgO: 12, SiO_2: 27) at a p_{CO2}/p_{CO} ratio of 10. The analysed ferric fraction was 0.40, while the predicted ferric fraction was 0.38. The agreement between the analysed and predicted ferric fractions was fair (± 0.05). Based on these two checks, it was considered acceptable to use the data of Larson and Chipman to give an indication of the ferric and ferrous contents of the slags at particular oxidation states. Ideally, a sample should have been taken at each equilibrium condition and the ferric and ferrous content of the sample analysed. However, with the shallow cell technique and the quantity of slag used, it was not feasible to obtain such samples.

5.3.3. *Slags containing 20wt% FeO_x*

The results of the experiments on the oxidation state dependence of the conductivity for slags containing 20wt% FeO_x are shown in Figure 101 as a function of the oxygen partial pressure.

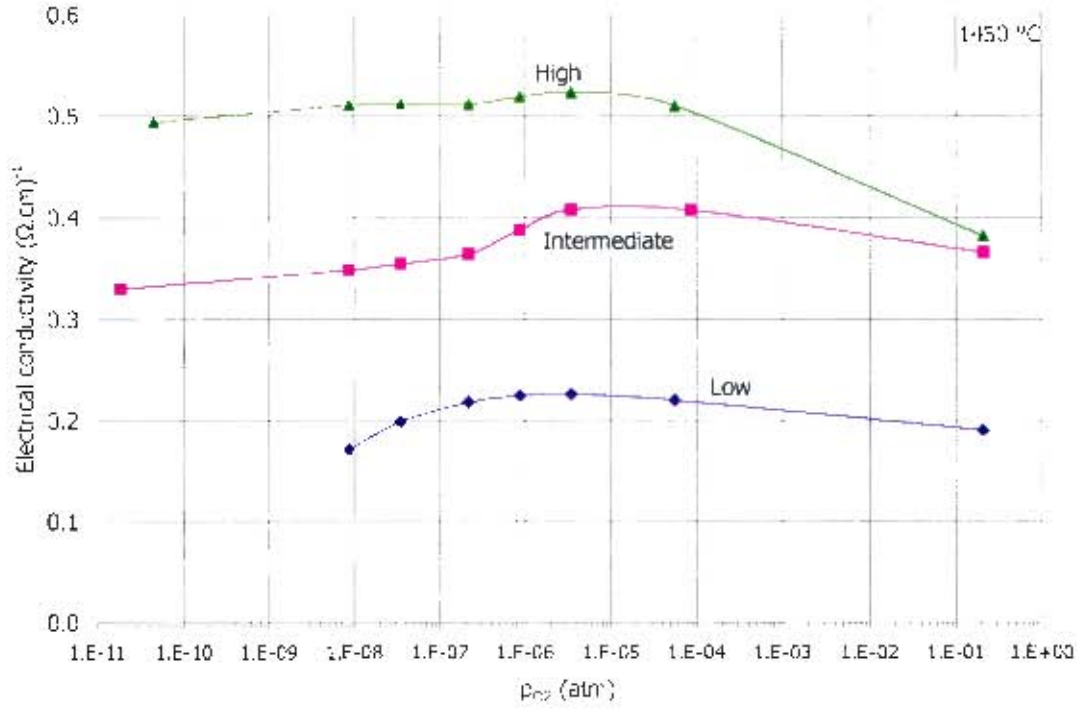

Figure 101: Variation of the electrical conductivity of slags containing 20wt% FeO_x with change in oxidation state at 1450 °C. Slags L20, I20 and H20

It is clear from Figure 101 that the electrical conductivity of the slags containing 20wt% FeO_x increased with increasing basicity. This was expected given that the number of charge carriers (Ca^{2+} and Mg^{2+}) increases with increasing basicity and the slags are more depolymerised. It is also evident that the conductivity was dependent on the oxidation state. This indicated that there was some electronic contribution to the overall conductivity.

The peaks in the conductivities for the three different basicity slags all occurred at an oxygen partial pressure of around 4×10^{-11} atm. As mentioned above, the conductivity results were also related to the ferric/ total iron fractions. Therefore, the results in Figure 101 have been replotted as a function of the ferric/total iron fraction and are shown in Figure 102:

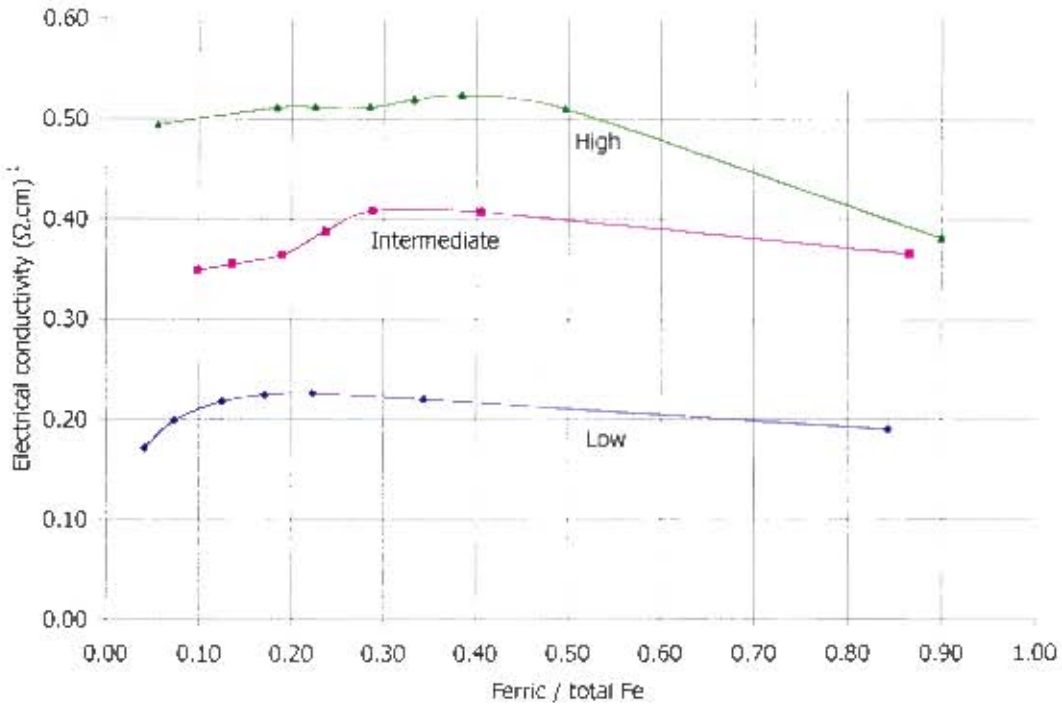

Figure 102: Electrical conductivity at 1450 °C of low, intermediate and high basicity slags containing 20wt% FeO_x as a function of the ferric / total iron fraction. Slags L20, I20 and H20

The trends in Figure 102 are very similar to those in Figure 101, however the peaks in the conductivity have shifted to different ferric fractions for the different basicity slags. Yang and Belton (1998) qualitatively explained that an increase in the basicity of a slag will increase the ferric fraction at a constant p_{O2}.

5.3.4. Slags containing 30wt% FeO_x

The data for the slags containing 30wt% FeO_x were treated in the same manner as above. Therefore the data for the low, intermediate and high basicity slags containing 30wt% FeO_x are shown in Figure 103 as a function of the oxygen partial pressure.

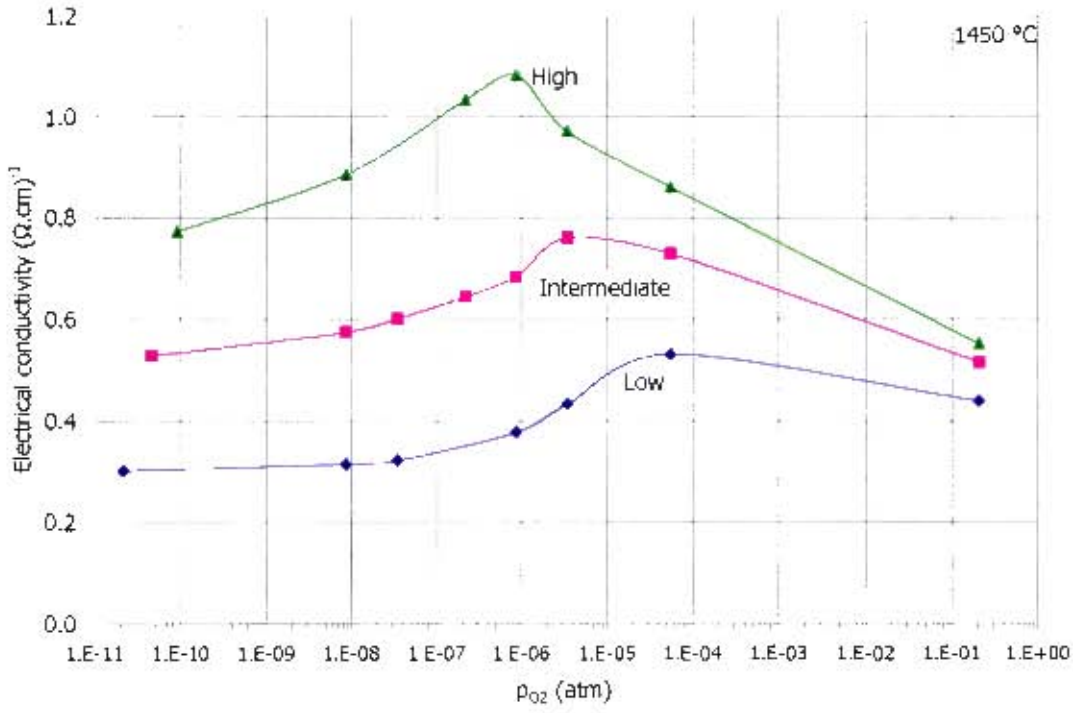

Figure 103: Variation of the electrical conductivity of slags containing 30wt% FeO, with change in oxidation state at 1450 °C. The captions indicate the basicities of the slags. Slags L30, I30 and H30

From Figure 103 it was evident that the electrical conductivity of the slags containing the same amount of iron increased with increasing basicity. This was expected for the same reasons as given previously. The electrical conductivity at oxidised conditions was very similar for the three basicity slags while at reduced conditions, the conductivity appeared to be more dependent on the basicity. The other trend evident is that the peak in the conductivity occurred at lower oxygen partial pressures as the basicity increased. The p_{O2} at which the maximum conductivity was reached decreased with basicity: 5×10^{-5}, 4×10^{-6} and 9×10^{-7} atm for the low, intermediate and high basicity slags respectively. The data are replotted as a function of the ferric fraction in Figure 104. The ferric fractions were estimated based on the data reported by Larson and Chipman (1953).

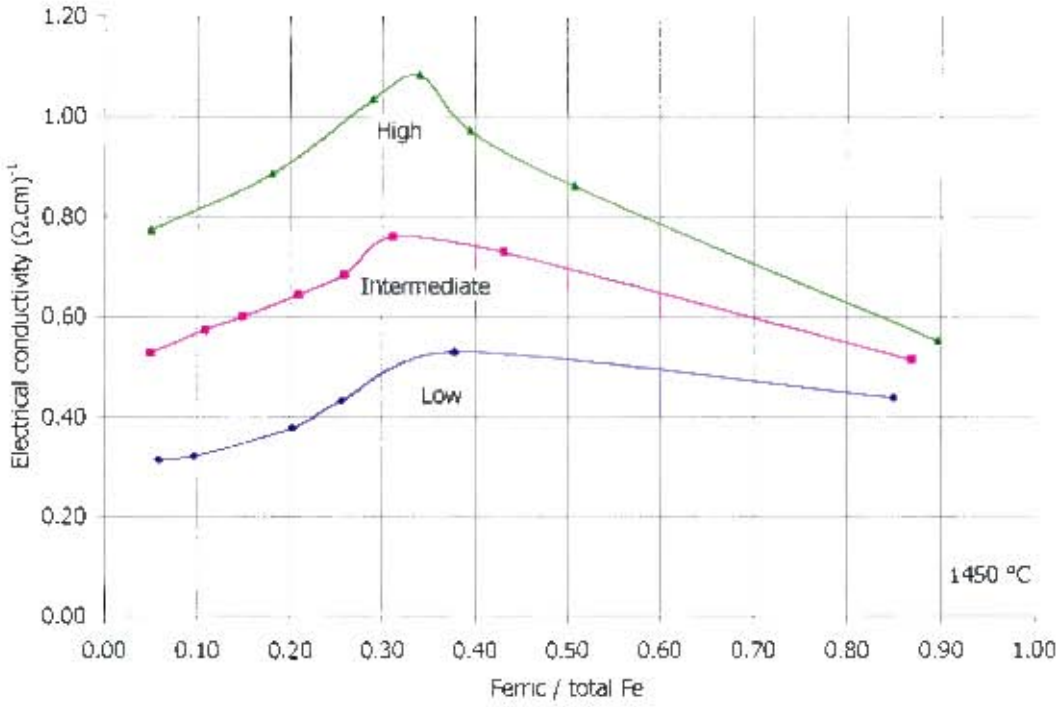

Figure 104: Electrical conductivity at 1450 °C of low, intermediate and high basicity slags containing 30wt% FeO_x as a function of the ferric / total iron fraction. Slags L30, I30 and H30

The trends in Figure 104 suggest that when the amounts of ferric and ferrous iron are taken into account, then the peaks in conductivity of the three basicity slags all occur at a ferric fraction of around 0.3 – 0.4.

5.3.5. Slags containing 40wt% FeO_x

The results of the oxidation state dependence of the conductivities of the slags containing 40wt% FeO_x are presented in the same manner as above. Therefore in Figure 105 the conductivities of the low, intermediate and high basicity slags are plotted as a function of the oxygen partial pressure.

The trends evident in Figure 105 are that the electrical conductivity generally increased with increasing basicity and the peaks in the conductivity occurred at lower oxygen partial pressures as the basicity increased. The one difference which was evident for the slags containing 40wt% FeO_x, was that the conductivities at the extremes for the intermediate basicity slag were higher than for the high basicity slag. This was not expected, however in order to present a better interpretation of the data in terms of slag structure the data was plotted as a function of the ferric fraction. As before the ferric and ferrous contents were estimated from the p_{O2} using the data of Larson and Chipman. This is shown in Figure 106.

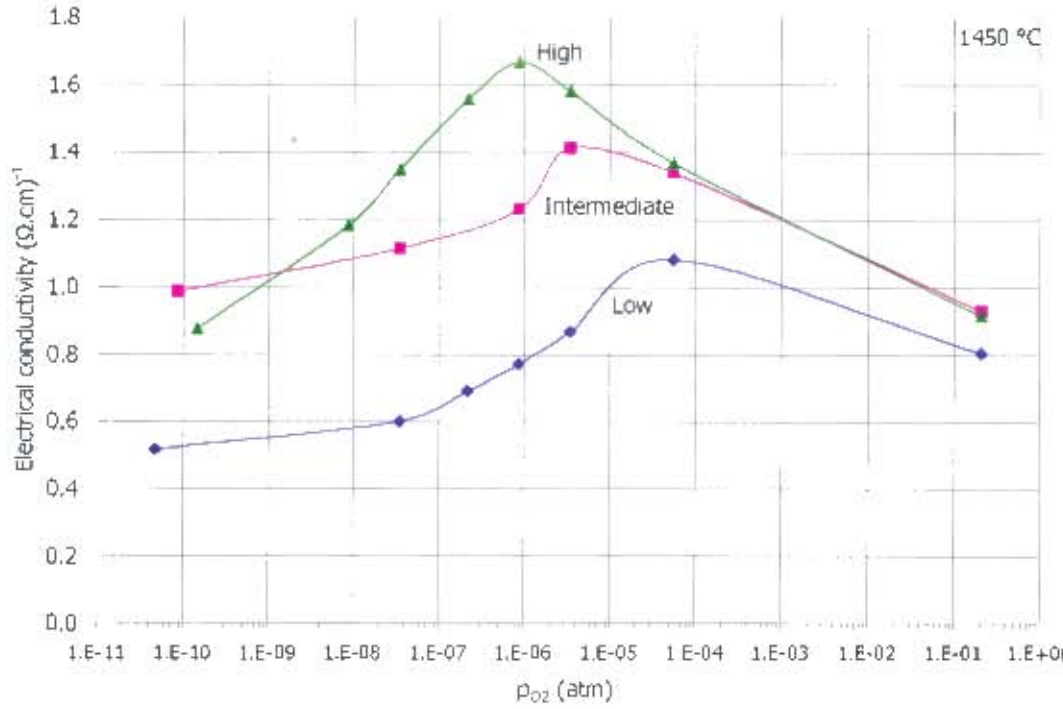

Figure 105: Variation of the electrical conductivity of slags containing 40wt% FeO_x with change in oxidation state at 1450 °C. Slags L40, I40 and H40

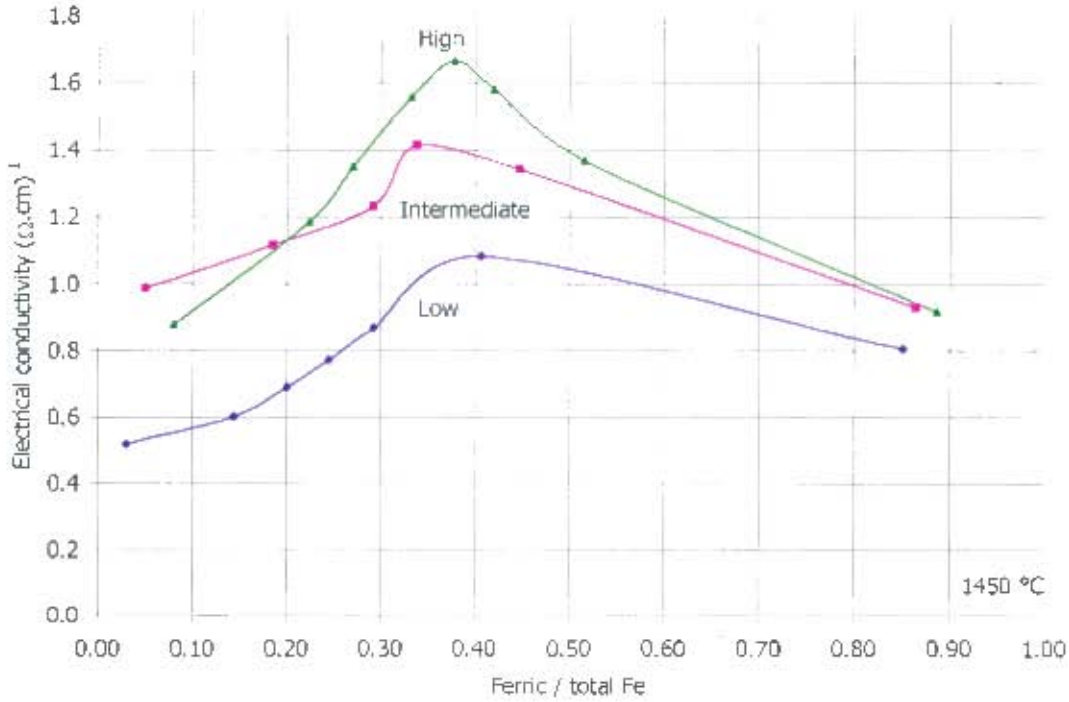

Figure 106: Electrical conductivity at 1450 °C of low, intermediate and high basicity slags containing 40wt% FeO_x as a function of the ferric / total iron fraction. Slags L40, I40 and H40

The trend apparent in Figure 106 is that the maximum in the conductivities for the three basicity slags occurred at ferric fractions of around 0.3-0.4. This was a similar value to that

for the 30wt% FeO_x slags. The conductivity of the intermediate basicity slag appeared to be higher than that of the high basicity slag at reduced conditions.

5.3.6. Numerical analysis of the oxidation state dependence of the conductivity results as a function of the ferric fraction, total iron content and basicity

The numerical analysis of the oxidation state dependent conductivity data provided a convenient way to summarise and compare the effect of the total iron content, basicity and the ferric/total iron fractions of the slags. It was decided that the analysis technique of Engell and Vygen (1968) would provide the information required. The reason for using the technique of Engell and Vygen was that it could handle the data at both reducing and oxidising conditions (in comparison to the techniques of Fontana *et al.* (1984) and Pastukhov *et al.* (1966) which only handled data at reduced conditions). The technique involved fitting a parabola to the data and analysing the fitting parameters according to the following equation:

Equation 25: $\kappa - \kappa_0 - ax + bx(1 \quad x)$

where $x = Fe^{3+}/Fe_{total}$

An example of the fitting procedure is presented in Figure 107 for the intermediate basicity slags with 30 and 40wt% FeO_x. It should be noted that none of the variables were constrained in the fitting procedure.

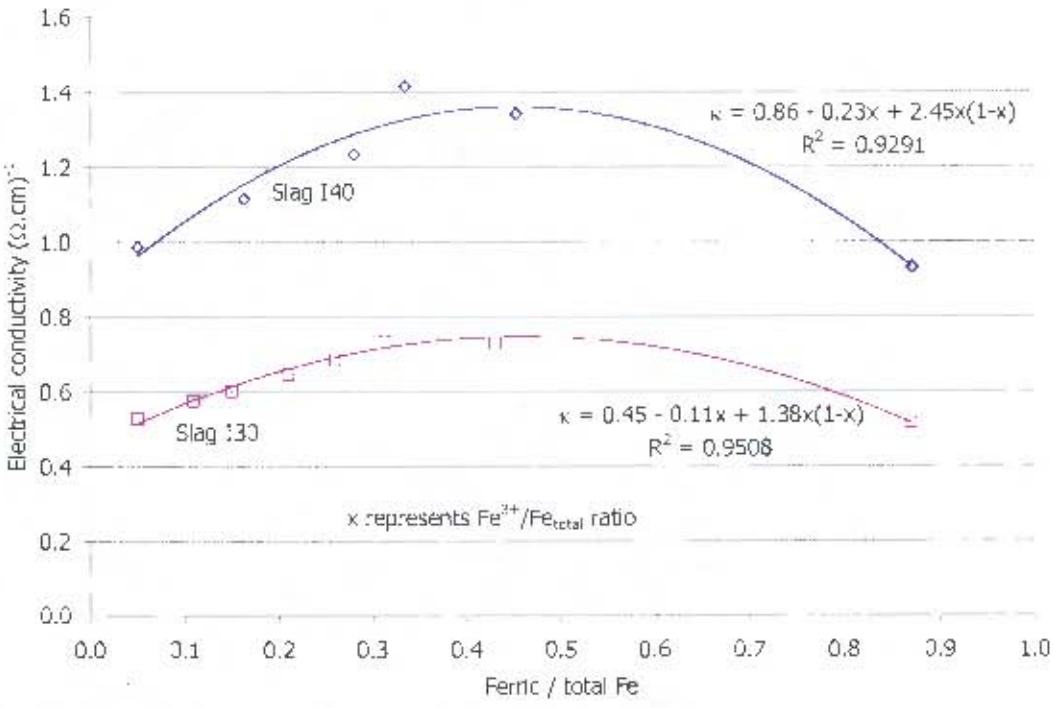

Figure 107: Modelling of the oxidation state dependence of the conductivity of the intermediate basicity slags containing 30 and 40 wt% FeO_x

The parabolic fit to the data gave reasonably close correlation. The fitted parameters for all the slags were calculated and are shown in Table 39. If one extrapolates the parabola to

x=1, a value for the conductivity is obtained where all the iron is present as ferric ions. These values have also been listed in the table. The correlation coefficients have also been included to provide an indication of the fit.

Table 39: Fitted parameters for oxidation state dependence of electrical conductivity of low, intermediate and high basicity slags

%FeO_x	basicity	κ_0	a	b	κ (x=1)	R^2
15	low	0.19	0.07	-0.01	0.12	0.9952
20	low	0.18	0.03	0.30	0.14	0.7139
	intermediate	0.32	-0.01	0.35	0.33	0.9097
	high	0.48	0.14	0.41	0.33	0.9923
30	low	0.23	-0.10	0.98	0.33	0.9207
	intermediate	0.45	0.11	1.38	0.34	0.9508
	high	0.73	0.40	1.74	0.33	0.8676
40	low	0.34	-0.21	2.41	0.54	0.9352
	intermediate	0.86	0.23	2.45	0.62	0.9291
	high	0.75	0.25	3.78	0.49	0.8774

From the values for κ_0, *a* and *b* presented in Table 39 several trends should be observed. Following the reasoning of Engell and Vygen, the ionic contribution is represented by the term $\kappa_0 - ax$ and the electronic contribution is represented by $bx(1-x)$.

Engell and Vygen suggested that the term κ_0 includes only the ionic contributions of Ca^{2+}, Fe^{2+} and Mg^{2+} cations (Al^{3+}, O^{2-} and Si^{4+} ions are assumed not to contribute). Generally at constant iron contents the values for κ_0 increase with increasing basicity (and hence Ca^{2+} and Mg^{2+} contents).

For a given slag, as the oxidation state increases and ferric ions form, the change in ionic conduction is represented by the parameter *a*. A positive value for *a* represents a decrease in the ionic contribution with increasing ferric and vice versa. The values of *a* for the low basicity slag containing 30 and 40wt% FeO_x were negative suggesting that the ionic conduction increased with increasing ferric content. This was unexpected as ferric ions at oxidised conditions were expected to be tetrahedrally co-ordinated in these slags and therefore enhance the slag polymerisation and decrease the conductivity. On closer examination of the literature though, data on the cation distributions of some $CaO\text{-}FeO_x\text{-}SiO_2$ melts in air were found. Pargamin *et al.* (1972) determined the cation distributions in two melts with increasing FeO_x contents. The melts had molar CaO/SiO_2 ratios of 0.58 and 1.3 and were equilibrated in air at 1550°C and then quenched. The quenched samples were then analysed by means of Mössbauer spectroscopy to determine the quantities of tetrahedrally co-ordinated ferric iron (Fe^{3+}(IV)), octahedrally co-ordinated ferric iron (Fe^{3+}(VI)) and ferrous iron (Fe^{2+}). The authors found that in the lower basicity slag (CaO/SiO_2 = 0.58) with increasing FeO_x content (up to 40wt%), the $Fe^{3+}(IV)/Fe_{total}$ fraction remained constant at around 0.2. In the higher basicity slag (CaO/SiO_2 = 1.3) the $Fe^{3+}(IV)/Fe_{total}$ fraction increased linearly with FeO_x content (10 to 40wt%) from 0.28 to 0.5. There are two implications of this work. The first is that the majority of the ferric ions are not in tetrahedral co-ordinations at oxidised conditions. The second implication is that the basicity of the slag possibly

determines the co-ordination of the ferric ions at oxidised conditions. With higher basicity slags it is likely that more of the ferric iron is tetrahedrally co-ordinated.

Therefore, it is suggested that in the low basicity slag (molar $(CaO+MgO)/(Al_2O_3+SiO_2)$ ratio = 0.63) the majority of the ferric cations are octahedrally co-ordinated in air. Fe^{3+}(VI) cations are considered to be network modifiers and this could qualitatively explain why the conductivities of the low basicity slags with 30 and 40 wt% FeO_x are higher in air than at reduced conditions.

If one now considers the conductivities of the intermediate and high basicity slags at oxidised conditions and their positive *a* values, it is suggested that the ferric ions become more tetrahedrally co-ordinated with increasing basicity. This in turn may lead to a decrease in the conductivity of slags in air owing to the partial network forming characteristics of the tetrahedrally co-ordinated ferric ions. This possibly explains why the conductivities of the intermediate and high basicity slags are lower in air than at reduced conditions.

Now considering the values of the electronic term coefficient *b*, it is seen that in the low basicity slag containing 15wt% FeO_x, there is negligible electronic contribution. This agrees with the discussion in Section 5.2 on the effect of iron addition, where it was suggested that more than ~16mol% or ~20wt% FeO_x is required for the facilitation of electronic conduction. The values of *b* for the slags containing 20wt% FeO_x ranged from 0.3 to 0.41 and increased with basicity. The values of *b* increased with increasing iron content and had values from 1-1.75 for slags with 30wt% FeO_x and values from 2.4 - 3.8 for slags containing 40wt% FeO_x. This gives some confirmation that the electronic contribution increases with increasing iron content.

The values calculated for the conductivity at x=1 increased with iron content. There was no clear trend of the effect of basicity on the κ (x=1) values. Limited conductivity data were found in the literature for iron-containing slags at oxidised conditions (in air). The majority of the data was provided by Morinaga *et al.* (1975) and Adachi and Ogino (1957). Therefore it was not possible to conclude what the effect of basicity should be on the conductivity of iron-containing slags at oxidised conditions.

The values found by Engell and Vygen (1968) for κ_0, *a* and *b* were larger than the values found in the current work, however their work was conducted at 1600 °C. It is reasoned that the higher values were due to temperature effects. The trends in the values were similar in that the values increased with increasing iron content. Also there was negligible electronic contribution until there was 15.5 mol% FeO_x and greater.

The fitted parameters are enlightening about the roles of the electronic and ionic conduction mechanisms and their contribution to the overall conductivity. Thus one can separate the contributions. An example of this is shown in Figure 108 for the intermediate basicity slag with 40wt% FeO_x.

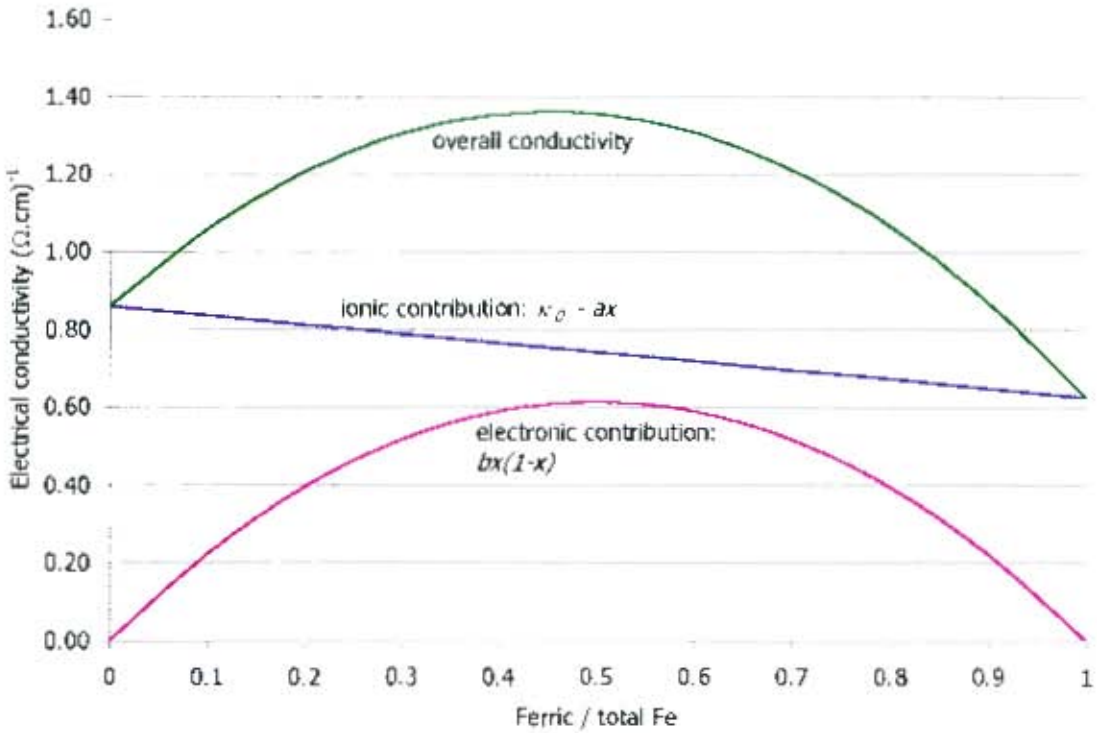

Figure 108: Separation of ionic and electronic contributions to overall conductivity for intermediate basicity slag with 40wt% FeO_x (based on Engell and Vygen model)

It was considered that the above treatment of the data would be a feasible approach to modelling the oxidation state dependence of the conductivity of iron containing slags. However there are several limitations in this type of analysis. The first is that one would need to estimate values for κ_0, a and b. Estimating κ_0 should be relatively simple given the amount of data available on the conductivity of slags at reduced conditions. Estimation of a is difficult as there is very little data available on slags at oxidised conditions and the data is not very consistent. Estimation of values for b is also difficult as a result of the scarcity of data on the oxidation state dependence of conductivity.

5.3.7. Calcium ferrite slag

The variation in the conductivity of the calcium ferrite slag with changing oxidation state provides information on the high basicity extreme of the slag systems of interest. As was seen in the Results chapter in Section 4.5, the conductivity reached a maximum at reduced conditions (at around $p_{O2} \approx 10^{-10}$ atm.). As was carried out for the silicate slags, the equivalent ferric fractions were calculated from the oxygen partial pressures. The ferric fractions were estimated using a correlation given by Takeda *et al.* (1980) relating the Fe^{3+}/Fe^{2+} ratio to a function of the wt% CaO and p_{O2} for calcium ferrite slags. The conductivity for the calcium ferrite slags is therefore presented as a function of the ferric / total iron fraction in Figure 109.

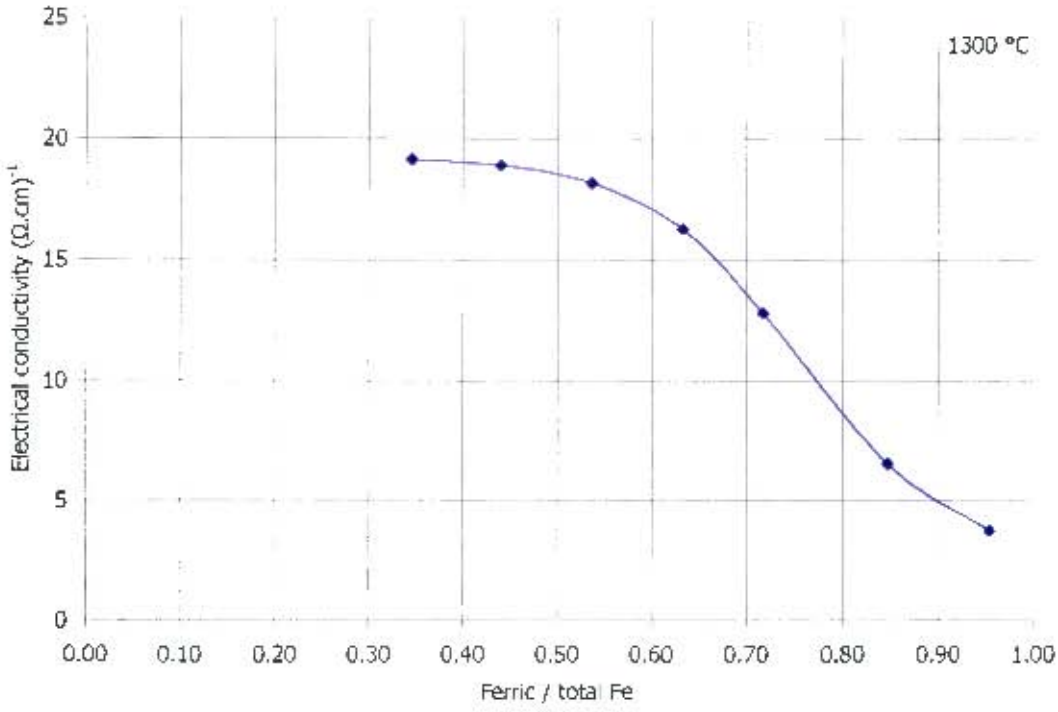

Figure 109: Variation of electrical conductivity at 1300 °C of calcium ferrite slag (25wt% CaO – 75%FeO_x) with ferric fraction

The electrical conductivity of the calcium ferrite slag increased with decreasing ferric / total Fe fraction and reached a maximum at around 0.35 where the initial experiment was ended. According to the data of Takeda *et al.* (1980) iron saturation should occur at a ferric fraction of around 0.22. It is likely that the conductivity would continue increasing until iron saturation occurred where a large increase in the conductivity would occur as a result of a highly conductive metallic phase. This was shown by the plot in Figure 91.

The other benefit of studying calcium ferrite slags was that they have been very well characterised. Both Yazawa *et al.* (1981) and Sumita *et al.* (1983) have provided structural information on calcium ferrite slags. Considering calcium ferrite slags in air, Sumita *et al.* (1983) suggested that in pure FeO_x the ferric ions were octahedrally co-ordinated and with addition of CaO the ferric ions became progressively more tetrahedrally co-ordinated. This increase in the proportion of tetrahedrally co-ordinated ferric ions with increasing CaO content agrees qualitatively with the findings of Pargamin *et al.* (1972) for co-ordination of ferric ions in silicate slags with increasing CaO/SiO_2 ratios.

Sumita *et al.* (1983) provided ion distributions for calcium ferrites as a function of the CaO content. For a slag with ~50 mol% CaO, the ferric ions were equally distributed between octahedral and tetrahedral co-ordinations. The calcium ferrite studied in this investigation had ~48 mol% CaO (~25wt% CaO), therefore it can be expected that in air approximately half the ferric ions were in tetrahedral co-ordinations and half in octahedral co-ordinations. Therefore considering the low conductivity at oxidised conditions, it is likely that the majority of the current is carried by Fe^{3+} (VI) and Ca^{2+} cations and a small amount is carried by the few Fe^{2+} cations that are present. The Fe^{3+} (IV) cations present will polymerise the slag and inhibit conduction. As the slag becomes more reduced, the number of Fe^{2+} cations increase

and hence electronic conduction is enhanced. It is not known how the distribution of octahedral and tetrahedral ferric cations is affected by the oxidation state.

5.3.8. *Iron silicate slags*

Although iron silicate slags were not investigated directly in this work, it was considered valuable to treat the iron silicate conductivity data provided in the literature more thoroughly. The reason for this is that the iron silicate data provides the other basicity extreme relative to calcium ferrite slags. The data of Pastukhov *et al.* (1966) and Fontana *et al.* (1984) were considered.

The ferric and ferrous fractions were estimated from the oxygen partial pressures using MPE (see Zhang *et al.* (2002)). The MPE values were in good agreement with the ferric fractions calculated by Fontana *et al.* using the thermodynamic model of Goel *et al.* (1980). Fontana *et al.* also presented data at constant p_{CO_2}/p_{CO} ratio which were also calculated as equivalent ferric and ferrous fractions. The resultant graph is shown in Figure 110.

The important trend observed in Figure 110 is that the electrical conductivity increased as the amount of ferric iron in the slag increased. Unfortunately no measurements were made at more oxidising conditions such that the peak in the conductivity could be observed. This was obviously limited by the formation of magnetite at more oxidised conditions at 1350 °C.

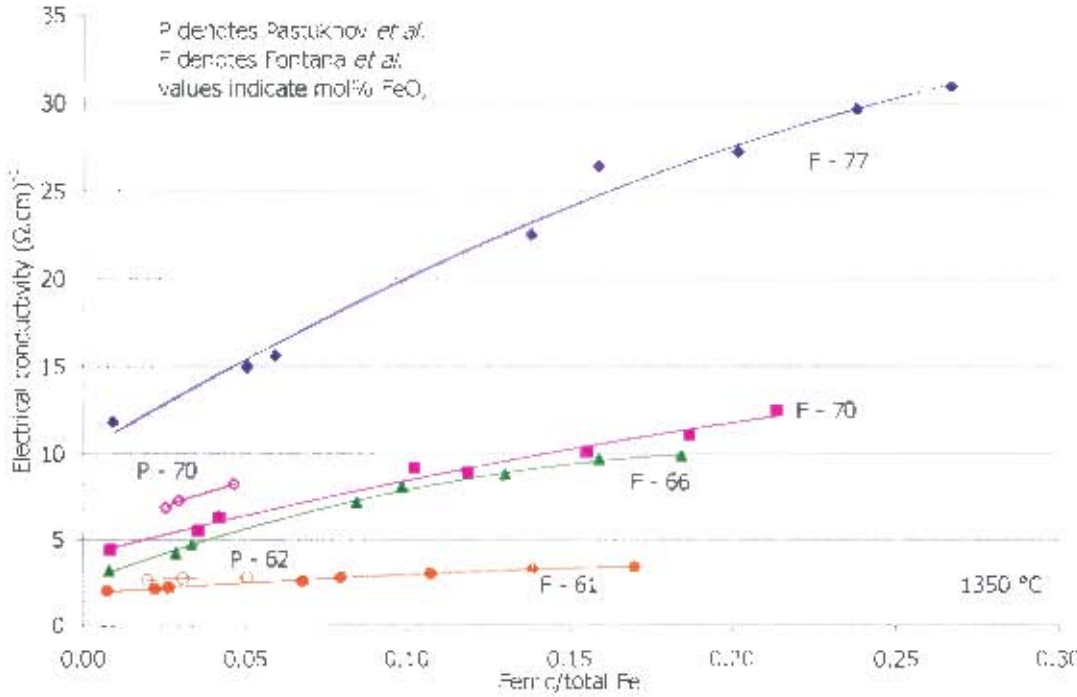

Figure 110: Electrical conductivity of iron silicate slags at 1350 °C as a function of the ferric / total iron fraction. Measurements by Fontana *et al.* (1984) and Pastukhov *et al.* (1966)

5.3.9. *Overall interpretation of oxidation state dependence of conductivity*

It should be clear from the above discussions that the electrical conductivity of iron containing slags is highly dependent on the proportions of ferric and ferrous ions present in

the slag. The effect of the oxidation state on the electrical conductivity of iron containing slags will be examined at the extremes, therefore at very reduced and very oxidised conditions and at the oxidation state where the maximum in the conductivity occurs. At each condition, the effect of oxidation state will also be specifically looked at in terms of calcium ferrite and iron silicate slags as these slags provide extremes in the basicity. The explanation of the trends found for basicities intermediate to the extremes should therefore follow from examination of trends for the extremes of the basicity.

5.3.9.1 Reduced conditions

At reduced conditions the majority of the iron in a slag will be present as ferrous ions. In the case of iron silicate slags, almost all the iron is ferrous (89-98% Fe^{2+} depending on total iron content), while in calcium ferrites at reduced conditions it is likely that around 70-90% of iron ions will be ferrous (depending on total iron content). Bockris *et al.* (1952) showed that ferrous ions were network modifiers.

From the conductivity and current efficiency results on iron silicate slags measured in iron crucibles, it was shown that as the iron oxide content of the slag increased, the electronic contribution increased. If one examines the ternary FeO-Fe_2O_3-SiO_2 phase diagram at iron saturation, it is seen that as the silica content of an iron silicate is decreased, the amount of ferric increases. Therefore the increase in the electronic contribution should be due to the increase in the total iron and the ferric fraction (as directly noted by Dukelow and Derge (1960)).

Now considering the conductivity and current efficiency measurements on calcium ferrite slags in iron crucibles, it was shown that the majority of the conduction was electronic. If one studies the ternary CaO-FeO-Fe_2O_3 phase diagram at iron saturation, it is seen that there is considerably more ferric iron than for iron silicate slags. This explains why there is significantly more electronic conduction in calcium ferrite slags and why the percentage of electronic conduction does not decrease very much with addition of lime.

In the silicate slags studied in the current work, at reduced conditions almost all the iron is ferrous, therefore there is little electronic conduction. The conduction would be due to the ionic contributions of the Ca^{2+}, Fe^{2+} and Mg^{2+} cations.

5.3.9.2 Oxidised conditions

At oxidised conditions the majority of the iron should be present as ferric ions. Ferric ions may be present in either octahedral or tetrahedral co-ordinations. Octahedral ferric ions are considered to be network modifiers while tetrahedral ferric ions are considered to be network formers. From the work of Pargamin *et al.* (1972), it was reasoned that the slag basicity and total iron content played a role in determining the relative quantities of the ferric and ferrous ions and the co-ordinations of the ferric ions. For calcium ferrite slags in air, Sumita *et al.* (1983) showed that the majority of the iron was ferric and that the ratio between Fe^{3+}(IV) and Fe^{3+}(VI) ions was linearly dependent on the total CaO content of the slag, with more Fe^{3+}(IV) at higher CaO contents.

Unfortunately no data was found concerning the conductivities of iron silicate slags at oxidised conditions. The conductivity data on the calcium ferrite slags in air showed that the

conductivity was lower than at reduced conditions. The correlation provided by Sumita *et al.* (1983) suggested that the conduction mechanism was primarily ionic and due to the Ca^{2+}, Fe^{2+} and Fe^{3+}(VI) ions.

The conductivities in air of the silicate slags studied in this work suggested that the magnitude of the conductivity at oxidised conditions was a function of the slag basicity, the total iron content and the co-ordination of the ferric ions. Following from the reasoning of Sumita *et al.* (1983), the conduction will be due to Ca^{2+}, Mg^{2+}, Fe^{2+} and Fe^{3+}(VI) cations. Fe^{3+}(IV) ions present will polymerise the slag and inhibit conduction.

5.3.9.3Conductivity maximum

It is not desired to place too much significance on the ferric fraction at which the maximum in the conductivity occurred owing to the uncertainty in the calculated values for the ferric fractions. However, it was considered worthwhile presenting some discussion on the subject. In terms of the electronic mechanism, one would expect that the maximum in the conductivity would occur at a ferric fraction of 0.5. This is where there are the equal quantities of ferric and ferrous ions and hence should be the most number of sites for electron / hole exchange. From the experiments, it was seen that the peaks in the conductivities in the case of the silicate slags occurred at ferric fractions of 0.3 to 0.4 and would most likely occur at around 0.25 for the calcium ferrite slag.

There are two possible reasons why the maximum in the conductivity does not occur at Fe^{3+}/Fe_{total} = 0.5. The first possibility is that although the electronic contribution has a maximum at a ferric fraction of 0.5, the underlying ionic contribution determines the shape of the total conductivity curve and therefore the apparent peak position. For example, consider the separation of the conductivity of the intermediate basicity slag with 40wt% FeO_x into its ionic and electronic contributions shown in Figure 108. The ionic contribution is higher at the reducing end than the oxidising end. The electronic contribution is parabolic with a maximum at a ferric fraction of 0.5. However, the sum of the ionic and electronic contributions results in the overall conductivity curve having a maximum below a ferric fraction of 0.5.

The second possibility is that not all of the ferric and ferrous ions are able to facilitate electron / hole exchange. In the case of solid wüstite and magnetite, the conductivity and the thermopower coefficient were related to c_+ and c_- which were referred to as the electrical valences by Gartstein and Mason (1982) and were not equal to the ferric and ferrous fractions. In the case of magnetite, it was shown that c_+ was the fraction of octahedrally co-ordinated ferric ions and c_- was the fraction of octahedrally co-ordinated ferrous ions (Wu and Mason (1981) and Nell and Wood (1991)).

Therefore it is suggested that in the case of molten slag systems containing iron oxide, electronic conduction is possibly also via ferric and ferrous ions in equivalent sites i.e. octahedrally co-ordinated sites. The iron cation distribution with changing oxidation state has not been treated thoroughly in the literature. Pargamin *et al.* (1972) provided some insight into the ferric cation distribution in air. The work of Mysen *et al.* (1984) was conducted on melts with low iron concentrations. However, it was shown that the ferric ions in silicate melts were predominantly tetrahedrally co-ordinated at oxidised conditions but as the Fe^{3+}/Fe_{total} fraction decreased from 0.5 to 0.3, the ferric ions changed co-ordination to

octahedral. Therefore the most number of equivalent sites for electronic conduction should occur between 0.3 and 0.5 as the ferric ions change co-ordination.

The next step in providing more detailed explanations of the ionic and electronic conduction mechanisms would necessitate more information on the iron cation distribution. The ionic mechanism is affected in terms of the melt polymerisation which is affected by the co-ordination of the ferric ions. Fe^{3+}(IV) ions enhance the polymerisation of the slag and therefore decrease the electrical conductivity, while Fe^{3+}(VI) ions act as network modifiers, depolymerise the slag and enhance the electrical conductivity. The electronic mechanism is likely to be affected if electronic conduction is only possible via ferric and ferrous cations in octahedral co-ordination.

To provide any further discussion concerning the conduction mechanisms in iron-containing slags would require more detailed information on the iron cation distributions at a range of oxidation states and higher iron levels than the work of Mysen *et al.* (1984). This would necessitate either Mössbauer spectroscopy of quenched samples or possibly measurements of the thermoelectric coefficient of the liquid melts (assuming that the relationship for the liquids between the thermoelectric coefficient and the electronically conducting cations is similar to the solid state relationships for wüstite and magnetite). It has also been assumed in the above discussion that ferrous ions are always octahedrally co-ordinated. In solid magnetite, ferrous ions may occupy both octahedral and tetrahedral positions.

Summary of the effect of oxidation state on the electrical conductivity of iron-containing slags

In slags with greater than around 15mol% FeO_x, the electrical conductivity is dependent on the ionic and electronic conduction mechanisms. The electronic contribution increases with increasing iron content. The electronic contribution arises from the exchange of electrons / holes between ferric and ferrous ions. As the slag chemistry determines the relative amounts of ferric and ferrous ions at a particular oxygen partial pressure, the slag chemistry affects the response of the conductivity to oxidation state. A typical response of the conductivity to changes in oxidation state is that at reduced and oxidised conditions the conductivity is lower (predominantly ionic conduction) than at intermediate oxidation states (predominantly electronic conduction). It is suggested that the co-ordination of the ferric ions in the slag will be an important factor determining the electronic and ionic contributions at more oxidised conditions.

5.4. Effect of chromium

From the results on the chromium containing slags, it was evident that the addition of chromium to the slags brought about a decrease in the conductivity. From the literature it was seen that where Al_2O_3-MgO-SiO_2 slags were below their liquidus temperatures, the addition of chromium caused a decrease in the conductivity. Rennie *et al.* (1972) suggested that this was due to the formation of a solid phase containing conducting cations. The movement of some of the conducting cations was therefore restricted. It was thought likely that a similar phenomenon would occur when chromium was added to the low basicity slag.

In order to quantify the effect of chromium, the type of solids that were likely to form with chromium addition were identified. Work (unpublished) has been conducted within CSIRO

Minerals on the compositions of the various phases present in chromium-containing slags at particular temperatures. It was found that spinel phase formed very readily with addition of chromium. From the measured compositions of the spinel phase present, it was found that a typical spinel composition for a slag similar in chemistry to the low basicity slag would be $Al_{0.7}Cr_{1.5}Fe_{0.5}Mg_{0.8}O_4$. Therefore the formation of spinel would lock up mainly Fe^{2+} and Mg^{2+} cations and the conductivity could decrease as a result.

The addition of chromium to the low basicity slags was modelled using MPE (Zhang *et al.* (2002)) to obtain an indication of the phases present and the quantity of each phase at a range of temperatures. The slags were modelled under an argon atmosphere to simulate the conditions of the slags. This gave an equivalent p_{O_2} of around 1 x 10^{-6} atm at 1500 °C. As was suggested in the literature review the chromium can be present as Cr^{3+} and Cr^{2+} ions depending on the oxidation state, therefore it was important to specify the oxidation state. The results are shown in Figure 111.

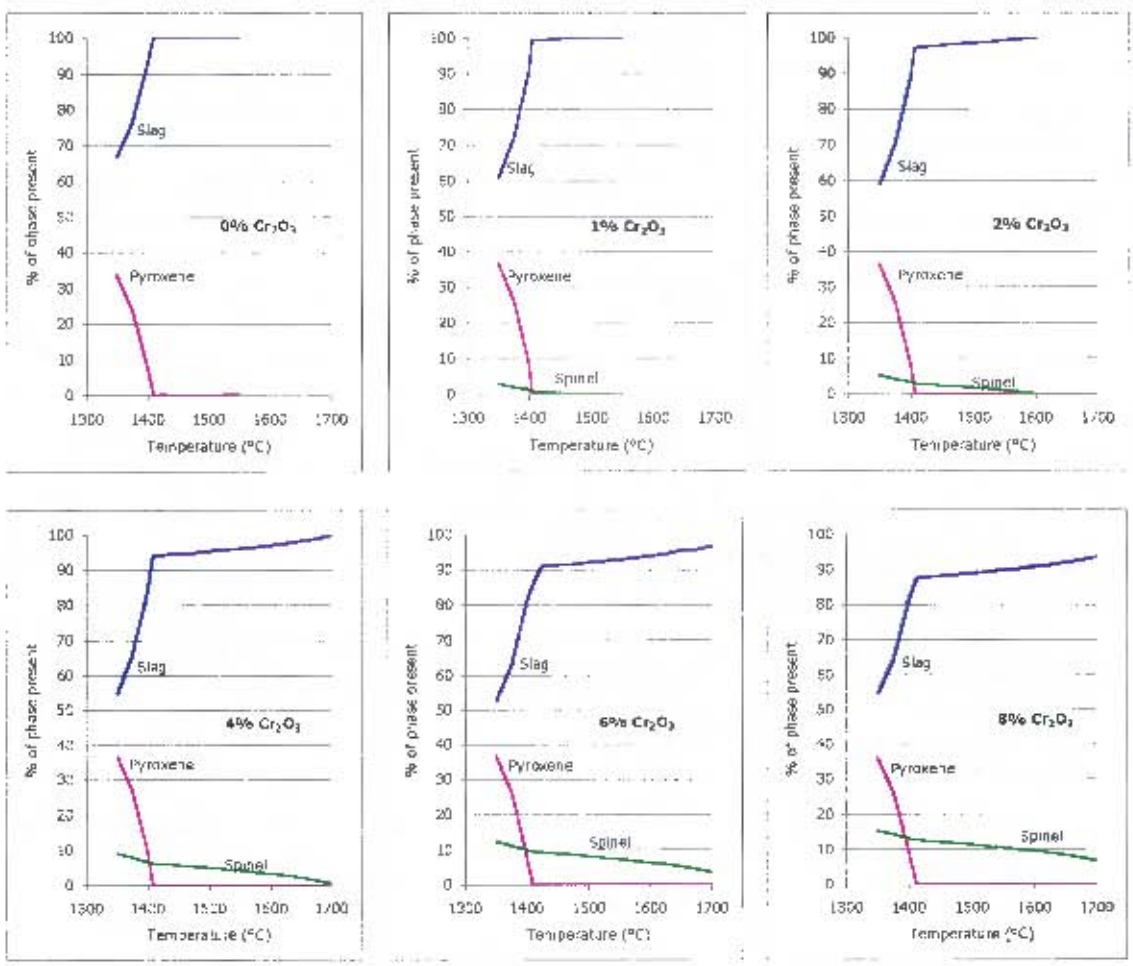

Figure 111: Phases present in 0, 1, 2, 4, 6 and 8wt% Cr_2O_3 containing slags as a function of temperature. Modelled using MPE (Zhang *et al.* (2002)) under an argon atmosphere

The most significant trend observed in Figure 111 is that the addition of chromium causes a spinel phase to form which has a very high melting point relative to the pyroxene phase. The amount of spinel at a constant temperature is directly related to the amount of chromium present. It should also be noted that the spinel melts gradually over a broad temperature range unlike the pyroxene which melts over a much smaller temperature range. The last point is

significant as this means that one will not necessarily observe a large change in the temperature dependence of the electrical conductivity where spinel and slag are the only phases present. Therefore if one considers the heatup profiles shown in the Results chapter (see Figure 81 and Figure 89), it is apparent why there was a large change in slope as the pyroxene phase melted out but an insignificant change in slope as the spinel melted out. This point is also shown in Figure 112 and Table 40 where the Arrhenius plots and the values for the activation energy and the pre-exponential factor are shown respectively.

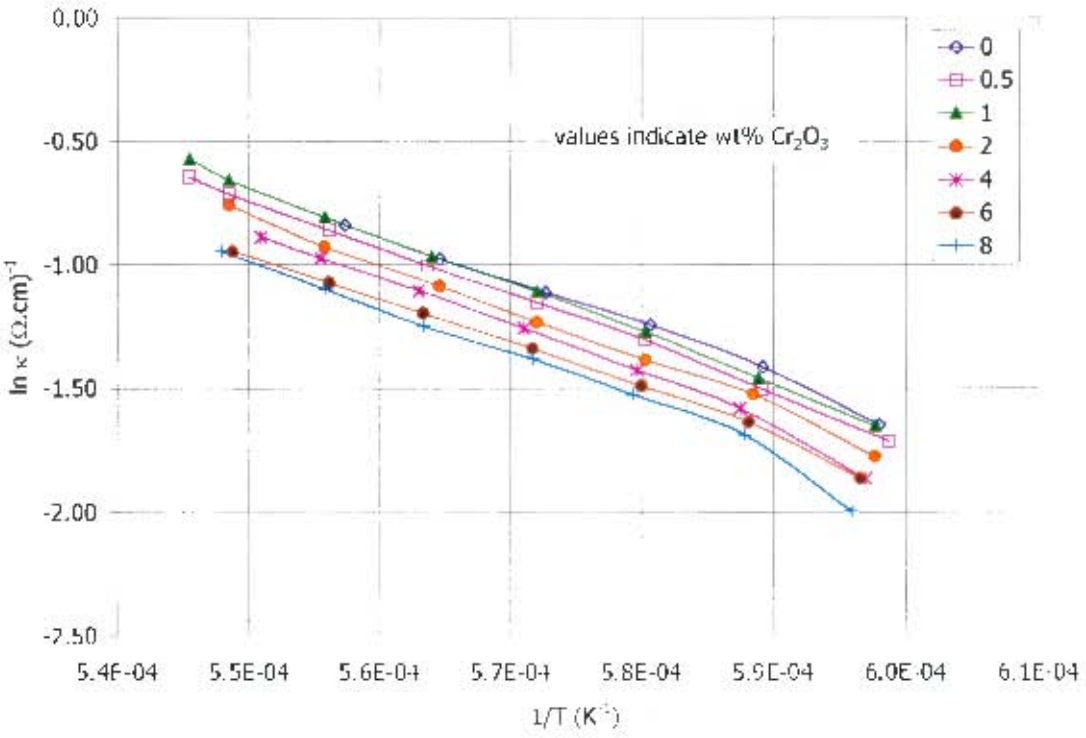

Figure 112: Arrhenius plots of ln κ vs reciprocal of temperature for chromium containing slags (conductivity measurements in Pt crucibles)

From the above graph it is evident that there is a change in slope between 1/T – $5.9x10^{-4}$ and $6.0x10^{-4}$ K^{-1}. This relates to the melting out of the pyroxene phase. Above 1425 °C (~$5.9x10^{-4}$ K^{-1}) there are no significant changes in the slope of the Arrhenius plots. The activation energies and pre-exponential factors calculated for the slags are summarised in Table 40.

Table 40: Activation energies and pre-exponential factors for chromium containing slags from the conductivity measurements made in Pt crucibles

Cr_2O_3 (wt%):	0	0.5	1	2	4	6	8
E, (kJ/mol)	147.4	159.3	162.7	158.3	157.6	146.0	157.6
ln A, $(\Omega.cm)^{-1}$	9.0	9.8	10.1	9.7	9.6	8.7	9.1
R^2	0.99880	0.99884	0.99913	0.99824	0.99959	0.99981	0.99977

From Table 40, it is seen that the activation energies for the slags containing 0.5 to 4% Cr_2O_3 are 10-15 kJ/mol higher than the chromium free slag. This possibly indicates that the melting of the spinel gives rise to the greater temperature dependence of the conductivity. It is likely that the lower activation energies for the slags containing 6 and 8% chromium arise because there are still significant amounts of spinel in the temperature range of the measurements. If one then

extrapolates the conductivity to higher temperatures, it is likely that the chromium containing slags may then have higher conductivities than the chromium free slag. This is shown in Figure 113 where the conductivities have been extrapolated based on the data presented in Table 40.

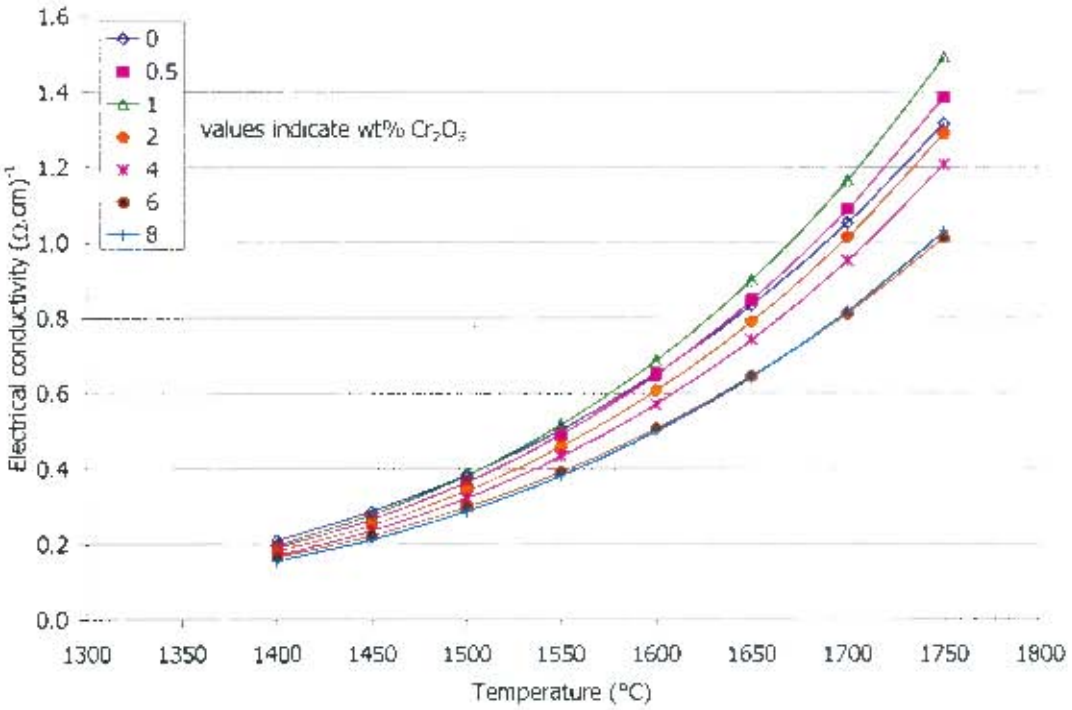

Figure 113: Extrapolation of conductivity data for chromium containing slags up to 1750°C

From the graph in Figure 113 it is suggested that at 1750°C the conductivities of the slags containing 0.5 and 1wt% Cr_2O_3 are higher than the chromium free slag. The conductivities of slags containing 2% Cr_2O_3 and more are still lower than the chromium free slag. Obviously extrapolating the conductivity far outside the temperature range in which it was measured is likely to give rise to errors. It was therefore of interest to measure the conductivity at higher temperatures to validate the trends shown in the extrapolation. The maximum temperature at which measurements were carried out in the platinum crucibles was 1550 °C. It was for this reason that measurements were also carried out in molybdenum crucibles in a high temperature furnace such that conductivity measurements could be made up to 1700 °C.

The measurements in the high temperature furnace also showed that the conductivity of the slags decreased with increasing chromium content (2 and 4wt% Cr_2O_3). The slag containing 2wt% chromium was likely to have been above its liquidus temperature at 1700 °C, whereas slag Cr4 was still below its liquidus. The fact that the conductivity of Slag Cr2 did not increase as the temperature increased above 1600 °c was unexpected as it was considered that once the spinel phase had melted out, the conducting cations that were associated with the spinel phase would then be available for conduction in the liquid phase. The conductivity of the Slag Cr2 should therefore have had the same, if not higher conductivities than the chromium-free slag. There are two possible reasons why this was not the case.

The first reason is that the measurements were carried out in molybdenum crucibles. From the analysed compositions of the slags after the experiments, it was clear that 1.3-1.5wt% Mo was

present in the slag. This made isolating the effect of chromium difficult when slags with 2 and 4wt% Cr_2O_3 were being tested. The effect of Mo in slags has not been directly quantified even though many authors have used molybdenum crucibles and electrodes for measurements. Rennie *et al.* (1972) suggested that since molybdenum is a transition metal, it was likely to bring about an increase in the conductivity. Drop quench testwork in molybdenum crucibles up to 1700 °C had also been carried out at CSIRO Minerals on chromium-containing slags to determine phase equilibria (unpublished). The analysis of the quenched samples showed small amounts of solid phases which were very rich in Cr and Mo (approximately 20wt% of each element and 2, 10 and 9wt% of Al, Fe and Mg respectively) at temperatures of up to 1700 °C. If similar solid phases were present in the slags used for conductivity measurements, they could provide an explanation for the decreased conductivity with increased chromium content.

The second possible reason for not finding an increase in the conductivity of Slag Cr2 with increased temperature (above the slag liquidus) was that the majority of the chromium was present in the trivalent form. If this were the case, then the spinel phase would be stabilised and the liquidus temperatures would be higher than indicated in the modelled phase distributions shown in Figure 111. Also, as was suggested by Liutikov and Tsylev, the Cr^{3+} cation is possibly a network former and will polymerise the slag and decrease the conductivity. Given that the experiments were conducted under an argon atmosphere, the possibility of there being a relatively large fraction of Cr^{3+} ions was good. Xiao *et al.* (2000) studied the oxidation state of chromium in molten slags, however none of the systems examined were similar enough to the present one to provide data on the oxidation state of the chromium.

Summary of the effect of chromium

From the above discussion, it is concluded that the decrease in conductivity with Cr_2O_3 addition to a slag is most likely the result of the precipitation of a solid phase containing large portions of conducting cations (such as Fe^{2+} and Mg^{2+}). Where slags containing chromium are above their liquidus temperatures, it was not possible to conclusively determine the effect of chromium from the current work due to complications of molybdenum dissolution and the possible formation of Mo-containing chromite spinels. It would however, seem apparent that a dramatic increase in the conductivity with increased chromium should not be expected where the slag is above its liquidus temperature.

5.5. Summary of the key findings

The key findings arising from the discussion are summarised below:

- In iron-free Al_2O_3-CaO-MgO-SiO_2 containing slags, the electrical conductivity increases with increasing basicity and temperature. In these slags, the activation energy for conduction and the natural logarithm of the pre-exponential factor are related by a compensation law. It also seems apparent that there is an inverse relationship between the basicity and the activation energy.
- When FeO_x is added to Al_2O_3-CaO-MgO-SiO_2 containing slags, the electrical conductivity increases. Slag basicity remains important in determining the electrical conductivity of iron-containing slags as the Ca^{2+} and Mg^{2+} cations provide ionic conduction. It appears likely that around 15 mol% FeO_x is required for electronic conduction to occur. The addition of iron

reduces the activation energy for conduction and brings about a shift of the temperature dependence data away from the compensation law found in iron-free slags. It was proposed that the deviation from the compensation law for iron-free slags was a possible indication of a change in conduction mechanism.

- The electrical conductivity of an iron-containing slag is dependent on the oxidation state of the slag. A typical response of the conductivity to a change in oxidation state is the following: starting at reduced conditions, the conductivity will increase with oxidation state, reach a peak at around Fe^{3+}/Fe_{total} = 0.3 to 0.5 and then decrease at more oxidised conditions. The electronic conduction mechanism is dependent on the amount of ferric and ferrous ions and the total iron content. The electronic contribution increases with increasing iron content. At reduced conditions, the majority of the iron is present as ferrous ions which are considered to be network modifiers. As the slag is oxidised, ferrous ions form ferric ions and electronic conduction increases as there are more sites available. At oxidised conditions, the majority of the iron is present as ferric ions. The co-ordination of ferric ions appears to be important in determining the effect on the conductivity. Where ferric ions are tetrahedrally co-ordinated it is likely that they will polymerise the slag and reduce the conductivity. Where ferric ions are octahedrally co-ordinated, it is likely that the ions are network modifiers and will generally increase the conductivity. It seems apparent that the slag basicity is important in determining the distribution of ferric and ferrous ions and therefore the conductivity at oxidised conditions. It is also likely that electronic conduction can only occur between ferric and ferrous ions in octahedral positions, in which case knowledge of the iron cation distribution would help in understanding the conduction mechanisms.
- The addition of chromium to a slag is likely to bring about a decrease in the electrical conductivity as a result of spinel phase formation. Depending on the composition of the spinel phase, conducting cations such as Fe and Mg could get locked up in the spinel phase and be unavailable for conduction in the liquid phase. In the case of the slags studied in this investigation (wt% Al_2O_3: 5, CaO: 5, FeO_x: 20, MgO: 20, SiO_2: 50 with additions of 0.5, 1, 2, 4, 6 and 8% chromium), the likely composition of spinel phase was $Al_{0.2}Cr_{1.5}Fe_{0.5}Mg_{0.8}O_4$. Therefore as spinels formed, Mg and Fe cations would become unavailable for conduction in the liquid phase. It was also of interest to determine the effect of chromium where slags were above their liquidus temperatures. Therefore experiments were carried out in molybdenum crucibles up to temperature of 1700 °C. It was suspected that the conductivity would increase as a result of Cr cations being conductive. However, it was not possible to conclusively determine the effect of chromium from the current work due to complications of molybdenum dissolution and the possible formation of Mo-containing chromite spinels at high temperatures (up to 1700 °C and theoretically above the slags' liquidus temperatures).

Chapter 6

MODELLING

The approach taken in modelling the electrical conductivity of slags was to initially consider slags containing transition metals and slags without transition metals separately. The iron oxide-free slag systems were considered first as it is known that only ionic conduction occurs, therefore the only variables affecting the conductivity are the slag chemistry and the temperature. Thereafter the conductivities of slags containing iron oxide were considered. In these slags mixed ionic and electronic conduction takes place and the conductivity is dependent on the slag chemistry, the temperature and the oxidation state. In order to attempt to account for the effect of chromium, the precipitation of a solid phase and its effect on the liquid slag composition was investigated.

The modelling would ideally have been fundamental in nature, however in order to accomplish this type of modelling, it would have been necessary to have considerably more information about the slag and its structure. For example, a fundamental approach would have required thermodynamic modelling of the slags to obtain values for the three types of oxygen (which give a good indication of the basicity or polymerisation of the slag). While this modelling can be (and was) carried out easily for binary silicates (see Lin and Pelton (1979)), it becomes considerably more complex for higher order systems. It was considered outside the scope of the current work to develop thermodynamic models for higher order systems such that predictions of the conductivity could be obtained.

The other more fundamental approach would be to relate the conductivity to the transport properties (mobilities) of the ions in the slag. This requires information about the diffusivities of ions in the slag of which there is less information than for conductivity. Also it has been shown in the literature (Goto (1984)), that the relationship between self (or tracer) diffusivities, ion mobilities and partial conductivities is not as easily explained than by the Nernst-Einstein equation.

The model developed for the iron-free Al_2O_3-CaO-MgO-SiO_2 systems was semi-empirical in nature where regressions were used to identify the best correlations of the conductivity to the compositions and temperature. The model developed for the iron oxide containing systems was necessarily semi-empirical in that information on the ferric and ferrous iron contents of the slag had to be considered in order to explain the change in conductivity with oxidation state. However, in modelling the conductivity, considerations such as the cation radii, state of polymerisation of the network, liquidus temperatures and oxygen partial pressures were always kept in mind.

In summary, it is believed that the models presented below will give reasonably accurate estimates of a slag's conductivity based on its temperature, composition and oxidation state. It is likely that more accurate models can be obtained by considering more fundamental aspects of the structure and

conditions of a slag. Hopefully the present modelling will stimulate further modelling of the conductivity of slags where the scope and time for thermodynamic modelling and other such activities permit.

6.1. Transition metal free slag systems

The electrical conductivity data considered for modelling was for systems that contained the components Al_2O_3, CaO, MgO and SiO_2. This included the data in the literature for binary, ternary and quaternary systems. The data used are those presented in the literature review chapter. As was mentioned in that chapter, it has been attempted to only consider conductivity data for slags that were above their liquidus temperatures. To give an indication of the amount of data available and the types of trends that occur, the data were plotted in Figure 114 at discrete temperatures against the mol% $(CaO + MgO)/(Al_2O_3 + SiO_2)$ ratio. There were limited conductivity data for slags at temperatures higher than 1600 °C and these points have been omitted from the graph.

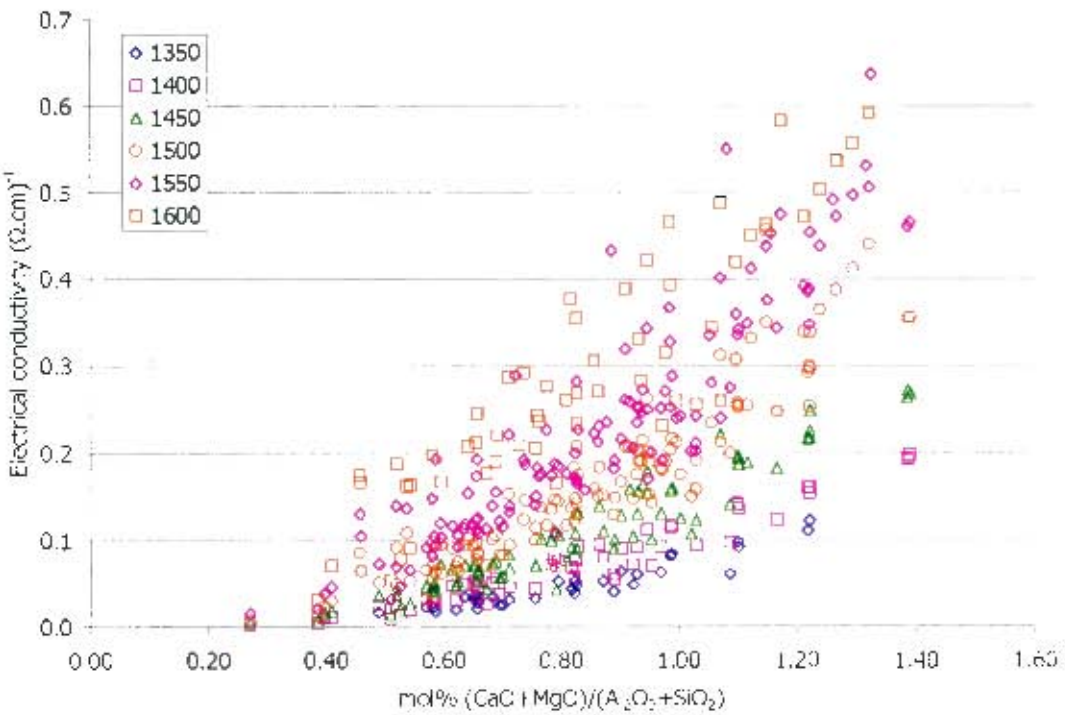

Figure 114: Electrical conductivity data for systems containing Al_2O_3, CaO, MgO and SiO_2 as a function of the mol% $(CaO+MgO)/(Al_2O_3+SiO_2)$ system from 1350-1600 °C

As expected, the trends in Figure 114 indicated that the conductivity increased with increasing temperature and with increasing CaO and MgO contents. The temperature dependence of the data was investigated further and it was found that the compensation law held for the relation between the pre-exponential factor and the activation energy for conduction. The compensation law relationship for the iron-free slags was shown in the Discussion chapter in Figure 94. The least squares fit for the data gave rise to the following equation for the compensation law:

Equation 26: $E_\sigma = 17.2 \ln A_\sigma - 6.85$

In modelling of the conductivities for the iron-free slags, the data set used contained the literature values and the few data points for iron-free systems measured in the current work. It is summarised as follows:

Table 41: Summary of data set considered for modelling conductivity of Al_2O_3-CaO-MgO-SiO_2 systems

Temperature °C	Number of data points	Electrical conductivity $(\Omega.cm)^{-1}$		
		Minimum	Maximum	Average
1350	34	0.016	0.122	0.048
1400	59	0.002	0.197	0.072
1450	78	0.004	0.271	0.106
1500	113	0.008	0.440	0.163
1550	129	0.015	0.637	0.232
1600	59	0.031	0.591	0.290
1650	13	0.208	0.687	0.389
1700	14	0.001	0.855	0.314
1750	5	0.340	1.000	0.681

The data for temperatures of 1650, 1700 and 1750 °C were not used in the regressions but the data points were compared with the predicted values from the model. Three approaches were considered in attempts to model the conductivity for the system. The first considered the conductivity as a function of the ratio of network modifiers to network formers. The second approach used multiple linear regressions of the natural logarithm of the conductivity as a function of the composition. The third approach made use of multiple linear regressions of the natural logarithm of the pre-exponential factor as a function of the composition and thereafter the compensation law was used to predict the activation energy. The approaches are detailed below:

6.1.1. Approach 1: Conductivity as function of ratio of network modifiers to network formers

The first approach was to relate the conductivity to a ratio of the network modifiers over the network formers, therefore similar to the approach of Winterhager *et al.* (1966). However to bring in the temperature dependence of the conductivity, one had to perform non-linear regressions at discrete temperatures and then relate the correlation parameters to the temperature. The approach is summarised in Equation 27.

Equation 27:
$$\kappa = \frac{(c_1)X_{CaO} + (m_1)X_{MgO}}{(a_1)X_{Al_2O_3} + (s_1)X_{SiO_2}}$$

Therefore the parameters c_1, m_1, a_1 and s_1 were determined at discrete temperatures and thereafter related to the temperature. The regression was performed using the Solver function of Microsoft Excel such that the slope of κ vs the function had a value of 1 and the intercept had a value of 0. The weighted (based on number of data points at each

temperature) correlation coefficient (R^2) was 0.6856 for data up to 1600 °C. The values of the parameters and their variation with temperature is shown in Figure 115.

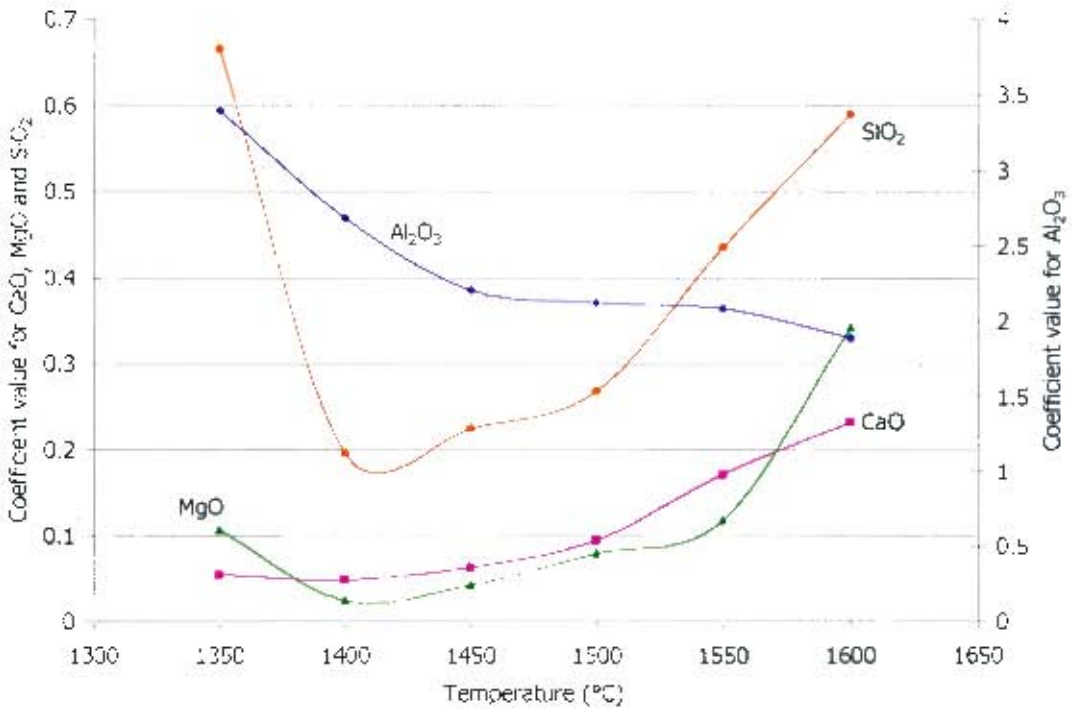

Figure 115: Regression parameters and their temperature dependence for model of conductivity of Al_2O_3-CaO-MgO-SiO_2 system as a ratio of network modifiers to network formers

Apart from the values at 1350 °C, the parameters for CaO, MgO and SiO_2 increased with temperature and the values for Al_2O_3 decreased with temperature. The increase in the values of the CaO and MgO are in accord with the concept that the higher the temperature, the greater the conductivity. The increase in the silica parameter with temperature may be misleading as the magnitude of the silica values is much lower than for the alumina values, therefore changes in the alumina values will have to be offset by changes in the silica values.

As a result of the relatively low values for the correlation coefficients (R^2 values), this approach was not considered further.

6.1.2. Approach 2: Multiple linear regression of ln κ as a function of the composition

The second approach was to perform multiple linear regressions of the natural logarithm of the conductivity data as a function of the composition. The regressions were carried out at discrete temperatures and thereafter the regression parameters were related to temperature. The modelling function is therefore expressed as the following:

Equation 28: $$\ln \kappa = \left(a_1 + \frac{a_2}{T}\right)X_{Al_2O_3} + \left(c_1 + \frac{c_2}{T}\right)X_{CaO} + \left(m_1 + \frac{m_2}{T}\right)X_{MgO} + \left(s_1 + \frac{s_2}{T}\right)X_{SiO_2}$$

This expression is related to the Arrhenius function as follows:

Equation 29: $$\ln\kappa = \ln\kappa_0 - \frac{E_\kappa}{RT}$$

where $$\ln\kappa_0 = (a_1)X_{Al_2O_3} + (c_1)X_{CaO} + (m_1)X_{MgO} + (s_1)X_{SiO_2}$$

and $$-\frac{E_\kappa}{RT} = \left(\frac{a_2}{T}\right)X_{Al_2O_3} + \left(\frac{c_2}{T}\right)X_{CaO} - \left(\frac{m_2}{T}\right)X_{MgO} + \left(\frac{s_2}{T}\right)X_{SiO_2}$$

The regressions were carried out using the LINEST function of Microsoft Excel. The regression parameters calculated are shown in Figure 116 as a function of the temperature.

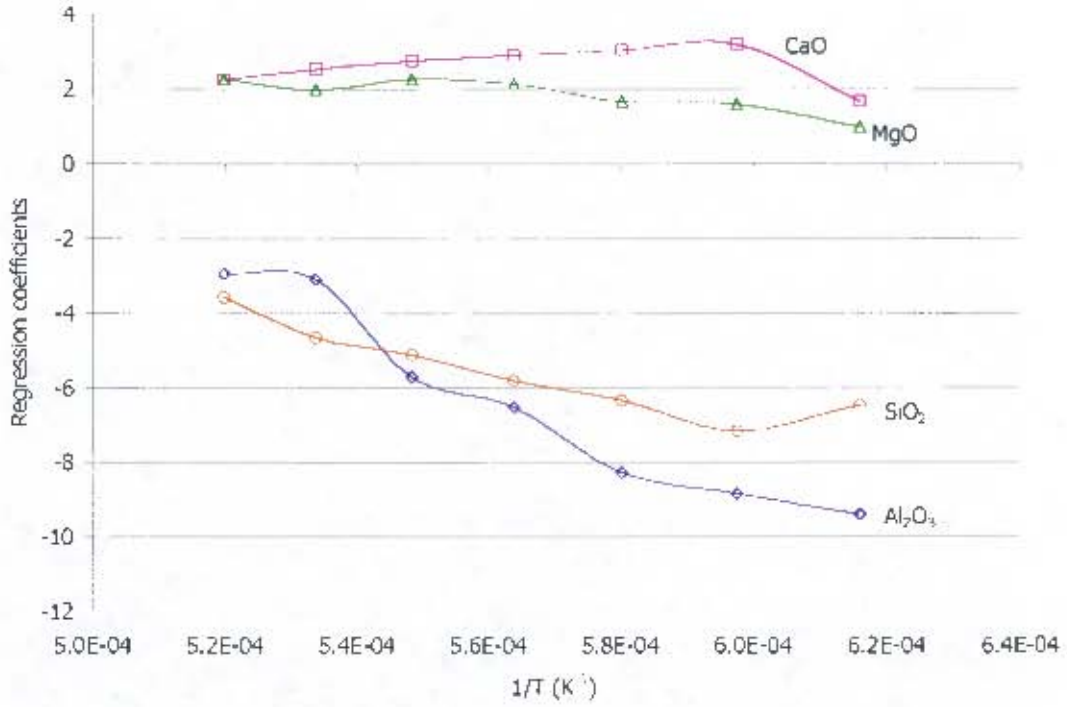

Figure 116: Regression parameters and their temperature dependence for modelling of the Al_2O_3-CaO-MgO-SiO_2 system: multiple linear regression approach

It should be noted from Figure 116 that the regression parameters for CaO and MgO are positive and the values for SiO_2 and Al_2O_3 are negative in the temperature range of interest. This agrees with the known effects of CaO, MgO, Al_2O_3 and SiO_2 on the electrical conductivity in slags. The values of the parameters also suggest that CaO is a more effective conductor than MgO up to temperatures of 1650 °C. One can also infer that Al_2O_3 decreases the conductivity more so than SiO_2 on a molar basis up to temperatures of 1550 °C.

Ignoring the parameters at 1350 °C, the regression parameters appeared to behave approximately linearly with the reciprocal of the temperature. This was expected given that the temperature dependence of the conductivity is governed by the Arrhenius relationship. From the slopes and intercepts of the curves for each component from 1400-1550 °C, the values for a_1, a_2, c_1, c_2, m_1, m_2, s_1 and s_2 were calculated. The values are summarised in Table 42.

Table 42: Model parameters based on multiple linear regression for Al_2O_3-CaO-MgO-SiO_2 containing slags

		Al_2O_3	CaO	MgO	SiO_2
		a	c	m	s
ln A	1	31.6	-2.2	10.5	17.1
- E_a / R	2	-68049	9006	-15049	-40544
E_a	kJ/mol	565.8	-74.9	125.1	337.1

The regression statistics (F and P values) suggested that the correlation parameters found were statistically significant. (The F value indicates whether the overall regression has statistically significant predictive capability and the P values indicate whether the variables selected have statistically significant predictive capability). The residuals were normally distributed. The positive slope of the CaO data relative to temperature was unexpected and resulted in a negative activation energy (see also Figure 2 where the relationship between the activation energy and the mol% CaO in the CaO-SiO_2 binary is not linear). The significance of this is that the model should not be extrapolated to pure CaO melts or melts containing very high CaO contents.

To give an indication of the fit of the model to the data, comparisons of the experimental data vs the calculated conductivities at discrete temperatures are shown in Figure 117.

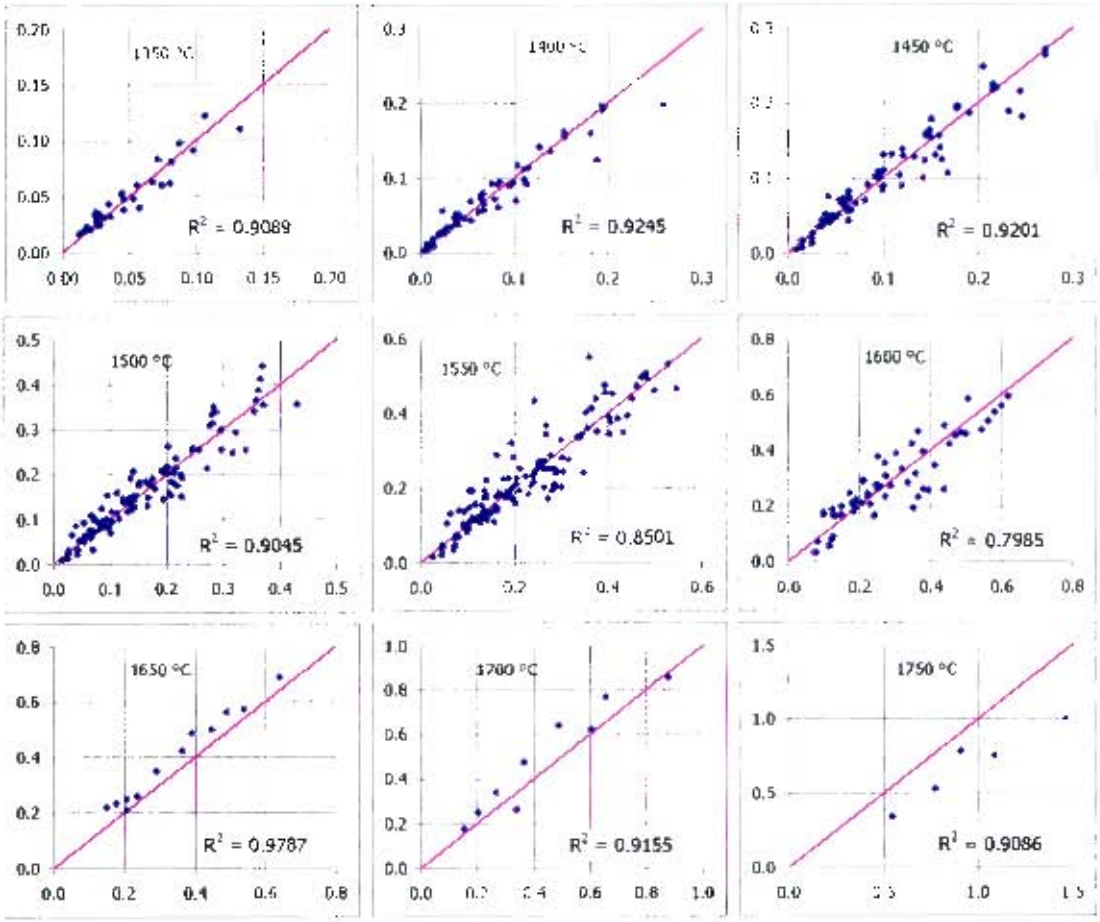

Figure 117: Comparisons of experimental vs calculated conductivities for the Al_2O_3-CaO-MgO-SiO_2 system from 1350 – 1750 °C. (Experimental values on y-axis and calculated values on x-axis, all values in $(\Omega.cm)^{-1}$, R^2 value for each temperature shown)

The conductivity values predicted by the model compared to the experimental values gave rise to a weighted (based on number of data points) correlation coefficient (R^2) value of 0.8358 for temperatures from 1350 to 1600 °C. It should be noted in Figure 117 that extrapolation of the model to the higher temperatures of 1650 to 1750 °C gave reasonable estimations of the conductivity (R^2 values of above 0.9), although especially in the case of the data at 1750 °C, the model is not accurate.

It is likely that the scatter in some of the trends could be reduced by identifying and omitting unreliable experimental data. However, in the model development all the data were considered and were equally weighted.

The temperature dependence of the model was still compensated. Values were calculated for ln A_λ and E_λ using Equation 29 for the slag compositions which resulted in the following compensation plot shown in Figure 118. The relationship was very similar to the one shown in Figure 94, however the calculated values for ln A_λ and E_λ were generally higher than those determined from the literature data.

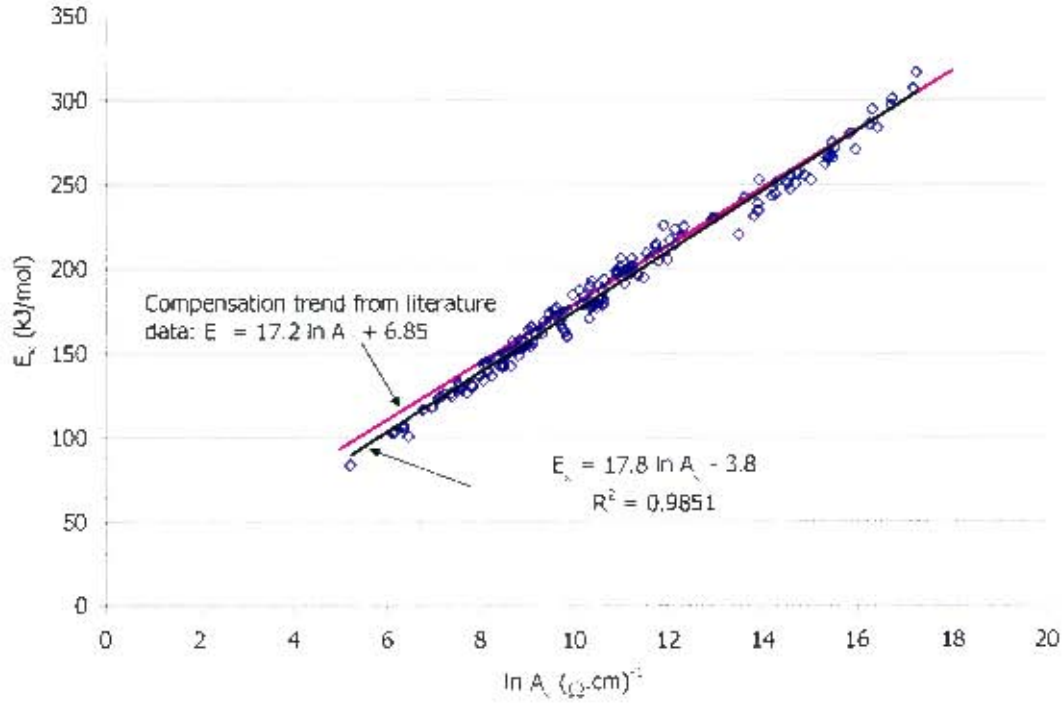

Figure 118: Compensation law plot based on model temperature dependence data for Al_2O_3-CaO-MgO-SiO_2 system. The compensation law relationship presented earlier for literature data is also shown.

As the compensation law was still found to be valid in modelling approach 2 (detailed above), the activation energy and pre-exponential factor were directly considered in the following approach (3).

6.1.3. Approach 3: Modelling of ln A_κ as a function of composition and calculation of activation energy for conduction from compensation law

The third approach was to relate the slag composition to the temperature dependence data such that either the activation energy or the natural logarithm of the pre-exponential factor could be found. From the compensation law given in Equation 26 and shown in Figure 94, given one of the factors, the other could be calculated. In this approach the temperature dependence of the conductivity is considered directly.

It was attempted to correlate ln A_κ to a function of the composition by means of a multiple linear regression as in approach 2 above, as well as by non-linear regression as in approach 1 above. In both cases unsatisfactory correlation was found between ln A_κ and the composition (correlation coefficients from around 0.2 to 0.4). Even though the temperature dependence data was compensated (which should smooth out some errors arising from excessively high or low pre-exponential factors), the degree of correlation to measured conductivities was poor.

Therefore the approach was abandoned. However, given that the temperature dependence of viscosity in silicate melts has been modelled in this way by Zhang and Jahanshahi (1998) and Urbain *et al.* (1981), it is possibly worthwhile isolating the cause for poor conductivity estimation by this method.

6.2. Iron oxide containing systems

The modelling of iron oxide containing systems is complicated by the number of variables (oxidation state, slag chemistry and temperature) and because mixed ionic and electronic conduction occurs. In order to simplify the modelling initially, the effect of temperature was disregarded by considering data at discrete temperatures.

Two approaches were considered for the modelling of the electrical conductivity of slags containing iron oxide. The first approach avoided direct consideration of the oxidation state dependence of the electrical conductivity, while the second approach directly considered the oxidation state dependence.

The numerical analysis technique used for discussion of the oxidation state dependence of the low, intermediate and high basicity slags (see Section 5.3.6) was also considered for modelling purposes. However, insufficient oxidation state dependent conductivity data were available to provide enough background information such that the model could be generalised to any iron-containing system. The benefit of this type of analysis is that one obtains a very good numerical description of the ionic and electronic components of the conductivity.

It should be noted in the sections below that very good correlation coefficients (R^2 values) are obtained for the iron-containing systems. The reasons for this are the very strong dependence of conductivity on iron content and the wide range of conductivity data available (from 0.1 to > 100 $(\Omega.cm)^{-1}$.

6.2.1. Approach 1: Oxidation state not considered, discrete temperatures

This approach considered only the data where measurements had been made at iron saturation or at relatively reduced conditions. Fortunately the majority of the electrical conductivity data was measured at these conditions. Also the current efficiency measurements had been made at these conditions.

Therefore in order to obtain estimates of the proportions of the conduction that were ionic and electronic, the current efficiency data were used. The current efficiency data shown in Figure 1 were fitted by means of exponential decay functions based on the iron oxide content and basicity of the slags. The fitted curves are shown in Figure 119. From these fitted curves, the current efficiency for any slag could be predicted based on the slag basicity and iron oxide content.

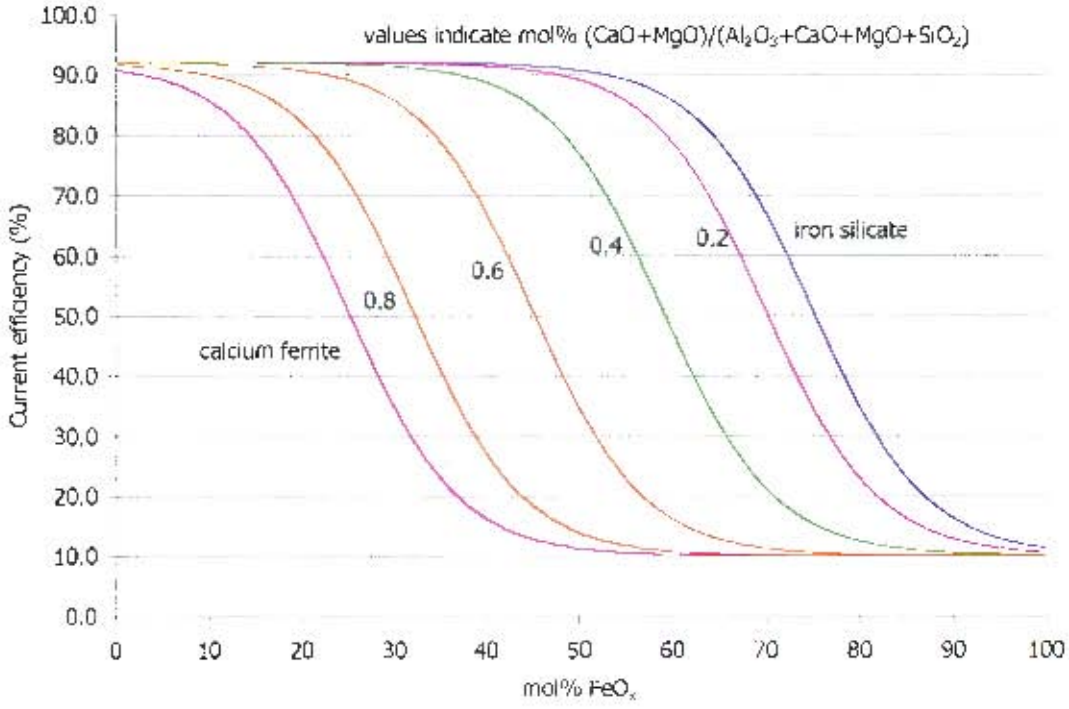

Figure 119: Fitted curves for current efficiency estimation based on slag chemistry and iron oxide content for slags at reduced conditions such as iron saturation. Based on the literature data presented in Figure 1.

The conductivity data were then modelled at discrete temperatures as a function of the composition and the amount of electronic and ionic conduction based on the current efficiency estimate. The following equation represents the model:

Equation 30: $\ln\kappa - (a_1)X_{Al_2O_3} + (c_1)X_{CaO} + (m_1)X_{MgO} + (s_1)X_{SiO_2} + (f_1)X_{FeO}\,\beta + (f_2)X_{FeO}\cdot(1-\beta)$

where β is the fraction of ionic conduction

$(1-\beta)$ is the fraction of electronic conduction based on the current efficiency

The model gave very good correlation of calculated and experimental data (R^2 values in excess of 0.97). However, the model was limited as it could not take into account the oxidation state of the slag and it was based on the assumption that the estimations of the

current efficiency were valid for a far wider range of compositions than actually measured. Therefore this approach was abandoned.

6.2.2. *Approach 2: Oxidation state directly considered, discrete temperatures*

In this approach the oxidation state of the slag was directly considered. This required information on the ferric and ferrous contents of the slags. In most cases in the literature, the quantities of ferric and ferrous ions were not reported, therefore it was necessary to estimate the ferric-ferrous values based on knowledge of the conditions under which the experiments were made and literature data concerning iron redox equilibria.

As mentioned above, the majority of the conductivity data for iron-oxide containing slags were measured at reduced conditions or in iron crucibles. Therefore the ferric and ferrous contents of the slags could be estimated based on the assumption that the slags were at iron saturation. For work carried out in molybdenum crucibles, the slags would also have been at relatively reduced conditions and it was assumed that ferric and ferrous values at iron saturation would provide a reasonable estimate. For measurements made in air, the oxygen partial pressure is obviously known. Therefore in the case of calcium ferrite slags in air, the correlation provided by Takeda *et al.* (1980) was used to calculate the ferric and ferrous contents. In the case of iron silicate slags, MPE (Zhang *et al.* (2002)) was used to obtain an estimate. In the cases of other basicity slags, the ferric and ferrous contents were estimated from the data given by Larson and Chipman (1953).

In order to give an example of how this data can be represented, the natural logarithm of the conductivity was plotted as a function of the ferric/ total iron fraction for iron silicate and calcium ferrite slags at a range of oxidation states in Figure 120.

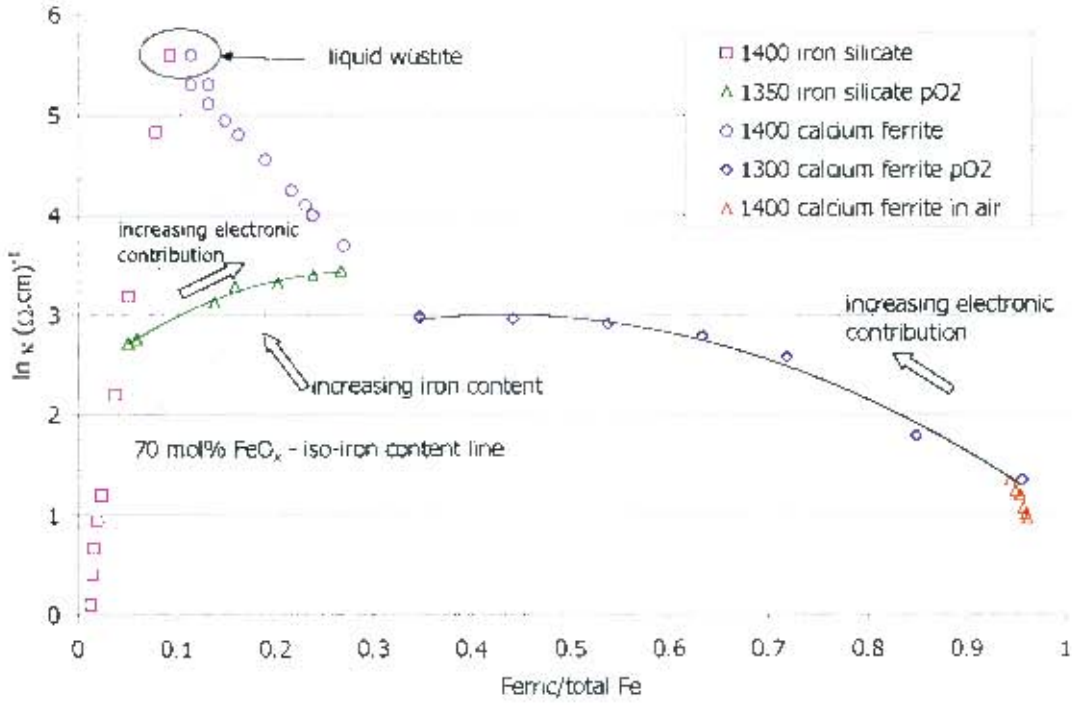

Figure 120: Conceptual representation of the oxidation state dependence of the electrical conductivity of iron silicate and calcium ferrite slags at a range of oxidation states and temperatures.

The following should be noted in Figure 120. The data connected by curved lines were measured at a range of oxidation states. The calcium ferrite and iron silicate data at reduced conditions were measured in iron crucibles. The calcium ferrite data at oxidised conditions were measured in air. The iso-iron content lines shown at reduced conditions are indicated to show the difference in conductivity between calcium ferrite and iron silicate slags containing the same amount of iron.

There are several important trends shown in Figure 120. Considering iron silicate slags first, the ferric content in the slag is very low. As the iron content is increased, one obtains greater amounts of ferric iron and the conductivity increases. If the oxidation state of a particular iron silicate slag is changed, one can expect the trend shown by the data in green triangles. The increase in the conductivity arises as a result of increasing ferric content and hence electronic conduction.

Now considering the calcium ferrite data at reduced conditions, the calcium ferrite slags contain considerably more ferric iron than iron silicate slags with the same amount of total iron. The greater amount of ferric iron and hence electronic conduction explains why the conductivity of the calcium ferrite slags is so much higher than the iron silicate slag conductivity. Where the oxidation state of a particular calcium ferrite slag was varied from reduced conditions to air, it is seen that the conductivity decreased with increasing ferric iron content. This is also due to electronic conduction where as the ferric iron increases and the ferrous iron decreases, the number of sites for electronic conduction decrease and the conductivity decreases.

There are parallels between the diagram in Figure 120 and the current efficiency data shown in Figure 1 for slags at iron saturation. When considered together the diagrams provide evidence that the electrical conductivity in iron oxide containing slags increases with increasing ferric fraction as a result of enhanced electronic conduction.

After conceptualising the data in this way, it was attempted to model the conductivity by means of the following expression:

Equation 31:

$$\ln \kappa = (a)X_{Al_2O_3} + (c)X_{CaO} + (m)X_{MgO} + (s)X_{SiO_2} + (f_1)X_{FeO}.Fe^{2+} + (f_2)X_{FeO}{}^2.Fe^{2+}.Fe^{3+} + (f_3).X_{FeO}.Fe^{3+}$$

Where Fe^{2+} and Fe^{3+} refer to the ferrous and ferric iron fractions respectively. The expression is very similar to the equation proposed by Engell and Vygen (1968) where:

$\kappa = \kappa_0 + ax - bx(1-x)$ and $x = Fe^{3+}/\text{total Fe}$

All the conductivity data for iron-oxide containing slags were considered in the modelling exercise including the oxidation state dependent data and the data measured in air. The data set considered for the modelling is summarised in Table 43.

Table 43: Summary of data set used for modelling of electrical conductivity in FeO_x containing slags

Temperature	Number of	Electrical conductivity (Ω.cm)$^{-1}$		Number of data at conditions:		
°C	data points	Minimum	Maximum	reduced	air	p_{O_2} dep
1300	157	0.04	98	115	22	20
1350	199	0.07	125	114	23	62
1400	114	0.02	269	64	27	23
1450	147	0.05	311	47	5	95
1500	81	0.05	324	52	6	23
1550	89	0.10	339	42	24	23
1600	106	0.07	352	33	7	66

A non-linear regression was performed using the Solver function of Microsoft Excel to obtain the best estimates for the parameters in the expression in Equation 31. The regressions were carried out at discrete temperatures so thereafter the parameters needed to be related to temperature.

The constraints specified in the model were that the slope of ln κ vs the function had a value of 1 and that the intercept had a value of 0. It was considered whether it was plausible to constrain the values for *a*, *c*, *m* and *s* to those values found in the model for the iron-free Al_2O_3-CaO-MgO-SiO_2 slags. However, it was reasoned that the regression parameter values for the iron-free slags were for silicate slags and attempting to apply them to slags such as calcium ferrites would be erroneous. Therefore the values for *a*, *c*, *m* and *s* were not constrained. The regression parameters calculated are shown as a function of the temperature in Figure 121. The averaged correlation coefficient found was 0.9779.

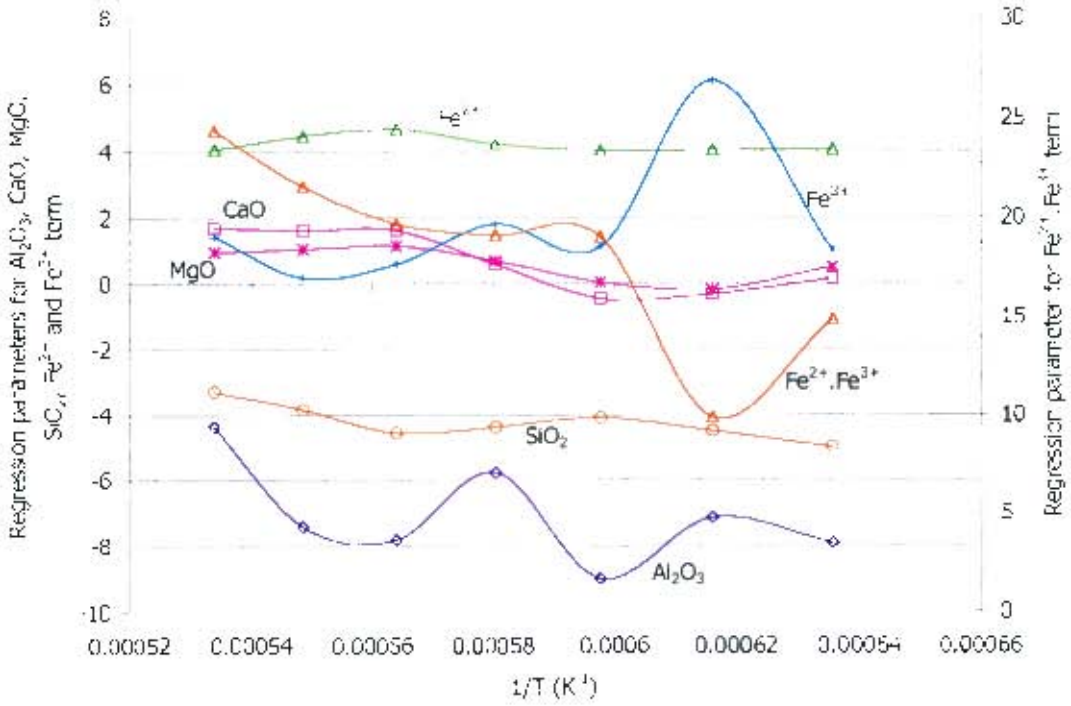

Figure 121: Regression parameters calculated for model of conductivity of iron-oxide containing slags

In Figure 121 the following trends are evident. The negative parameter values for Al_2O_3 and SiO_2 indicate their effect of decreasing the conductivity. The parameter values for CaO and MgO are mostly positive although some of the values are negative. A possible reason for the negative values is that in high iron containing slags, the addition of CaO or MgO decreases the conductivity as a result of a decrease in electronic conduction. The positive values for all the iron terms indicate their effect if increasing the conductivity.

It was expected that the regression parameters would be close to linear with respect to temperature, however this was not the case. The parameter values for the Al_2O_3, Fe^{3+} and $Fe^{2+}.Fe^{3+}$ terms were particularly non-linear. It was found that the alumina parameter had little impact on the overall correlation coefficients as a result of being present only in small quantities. The $Fe^{2+}.Fe^{3-}$ term was strongly dependent on the type of data available at each temperature. For example, the data at 1600°C were predominantly Engell and Vygen's oxidation state dependent data, therefore the $Fe^{2-}.Fe^{3+}$ term was biased around the magnitude of the authors' data. The Fe^{3+} and $Fe^{2+}.Fe^{3+}$ parameter values were far outside the expected range at 1350 °C (~0.00061 K^{-1}).

By constraining the Fe^{3+} parameter at 1350 °C to a value of around 2, the $Fe^{2+}.Fe^{3+}$ term was in better agreement with the rest of the $Fe^{2+}.Fe^{3+}$ values. The resultant overall parameters are shown in Figure 122. The average correlation coefficient decreased to 0.9777.

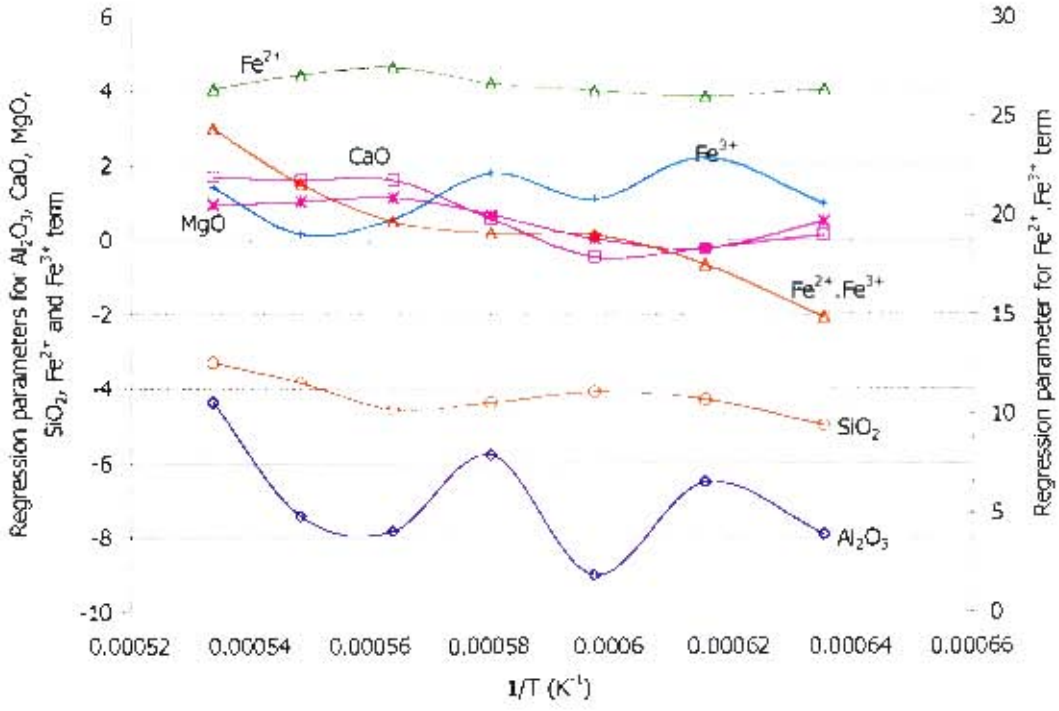

Figure 122: Adjusted regression parameters for model of conductivity of iron-oxide containing slags

In order to obtain a description of the temperature dependence of the parameters, the parameters were linearised with respect to temperature. Admittedly a least squares fit to some of the parameters (Al_2O_3, Fe^{2+} and Fe^{3+}) was not very good, however reasonable correlation coefficients were obtained when comparing experimental and calculated

conductivity values. The average correlation coefficient decreased to 0.9736. The following parameter values were therefore used:

Table 44: Temperature dependence of parameters for model of conductivity of iron-containing slags

Parameter	slope	intercept
a	-20263	4.8
c	-21634	13.3
f_1	3869	6.4
f_2	78130	64.9
f_3	7001	-2.9
m	-10400	6.6
s	-11487	2.5

where, for example, the value for *a* at temperature T (K) is given by *a = slope/T + intercept*. The values for the parameters and the slag composition are then substituted into Equation 31 and the conductivity can be calculated. To give an indication of the fit of the model to the data, comparisons of the experimental data vs the calculated conductivities at discrete temperatures are shown in Figure 123.

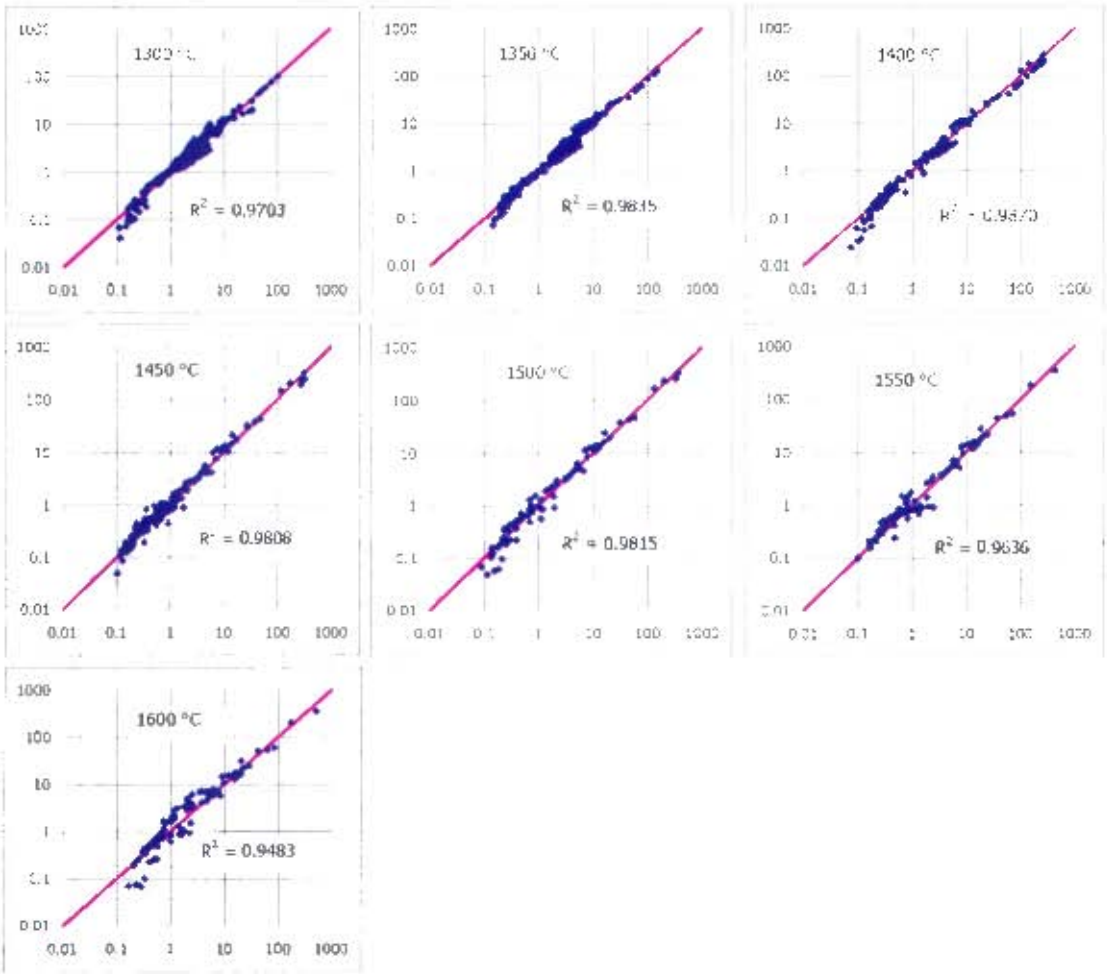

Figure 123: Fit of model to experimental data for iron-containing slags. (Experimental values on y-axis and calculated values on x-axis, all values in $(\Omega.cm)^{-1}$, R^2 value for each temperature shown)

In order to show how the model fits oxidation state dependent data, the model was used to predict conductivity values for the low, intermediate and high basicity slags and the calcium ferrite slag at a range of oxidation states. The model values are compared with the experimental values in Figure 124.

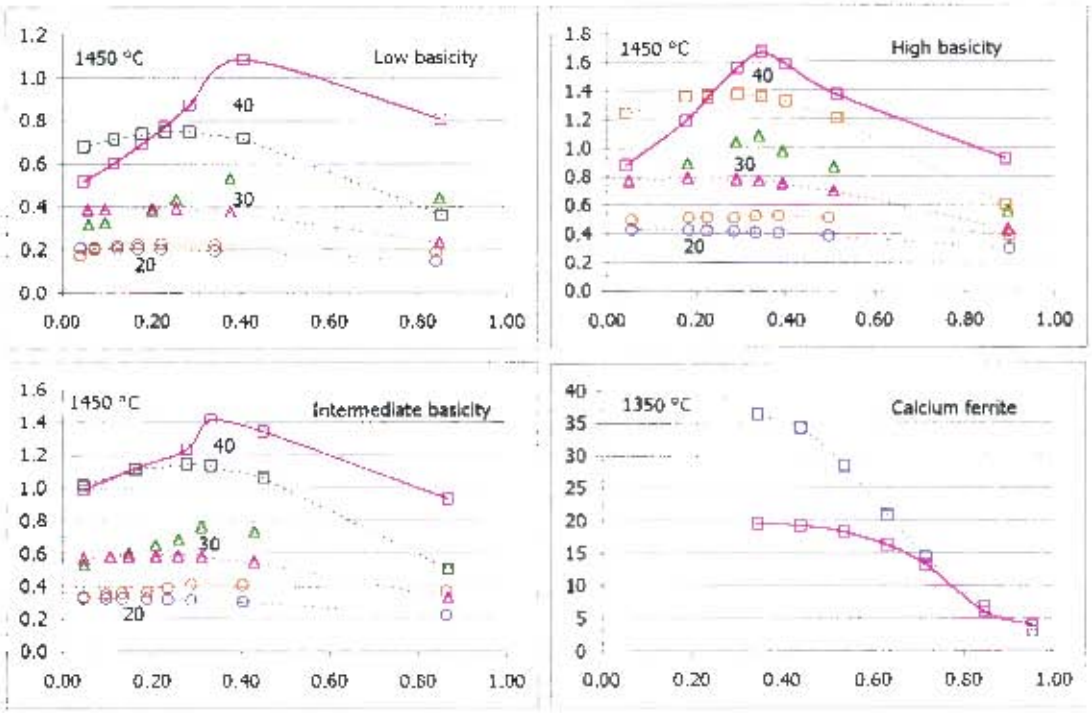

Figure 124: Comparison of model (dotted lines) and experimental (solids lines) conductivity values for the low, intermediate and high basicity slags and the calcium ferrite slag at a range of oxidation states. Iron levels and temperatures are indicated on the diagrams. Ferric/total iron fractions are indicated on the x-axes and electrical conductivity values in $(\Omega.cm)^{-1}$ are indicated on the y-axes. Symbols used at particular iron levels are the same for the model and experimental values.

From the graphs in Figure 124, it is seen that the model predicts the correct response to the oxidation state in terms of the conductivity being lower at very reduced and oxidised conditions and reaching a peak at intermediate ferric fractions. The model also correctly accounts for the increase in conductivity with increasing iron content. However, the magnitude of the conductivity at particular oxidation states is quite different when comparing model and experimental values. It is very evident in the case of the low, intermediate and high basicity slags that the model values at oxidised conditions are significantly lower than the measured values. The reason for this is that the amount of literature data available for the conductivity of iron-containing systems in air is limited, whereas there are many data at reduced conditions. Therefore the model is biased towards satisfying the conductivities at reduced conditions. The reason for the higher model conductivity values for the calcium ferrite slag at reduced conditions is because the literature data suggests higher conductivities at those conditions (see Section 4.5 and the data of Dancy and Derge (1966)).

Of some encouragement in Figure 121 and Figure 122 was that the parameter values for Al_2O_3, CaO, MgO and SiO_2 were in the same ranges as for the iron-free slag conductivity model. For example, in Figure 121 and in Figure 116, in both cases the parameter values for

silica were around –6 to –4. The relationship of the parameter values to temperature was slightly different. Nonetheless, it was felt that the conductivity data for the iron-free and iron-containing slags could be modelled together and provide a more general and hopefully more accurate model. The inclusion of the iron-free data would also hopefully improve the temperature dependence of the regression parameters. The details of this unified model are given in Section 6.3.

6.3. Unified model for conductivity of slags containing Al_2O_3, CaO, MgO, SiO_2 and FeO_x

The magnitude of the regression parameters for Al_2O_3, CaO, MgO and SiO_2 were similar in both the iron-free system and the iron-containing system. It was thus suggested that all the data be combined for the iron-free and iron-containing systems. It was hoped that the temperature dependence of the regression parameters would be also improved. The other benefit of a unified model is that its range of applicability is broader, however the accuracy of separate models is sacrificed.

The unified model was derived using the same multiple linear regression technique employed in the case of the iron-free and iron-containing slags. The equation used for the regression was the same as that given in Equation 31. The two data sets, summarised in Table 41 and Table 43, were combined and the regressions were carried out at discrete temperatures. The regression parameters obtained and their dependence on temperature is shown in Figure 125. The average correlation coefficient for all temperatures was 0.9774.

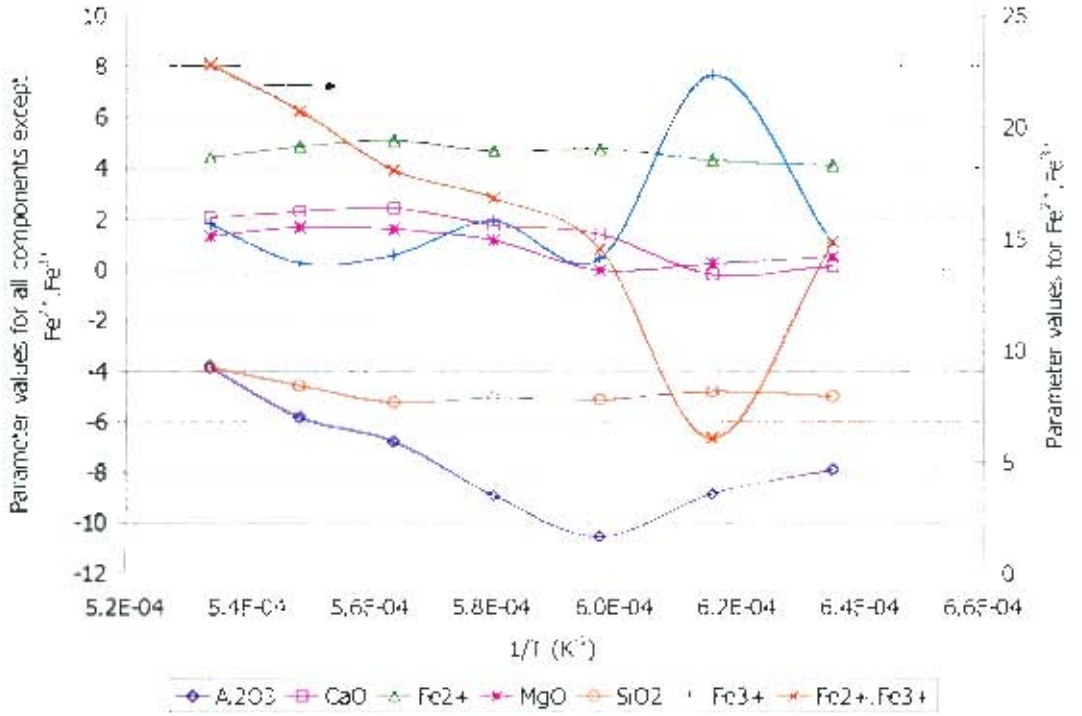

Figure 125: Parameter values for unified model for electrical conductivity of slags containing Al_2O_3, CaO, FeO_x, MgO and SiO_2.

If one compares Figure 125 with Figure 121, it appears that the temperature dependence of the parameters has improved with the exception of the values for the Fe^{3+} and $Fe^{2+}.Fe^{3+}$ terms at 1350 °C ($1/T \sim 6.1 \times 10^{-4} K^{-1}$). By manipulating the constraints for Fe^{3+} in the Solver function of Microsoft Excel, it was determined that the Fe^{3+} and $Fe^{2+}.Fe^{3+}$ values were inversely related. This meant that if the regression parameter at 1350 °C for Fe^{3+} was constrained at around 3, then the values for the both terms were in better agreement with the rest of the regression parameters. As a result of the inverse relationship between the two parameters, the change in the correlation coefficient at 1350 °C was minimal (R^2 changed from 0.9922 to 0.9912). The adjusted regression parameters are shown in Figure 126. The average correlation coefficient for all the temperatures was 0.9773.

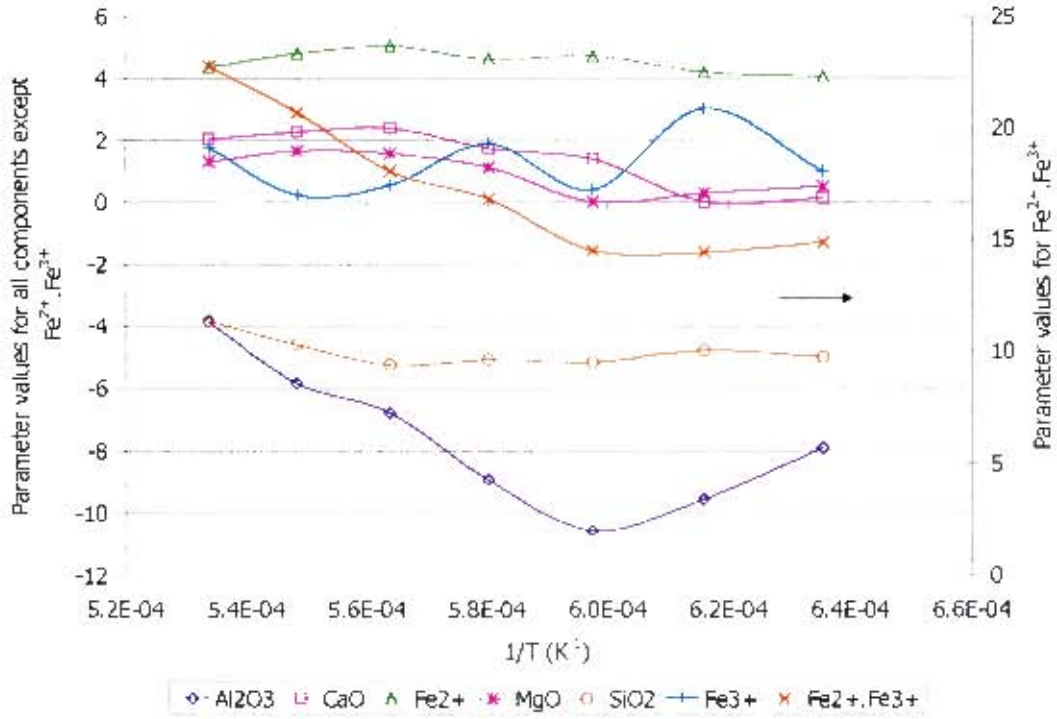

Figure 126: Adjusted regression parameters for the unified model for the electrical conductivity of slags containing Al_2O_3, CaO, FeO_x, MgO and SiO_2.

The adjusted regression parameters in Figure 126 appeared to be better functions of temperature. The parameters were linearised with respect to temperature in order to obtain a single equation for the model. The parameters and their temperature dependence are shown in Table 45. Through the linearisation of the parameters, the average correlation coefficient decreased to 0.9743.

Table 45: Temperature dependence of parameters for unified model for conductivity of Al_2O_3-CaO-FeO_x-MgO-SiO_2 containing slags

parameter	slope	intercept
a	-47348	19.9
c	-24087	15.4
f_1	-9140	10.0
f_2	-82447	65.4
f_3	6642	-2.6
m	-14151	9.2
s	-7478	-0.5

where, for example, the value for *a* at temperature T (K) is given by *a = slope/T + intercept*. The values for the parameters and the slag composition are then substituted into Equation 31 and the conductivity can be calculated. As has been done previously in the chapter, the fit of the model to the experimental data is shown in Figure 127.

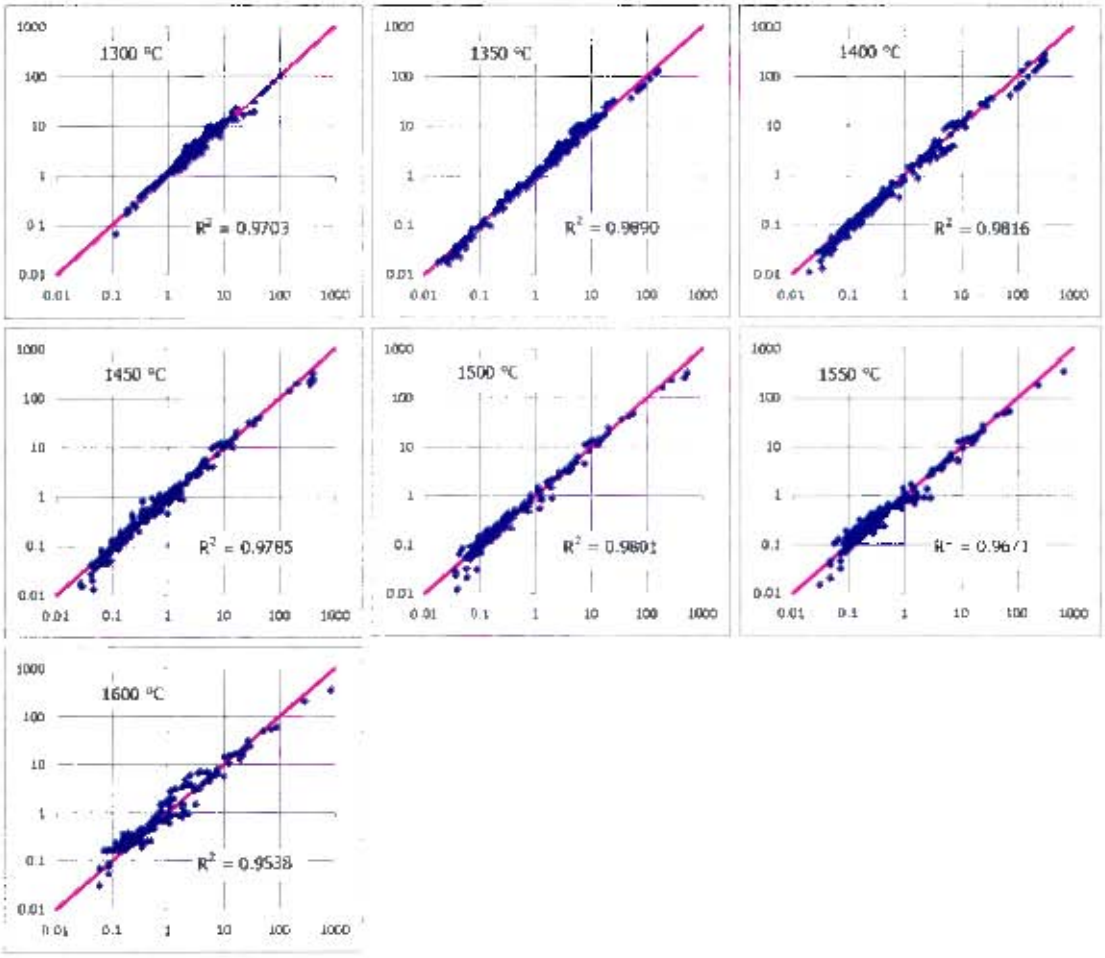

Figure 127: Fit of unified model to experimental data for Al_2O_3, CaO, FeO_x, MgO, SiO_2 containing slags. (Experimental values on y-axis and calculated values on x-axis, all values in $(\Omega.cm)^{-1}$, R^2 value for each temperature shown)

It is seen in Figure 127 that the fit of the model to the data is good (average R^2 value of 0.9743). As before the oxidation state dependence of the conductivity was of interest. The fit of the model to the measured data for the low, intermediate and high basicity slags was very similar to that shown in Figure 124 and will not be shown again. In order to show that the model was capable of

predicting oxidation state data reasonably well, the conceptual graph shown in Figure 120 was reproduced but using model predicted data instead of experimental data. The model-predicted conceptual graph is shown in Figure 128.

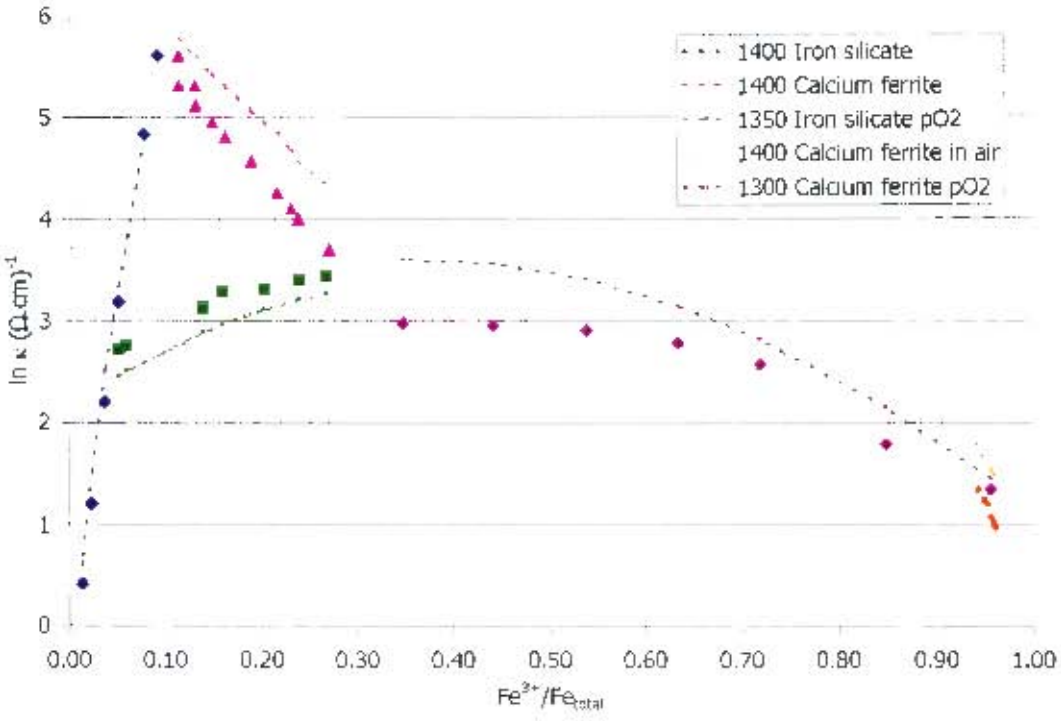

Figure 128: Model-generated conceptual graph showing oxidation state dependence of electrical conductivity of iron silicate and calcium ferrite slags. Compare with Figure 120. Experimental data is shown by dot points and model calculated trends are shown by dotted lines.

From Figure 128 it is seen that the magnitude of the conductivity for calcium ferrite slags is over estimated by the model. The model slightly under estimates the magnitude of the conductivity for iron silicate slags. However, it should be noted that the trends in Figure 128 are correctly predicted with respect to the response of the conductivity to changes in the oxidation state for the slags.

6.4. Comments on the temperature dependence of the conductivity in modelling of iron-containing slag systems

The effect of temperature on the conductivity of FeO_x containing systems was examined briefly in Section 5.2, where the relation between the activation energy and pre-exponential factor for iron-containing slags was shown in Figure 98. Given that modelling of the conductivity based on the activation energy or pre-exponential factor for the iron-free slags was not as straightforward as hoped (see Section 6.1.3), this approach in modelling of the conductivity in iron-containing systems was not fully attempted. However, the relationship between the activation energy, pre-exponential factor and iron content are shown in Figure 129. The activation energies and pre-exponential factors were either obtained directly from literature data (where reported), or calculated from literature data where conductivity values were reported for a range of temperatures.

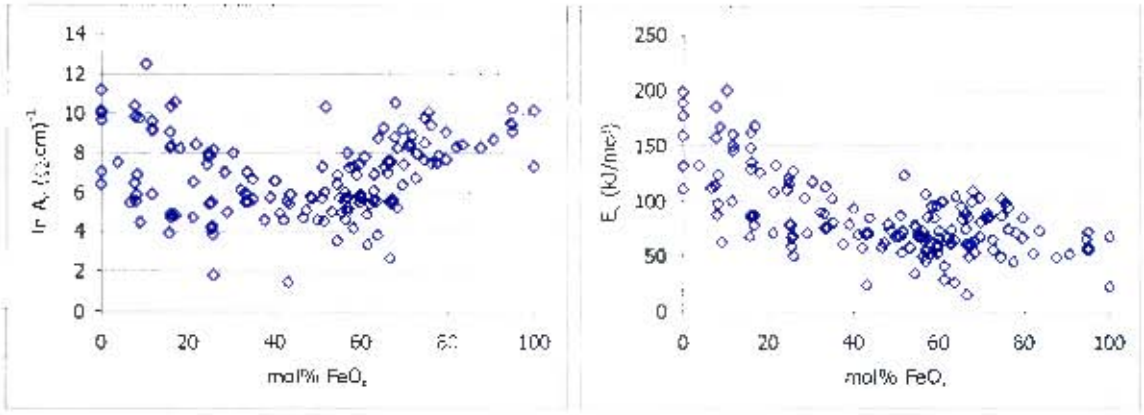

Figure 129: Dependence of the natural logarithm of the pre-exponential factor and activation energy on the total iron content in iron-containing slags.

It is seen in Figure 129 that the relation between the pre-exponential factor and the iron content appears to be parabolic in nature. The activation energy for conduction decreases with increasing iron content. Given the variation of activation energies for iron-containing systems of differing basicities (see Figure 100), this modelling approach was not expanded further for iron-containing slags, however it is likely that an approach of this nature could be of benefit.

6.5. Modelling of the effect of chromium

In the literature review (see Section 2.9), several mixing models were examined which have been used to calculate the conductivity of multiphase systems. To apply most of these mixing models, the volume fraction and conductivity of each phase are required. The difficulty in applying these mixing models to the chromium containing slag systems was that the volume fraction and conductivity of each phase were not easily calculable. Therefore an alternative approach was used.

The effect of chromium was quantified by determining the amount and composition of spinel phase that would form as a result of the chromium addition. As was mentioned in Section 5.4, for the low basicity slag studied in this investigation (composition (wt%): Al_2O_3: 5, CaO: 5, FeO_x: 20, MgO: 20, SiO_2: 50), the composition of the spinel phase was likely to be $Al_{0.7}Cr_{1.5}Fe_{0.3}Mg_{0.4}O_4$. Given this constraint, the quantity of spinel was estimated from MPE (Zhang *et al.* (2002)). Based on the quantity and the composition of spinel phase, the change in the liquid slag composition was calculated. Obviously, the precipitation of spinel phase would lead to a decrease in the Al_2O_3, FeO_x and MgO in the liquid slag. The resultant liquid slag composition was then substituted into the model developed in Section 6.3 to give an indication of the conductivity. The conductivities of the spinel phase and the Cr ions in the liquid slag were assumed to be negligible. The calculated conductivities of the chromium containing slags were plotted against the experimentally measured values in Figure 130.

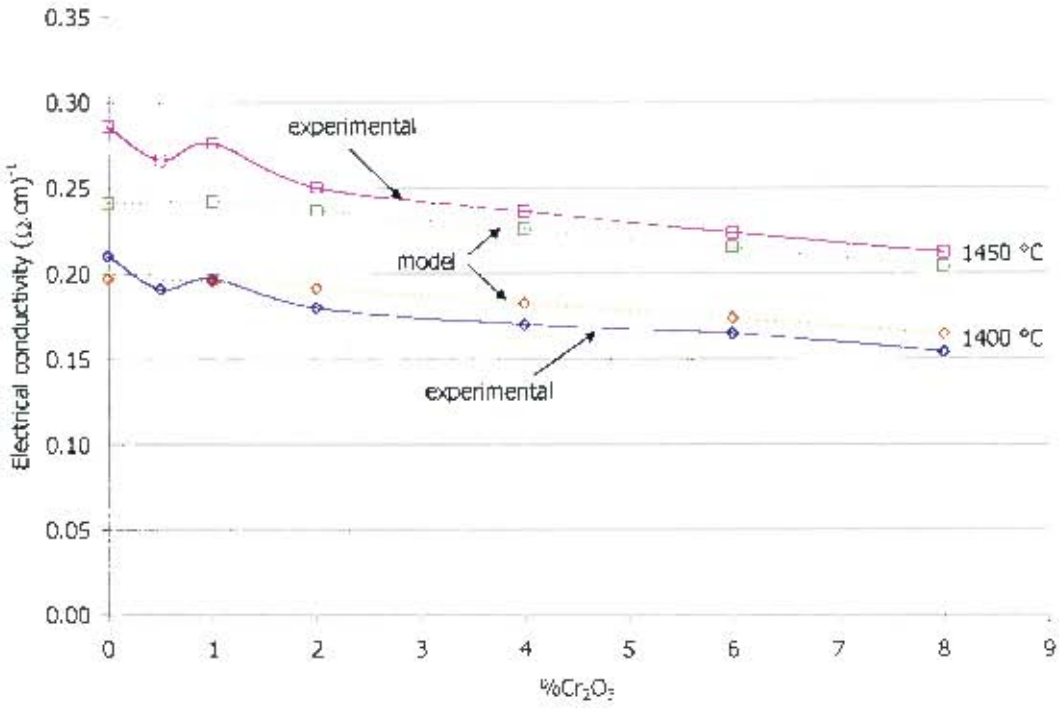

Figure 130: Comparison of experimental (solid lines) and calculated (dotted lines) conductivities for Cr_2O_3 containing slags at 1400 and 1450 °C.

It is seen in Figure 130 that the calculated conductivity values decreased with chromium addition in the same manner that the measured values did. This suggested that the approach in modelling the effect of chromium was acceptable. The magnitudes of the conductivity were slightly different, where at 1400 °C, the model values were higher than the measured values and the reverse was true for the conductivities at 1450 °C.

The shortcomings of this modelling approach are the assumptions that the Cr ions in the liquid slag do not contribute to the overall conductivity and that the spinel phase conductivity is negligible. In order to account for the Cr ion and spinel phase contributions to the conductivity, considerably more experimental work would be required.

6.6. Summary of the modelling of the electrical conductivity of slags

6.6.1. Al_2O_3-CaO-MgO-SiO_2 slags

Three approaches were considered in attempts to model the conductivity for the system. The first considered the conductivity as a function of the ratio of network modifiers to network formers. The second approach used multiple linear regressions of the natural logarithm of the conductivity as a function of the composition. The third approach made use of multiple linear regressions of the natural logarithm of the pre-exponential factor as a function of the composition and thereafter the compensation law was used to predict the activation energy.

The second approach provided the best description for the conductivities of the system at temperatures in the range 1350 – 1750 °C. The model is summarised in Equation 32:

Equation 32:

$$\ln\kappa = \left(31.6 - \frac{68048}{T}\right)X_{Al_2O_3} + \left(-2.2 + \frac{9006}{T}\right)X_{CaO} + \left(10.5 - \frac{15049}{T}\right)X_{MgO} + \left(17.1 - \frac{40544}{T}\right)X_{SiO_2}$$

where X_i is the mole fraction of component *i* and T is in K.

The literature conductivity data was relatively well described by the model with a weighted average correlation coefficient of 0.8358.

6.6.2. Iron-containing slags

Two approaches were considered for the modelling of the electrical conductivity of slags containing iron oxide. The first approach avoided direct consideration of the oxidation state dependence of the electrical conductivity, while the second directly considered the oxidation state dependence. The first approach was limited in that it only considered conductivity data for slags that were at reduced conditions. Therefore more effort was put into the second approach where the oxidation state of the slag was considered. A regression technique was used to calculate the model parameters.

The model developed is summarised in Equation 33:

Equation 33:

$$\ln\kappa = \left(4.8 - \frac{20263}{T}\right).X_{Al_2O_3} + \left(13.3 - \frac{21634}{T}\right).X_{CaO} + \left(6.6 - \frac{10400}{T}\right).X_{MgO} + \left(2.5 - \frac{11487}{T}\right).X_{SiO_2} + \left(6.4 - \frac{3869}{T}\right)X_{FeO}.Fe^{2+} + \left(64.9 - \frac{78130}{T}\right).X_{FeO}{}^2.Fe^{2+}.Fe^{3+} + \left(-2.9 + \frac{7001}{T}\right).X_{FeO}.Fe^{3+}$$

where X_i is the mole fraction of component *i*, T is in K and Fe^{2+} and Fe^{3+} are the ferrous and ferric fractions respectively.

Very good correlation (average correlation coefficient of 0.9736) was obtained between experimental and calculated values, however the temperature dependence of the regression parameters was not well described. It was noted that the magnitude of the parameters for Al_2O_3, CaO, MgO and SiO_2 were very similar in the iron-free and iron-containing slag systems. It was therefore decided to combine all the data for the iron-free and iron-containing slag systems in a unified model.

6.6.3. Unified model for iron-free and iron-containing systems

The benefits of a unified model were attractive in that one equation would be able to provide conductivity values for a slag containing two or more of the following components: Al_2O_3, CaO, MgO, SiO_2 and FeO_x. A regression technique was again employed and the model was described by the following equation:

Equation 34:

$$\ln\kappa = \left(19.9 - \frac{47348}{T}\right).X_{Al_2O_3} + \left(15.4 - \frac{24087}{T}\right).X_{CaO} + \left(9.2 - \frac{14151}{T}\right).X_{MgO} + \left(-0.5 - \frac{7478}{T}\right).X_{SiO_2} + \left(10.0 - \frac{9140}{T}\right)X_{FeO}.Fe^{2+} + \left(65.4 - \frac{82447}{T}\right).X_{FeO}{}^2.Fe^{2+}.Fe^{3+} + \left(-2.6 + \frac{6642}{T}\right).X_{FeO}.Fe^{3+}$$

where X_i is the mole fraction of component i, T is in K and Fe^{2+} and Fe^{3+} are the ferrous and ferric fractions respectively.

The correlation of experimental to calculated conductivity values was very good (average correlation coefficient of 0.9743). The description of the oxidation state dependence of the conductivity was good in that the trends observed experimentally could be reproduced by the model. However, in the case of some of the oxidation state data, the conductivity values at oxidised conditions were calculated to be lower than the experimental values. This was as a result of the scarcity of data for iron-containing systems at oxidised conditions.

6.6.4. Modelling of the conductivity of chromium containing slags

The conductivities of chromium containing slags were modelled by calculating the change in the liquid phase composition as a result of spinel phase formation with chromium addition. Assumptions were made that the spinel phase and the Cr ions in the liquid slag did not contribute to the conductivity. The conductivity of the liquid phase was then calculated using the model given in Equation 34. The trend of decreasing conductivity with increasing chromium content was reproduced by modelling in this way. Further experimental work will need to be carried out in order to determine the contributions of the spinel phase and the Cr ions in the liquid slag.

6.6.5. General comments

The modelling of the conductivity of slags has been relatively empirical in nature. The motivation for modelling in this manner was that relatively good descriptions for the conductivities of a wide range of slag systems could be obtained. If more fundamental modelling was to have taken place, it was likely that examination of more specific slag systems would have been required (including additional experimental work) and the application of a fundamental model would therefore have been more limited. It is hoped that, through consideration of some of the fundamental aspects in addition to the empirical modelling, greater understanding of the electrical conductivity of slags has been achieved.

Chapter 7

CONCLUSIONS

The work carried out in this investigation arose from the need for a better understanding of the factors affecting the electrical conductivity of melter type slags. The key research areas were identified in Section 2.10 and the findings made with respect to these research areas are discussed below. Finally, the origins of this research project are discussed in light of the information obtained through this investigation

7.1. Effect of iron oxide on slag conductivity

Initially iron-free slag systems were examined to gain a good appreciation of the effects of temperature and basicity on the electrical conductivity of slags. Briefly, the higher the temperature and basicity, the higher the conductivity of the slag. In iron-free slags, the activation energy for conduction and the natural logarithm of the pre-exponential factor were found to be related by a compensation law.

The addition of iron oxide increased the electrical conductivity of a slag. At low iron concentrations in the slag, the increase in the conductivity is likely to arise from the increased depolymerisation of the slag, the increased number of conducting cations and enhanced cation mobilities. At higher iron concentrations (greater than around 15 mol% FeO_x), it is likely that electronic conduction occurs in addition to the increased ionic conduction. The electronic conduction arises from the exchange of electrons / holes between ferric and ferrous ions. There were several indications that electronic conduction was taking place. The most obvious was that the slag conductivity varied with oxidation state. A more indirect and unproven indication was that the temperature dependence data (activation energy and pre-exponential factor) shifted away from the compensation law found for iron-free slags. It was proposed that the deviation from the compensation law indicated a change in conduction mechanism. The activation energy for conduction decreased with addition of iron oxide.

The variation of slag conductivity with oxidation state gave a good indication of the contributions of the ionic and electronic mechanisms. It was observed that the slag chemistry played an important part in determining both the ionic and electronic contributions, where the higher the slag basicity, the greater the ionic and electronic contributions. It was hypothesised that the iron content was the most important factor determining the slag conductivity, however for a given iron content, the slag chemistry played an important role in determining the overall conductivity.

The quantitative prediction of conductivity is dealt with below.

7.2. Effect of oxidation state

As mentioned above, conductivity in slags containing approximately 15mol% FeO_x or more is due to both electronic and ionic conduction. Where electronic conduction takes place, the electrical conductivity of the iron-containing slag is dependent on the oxidation state of the slag. A typical response of the conductivity to a change in oxidation state is the following: starting at reduced conditions, the conductivity will increase with oxidation state, reach a peak at around Fe^{3+}/Fe_{total} = 0.3 to 0.5 and then decrease at more oxidised conditions. The electronic conduction mechanism is dependent on the amount of ferric and ferrous ions and the total iron content. The electronic contribution increases with increasing iron content. At reduced conditions, the majority of the iron is present as ferrous ions which are considered to be network modifiers. As the slag is oxidised, ferrous ions form ferric ions and electronic conduction increases as there are more sites available for electron / hole transfer. At oxidised conditions, the majority of the iron is present as ferric ions. The co-ordination of ferric ions appears to be important in determining the effect on the conductivity. Where ferric ions are tetrahedrally co-ordinated it is likely that they will polymerise the slag and reduce the conductivity. Where ferric ions are octahedrally co-ordinated, it is likely that the ions are network modifiers and will generally increase the conductivity. It is also likely that electronic conduction can only occur between ferric and ferrous ions in octahedral positions, in which case knowledge of the iron cation distribution would help in understanding the conduction mechanisms.

Therefore, the likely manner in which the slag basicity affects the oxidation state dependence of the electrical conductivity is that it determines the distribution and co-ordination of ferric and ferrous ions and in this way affects the electronic conduction mechanism.

In terms of quantifying the slag conductivity of iron-containing slags, an empirical model was developed based on the slag composition, temperature and oxidation state.

7.3. Effect of chromium

The addition of chromium to a slag containing Al_2O_3-CaO-FeO_x-MgO-SiO_2 is likely to bring about a decrease in the electrical conductivity of the slag. It is likely that the decrease is caused by the precipitation of a spinel phase containing Al, Fe and Mg ions. The locking up of conducting Fe and Mg cations in the spinel phase is considered to cause the decrease in the conductivity. In the case of the slags studied in this investigation (wt% Al_2O_3: 5, CaO: 5, FeO_x: 20, MgO: 20, SiO_2: 50 with additions of 0.5, 1, 2, 4, 6 and 8% chromium), the likely composition of spinel phase was $Al_{0.2}Cr_{1.5}Fe_{0.5}Mg_{0.8}O_4$. Therefore as spinels formed, Mg and Fe cations would become unavailable for conduction in the liquid phase. It was also of interest to determine the effect of chromium where slags were above their liquidus temperatures. Therefore experiments were carried out in molybdenum crucibles up to temperatures of 1700 °C. It was suspected that the conductivity would increase as a result of Cr cations being conductive. However, it was not possible to conclusively determine the effect of chromium from the current work due to complications of molybdenum dissolution and the possible formation of Mo-containing chromite spinels at high temperatures (up to 1700 °C and theoretically above the Mo-free slags' liquidus temperatures).

7.4. Modelling

7.4.1. Al_2O_3-CaO-MgO-SiO_2 slags

Multiple linear regressions were used to correlate the natural logarithm of the conductivity as a function of the composition for Al_2O_3-CaO-MgO-SiO_2 slags. This approach provided a reasonable description of the conductivities of the system at temperatures in the range 1350 – 1750 °C. The model is summarised in Equation 32:

Equation 32:

$$\ln\kappa = \left(31.6 - \frac{68048}{T}\right)X_{Al_2O_3} + \left(-2.2 + \frac{9006}{T}\right)X_{CaO} + \left(10.5 - \frac{15049}{T}\right)X_{MgO} + \left(17.1 - \frac{40544}{T}\right)X_{SiO_2}$$

where X_i is the mole fraction of component *i* and T is in K.

The literature conductivity data was relatively well described by the model with a weighted average correlation coefficient of 0.8358.

Poor correlations were achieved when attempting to use the compensation law to develop a model for the conductivity (correlation coefficients in the range 0.2 to 0.4).

7.4.2. Iron-containing slags

Two approaches were considered for the modelling of the electrical conductivity of slags containing iron oxide. The first approach avoided direct consideration of the oxidation state dependence of the electrical conductivity, while the second directly considered the oxidation state dependence. The first approach was limited in that it only considered conductivity data for slags that were at reduced conditions. Therefore more effort was put into the second approach where the oxidation state of the slag was considered. A regression technique was used to calculate the model parameters.

The model developed is summarised in Equation 33:

Equation 33:

$$\ln\kappa = \left(4.8 - \frac{20263}{T}\right).X_{Al_2O_3} + \left(13.3 - \frac{21634}{T}\right).X_{CaO} + \left(6.6 - \frac{10400}{T}\right).X_{MgO} + \left(2.5 - \frac{11487}{T}\right).X_{SiO_2} + \left(6.4 - \frac{3869}{T}\right)X_{FeO}.Fe^{2+} + \left(64.9 - \frac{78130}{T}\right).X_{FeO}{}^2.Fe^{2+}.Fe^{3+} + (-2.9 + \frac{7001}{T}).X_{FeO}.Fe^{3+}$$

where X_i is the mole fraction of component *i*, T is in K and Fe^{2+} and Fe^{3+} are the ferrous and ferric fractions respectively.

Very good correlation (average correlation coefficient of 0.9736) was obtained between experimental and calculated values, however the temperature dependence of the regression parameters was not well described. The model provided the correct trends of the response of the slag conductivity to changes in oxidation state. It was noted that the magnitude of the parameters for Al_2O_3, CaO, MgO and SiO_2 were very similar in the iron-free and iron-containing slag systems. It was therefore decided to combine all the data for the iron-free and iron-containing slag systems in a unified model.

7.4.3. Unified model for iron-free and iron-containing systems

The benefits of a unified model were attractive in that one equation could provide conductivity values for a slag containing two or more of the following components: Al_2O_3, CaO, MgO, SiO_2 and FeO_x. A regression technique was again employed and the model was described by the following equation:

Equation 34:

$$\ln\kappa = \left(19.9 - \frac{47348}{T}\right).X_{Al_2O_3} + \left(15.4 - \frac{24087}{T}\right).X_{CaO} + \left(9.2 - \frac{14151}{T}\right).X_{MgO} + \left(-0.5 - \frac{7478}{T}\right).X_{SiO_2} + \left(10.0 - \frac{9140}{T}\right)X_{FeO}.Fe^{2+} + \left(65.4 - \frac{82447}{T}\right).X_{FeO}{}^2.Fe^{2+}.Fe^{3+} + (-2.6 + \frac{6642}{T}).X_{FeO}.Fe^{3+}$$

where X_i is the mole fraction of component i, T is in K and Fe^{2+} and Fe^{3+} are the ferrous and ferric fractions respectively.

The correlation of experimental to calculated conductivity values was very good (average correlation coefficient of 0.9743). The description of the oxidation state dependence of the conductivity was good in that the trends observed experimentally could be reproduced by the model. However, in the case of some of the oxidation state data, the conductivity values at oxidised conditions were calculated to be lower than the experimental values. This was as a result of the scarcity of data for iron-containing systems at oxidised conditions.

7.4.4. Modelling of the conductivity of chromium containing slags

The conductivities of chromium containing slags were modelled by calculating the change in the liquid phase composition as a result of spinel phase formation with chromium addition. Assumptions were made that the spinel phase and the Cr ions in the liquid slag did not contribute to the conductivity. The conductivity of the liquid phase was then calculated using the model given in Equation 34. The trend of decreasing conductivity with increasing chromium content was reproduced by modelling in this way. Further experimental work will need to be carried out in order to determine the contributions of the spinel phase and the Cr ions in the liquid slag.

7.4.5. General comments

The modelling of the conductivity of slags has been relatively empirical in nature. The motivation for modelling in this manner was that relatively good descriptions for the conductivities of a wide range of slag systems could be obtained. If more fundamental modelling was to have taken place, it was likely that examination of more specific slag systems would have been required (including additional experimental work) and the application of a fundamental model would therefore have been more limited. It is hoped that, through consideration of some of the fundamental aspects in addition to the empirical modelling, greater understanding of the electrical conductivity of slags has been achieved.

7.5. Relevance of research conducted

In the Introduction (Chapter 1), the background of the project was explained. The background was largely based on the problems being experienced in the six-in-line- electric furnaces of the

platinum producers in South Africa. It was considered worthwhile exploring the problems mentioned in light of the greater understanding obtained of the electrical conductivity of melter type slags.

The major problem mentioned was the increased slag conductivity which resulted in shallower immersion depths of the electrodes. The shallower immersion depths resulted in reduced smelting rates, increased furnace roof temperatures, tapping problems and increased bottom build-ups. From the research carried out, it appears unlikely that the increased levels of chromium in the furnace slag at that time contributed to an increase in the slag conductivity. What becomes apparent from the investigation is that the return of iron-rich converter slag to the furnaces was the largest contributor to the increased slag conductivity. When return of the converter slag to the furnaces was discontinued, many of the problems in operating the furnace were resolved. However, converter slag has traditionally been returned to the six-in-line furnaces without problems, which leads to the question of why the increase in the chromium content of the furnace slag over time exacerbated the problem of increased slag conductivity.

It is surmised that the oxidised iron in the converter slag return and the higher levels of chromium promote the formation of high melting point magnetite and chromium based spinels in the furnaces. The presence of these spinels in the furnaces has been observed to bring about the following problems: formation of a highly viscous intermediate layer between matte and slag and increased bottom build-up as the spinels deposit on the hearth. Relating this back to the question of increased conductivity, the intermediate layer is highly viscous and settling of matte droplets through the layer is slow. It is a possibility that the intermediate layer is highly conductive as a result of the entrained matte and depending of the thickness of the layer, a shorter current path may be available to the current. The other consideration is that the hearth build-up reduces the height (and volume) available in the furnace so the levels of slag in the furnace are likely to be reduced. With a lower slag level, the electrodes are effectively closer to the matte (and intermediate layer) and conductivity is likely to increase. The final consideration is that the furnace operators are forced to run at higher temperatures in order to try to melt intermediate layers, get heat down to the matte and melt hearth build-ups and as shown in this investigation, increased temperatures leads to increased slag conductivity.

If one now considers the effect of increased UG2 concentrate addition to the furnaces on the slag conductivity, without the return of iron-rich converter slag, then it is expected that the slag conductivity will decrease (relative to slags arising from Merensky concentrates). The reason for this is that the iron content in UG2 concentrates is lower then Merensky concentrates and the higher levels of chromium in UG2 concentrates will promote formation of spinels and also decrease the conductivity. As stated above, the high melting point spinels will still promote formation of hearth build-ups and intermediate layers and again furnace operators are forced to run at higher slag temperatures in order to attempt to deal with the problems. The increased slag temperatures result in increased conductivity and shallower immersion depths.

Addressing the problem of increased chromium in the furnaces purely on the basis of manipulation of the conductivity is not feasible as the other physicochemical properties of the slag need to be considered. This type of investigation forms part of the larger AMIRA P479A project, but it is hoped that the findings of the investigation on conductivity will be useful.

Chapter 8

RECOMMENDATIONS

Several recommendations arose through the review of the work carried out in the investigation. In many cases, the time and financial constraints did not allow for the additional work to be carried out, but the following are considered to be worthwhile objectives for future work:

- Conduct measurements of the conductivity of iron-containing slags in air to obtain consistent data and thereby improve the model for iron-containing slags. The amount and quality of data at reduced conditions is good, however the same cannot be said for data at oxidised conditions. The advantage of having data at both reduced and oxidised conditions will be that the end points for oxidation state dependent modelling will be well defined. It follows from this that the description of the electrical conductivity at intermediate oxidation states is easier.
- Carry out work to determine the iron cation distributions in iron-containing slags at a range of oxidation states. The difficulty experienced in this investigation with respect to application of fundamental conduction models was that there was not enough information on the slag structure. By means of Mössbauer spectroscopy it should be possible to obtain iron cation distributions in quenched slag samples. This knowledge would give a very good indication of the likely conduction mechanisms taking place and facilitate fundamental modelling.
- It would probably have been advisable to carry out the oxidation state work in an inert crucible. Obviously the equilibration times would be considerably longer than with the technique used in this investigation. However, the advantages of an inert conductivity cell would allow for temperature dependence data to be obtained at each oxidation state and provide further insight into the conduction mechanisms.
- There are obvious difficulties in carrying out high temperature work above 1600 °C, such as the problems experienced in the investigation of the effect of chromium. However, it would be advantageous if one could find suitable inert materials to perform experiments on chromium containing slags at very high temperatures (around 1700 °C). Then one should be able to isolate the effect of chromium (without having to consider the effect of molybdenum as well).
- Application of the knowledge gained in this investigation to obtain a greater understanding of the control and operation of industrial furnaces.
- Carry out more fundamental modelling such as description of slag structure in terms of the three types of oxygen. This in conjunction with information of the distribution and co-ordination of the iron ions would provide a very good basis for a more fundamental approach to the modelling of conductivity.

Chapter 9

REFERENCES

Adachi A. and Ogino K., Electrical conductivity of oxidised slags, Technology Reports of the Osaka University, vol. 7, no. 244, pp 121-126, 1957.

Attwood S.S., Electric and Magnetic Fields, 3rd edition, John Wiley and Sons Inc., New York, 1949.

Banisi S., Finch J.A. and Laplante A.R., Electrical conductivity of dispersions: a review, Minerals Engineering, volume 6, number 4, pp 369-385, 1993.

Berryman R.A. and Sommerville I.D., Anionic modification of electrical conductivity in liquid silicates, Proceedings of the 3rd International Symposium on Metallurgical Slags and Fluxes held in Glasgow, pp 202-206, June 1988.

Bobok L., Bodnár L. and Schmiedl J., Merná elektická vodivost' troskovych sústav Fe-O-SiO_2-X, Hutnicke listy, vol. 37, pp. 419-424, 1982.

Bockris J. O'M., Kitchener J.A., Ignatowicz S. and Tomlinson J.W., The electrical conductivity of silicate melts: systems containing Ca, Mn and Al, Discussions of the Faraday Society, no. 4, pp. 265-281, 1948.

Bockris J. O'M., KitchenerJ.A., Ignatowicz S. and Tomlinson J.W., Electrical conductance in liquid silicates, Transactions of the Faraday Society, vol 48, pp 75 – 91, 1952

Britten S.C. and Pal U.B., Solid-state amperometric sensor for the in-situ monitoring of slag composition and transport properties, Metallurgical and Materials Transactions B, volume 31B, pp 733-753, August 2000.

Chakraborty S., Chapter 10: Diffusion in silicate melts, Reviews in Mineralogy: Volume 32, Structure, dynamics and properties of silicate melts, JF Stebbins, PF McMillan, DB Dingwell editors, The Mineralogy Society, 1995.

Constable S. and Roberts J.J., Simultaneous modeling of thermopower and electrical conduction in olivine, Physics and Chemistry of Minerals, vol. 24, pp. 319-325, 1997.

Dancy E.A. and Derge G.J., The electrical conductivity of FeO_x – CaO slags, Transactions of the Metallurgical Society of AIME, vol 236, pp 1642 – 1648, 1966.

Desrosiers R., Ajersch F. and Grau A., Electrical conductivity of industrial slags of high titania content, International Symposium on Metallurgical Slags, Halifax, Nova Scotia, 26-27 August 1980, CIMM, pp 29, 1980.

Dickson W.R. and Dismukes E.B., The electrolysis of FeO-CaO-SiO_2 melts, Transactions of the Metallurgical Society of AIME, vol. 224, pp 505-511, June 1962.

Dietzel, Z. Elektrochem., vol. 48, no. 9, 1942.

Dobos D., Electrochemical data: a handbook for electrochemists in industry and universities, Elsevier, New York, 1975.

Dosdale T. and Brook R.J., Comparison of diffusion data and of activation energies, Journal of the American Ceramic Society, vol. 66, no. 6, pp 392-395, 1983.

Downing J.H. and Urban L., Electrical conduction in submerged arc furnaces, Journal of Metals, pp 337-344, 1966.

Ducret A.C., Khetpal D., and Sadoway D.R., Electrical Conductivity and Transference Number Measurements of FeO - CaO - MgO - SiO2 Melts, Molten Salts, Proceedings of the Thirteenth International Symposium, P.C. Trulove, H.C. De Long, and R.A. Mantz, eds., The Electrochemical Society, Pennington NJ, pp. xxx-xxx. 2002

Dukelow D.A. and Derge G., Electrochemical characteristics of FeO-MnO-SiO_2 melts, Transactions of the Metallurgical Society of AIME, vol 218, pp 136-141, February 1960.

Elliot S.R., The chemistry and physics of solids, John Wiley and Sons, Chichester, pp. 513-518, 1998.

Engell H.J. and Vygen P., Ionen- und elektronenleitung in CaO-FeO-Fe_2O_3-SiO_2 schmelzen, Berichte der Bunsengesell fur Physikalische Chemie, volume 72, no. 1, pp 5-12, 1968.

Eric R.H., Hejja A.A. and Stange W., Liquidus temperatures and electrical conductivities of synthetic ferromanganese slags, Minerals Engineering Vol. 4, no 12, pp 1315-1332, 1991.

Fay H., The electrical conductivity of liquid Al_2O_3, Journal of Physical Chemistry, vol. 70, pp. 890-893, 1966.

Fontana A., Segers L. and Winand R., Electrochemical behaviour of a platinum electrode in SiO_2-CaO-MnO molten slags, Electrochimica Acta, volume 30, no. 6, pp. 827-833, 1985.

Fontana A., Segers L., Twite K. and Winand R., Electrical conductivity of ferrous silicate melts from slag cleaning operations, TMS-AIME Paper Selection, Paper no A84-38, 1984.

Fortner J., Karpov V.G. and Saboungi M.-L., Meyer-Neldel Rule for liquid semiconductors, Applied Physical Letters, volume 66, number 8, pp 997-999, Feb 20 1995.

Gartstein E. and Mason T.O., Reanalysis of wüstite electrical properties, Journal of the American Ceramic Society, vol. 65, pp C24 – C26, February 1982.

Geiger G.H. and Wagner Jr., J.B., Studies of electrical conductivity of hematite containing titanium or calcium and reduction of the doped hematite to magnetite in CO/CO_2 mixtures, Transactions of the Metallurgical Society of AIME, volume 233, pp 2092-2100, December 1965.

Gleitzer C., Electrical properties of anhydrous iron oxides, Key Engineering Materials, Volumes 125-126, pp 355-418, 1997.

Glover P.W.J., Hole M.J. and Pous J., A modified Archie's law for two conducting phases, Earth and Planetary Science Letters, volume 180, issues 3-4, pp 369-383, August 15 2000.

Goel R.P., Kellogg H.H. and Larrain J., Mathematical description of the thermodynamic properties of the systems FeO and Fe-O-SiO_2, Metallurgical Transactions B, vol. 11B, pp 107-117, March 1980.

Goto K.S., A review of the electrolytic properties of metallurgical slags, Proceedings of the 2nd International Symposium on Metallurgical Slags and Fluxes held in Lake Tahoe, pp 839-862, Nov 1984.

Goto K.S., Sasabe M. and Kawakami M., Relation between tracer diffusivity and electrical conductivity on multi-component oxide slags at 900 °C to 1600 °C, Transactions of the ISIJ, vol. 17, pp 213-214, 1977.

Gudenau H.W. and Petry J., Ein Versuchsaufbau zur Messung von Viskosität und elektrischer Leitfähigkeit flüssiger Schlacken im sauren Bereich des Vierstoffsystems Fe_2O_3-FeO-SiO_2-CaO, Fachberichte Hüttenpraxis Metallweiterverarbeitung, vol. 19, pp. 32-36, 1981.

Hagel W.C. and Seybolt A.U., Cation diffusion in Cr_2O_3, Journal of the Electrochemical Society, volume 108, no. 12, pp 1146-1152, December 1961.

Harris P.S., Compensation effect and experimental error, Nature, vol. 243, pp. 401-402, June 15, 1973.

Hejja A.A., Eric R.H. and Howat D.D., Electrical conductivity, viscosity and liquidus temperature of slags in electric smelting of copper-nickel concentrates, EPD Congress 1994, edited by G. Warren, TMS, pp 621- 640, 1994.

Hino M., Hirayama Y., Nitta T. and Ban-ya S., AC Impedance analysis of the kinetics of reactions between molten Cu or Fe and CaO-Al_2O_3 slag, ISIJ International, vol. 32, no. 1, pp 43-49, 1992.

Hodge J.D. and Bowen H.K.,High-temperature thermoelectric power measurements in wüstite, Journal of the American Ceramic Society, vol. 64, no. 8, pp 431-436, August 1981.

Hoster T. and Pötschke J., Die elektrische Leitfähigkeit FeO-haltiger CaO-Al_2O_3-SiO_2-Schlacken mit Basizitäten $\leq$ 1.5 bei 1450 bis 1650 °C, Archiv für das Eisenhüttenwesen, vol. 54, no. 10, October 1983.

Inouye H., Tomlinson J.W. and Chipman J., The electrical conductivity of wüstite melts, Transactions of the Faraday Society, vol 49, pp 796 – 801, 1953.

Janz G.J. and Tomkins R.P.T., Conductance cell calibrations: Current practices, Journal of the Electrochemical Society, vol 104, pp 55C-59C, 1977.

Jiao Q. and Themelis N.J., Correlations of electrical conductivity to slag composition and temperature, Metallurgical Transactions B, vol. 19B, pp 133-140, 1988.

Jones G. and Bradshaw B.C., Journal of the American Chemical Society, volume 55, pp. 1780-1800, 1933.

Jowsa J. and Gzielo A., Applicability of measuring methods used for determination of electrical conductivity of slags, Archives of Metallurgy, volume 33, issue 4, pp 607-618, 1988.

Kato M. and Minowa S., Electrical conductivity measurements of slag at elevated temperature, Properties of slag at elevated temperature (Part II), Transactions of the Iron and Steel Institute of Japan, volume 9, no. 1, pp 39-46, 1969.

Kawahara M., Morinaga K. and Yanagase T., Behaviour of MgO and NiO in molten slags, Canadian Metallurgical Quarterly, vol 22, no 2, pp 143-147, 1983.

Keller H. and Schwerdtfeger K., Tracer diffusivity of Si^{31} in $CaO-SiO_2$ melts at 1600 °C, Metallurgical Transactions B, vol. 10B, pp 551-554, 1979a.

Keller H., Schwerdtfeger K. and Hennesen K., Tracer diffusivity of Ca^{45} and electrical conductivity in $CaO-SiO_2$ melts, Metallurgical transactions B, vol 10B, pp 67-70, March 1979b.

Keller H., Schwerdtfeger K., Petri H., Hölzle R. and Hennesen K., Tracer diffusivity of O^{18} in $CaO-SiO_2$ melts at 1600 °C, Metallurgical Transactions B, vol. 13B, pp 237-240, 1982.

Kemeny G. and Rosenberg B., Compensation law in thermodynamics and thermal death, Nature, vol. 243, pp. 400-401, June 15, 1973.

Kim K.B. and Sadoway D.R., Electrical conductivity measurements of molten alkaline-earth fluorides, Journal of the Electrochemical Society, vol. 139, no.4, pp. 1027-1033, April 1992.

Kohlrausch F., Holborn L. and Diesselhorst H., Wied. Ann. Phys., vol. 64, pp. 417, 1898.

Kohlrausch F. and Holborn L., "Das Leitvermoegen der Elektrolyte.", Teubner, 1916.

Larson H. and Chipman J., Oxygen activity in iron oxide slags, Transactions of the AIME, vol. 197, pp 1089-1096, 1953.

Levenspiel O., Chemical Reaction Engineering, 2nd edition, John Wiley and Sons, New York, p.23, 1972.

Lin P.L. and Pelton A.D., A structural model for binary silicate systems, Metallurgical Transactions B, volume 10B, pp 667-675, December 1979.

Liutikov R.A. and Tsylev L.M., Effect of chromium oxides on the viscosity and specific conductivity of silica-magnesia-alumina melts, Russian Mining and Metallurgy, vol. 2, pp 54-58, 1963.

Macdonald J.R. and Johnson W.B., Fundamentals of impedance spectroscopy in: Impedance Spectroscopy; Emphasizing Solid Materials and Systems, John Wiley & Sons, New York, 1987.

Mackenzie J.D., Oxide Melts, Advances in Inorganic Chemistry and Radiochemistry, volume 4, pp. 293-318, 1962.

Mackey P.J., The physical chemistry of copper smelting slags – a review, Canadian Metallurgical Quarterly, vol. 21, no 3, pp 221-260, 1982.

Mason T.O. and Bowen H.K., Cation distribution and defect chemistry of iron-aluminate spinels, Journal of the American Ceramic Society, vol. 64, no.2, pp 86-90, 1981a.

Mason T.O. and Bowen H.K., Electronic conduction and thermopower of magnetite and iron-aluminate spinels, Journal of the American Ceramic Society, Volume 64, No. 4, pp 237-242, 1981b.

Masson C.R., An approach to the problem of ionic distribution in liquid silicates, Proceedings of the Royal Society, vol. A265, pp 201-221, 1965.

Masson C.R., The chemistry of slags, Proceedings of the 2nd International Symposium on Metallurgical Slags and Fluxes held in Lake Tahoe, pp 1 - 45, Nov 1984.

Mills K.C., The influence of structure on the physico-chemical properties of slags, ISIJ International, vol 33, no 1, pp 148-155, 1993.

Min'ko N.I. and Nevedomskii V.A., Properties of molten silicon-manganese slags, Melts, volume 3, no. 6, pp 359-364, 1991.

Mitchell A. and J Cameron J., The electrical conductivity of some liquids in the system CaF_2 + CaO + Al_2O_3, Metallurgical Transactions, vol. 2, pp 3361 – 3366, 1971.

Morinaga K., Suginohara Y. and Yanagase T., The electrical conductivity of CaO-SiO_2-Fe_2O_3 and Na_2O-SiO_2-Fe_2O_3 melts, Journal of the Japanese Institute of Metals, vol. 39, no. 12, pp 1312 – 1317, 1975.

Mysen B.O., Virgo D. and Seifert F.A., Redox equilibrium of iron in alkaline earth silicate melts: relationships between melt structure, oxygen fugacity, temperature and properties of iron-bearing silicate liquids, American Mineralogist, vol. 69, pp. 834-847, 1984.

Mysen B.O., Virgo D., Neumann E.-R., Seifert F.A., Redox equilibria and the structural states of ferric and ferrous iron in melts in the system CaO-MgO-Al_2O_3-SiO_2-FeO: relationships between redox equilibria, melt structure and liquidus phase equilibria, American Mineralogist, volume 70, pp 317-331, 1985.

Narita K., Onoye T., Ishii T. and Uemura K., The electrical conductivity of CaO-SiO_2-Fe_tO Slag, Tetsu-to-Hagane, vol. 61, no. 14, pp. 2943-2951, 1975.

Nell J. and Wood B.J. High temperature electrical measurements and thermodynamic properties of Fe_3O_4 – $FeCr_2O_4$ – $MgCr_2O_4$ – $FeAl_2O_4$ spinels, American Mineralogist, volume 76, pp 405-426, 1991.

Nesterenko S.V. and Khomenko V.M., Study of the effects of alkalis on the surface tension and the electrical conductivity of slags of the CaO-MgO-SiO_2 system containing 5% Al_2O_3, Russian Metallurgy, vol. 2, pp 42 – 45, 1985.

Ossin D.I., Howat D.D. and Jochens P.R., Liquidus temperatures, viscosities and electrical conductivities of lime containing slags produced during the smelting of high-carbon ferrochromium and ferrochromium-silicide alloys, Electric Furnace Proceedings, pp 94-101, 1971.

Pal U., Debroy T. and Simkovich G., Electrical conductivity of PbO-SiO_2 liquids containing Pb precipitates, Canadian Metallurgical Quarterly, vol. 23, no 3, pp 295-302, 1980.

Pal U., Debroy T. and Simkovich G., Electronic and ionic transport in liquid PbO-SiO_2 systems, Metallurgical Transactions B, vol. 16B, pp 77-82, March 1985.

Panish M.B., The electrical conductivity of molten silica, Journal of Physical Chemistry, vol. 63, pp. 1337-1338, 1959.

Pargamin L., Lupis C.H.P. and Flinn P.A., Mössbauer analysis of the distribution of iron cations in silicate slags, Metallurgical Transactions, volume 3, pp 2093-2105, August 1972.

Partzsch G.M., Schilling F.R. and Arndt J., The influence of partial melting on the electrical behaviour of crustal rocks: laboratory examinations, model calculations and geological interpretations, Tectonophysics, volume 317, pp 189-203, 2000.

Pastukhov E.A., Esin O.A. and Chuchmarev S.K., The electrical conductivity of molten silicates containing iron oxides, Soviet Electrochemistry, vol 2, pp 193-198, 1966.

Persson J.A. and Treilhard D.G., Electrothermic smelting of copper and nickel sulphides and other metal bearing constituents, Journal of Metals, pp 34-39, January 1973.

Pratt K.W., Koch W.F., Wu Y.C. and Berezansky P.A., Molality-based primary standards of electrolytic conductivity, Pure and Applied Chemistry, vol. 73, no. 11, pp. 1783-1793, 2001.

Rennie M.S., Howat D.D. and Jochens P.R., The effects of chromium oxide, iron oxide and calcium oxide on the liquidus temperatures, viscosities and electrical conductivities of slags in the systems $MgO-Al_2O_3-SiO$, SAIMM Journal, pp 1-9, August 1972.

Rice S.A., A conjecture concerning the electrical conductance of metal-molten salt mixtures, Discussions of the Faraday Society, volume 32, pp 181-187, 1962.

Riebling, E.F. and Logel P.C., Dipping electrode electrical conductance instrument for use to 1700°C, Review of Scientific Instruments, vol. 36 no 4, pp 425-428, 1965.

Robbins G.D., Measurement of electrical conductivity in molten fluorides. A survey., Journal of the Electrochemical society, vol 116, pp 813-817, 1969.

Sarkar S.B., Electrical conductivity of molten high-alumina blast furnace slags, ISIJ International, vol 29, no 4, pp 348-351, 1989.

Schiefelbein S.L. and Sadoway D.R., A high-accuracy, calibration-free technique for measuring the electrical conductivity of molten oxides, Metallurgical and Materials Transactions B, vol. 28B, pp 1141-1149, December 1997.

Schiefelbein S.L., High accuracy electrical conductivity measurements of corrosive melts using the coaxial cylinders technique, Sixth international conference on molten slags, fluxes and salts, Stockholm, Sweden – Helsinki Finland, 12-17 June 2000, CD-rom.

Segers L., Fontana A. and Winand R., Conductivites electriques de melanges de silicate fondus du systeme $CaO-SiO_2-MnO$, Electrochimica Acta, volume 23, pp 1281-1286, 1978.

Segers L., Fontana A. and Winand R., Electrical conductivity of molten slags of the system $SiO_2 - Al_2O_3 - MnO - CaO - MgO$, Canadian Metallurgical Quarterly, vol 22, no 4, pp 429-435, 1983.

Shluger A.L. and Stoneham A.M., Small polarons in real crystals: concepts and problems, Journal of Physics: Condensed matter, vol. 5, pp 3049-3086, 1993.

Simnad M.T., Derge G. and George I., Ionic nature of liquid iron-silicate slags, Journal of Metals, vol 6, pp 1386-1390, December 1954.

Slag Atlas, 1st edition, Verlag Stahleisen, Düsseldorf, 1981.

Slag Atlas, chapter 14 – electrical conductivity, 2nd edition, Verlag Stahleisen, Düsseldorf, 1995.

Solomons C., Electrochemical measurement, Techniques of metals research, vol 2, Wiley, New York, pp 35-79, 1979.

Sommerville I.D. and Bell H.B., The behaviour of titania in metallurgical slags, Canadian Metallurgical Quarterly, vol. 21, no 2, pp 145-155, 1980.

Sumita S., Morinaga K. and Yanagase T., Physical properties and structures of binary ferrite melts, Transactions of the Japan Institute of Metals, vol. 24, no. 1, pp 35-41, 1983.

Sun S. and Jahanshahi S., Oxygen transport in iron oxide containing melts and the role of electronic conduction, 6th International Conference of Molten Salt Chemistry and Technology, 2001.

Takeda Y., Nakazawa S. and Yazawa A., Thermodynamics of calcium ferrite slags at 1200 and 1300 °C, Canadian Metallurgical Quarterly, volume 19, pp 297-305, 1980.

Timucin M. and Morris A.E., Phase equilibria and thermodynamic studies in the system CaO-FeO-Fe_2O_3-SiO_2, Metallurgical Transactions, vol. 1, pp 3193-3201, November 1970.

Urbain G., Cambier F., Deletter M. and Anseau M.R., Viscosity of silicate melts, Transactions and Journal of the British Ceramic Society , vol. 80, issue 4, pp 139-141, 1981.

Van Arkel A.E., Flood E.A. and Bright N.F.H.,The electrical conductivity of molten oxides, Canadian Journal of Chemistry, vol. 31, no. 11, pp 1009-1019, 1953.

Van der Colf J. and Howat D.D., Viscosities, electrical resistivities and liquidus temperatures of slags in the system CaO – MgO – Al_2O_3 – TiO_2 – SiO_2 under reducing conditions, Journal of the SAIMM, pp 327-333, June 1979.

Victorovich G.S., Diaz C. and Vallbacka D.K., Electrical conductivity of ferromagnesian silicates, Proceedings of the 2nd International Symposium on Metallurgical Slags and Fluxes held in Lake Tahoe, pp 907-924, Nov 1984.

Wejnarth A., The current conducting properties of slags in electric furnaces part 1, Transactions of the American Electrochemical Society, vol 65, pp 177-187, 1934a.

Wejnarth A., The current conducting properties of slags in electric furnaces part 2, Transactions of the American Electrochemical Society, vol 66, pp 329-343, 1934b.

Winchell P., The compensation law for diffusion in silicates, High temperature science, volume 1, pp 200-215, 1969.

Winterhager H., Greiner L. and Kammel R., Untersuchungen über die Dichte und die elektrische Leitfähigkeit von Schmelzen der Systeme CaO-Al_2O_3-SiO_2 und CaO-MgO-Al_2O_3-SiO_2, Köln/Opladen, 1966. (Forschungsberichte des Landes Nordrhein-Westfalen 1630).

Woollacott L.C., Howat D.D. and Jochens P.R., The viscosities and electrical conductivities of slags associated with the production of high-carbon ferromanganese alloys, Infacon 74 – proceedings of the 1st International Ferro-alloys Congress, Johannesburg, SAIMM, pp 227-232, 1974.

Wu C.C. and Mason T.O., Thermopower measurements of cation distribution in magnetite, Journal of the American Ceramic Society, vol. 64, no. 9, pp 520-522, 1981.

Xiao Y., Reuter M. and Holappa L., Oxidation state of chromium in molten slags, Sixth international conference on molten slags, fluxes and salts, Stockholm, Sweden – Helsinki Finland, 12-17 June 2000, CD-rom.

Yang L. and Belton G.R.,Iron redox equilibria in CaO-Al_2O_3-SiO_2 and MgO-CaO-Al_2O_3-SiO_2 slags, Metallurgical and Materials Transactions B, vol 29B, pp 837-845, August 1998.

Yazawa A. and Takeda Y., Equilibrium reactions between liquid copper and calcium ferrite slag, Transactions of the Japan Institute of Metals, vol. 23, no 6, pp 328-333, 1982.

Yazawa A., Takeda Y. and Waseda Y., Thermodynamic properties and structure of ferrite slags and their process implications, Canadian Metallurgical Quarterly, volume 20, no. 2, pp 129-134, 1981.

Young E.W.A., Gerretsen J.H. and de Wit J.H.W., The oxygen partial pressure dependence of the defect structure of chromium (III) oxide, Journal of the Electrochemical Society, vol. 134, no. 9, pp. 2257-2260, September 1987.

Zhang L. and Jahanshahi S., Modelling viscosity of alumina-containing silicate melts, Sixth international conference on molten slags, fluxes and salts, Stockholm, Sweden – Helsinki Finland, 12-17 June 2000.

Zhang L. and Jahanshahi S., Review and modelling of viscosity of silicate melts: Part I. Viscosity of binary and ternary silicates containing CaO, MgO and MnO, Metallurgical and Materials Transactions B, volume 29B, pp 177-186, 1998a.

Zhang L. and Jahanshahi S., Review and modelling of viscosity of silicate melts: Part II. Viscosity of melts containing iron oxide in the CaO-MgO-MnO-FeO-Fe_2O_3-SiO_2 system, Metallurgical and Materials Transactions B, volume 29B, pp 187-195, 1998b.

Zhang L., Jahanshahi S., Sun S., Chen C., Bourke B., Wright S., and Somerville M., CSIRO's multiphase reaction models and their industrial applications, Journal of Metals, vol. 54, no. 11, pp. 51-56, 2002.

APPENDICES

A. Literature review

B. Materials and methods

C. Results

Key to the oxidation state dependent data and graphs

The first table contains the raw data indicating the gas atmosphere, measured resistance and the calculated conductivity. The calibration details are also given in the table. To the right of the table is a graph indicating the response of the conductivity to the change in gas atmosphere.

The next table indicates the average rate of change in the measured resistance determined at the point of assumed equilibrium. Based on the average rate of change, a new conductivity value is calculated if the slag was left to equilibrate for a further 30 minutes. The percentage change between the original and changed conductivity is shown.

The next graph contains the data of the average rate of change in the measured resistances based on a five minute moving average. The points where equilibrium was assumed have been indicated by an arrow with a label indicating the gas atmosphere at that point.

The final graph indicates the trends in the conductivity vs ferric / total Fe if calculated from the original measured data and if calculated if the slag was allowed to equilibrate for a further 30 minutes.

A. LITERATURE REVIEW

A.1. Frequencies of authors' measurements

Reference	Frequency	Other comments
Hejja *et al.* (1994)	150 kHz or 10 kHz?	variable series of capacitances connected in parallel with measuring cell to counteract capacitive effects of the slag
Eric *et al.* (1991)	150 kHz or 10 kHz?	variable series of capacitances connected in parallel with measuring cell to counteract capacitive effects of the slag
Rennie *et al.* (1972)	10 kHz	Indepedent of f down to 2 kHz but greatest precision at 10 kHz, calibration with KCl found capacitive effects and therefore calibration results were extrapolated to infinite frequency resistance plotted vs 1/f
Robbins (1969)	survey	look at frequency depedence of molten flourides and calibration - of direct relevance to discussion
Segers *et al.* (1983)	10 kHz	calibration with aqueous solutions at 100 kHz but measurements on slag at 10 KHz
Victorovich *et al.* (1984)	1 kHz	calibration of 1N KCl at this frequency - cell constant possibly has error because of low frequency measurements made at a sequence of depths
Downing and Urban (1966)	10 kHz	cell constant calibration at 10 kHz in 0.1M KCl
Inouye *et al.* (1953)	???	calibration with 0.1N KCl
Bockris *et al.* (1952)	???	took into account frequency effects
Sarkar (1989)	1 kHz	calibration with KCl solutions
Dancy and Derge (1966)	not mentioned	
Keller *et al.* (1979)	30-100 kHz	calibration with 1n KCl, 0.02N KCl, saturated NaCl and KCl at 850 °C
Solomons (1979)		mentions effect of frequency on bridges
Mitchell and Cameron (1971)	1 kHz	
Schiefelbein and Sadoway (1997)	EIS	from scan determine frequency at which Z" is minimum and use corresponding value of Z' do this for different immersion depths well defined cell, therefore no need to calibrate
Desrosiers *et al.* (1980)	1 kHz	0.01, 0.1 and 1.0 M KCl
Pal *et al.* (1980)	> 1 kHz	to avoid polarisation calibration with 0.01N KCl
Pal *et al.* (1985)	> 1 kHz	to avoid polarisation calibration with 0.01N KCl
Berryman and Sommerville (1988)	1 kHz	
Pastukhov *et al.* (1966)	0.1 - 10 kHz	frequency independence in FeO melts
Fontana *et al.* (1984)	> 0.1 kHz	Indepedent of f for slags investigated
Engell and Vygen (1968)	50 kHz	found measured frequency constant from 40 kHz to 100 kHz calibration with KCl solutions
Woollacott *et al.* (1974)	10 kHz	
Britten and Pal (2000)	EIS	see page 745
Botor *et al.* (1997)	10 kHz	
Kato and Minowa (1969)	1 kHz	
Ziolek and Bogacz (1987)	6 kHz	frequency independence from 1 to 20 kHz
Ossin *et al.* (1971)	10 kHz	
Hoster and Pötschke (1983)	17.3 kHz	calibrated with KCl solutions
Segers *et al.* (1978)		mention frequency f_0 where the real part is constant i.e. no Z" 10 kHz for silicate slags, 60 kHz for KNO_3 and 150 kHz for KCl solutions
Jowsa and Gzielo (1988)	5 - 12 kHz	discussion of three techniques - ac bridge, voltmeter-ammeter, galvanostatic
Hino *et al.* (1992)	EIS	some notes on principle
Partzsch *et al.* (2000)	EIS	partial melting
Fontana *et al.* (1985)	EIS	
Kim and Sadoway (1992)	frequency scan	related to Schiefelbeins technique
Narita *et al.* (1975)		graph of frequency dependence
Winterhager *et al.* (1966)	50 kHz	calibration with H_2SO_4 and KNO_3

In the table EIS refers to Electrochemical Impedance Spectroscopy.

B. MATERIALS AND METHODS

B.1. Calibration of thermocouple

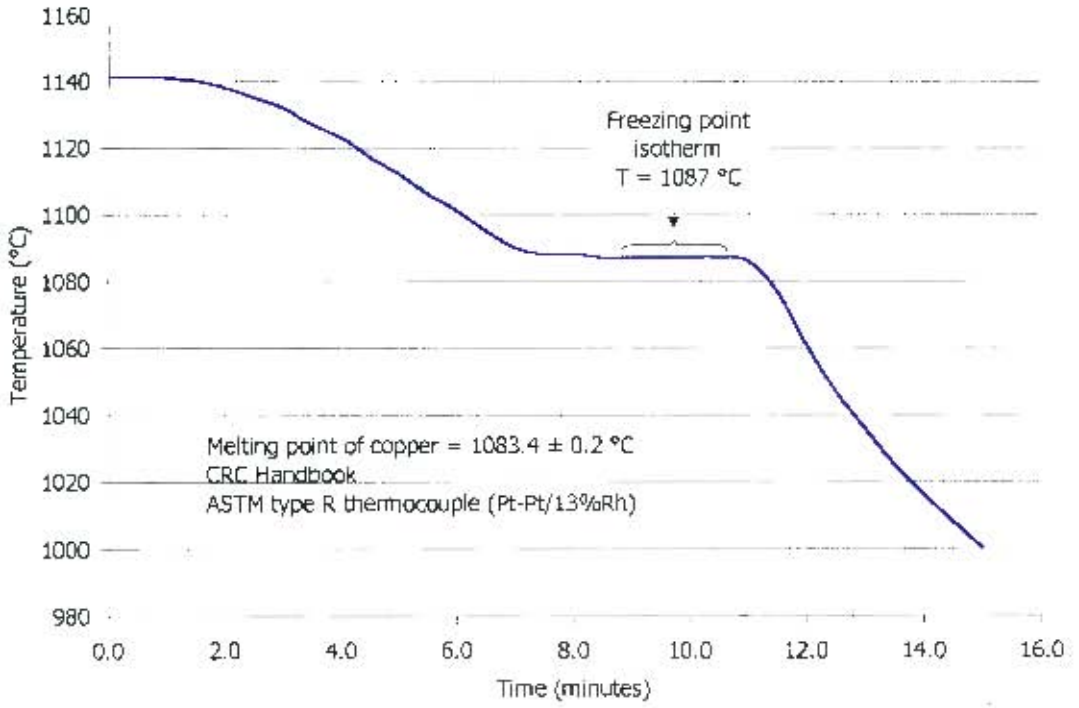

The accuracy of the thermocouple was checked against the freezing point of copper and was found to be approximately 3.5 °C higher than the standard value. The calibration of the thermocouple was carried out towards the end of the experimental programme, therefore it would have been more accurate in the earlier experiments.

B.2. Hot zone of furnace

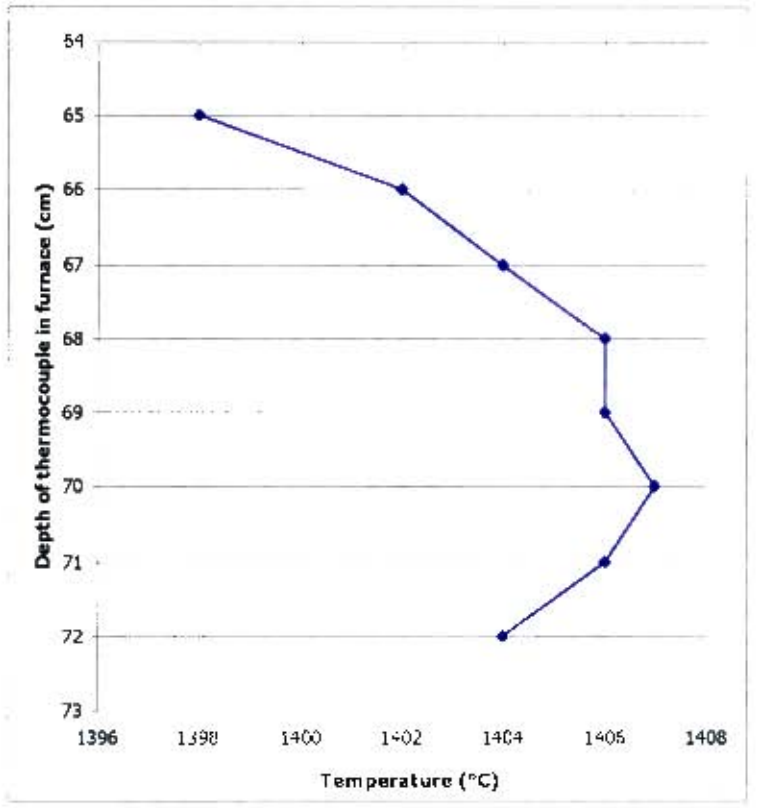

The hot zone of the standard furnace extended from a depth of 67 to 72 cm below the top end cap of the furnace. In this region the temperature varied by around ±2 °C (taking 1406°C as the setpoint)

B.3. Calibration of gas flow meters

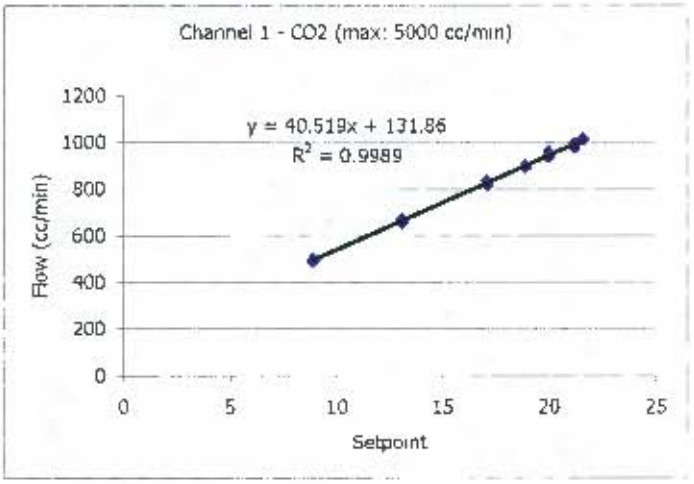

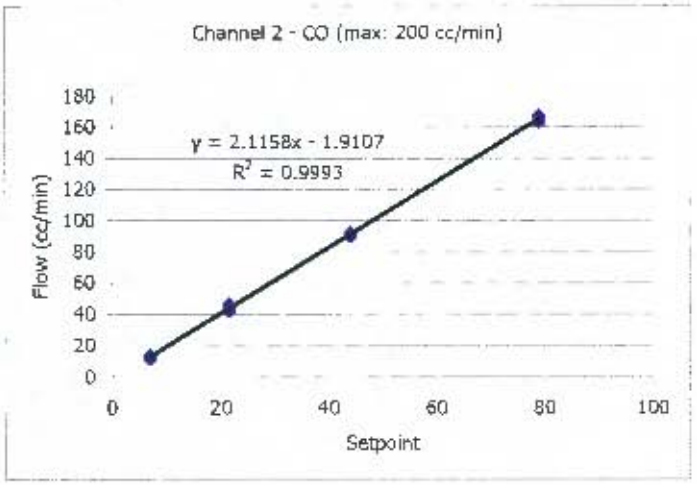

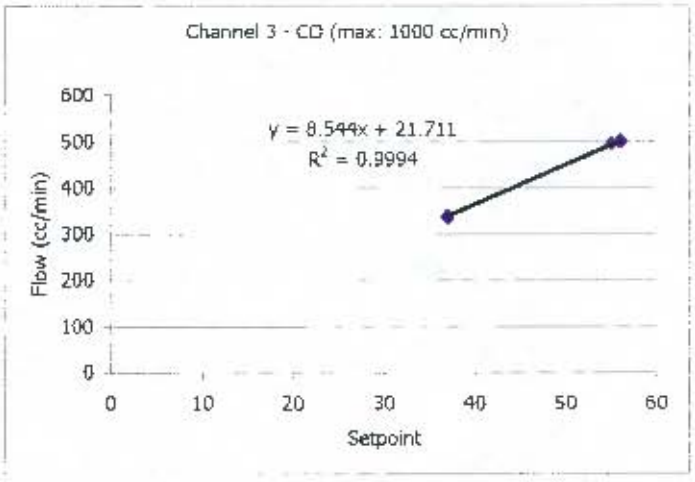

The gas was controlled through three channels. Typically the CO_2 flow rate required was larger than the CO flow rate, therefore the larger capacity controller in channel 1 was used (max: 5000 cc/min). Then two different controllers were used for the CO flow rate: for very low flow rates channel 2 was used (max: 200 cc/min) and for higher flow rates, channel 3 was used (max: 1000 cc/min). The graphs show the linear relationship between the setpoint and the actual flow rate.

B.4. Resistance of electrodes

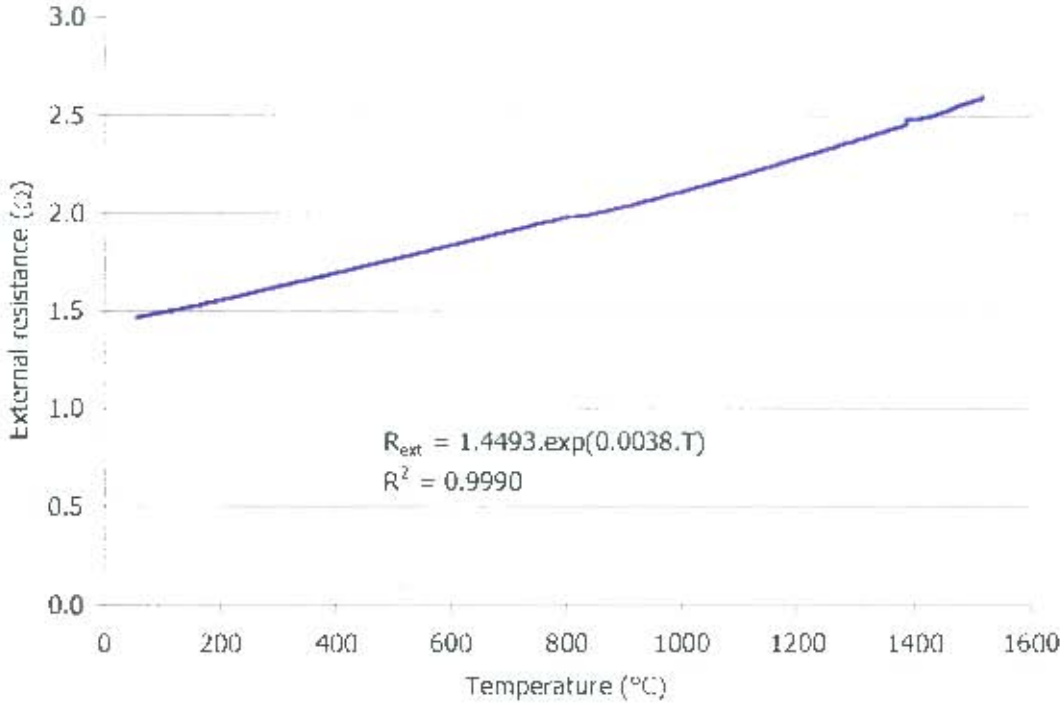

The external resistance offered by the leads and the electrodes was measured by twisting the tips of the electrodes together, placing the electrodes in the empty furnace, sealing the furnace and then ramping up the temperature while measuring the resistance. The exponential equation was used in calculation of the external resistance.

C. APPENDIX – RESULTS

C.1. Low basicity slag

C.1.1. Compositions

Intended and analysed compositions of FeO_x- free low basicity slag

Slag L0	intended		analysed	
Component	wt%	mol%	wt%	mol%
Al_2O_3	6.3	3.3	6.6	3.6
CaO	6.3	6.1	6.5	6.4
MgO	25.0	33.8	23.2	32.0
SiO_2	62.5	56.7	62.8	58.0
Total	100	100.0	99.1	100.0

From the analysis it was evident that the MgO content was lower than intended while the other components were slightly higher than intended. A possible cause for this was the purity of the MgO. The only significant minor impurity was 0.15wt% Na_2O which was regarded as insufficient to affect the conductivity.

Slag L15	Intended		Initial analysed		Final analysed	
Component	wt%	mol%	wt%	mol%	wt%	mol%
Al_2O_3	5.3	2.9	6.2	3.5	6.1	3.4
CaO	5.3	5.4	5.6	5.7	5.6	5.7
FeO_x	15.0	11.8	14.6	11.6	13.6	10.8
MgO	21.3	29.8	19.8	28.1	21.6	30.4
SiO_2	53.1	50.0	53.8	51.1	52.7	49.8
Total	100.0	100.0	100.1	100.0	99.6	100.0
(C+M)/(A+S)	0.45	0.66	0.42	0.62	0.46	0.68

	wt%	mol%
gain in MgO	1.8	2.3
change in B	0.04	0.06

Experiment duration (hr)	4.9
Final CO_2/CO ratio	1

Slag L20	Intended		Initial analysed		Final analysed	
Component	wt%	mol%	wt%	mol%	wt%	mol%
Al_2O_3	5.0	2.8	6.0	3.4	5.8	3.3
CaO	5.0	5.1	5.2	5.4	5.2	5.3
FeO_x	20.0	16.0	19.4	15.7	18.0	14.3
MgO	20.0	28.4	18.6	26.7	21.8	30.8
SiO_2	50.0	47.7	50.4	48.7	48.9	46.4
Total	100.0	100.0	99.6	100.0	99.6	100.0
(C+M)/(A+S)	0.45	0.66	0.42	0.62	0.49	0.73

	wt%	mol%
gain in MgO	3.2	4.0
change in B	0.07	0.11

Experiment duration (hr)	5.4
Final CO_2/CO ratio	1

C. APPENDIX – RESULTS

C.1. Low basicity slag

C.1.1. Compositions

Intended and analysed compositions of FeO-free low basicity slag

Slag L0	intended		analysed	
Component	wt%	mol%	wt%	mol%
Al_2O_3	6.3	3.3	6.6	3.6
CaO	6.3	6.1	6.5	6.4
MgO	25.0	33.8	23.2	32.0
SiO_2	62.5	56.7	62.8	58.0
Total	100	100.0	99.1	100.0

From the analysis it was evident that the MgO content was lower than intended while the other components were slightly higher than intended. A possible cause for this was the purity of the MgO. The only significant minor impurity was 0.15wt% Na_2O which was regarded as insufficient to affect the conductivity.

Slag L15	Intended		Initial analysed		Final analysed	
Component	wt%	mol%	wt%	mol%	wt%	mol%
Al_2O_3	5.0	2.9	6.2	3.5	6.1	3.4
CaO	5.3	5.4	5.6	5.7	5.6	5.7
FeO_x	15.0	11.8	14.6	11.6	13.6	10.8
MgO	21.3	29.8	19.8	28.1	21.6	30.4
SiO_2	53.1	50.0	53.8	51.1	52.7	49.8
Total	100.0	100.0	100.1	100.0	99.6	100.0
(C+M)/(A+S)	0.45	0.66	0.42	0.62	0.46	0.68

	wt%	mol%
gain in MgO	1.6	2.3
change in B	0.04	0.06

Experiment duration (hr)	4.5
Final CO_2/CO ratio	1

Slag L20	Intended		Initial analysed		Final analysed	
Component	wt%	mol%	wt%	mol%	wt%	mol%
Al_2O_3	5.0	2.8	6.0	3.4	5.8	3.3
CaO	5.0	5.1	5.2	5.4	5.2	5.3
FeO_x	20.0	16.0	19.4	15.7	18.0	14.3
MgO	20.0	28.4	19.6	26.7	21.8	30.8
SiO_2	50.0	47.7	50.4	48.7	48.5	46.4
Total	100.0	100.0	99.6	100.0	99.6	100.0
(C+M)/(A+S)	0.45	0.66	0.42	0.62	0.49	0.73

	wt%	mol%
gain in MgO	3.2	4.0
change in B	0.07	0.11

Experiment duration (hr)	5.4
Final CO_2/CO ratio	1

L40 rep 1	Intended		Initial analysed		Final analysed	
Component	wt%	mol%	wt%	mol%	wt%	mol%
Al_2O_3	3.8	2.2	5.0	3.0	4.0	2.4
CaO	3.8	4.0	3.9	4.3	4.1	4.4
FeO_x	40.0	33.6	37.8	32.7	34.2	28.8
MgO	15.0	22.5	13.7	21.1	18.5	27.9
SiO_2	37.5	37.7	37.4	38.8	36.2	36.5
Total	100.0	100.0	97.8	100.0	97.1	100.0
(C+M)/(A+S)	0.45	0.66	0.41	0.61	0.56	0.83

	wt%	mol%
gain in MgO	4.8	6.7
change in B	0.15	0.22

Experiment duration (hr)	6
Final CO_2/CO ratio	10

L40 rep 2	Intended		Initial analysed		Final analysed	
Component	wt%	mol%	wt%	mol%	wt%	mol%
Al_2O_3	3.8	2.2	5.0	3.0	3.7	2.2
CaO	3.8	4.0	3.9	4.3	3.9	4.2
FeO_x	40.0	33.6	37.8	32.7	33.8	28.3
MgO	15.0	22.5	13.7	21.1	19.6	29.3
SiO_2	37.5	37.7	37.4	38.8	36.0	36.1
Total	100.0	100.0	97.8	100.0	97.0	100.0
(C+M)/(A+S)	0.45	0.66	0.41	0.61	0.59	0.87

	wt%	mol%
gain in MgO	5.9	8.1
change in B	0.18	0.27

Experiment duration (hr)	6
Final CO_2/CO ratio	10

C.1.2. Temperature dependence measurements

Slag L0

Temperature	Resistance measured	Electrical conductivity	$1/T * 10^4$	ln σ
°C	Ω	$(\Omega.cm)^{-1}$	K^{-1}	$(\Omega.cm)^{-1}$
1475	18.3	0.063	5.72	-2.77
1498	16.2	0.073	5.65	-2.62
1518	14.6	0.083	5.58	-2.49
1548	12.3	0.104	5.49	-2.27
1526	13.6	0.091	5.56	-2.40
1475	18.2	0.063	5.72	-2.76
1466	19.4	0.059	5.75	-2.83
1456	21.0	0.054	5.78	-2.93
1445	22.5	0.050	5.82	-3.00
Calibration slope		-1.013	E_0	184.9
Calibration intercept		0.024	ln A_0	9.9
			rsq	0.997555425

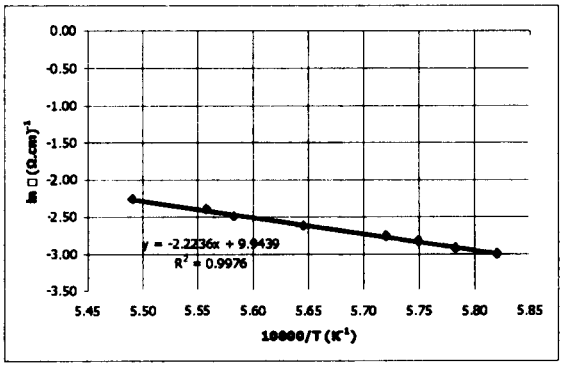

Slag L30	Intended		Initial analysed		Final analysed	
Component	wt%	mol%	wt%	mol%	wt%	mol%
Al_2O_3	4.4	2.5	5.5	3.2	5.3	3.1
CaO	4.4	4.6	4.5	4.8	4.6	4.8
FeO_x	30.0	24.6	29.3	24.6	26.3	21.6
MgO	17.5	25.5	16.0	23.9	20.0	29.3
SiO_2	43.8	42.8	43.4	43.4	41.9	41.1
Total	100.0	100.0	98.7	100.0	98.2	100.0
(C+M)/(A+S)	0.45	0.66	0.42	0.62	0.52	0.77

	wt%	mol%
gain in MgO	4.0	5.4
change in B	0.10	0.16

Experiment duration (hr)	7
Final CO_2/CO ratio	2

L30 rep 1	Intended		Initial analysed		Final analysed	
Component	wt%	mol%	wt%	mol%	wt%	mol%
Al_2O_3	4.4	2.5	5.5	3.2	4.5	2.6
CaO	4.4	4.6	4.5	4.8	4.6	4.8
FeO_x	30.0	24.6	29.3	24.6	25.6	21.0
MgO	17.5	25.5	16.0	23.9	20.9	30.5
SiO_2	43.8	42.8	43.4	43.4	42.0	41.2
Total	100.0	100.0	98.7	100.0	97.6	100.0
(C+M)/(A+S)	0.45	0.66	0.42	0.62	0.55	0.81

	wt%	mol%
gain in MgO	4.9	6.5
change in B	0.13	0.19

Experiment duration (hr)	7
Final CO_2/CO ratio	2

L30 rep 2	Intended		Initial analysed		Final analysed	
Component	wt%	mol%	wt%	mol%	wt%	mol%
Al_2O_3	4.4	2.5	5.5	3.2	4.5	2.6
CaO	4.4	4.6	4.5	4.8	4.6	4.8
FeO_x	30.0	24.6	29.3	24.6	26.8	21.6
MgO	17.5	25.5	16.0	23.9	21.2	30.4
SiO_2	43.8	42.8	43.4	43.4	42.2	40.7
Total	100.0	100.0	98.7	100.0	99.4	100.0
(C+M)/(A+S)	0.45	0.66	0.42	0.62	0.55	0.81

	wt%	mol%
gain in MgO	5.2	6.5
change in B	0.13	0.20

Experiment duration (hr)	7
Final CO_2/CO ratio	2

Slag L40	Intended		Initial analysed		Final analysed	
Component	wt%	mol%	wt%	mol%	wt%	mol%
Al_2O_3	3.8	2.2	5.0	3.0	4.9	2.9
CaO	3.8	4.0	3.9	4.3	4.0	4.2
FeO_x	40.0	33.6	37.8	32.7	35.3	29.5
MgO	15.0	22.5	13.7	21.1	18.2	27.1
SiO_2	37.5	37.7	37.4	38.8	36.3	36.2
Total	100.0	100.0	97.8	100.0	98.6	100.0
(C+M)/(A+S)	0.45	0.66	0.41	0.61	0.54	0.80

	wt%	mol%
gain in MgO	4.5	6.0
change in B	0.12	0.19

Experiment duration (hr)	6
Final CO_2/CO ratio	10

Slag L10

Temperature	Resistance measured	Electrical conductivity	1/T * 10^4	ln □
°C	Ω	$(\Omega.cm)^{-1}$	K^{-1}	$(\Omega.cm)^{-1}$
1474	13.1	0.095	5.72	-2.36
1498	11.3	0.115	5.65	-2.16
1524	9.9	0.138	5.56	-1.98
1540	9.2	0.153	5.52	-1.88
1500	11.1	0.118	5.64	-2.14
1455	14.2	0.085	5.79	-2.46
1477	12.7	0.098	5.71	-2.32
Calibration slope		-1.013	$E_□$	184.5
Calibration intercept		0.024	ln $A_□$	10.4
			rsq	0.996164708

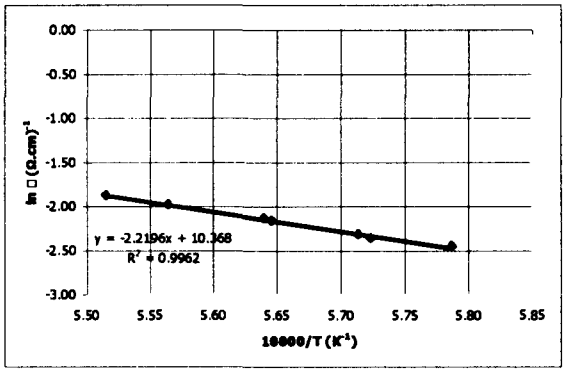

Slag L15

Temperature	Resistance measured	Electrical conductivity	1/T * 10^4	ln □
°C	Ω	$(\Omega.cm)^{-1}$	K^{-1}	$(\Omega.cm)^{-1}$
1451	10.0	0.134	5.80	-2.01
1474	9.1	0.154	5.72	-1.87
1499	8.2	0.181	5.64	-1.71
1524	7.4	0.209	5.56	-1.56
1550	6.8	0.244	5.49	-1.41
1502	8.0	0.185	5.63	-1.69
1455	9.9	0.137	5.79	-1.99
1427	11.3	0.114	5.88	-2.17
Calibration slope		-1.013	$E_□$	159.4
Calibration intercept		0.024	ln $A_□$	9.1
			rsq	0.999722658

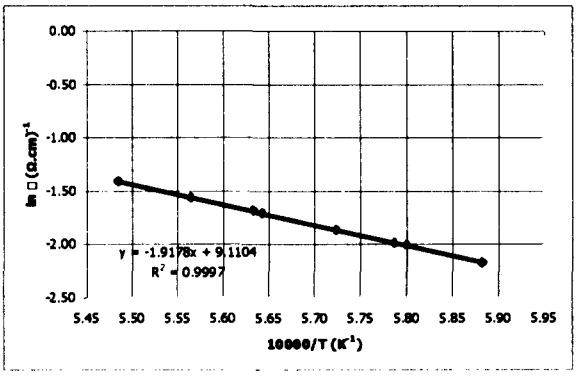

Slag L20

Temperature	Resistance measured	Electrical conductivity	1/T * 10^4	ln □
°C	Ω	$(\Omega.cm)^{-1}$	K^{-1}	$(\Omega.cm)^{-1}$
1399	7.7	0.192	5.98	-1.65
1424	6.7	0.242	5.89	-1.42
1449	6.1	0.287	5.81	-1.25
1473	5.7	0.328	5.73	-1.12
1498	5.3	0.375	5.65	-0.98
1521	5.0	0.430	5.57	-0.84
Calibration slope		-1.013	$E_□$	147.4
Calibration intercept		0.024	ln $A_□$	9.0
			rsq	0.9988

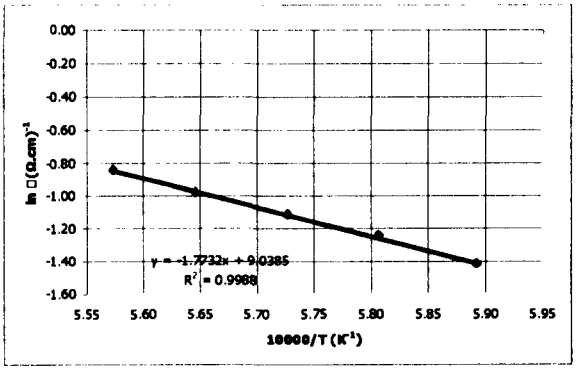

C.1.3. Oxidation state measurements

Slag L15

P_{CO_2}/P_{CO}	P_{O_2}	Resistance measured	Electrical conductivity
	atm	Ω	$(\Omega.cm)^{-1}$
air	2.1E-01	31.0	0.132
80	5.6E-05	26.0	0.161
20	3.5E-06	25.1	0.167
10	8.7E-07	24.7	0.170
5	2.2E-07	24.1	0.175
2	3.5E-08	23.6	0.180
1	8.7E-09	23.4	0.181
Calibration slope			-1.02
Calibration Intercept			1.37

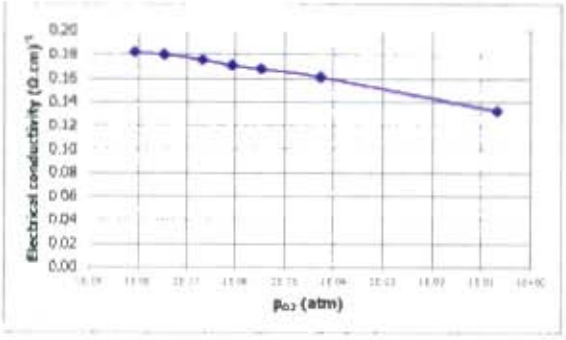

P_{CO_2}/P_{CO}	Time	$R_{measured}$	average $\Delta R/\Delta t$	k_{ini}	k_{fit}	%change
ratio	minutes	Ω	Ω/min	$(\Omega.cm)^{-1}$	$(\Omega.cm)^{-1}$	
air	51	31.00	-0.015	0.132	0.134	1.7
80	105	26.02	-0.021	0.161	0.165	2.8
20	149	25.09	-0.032	0.167	0.175	4.5
10	180	24.69	-0.007	0.170	0.172	1.0
5	214	24.10	-0.014	0.175	0.179	2.0
2	249	23.57	-0.006	0.180	0.181	0.9
1	279	23.36	-0.010	0.181	0.184	1.5

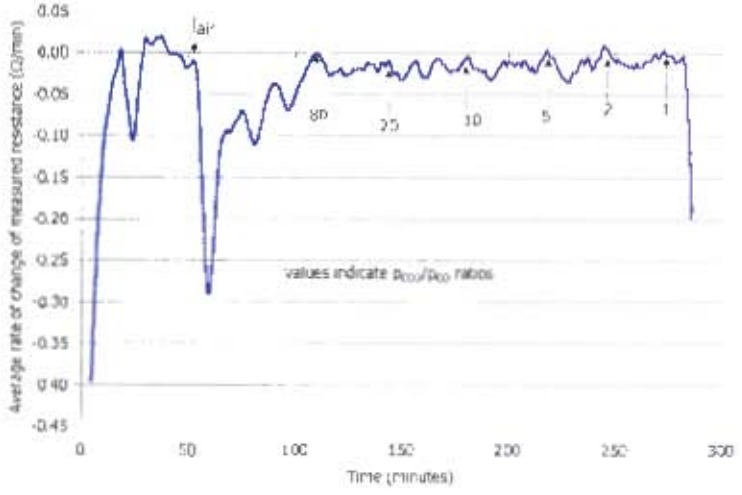

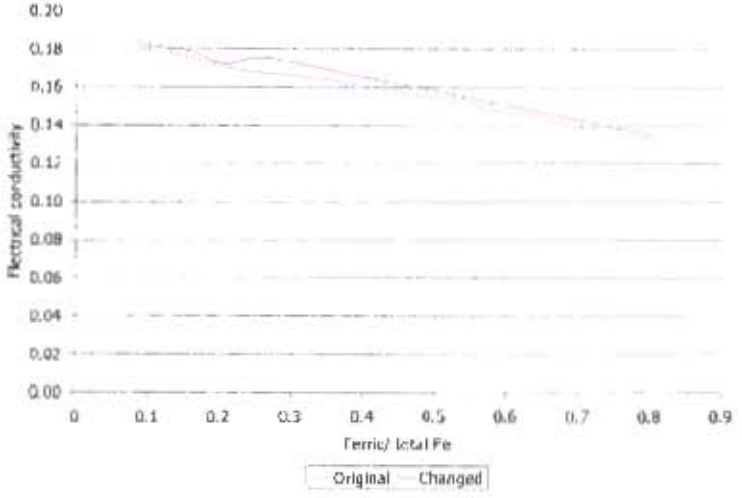

Slag L20

P_{CO2}/P_{CO}	P_{O2}	Resistance measured	Electrical conductivity
	atm	Ω	$(\Omega cm)^{-1}$
air	2.1E-01	22.8	0.190
80	5.6E-05	20.1	0.220
20	3.5E-06	19.6	0.225
10	8.7E-07	19.7	0.224
5	2.2E-07	20.2	0.217
2	3.5E-08	21.9	0.198
1	8.7E-09	25.0	0.171
Calibration slope			-1.02
Calibration intercept			1.40

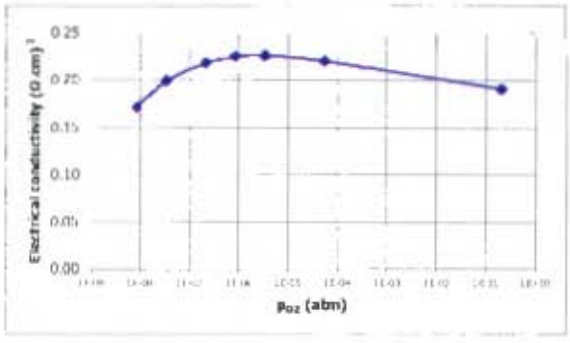

P_{CO2}/P_{CO}	Time	$R_{measured}$	average $\Delta R/\Delta t$	k_{eq}	k_{10}	%change
ratio	minutes	Ω	Ω/min	$(\Omega cm)^{-1}$	$(\Omega cm)^{-1}$	
air	47	22.72	-0.006	0.190	0.192	0.9
80	90	20.08	-0.012	0.219	0.224	2.1
20	121	19.64	0.004	0.225	0.224	0.7
10	156	19.73	0.005	0.224	0.222	0.8
5	203	20.47	0.016	0.215	0.209	2.6
2	250	21.92	0.036	0.198	0.188	5.3
1	322	24.95	-0.011	0.171	0.174	1.5

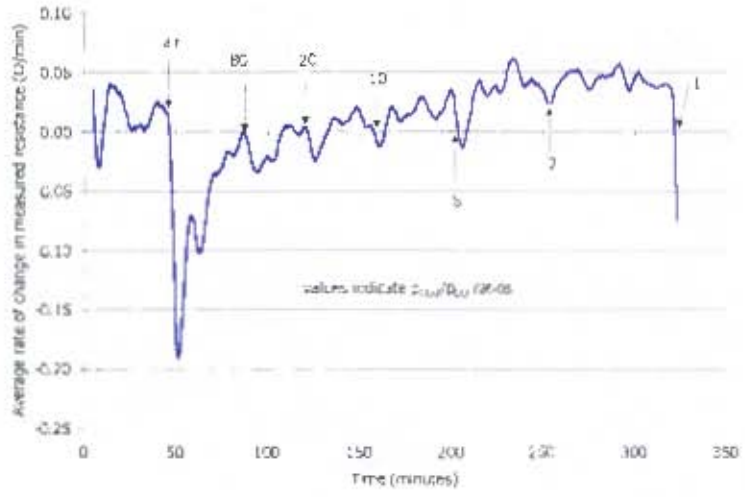

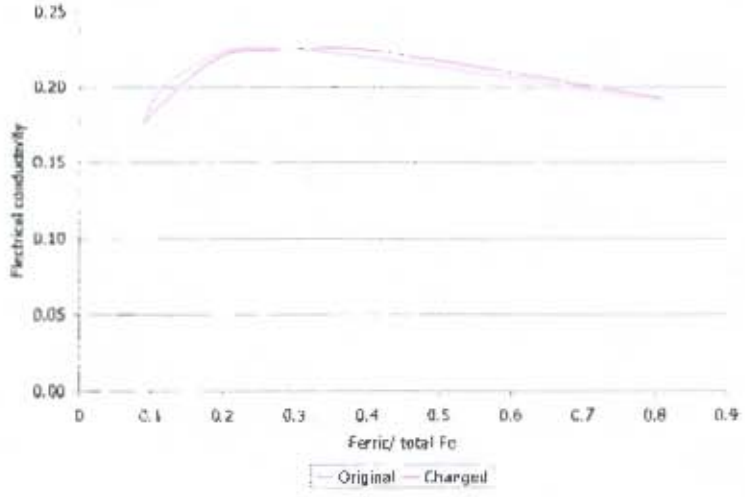

Slag L3D initial

P_{CO_2}/P_{CO}	P_{O_2}	Resistance measured	Electrical conductivity
	atm	Ω	$(\Omega.cm)^{-1}$
air	7.1E-01	15.3	0.313
80	5.6E-05	13.4	0.370
20	3.5E-06	15.9	0.301
10	8.7E-07	18.3	0.252
5	2.2E-07	20.1	0.227
2	3.5E-08	20.8	0.217
Calibration slope			-1.02
Calibration intercept			1.44

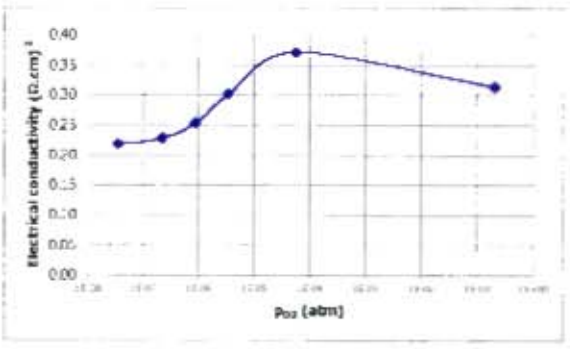

P_{CO_2}/P_{CO}	Time	$R_{measured}$	average $\Delta R/\Delta t$	k_{eq}	k_{SI}	%change
ratio	minutes	Ω	Ω/min	$(\Omega.cm)^{-1}$	$(\Omega.cm)^{-1}$	
air	/	15.34	-0.018	0.313	0.328	4.6
80	22	13.39	0.000	0.370	0.371	0.1
20	85	15.85	0.015	0.301	0.291	3.3
10	144	18.35	0.010	0.252	0.248	1.9
5	187	20.05	0.022	0.227	0.219	3.8
2	207	20.82	0.010	0.217	0.214	1.7

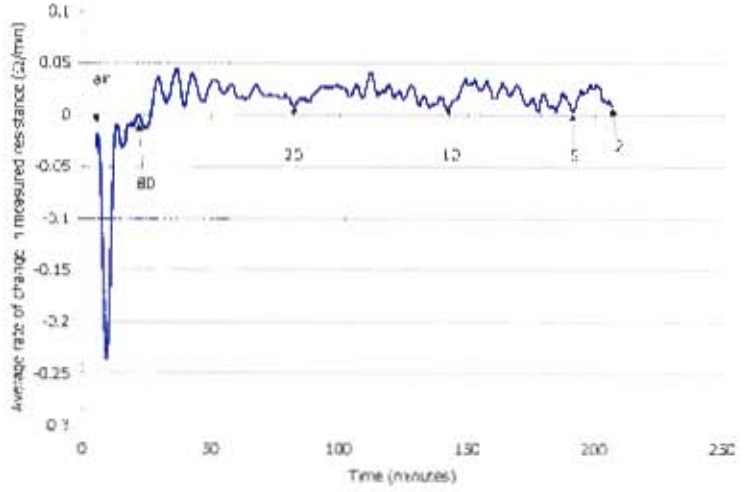

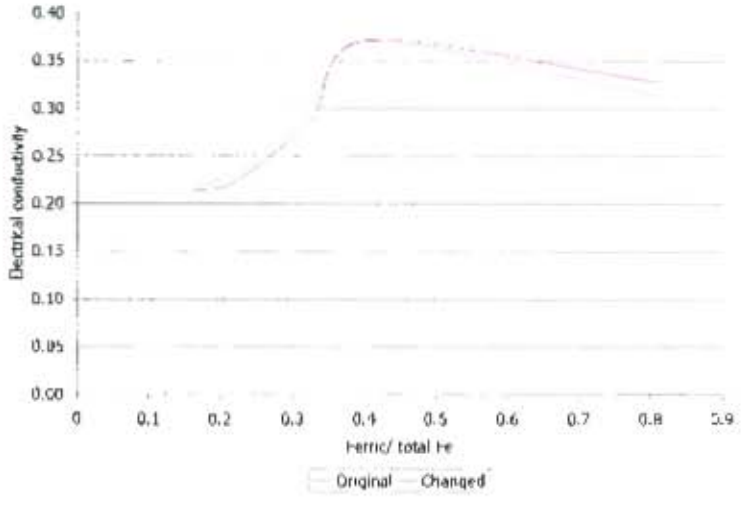

Slag L30 repeat

P_{CO2}/P_{CO}	P_{O2}	Resistance measured	Electrical conductivity
	atm	Ω	$(\Omega.cm)^{-1}$
air	2.1E-01	12.0	0.408
80	5.6E-05	10.3	0.525
20	3.5E-06	10.5	0.511
10	8.7E-07	12.3	0.415
2	3.5E-08	14.1	0.347
1	8.7E-09	14.7	0.331
0.1	2.2E-11	15.8	0.303
Calibration slope			1.02
Calibration intercept			1.44

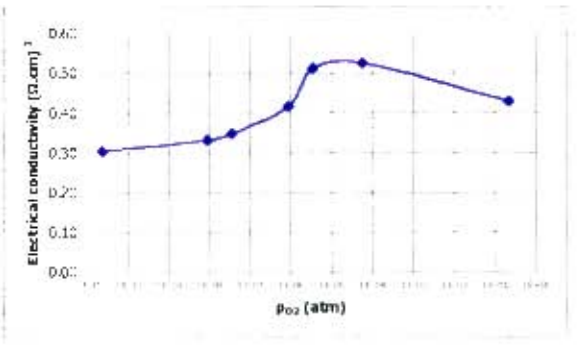

P_{CO2}/P_{CO}	Time	$R_{measured}$	average $\Delta R/\Delta t$	k_{60}	k_{30}	%change
ratio	minutes	Ω	Ω/min	$(\Omega\ cm)^{-1}$	$(\Omega.cm)^{-1}$	
air	9	11.97	-0.004	0.428	0.434	1.4
80	65	10.26	-0.006	0.525	0.538	2.4
10	212	12.25	0.006	0.415	0.408	-1.7
2	295	14.12	0.008	0.347	0.339	-2.1
1	350	14.68	0.004	0.331	0.327	-1.0
$CO+N_2$	395	15.76	-0.002	0.303	0.305	0.5

Note: conductivity measurement for p_{CO2}/p_{CO} = 20 has been omitted as it was not taken at equilibrium

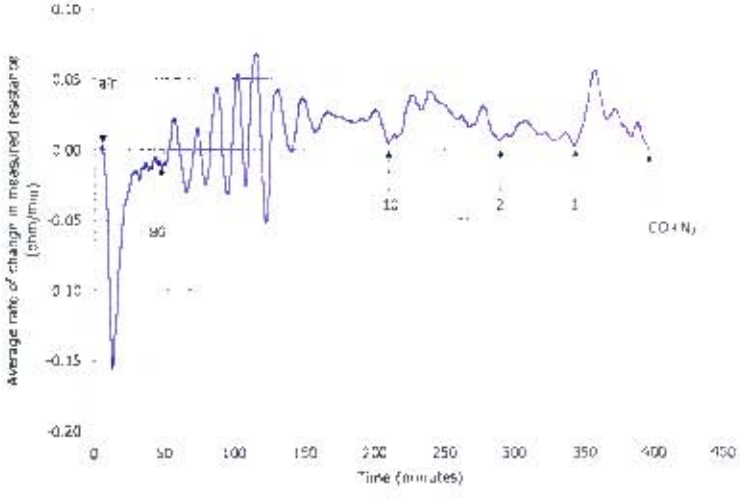

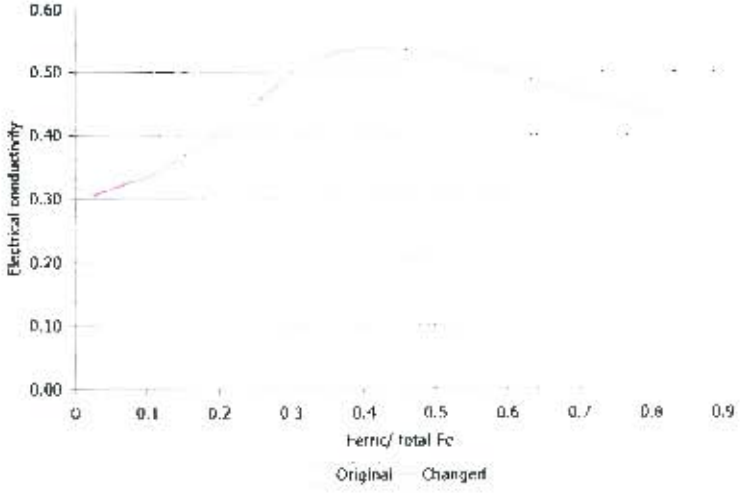

Slag L30 repeat 2

P_{CO_2}/P_{CO}	P_{O_2}	Resistance measured	Electrical conductivity
	atm	Ω	$(\Omega.cm)^{-1}$
air	0.21	11.55	0.448
80	5.6E-05	10.14	0.533
20	3.5E-06	11.89	0.431
10	8.7E 07	14.18	0.345
Calibration slope			-1.07
Calibration intercept			1.44

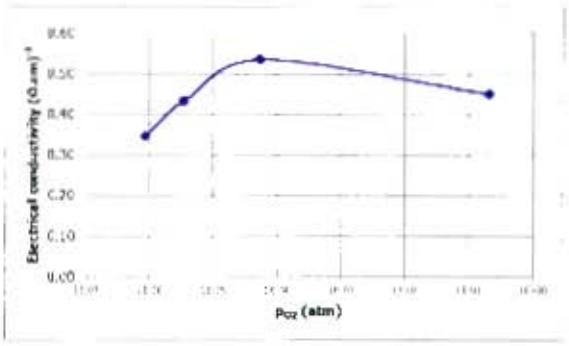

Time	$R_{measured}$	average $\Delta R/\Delta t$	k_{exp}	k_{fit}	%change
minutes	Ω	Ω/min	$(\Omega.cm)^{-1}$	$(\Omega.cm)^{-1}$	
14	11.52	-0.01624	0.443	0.468	5.8
58	10.14	-0.00108	0.524	0.526	0.4
158	11.89	-0.00524	0.425	0.432	1.7
273	14.18	0.013	0.341	0.330	-3.3

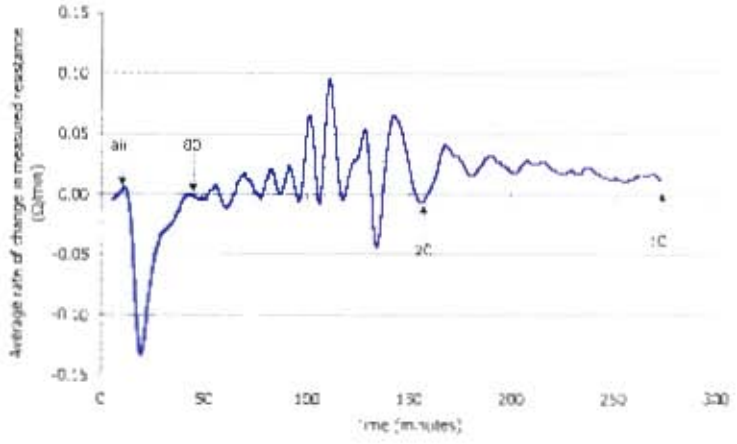

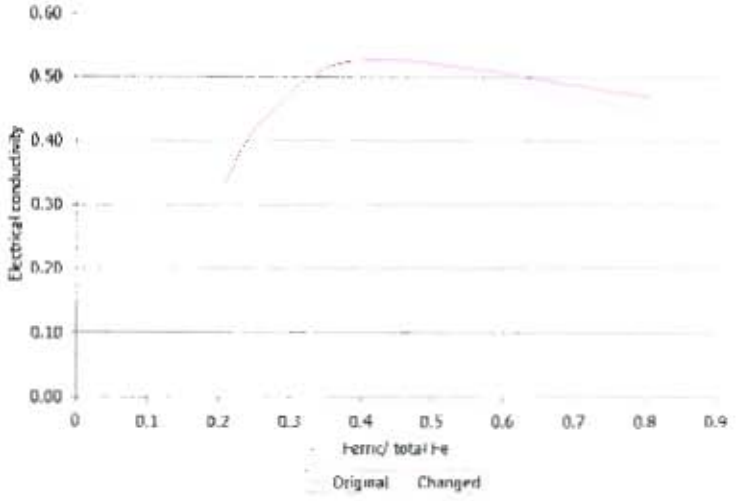

Slag L40 initial

P_{CO_2}/P_{CO}	P_{O_2}	Resistance measured	Electrical conductivity
	atm	Ω	$(\Omega cm)^{-1}$
air	2.1E-01	7.8	0.802
80	5.6E-05	6.7	1.015
20	4.5E-06	7.6	0.805
10	8.7E-07	8.4	0.733
Calibration slope			1.02
Calibration intercept			1.46

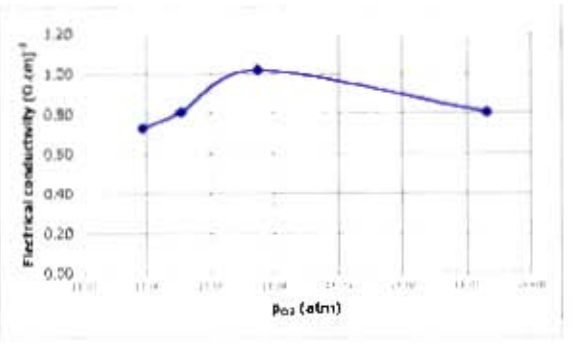

P_{CO_2}/P_{CO}	Time	$R_{measured}$	average $\Delta R/\Delta t$	k_{es}	k_{ec}	Exchange
ratio	minutes	Ω	Ω/min	$(\Omega.cm)^{-1}$	$(\Omega.cm)^{-1}$	
air	10	7.63	-0.501	0.802	0.808	0.6
80	43	6.74	-0.001	1.015	1.023	0.8
20	167	7.81	0.003	0.805	0.792	1.6

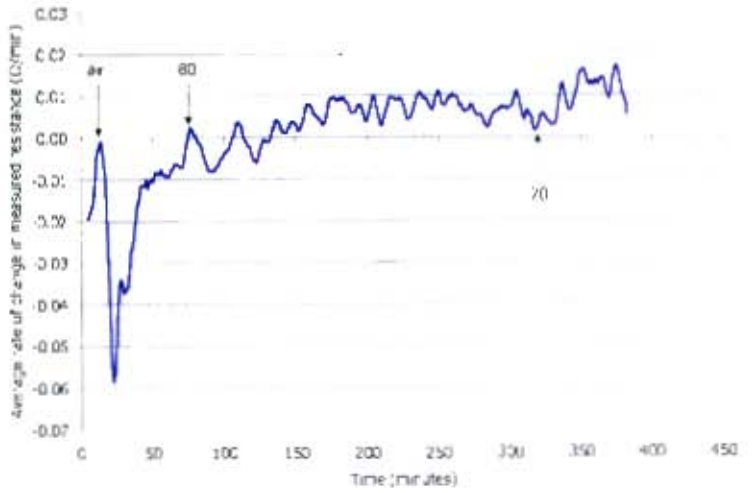

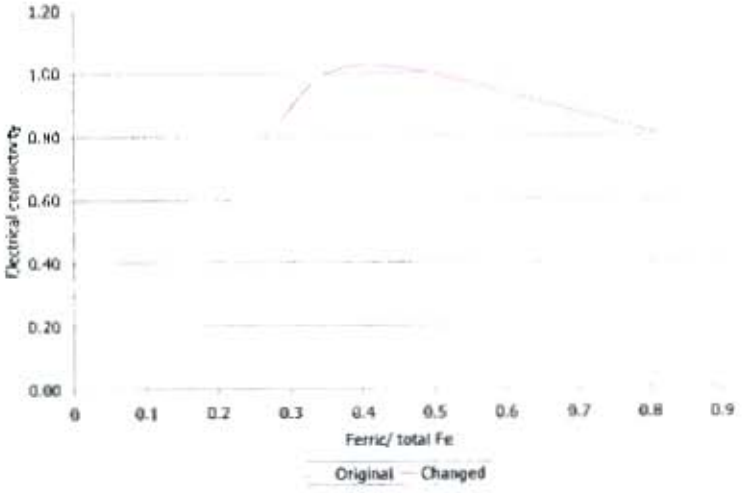

Slag L40 repeat 1

P_{CO2}/P_{CO}	P_{O2}	Resistance measured	Electrical conductivity
	atm	Ω	$(\Omega.cm)^{-1}$
air	2.1E 01	8.0	0.783
80	5.6E 05	6.4	1.103
10	8.7E 07	7.7	0.824
2	3.5E-08	9.6	0.600
0.1	4.7E-11	10.9	0.504
Calibration slope			-1.02
Calibration intercept			1.48

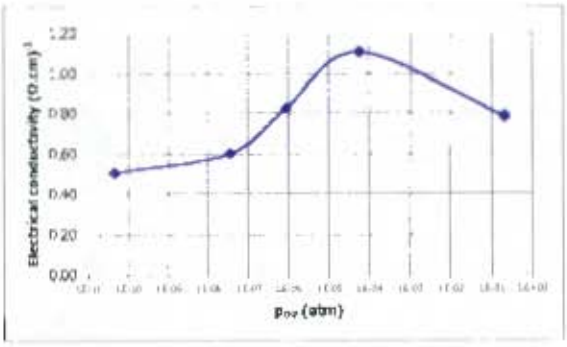

P_{CO2}/P_{CO} ratio	Time minutes	$R_{measured}$ Ω	average $\Delta R/\Delta t$ Ω/min	k_{exp} $(\Omega.cm)^{-1}$	k_{30} $(\Omega.cm)^{-1}$	%change
air	10	7.98	0.010	0.778	0.738	-5.2
80	43	6.42	-0.001	1.102	1.108	0.6
20	167	6.28	-0.001	1.145	1.152	0.6
10	191	7.77	0.013	0.841	0.754	-7.0
5	0	9.56	0.007	0.599	0.582	-2.9
$CO+N_2$	0	10.85	-0.001	0.504	0.506	0.4

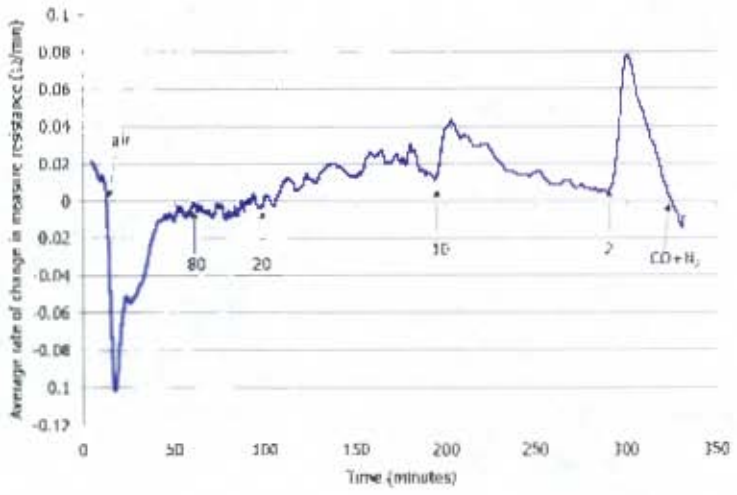

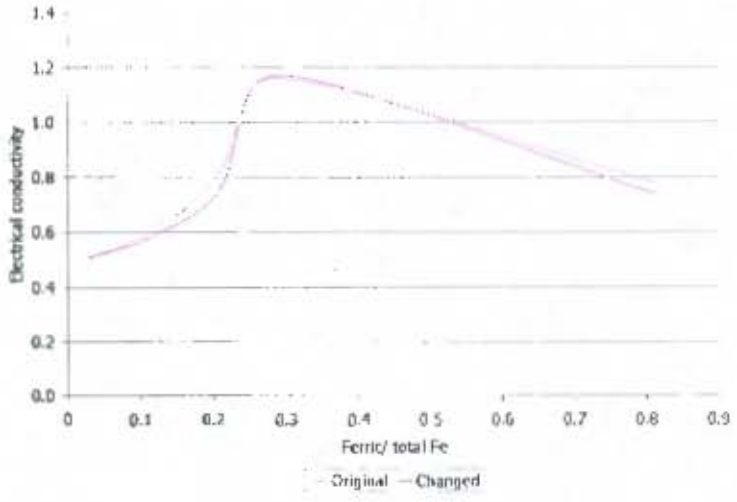

Slag L40 repeat 2

P_{CO2}/P_{CO}	P_{O2}	Resistance measured	Electrical conductivity
	atm	Ω	$(\Omega.cm)^{-1}$
air	2.1E-01	7.7	0.827
80	5.6E-05	6.3	1.132
20	3.5E-06	7.1	0.938
5	2.2E-07	8.7	0.688
0.1	4.7E-11	10.5	0.528
Calibration slope			-1.02
Calibration intercept			1.48

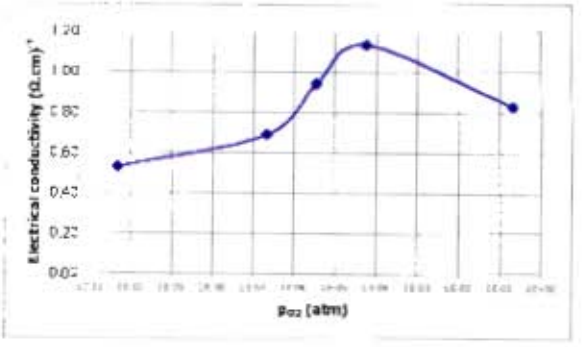

P_{CO2}/P_{CO} ratio	Time minutes	$R_{measured}$ Ω	average ΔR/Δt Ω/min	k_{eq} $(\Omega.cm)^{-1}$	k_{act} $(\Omega.cm)^{-1}$	%change
air	10	7.67	-0.005	0.827	0.851	2.9
80	56	6.32	-0.004	1.132	1.166	3.0
20	185	7.08	0.012	0.938	0.870	-7.3
5	273	8.68	0.007	0.688	0.665	-3.3
$CO+N_2$	317	10.49	0.000	0.528	0.528	0.1

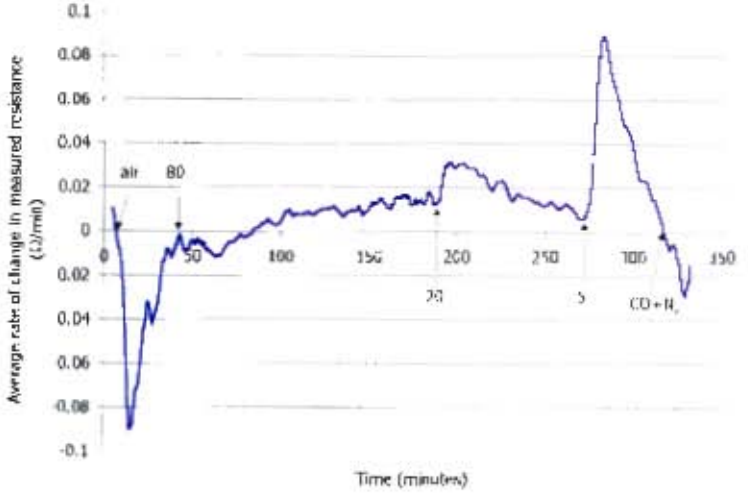

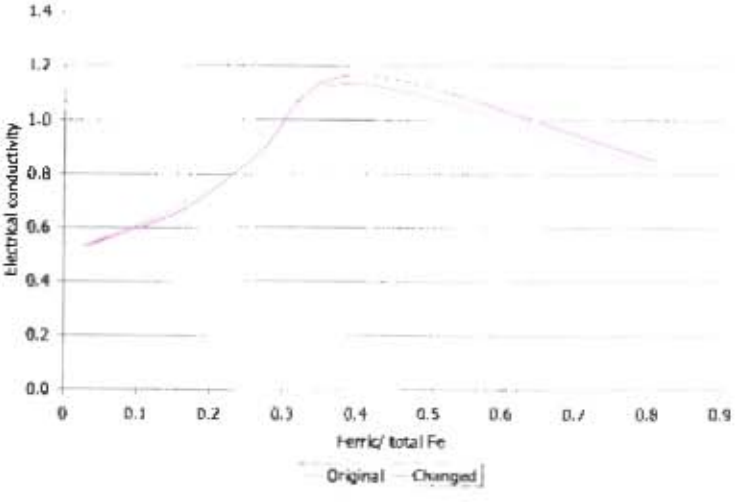

C.2. Intermediate basicity slag

C.2.1. Compositions

The intended and analysed compositions of slag I0 are shown in the table below as the other intermediate basicity slags were made up using slag I0.

Slag I0	intended		analysed	
Component	wt%	mol%	wt%	mol%
Al_2O_3	6.3	3.4	6.1	3.3
CaO	20.0	19.7	19.3	19.1
MgO	20.0	27.4	19.8	27.3
SiO_2	53.8	49.5	54.6	50.4
Total	100.0	100.0	99.8	100.0

The analysed composition was in good agreement with the intended composition although the silica content was slightly higher.

Slag I20	Intended		Initial analysed		Final analysed	
	wt%	mol%	wt%	mol%	wt%	mol%
Al_2O_3	5.0	2.8	5.9	3.4	5.9	3.3
CaO	16.0	16.5	15.8	16.6	16.2	16.6
FeO_x	20.0	16.1	20.7	17.0	18.0	14.4
MgO	16.0	23.0	14.9	21.8	18.6	26.6
SiO_2	43.0	41.5	41.8	41.1	40.7	39.0
Total	100.0	100.0	99.0	100.0	99.4	100.0
(C+M)/(A+S)	0.67	0.89	0.64	0.86	0.75	1.02

	wt%	mol%			
gain in MgO	3.8	4.8		Experiment duration (	5.9
change in B	0.11	0.16		Final CO_2/CO ratio	CO + N_2

Slag I30	Intended		Initial analysed		Final analysed	
	wt%	mol%	wt%	mol%	wt%	mol%
Al_2O_3	4.4	2.5	5.5	3.3	5.4	3.1
CaO	14.0	14.8	13.6	14.8	14.3	14.9
FeO_x	30.0	24.8	30.2	25.7	25.6	20.8
MgO	14.0	20.6	12.7	19.3	18.0	26.1
SiO_2	37.6	37.2	36.2	36.8	36.1	35.1
Total	100.0	100.0	98.2	100.0	99.3	100.0
(C+M)/(A+S)	0.67	0.89	0.63	0.85	0.78	1.07

	wt%	mol%			
gain in MgO	5.2	6.8		Experiment duration (	6
change in B	0.14	0.22		Final CO_2/CO ratio	CO + N_2

Slag I40	Intended		Initial analysed		Final analysed	
	wt%	mol%	wt%	mol%	wt%	mol%
Al_2O_3	3.8	2.2	4.9	3.0	5.2	3.0
CaO	12.0	13.0	11.6	13.1	12.5	13.2
FeO_x	40.0	33.9	39.1	34.4	37.6	31.1
MgO	12.0	18.1	10.8	16.9	15.4	22.6
SiO_2	32.3	32.7	30.9	32.5	30.5	30.1
Total	100.0	100.0	97.3	100.0	101.1	100.0
(C+M)/(A+S)	0.67	0.89	0.62	0.84	0.78	1.08

	wt%	mol%
gain in MgO	4.6	5.7
change in B	0.16	0.24

Experiment duration (	4
Final CO_2/CO ratio	10

I40 rep	Intended		Initial analysed		Final analysed	
	wt%	mol%	wt%	mol%	wt%	mol%
Al_2O_3	3.8	2.2	4.9	3.0	3.9	2.3
CaO	12.0	13.0	11.6	13.1	11.9	13.0
FeO_x	40.0	33.9	39.1	34.4	33.1	28.1
MgO	12.0	18.1	10.8	16.9	16.6	25.2
SiO_2	32.3	32.7	30.9	32.5	30.8	31.3
Total	100.0	100.0	97.3	100.0	96.4	100.0
(C+M)/(A+S)	0.67	0.89	0.62	0.84	0.82	1.13

	wt%	mol%
gain in MgO	5.8	8.3
change in B	0.20	0.29

Experiment duration (	4
Final CO_2/CO ratio	10

C.2.2. Temperature dependence measurements

Slag I0

Temperature	Resistance measured	Electrical conductivity	$1/T * 10^4$	ln □
°C	Ω	$(\Omega.cm)^{-1}$	K^{-1}	$(\Omega.cm)^{-1}$
1407	18.4	0.062	5.95	-2.78
1429	14.6	0.082	5.87	-2.50
1450	12.3	0.102	5.80	-2.28
1474	10.5	0.126	5.72	-2.07
1498	9.2	0.151	5.65	-1.89
1525	8.2	0.180	5.56	-1.71
1550	7.5	0.208	5.49	-1.57
1501	9.0	0.156	5.64	-1.85
1454	11.5	0.112	5.79	-2.19
1405	15.6	0.076	5.96	-2.58
Calibration slope		-1.013	$E_□$	181.0
Calibration intercept		0.024	ln $A_□$	10.4
			rsq	0.99255023

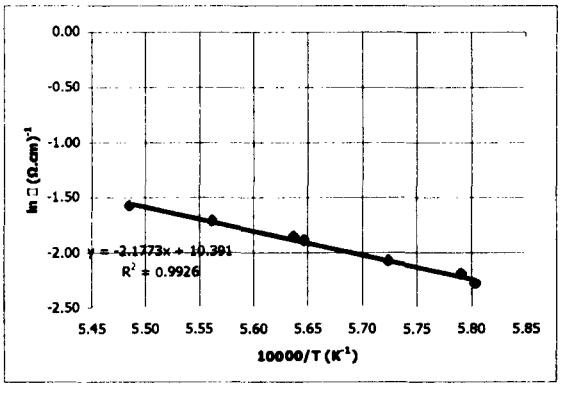

Slag I10

Temperature	Resistance measured	Electrical conductivity	1/T * 10^4	ln □
°C	Ω	$(\Omega.cm)^{-1}$	K^{-1}	$(\Omega.cm)^{-1}$
1407	11.2	0.115	5.95	-2.16
1426	10.0	0.134	5.89	-2.01
1449	8.9	0.158	5.81	-1.85
1475	8.0	0.185	5.72	-1.69
1500	7.2	0.221	5.64	-1.51
1525	6.6	0.255	5.56	-1.37
1550	6.1	0.291	5.49	-1.23
1503	7.2	0.219	5.63	-1.52
1454	8.9	0.159	5.79	-1.84
1403	11.4	0.112	5.97	-2.19
Calibration slope		-1.013	$E_□$	166.0
Calibration intercept		0.024	ln $A_□$	9.7
			rsq	0.99877115

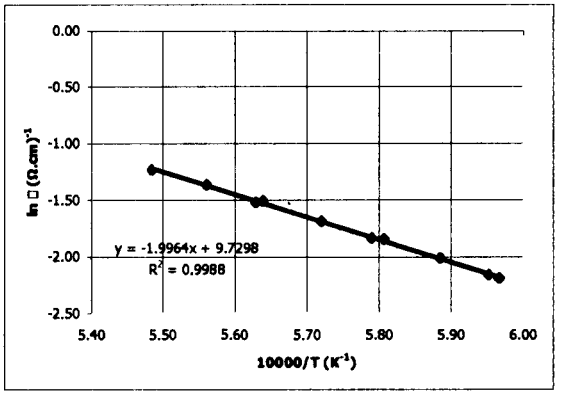

Slag I20

Temperature	Resistance measured	Electrical conductivity	1/T * 10^4	ln □
°C	Ω	$(\Omega.cm)^{-1}$	K^{-1}	$(\Omega.cm)^{-1}$
1407	6.3	0.267	5.95	-1.32
1426	5.8	0.309	5.89	-1.17
1450	5.4	0.353	5.80	-1.04
1475	5.1	0.400	5.72	-0.92
1499	4.9	0.452	5.64	-0.79
1523	4.6	0.509	5.57	-0.68
1551	4.4	0.582	5.48	-0.54
1501	4.8	0.464	5.64	-0.77
1453	5.4	0.355	5.79	-1.04
1403	6.2	0.271	5.97	-1.31
Calibration slope		-1.013	$E_□$	134.3
Calibration intercept		0.024	ln $A_□$	8.3
			rsq	0.99776293

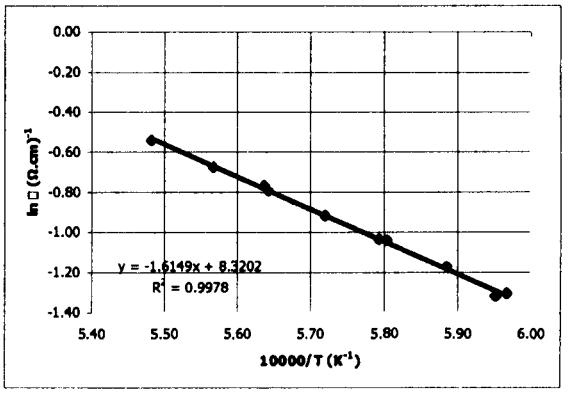

Slag I30

Temperature	Resistance measured	Electrical conductivity	1/T * 10^4	ln □
°C	Ω	$(\Omega.cm)^{-1}$	K^{-1}	$(\Omega.cm)^{-1}$
1405	4.5	0.519	5.96	-0.66
1429	4.3	0.596	5.87	-0.52
1452	4.1	0.667	5.80	-0.41
1477	4.0	0.746	5.71	-0.29
1501	3.8	0.833	5.64	-0.18
1523	3.8	0.918	5.57	-0.09
1551	3.7	1.046	5.48	0.05
1504	3.8	0.849	5.63	-0.16
1453	4.1	0.679	5.79	-0.39
Calibration slope		-1.013	$E_□$	119.6
Calibration intercept		0.024	ln $A_□$	7.9
			rsq	0.99863542

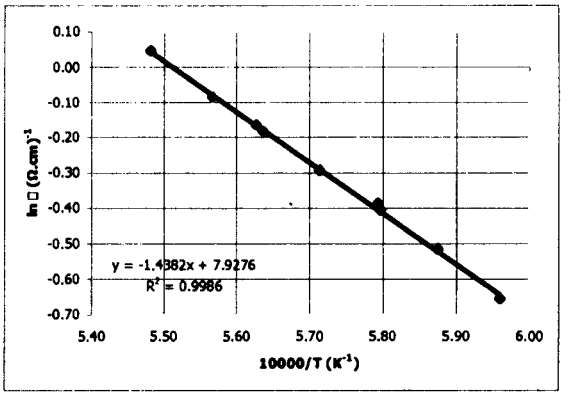

C.2.3. Oxidation state measurements

Slag I20

P_{CO2}/P_{CO}	P_{O2}	Resistance measured	Electrical conductivity
	atm	Ω	$(\Omega.cm)^{-1}$
air	2.1E-01	13.3	0.353
80	5.6E-05	12.9	0.392
20	3.5E-06	12.2	0.393
10	8.7E-07	12.7	0.374
5	2.2E-07	13.4	0.352
2	3.5E-08	13.7	0.343
1	8.7E-09	13.9	0.337
0.05	1.9E-11	14.5	0.320
Calibration slope			-1.02
Calibration intercept			1.41

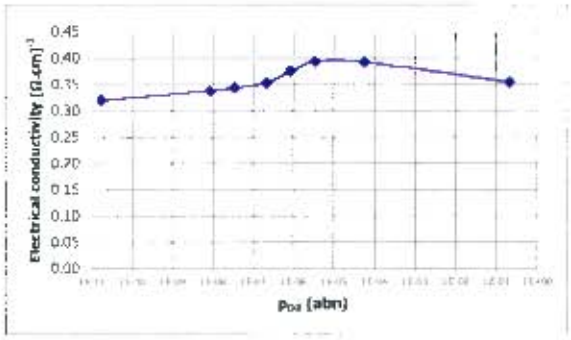

P_{CO2}/P_{CO}	Time	$R_{measured}$	Average $(\Delta R/\Delta t)$	κ_{eq}	κ_{20}	%change
ratio	minutes	Ω	(Ω/min)	$(\Omega.cm)^{-1}$	$(\Omega.cm)^{-1}$	
air	12	13.35	0.003	0.353	0.351	-0.8
80	54	12.26	0.002	0.392	0.390	-0.5
20	112	12.24	0.001	0.393	0.392	-0.3
10	175	12.74	0.007	0.374	0.366	-2.1
5	251	13.38	0.007	0.352	0.345	-1.9
2	292	13.66	0.011	0.343	0.333	-2.9
1	329	13.86	-0.001	0.337	0.338	0.2
$CO + N_2$	357	14.47	-0.002	0.320	0.322	0.5

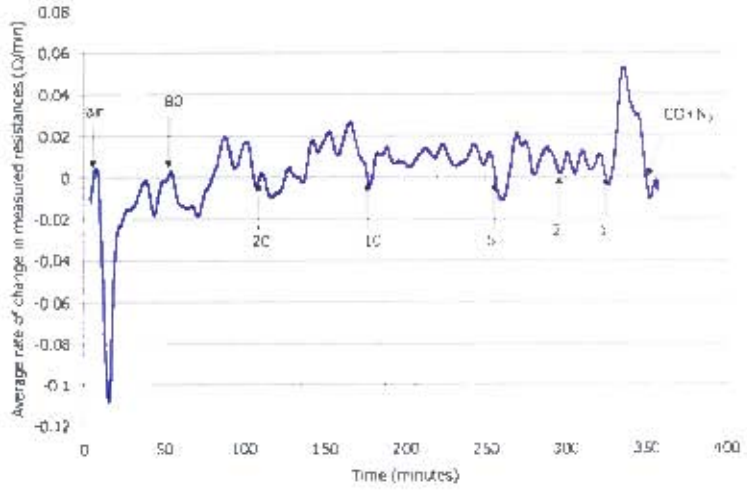

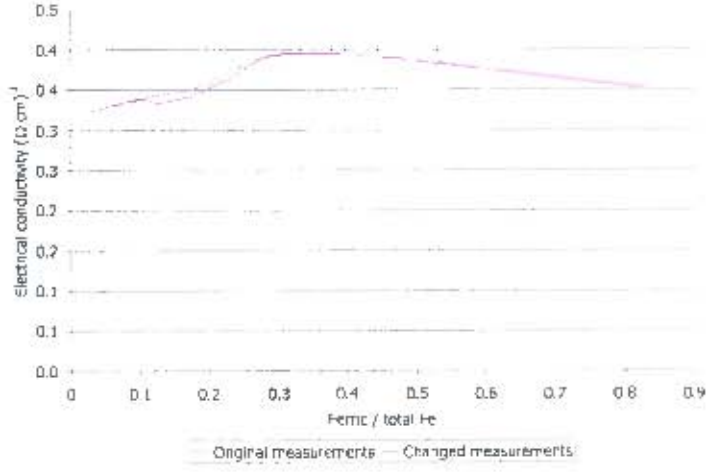

Slag I30

P_{CO2}/P_{CO}	P_{O2} atm	Resistance measured Ω	Electrical conductivity $(\Omega.cm)^{-1}$
air	7.1E-01	10.5	0.514
80	5.6E-05	8.7	0.729
20	3.5E-06	8.0	0.760
10	8.7E-07	8.6	0.683
5	2.2E-07	9.0	0.644
2	3.5E-08	9.4	0.600
1	8.7E-09	9.7	0.574
0.1	4.7E-11	10.3	0.527
Calibration slope			-1.02
Calibration intercept			1.45

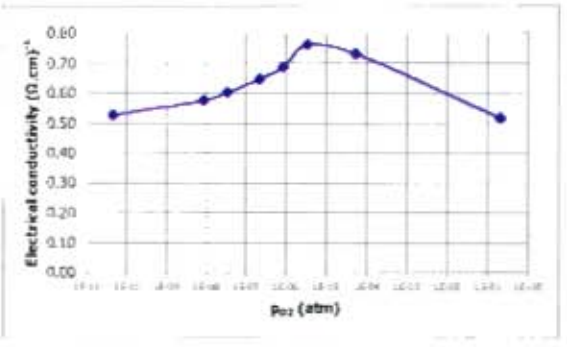

P_{CO2}/P_{CO} ratio	Time minutes	$R_{measured}$ Ω	Average $(\Delta R/\Delta t)$ (Ω/min)	κ_{eq} $(\Omega.cm)^{-1}$	κ_{30} $(\Omega.cm)^{-1}$	%change
air	20	10.53	0.001	0.514	0.512	-0.4
80	66	8.23	0.000	0.729	0.727	-0.2
20	115	8.00	0.002	0.760	0.754	-0.9
10	202	8.59	0.007	0.683	0.660	-3.4
5	244	8.96	0.007	0.644	0.622	-3.5
2	293	9.41	0.003	0.600	0.592	-1.3
1	336	9.72	0.002	0.574	0.570	-0.7
$CO + N_2$	356	10.34	-0.002	0.527	0.530	0.7

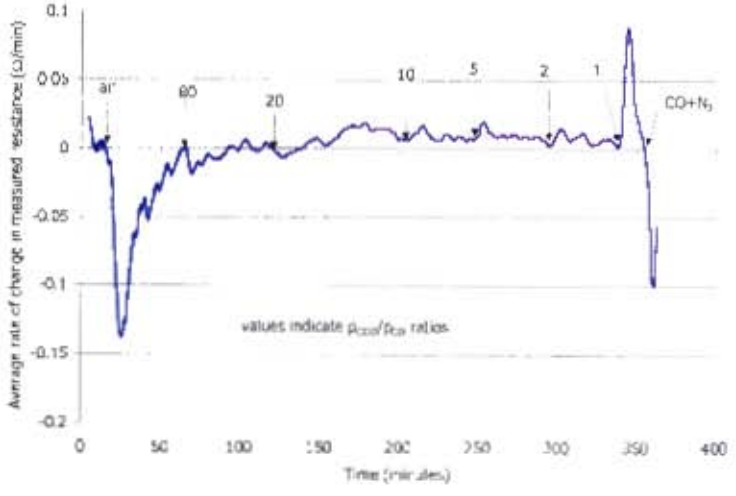

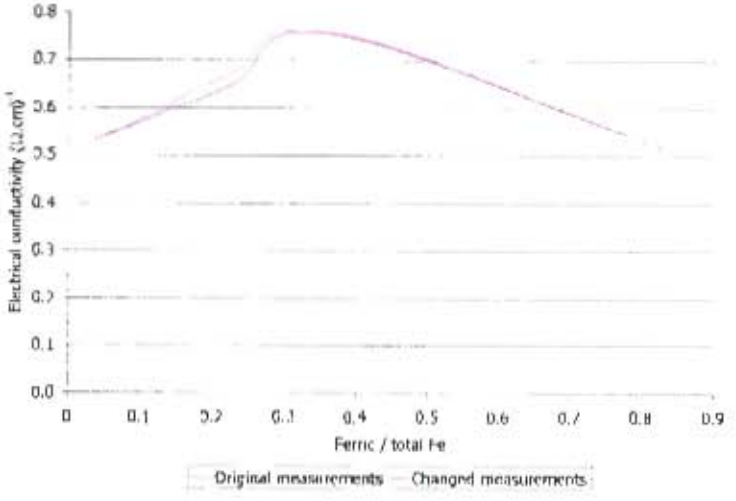

Slag 140 initial

P_{CO2}/P_{CO}	P_{O2}	Resistance measured	Electrical conductivity
	atm	Ω	$(\Omega.cm)^{-1}$
air	2.1E 01	6.8	1.017
80	5.6E 05	5.7	1.386
20	3.5E-06	5.7	1.395
10	8.7E-07	6.1	1.220
Calibration slope			-1.02
Calibration intercept			1.49

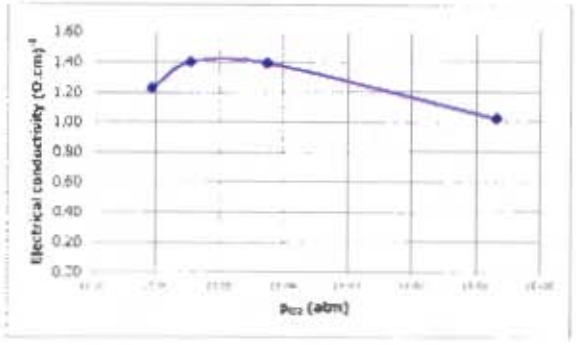

P_{CO2}/P_{CO}	Time	$R_{measured}$	Average $(\Delta R/\Delta t)$	κ_{eq}	κ_{10}	%change
ratio	minutes	Ω	(Ω/min)	$(\Omega.cm)^{-1}$	$(\Omega.cm)^{-1}$	
air	15	6.79	-0.011	1.017	1.104	8.6
80	64	5.69	-0.002	1.386	1.418	2.3
20	142	5.61	0.000	1.424	1.419	-0.3
10	222	6.10	0.002	1.220	1.194	-2.1

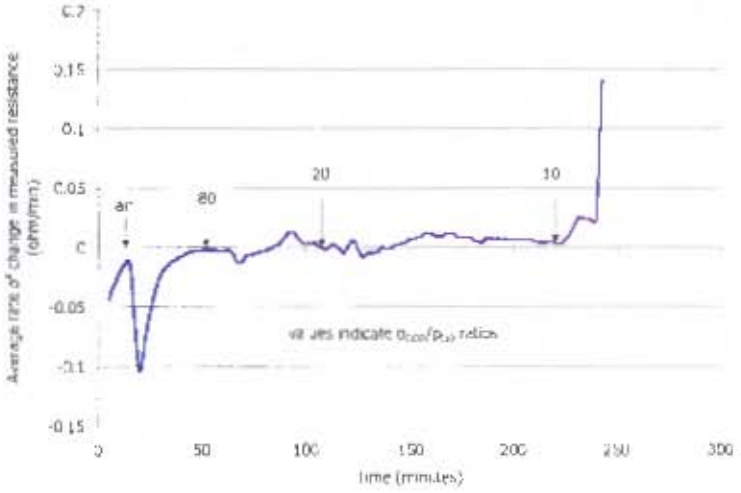

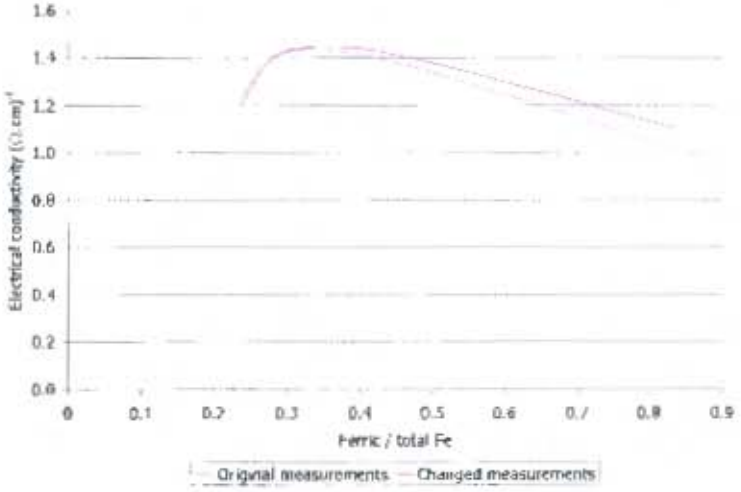

Slag 140 repeat

P_{CO2}/P_{CO}	P_{O2}	Resistance measured	Electrical conductivity
	atm	Ω	$(\Omega.cm)^{-1}$
air	2.1E-01	7.6	0.856
80	5.6E-05	5.9	1.296
20	3.5E-06	5.6	1.432
10	8.7E-07	6.0	1.242
2	1.5E-08	6.4	1.114
0.1	8.7E-11	6.9	0.985
Calibration slope			-1.02
Calibration intercept			1.49

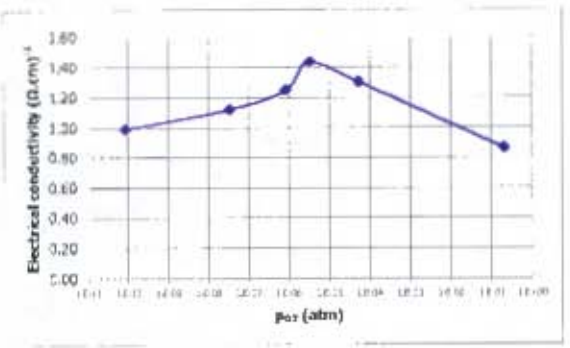

P_{CO2}/P_{CO}	Time	$R_{measured}$	Average $(\Delta R/\Delta t)$	κ_{eq}	κ_{140}	%change
ratio	minutes	Ω	(Ω/min)	$(\Omega.cm)^{-1}$	$(\Omega.cm)^{-1}$	
air	15	7.56	-0.009	0.856	0.907	6.0
80	82	5.90	-0.003	1.296	1.333	2.8
20	145	5.59	0.000	1.432	1.437	0.4
10	238	6.04	0.001	1.242	1.228	-1.1
2	275	6.43	0.003	1.114	1.088	-2.3
$CO - N_2$	292	6.92	0.001	0.985	0.981	-0.4

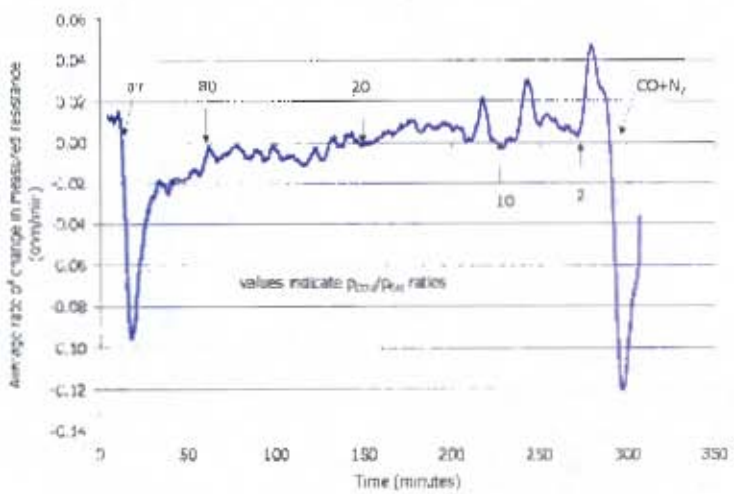

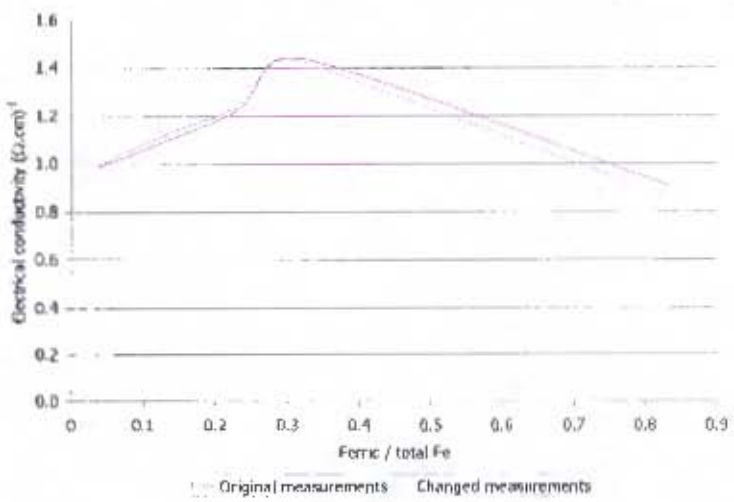

L40 rep 1	Intended		Initial analysed		Final analysed	
Component	wt%	mol%	wt%	mol%	wt%	mol%
Al_2O_3	3.8	2.2	5.0	3.0	4.0	2.4
CaO	3.8	4.0	3.9	4.3	4.1	4.4
FeO_x	40.0	33.6	37.8	32.7	34.2	28.8
MgO	15.0	22.5	13.7	21.1	18.5	27.9
SiO_2	37.5	37.7	37.4	38.8	36.2	36.5
Total	100.0	100.0	97.8	100.0	97.1	100.0
(C+M)/(A+S)	0.45	0.66	0.41	0.61	0.56	0.83

	wt%	mol%
gain in MgO	4.8	6.7
change in B	0.15	0.22

Experiment duration (hr)	6
Final CO_2/CO ratio	10

L40 rep 2	Intended		Initial analysed		Final analysed	
Component	wt%	mol%	wt%	mol%	wt%	mol%
Al_2O_3	3.8	2.2	5.0	3.0	3.7	2.2
CaO	3.8	4.0	3.9	4.3	3.9	4.2
FeO_x	40.0	33.6	37.8	32.7	33.8	28.3
MgO	15.0	22.5	13.7	21.1	19.6	29.3
SiO_2	37.5	37.7	37.4	38.8	36.0	36.1
Total	100.0	100.0	97.8	100.0	97.0	100.0
(C+M)/(A+S)	0.45	0.66	0.41	0.61	0.59	0.87

	wt%	mol%
gain in MgO	5.9	8.1
change in B	0.18	0.27

Experiment duration (hr)	6
Final CO_2/CO ratio	10

C.1.2. Temperature dependence measurements

Slag L0

Temperature	Resistance measured	Electrical conductivity	$1/T * 10^4$	ln □
°C	Ω	$(\Omega.cm)^{-1}$	K^{-1}	$(\Omega.cm)^{-1}$
1475	18.3	0.063	5.72	-2.77
1498	16.2	0.073	5.65	-2.62
1518	14.6	0.083	5.58	-2.49
1548	12.3	0.104	5.49	-2.27
1526	13.6	0.091	5.56	-2.40
1475	18.2	0.063	5.72	-2.76
1466	19.4	0.059	5.75	-2.83
1456	21.0	0.054	5.78	-2.93
1445	22.5	0.050	5.82	-3.00
Calibration slope		-1.013	E_0	184.9
Calibration intercept		0.024	ln A_0	9.9
			rsq	0.997555425

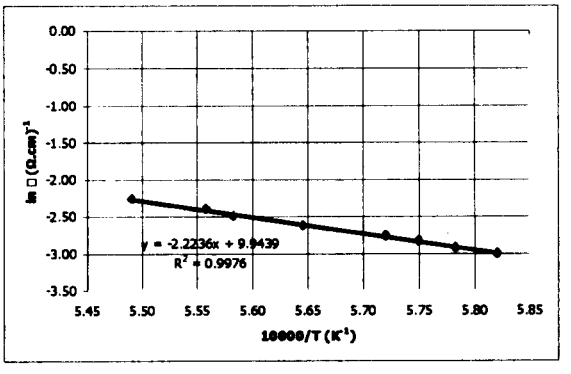

Slag L30	Intended		Initial analysed		Final analysed	
Component	wt%	mol%	wt%	mol%	wt%	mol%
Al_2O_3	4.4	2.5	5.5	3.2	5.3	3.1
CaO	4.4	4.6	4.5	4.8	4.6	4.8
FeO_x	30.0	24.6	29.3	24.6	26.3	21.6
MgO	17.5	25.5	16.0	23.9	20.0	29.3
SiO_2	43.8	42.8	43.4	43.4	41.9	41.1
Total	100.0	100.0	98.7	100.0	98.2	100.0
(C+M)/(A+S)	0.45	0.66	0.42	0.62	0.52	0.77

	wt%	mol%
gain in MgO	4.0	5.4
change in B	0.10	0.16

Experiment duration (hr)	7
Final CO_2/CO ratio	2

L30 rep 1	Intended		Initial analysed		Final analysed	
Component	wt%	mol%	wt%	mol%	wt%	mol%
Al_2O_3	4.4	2.5	5.5	3.2	4.5	2.6
CaO	4.4	4.6	4.5	4.8	4.6	4.8
FeO_x	30.0	24.6	29.3	24.6	25.6	21.0
MgO	17.5	25.5	16.0	23.9	20.9	30.5
SiO_2	43.8	42.8	43.4	43.4	42.0	41.2
Total	100.0	100.0	98.7	100.0	97.6	100.0
(C+M)/(A+S)	0.45	0.66	0.42	0.62	0.55	0.81

	wt%	mol%
gain in MgO	4.9	6.5
change in B	0.13	0.19

Experiment duration (hr)	7
Final CO_2/CO ratio	2

L30 rep 2	Intended		Initial analysed		Final analysed	
Component	wt%	mol%	wt%	mol%	wt%	mol%
Al_2O_3	4.4	2.5	5.5	3.2	4.5	2.6
CaO	4.4	4.6	4.5	4.8	4.6	4.8
FeO_x	30.0	24.6	29.3	24.6	26.8	21.6
MgO	17.5	25.5	16.0	23.9	21.2	30.4
SiO_2	43.8	42.8	43.4	43.4	42.2	40.7
Total	100.0	100.0	98.7	100.0	99.4	100.0
(C+M)/(A+S)	0.45	0.66	0.42	0.62	0.55	0.81

	wt%	mol%
gain in MgO	5.2	6.5
change in B	0.13	0.20

Experiment duration (hr)	7
Final CO_2/CO ratio	2

Slag L40	Intended		Initial analysed		Final analysed	
Component	wt%	mol%	wt%	mol%	wt%	mol%
Al_2O_3	3.8	2.2	5.0	3.0	4.9	2.9
CaO	3.8	4.0	3.9	4.3	4.0	4.2
FeO_x	40.0	33.6	37.8	32.7	35.3	29.5
MgO	15.0	22.5	13.7	21.1	18.2	27.1
SiO_2	37.5	37.7	37.4	38.8	36.3	36.2
Total	100.0	100.0	97.8	100.0	98.6	100.0
(C+M)/(A+S)	0.45	0.66	0.41	0.61	0.54	0.80

	wt%	mol%
gain in MgO	4.5	6.0
change in B	0.12	0.19

Experiment duration (hr)	6
Final CO_2/CO ratio	10

C.3. High basicity slag

C.3.1. Compositions

As the other high basicity slags were made up from the master slag H0, the intended and analysed compositions of slag H0 are provided in the table below:

Table: Intended and analysed compositions of the high basicity master slag H0

Slag H0	Intended		Analysed	
Component	wt%	mol%	wt%	mol%
Al_2O_3	5.0	2.7	5.3	2.9
CaO	30.0	29.2	28.7	28.2
MgO	20.0	27.1	19.6	26.8
SiO_2	45.0	40.9	45.8	42.1
Total	100	100.0	99.3	100.0
(C+M)/(A+S)	1.00	1.29	0.94	1.22

The lime and magnesia contents of the analysed slag were slightly lower than intended which meant that the wt% basicity ratio was 0.94 instead of 1.00.

Slag H20	Intended		Initial analysed		Final analysed	
	wt%	mol%	wt%	mol%	wt%	mol%
Al_2O_3	4.0	2.3	4.8	2.7	4.5	2.5
CaO	24.0	24.6	23.1	24.0	21.8	22.1
FeO_x	20.0	16.0	19.0	15.5	18.5	14.7
MgO	16.0	22.8	15.4	22.4	19.2	27.2
SiO_2	36.0	34.4	36.4	35.4	35.3	33.5
Total	100.0	100.0	98.6	100.0	99.3	100.0
(C+M)/(A+S)	1.00	1.29	0.93	1.22	1.03	1.37

	wt%	mol%		
gain in MgO	3.8	4.8	Experiment duration (	6
change in B	0.09	0.15	Final CO_2/CO ratio	CO + N_2

Slag H30	Intended		Initial analysed		Final analysed	
	wt%	mol%	wt%	mol%	wt%	mol%
Al_2O_3	3.5	2.0	4.3	2.6	4.2	2.4
CaO	21.0	22.1	19.6	21.3	20.7	21.2
FeO_x	30.0	24.6	29.6	25.1	24.3	19.5
MgO	14.0	20.5	13.0	19.7	18.8	26.8
SiO_2	31.5	30.9	30.8	31.3	31.3	30.0
Total	100.0	100.0	97.3	100.0	99.3	100.0
(C+M)/(A+S)	1.00	1.29	0.93	1.21	1.11	1.48

	wt%	mol%		
gain in MgO	5.8	7.2	Experiment duration (	5.3
change in B	0.18	0.27	Final CO_2/CO ratio	CO + N_2

H30	Intended		Initial analysed		Final analysed	
	wt%	mol%	wt%	mol%	wt%	mol%
Al_2O_3	3.5	2.0	4.3	2.6	3.7	2.1
CaO	21.0	22.1	19.6	21.3	21.0	21.9
FeO_x	30.0	24.6	29.6	25.1	23.8	19.4
MgO	14.0	20.5	13.0	19.7	18.4	26.8
SiO_2	31.5	30.9	30.8	31.3	30.6	29.8
Total	100.0	100.0	97.3	100.0	97.5	100.0
(C+M)/(A+S)	1.00	1.29	0.93	1.21	1.15	1.52

	wt%	mol%
gain in MgO	5.4	7.1
change in B	0.22	0.31

Experiment duration (	5.3
Final CO_2/CO ratio	$CO + N_2$

H30 rep	Intended		Initial analysed		Final analysed	
	wt%	mol%	wt%	mol%	wt%	mol%
Al_2O_3	3.5	2.0	4.3	2.6	3.8	2.2
CaO	21.0	22.1	19.6	21.3	21.6	22.6
FeO_x	30.0	24.6	29.6	25.1	23.1	18.9
MgO	14.0	20.5	13.0	19.7	17.3	25.2
SiO_2	31.5	30.9	30.8	31.3	32.0	31.2
Total	100.0	100.0	97.3	100.0	97.8	100.0
(C+M)/(A+S)	1.00	1.29	0.93	1.21	1.09	1.43

	wt%	mol%
gain in MgO	4.3	5.5
change in B	0.16	0.22

Experiment duration (	5.3
Final CO_2/CO ratio	$CO + N_2$

Slag H40 initial	Intended		Initial analysed		Final analysed	
	wt%	mol%	wt%	mol%	wt%	mol%
Al_2O_3	3.0	1.8	4.0	2.4	3.8	2.2
CaO	18.0	19.4	16.9	18.9	17.5	18.3
FeO_x	40.0	33.7	37.9	33.0	32.3	26.4
MgO	12.0	18.0	11.4	17.6	18.6	27.1
SiO_2	27.0	27.2	27.0	28.1	26.6	26.0
Total	100.0	100.0	97.2	100.0	98.7	100.0
(C+M)/(A+S)	1.00	1.29	0.91	1.20	1.19	1.61

	wt%	mol%
gain in MgO	7.2	9.5
change in B	0.27	0.42

Experiment duration (	5.6
Final CO_2/CO ratio	$CO + N_2$

Slag H40 repeat	Intended		Initial analysed		Final analysed	
	wt%	mol%	wt%	mol%	wt%	mol%
Al_2O_3	3.0	1.8	4.0	2.4	3.3	2.0
CaO	18.0	19.4	16.9	18.9	17.6	18.9
FeO_x	40.0	33.7	37.9	33.0	34.7	29.1
MgO	12.0	18.0	11.4	17.6	15.6	23.2
SiO_2	27.0	27.2	27.0	28.1	26.7	26.8
Total	100.0	100.0	97.2	100.0	98.0	100.0
(C+M)/(A+S)	1.00	1.29	0.91	1.20	1.10	1.47

	wt%	mol%
gain in MgO	4.2	5.6
change in B	0.19	0.27

Experiment duration (	2.9
Final CO_2/CO ratio	10

C.3.2. Temperature dependence measurements

Slag H0

Temperature	Resistance measured	Electrical conductivity	1/T * 10^4	ln □
°C	Ω	$(\Omega.cm)^{-1}$	K^{-1}	$(\Omega.cm)^{-1}$
1396	9.51	0.143	5.99	-1.95
1417	8.07	0.181	5.92	-1.71
1452	6.60	0.249	5.80	-1.39
1477	6.00	0.296	5.71	-1.22
1502	5.56	0.343	5.63	-1.07
1527	5.19	0.397	5.56	-0.92
1551	4.90	0.455	5.48	-0.79
Calibration slope		-1.013	$E_□$	157.9
Calibration intercept		0.024	ln $A_□$	9.6
			rsq	0.99951078

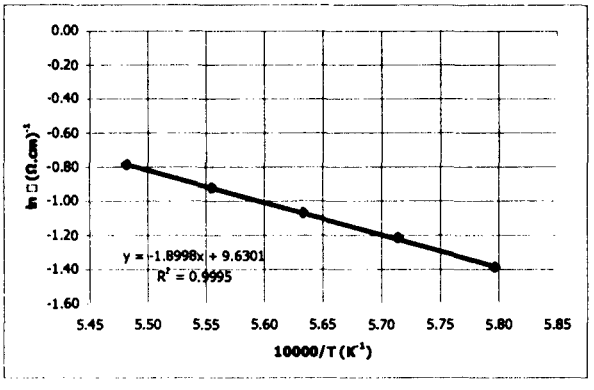

Slag H10

Temperature	Resistance measured	Electrical conductivity	1/T * 10^4	ln □
°C	Ω	$(\Omega.cm)^{-1}$	K^{-1}	$(\Omega.cm)^{-1}$
1401	7.00	0.224	5.97	-1.50
1430	6.18	0.277	5.87	-1.28
1452	5.65	0.327	5.80	-1.12
1477	5.25	0.381	5.71	-0.97
1502	4.90	0.444	5.63	-0.81
1526	4.61	0.517	5.56	-0.66
1552	4.39	0.592	5.48	-0.52
Calibration slope		-1.013	$E_□$	160.2
Calibration intercept		0.024	ln $A_□$	10.0
			rsq	0.99901703

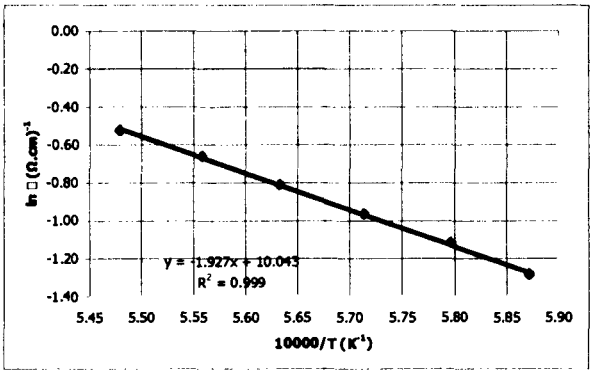

Slag H15

Temperature	Resistance measured	Electrical conductivity	1/T * 10⁴	ln □
°C	Ω	$(\Omega.cm)^{-1}$	K^{-1}	$(\Omega.cm)^{-1}$
1408	5.88	0.301	5.95	-1.20
1425	5.52	0.339	5.89	-1.08
1452	5.17	0.389	5.80	-0.94
1476	4.86	0.446	5.72	-0.81
1500	4.57	0.520	5.64	-0.65
1524	4.36	0.591	5.56	-0.53
1546	4.20	0.664	5.50	-0.41
1503	4.51	0.537	5.63	-0.62
1456	4.98	0.420	5.78	-0.87
Calibration slope		-1.013	$E_□$	144.9
Calibration intercept		0.024	ln $A_□$	9.2
			rsq	0.99571627

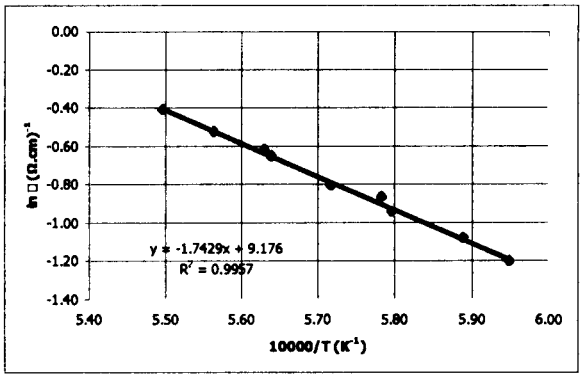

Slag H20

Temperature	Resistance measured	Electrical conductivity	1/T * 10⁴	ln □
°C	Ω	$(\Omega.cm)^{-1}$	K^{-1}	$(\Omega.cm)^{-1}$
1405	5.21	0.375	5.96	-0.98
1427	4.94	0.423	5.88	-0.86
1452	4.70	0.475	5.80	-0.74
1475	4.46	0.545	5.72	-0.61
1498	4.27	0.613	5.65	-0.49
1524	4.12	0.691	5.56	-0.37
1548	4.00	0.768	5.49	-0.26
1500	4.27	0.617	5.64	-0.48
1453	4.63	0.492	5.79	-0.71
1404	5.23	0.373	5.96	-0.99
Calibration slope		-1.013	$E_□$	128.4
Calibration intercept		0.024	ln $A_□$	8.2
			rsq	0.99895134

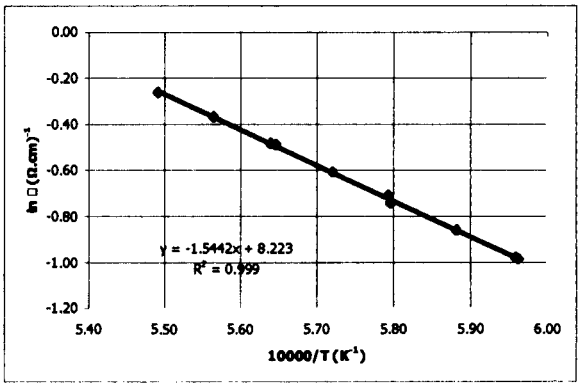

Slag H30

Temperature	Resistance measured	Electrical conductivity	1/T * 10⁴	ln □
°C	Ω	$(\Omega.cm)^{-1}$	K^{-1}	$(\Omega.cm)^{-1}$
1407	4.10	0.645	5.95	-0.44
1427	4.02	0.692	5.88	-0.37
1450	3.90	0.763	5.80	-0.27
1475	3.80	0.849	5.72	-0.16
1501	3.70	0.950	5.64	-0.05
1524	3.61	1.055	5.56	0.05
1550	3.53	1.193	5.49	0.18
1453	3.85	0.797	5.79	-0.23
Calibration slope		-1.013	$E_□$	109.1
Calibration intercept		0.024	ln $A_□$	7.4
			rsq	0.99557777

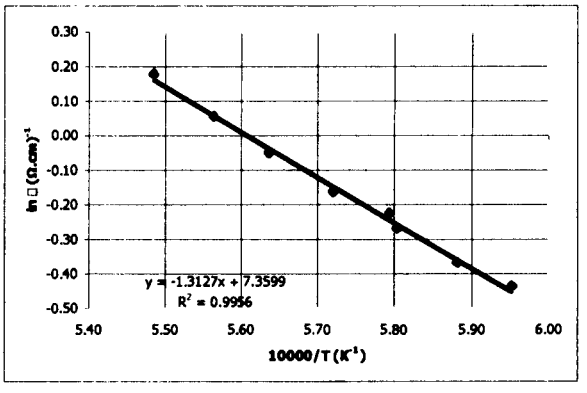

C.3.3. Oxidation state measurements

Slag H20

P_{CO_2}/P_{CO}	P_{O_2}	Resistance measured	Electrical conductivity
	atm	Ω	$(\Omega.cm)^{-1}$
air	2.1E-01	13.1	0.381
80	5.6E-05	10.5	0.509
20	3.5E-06	10.3	0.522
10	8.7E-07	10.4	0.518
5	2.2E-07	10.5	0.511
2	3.5E-08	10.5	0.511
1	8.7E-09	10.5	0.510
0.1	4.5E-11	10.8	0.493
Calibration slope			-1.02
Calibration intercept			1.44

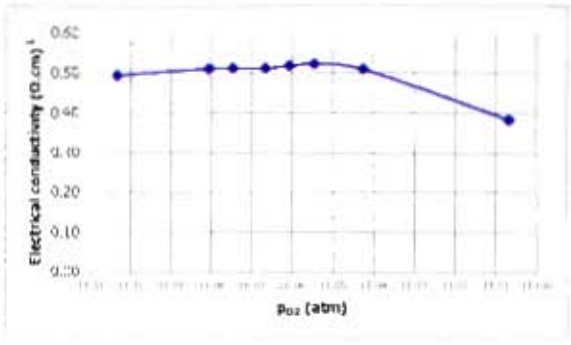

P_{CO_2}/P_{CO}	Time	$R_{measured}$	Average $(\Delta R/\Delta t)$	σ_{eq}	σ_{av}	%change
ratio	minutes	Ω	(Ω/min)	$(\Omega.cm)^{-1}$	$(\Omega.cm)^{-1}$	
air	18	13.1	-0.011	0.381	0.393	3.1
80	67	10.5	-0.005	0.509	0.519	1.9
20	133	10.3	0.003	0.522	0.515	-1.4
10	178	10.4	0.000	0.518	0.519	0.1
5	223	10.5	0.008	0.511	0.495	-3.0
2	283	10.5	0.002	0.511	0.508	-0.6
1	332	10.5	0.000	0.510	0.511	0.0
CO + N_2	345	10.7	-0.002	0.496	0.500	0.9

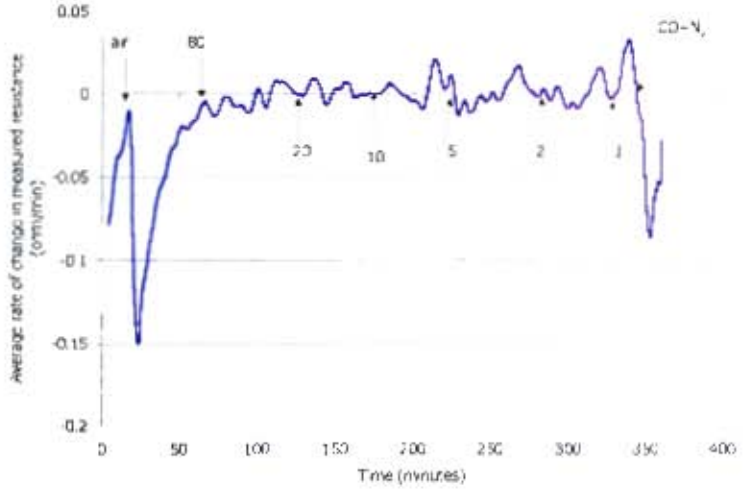

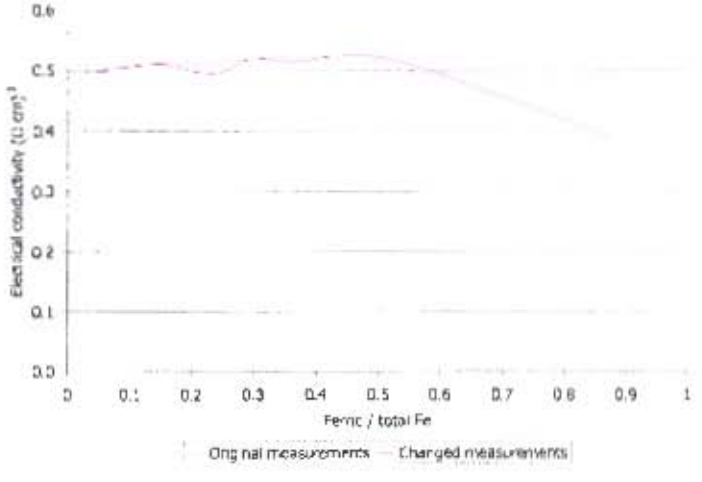

Slag H30 initial

P_{CO_2}/P_{CO}	P_{O_2}	Resistance measured	Electrical conductivity
	atm	Ω	$(\Omega\,cm)^{-1}$
air	2.1E-01	10.3	0.540
80	5.6E-05	7.6	0.845
20	3.5E-06	7.1	0.935
10	8.7E-07	6.6	1.053
5	2.2E-07	6.7	1.025
1	8.7E-09	7.6	0.830
0.1	9.2E-11	8.4	0.722
Calibration slope			-1.02
Calibration intercept			1.48

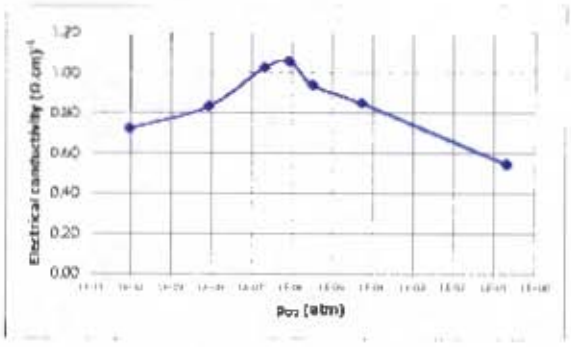

P_{CO_2}/P_{CO} ratio	Time minutes	$R_{measured}$ Ω	Average $(\Delta R/\Delta t)$ Ω/min	κ_{est} $(\Omega.cm)^{-1}$	κ_{30} $(\Omega.cm)^{-1}$	%change
air	33	10.3	-0.006	0.540	0.553	2.4
80	89	7.5	-0.003	0.849	0.867	2.1
20	122	7.1	-0.008	0.941	0.993	5.5
10	162	6.6	-0.003	1.053	1.079	2.5
5	226	6.7	0.000	1.025	1.025	0.0
1	287	7.6	0.003	0.835	0.820	-1.9
$CO + N_2$	310	8.7	-0.002	0.680	0.687	1.0

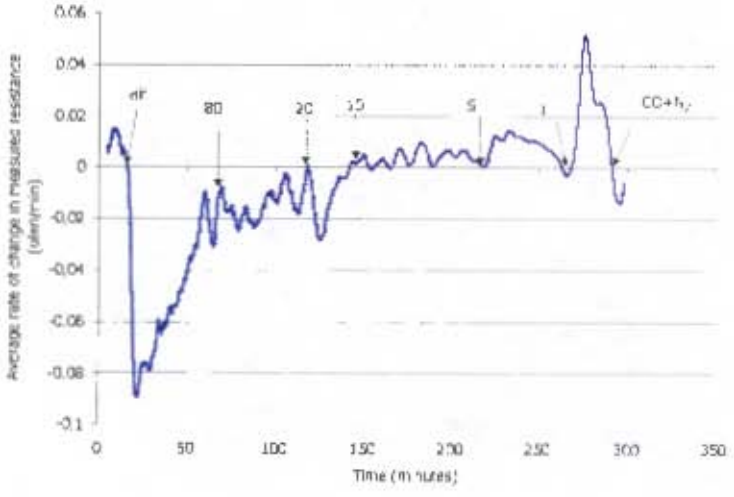

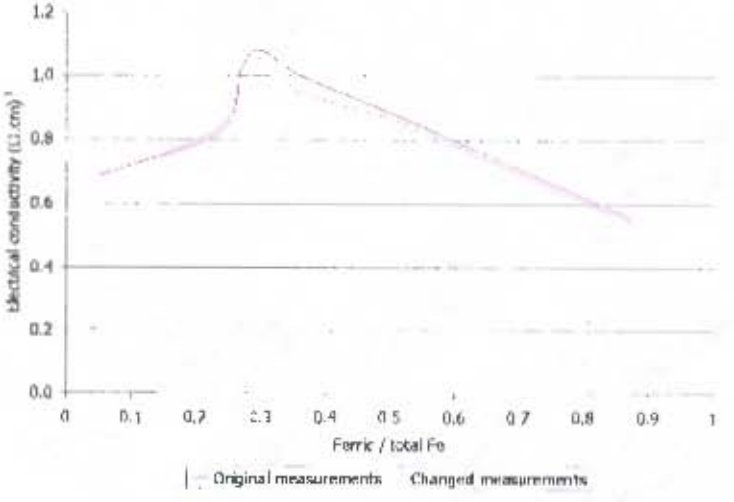

Slag H30 repeat

P_{CO_2}/P_{CO}	P_{O_2}	Resistance measured	Electrical conductivity
	atm	Ω	$(\Omega.cm)^{-1}$
air	2.1E-01	10.0	0.560
80	5.6E 05	7.4	0.874
20	3.5E-06	6.8	0.991
10	8.7E-07	6.4	1.109
5	2.2E-07	6 6	1 039
1	8.7E-09	7.0	0 945
0.1	9.2E 11	7 7	0 827
Calibration slope			-1 02
Calibration intercept			1.48

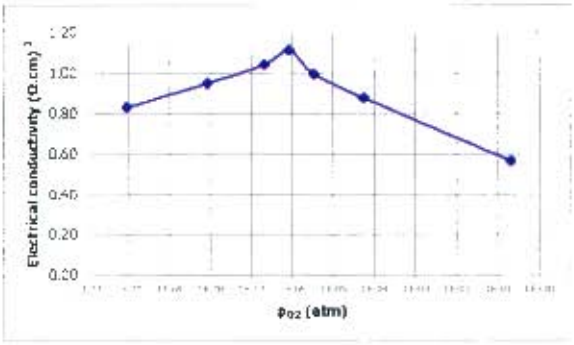

P_{CO_2}/P_{CO}	Time	$R_{measured}$	Average $(\Delta R/\Delta t)$	κ_{exp}	κ_{30}	%change
ratio	minutes	Ω	(Ω/min)	$(\Omega.cm)^{-1}$	$(\Omega.cm)^{-1}$	
air	17	10.0	-0.001	0.566	0.569	0.6
80	70	7.5	-0.008	0.861	0.909	5.6
20	119	6.7	-0.001	1.023	1.030	0.7
10	147	6.4	0.001	1.109	1.099	-1.0
5	215	6.6	0.002	1.039	1.020	-1.8
1	268	7.0	-0.002	0.945	0.958	1.3
$CO + N_2$	291	7.6	0.001	0.829	0.823	-0.8

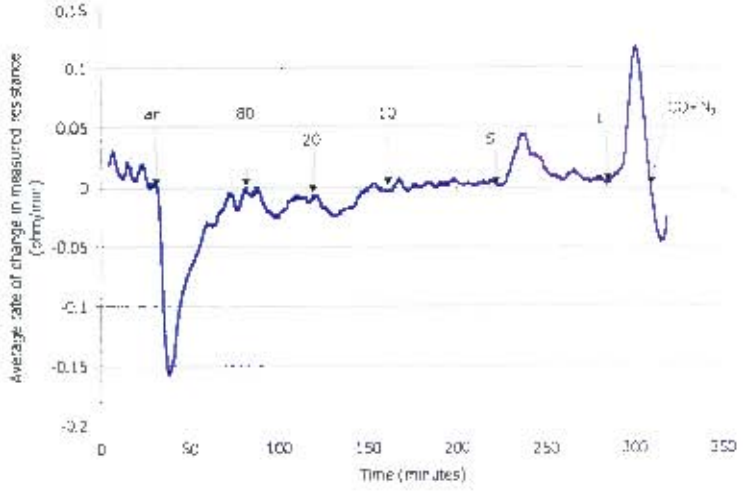

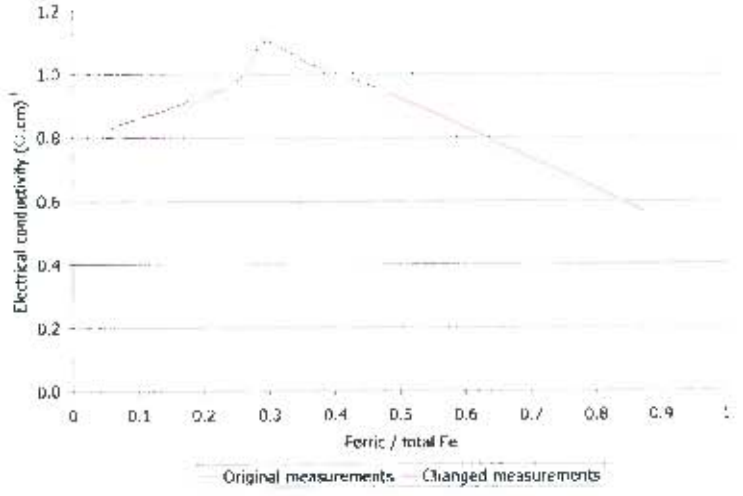

Slag H40 initial

P_{CO_2}/P_{CO}	P_{O_2}	Resistance measured	Electrical conductivity
	atm	Ω	$(\Omega\ cm)^{-1}$
air	2.1E-01	7.6	0.865
80	5.6E-05	5.9	1.328
20	3.5E-06	5.4	1.556
10	8.7E-07	5.2	1.657
5	2.2E-07	5.4	1.558
2	3.5E-08	5.8	1.350
1	8.7E-09	6.3	1.185
0.13	1.5E-10	7.5	0.877
Calibration slope			-1.03
Calibration intercept			1.51

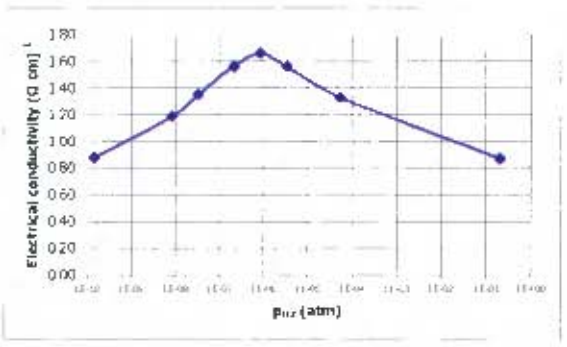

P_{CO_2}/P_{CO} ratio	Time minutes	$R_{measure}$ Ω	Average $(\Delta R/\Delta t)$ (Ω/min)	κ_{eq} $(\Omega.cm)^{-1}$	κ_{fit} $(\Omega.cm)^{-1}$	%change
air	19	7.61	0.000	0.865	0.864	-0.2
80	63	5.89	-0.001	1.328	1.341	1.0
20	106	5.41	-0.004	1.556	1.620	4.1
10	158	5.24	0.000	1.658	1.653	-0.3
5	203	5.41	0.000	1.558	1.550	-0.5
2	254	5.83	0.002	1.350	1.323	-2.0
1	295	6.28	0.003	1.185	1.156	-2.5
$CO + N_2$	315	7.54	0.001	0.877	0.874	-0.4

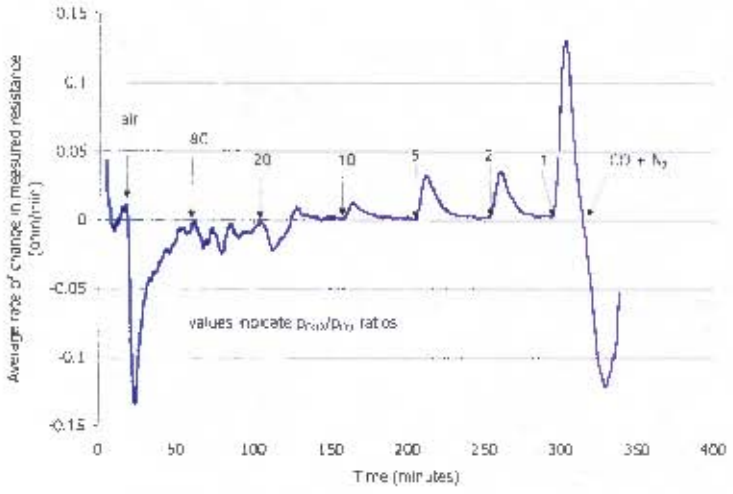

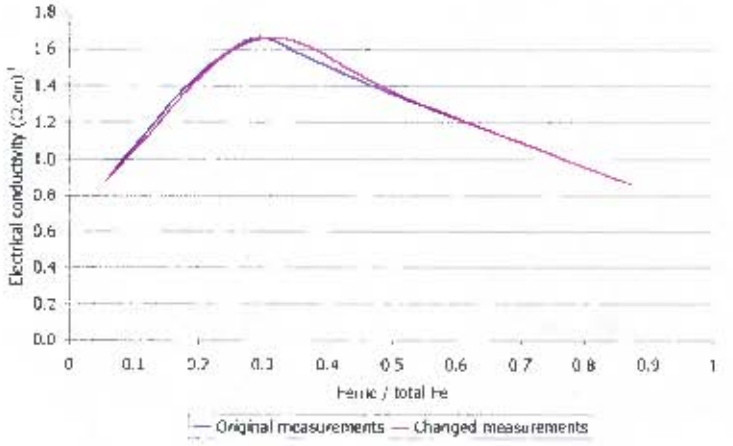

C.4. Chromium containing slags

Slag Cr0				
0% Cr_2O_3				
Temperature	Resistance measured	Electrical conductivity	10^4 / T	$\ln \sigma$
°C	Ω	$(\Omega\ m)^{-1}$	K^{-1}	$(\Omega\ m)^{-1}$
1399	7.75	0.192	5.08	-1.65
1441	6.69	0.242	5.89	-1.42
1449	6.07	0.287	5.81	-1.25
1473	5.67	0.328	5.73	-1.12
1498	5.31	0.375	5.66	-0.98
1521	4.99	0.415	5.57	-0.84
Calibration slope		-1.013	E	147.4
Calibration intercept		0.024	ln A	9.04
			R^2	0.9988

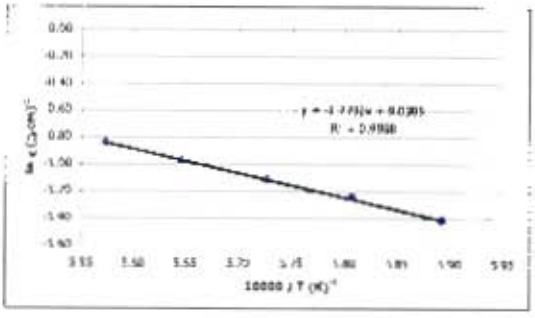

Slag Cr0.5				
0.5% Cr_2O_3				
Temperature	Resistance measured	Electrical conductivity	10^4 / T	$\ln \sigma$
°C	Ω	$(\Omega\ m)^{-1}$	K^{-1}	$(\Omega\ m)^{-1}$
1397	8.09	0.180	5.08	-1.72
1424	7.06	0.221	5.89	-1.51
1450	6.36	0.270	5.80	-1.31
1475	5.79	0.315	5.72	-1.16
1501	5.38	0.366	5.64	-1.00
1525	5.04	0.422	5.55	-0.86
1550	4.75	0.488	5.49	-0.72
Calibration slope		-1.013	E	159.3
Calibration intercept		0.024	ln A	9.80
			R	0.9998

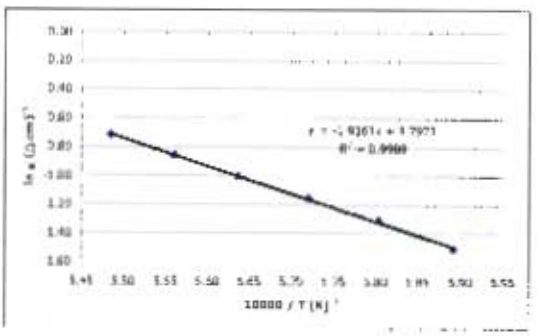

Slag Cr1				
1% Cr_2O_3				
Temperature	Resistance measured	Electrical conductivity	10^4 / T	$\ln \sigma$
°C	Ω	$(\Omega\ m)^{-1}$	K^{-1}	$(\Omega\ m)^{-1}$
1402	7.27	0.191	5.98	-1.66
1425	6.88	0.232	5.89	-1.46
1452	6.16	0.279	5.80	-1.28
1475	5.66	0.329	5.72	-1.11
1502	5.21	0.379	5.64	0.97
1525	4.93	0.444	5.56	-0.81
1552	4.64	0.517	5.49	-0.66
Calibration slope		-1.013	E	162.7
Calibration intercept		0.024	ln A	10.07
			R^2	0.9991

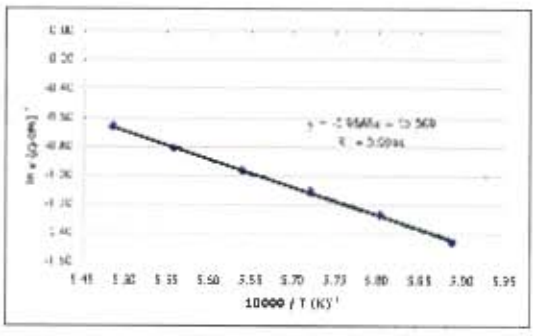

Slag Cr2				
2% Cr_2O_3				
Temperature	Resistance measured	Electrical conductivity	10^4 / T	$\ln \sigma$
°C	Ω	$(\Omega\ m)^{-1}$	K^{-1}	$(\Omega\ m)^{-1}$
1400	8.45	0.185	5.98	-1.78
1425	7.17	0.217	5.89	-1.53
1450	6.60	0.249	5.80	-1.39
1475	6.06	0.295	5.72	-1.24
1498	5.61	0.332	5.65	-1.09
1526	5.21	0.394	5.56	-0.93
1550	4.84	0.467	5.49	-0.76
Calibration slope		-1.013	E	159.3
Calibration intercept		0.024	ln A	9.67
			R^2	0.9982

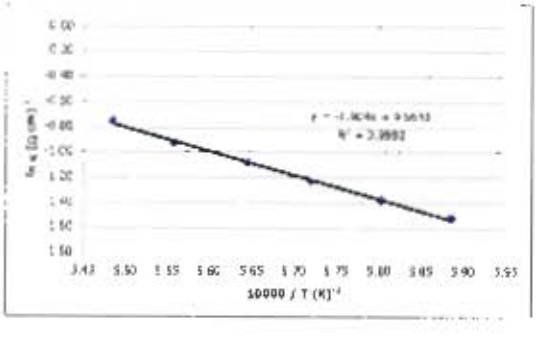

Slag H40 repeat

P_{CO_2}/P_{CO}	P_{O_2}	Resistance measured	Electrical conductivity
	atm	Ω	$(\Omega.cm)^{-1}$
air	2.1E-01	7.1	0.976
80	5.6E-05	5.7	1.414
20	3.5E-06	5.3	1.609
10	8.7E-07	5.2	1.679
Calibration slope			-1.03
Calibration intercept			1.51

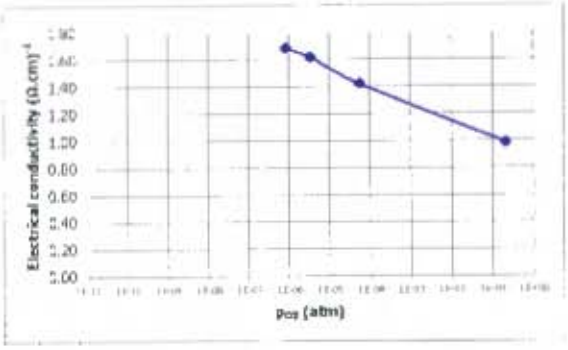

P_{CO_2}/P_{CO}	Time	$P_{measured}$	Average $(\Delta R_i/\Delta t)$	κ_{exp}	κ_{fit}	%change
ratio	minutes	Ω	(Ω/min)	$(\Omega.cm)^{-1}$	$(\Omega.cm)^{-1}$	
air	19	7.05	-0.003	0.975	0.999	2.4
80	65	5.69	-0.002	1.414	1.444	2.2
20	123	5.30	-0.005	1.618	1.714	5.9
10	175	5.21	0.001	1.679	1.658	1.3

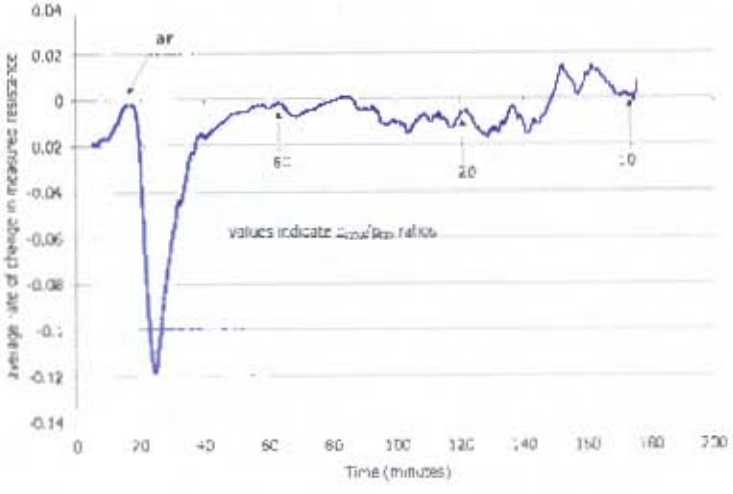

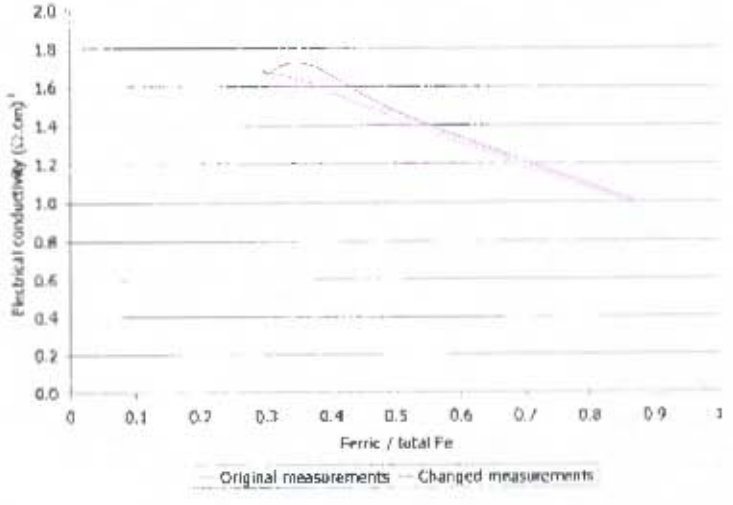

Slag Cr4				
4% Cr_2O_3				
Temperature	Resistance measured	Electrical conductivity	10^4 / T	$\ln \sigma$
°C	Ω	$(\Omega\ cm)^{-1}$	K^{-1}	$(\Omega\ cm)^{-1}$
1402	8.99	0.154	5.97	-1.87
1429	7.44	0.205	5.87	-1.58
1452	6.76	0.240	5.80	-1.43
1478	6.15	0.284	5.71	-1.26
1503	5.68	0.330	5.63	-1.11
1527	5.33	0.377	5.56	-0.97
1542	5.12	0.411	5.51	-0.89
Calibration slope		-1.013	E_σ	157.6
Calibration intercept		0.024	$\ln A_\sigma$	9.56
			R^2	0.9996

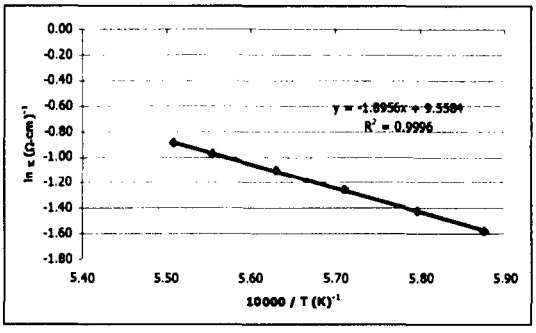

Slag Cr6				
6% Cr_2O_3				
Temperature	Resistance measured	Electrical conductivity	10^4 / T	$\ln \sigma$
°C	Ω	$(\Omega\ cm)^{-1}$	K^{-1}	$(\Omega\ cm)^{-1}$
1403	8.98	0.155	5.97	-1.87
1427	7.71	0.194	5.88	-1.64
1451	7.04	0.225	5.80	-1.49
1476	6.44	0.262	5.72	-1.34
1502	5.96	0.302	5.63	-1.20
1525	5.60	0.342	5.56	-1.07
1549	5.28	0.388	5.49	-0.95
Calibration slope		-1.013	E_σ	146.0
Calibration intercept		0.024	$\ln A_\sigma$	8.69
			R^2	0.9998

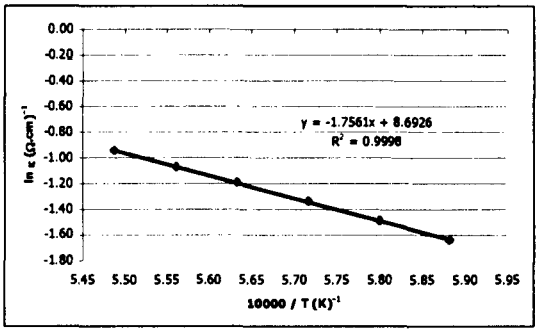

Slag Cr8				
8% Cr_2O_3				
Temperature	Resistance measured	Electrical conductivity	10^4 / T	$\ln \sigma$
°C	Ω	$(\Omega\ cm)^{-1}$	K^{-1}	$(\Omega\ cm)^{-1}$
1405	9.90	0.135	5.96	-2.00
1428	7.98	0.184	5.88	-1.69
1453	7.20	0.217	5.79	-1.53
1476	6.61	0.250	5.72	-1.39
1502	6.15	0.286	5.63	-1.25
1526	5.69	0.332	5.56	-1.10
1552	5.29	0.386	5.48	-0.95
Calibration slope		-1.013	E_σ	152.6
Calibration intercept		0.024	$\ln A_\sigma$	9.10
			R^2	0.9993